

An Advanced Course in Nuclear Engineering

Yoshiaki Oka *Editor*

Nuclear Reactor Design



Springer

An Advanced Course in Nuclear Engineering

Series Editors: Yoshiaki Oka, Tokyo, Japan
Haruki Madarame, Tokyo, Japan
Mitsuru Uesaka, Tokyo, Japan

For further volumes:
<http://www.springer.com/series/10746>

An Advanced Course in Nuclear Engineering

Since the beginning of the twenty-first century, expectations have been rising for nuclear power generation in the world because the need for a safe and stable energy supply is increasing against the background of global environmental issues and the depletion of oil-based energy sources. The situation is calling for the development of human resources with advanced knowledge and techniques of nuclear energy. The role of nuclear energy remains unchanged in the world even after Fukushima Daiichi Nuclear Power Plant accident. Needs for education and human resource development of nuclear professionals who understand and manage the nuclear power have increased worldwide.

This series of books is really the renaissance of publication covering the full fields of, and reflecting recent advances in, nuclear engineering and technology in these three past decades in the world.

Anyone who tries to solve and counter practical problems and unknown application problems encountered in using nuclear energy will face the need to return to the basics. This requires the capability to envision various images of the subject. The systematic acquisition of knowledge of nuclear energy is fundamental to nuclear R&D and the development of the nuclear industry. This series of books is designed to serve that purpose.

We have been publishing this series as a set of standard books for systematically studying nuclear energy from the basics to actual practice, with the aim of nurturing experts and engineers who can act from a global perspective. While being aware of the situation surrounding nuclear energy, students need not only to familiarize themselves with basic knowledge but also to acquire practical expertise, including flexible knowledge and first-hand techniques that allow them to understand field practices without experiencing any gap.

This series consists of three courses on nuclear energy: the basic course, the frontier course, and the practical course. The content is based on the education at the Nuclear Professional School and the Department of Nuclear Engineering and Management, both established by the University of Tokyo with the aim of developing high-level human resources specializing in nuclear energy to cope with the new century of nuclear energy. The books were written mainly by faculty members of the University of Tokyo and researchers at the Japan Atomic Energy Agency and in related industries.

We would like to extend our gratitude to all those who have kindly taken the time to contribute to or cooperate in the creation and publication of this book series.

Yoshiaki Oka, Haruki Madarame, and Mitsuru Uesaka

Department of Nuclear Engineering and Management, and Nuclear Professional School,
School of Engineering, The University of Tokyo

Yoshiaki Oka
Editor

Nuclear Reactor Design



Springer

Editor
Yoshiaki Oka
Cooperative Major in Nuclear Energy
Graduate School of Advanced Science
and Engineering
Waseda University
Tokyo, Japan

Professor Emeritus
The University of Tokyo
Tokyo, Japan

Content Editor
Takashi Kiguchi
Japan Nuclear Energy Safety Organization
Tokyo, Japan

Original Japanese edition
Genshiryoku Kyokasho: Genshiro Sekkei
Edited by Yoshiaki Oka, Copyright © 2010 Published by Ohmsha, Ltd.
3-1 Kanda Nishikicho, Chiyoda-ku, Tokyo, Japan

ISSN 2195-3708 ISSN 2195-3716 (electronic)
ISBN 978-4-431-54897-3 ISBN 978-4-431-54898-0 (eBook)
DOI 10.1007/978-4-431-54898-0
Springer Tokyo Heidelberg New York Dordrecht London

Library of Congress Control Number: 2014932983

© Authors 2014

This work is subject to copyright. All rights are reserved by the Publisher, whether the whole or part of the material is concerned, specifically the rights of translation, reprinting, reuse of illustrations, recitation, broadcasting, reproduction on microfilms or in any other physical way, and transmission or information storage and retrieval, electronic adaptation, computer software, or by similar or dissimilar methodology now known or hereafter developed. Exempted from this legal reservation are brief excerpts in connection with reviews or scholarly analysis or material supplied specifically for the purpose of being entered and executed on a computer system, for exclusive use by the purchaser of the work. Duplication of this publication or parts thereof is permitted only under the provisions of the Copyright Law of the Publisher's location, in its current version, and permission for use must always be obtained from Springer. Permissions for use may be obtained through RightsLink at the Copyright Clearance Center. Violations are liable to prosecution under the respective Copyright Law.

The use of general descriptive names, registered names, trademarks, service marks, etc. in this publication does not imply, even in the absence of a specific statement, that such names are exempt from the relevant protective laws and regulations and therefore free for general use.

While the advice and information in this book are believed to be true and accurate at the date of publication, neither the authors nor the editors nor the publisher can accept any legal responsibility for any errors or omissions that may be made. The publisher makes no warranty, express or implied, with respect to the material contained herein.

Printed on acid-free paper

Springer is part of Springer Science+Business Media (www.springer.com)

Preface

Nuclear reactor design is based on knowledge and data from many nuclear engineering fields including nuclear reactor physics, nuclear thermal hydraulics, and nuclear safety.

In nuclear reactor design, reactor performance is evaluated by numerical analysis for requirements of nuclear and thermal limitations, stability, controllability, and safety, referred to as conceptual design. To approximate reactor performance, the design then proceeds to hardware design of reactor facilities using knowledge from mechanical engineering, electrical engineering, and nuclear structural engineering. The consequent reactor power plant facilities are mainly described in another textbook of this series titled Nuclear Plant Engineering. Knowledge of nuclear reactor fuel and materials is referenced in the conceptual design for reactor performance and in the hardware design which include in particular the fuel assemblies, reactor vessel, and its internal structures. The conceptual and hardware designs may be repeated if necessary.

To understand nuclear reactor design, it is necessary not only to be aware of the structures and compositions of the facilities constructed by the conceptual and hardware designs but also to comprehend the processes and methods used to reach the nuclear reactor design. This book describes an approach to design and calculation methods, focused on core design. Many pages have been devoted to core calculation methods and light water reactor core design. We hope that this book will help professionals as well as beginners understand and review the methods and core design.

Features of each chapter are summarized as follows.

“Fuel Burnup and Reactivity Control” of Chap. 1 is not only a key component of nuclear reactor physics but also of core design, reactor operation management, and safety. Details, including calculation methods, are described. Because the textbook of this series titled *Nuclear Reactor Physics* does not cover the topics in this chapter, it is recommended that readers interested in nuclear reactor physics read Chap. 1.

Section 2.1, “Nuclear Design Calculation,” first describes nuclear data and neutron cross sections and their processing methods for the nuclear calculation.

Next, the lattice calculation, lattice burnup calculation, core diffusion calculation, nuclear and thermal-hydraulic-coupled calculation, core burnup calculation, and space-dependent kinetics calculation are described. From this description, readers will be able to understand the nuclear design calculation methods used in practice. Section 2.2, “Reactor Core, Plant Dynamics and Safety Calculations,” is intended to provide an understanding of the key points of plant dynamics and safety calculation methods as well as core calculation methods. Core design calculations are performed to determine core characteristics at normal conditions in combination with nuclear and thermal-hydraulic calculations. The single-channel thermal-hydraulic calculation model with fuel rods and its hydraulic equivalent coolant path provides the simplest model for heat transfer flow of the core beyond the fuel rods. The three-dimensional nuclear and thermal-hydraulic-coupled core burnup calculation, in combination with nuclear and heat transfer calculations, is used in core management as well as core design. The plant dynamics calculation is concerned with plant control, stability, and safety analysis. First, the node junction model, which is a basic model for the heat transfer calculation in the plant system including the reactor, coolant pipes, valves, and pumps, is described and then reactor control system design, plant startup analysis, and reactor stability analysis methods are treated. The basic concept of reactor safety analysis methods is also touched upon. Supercritical light water-cooled reactors are introduced as an example, and the nature of consideration and analysis methods is the same as that of light water reactors. The actual facilities and systems of light water reactors are complex. We believe that the descriptions in this book, rather than focusing on details, are better suited to understanding the general nature of reactors. More detailed analysis models and large-scale conventional codes are used in practical safety analysis. Their explanations are left to books for professionals; this book is expected to help in understanding the basic analysis methods. At the very end of Sect. 2.2, the FEMAXI-6 code is described for fuel rod behavior analysis. Fuel rod behavior and integrity concerning pellet and cladding are associated with core characteristics as burnup and core safety from the point of view of security of fuel integrity at abnormal transients. Such a series of analysis methods in the core, plant, and fuel rod behavior should be able to be understood as their individual concepts and then in their overall connection.

Section 3.1 is “Development and Improvement of Light Water Reactors,” and Sects. 3.2 and 3.3 present core design and core fuel management of boiling water reactors (BWRs) and pressurized water reactors (PWRs), respectively. Basic core design flow, core configuration setup, fuel lattice, fuel assembly design, reactivity characteristics, power distribution control, transitions and future trends in core design, core management, fuel management, and core design of conventional light water reactor are described.

“Design of Advanced Reactors,” Chap. 4, describes fast reactors and high-temperature gas-cooled reactors, focusing on core design. Detailed descriptions of each reactor type are left to other books; this book is expected, instead, to help in understanding the core design concept of each reactor. For example, advanced reactors are characterized by single-phase flow cooling, high-temperature core

cooling, and different fuel compositions. The design criteria and principles are also different from those of light water reactors. Understanding the difference may lead to a deeper comprehension of reactor design. This book also describes experiences with the HTTR experimental reactor as a high-temperature gas-cooled reactor.

This book systematically describes consideration and calculation methods about nuclear reactor design, mainly core design. We hope it will be useful for readers actually working in the nuclear power industry, research and development, and safety, as well as for students.

In addition to the authors, sincere appreciation goes to Shuichi Hasegawa, Haruka Moriguchi, Yumiko Kawamata, Moe Sekiguchi and the committee members of University of Tokyo, Shigeaki Okamura of JAEA, Yuko Sumino and Nobuko Hirota of Springer Japan who helped to publish the book. I am also grateful for the editing assistance of Takashi Kiguchi and in English of Carol Kikuchi.

Tokyo, Japan
November 2013

Yoshiaki Oka

Contents

1 Fuel Burnup and Reactivity Control	1
Shigeo Ohki	
1.1 Fuel Burnup Analysis	1
1.1.1 Burnup Equations	2
1.1.2 Solutions of the Burnup Equations	4
1.1.3 Reactivity Changes with Burnup	6
1.1.4 Burnup	8
1.2 Fission Product Poisoning	9
1.2.1 ^{135}Xe	10
1.2.2 ^{149}Sm	14
1.2.3 ^{135}Xe Transients with Power Level Changes	18
1.3 Effects of Burnable Poison and Chemical Shim	18
1.3.1 Burnable Poison	18
1.3.2 Chemical Shim	19
1.4 Control Rod Worth	19
1.4.1 Features of Control Rod Types	20
1.4.2 Calculation of Control Rod Worth	21
1.4.3 Shadowing Effect of Control Rods	22
1.5 Inherent Reactivity Effects	22
1.5.1 Definition of Power and Temperature Coefficients	22
1.5.2 Temperature Coefficients by the Six-Factor Formula	24
1.5.3 Other Temperature Coefficients	36
1.5.4 Control Reactivity Balance	37
1.6 Perturbation Theory for Reactivity Calculations	38
1.6.1 Mathematical Preparation	38
1.6.2 Perturbation Theory	41
1.6.3 Application of Perturbation Theory: Reactivity Worth of Partially Inserted Control Rod	44
References	46

2 Nuclear Reactor Calculations	49
Keisuke Okumura, Yoshiaki Oka, and Yuki Ishiwatari	
2.1 Nuclear Design Calculations	49
2.1.1 Fundamental Neutron Transport Equation	49
2.1.2 Neutron Spectrum	51
2.1.3 Nuclear Data and Cross Sections	52
2.1.4 Lattice Calculation	60
2.1.5 Core Calculation	71
2.2 Reactor Core, Plant Dynamics and Safety Calculations	94
2.2.1 Reactor Core Calculation	94
2.2.2 Plant Dynamics Calculation	103
2.2.3 Safety Analysis	115
2.2.4 Fuel Rod Analysis	117
References	125
3 Light Water Reactor Design	127
Yoshiaki Oka, Sadao Uchikawa, and Katsuo Suzuki	
3.1 Development and Improvement of Light Water Reactors	127
3.1.1 Pressurized Water Reactors	127
3.1.2 Boiling Water Reactors	130
3.2 BWR Core Design and Core and Fuel Management	131
3.2.1 General Core Design	131
3.2.2 Core Design Set-Up	138
3.2.3 Design of Fuel Lattice and Assembly	144
3.2.4 Characteristics of Reactivity	150
3.2.5 Control of Power Distribution	155
3.2.6 History and Future Trends in Core Design	161
3.2.7 Core Management	171
3.2.8 Fuel Management	175
3.3 PWR Core Design and Core-Fuel Management	178
3.3.1 General Core Design	178
3.3.2 Core Size and Figure Set-up	182
3.3.3 Design of Fuel Lattice and Assembly	184
3.3.4 Reactivity Characteristics	187
3.3.5 Power Distribution Control	198
3.3.6 Evolution and Future Trends of Core Design	208
3.3.7 Core Management	220
3.3.8 Fuel Management	223
References	227
4 Design of Advanced Reactors	231
Hiroo Osada and Kiyonobu Yamashita	
4.1 Design of Fast Reactors	231
4.1.1 Basic Procedure of Core Design	234
4.1.2 Core Geometry, Operation and Management	238

4.1.3	Design of Fuel Element and Fuel Assembly	243
4.1.4	Nuclear Design	249
4.1.5	Reactivity Characteristics	250
4.1.6	Power Distribution Characteristics	256
4.1.7	Thermal-Hydraulic Design	257
4.1.8	Transitions in Core Design and Tendency in the Future	262
4.2	Design of High Temperature Gas-Cooled Reactors	267
4.2.1	Overview	267
4.2.2	Core, Fuel, and Control Rod Designs	271
4.2.3	Method of Achieving High Outlet Coolant Temperature	277
4.2.4	Nuclear Design	282
4.2.5	Thermohydraulic Design	293
4.2.6	Mechanical Design	298
4.2.7	Annular Core Design	299
	References	301
	Answers for Exercises	305
	Index	323

Contributors

Editor

Yoshiaki Oka (Waseda University, Emeritus professor of University of Tokyo)

Consulting editor

Takashi Kiguchi (Japan Nuclear Energy Safety Organization)

Authors

Shigeo Ohki (Japan Atomic Energy Agency)	Chapter 1
Keisuke Okumura (Japan Atomic Energy Agency)	Chapter 2.1
Yoshiaki Oka (Waseda University)	Chapter 2.2 & 3.1
Yuki Ishiwatari (University of Tokyo/Hitachi GE Nuclear Energy Ltd.)	Chapter 2.2
Sadao Uchikawa (Japan Atomic Energy Agency)	Chapter 3.2
Katsuo Suzuki (Mitsubishi Heavy Industries)	Chapter 3.3
Hiroo Osada (Mitsubishi FBR Systems Inc.)	Chapter 4.1
Kiyonobu Yamashita (Japan Atomic Energy Agency)	Chapter 4.2

Chapter 1

Fuel Burnup and Reactivity Control

Shigeo Ohki

Abstract Nuclear fuel burnup and reactivity control are important points in the core design of nuclear reactors.

The fuel burnup analysis generally evaluates the time-dependent core power distribution and reactivity by solving burnup equations for the atomic density change of nuclides contained in the fuel as well as solving multi-group diffusion equations for neutron flux distribution and effective neutron multiplication factor. The core power distribution is necessary information for thermal-hydraulic and fuel designs.

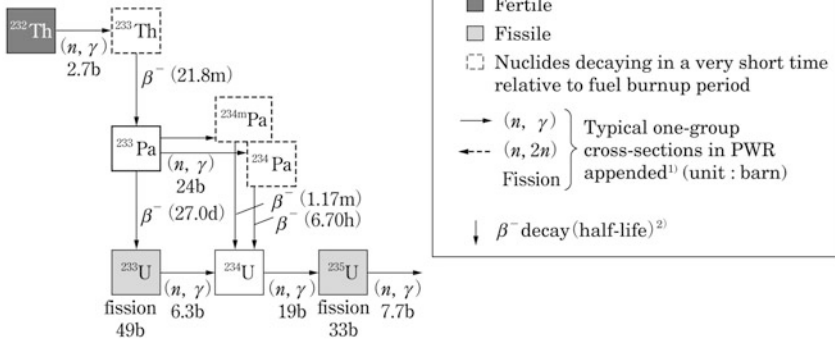
The core design for reactivity control predicts reactivity change during reactor operation and determines its optimal control methods based on calculations of reactivity change with fuel burnup, fission product (FP) accumulation (poisoning effect), inherent reactivity feedback by temperature changes of fuel and coolant, etc. Among the general methods available for reactivity control, the insertion and withdrawal of neutron absorbers, generally referred to as control rods, is the approach usually taken for power reactors. A burnable poison, (a nuclide that has a large neutron absorption cross section) or a chemical shim (a neutron-absorbing chemical, usually boric acid, which is concentrated in the moderator or coolant) is employed for reactivity control depending on reactor types.

Fuel burnup and reactivity control based on fundamental theories with numerical expressions will be briefly reviewed in this chapter.

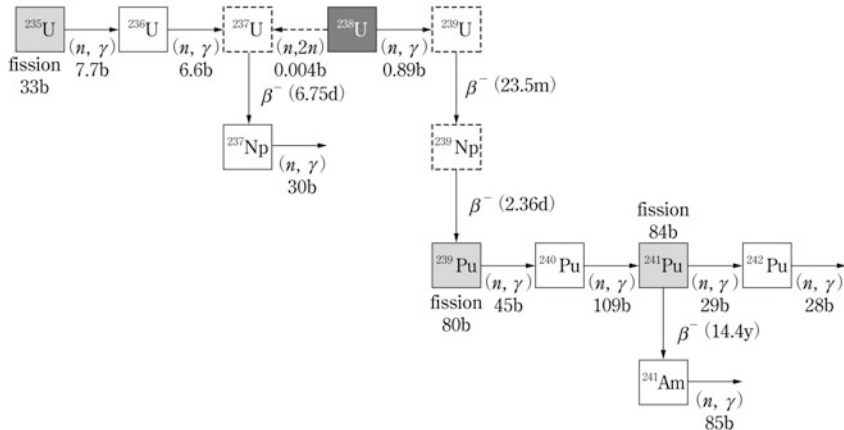
1.1 Fuel Burnup Analysis

During reactor operation, neutron interactions with fuel give rise to various nuclear reactions such as fission of fissile nuclides, conversion of fertile nuclides into fissile ones, and production of FPs. This section solves the burnup equation to determine atomic number densities of fissile and fertile nuclides in fuel, and considers the changes with fuel burnup. Fission products are mainly treated in Sect. 1.2.

Burnup Chain from Thorium



Burnup Chain from Uranium

**Fig. 1.1** Burnup chain from thorium and uranium

1.1.1 Burnup Equations

From an engineering viewpoint ^{233}U , ^{235}U , and ^{239}Pu (and ^{241}Pu) are fissile nuclides and most nuclear reactors in operation or under planning use one of them. Among these fissile nuclides only ^{235}U (0.72 % isotopic abundance in natural uranium) exists as a natural resource and the others are artificially produced in nuclear reactors through conversion of fertile nuclides: ^{232}Th to ^{233}U and ^{238}U to ^{239}Pu (and ^{241}Pu). A burnup chain (nuclear transmutation and decay chain) including those nuclides is shown in Fig. 1.1.

Let us derive the burnup equation of each nuclide from the burnup chain of uranium, presented by characteristic expressions which include terms for: atomic number density at position \vec{r} and time t , $N(\vec{r}, t)$; absorption, capture, and $(n, 2n)$

reaction cross sections, σ_a , σ_c , and $\sigma_{n,2n}$ respectively; decay constant, λ ; and neutron flux, $\phi(\vec{r}, t)$. The absorption cross section is the sum of the cross sections of all neutron absorption reactions such as fission, capture, and $(n, 2n)$. For simplicity of calculation, the one-group neutron energy is assumed.

Recalling the volumetric reaction rate (reaction rate per unit time and volume) expressed by $\sigma\phi N$ (λN in case of decay) and making a balanced relation between the production and destruction rates of a target nuclide, the burnup equations can be given by the following equations, where nuclides are identified by a two-digit superscript indicating the last digit in the atomic number and the last digit in the mass number, respectively.

$$^{235}\text{U} : \quad \frac{\partial N^{25}}{\partial t} = -\sigma_a^{25} \phi N^{25} \quad (1.1)$$

$$^{236}\text{U} : \quad \frac{\partial N^{26}}{\partial t} = \sigma_c^{25} \phi N^{25} - \sigma_a^{26} \phi N^{26} \quad (1.2)$$

$$^{237}\text{U} : \quad \frac{\partial N^{27}}{\partial t} = \sigma_c^{26} \phi N^{26} + \sigma_{n,2n}^{28} \phi N^{28} - \lambda^{27} N^{27} \quad (1.3)$$

$$^{237}\text{Np} : \quad \frac{\partial N^{37}}{\partial t} = \lambda^{27} N^{27} - \sigma_a^{37} \phi N^{37} \quad (1.4)$$

$$^{238}\text{U} : \quad \frac{\partial N^{28}}{\partial t} = -\sigma_a^{28} \phi N^{28} \quad (1.5)$$

$$^{239}\text{U} : \quad \frac{\partial N^{29}}{\partial t} = \sigma_c^{28} \phi N^{28} - \lambda^{29} N^{29} \quad (1.6)$$

$$^{239}\text{Np} : \quad \frac{\partial N^{39}}{\partial t} = \lambda^{29} N^{29} - \lambda^{39} N^{39} \quad (1.7)$$

$$^{239}\text{Pu} : \quad \frac{\partial N^{49}}{\partial t} = \lambda^{39} N^{39} - \sigma_a^{49} \phi N^{49} \quad (1.8)$$

$$^{240}\text{Pu} : \quad \frac{\partial N^{40}}{\partial t} = \sigma_c^{49} \phi N^{49} - \sigma_a^{40} \phi N^{40} \quad (1.9)$$

$$^{241}\text{Pu} : \quad \frac{\partial N^{41}}{\partial t} = \sigma_c^{40} \phi N^{40} - (\lambda^{41} + \sigma_a^{41} \phi) N^{41} \quad (1.10)$$

$$^{242}\text{Pu} : \frac{\partial N^{42}}{\partial t} = \sigma_c^{41}\phi N^{41} - \sigma_a^{42}\phi N^{42} \quad (1.11)$$

$$^{241}\text{Am} : \frac{\partial N^{51}}{\partial t} = \lambda^{41}N^{41} - \sigma_a^{51}\phi N^{51} \quad (1.12)$$

The following approximation can be used for a short-lived nuclide which has a very short half-life relative to fuel burnup period in nuclear reactors. The short-lived nuclide decays immediately after it is produced and it reaches a balanced state between production and destruction like a radioactive equilibrium. If the time differentials of ^{237}U , ^{239}Pu , and ^{239}Np are set to be zero, the burnup equations of ^{237}Np and ^{239}Pu are represented by the next equations.

$$^{237}\text{Np} : \frac{\partial N^{37}}{\partial t} = \sigma_c^{26}\phi N^{26} + \sigma_{n,2n}^{28}\phi N^{28} - \sigma_a^{37}\phi N^{37} \quad (1.13)$$

$$^{239}\text{Pu} : \frac{\partial N^{49}}{\partial t} = \sigma_c^{28}\phi N^{28} - \sigma_a^{49}\phi N^{49} \quad (1.14)$$

It is considered that the short-lived nuclides decay instantaneously in this burnup chain.

1.1.2 Solutions of the Burnup Equations

In the burnup equations, the atomic number density $N(\vec{r}, t)$ and the neutron flux $\phi(\vec{r}, t)$ are generally a function of space and time. Nuclear fuel does not uniformly burn at the location in actual nuclear reactors and neutron flux varies with time (neutron flux should be increased according to depletion of fissile nuclides to maintain a specified reactor power). For simplicity, the space-independent burnup equations are solved assuming a constant neutron flux with time.

In Eq. (1.1) for ^{235}U , both sides are divided by N^{25} and this equation can be integrated from time 0 to t (separation of variables) to give Eq. (1.15).

$$N^{25}(t) = N^{25}(0) e^{-\sigma_a^{25}\phi t} \quad (1.15)$$

As an example, the hypothetical case is considered for a pure ^{235}U -fueled reactor operated at a constant neutron flux of $2.0 \times 10^{14}\text{n/cm}^2\text{s}$ for 1 year. The depletion rate of ^{235}U during the operation is calculated, using the cross section of Fig. 1.1, in the following.

$$\begin{aligned}\frac{N^{25}(0) - N^{25}(t)}{N^{25}(0)} &= 1 - e^{-\sigma_a^{25}\phi t} \\ &= 1 - \exp [-(33 + 7.7) \times 10^{-24} \times 2 \times 10^{14} \times 3.156 \times 10^7] \\ &= 23\%\end{aligned}$$

Next, the burnup equation of ^{236}U [Eq. (1.2)] is considered which can be solved in several ways. Here the term of $N^{26}(t)$ is transposed into the left-hand side and each term is multiplied by the integrating factor $\exp [\sigma_a^{26}\phi t]$ to obtain

$$\frac{\partial N^{26}}{\partial t} e^{\sigma_a^{26}\phi t} + N^{26}(t) (\sigma_a^{26}\phi e^{\sigma_a^{26}\phi t}) = \sigma_c^{25}\phi N^{25}(t) e^{\sigma_a^{26}\phi t}.$$

It should be noted that the left-hand side is a time-differentiated form of $N^{26}(t) \exp [\sigma_a^{26}\phi t]$. It follows therefore that

$$\frac{\partial}{\partial t} [N^{26}(t) e^{\sigma_a^{26}\phi t}] = \sigma_c^{25}\phi N^{25}(t) e^{\sigma_a^{26}\phi t}.$$

Equation (1.16) is given by integrating both sides of the above expression from time 0 to t and substituting Eq. (1.15).

$$N^{26}(t) = N^{26}(0) e^{-\sigma_a^{26}\phi t} + N^{25}(0) \frac{\sigma_c^{25}}{\sigma_a^{25} - \sigma_a^{26}} (e^{-\sigma_a^{26}\phi t} - e^{-\sigma_a^{25}\phi t}) \quad (1.16)$$

The burnup equations of ^{238}U and ^{239}Pu [Eqs. (1.5) and (1.14)] are identical to those of ^{235}U and ^{236}U . As a consequence, the solutions are given by the next expressions.

$$N^{28}(t) = N^{28}(0) e^{-\sigma_a^{28}\phi t} \quad (1.17)$$

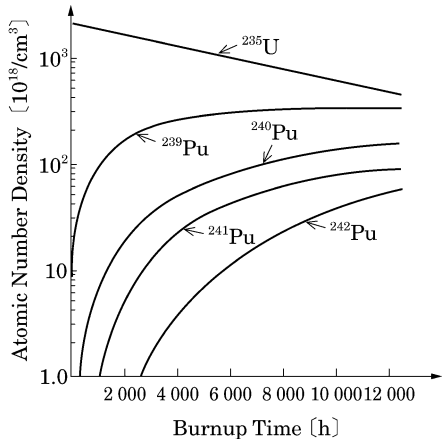
$$N^{49}(t) = N^{49}(0) e^{-\sigma_a^{49}\phi t} + N^{28}(0) \frac{\sigma_c^{28}}{\sigma_a^{49} - \sigma_a^{28}} (e^{-\sigma_a^{28}\phi t} - e^{-\sigma_a^{49}\phi t}) \quad (1.18)$$

Continuing for the burnup equation of ^{240}Pu , the term of $N^{40}(t)$ is transposed into the left-hand side and each term is multiplied by the integrating factor $\exp [\sigma_a^{40}\phi t]$ to obtain

$$\frac{\partial}{\partial t} [N^{40}(t) e^{\sigma_a^{40}\phi t}] = \sigma_c^{49}\phi N^{49}(t) e^{\sigma_a^{40}\phi t}.$$

Equation (1.19) is obtained by integrating both sides of the above expression from time 0 to t and substituting Eq. (1.18).

Fig. 1.2 Depletion of ^{235}U and buildup of Pu isotopes for a representative LWR fuel composition [4]



$$\begin{aligned}
 N^{40}(t) &= N^{40}(0)e^{-\sigma_a^{40}\phi t} + e^{-\sigma_a^{40}\phi t} \int_0^t dt [\sigma_c^{49}\phi N^{49}(t)e^{\sigma_a^{40}\phi t}] \\
 &= N^{40}(0)e^{-\sigma_a^{40}\phi t} + N^{49}(0) \frac{\sigma_c^{49}}{\sigma_a^{49} - \sigma_a^{40}} (e^{-\sigma_a^{40}\phi t} - e^{-\sigma_a^{49}\phi t}) \\
 &\quad + N^{28}(0) \sigma_c^{28} \sigma_c^{49} \left[\frac{e^{-\sigma_a^{40}\phi t}}{(\sigma_a^{49} - \sigma_a^{40})(\sigma_a^{28} - \sigma_a^{40})} \right. \\
 &\quad \left. + \frac{e^{-\sigma_a^{49}\phi t}}{(\sigma_a^{28} - \sigma_a^{49})(\sigma_a^{40} - \sigma_a^{49})} \right. \\
 &\quad \left. + \frac{e^{-\sigma_a^{28}\phi t}}{(\sigma_a^{40} - \sigma_a^{28})(\sigma_a^{49} - \sigma_a^{28})} \right]
 \end{aligned} \tag{1.19}$$

The same method can be applied to ^{241}Pu , ^{242}Pu , and the nuclides downstream in the burnup chain. Equations (1.17)–(1.19) can be perceived to have a regularity, and the general solution to them is known as the Bateman solution [3].

Figure 1.2 shows the depletion behavior of ^{235}U and the production behavior of Pu isotopes for a representative LWR fuel. While ^{235}U exponentially decreases, the neutron capture of ^{238}U produces ^{239}Pu , which in turn is converted by neutron capture into ^{240}Pu and higher Pu isotopes. It is seen that the buildup of Pu isotopes is approaching an equilibrium state.

1.1.3 Reactivity Changes with Burnup [5]

In a uranium-fueled thermal reactor, the reactivity changes with burnup are associated with the following factors:

- (i) Depletion of ^{235}U ;
- (ii) Buildup of ^{239}Pu ;

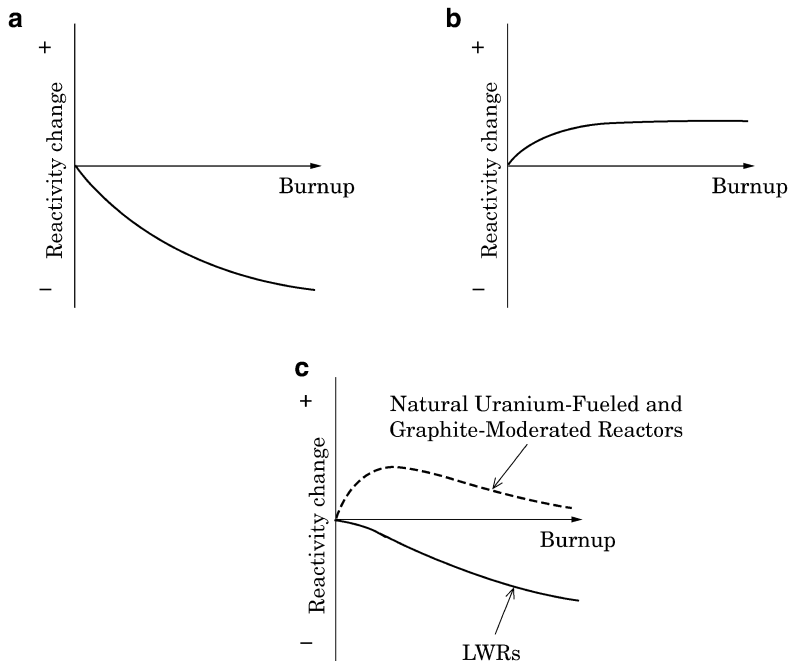


Fig. 1.3 Reactivity change due to ^{235}U depletion and ^{239}Pu buildup. (a) Reactivity decrease due to ^{235}U depletion, (b) reactivity increase due to ^{239}Pu buildup, (c) reactivity change of ^{235}U and ^{239}Pu

- (iii) Buildup of ^{241}Pu ;
- (iv) Buildup of non-fissile nuclides, ^{240}Pu , ^{236}U , and ^{242}Pu ;
- (v) Buildup of highly thermal neutron-absorbing FPs (^{135}Xe and ^{149}Sm); and
- (vi) Buildup of other FPs.

Items (i) and (ii) mainly lead to reactivity changes by increase or decrease in amounts of fissile nuclides. Reactivity drops due to exponential depletion of ^{235}U and reactivity rises due to buildup of ^{239}Pu as shown in Fig. 1.3a, b, respectively. The combined reactivity change of ^{235}U and of ^{239}Pu is presented in Fig. 1.3c. In an enriched-uranium fueled LWR, the effect of ^{235}U is generally larger than that of ^{239}Pu and it results in a reactivity decrease with burnup. In the case of a fuel type of natural uranium and high conversion ratio for graphite-moderated reactors, there is an early reactivity increase and then a decrease with burnup because ^{235}U and ^{239}Pu produce comparable reactivity effects and the fissile replacement of ^{235}U by ^{239}Pu proceeds.

^{240}Pu , ^{241}Pu , and ^{242}Pu are produced with burnup by neutron capture. ^{240}Pu has a large thermal-neutron absorption cross section and has a negative reactivity effect. ^{241}Pu produced by the subsequent neutron capture is a fissile nuclide and has a positive reactivity effect. On the other hand, ^{242}Pu produces a small negative reactivity because its production amount and cross section are small.

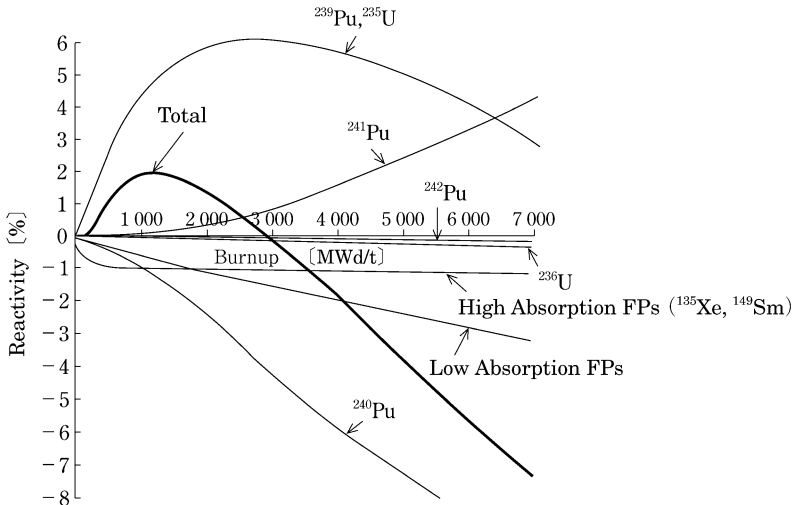


Fig. 1.4 Reactivity change with burnup in a natural uranium-fueled, graphite-moderated reactor [6]

^{236}U produced from ^{235}U by neutron capture also gives a small negative reactivity effect.

It is also necessary to consider the negative reactivity effect by buildup of FPs, which can be classified as two significant FPs and other FPs. The former are ^{135}Xe and ^{149}Sm which have very large absorption cross sections. Within a short time after burnup (usually within several hours to several days), they reach an individual equilibrium concentration by the balance between production and destruction because of the strong neutron absorption, and they have a constant negative reactivity effect. The other FPs continue to be accumulated with burnup because of low absorption cross sections and to increase the negative reactivity.

Typical reactivity changes for such individual reactivity effects are shown in Fig. 1.4 for natural uranium-fueled, graphite-moderated reactors. After an initial increase in reactivity due to the buildup of ^{239}Pu , there is a gradual reduction in reactivity due to the depletion of ^{235}U and the buildup of neutron absorbing materials. These analyses of reactivity changes with fuel burnup are used to determine the fissile amount for criticality during reactor operation and to determine the reactivity worth of control rods.

1.1.4 Burnup

The concept of burnup (unit: MWd/t) is a fairly general measure of fuel depletion, which is defined as thermal energy output (unit: MWd) per unit mass (unit metric ton, t) of heavy metal content in the initial fuel.

For a reactor which loads a heavy metal content of 100 t and operates at a thermal power of 3,000 MW for 1,000 days, the average burnup of the discharge fuel will be 30,000 MWd/t.

The thermal energy production by fission of 1 g heavy metal fuel, assuming that the fuel is ^{235}U and its fission energy is 200 MeV, is as follows.

$$1 \text{ g} \times \frac{0.6022 \times 10^{24} \text{ atom/mol}}{235 \text{ g/mol}} \times 200 \text{ MeV/fission} \times \frac{1.602 \times 10^{-19} \text{ J/eV}}{24 \times 3600 \text{ s/d}} \\ = 0.95 \text{ MWd}$$

The fission of 1 g heavy metal corresponds to about 1 MWd. For a discharge fuel of 30,000 MWd/t burnup, this means that about 30 kg per initial heavy metal of 1 t has fissioned (that is, about 3 % of the initial heavy metal has fissioned).

The average burnup of typical LWRs is 30,000–50,000 MWd/t. Fast breeder reactors are being designed with the average burnup of 100,000–150,000 MWd/t as a development target.

1.2 Fission Product Poisoning

As mentioned before, FPs accumulate and decrease reactivity during reactor operation. This is known as FP poisoning. Among the FPs, ^{135}Xe and ^{149}Sm in particular, have significant absorption cross sections for thermal neutrons: 2.65×10^6 and 4.02×10^4 b at a neutron speed of 2,200 m/s (= neutron energy of 0.0253 eV), respectively. These absorption cross sections rapidly decline over 0.1–1 eV. Such FP poisoning is therefore a specific characteristic of thermal reactors.

^{135}Xe and ^{149}Sm have a substantial impact on operation and control of thermal reactors because they give rise to a characteristic behavior in reactivity change during reactor startup, power change in operation, shutdown, and re-startup.

The reactivity change can be evaluated based on the six-factor formula [5] for understanding the FP poisoning. An infinite homogeneous thermal reactor is assumed here for convenience. Initially, the infinite multiplication factor of the unpoisoned reactor (i.e., before production of ^{135}Xe and ^{149}Sm) is given as Eq. (1.20).

$$k_{\infty} = \eta f p \epsilon, f = \frac{\bar{\Sigma}_{aF}}{\bar{\Sigma}_{aF} + \bar{\Sigma}_{aM}} \quad (1.20)$$

With poisons present (after production of ^{135}Xe and ^{149}Sm), k_{∞} becomes

$$k'_{\infty} = \eta f' p \epsilon, f' = \frac{\bar{\Sigma}_{aF}}{\bar{\Sigma}_{aF} + \bar{\Sigma}_{aM} + \bar{\Sigma}_{aP}} \quad (1.21)$$

where $\overline{\Sigma}_{aF}$, $\overline{\Sigma}_{aM}$, and $\overline{\Sigma}_{aP}$ are the macroscopic thermal absorption cross sections of the fuel, moderator and structure, and the poisons, respectively. Thus the reactivity change due to the poison production can be written as

$$\begin{aligned}\rho &= \frac{k'_\infty - k_\infty}{k_\infty k'_\infty} = \frac{f' - f}{ff'} \frac{1}{\eta p \epsilon} = - \frac{\overline{\Sigma}_{aP}}{\overline{\Sigma}_{aF}} \frac{1}{\eta p \epsilon} \\ &= - \frac{\overline{\Sigma}_{aP}}{v \overline{\Sigma}_f p \epsilon}\end{aligned}\quad (1.22)$$

where v is the average number of neutrons released per fission and $\overline{\Sigma}_f$ is the macroscopic thermal fission cross section of the fuel.

Each atomic number density of ^{135}Xe and ^{149}Sm must be known to calculate the FP poisoning using Eq. (1.22). The atomic number density is determined by time-dependent equations of production and destruction as described in the following sections.

1.2.1 ^{135}Xe

The production process of ^{135}Xe is presented in Fig. 1.5. In the decay chain of mass number 135 related to ^{135}Xe production, ^{135}Sb , ^{135}Te , ^{135}I , and ^{135}Xe are the main FPs. Because ^{135}Sb and ^{135}Te are short-lived nuclides, they can be assumed to decay very rapidly to ^{135}I .

The time-dependent nuclide concentrations of ^{135}I and ^{135}Xe are represented by $I(t)$ and $X(t)$, respectively, the fission yields (FP yields per fission shown in Table 1.1) are represented by γ_I and γ_{Xe} , and the decay constants are represented by λ_I and λ_{Xe} . Assuming the thermal absorption cross section of ^{135}Xe is $\overline{\sigma}_a^{Xe}$ and time-independent neutron flux is ϕ , the production-destruction equations of $I(t)$ and $X(t)$ can be represented as follows.

$$\frac{dI}{dt} = \gamma_I \overline{\Sigma}_f \phi - \lambda_I I \quad (1.23)$$

$$\frac{dX}{dt} = \lambda_I I + \gamma_{Xe} \overline{\Sigma}_f \phi - \lambda_{Xe} X - \overline{\sigma}_a^{Xe} \phi X \quad (1.24)$$

[1] Solution at initial startup

When the reactor is started up from a clean condition in which $I(0) = X(0) = 0$, the ^{135}I and ^{135}Xe concentrations can be obtained as shown in Eqs. (1.25) and (1.26).

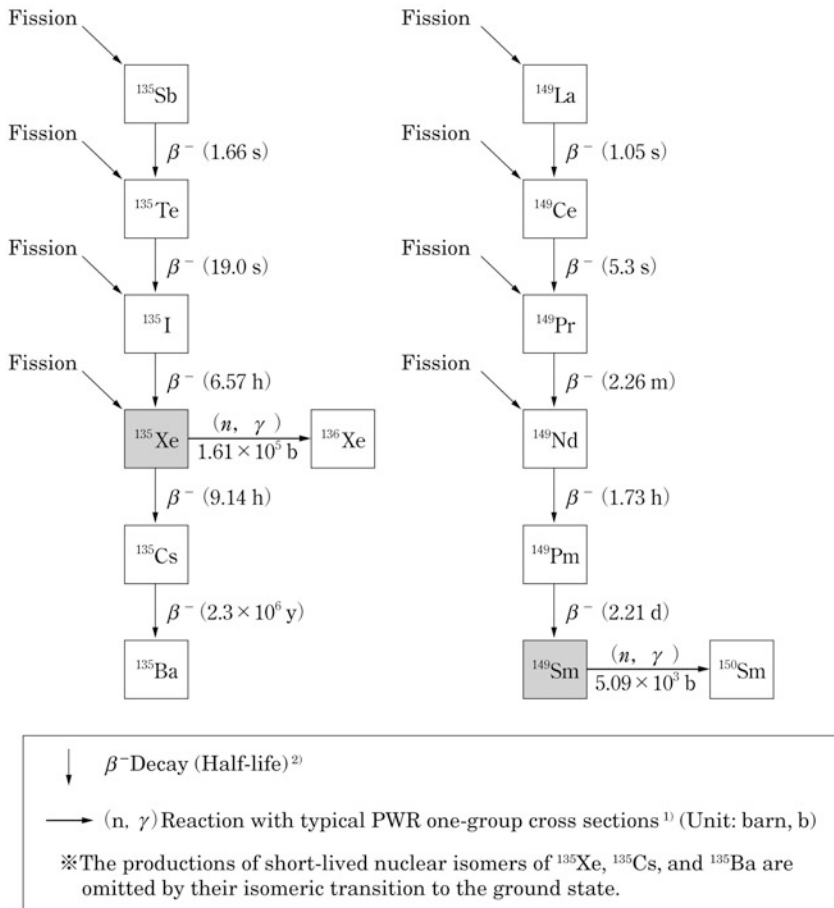


Fig. 1.5 Production processes of ^{135}Xe and ^{149}Sm

Table 1.1 Fission yields by thermal fission [8]

Fission product	Decay constant [2] (s^{-1})	Fission yield (number of a fission product produced per fission)		
		^{233}U	^{235}U	^{239}Pu
^{135}I	2.93×10^{-5}	0.0491	0.0629	0.0645
^{135}Xe	2.11×10^{-5}	0.0128	0.0024	0.0115
^{149}Nd	1.11×10^{-4}	0.0078	0.0107	0.0124

The fission yields of ^{135}I and ^{149}Nd are the cumulative fission yields including nuclides in the upper part of each β^- decay chain. The fission yield of ^{135}Xe is the independent fission yield representing the direct production by fission

$$I(t) = \frac{\gamma_I \bar{\Sigma}_f \phi}{\lambda_I} (1 - e^{-\lambda_I t}) \quad (1.25)$$

$$\begin{aligned} X(t) = & \frac{(\gamma_I + \gamma_{Xe}) \bar{\Sigma}_f \phi}{\lambda_{Xe} + \bar{\sigma}_a^{Xe} \phi} (1 - e^{-(\lambda_{Xe} + \bar{\sigma}_a^{Xe} \phi)t}) \\ & + \frac{\gamma_I \bar{\Sigma}_f \phi}{\lambda_{Xe} + \bar{\sigma}_a^{Xe} \phi - \lambda_I} (e^{-(\lambda_{Xe} + \bar{\sigma}_a^{Xe} \phi)t} - e^{-\lambda_I t}) \end{aligned} \quad (1.26)$$

Within enough time after the reactor startup, the concentrations approach equilibrium values, I_{eq} and X_{eq} , which can be found at $t \rightarrow \infty$ in Eqs. (1.25) and (1.26) as follows.

$$I_{eq} = \frac{\gamma_I \bar{\Sigma}_f \phi}{\lambda_I} \quad (1.27)$$

$$X_{eq} = \frac{(\gamma_I + \gamma_{Xe}) \bar{\Sigma}_f \phi}{\lambda_{Xe} + \bar{\sigma}_a^{Xe} \phi} \quad (1.28)$$

These equations can be directly obtained by placing the time derivatives in Eqs. (1.23) and (1.24) equal to zero.

Upon inserting Eq. (1.28) into Eq. (1.22), the reactivity change due to equilibrium ^{135}Xe is found to be

$$\rho_{Xe}^{eq} = -\frac{\bar{\sigma}_a^{Xe} X_{eq}}{\nu \bar{\Sigma}_f p \epsilon} = -\frac{\gamma_I + \gamma_{Xe}}{\nu p \epsilon} \frac{\phi}{\lambda_{Xe} / \bar{\sigma}_a^{Xe} + \phi} . \quad (1.29)$$

If, $\phi \ll \lambda_{Xe} / \bar{\sigma}_a^{Xe}$ the negative reactivity increases linearly with ϕ . On the other hand, if $\phi \gg \lambda_{Xe} / \bar{\sigma}_a^{Xe}$, the negative reactivity takes its maximum value

$$\phi \gg \lambda_{Xe} / \bar{\sigma}_a^{Xe} \quad \rho_{Xe}^{eq} \rightarrow -\frac{\gamma_I + \gamma_{Xe}}{\nu p \epsilon} .$$

To estimate the magnitude of the maximum value, suppose that a thermal reactor is fueled with ^{235}U and contains no resonance absorbers and fast fission materials. In this case, $p = \epsilon = 1$, and the negative reactivity gives

$$-\frac{\gamma_I + \gamma_{Xe}}{\nu} = -\frac{0.0629 + 0.0024}{2.42} = -2.7\% \Delta k/k$$

by using the fission yield from ^{235}U in Table 1.1 and $\nu = 2.42$. This is a considerably large reactivity which is about -4.2 dollars for the delayed neutron fraction of 0.0064 in thermal fission of ^{235}U .

[2] Solution after shutdown

Although the production of ^{135}I and ^{135}Xe by fission and the transmutation of ^{135}Xe by thermal neutron absorption cease when the reactor is shut down, ^{135}Xe continues to be produced as the result of the decay of ^{135}I present in the system. It eventually disappears by its own decay.

After shutdown, the production-destruction equations of ^{135}I and ^{135}Xe are given by the next expressions.

$$\frac{dI}{dt} = -\lambda_I I \quad (1.30)$$

$$\frac{dX}{dt} = \lambda_I I - \lambda_{xe} X \quad (1.31)$$

If the concentrations at shutdown are I_0 and X_0 , the concentrations at a later time t can be written as follows.

$$I(t) = I_0 e^{-\lambda_I t} \quad (1.32)$$

$$X(t) = X_0 e^{-\lambda_{xe} t} + \frac{\lambda_I I_0}{\lambda_I - \lambda_{xe}} (e^{-\lambda_{xe} t} - e^{-\lambda_I t}) \quad (1.33)$$

If ^{135}I and ^{135}Xe had reached equilibrium prior to shutdown, then I_0 and X_0 would be given by Eqs. (1.27) and (1.28), and the concentration of ^{135}Xe becomes

$$X(t) = \frac{(\gamma_I + \gamma_{xe}) \bar{\Sigma}_f \phi}{\lambda_{xe} + \bar{\sigma}_a^{xe} \phi} e^{-\lambda_{xe} t} + \frac{\gamma_I \bar{\Sigma}_f \phi}{\lambda_I - \lambda_{xe}} (e^{-\lambda_{xe} t} - e^{-\lambda_I t}) \quad (1.34)$$

The resulting reactivity change due to ^{135}Xe at a later time t after shutdown is given by Eq. (1.35).

$$\rho_{xe}(t) = -\frac{1}{v p \epsilon} \left[\frac{(\gamma_I + \gamma_{xe}) \phi}{\lambda_{xe} / \bar{\sigma}_a^{xe} + \phi} e^{-\lambda_{xe} t} + \frac{\gamma_I \phi}{\lambda_I / \bar{\sigma}_a^{xe} - \lambda_{xe} / \bar{\sigma}_a^{xe}} (e^{-\lambda_{xe} t} - e^{-\lambda_I t}) \right] \quad (1.35)$$

Figure 1.6 shows the reactivity change due to ^{135}Xe buildup in a ^{235}U -fueled thermal reactor after shutdown as calculated by Eq. (1.35). The buildup of ^{135}Xe rises to a maximum, which occurs at about 10 h after shutdown, and then decreases to zero. It should be particularly noted that the buildup of ^{135}Xe is greatest in reactors which have been operating at the highest flux before shutdown. This gives rise to a reactor dead time in the operation of high-flux reactors, during which time the reactor cannot be restarted. This situation is indicated in Fig. 1.6 during the time interval from t_a to t_b , where the horizontal line represents a hypothetical reactivity margin of $0.2 \Delta k/k$ by withdrawal of all

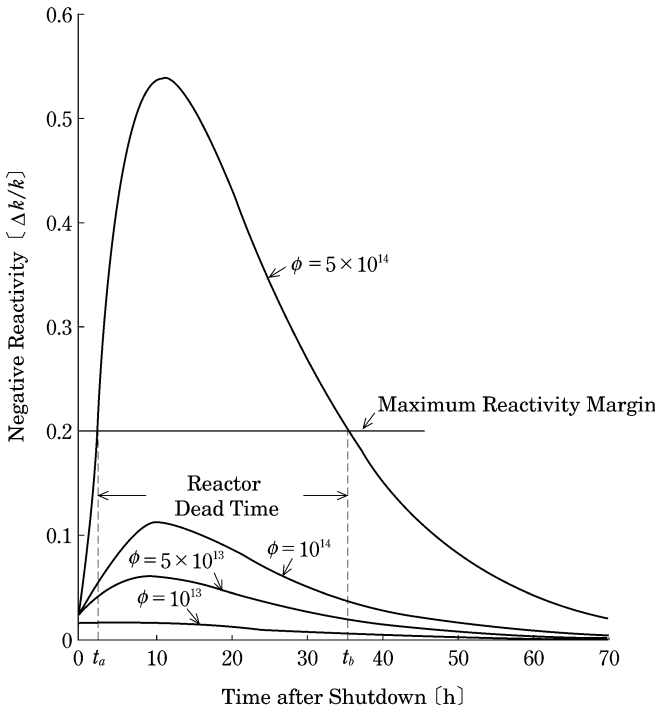


Fig. 1.6 Negative reactivity due to ^{135}Xe buildup after shutdown [7]

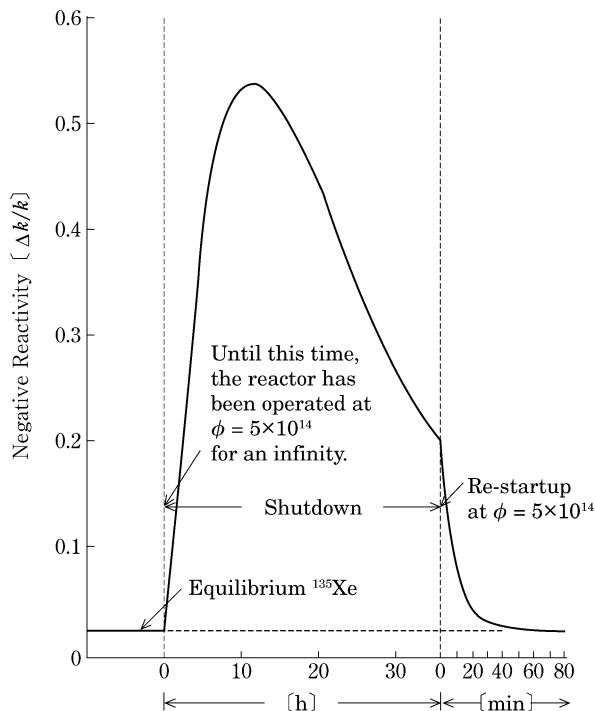
control rods. As a countermeasure to reduce the reactor dead time, a gradual reduction in reactor power and the shutdown at a low neutron flux can suppress the buildup of ^{135}Xe .

Figure 1.7 shows the negative reactivity change due to ^{135}Xe in a reactor that is returned to full power just at the end of the dead time. If a reactor is restarted while a large amount of ^{135}Xe is present in the system, it should be noted that the subsequent burnout of this poison substantially increases the reactivity of the reactor.

1.2.2 ^{149}Sm

In the same way as for ^{135}Xe , the production-destruction equations of ^{149}Sm are solved and some features of its negative reactivity from reactor startup to after shutdown can be discussed. ^{135}Xe has a significantly large thermal absorption cross section and undergoes β^- decay with a half-life of about 9 h as well. On the other hand, ^{149}Sm is a stable nuclide with a large thermal absorption cross section and this is the major difference between the both poisons.

Fig. 1.7 Positive reactivity insertion due to ^{135}Xe burnout at re-startup [7]



In the production processes of ^{149}Sm described in Fig. 1.5, ^{149}La , ^{149}Ce , ^{149}Pr , and ^{149}Nd are the main relevant FPs. They decay comparatively rapidly to ^{149}Pm due to their short half-lives. The production-destruction equations are set up with due attention paid to ^{149}Pm and ^{149}Sm . The nuclide concentrations of ^{149}Pm and ^{149}Sm are denoted by $P(t)$ and $S(t)$, the decay constant of ^{149}Pm is λ_{Pm} , the thermal absorption cross section of ^{149}Sm is $\bar{\sigma}_a^{Sm}$, and the fission yield of ^{149}Nd is γ_{Nd} . Thus the production-destruction equations of ^{149}Pm and ^{149}Sm can be written as below.

$$\frac{dP}{dt} = \gamma_{Nd} \bar{\Sigma}_f \phi - \lambda_{Pm} P \quad (1.36)$$

$$\frac{dS}{dt} = \lambda_{Pm} P - \bar{\sigma}_a^{Sm} \phi S \quad (1.37)$$

[1] Solution at initial startup

Here, a reactor is considered that is starting up from a clean condition in which there are no FPs. Solving Eqs. (1.36) and (1.37) with the initial conditions of $P(0) = S(0) = 0$ gives the next solutions.

$$P(t) = \frac{\gamma_{Nd} \bar{\Sigma}_f \phi}{\lambda_{Pm}} (1 - e^{-\lambda_{Pm} t}) \quad (1.38)$$

$$S(t) = \frac{\gamma_{Nd} \bar{\Sigma}_f}{\bar{\sigma}_a^{Sm}} (1 - e^{-\bar{\sigma}_a^{Sm} \phi t}) + \frac{\gamma_{Nd} \bar{\Sigma}_f \phi}{\bar{\sigma}_a^{Sm} \phi - \lambda_{Pm}} (e^{-\bar{\sigma}_a^{Sm} \phi t} - e^{-\lambda_{Pm} t}) \quad (1.39)$$

The equilibrium concentrations, P_{eq} and S_{eq} , are found to be Eqs. (1.40) and (1.41).

$$P_{eq} = \frac{\gamma_{Nd} \bar{\Sigma}_f \phi}{\lambda_{Pm}} \quad (1.40)$$

$$S_{eq} = \frac{\gamma_{Nd} \bar{\Sigma}_f}{\bar{\sigma}_a^{Sm}} \quad (1.41)$$

The reactivity change due to the equilibrium ^{149}Sm is then expressed as Eq. (1.42).

$$\rho_{Sm}^{eq} = -\frac{\bar{\sigma}_a^{Sm} S_{eq}}{\nu \bar{\Sigma}_f p \epsilon} = -\frac{\gamma_{Nd}}{\nu p \epsilon} \quad (1.42)$$

It should be particularly noted that this reactivity change is independent of the neutron flux in contrast to ^{135}Xe . In a ^{235}U -fueled thermal reactor, this reactivity change is

$$-\frac{\gamma_{Nd}}{\nu} = -\frac{0.0107}{2.42} = -0.44\% \Delta k/k.$$

In comparison with ^{135}Xe , this is a secondary reactivity effect which is about -0.69 dollars for the delayed neutron fraction.

[2] Solution after shutdown

After shutdown, ^{149}Sm builds up as the accumulated ^{149}Pm decays. However, unlike ^{135}Xe , which undergoes β^- decay, ^{149}Sm is stable and remains in the reactor.

The production-destruction equations of the ^{149}Pm and ^{149}Sm concentrations after shutdown are given below.

$$\frac{dP}{dt} = -\lambda_{Pm} P \quad (1.43)$$

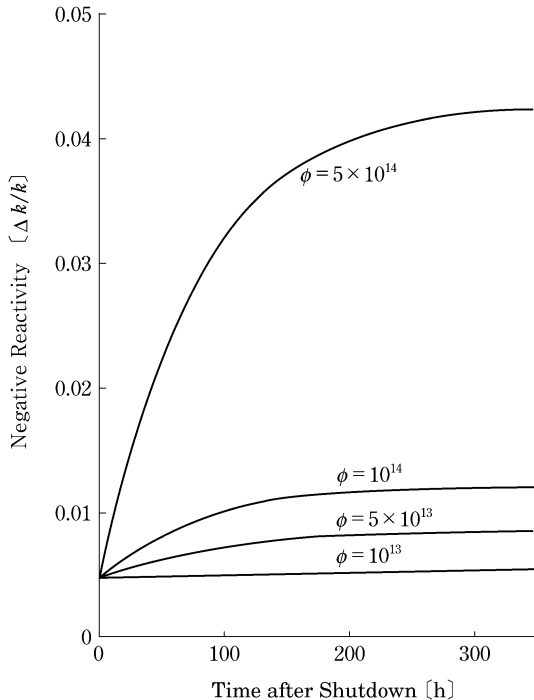
$$\frac{dS}{dt} = \lambda_{Pm} P \quad (1.44)$$

With the concentrations at shutdown denoted by P_0 and S_0 , respectively, the concentrations at the later time t become Eqs. (1.45) and (1.46).

$$P(t) = P_0 e^{-\lambda_{Pm} t} \quad (1.45)$$

$$S(t) = S_0 + P_0 (1 - e^{-\lambda_{Pm} t}) \quad (1.46)$$

Fig. 1.8 Negative reactivity due to ^{149}Sm after shutdown [7]



If ^{149}Pm and ^{149}Sm are at their equilibrium concentrations at shutdown, P_0 and S_0 are given by Eqs. (1.40) and (1.41). Equation (1.46) can then be rewritten as the following.

$$S(t) = \frac{\gamma_{Nd} \bar{\Sigma}_f}{\bar{\sigma}_a^{Sm}} \left[1 + \frac{\bar{\sigma}_a^{Sm} \phi}{\lambda_{Pm}} (1 - e^{-\lambda_{Pm} t}) \right] \quad (1.47)$$

The post-shutdown reactivity change due to ^{149}Sm at the later time t is obtained as Eq. (1.48).

$$\rho_{Sm}(t) = -\frac{\gamma_{Nd}}{vp\varepsilon} \left[1 + \frac{\phi}{\lambda_{Pm} / \bar{\sigma}_a^{Sm}} (1 - e^{-\lambda_{Pm} t}) \right] \quad (1.48)$$

The reactivity change of Eq. (1.48) is shown in Fig. 1.8 for a ^{235}U -fueled thermal reactor after shutdown. It is observed that, like ^{135}Xe , the post-shutdown buildup of ^{149}Sm increases with increasing the neutron flux before shutdown. The buildup is, however, saturated to an asymptotic value dependent on the flux because ^{149}Sm does not decay. The ^{149}Sm poisoning is small compared with ^{135}Xe poisoning and does not have a large effect on the reactor

dead time. In addition, ^{149}Pm has a relatively long half-life of 2.21 days so that the ^{149}Sm buildup proceeds comparatively slowly.

When a reactor is restarted after shutdown, the burnout of the accumulated ^{149}Sm gives a positive reactivity to the system toward the equilibrium value at operation. This effect occurs regardless of how long after shutdown the re-startup occurs.

1.2.3 ^{135}Xe Transients with Power Level Changes

The ^{135}Xe buildup occurs when a reactor is brought to a low power level as well as at shutdown and then the ^{135}Xe concentration begins to decrease soon, or vice versa, when the power level is increased. This is called the “Xe transient” which is characterized by times of the order of about 8 h [9] and therefore it should be controlled properly.

In a large power reactor, local changes in the power distribution by such factors as control rod movement can lead to spatial oscillations even though the reactor power is kept constant. In the region of increased power density, ^{135}Xe burns out more rapidly and then its concentration decreases. This decrease leads to a higher reactivity in this region, which, in turn, leads to an increased neutron flux. This again leads to a more increased power density in this region. Meanwhile, in the region of decreased power density, the ^{135}Xe concentration increases due to its reduced burnup. This increased concentration decreases the local reactivity, which reduces the neutron flux, in turn, decreasing the local power density again. In a short time, however, the decreased ^{135}Xe concentration begins to increase and contrarily the increased concentration begins to decrease. In this way, the local power continues to oscillate between different regions. Calculations show that these oscillations have a period from about 15–30 h. Actually this type of oscillation is easily controlled in practical reactor operations by negative reactivity feedback (moderator void coefficient and Doppler coefficient) and a procedure of control rod movement.

1.3 Effects of Burnable Poison and Chemical Shim

The excess reactivity must be included in an initial reactor core in order to obtain the normal power during the required operation period. This reactivity control is mainly provided by control rods. The combined use of burnable poison and chemical shim lessens the need for control rods in thermal reactors and is intended to ensure a long operation period of the reactor.

1.3.1 Burnable Poison

A substance which has a large neutron absorption cross section is loaded into the reactor core or is directly mixed in fuel to suppress the large excess reactivity

at the initial burnup. This neutron absorber is converted into a nuclide with a low absorption cross section as the result of neutron absorption. Thus, the increase in reactivity accompanying the burnup of the poison compensates to some extent for the decrease in reactivity due to fuel burnup. This poison is called a burnable poison or a burnable neutron absorber.

Gadolinium (Gd) and boron (B) are representative burnable poisons. Boiling water reactors (BWRs) and pressurized water reactors (PWRs) use gadolinia (Gd_2O_3) mixed with the UO_2 fuel. In past PWRs, borosilicate glass ($\text{B}_2\text{O}_3\text{-SiO}_2$) was inserted into the control rod guide tubes which were not being used for control rods. Recently, investigation showed that erbium (Er), which has a lower neutron absorption cross section compared with Gd but can suppress the excess reactivity for a long time, can be mixed in the form of erbia (Er_2O_3) with the UO_2 fuel as a burnable poison.

Burnable poisons are zoned both radially and axially for flattening neutron flux in the more advanced core designs.

1.3.2 *Chemical Shim*

In PWRs, the reactivity control is accomplished in part by varying the concentration of boric acid (H_3BO_3) dissolved in the coolant. Such a chemical shim cannot be made to respond as quickly as control rods. Therefore, the chemical shim is used to control the long-term reactivity changes due to such factors as fuel burnup and Xe transients. It substantially reduces the number of control rods required in the reactor. Furthermore, because boric acid is more or less uniformly distributed through the reactor core, its concentration changes can be made without disturbing the neutron flux in the core.

Figure 1.9 shows an example of the changes of the boric acid concentration in a PWR. It is observed in the figure that the chemical shim compensates for the negative reactivity due to ^{135}Xe and ^{149}Sm and for the reactivity decrease with fuel burnup.

If a chemical shim is present, a decrease in coolant density due to temperature rise will also lead to a decrease in boric acid concentration. Thus it has a positive reactivity effect on moderator temperature coefficient as shown in Fig. 1.10. The requirement for a negative moderator temperature coefficient will limit the amount of boric acid concentration allowed.

1.4 Control Rod Worth

Control rods play a central role in reactivity control for various types of reactors; they are used in the reactivity control for the power level changes, the reactivity compensation for the long-term fuel burnup, and the reactor scram in an emergency. Boron is generally used as a neutron absorber for control rods using the (n, α) reaction of the isotope ^{10}B .

Fig. 1.9 Boric acid concentration changes of chemical shim (PWR) [4]

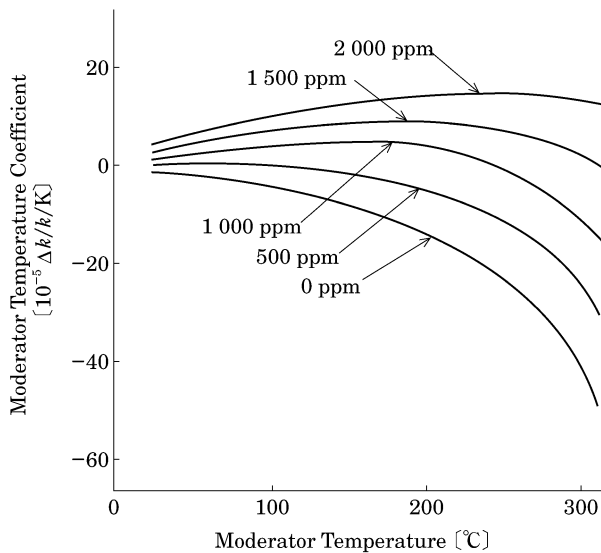
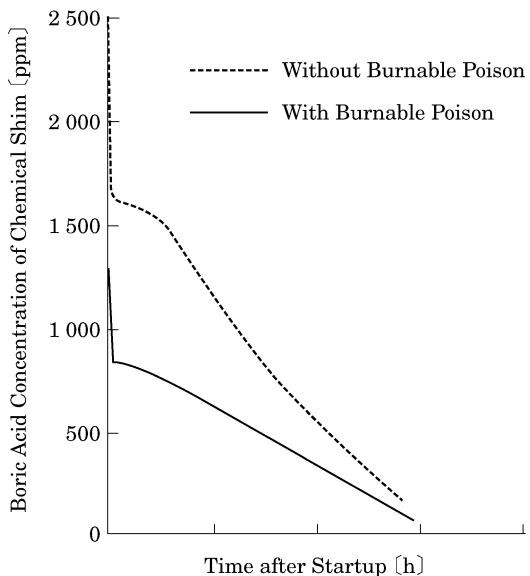


Fig. 1.10 Effect of chemical shim on moderator temperature coefficient (PWR) [10]

1.4.1 Features of Control Rod Types

In PWRs, the control rods for the 17×17 lattice fuel assembly are combined in clusters of 48 rods which are inserted from the top of the reactor vessel. Such a great number of rods with a relatively low reactivity worth keeps the neutron flux as

uniform as possible throughout the core. The control neutron absorber is an alloy of Ag-In-Cd, which features a somewhat weaker neutron absorption that produces less flux peaking and has a neutron absorption over a considerable range of neutron energies.

The control rods of BWRs consist of two crossed blades fitting into each corner between the fuel assemblies. The cruciform rods raise the surface-to-volume ratio of the control elements. Boron carbide (B_4C) or hafnium (Hf) is employed as a control rod material. Hf loaded control rods absorb neutrons by resonance capture reactions of Hf isotopes. The control rods of BWRs are driven up from the bottom of the core. The bottom-entry arrangement makes the reactivity worth of control rods greater in the lower part of the core than in the upper part where the void ratio is high and the neutron spectrum is hard.

In fast reactors, the control assemblies composed of B_4C rods, rather than the control rods inserted into fuel assemblies, replace some fuel assemblies in the core because the mean free path of neutrons is long.

1.4.2 Calculation of Control Rod Worth

The reactivity worth of control rods (control rod worth), ρ_W , can be defined as

$$\rho_W = \rho_0 - \rho_i \quad (1.49)$$

where ρ_0 and ρ_i are the system reactivity at control rod withdrawal and insertion, respectively. This definition is mainly used when measuring the insertion depth of control rods required to change the reactor power level. Another definition of control rod worth can be used to compensate for the reactivity change due to a long-time fuel burnup. In the former definition, there is no variation in physical properties of the core materials even though the control rods are inserted. Meanwhile, the physical properties vary with the fuel burnup in the latter definition. But, it was eventually found that the two definitions of control rod worth were equivalent. It is now common practice to use the first definition [11].

The calculation of control rod worth is one of the most difficult problems in the core calculation of nuclear reactors. Recently, the control rod worth has been directly evaluated through numerical calculations with a three-dimensional core representation. Many theoretical evaluations were conducted in early designs because of limitations in calculation capability. One approach was to determine the reactivity worth by using the changes in the bucklings of the system with a boundary condition at the control rod surface [12]. Another one was to calculate the reactivity worth of a large number of control rods in a regular array or cruciform control rods by applying the Wigner-Seitz method [13]. At present, such theoretical approaches are seldom applied.

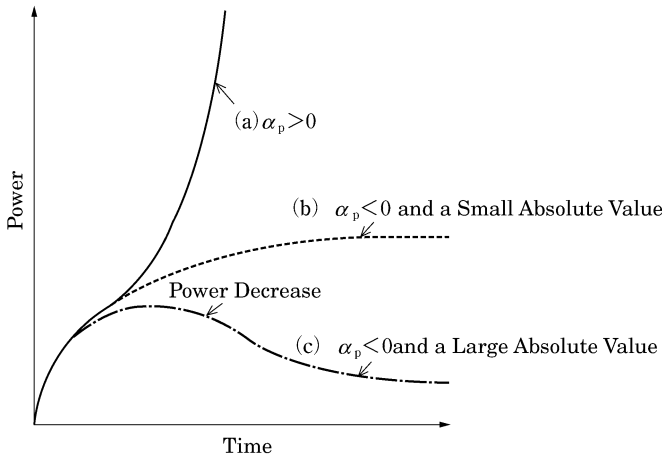


Fig. 1.11 Reactor power variation after a positive reactivity insertion [14]

1.4.3 Shadowing Effect of Control Rods

The insertion of a control rod depresses the neutron flux in its vicinity and makes the curvature of the flux greater. The gradient of the flux will contrarily increase at a radial distance. Usually, multiple control rods are placed in the core. The control rods will distort the neutron flux around each other and will have an effect on the reactivity worth. The term “shadowing effect” has been used to describe this. The worth of the control rods will be less than the sum of the separate rod worth values or greater than the sum depending on the control rod locations. It is important to determine the shadowing effect of control rods.

1.5 Inherent Reactivity Effects

1.5.1 Definition of Power and Temperature Coefficients

An important cause of reactivity variation in an operating reactor is change in the temperature of the system; that is in the fuel, moderator, coolant, and structure. The “power coefficient,” defined as Eq. (1.50), describes the variation in reactivity due to a change in reactor power. It must be essentially negative since it is an important factor for the inherent stability of the reactor.

$$\alpha_P = \frac{\partial \rho}{\partial P} \quad (1.50)$$

Figure 1.11 shows the variation in reactor power with time after a positive reactivity insertion by control rod withdrawal. If the power coefficient is negative,

the instantaneous rise of reactivity to supercritical decreases as the power increases, and then reaches criticality. If the power coefficient is positive, the reactor power will infinitely increase. If the absolute value of the negative power coefficient is too large, it is not easy to elevate the power level and a lot of control rod worth must be required as well; this will be a hard-to-operate and uneconomical reactor. The “temperature coefficient” corresponding to the temperature of each core component i ($i = \text{fuel, moderator, coolant, and structure}$), α_{T_i} , is defined as

$$\alpha_{T_i} = \frac{\partial \rho}{\partial T_i} \quad (1.51)$$

where T_i is again the temperature associated with each core component. The power coefficient can be expressed with the temperature coefficients as

$$\alpha_P = \frac{\partial \rho}{\partial P} = \sum_i \frac{\partial \rho}{\partial T_i} \frac{\partial T_i}{\partial P} = \sum_i \alpha_{T_i} \frac{\partial T_i}{\partial P} \quad (1.52)$$

where $\frac{\partial T_i}{\partial P}$ is the variation in the temperature of the i core component due to a power change and it is evaluated by thermal-hydraulic analyses (the thermal-hydraulic analyses are not discussed here).

In a reactor designed to have a negative power coefficient, the reactivity of the system decreases as the power level increases. From a different viewpoint, since the reactivity increases with the decrease in power or temperature of the system, the reactivity essentially suppressed by control rods becomes a maximum at the cold shutdown for the fuel loading and discharge.

The reactivity decrease of the system due to an increase in power or temperature can be presented by using the power coefficient or temperature coefficient. Here a reactor is considered from the cold shutdown condition to the hot shutdown condition. The reactor power is zero and the temperature of the system uniformly increases. The reactivity decrease of the system can be written by integrating the temperature coefficient from the cold shutdown temperature to the hot shutdown temperature as

$$\rho_{TD} = \sum_i \int_{\text{Cold Temperature}}^{\text{Hot Temperature}} \alpha_{T_i} dT_i \quad (1.53)$$

which is called the “temperature defect”. Since the entire reactor core is essentially characterized by an identical temperature, the temperature coefficient can be called the “isothermal temperature coefficient”.

The decrease in reactivity from the hot shutdown (zero power) condition to the normal power condition can be obtained by integrating the power coefficient in the same way, which is called the “power defect”. The power defect can be represented using Eq. (1.52) as

$$\rho_{PD} = \int_{\text{Zero Power}}^{\text{Normal Power}} \alpha_P dP = \sum_i \int_{\text{Hot Temperature}}^{\text{Normal Temperature of Element } i} \alpha_{T_i} dT_i . \quad (1.54)$$

The temperature defect and power defect are part of the reactivity that the control rods should compensate.

1.5.2 Temperature Coefficients by the Six-Factor Formula [14]

The temperature coefficient in a thermal reactor can be derived by using the six-factor formula,

$$k = \eta f p \varepsilon P_{TNL} P_{FNL} . \quad (1.55)$$

In this, k is the effective multiplication factor, η is the average number of fission neutrons emitted per thermal neutron absorbed by fuel, f is the thermal utilization factor, p is the resonance escape probability, ε is the fast fission factor, and P_{TNL} and P_{FNL} are the non-leakage probabilities of thermal and fast neutrons, respectively.

Recalling the definition of reactivity

$$\rho = \frac{k-1}{k} \quad (1.56)$$

and assuming k is close to unity, the temperature coefficient can be expressed approximately in the form of the sum of each temperature coefficient of the six factors as

$$\begin{aligned} \alpha_{T_i} &= \frac{\partial \rho}{\partial T_i} = \frac{1}{k^2} \frac{\partial k}{\partial T_i} \simeq \frac{1}{k} \frac{\partial k}{\partial T_i} \\ &= \frac{1}{\eta} \frac{\partial \eta}{\partial T_i} + \frac{1}{f} \frac{\partial f}{\partial T_i} + \frac{1}{p} \frac{\partial p}{\partial T_i} + \frac{1}{\varepsilon} \frac{\partial \varepsilon}{\partial T_i} + \frac{1}{P_{TNL}} \frac{\partial P_{TNL}}{\partial T_i} + \frac{1}{P_{FNL}} \frac{\partial P_{FNL}}{\partial T_i} \\ &\equiv \alpha_{T_i}^\eta + \alpha_{T_i}^f + \alpha_{T_i}^p + \alpha_{T_i}^\varepsilon + \alpha_{T_i}^{P_{TNL}} + \alpha_{T_i}^{P_{FNL}} . \end{aligned} \quad (1.57)$$

The principal temperature effects of most thermal reactors are the variation in resonance absorption (the Doppler effect) and the fuel expansion due to a change of fuel temperature, the variation in neutron spectrum and the moderator expansion due to a change of moderator temperature, and the expansion of other materials such as coolant (apart from moderator) or structure. These phenomena are discussed through η , f , and p . Since the temperature coefficients of ε , P_{TNL} , and P_{FNL} are generally small, on the order of $10^{-6} \Delta k/k/K$, they are omitted in the discussion.

[1] Fuel temperature coefficient

The temperature coefficient α_{T_F} at fuel temperature T_F is considered. The Doppler effect is shown through the resonance escape probability p and the fuel expansion effect is shown through f and p .

(1) Fuel temperature coefficient of resonance escape probability

The resonance escape probability can be given by [14, 15]

$$p = \exp \left[-\frac{N_F V_F}{\xi_M \Sigma_{sM} V_M} I \right] \quad (1.58)$$

where N_F and V_F are the atomic density and volume fraction of the fuel, and $\xi_M \Sigma_{sM}$ and V_M are the moderating power and volume fraction of the moderator. I is the resonance integral for the normalized moderated neutron flux which behaves as $1/E$ beyond the resonance, given by the following.

$$I = \int \sigma_{aF}(E) \phi(E) dE \quad \left[\phi(E) \sim \frac{1}{E} \right] \quad (1.59)$$

An experimental formula [16] for the temperature dependence I of is known as

$$\begin{aligned} I(T_F) &= I(300\text{K}) [1 + \beta''(\sqrt{T_F} - \sqrt{300})] \\ I(300\text{K}) &= 11.6 + 22.8 \frac{S_F}{M_F} \\ {}^{238}\text{UO}_2 : \beta'' &= 61 \times 10^{-4} + 47 \times 10^{-4} \frac{S_F}{M_F} \\ {}^{232}\text{ThO}_2 : \beta'' &= 97 \times 10^{-4} + 120 \times 10^{-4} \frac{S_F}{M_F} \end{aligned} \quad (1.60)$$

where T_F is the fuel temperature (unit: K), and S_F and M_F are, respectively, the surface area (unit: cm^2) and mass (unit: g) of the fuel element. Thus, the temperature dependence of I indeed shows the Doppler effect. That is, since the vibration of the nuclei increases with the fuel temperature, the relative velocity of the interacting neutron to the nucleus changes and hence the neutron energy range for the resonance reaction is broadened. Then, the Doppler effect mitigates the depression of the neutron flux due to large resonance absorption cross sections of a large amount of nuclides in the reactor (the energy self-shielding effect) and increases the resonance absorption reaction.

The temperature coefficient $\alpha_{T_F}^{p(\text{Doppler})}$ of the resonance escape probability p due to the Doppler effect can be obtained by differentiating I with T_F as the following.

$$\begin{aligned}\therefore \alpha_{T_F}^{p(\text{Doppler})} &= \frac{1}{p} \frac{\partial p}{\partial I} \frac{\partial I}{\partial T_F} \\ &= -\frac{N_F V_F}{\xi_M \Sigma_{sM} V_M} I(300\text{K}) \frac{\beta''}{2\sqrt{T_F}} \\ &= -\ln \left[\frac{1}{p(300\text{K})} \right] \frac{\beta''}{2\sqrt{T_F}}\end{aligned}\quad (1.61)$$

Since $p < 1$, $\ln(1/p) > 0$ and $\alpha_{T_F}^{p(\text{Doppler})}$ becomes negative. It can be noted that the magnitude of the absolute value is about 10^{-4} – $10^{-5} \Delta k/k/\text{K}$.

Next, the effect of the fuel expansion is considered assuming the ratio of the fuel volume fraction is constant. Suppose that the fuel will axially expand causing a decrease in the fuel atomic density. The temperature coefficient of the atomic density can be represented by the coefficient of linear expansion as Eq. (1.62).

$$\frac{1}{N_F} \frac{dN_F}{dT_F} = -\theta_F \quad (1.62)$$

The linear expansion coefficient of a material in the cube of length l is generally defined as

$$\theta = \frac{1}{l} \frac{dl}{dT} .$$

Equation (1.62) is derived from the relation between axial length and atomic density

$$N \propto \frac{1}{l} .$$

The temperature coefficient of the resonance escape probability due to the fuel expansion can be given by taking note of the variation in fuel atomic density due to a temperature change and by using Eq. (1.62) as

$$\alpha_{T_F}^{p(\text{Expansion})} = \frac{1}{p} \frac{\partial p}{\partial N_F} \frac{\partial N_F}{\partial T_F} = \frac{\ln p}{N_F} \frac{\partial N_F}{\partial T_F} = \theta_F \ln \left(\frac{1}{p} \right) . \quad (1.63)$$

Since $\ln(1/p) > 0$, $\alpha_{T_F}^{p(\text{Expansion})}$ is positive. The magnitude of the absolute value is small, about $10^{-5} \Delta k/k/\text{K}$ for a solid fuel. This shows physically that the decrease in the density of resonance nuclides leads to the increase in the resonance escape probability.

(2) Fuel temperature coefficient of thermal utilization factor

Considering fuel and moderator (coolant) for simplicity, the thermal utilization factor f is given by the next formula

$$f = \frac{\bar{\Sigma}_a^F V_F}{\bar{\Sigma}_a^F V_F + \bar{\Sigma}_a^M V_M} \zeta \quad (1.64)$$

where $\bar{\Sigma}_a^F$ and $\bar{\Sigma}_a^M$ are the macroscopic absorption cross sections for thermal neutrons of fuel and moderator, respectively, and V_F and V_M are their volume fractions. ζ is called the thermal disadvantage factor [17] originating from heterogeneity of the fuel lattice cell and it is defined as

$$\zeta = \phi_M / \phi_F .$$

It is noted that the thermal disadvantage factor is also dependent on the fuel and moderator temperatures. Although structure materials were omitted in Eq. (1.64) for simplicity, the following discussions essentially do not change even if considering the structure.

In recalling the axial expansion of the fuel, it should be noted that, in the numerator and denominator of Eq. (1.64), there will be a variation in the atomic density in the macroscopic cross section of the fuel due to an increase in the fuel temperature. Considering the fuel temperature dependence of the thermal disadvantage factor additionally, the fuel temperature coefficient of the thermal utilization factor is given as

$$\begin{aligned} \alpha_{T_F}^f &= \frac{1}{f} \frac{\partial f}{\partial T_F} = (1-f) \left(\frac{1}{N_F} \frac{\partial N_F}{\partial T_F} - \frac{1}{\zeta} \frac{\partial \zeta}{\partial T_F} \right) \\ &= (1-f) (-\theta_F - \alpha_{T_F}^\zeta) . \end{aligned} \quad (1.65)$$

The first term in the second parenthesis in the final expression is determined by the linear expansion coefficient and has a negative effect of about 10^{-5} $\Delta k/k/K$ for a solid fuel. Physically, this shows the probability of the thermal neutron absorption in the fuel will decrease due to a decrease in the fuel density. The second term is discussed later with the thermal disadvantage factor term in the moderator temperature coefficient.

As mentioned above, the fuel temperature coefficient was discussed with the Doppler effect and the fuel expansion effects through p and f . A negative temperature coefficient by the Doppler effect is dominant among them. Furthermore, because the fuel temperature responds immediately to changes in reactor power compared with the moderator temperature, the fuel temperature coefficient is thus often described as the prompt temperature coefficient. In this connection, it is of greatest importance that the temperature coefficient becomes negative owing to the Doppler effect.

[2] Moderator temperature coefficient

An increase in the moderator temperature T_M leads to a reduction in thermal neutron absorption due to moderator expansion and an increase in resonance absorption due to the moderating power decrease as well. They are described through f and p , respectively. Because the thermal neutron spectrum changes depending on the moderator temperature (spectral shift), there is a variation in the thermal cross sections averaged by the thermal neutron spectrum. This is discussed with η and f .

(1) Moderator temperature coefficient of resonance escape probability

In Eq. (1.58), an increase in the moderator temperature causes a reduction in the moderator atomic density (the moderator volume fraction is constant) and results in a reduction in the resonance escape probability. This means that the resonance absorption of neutrons rises due to the reduction in the neutron moderating power. The moderator temperature coefficient of the resonance escape probability is given by

$$\alpha_{T_M}^p = \frac{1}{p} \frac{\partial p}{\partial N_M} \frac{\partial N_M}{\partial T_M} = -\frac{\ln p}{N_M} \frac{\partial N_M}{\partial T_M} = -3\theta_M \ln\left(\frac{1}{p}\right) \quad (1.66)$$

which shows a negative value. An expansion of the moderator in liquid or gas is described by the relation between the temperature coefficient of atomic density and the linear expansion coefficient as

$$\frac{1}{N_M} \frac{dN_M}{dT_M} = -3\theta_M \quad (1.67)$$

where the volume expansion coefficient ($= 3\theta_M$) can be used instead of the linear expansion coefficient.

Figure 1.12 shows the volume expansion coefficients of liquid moderators. The moderator temperature coefficient of the resonance escape probability is about $10^{-4}\Delta k/k/K$ and has a large negative reactivity effect.

(2) Moderator temperature coefficient of thermal utilization factor

The moderator temperature coefficient of the thermal utilization factor can be approached in the same way. A variation in the moderator atomic density due to an increase in the moderator temperature (the moderator volume fraction is constant) can be described with the linear expansion coefficient of the moderator and also by considering the moderator temperature dependence of the thermal disadvantage factor. In addition, the thermal absorption cross sections of both the fuel and moderator change in order to shift the thermal neutron spectrum due to an increase in the moderator temperature. The moderator temperature coefficient can be therefore obtained by Eq. (1.68).

$$\alpha_{T_M}^f = \frac{1}{f} \frac{\partial f}{\partial T_M} = (1-f) \left(3\theta_M - \alpha_{T_M}^\zeta + \frac{1}{\bar{\sigma}_a^F} \frac{\partial \bar{\sigma}_a^F}{\partial T_M} - \frac{1}{\bar{\sigma}_a^M} \frac{\partial \bar{\sigma}_a^M}{\partial T_M} \right) \quad (1.68)$$

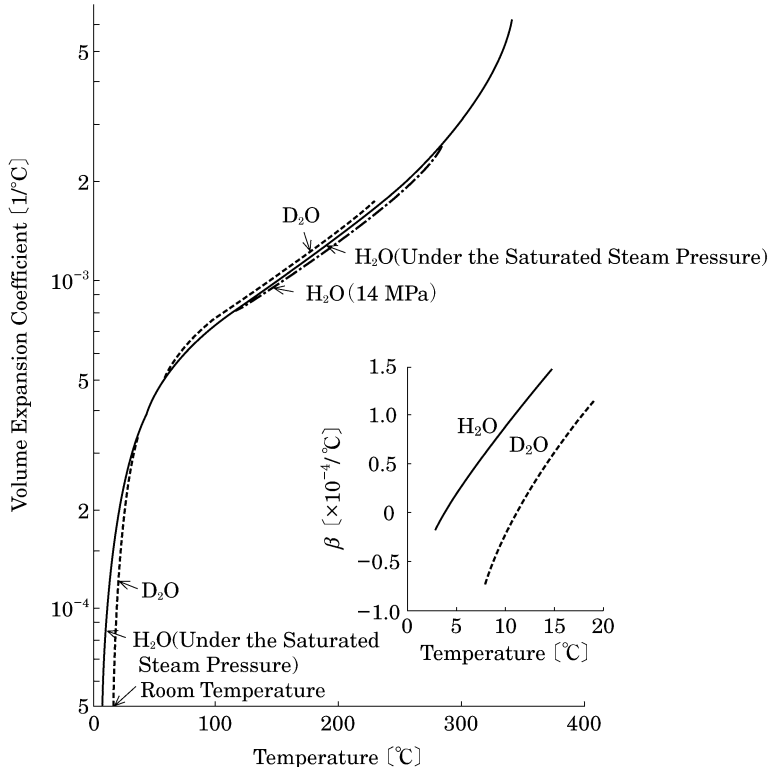


Fig. 1.12 Volume expansion coefficients of liquid moderators [14]

The temperature dependence of the thermal cross sections is given by Eq. (1.69) [18].

$$\bar{\sigma}(T_n) = \frac{\sqrt{\pi}}{2} g(T_n) \left(\frac{T_0}{T_n} \right)^{1/2} \sigma(T_0) \quad (1.69)$$

This equation can be obtained by integrating a $1/v$ cross section for the thermal neutron spectrum in a Maxwellian distribution characterized by effective neutron temperature T_n of the system. $g(T_n)$, called the non- $1/v$ factor (Westcott factor), represents the extent of the difference from the $1/v$ behavior of resonance cross sections in the range of thermal neutron energies. The non- $1/v$ factor depends on the neutron temperature because the thermal neutron spectrum and resonance cross section vary with temperature. $\sigma(T_0)$ is the cross section at the neutron speed of $v = 2200 \text{ m/s}$ and it is employed as a reference mark. The corresponding neutron energy and temperature (T_0) are 0.0253 eV and 293.61 K, respectively.

The neutron temperature T_n may be considered to be the same as the moderator temperature T_M to determine the thermal neutron spectrum. However, since the thermal neutron spectrum is practically hardened by thermal neutron absorption (absorption hardening), the neutron temperature is somewhat different from the moderator temperature. The neutron temperature can be regarded as approximately proportional to the moderator temperature by using a proportionality constant a , given by

$$T_n = aT_M \quad (1.70)$$

where a is about 1.2–1.3 for a light water-moderated reactor [14, 19].

Thus the moderator temperature coefficient of the thermal cross section can be written as

$$\frac{1}{\bar{\sigma}} \frac{\partial \bar{\sigma}}{\partial T_M} = \frac{1}{g} \frac{\partial g}{\partial T_n} \frac{\partial T_n}{\partial T_M} - \frac{1}{2T_n} \frac{\partial T_n}{\partial T_M} = a \alpha_{T_n}^g - \frac{1}{2T_M} . \quad (1.71)$$

Applying Eq. (1.71) to Eq. (1.68) gives the moderator temperature coefficient concerning the thermal utilization factor

$$\alpha_{T_M}^f = (1-f)(3\theta_M - \alpha_{T_M}^\zeta + a\alpha_{T_n}^{g^F}) \quad (1.72)$$

where the temperature coefficient of the non- $1/v$ factor was removed for a $1/v$ absorber such as the light water moderator. The first term in the second parenthesis on the right-hand side is positive. Physically, this results from the effect to raise the absorption probability of thermal neutrons in the fuel due to a decrease in moderator density caused by a moderator temperature increase. Its magnitude is large, about $10^{-4} \Delta k/k/K$ for liquid moderators. For the second term in the second parenthesis on the right-hand side, let us consider a special case in which the fuel and moderator temperatures uniformly change; then the moderator temperature coefficient of the disadvantage factor in Eq. (1.72) can be summed with the fuel temperature coefficient of the disadvantage factor in Eq. (1.65), that is,

$$\alpha_T^\zeta = \alpha_{T_F}^\zeta + \alpha_{T_M}^\zeta . \quad (1.73)$$

It turns out that α_T^ζ is always negative [14]. This is due to the fact that the thermal diffusion length increases with temperature. As the diffusion length increases, the neutron flux in the lattice fuel cell tends to flatten, that is, the depression of the flux across the cell becomes less pronounced, and this leads to a smaller value of the disadvantage factor. As a result, there is a positive reactivity effect on the temperature coefficient of the thermal utilization factor. Further details are not discussed here.

The third term in the second parenthesis on the right-hand side of Eq. (1.72) is the effect of the non- $1/v$ absorption cross section of fuel.

Table 1.2 Non- $1/v$ factors of major fuel nuclides [18]

T_n (°C)	^{233}U		^{235}U		^{238}U		^{239}Pu	
	g_a	g_f	g_a	g_f	g_a	g_a	g_f	
20	0.9983	1.0003	0.9780	0.9759	1.0017	1.0723	1.0487	
100	0.9972	1.0011	0.9610	0.9581	1.0031	1.1611	1.1150	
200	0.9973	1.0025	0.9457	0.9411	1.0049	1.3388	1.2528	
400	1.0010	1.0068	0.9294	0.9208	1.0085	1.8905	1.6904	
600	1.0072	1.0128	0.9229	0.9108	1.0122	2.5321	2.2037	
800	1.0146	1.0201	0.9182	0.9036	1.0159	3.1006	2.6595	
1,000	1.0226	1.0284	0.9118	0.8956	1.0198	3.5353	3.0079	

Table 1.3 η values of major fuel nuclides [18]

T_n (°C)	^{233}U	^{235}U	^{239}Pu
20	2.2837	2.0651	2.0347
100	2.2880	2.0632	1.9978
200	2.2908	2.0595	1.9468
400	2.2922	2.0504	1.8604
600	2.2917	2.0423	1.8107
800	2.2915	2.0366	1.7845
1,000	2.2919	2.0328	1.7701

The temperature coefficient is generally quite small, on the order of $10^{-6} \Delta k/k/\text{K}$ for ^{233}U and ^{235}U . However, ^{239}Pu has a high dependence of its non- $1/v$ factors on the neutron temperature, as shown in Table 1.2, and the moderator temperature coefficient of f has a large positive reactivity effect (order of $10^{-4} \Delta k/k/\text{K}$). Hence, this effect should not be neglected as ^{239}Pu builds up with fuel burnup.

(3) Moderator temperature coefficient of η value

As shown in Table 1.3, the dependence of η on the neutron temperature is small for ^{233}U and ^{235}U and it has an effect on the order of only $10^{-5} \Delta k/k/\text{K}$ on the moderator temperature coefficient. Meanwhile, ^{239}Pu has a high dependence and a significant negative reactivity effect of about $10^{-4} \Delta k/k/\text{K}$ on the moderator temperature coefficient. For each individual fissile nuclide, the η value is given by

$$\eta = \frac{\nu \bar{\sigma}_f}{\bar{\sigma}_a} \quad (1.74)$$

in which the moderator temperature coefficient is expressed as the difference in neutron temperature dependence between the non- $1/v$ fission factor and non- $1/v$ absorption factor, like

$$\alpha_{T_M}^\eta = a \alpha_{T_n}^\eta = a (\alpha_{T_n}^{g_f} - \alpha_{T_n}^{g_a}) \quad (1.75)$$

(4) Overall considerations of moderator temperature coefficient

In the above, the principal effects of the moderator temperature coefficient have been looked at based on the six-factor formula. For a liquid moderator, two prominent effects were seen. (i) Due to the large expansion coefficient, the temperature coefficients of p and f have a negative or positive reactivity effect, respectively, to the extent of $10^{-4}\Delta k/k/K$. (ii) When ^{239}Pu builds up with fuel burnup, the resonance of ^{239}Pu leads to a negative or positive reactivity effect, respectively, on the temperature coefficients of η and f to the same extent, $10^{-4}\Delta k/k/K$.

As first mentioned, the temperature coefficients must be essentially negative for stable operation of the reactors. As a practical result of the effects, (i) and (ii), necessary conditions for a negative reactivity effect are discussed below.

(i) Moderator expansion effect on p and f

Here, an explanation is given as to the reason for placing a design point on the under-moderated region being discussed. The moderator temperature coefficient is mainly determined by the balance of the temperature coefficients of p in Eq. (1.66) and f regarding the first term in the second parenthesis of the right-hand side in Eq. (1.72). It can be then written as Eq. (1.76).

$$\alpha_{T_M} \approx 3\theta_M \left[-\ln\left(\frac{1}{p}\right) + (1-f) \right] \quad (1.76)$$

When p approaches 1, the following holds

$$\ln\left(\frac{1}{p}\right) \approx 1-p$$

and the moderator temperature coefficient can be approximated as

$$\alpha_{T_M} \approx 3\theta_M(p-f) . \quad (1.77)$$

If f exceeds p , it may provide a negative moderator temperature coefficient.

Figure 1.13 illustrates the infinite multiplication factor and the four factors as a function of the ratio (denoted by x) of the atomic number densities of fuel and moderator. A decrease in moderator density due to a rise in moderator temperature corresponds to the increase of x . As mentioned up to now, the figure indicates that the variation of the effective multiplication factor due to an increase in moderator temperature is determined by p and f (η in the four-factor formula is out of the range of this figure, but almost constant with x without the resonance effect of nuclides such as ^{239}Pu).

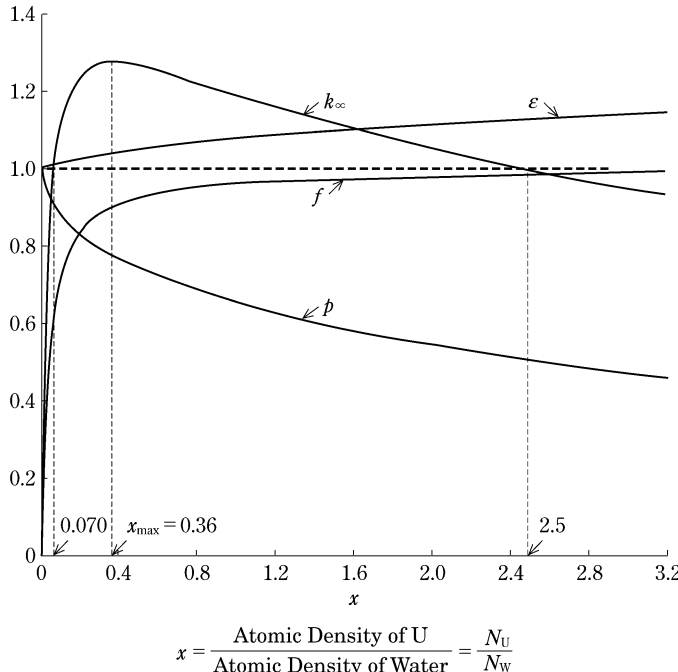


Fig. 1.13 Infinite multiplication factor as a function of the ratio of atomic number densities of fuel and moderator [20] (for a homogeneous mixture of 2 %-enriched uranium and light water)

To make the moderator temperature coefficient negative in Fig. 1.13, in other words, to decrease the infinite multiplication factor with an increase of x , x should be larger than x_{\max} at the maximum of the infinite multiplication factor.

The region above x_{\max} , in which the ratio of the moderator atomic density is smaller than that at x_{\max} , is called the under-moderated region. As an optimal point, a reactor may be designed with an as-small-as-possible fuel concentration which gives the largest value of the infinite multiplication factor. However, it is usual to place the design point slightly toward the under-moderated region from the maximum in order to make the moderator temperature coefficient negative from the viewpoint of reactor safety. In the region below x_{\max} (the over-moderated region), the infinite multiplication factor increases with x , that is, the moderator temperature coefficient is positive.

Further, it is easy to confirm that Fig. 1.13 includes the positive or negative relation of the moderator temperature coefficient in Eqs. (1.76) or (1.77).

(ii) ^{239}Pu buildup effect on η and f [21]

The multiplication of η and f in uranium fuel, including ^{239}Pu produced during burnup, can be written as Eq. (1.78).

$$\eta f = \frac{\nu \bar{\Sigma}_f^{\text{U}235} + \nu \bar{\Sigma}_f^{\text{Pu}239}}{\bar{\Sigma}_a^{\text{U}235} + \bar{\Sigma}_a^{\text{U}238} + \bar{\Sigma}_a^{\text{Pu}239} + \bar{\Sigma}_a^{\text{Others}}} \quad (1.78)$$

Recalling that the non- $1/v$ factors of ^{239}Pu give the moderator temperature coefficient of ηf , then

$$\begin{aligned} \alpha_{T_M}^{\eta f} &= \frac{1}{\eta f} \frac{\partial(\eta f)}{\partial T_M} \\ &= \frac{\nu \bar{\Sigma}_f^{\text{Pu}239}}{\nu \bar{\Sigma}_f^{\text{U}235} + \nu \bar{\Sigma}_f^{\text{Pu}239}} a \alpha_{T_n}^{g_f^{\text{Pu}239}} - \frac{\bar{\Sigma}_a^{\text{Pu}239}}{\bar{\Sigma}_a^{\text{U}235} + \bar{\Sigma}_a^{\text{U}238} + \bar{\Sigma}_a^{\text{Pu}239} + \bar{\Sigma}_a^{\text{Others}}} a \alpha_{T_n}^{\eta_{\text{Pu}239}} \\ &\equiv F a \alpha_{T_n}^{g_f^{\text{Pu}239}} - A a \alpha_{T_n}^{\eta_{\text{Pu}239}} . \end{aligned} \quad (1.79)$$

The right-hand side were partially substituted by F and A , which represent the contribution rates of ^{239}Pu to fission neutron production and absorption of thermal neutrons, respectively. Further, referring to Eq. (1.75) and applying the temperature coefficient of η to ^{239}Pu gives Eq. (1.80).

$$\alpha_{T_M}^{\eta f} = (F - A) a \alpha_{T_n}^{g_f^{\text{Pu}239}} + A a \alpha_{T_n}^{\eta_{\text{Pu}239}} \quad (1.80)$$

A rough approximation is

$$F = \frac{\nu \bar{\Sigma}_f^{\text{Pu}239}}{\nu \bar{\Sigma}_f^{\text{U}235} + \nu \bar{\Sigma}_f^{\text{Pu}239}} \approx \frac{\bar{\Sigma}_a^{\text{Pu}239}}{\bar{\Sigma}_a^{\text{U}235} + \bar{\Sigma}_a^{\text{Pu}239}} \quad (1.81)$$

and then

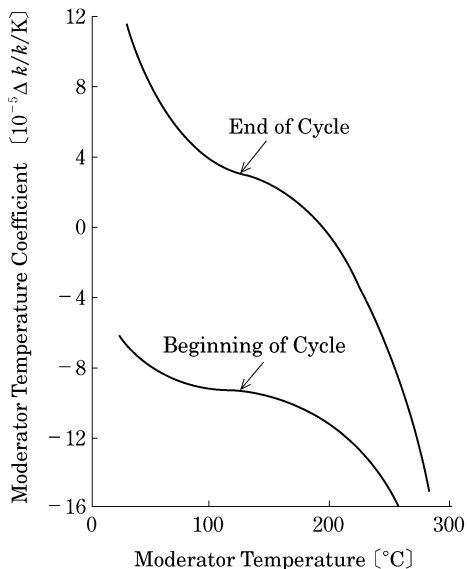
$$\frac{A}{F} \approx \frac{\bar{\Sigma}_a^{\text{U}235} + \bar{\Sigma}_a^{\text{Pu}239}}{\bar{\Sigma}_a^{\text{U}235} + \bar{\Sigma}_a^{\text{U}238} + \bar{\Sigma}_a^{\text{Pu}239} + \bar{\Sigma}_a^{\text{Others}}} \equiv f_{\text{fissile}} . \quad (1.82)$$

Inserting Eq. (1.82) into Eq. (1.80) gives

$$\therefore \alpha_{T_M}^{\eta f} \approx F a [(1 - f_{\text{fissile}}) \alpha_{T_n}^{g_f^{\text{Pu}239}} + f_{\text{fissile}} \alpha_{T_n}^{\eta_{\text{Pu}239}}] . \quad (1.83)$$

Therefore, the moderator temperature coefficient of ηf in ^{239}Pu buildup can be expressed in an easy form by the thermal utilization factor of fissile nuclides f_{fissile} through the approximation of Eq. (1.81).

Fig. 1.14 An example of the shift of moderator temperature coefficient to positive with fuel burnup in a LWR [22]



For example, consider

$$\begin{aligned}\alpha_{T_n}^{g_{\text{Pu239}}} &= +1.4 \times 10^{-3} \Delta k/k/\text{K} \\ \alpha_{T_n}^{\eta_{\text{Pu239}}} &= -5 \times 10^{-4} \Delta k/k/\text{K} .\end{aligned}$$

According to both temperature coefficients, it is necessary that $f_{\text{fisile}} > 0.74$ for $\alpha_{T_M}^{\eta f} < 0$ in Eq. (1.83). The thermal absorption rate of fissile nuclides should be large to make the reactivity effect negative against ^{239}Pu build up. By contrast, a small thermal absorption rate of fissile nuclides for natural uranium or very low-enriched fuel may lead to emergence of factors to make the moderator temperature coefficient positive due to ^{239}Pu buildup. Figure 1.14 shows an example that the moderator temperature coefficient in a LWR shifts to positive values with fuel burnup.

[3] Coolant temperature coefficient

Since the moderator also serves as a coolant in LWRs, the coolant temperature coefficient is identical to the moderator temperature coefficient. In thermal reactors with different moderator and coolant materials such as graphite-moderated reactors, the coolant temperature coefficient is separately used. As mentioned before, the moderator temperature coefficient in thermal reactors is determined by the net effect of both the negative and positive temperature coefficients of p and f , respectively. In thermal reactors with a separate moderator material, since coolant expansion does not lead to a sufficient reduction in the neutron moderating power, it should be noted that the positive effect of f may become dominant for the coolant temperature coefficient.

The coolant temperature coefficient is also used in fast reactors with no moderator. The mechanism of reactivity change is different from that in thermal reactors (see Sect. 1.4).

[4] Structure temperature coefficient

The expansion effect due to a temperature rise in structures is concerned with thermal utilization factor in the six-factor formula. Since structures are usually solids, their temperature coefficient is small. In the evaluation of the fuel or moderator temperature coefficient, it was assumed that the atomic density of fuel or moderator decreases with each temperature rise assuming a constant fuel or moderator volume fraction. This assumption was made because the variation in volume of structures due to a change in temperature is small and therefore almost a constant volume fraction of fuel or coolant is maintained. Hence, the structure temperature coefficient was disregarded in the discussion above.

However, the structure temperature coefficient should be necessarily regarded in the practical evaluation. Generally, a volume expansion due to a temperature rise of structures leads to a decrease in atomic density and an increase in the thermal utilization factor, and therefore has a positive reactivity effect. The structure expansion essentially presses liquid or gas coolant out of the system. It is somewhat complicated to formulate the structure temperature coefficient.

1.5.3 Other Temperature Coefficients

The following gives an overview of other reactivity coefficients defined according to features of the reactor type, regarding an increase in reactor power.

[1] Void coefficient

This coefficient describes a reactivity change due to formation of voids in a liquid coolant. It is used in BWRs to control the reactivity by changing the void fraction. The mechanism of the reactivity change is identical to that discussed in the moderator temperature coefficient.

In sodium-cooled fast reactors, the void reactivity of sodium is evaluated on the basis of coolant boiling caused by hypothetical accidents.

[2] Pressure coefficient

Since PWRs and BWRs are operated at high pressure, the reactivity coefficient to pressure change (pressure coefficient) should be defined. The coolant density increases with pressure and the voids in BWRs are collapsed. The mechanism of the reactivity change is diametrically opposite to that of the moderator temperature coefficient.

[3] Core expansion effect

In a system with a large neutron leakage, an increase in leakage due to expansion or deformation of structure can have a remarkable negative reactivity effect. This effect is especially important for small fast reactors.

Table 1.4 Examples of control reactivity balance for the PWR and BWR [4]

Item	(Unit: % $\Delta k/k$)	
	PWR	BWR
Excess reactivity		
No burnup and cold shutdown	22	25
No burnup and normal power	17	
Xe and Sm equilibrium	14	
Control reactivity worth		
Control rod worth (one rod stuck)	12	17
Burnable poison	7	12
Chemical shim	7	–
Sum	26	29
Shutdown margin	4	4

1.5.4 Control Reactivity Balance

The reactivity changes due to changes in temperature and fuel burnup in reactors have been described in this chapter. Control rods, burnable poisons, and chemical shim were introduced as methods to control the reactivity. In the reactor core design, it is necessary to manifest that there is enough margin in such control elements to the total reactivity requirement for control. This is called an evaluation of control reactivity balance.

Table 1.4 shows examples of the control reactivity balance for the PWR and BWR. The total reactivity requirement for control, that is, the core reactivity with all control elements withdrawn from the core, is the excess reactivity. Because the reactivity of the system is reduced due to the consumption of fissile nuclides and the accumulation of FPs with fuel burnup (burnup defect) and also because the temperature defect and power defect of the reactivity lead to a negative feedback effect, the excess reactivity is largest at no burnup and cold shutdown. Temperature defect, power defect, reactivity worth of Xe and Sm, and burnup defect are included in the excess reactivity.

The control reactivity worth is estimated by piling up the reactivity worth of the individual control elements; i.e., the control rods, burnable poisons, and chemical shim (for the PWR). The control rod worth is the sum of the reactivity worth values of individual control rods, as a conservative margin, with the exception of the most reactive control rod stuck in the full out position from the core. This is called the “stuck-rod criterion”.

The so-called “shutdown margin” is obtained by subtracting the excess reactivity at no burnup and cold shutdown from the control reactivity worth. The control elements must necessarily provide a shutdown margin.

A suitable design margin is practically evaluated from the accuracy in nuclear design for the excess reactivity and control reactivity worth and it is considered for the control reactivity balance.

1.6 Perturbation Theory for Reactivity Calculations

Highly practical methods for reactivity calculations are discussed in the last section of this chapter. In the design of power reactors or operation of research reactors, it is often necessary to evaluate the effect of small changes (perturbations) on the behavior of the reactors. A local change of reactivity in power reactors, insertion of irradiation pieces in research reactors, and so on should be treated as a local perturbation. In principle, the reactivity change due to a perturbation can be evaluated by repeatedly performing the two- or three-dimensional multi-group calculation. For a small perturbation, however, the reactivity change may be lost in the computations as the result of round-off errors. Enormous calculations are required to obtain the distribution of reactivity coefficients in the core. Such problems can be handled by perturbation theory.

1.6.1 Mathematical Preparation

It is convenient to begin with the multi-group diffusion equation in a steady state.

$$-\vec{\nabla} \cdot D_g \vec{\nabla} \phi_g + \Sigma_{tg} \phi_g - \sum_{g'} \Sigma_{sg'g} \phi_{g'} = \frac{1}{k} \chi_g \sum_{g'} v_{g'} \Sigma_{fg'} \phi_{g'} \quad (1.84)$$

D_g : diffusion coefficient in energy group g

Σ_{tg} : macroscopic total cross section in group g

$\Sigma_{sg'g}$: macroscopic scattering cross section from group g' to group g

v : average number of neutrons released per fission

Σ_{fg} : macroscopic fission cross section in group g

χ_g : fission spectrum in group g

ϕ_g : neutron flux in group g

k : effective multiplication factor

Equation (1.84) can be represented in the matrix form expanded in the energy group as

$$\mathbf{M}\phi = \frac{1}{k} \mathbf{F}\phi \quad (1.85)$$

where the matrix elements of \mathbf{M} and \mathbf{F} , and the elements of vector ϕ are given by the followings.

$$(\mathbf{M})_{gg'} = (-\vec{\nabla} \cdot D_g \vec{\nabla} + \Sigma_{tg}) \delta_{gg'} - \Sigma_{sg'g} \quad (1.86)$$

$$(\mathbf{F})_{gg'} = \chi_g \nu_{g'} \Sigma_f g' \quad (1.87)$$

$$(\phi)_g = \phi_g \quad (1.88)$$

Since \mathbf{M} and \mathbf{F} are matrices and the former includes differential operators, the product order is not commutative. \mathbf{M} and \mathbf{F} are called the operators on ϕ and the effective multiplication factor k is called the eigenvalue.

The inner product between two arbitrary functions f and g which are vectors in the energy group is defined as

$$(f, g) \equiv \int_V \sum_g f_g^* (\vec{r}) g_g (\vec{r}) d^3 r \quad (1.89)$$

where f_g^* denotes the complex conjugate of f_g . Since physical quantities used in nuclear reactor physics are normally real numbers, the complex conjugate need not actually to be considered (although necessary in mathematics).

The inner product to define the operator \mathbf{M}^\dagger adjoint to the operator \mathbf{M} is used as Eq. (1.90).

$$(\mathbf{M}^\dagger f, g) = (f, \mathbf{M}g) \quad (1.90)$$

The adjoint operator of \mathbf{F} can be defined in the same way.

In general, there is a corresponding solution ϕ^\dagger (the adjoint neutron flux) to the adjoint equation

$$\mathbf{M}^\dagger \phi^\dagger = \frac{1}{k} \mathbf{F}^\dagger \phi^\dagger \quad (1.91)$$

Here, it is noted that the eigenvalue is the same as that in Eq. (1.85). This can be found as the following. First, Eq. (1.91) is written as

$$\mathbf{M}^\dagger \phi^\dagger = \frac{1}{k^\dagger} \mathbf{F}^\dagger \phi^\dagger \quad (\ddagger)$$

The inner product of Eq. (1.85) is taken with the adjoint flux ϕ^\dagger as

$$(\phi^\dagger, \mathbf{M}\phi) = \frac{1}{k} (\phi^\dagger, \mathbf{F}\phi) \quad .$$

From the definition of the adjoint operator in Eq. (1.90), the following is given.

$$(\mathbf{M}^\dagger \phi^\dagger, \phi) = \frac{1}{k} (\mathbf{F}^\dagger \phi^\dagger, \phi)$$

Applying Eq. (※) to the left-hand side gives

$$\frac{1}{k^{\dagger*}} (\mathbf{F}^\dagger \phi^\dagger, \phi) = \frac{1}{k} (\mathbf{F}^\dagger \phi^\dagger, \phi)$$

and it is found that $k = k^{\dagger*}$. Since the eigenvalue in the multi-group diffusion equation is a real number, $k = k^\dagger$, therefore it is evident that the eigenvalue in Eq. (1.85) agrees with that in its adjoint equation.

Next, it is necessary to discuss some characteristics of the adjoint operator. An inner product for one-group macroscopic cross section can be written as

$$(f, \Sigma g) = \int_V f^* \Sigma g d^3r = \int_V (\Sigma f)^* g d^3r = (\Sigma f, g) . \quad (1.92)$$

It is found that $\Sigma^\dagger = \Sigma$ and thus the operator and its adjoint operator are identical. Such operators are said to be self-adjoint.

Then, the spatial derivatives in the leakage term of the multi-group diffusion equation are considered, that is,

$$\begin{aligned} (f, \vec{V} \cdot D\vec{V}g) &= \int_V f^* \vec{V} \cdot D\vec{V}g d^3r \\ &= \int_V \vec{V} \cdot [f^* D\vec{V}g] d^3r - \int_V (\vec{V}f^*) \cdot D\vec{V}g d^3r \end{aligned}$$

where the Integration by Parts formula was used to move the operand function of the differential operator from g to f . The first term on the right-hand side can be converted into an integral over the surface using Gauss' theorem. Since the functions f and g are regarded as zero on the surface, the surface integral vanishes. Repeating this procedure for the second term gives

$$\begin{aligned} (f, \vec{V} \cdot D\vec{V}g) &= - \int_V (\vec{V}f^*) \cdot D\vec{V}g d^3r \\ &= - \int_V \vec{V} \cdot [(\vec{V}f^*) Dg] d^3r + \int_V (\vec{V} \cdot D\vec{V}f^*) g d^3r \\ &= \int_V (\vec{V} \cdot D\vec{V}f^*) g d^3r \\ &= (\vec{V} \cdot D\vec{V}f, g) . \end{aligned} \quad (1.93)$$

It is found that $(\vec{V} \cdot D\vec{V})^\dagger = \vec{V} \cdot D\vec{V}$ and thus the leakage term is also self-adjoint.

From Eqs. (1.92) and (1.93), it is apparent that the operators in the static one-group diffusion equation are self-adjoint. In the one-group theory, the diffusion equation and adjoint equation are identical, namely, the neutron flux and its adjoint flux are identical except for the normalization factor.

Not being self-adjoint is encountered in multi-group operators or the time differential operators, that is,

$$\mathbf{M}^\dagger = \mathbf{M}^{T*} \quad (1.94)$$

$$\left(\frac{\partial}{\partial t} \right)^\dagger = - \frac{\partial}{\partial t} \quad (1.95)$$

where T implies the transpose matrix. Equation (1.94) is derived in the following. Since the time differential operators are out of the scope of this book, the references [23–25] should be consulted for Eq. (1.95).

The relation between the multi-group operator \mathbf{M} and its adjoint operator \mathbf{M}^\dagger , which meets the definition of the adjoint operator in Eq. (1.90), can be determined to find Eq. (1.94). It can be readily expressed with the matrix elements in energy group. Disregarding the spatial dependence of the operators for simplicity, the right-hand side of Eq. (1.90) is rewritten as

$$(f, \mathbf{M}g) = \sum_g f_g^* (\mathbf{M}g)_g = \sum_{g, g'} f_g^* M_{gg'} g_{g'} = \sum_{g, g'} (M_{gg'}^* f_g)^* g_{g'}$$

and the left-hand side is rewritten as

$$(\mathbf{M}^\dagger f, g) = \sum_{g'} (\mathbf{M}^\dagger f)_{g'}^* g_{g'} = \sum_{g, g'} (M_{g g'}^\dagger f_g)^* g_{g'}.$$

Hence,

$$M_{g g'}^\dagger = M_{g g'}^*$$

$$\therefore \mathbf{M}^\dagger = \mathbf{M}^{T*}.$$

The matrix elements of the adjoint operators \mathbf{M}^\dagger and \mathbf{F}^\dagger are concretely represented by the next two equations.

$$(M^\dagger)_{gg'} = (-\vec{\nabla} \cdot D_g \vec{\nabla} + \Sigma_t g) \delta_{gg'} - \Sigma_s g g' \quad (1.96)$$

$$(F^\dagger)_{gg'} = \nu_g \Sigma_f g \chi_{g'} \quad (1.97)$$

As mentioned above, the multi-group diffusion equation was represented in the form of a matrix and the adjoint operators were introduced. These are very useful in deriving the perturbation theory to calculate reactivity changes.

1.6.2 Perturbation Theory

The change in reactivity caused by a small change (perturbation) occurring in reactors can be expressed by perturbation theory. Suppose that a perturbation (denoted by δ) appears in the multi-group diffusion operators as

$$\mathbf{M}' = \mathbf{M} + \delta \mathbf{M} \quad (1.98)$$

$$\mathbf{F}' = \mathbf{F} + \delta \mathbf{F} \quad (1.99)$$

where \mathbf{M} and \mathbf{F} are the operators before the perturbation and \mathbf{M}' and \mathbf{F}' are those after the perturbation.

The multi-group diffusion equation before the perturbation and its adjoint equation are written as

$$\mathbf{M}\phi = \frac{1}{k} \mathbf{F}\phi \quad (1.100)$$

$$\mathbf{M}^\dagger \phi^\dagger = \frac{1}{k} \mathbf{F}^\dagger \phi^\dagger \quad (1.101)$$

and the multi-group diffusion equation after the perturbation is written as

$$\mathbf{M}'\phi' = \frac{1}{k'} \mathbf{F}'\phi' \quad (1.102)$$

The dagger symbol \dagger is superscripted for the adjoint operator and adjoint neutron flux, and the prime symbol $'$ is used for the operator, flux, and effective multiplication factor after the perturbation. It should also be remembered that the effective multiplication factor in the adjoint equation is identical to that in the original diffusion equation.

The change in reactivity is calculated from the change from k to k' . This reactivity change becomes the expression of the perturbation theory through a mathematical formulation with $\delta\mathbf{M}$ and $\delta\mathbf{F}$. Taking the inner product with ϕ' on both sides of Eq. (1.102) gives

$$(\phi^\dagger, \mathbf{M}'\phi') = \frac{1}{k'} (\phi^\dagger, \mathbf{F}'\phi')$$

Substituting \mathbf{M}' and \mathbf{F}' by Eqs. (1.98) and (1.99) respectively gives

$$(\phi^\dagger, \mathbf{M}\phi') + (\phi^\dagger, \delta\mathbf{M}\phi') = \frac{1}{k'} (\phi^\dagger, \mathbf{F}\phi') + \frac{1}{k'} (\phi^\dagger, \delta\mathbf{F}\phi')$$

Using the definition of the adjoint operator [Eq. (1.90)] and the adjoint equation [Eq. (1.101)], the first term in the left-hand side can be transformed as

$$(\phi^\dagger, \mathbf{M}\phi') = (\mathbf{M}^\dagger\phi^\dagger, \phi') = \frac{1}{k} (\mathbf{F}^\dagger\phi^\dagger, \phi') = \frac{1}{k} (\phi^\dagger, \mathbf{F}\phi')$$

and then

$$\frac{1}{k} (\phi^\dagger, \mathbf{F}\phi') + (\phi^\dagger, \delta\mathbf{M}\phi') = \frac{1}{k'} (\phi^\dagger, \mathbf{F}\phi') + \frac{1}{k'} (\phi^\dagger, \delta\mathbf{F}\phi')$$

is given. Hence, the change in reactivity caused by the perturbation can be found as

$$\rho = \frac{k' - k}{kk'} = \frac{1}{k} - \frac{1}{k'} = \frac{\left(\phi^\dagger, \left[\frac{1}{k'} \delta\mathbf{F} - \delta\mathbf{M} \right] \phi \right)}{(\phi^\dagger, \mathbf{F}\phi')}$$

By approximating $1/k'$ multiplied by $\delta\mathbf{F}$ in the numerator of the right-hand side as unity, the reactivity change becomes

$$\rho = \frac{(\phi^\dagger, [\delta\mathbf{F} - \delta\mathbf{M}] \phi')}{(\phi^\dagger, \mathbf{F} \phi')} . \quad (1.103)$$

This expression is called the exact perturbation theory and the non-matrix form is given by Eq. (1.104).

$$\rho = \frac{\int_V \sum_g \phi_g^\dagger(\vec{r}) \left[\begin{array}{l} \chi_g \sum_{g'} \delta(v_{g'} \Sigma_{fg'}(\vec{r})) \phi'_{g'}(\vec{r}) \\ + \vec{V} \cdot \delta D_g(\vec{r}) \vec{V} \phi'_g(\vec{r}) - \delta \Sigma_{tg}(\vec{r}) \phi'_g(\vec{r}) \\ + \sum_g \delta \Sigma_{sg'g}(\vec{r}) \phi'_{g'}(\vec{r}) \end{array} \right] d^3 r}{\int_V \sum_g \phi_g^\dagger(\vec{r}) \chi_g \sum_{g'} v_{g'} \Sigma_{fg'}(\vec{r}) \phi'_{g'}(\vec{r}) d^3 r} \quad (1.104)$$

To evaluate the reactivity change using the exact perturbation theory, it is necessary to know the neutron flux after the perturbation as well as the adjoint flux before the perturbation and changes of the macroscopic cross sections and diffusion coefficient. In other words, the change in neutron flux caused by the perturbation should be considered.

If the perturbation is small enough and its effect on neutron flux is similarly small, the neutron flux after the perturbation can be approximated to that before the perturbation. Equation (1.103) can be written as Eq. (1.105) which is called the first-order perturbation theory.

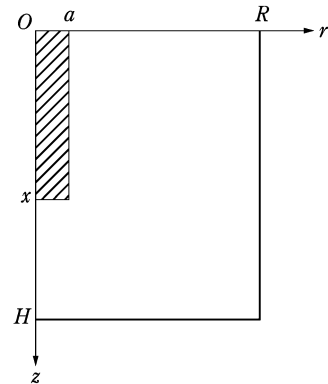
$$\rho = \frac{(\phi^\dagger, [\delta\mathbf{F} - \delta\mathbf{M}] \phi)}{(\phi^\dagger, \mathbf{F} \phi)} \quad (1.105)$$

Further, this equation becomes simpler in one-group theory because the neutron flux is self-adjoint. The equation in the one-group first-order perturbation theory can be detailed as Eq. (1.106).

$$\rho = \frac{\int_V [\delta(v \Sigma_f(\vec{r})) \phi^2(\vec{r}) - \delta D(\vec{r}) (\vec{V} \phi(\vec{r}))^2 - \delta \Sigma_a(\vec{r}) \phi^2(\vec{r})] d^3 r}{\int_V v \Sigma_f(\vec{r}) \phi^2(\vec{r}) d^3 r} \quad (1.106)$$

The reactivity change in the perturbation theory is expressed with the neutron flux and its adjoint flux operating to cause the change in the macroscopic cross sections. The product of the neutron flux and the change in the macroscopic cross sections represents the change in reactor rate. The adjoint neutron flux is interpreted to be multiplied as an importance. This physical interpretation of the adjoint flux can be clearly made in considering a time-dependent problem. For more details, the references [23–25] should be consulted.

Fig. 1.15 Control rod partially inserted along the axis of a cylindrical reactor



1.6.3 Application of Perturbation Theory: Reactivity Worth of Partially Inserted Control Rod [26]

An application of the one-group first-order perturbation theory is discussed here.

A bare cylindrical reactor of extrapolated radius R and height H is considered, in which a central control rod of radius a is partially inserted, as shown in Fig. 1.15. The insertion depth of the control rod from the origin in the top of the cylindrical reactor is denoted by x . If the control rod is a relatively weak absorber of neutrons and the control rod insertion has a small effect on the change in neutron flux distribution, then the first-order perturbation theory can be applied to obtain the reactivity worth of the partially inserted control rod.

The macroscopic absorption cross section is assumed to increase by $\delta \Sigma_a$ in the region of $0 \leq z \leq x$ and $0 \leq r \leq a$. In this coordinate system, the unperturbed neutron flux is

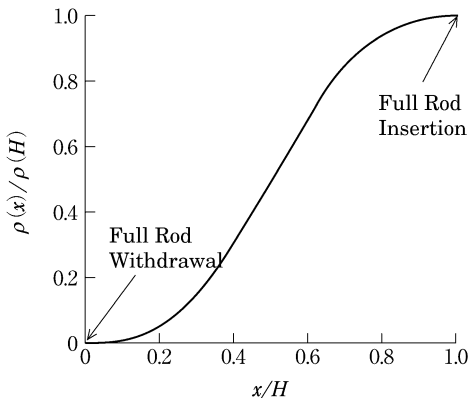
$$\phi(r, z) = A J_0 \left(\frac{2.405r}{R} \right) \sin \left(\frac{\pi z}{H} \right) \quad (1.107)$$

where A is a constant. Introducing Eq. (1.107) into Eq. (1.106) and noting that the differential volume element d^3r is $2\pi r dr dz$, the reactivity change due to the rod insertion of x can be obtained as Eq. (1.108).

$$\rho(x) = \frac{-2\pi A^2 \delta \Sigma_a \int_0^a r J_0^2 \left(\frac{2.405r}{R} \right) dr \int_0^x \sin^2 \left(\frac{\pi z}{H} \right) dz}{\int_V v \Sigma_f \phi^2 d^3r} \quad (1.108)$$

Comparing this with the reactivity change $\rho(H)$ when the control rod is fully inserted, the relative reactivity worth of the control rod is given by Eq. (1.109) which is illustrated in Fig. 1.16.

Fig. 1.16 Relative reactivity worth of control rod as a function of its insertion depth



$$\frac{\rho(x)}{\rho(H)} = \frac{\int_0^x \sin^2\left(\frac{\pi z}{H}\right) dz}{\int_0^H \sin^2\left(\frac{\pi z}{H}\right) dz} = \frac{x}{H} - \frac{1}{2\pi} \sin\left(\frac{2\pi x}{H}\right) \quad (1.109)$$

This is called the S-curve of control rod worth. The maximum change in the reactivity occurs when the end of the control rod is at the center of the reactor.

This case shows that the perturbation theory can be used to provide a satisfactory estimate of the reactivity worth as a function of location in the perturbation region.

Exercises of Chapter 1

1. Consider the hypothetical case of an infinite-sized thermal reactor initially fueled with enriched uranium which operates at a constant neutron flux. For a constant atomic density of ^{238}U : (a) derive the equations that determine the time dependence of the ^{235}U and ^{239}Pu concentrations in the reactor and (b) plot the behavior as a function of time.
2. (a) Derive the equations that determine the transient behavior of the ^{135}I and ^{135}Xe concentrations in an infinite-size thermal reactor which operates at a neutron flux ϕ_0 when the flux is changed to ϕ_1 and (b) plot the behavior as a function of time.
3. Explain the main reactivity feedback effects and reactivity control methods for each system of the BWR, PWR, high-temperature gas-cooled reactor (HTGR), and liquid-metal fast breeder reactor (LMFBR).
4. Consider a light water-cooled graphite-moderated thermal reactor fueled with very low-enriched uranium which operates with burnup. Explain the causes of the results in the cases of (a) a positive coolant void coefficient and (b) a positive moderator temperature coefficient [27].
5. Consider a ^{235}U fueled thermal reactor which is a homogeneous cubic reactor of side length L . Assume that the temperature suddenly increases by the amount ΔT

throughout a cubic region of side length $L/6$ along the center of the reactor. Compute the reactivity change introduced into the reactor by this local temperature rise using the one-group first-order perturbation theory. Ignore the change in neutron leakage due to the temperature rise [26].

References

1. Suyama K, Kataura J, Ohkawachi Y, Ishikawa M (1999) Libraries based on JENDL-3.2 for ORIGEN2 code: ORLIBJ32, JAERI-Data/Code 99-003. Japan Atomic Energy Research Institute (in Japanese)
2. Horiguchi T, Tachibana T, Koura H, Kataura J (2004) Chart of the nuclides 2004. Japanese Nuclear Data Committee, Japan Atomic Energy Research Institute
3. Bateman H (1910) The solution of a system of differential equations occurring in the theory of radio-active transformations. Proc Cambridge Philos Soc 15:423
4. Knief RA (1992) Nuclear engineering. Taylor and Francis, Bristol
5. Sugi T (1994) Nuclear reactor training lecture text: nuclear reactor physics. Japan Atomic Energy Research Institute, pp 119–124 (in Japanese)
6. Jakeman D (1966) Physics of nuclear reactors. The English Universities Press, London
7. Lamarche JR (1966) Introduction to nuclear reactor theory, section 13.2. Addison-Wesley, Reading
8. Tasaka K et al (1990) JNDC nuclear data library of fission products, -second version-, JAERI 1320. Japan Atomic Energy Research Institute
9. Duderstadt JJ, Hamilton LJ (1976) Nuclear reactor analysis, section 15-I. Wiley, New York
10. Duderstadt JJ, Hamilton LJ (1976) Nuclear reactor analysis, section 14-IV. Wiley, New York
11. Lamarche JR (1966) Introduction to nuclear reactor theory, section 14-1. Addison-Wesley, Reading
12. Lamarche JR (1966) Introduction to nuclear reactor theory, section 14-2. Addison-Wesley, Reading
13. Lamarche JR (1966) Introduction to nuclear reactor theory, section 14-7. Addison-Wesley, Reading
14. Lamarche JR (1966) Introduction to nuclear reactor theory, section 13-1. Addison-Wesley, Reading
15. Lamarche JR (1966) Introduction to nuclear reactor theory, section 11-3. Addison-Wesley, Reading
16. Duderstadt JJ, Hamilton LJ (1976) Nuclear reactor analysis, section 14-V. Wiley, New York
17. Lamarche JR (1966) Introduction to nuclear reactor theory, section 11-2. Addison-Wesley, Reading
18. Lamarche JR (1966) Introduction to nuclear reactor theory, section 8-2. Addison-Wesley, Reading
19. Lamarche JR (1966) Introduction to nuclear reactor theory, section 8-1. Addison-Wesley, Reading
20. Lamarche JR (1966) Introduction to nuclear reactor theory, section 9-6. Addison-Wesley, Reading
21. Sugi T (1994) Nuclear reactor training lecture text: nuclear reactor physics. Japan Atomic Energy Research Institute, pp 159–162 (in Japanese)
22. Togo Y, Ishikawa M, Shiba M (1977) Document collection of safety measures in postulated accidents of light water reactors. ISU Inc., Japan (in Japanese)
23. Lewins J (1965) Importance: the adjoint function. Pergamon, Oxford
24. Otsuka M (1972) Nuclear reactor physics. Kyoritsu, Tokyo (in Japanese)

25. Bell GI, Glasstone S (1970) Nuclear reactor theory, section 6-1. Van Nostrand Reinhold Co., New York
26. Lamarsh JR (1966) Introduction to nuclear reactor theory, section 15–6. Addison-Wesley, Reading
27. Japan Atomic Energy Agency (2007) The 38th nuclear reactor chief engineer examination (in Japanese)

Chapter 2

Nuclear Reactor Calculations

Keisuke Okumura, Yoshiaki Oka, and Yuki Ishiwatari

Abstract The most fundamental evaluation quantity of the nuclear design calculation is the effective multiplication factor (k_{eff}) and neutron flux distribution. The excess reactivity, control rod worth, reactivity coefficient, power distribution, etc. are undoubtedly inseparable from the nuclear design calculation. Some quantities among them can be derived by secondary calculations from the effective multiplication factor or neutron flux distribution. Section 2.1 treats the theory and mechanism to calculate the effective multiplication factor and neutron flux distribution in calculation programs (called *codes*). It is written by Keisuke Okumura.

The nuclear reactor calculation is classified broadly into the reactor core calculation and the nuclear plant characteristics calculation. The former is done to clarify nuclear, thermal, or their composite properties. The latter is done to clarify dynamic and control properties, startup and stability, and safety by modeling pipes and valves of the coolant system, coolant pump, their control system, steam turbine and condenser, etc. connected with the reactor pressure vessel as well as the reactor core. The reactor core, plant dynamics, safety analysis and fuel rod analysis are described in Sect. 2.2. It is written by Yoshiaki Oka and Yuki Ishiwatari.

2.1 Nuclear Design Calculations

2.1.1 Fundamental Neutron Transport Equation

The collective behavior of neutrons in a reactor core is described by the neutron transport equation presented in Eq. (2.1) which is also referred to as the Boltzmann equation.

$$\frac{1}{v} \frac{\partial}{\partial t} \phi(\vec{r}, \vec{\Omega}, E, t) = S(\vec{r}, \vec{\Omega}, E, t) - \vec{\Omega} \cdot \nabla \phi(\vec{r}, \vec{\Omega}, E, t) - \Sigma_t(\vec{r}, E, t) \phi(\vec{r}, \vec{\Omega}, E, t) \quad (2.1)$$

Here, S is the neutron source, Σ_t is the macroscopic total cross section, and ϕ is the angular neutron flux being calculated. This equation represents the balance between gain and loss in the unit volume of neutrons that are characterized by a specific kinetic energy E (velocity v) and are traveling in a specific direction $\vec{\Omega}$ at a time t and a position \vec{r} . That is, the time change of the target neutrons (the first term in the LHS) is given by the balanced relation among: the gain of neutrons appearing from the neutron source S (the first in the RHS), the net loss of neutrons traveling (the second term in the RHS), and the loss of neutrons due to nuclear collisions (the third term in the RHS). It should be noted that the changes in angle and energy of neutrons are also included in the gain and loss.

The target neutrons are gained from three mechanisms: scattering, fission, and external neutron sources. Each gain is represented in

$$\begin{aligned} S(\vec{r}, \vec{\Omega}, E, t) &= \int_0^\infty dE' \int_{4\pi} \Sigma_s(\vec{r}, \vec{\Omega}' \rightarrow \vec{\Omega}, E' \rightarrow E, t) \phi(\vec{r}, \vec{\Omega}', E', t) d\Omega' \\ &\quad + \frac{\chi(E)}{4\pi} \int_0^\infty dE' \int_{4\pi} \chi(E) v \Sigma_f(\vec{r}, E', t) \phi(\vec{r}, \vec{\Omega}', E', t) d\Omega' \\ &\quad + S_{ex}(\vec{r}, \vec{\Omega}, E, t) \end{aligned} \quad (2.2)$$

where Σ_s and Σ_f are the macroscopic scattering and fission cross sections, respectively. v is the average number of neutrons released per fission and the product $v\Sigma_f$ is treated as a production cross section. The cross sections are described in the next section.

The first term in the RHS of Eq. (2.2) is called the *scattering source* and it totals the number of the target neutrons scattering into E and $\vec{\Omega}$ from another energy E' and direction $\vec{\Omega}'$ by integrating the number for E' and $\vec{\Omega}'$. The second term is the fission source and it indicates that the neutrons produced by fission over the whole range of energies are distributed with the isotropic probability in direction ($1/4\pi$) and the probability $\chi(E)$ in energy. $\chi(E)$ is called the *fission spectrum* and it is dependent on the nuclide undergoing fission and the energy of incident neutrons. For instance, the fission spectrum in an enriched uranium-fueled LWR is well described by the function of Eq. (2.3).

$$\chi(E) = \sinh \sqrt{2.29E} \exp(-E/0.965) \quad (2.3)$$

Since $\chi(E)$ is a probability distribution function, it is normalized so that

$$\int_0^\infty \chi(E) dE = 1.0 \quad (2.4)$$

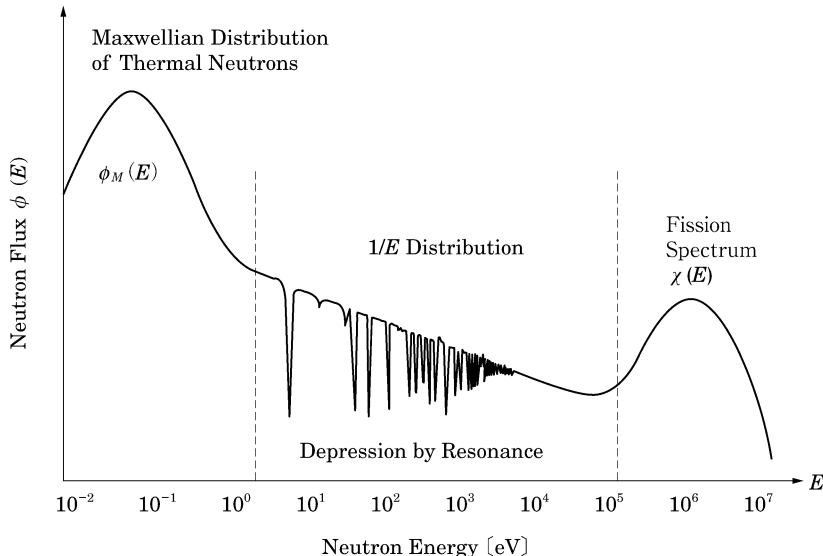


Fig. 2.1 Neutron spectrum of a thermal reactor

The third term in the RHS of Eq. (2.2), S_{ex} , expresses the external neutron source for reactor startup which may be such species as ^{252}Cf or Am-Be. Therefore, it is not used in the nuclear design calculation of a reactor in operation.

More details of the neutron transport equation are not handled here. If the cross section data (Σ_t , Σ_s , and $v\Sigma_f$) in Eqs. (2.1) and (2.2) are provided, the angular neutron flux $\phi(\vec{r}, \vec{\Omega}, E, t)$, which depends on location, traveling direction, energy, and time, can be calculated by properly solving the equation.

The information on traveling direction of neutrons is finally unimportant in the nuclear design calculation. The scalar neutron flux integrated over the angle is rather meaningful.

$$\phi(\vec{r}, E, t) = \int_0^{4\pi} \phi(\vec{r}, \vec{\Omega}, E, t) d\Omega \quad (2.5)$$

2.1.2 Neutron Spectrum

The function characterizing the energy dependence of neutron flux $\phi(\vec{r}, E, t)$ is called the *neutron spectrum* and it varies with fuel enrichment, moderator density, void fraction, burnup, and so on. Figure 2.1 shows a neutron spectrum of a thermal reactor. The neutron spectrum of thermal reactors is divided into three distinct energy regions. In the high-energy region above 10^5 eV, since the prompt neutrons released by fission are dominant, the neutron spectrum is approximately

proportional to the fission spectrum $\chi(E)$. In the energy region below several hundred of keV, the fast neutrons from fission lose their energies mainly through elastic scattering reaction with light moderator nuclides such as hydrogen.

According to neutron slowing-down theory [1], when fast neutron sources are in an infinite homogeneous medium which is an ideal moderator with negligible absorption, the neutron energy spectrum behaves as $1/E$.

$$\phi(E) \propto \frac{1}{E} \quad (2.6)$$

In the practical medium of fuel and moderator, the $1/E$ distribution is characterized by the occurrence of fairly sharp depressions due to the resonance absorption of ^{238}U , etc. as shown in Fig. 2.1. Moreover, if the resonance absorption is large, the neutron flux becomes somewhat smaller than the $1/E$ distribution in the low energy region.

If neutrons are moderated below several eV of kinetic energy, the kinetic energy by thermal vibration of nuclei cannot be ignored. In other words, if the kinetic energies of neutrons become appropriately small, the neutrons collide with thermally vibrating moderator nuclei and their kinetic energies become reversely large. This is called *up-scattering* against moderation (*down-scattering*). In this energy region, the neutron spectrum is characterized in a thermal equilibrium at a temperature T by a balance between down-scattering and up-scattering. Further, in the ideal infinite medium without absorption, the thermal equilibrium neutron spectrum is described by the following Maxwellian distribution function

$$\phi_M(E) \propto E \cdot \exp\left(-\frac{E}{kT}\right) \quad (2.7)$$

where k is the Boltzmann constant. At room temperature ($T = 300$ K), ϕ_M is maximized at $E = 0.0253$ eV for which the corresponding velocity is 2,200 m/s.

On being absorbed, the thermal neutron spectrum deviates a little from $\phi_M(E)$ forward the high energy region because absorption cross sections are larger in lower energies. This is called *absorption hardening*. To compensate the Maxwellian distribution for the absorption hardening, neutron temperature, which is a little higher than moderator temperature, is used as T of Eq. (2.7).

2.1.3 Nuclear Data and Cross Sections

[1] Macroscopic cross sections

The cross section used in the neutron transport equation, Σ , is called the macroscopic cross section and its unit is (cm^{-1}). The macroscopic cross section of nuclear reaction x is the sum of the product of atomic number density N^i and microscopic cross section σ_x^i of a constituent nuclide i of the material at a position \vec{r} . It is expressed as Eq. (2.8).

Table 2.1 Classification of key nuclear reactions in nuclear reactors

Classification	Reaction	Transcription	Cross section symbol	Reaction example
Scattering (σ_s)	Elastic scattering	(n, n)	σ_e	$^1\text{H}(n, n)$
	Inelastic scattering	(n, n')	σ_{in}	$^{238}\text{U}(n, n')$
Absorption (σ_a)	Radiative capture	(n, γ)	σ_γ	$^{238}\text{U}(n, \gamma)$
	Fission	(n, f)	σ_f	$^{235}\text{U}(n, f)$
	Charged-particle emission	(n, p)	σ_p	$^{14}\text{N}(n, p)$
		(n, α)	σ_α	$^{10}\text{B}(n, \alpha)$
	Neutron emission	$(n, 2n)^a$	$\sigma_{(n, 2n)}$	$^9\text{Be}(n, 2n)$

^aThe $(n, 2n)$ reaction can be treated as a special scattering reaction. Here this reaction, which transmutes the nuclide, is classified as an absorption reaction

$$\Sigma_x(\vec{r}, E, t) = \sum_i N^i(\vec{r}, t) \sigma_x^i(E) \quad (2.8)$$

The atomic number density N^i can be given by

$$N^i(\vec{r}, t) = \frac{\rho^i(\vec{r}, t)}{M^i} N_A \quad (2.9)$$

where ρ^i is the density occupied by i in the material, M^i is the atomic mass, and N_A is Avogadro's number. Variation of atomic number density with position and time should be considered in power reactors, reflecting fuel burnup or coolant void fraction.

[2] Microscopic cross sections

Interactions between neutrons and nuclei in nuclear reactors can be classified broadly into scattering and absorption reactions as shown in Table 2.1. Scattering is further classified into elastic scattering in which the kinetic energy is conserved before and after the reaction, and inelastic scattering in which a part of the kinetic energy is used in exciting a target nucleus. In absorption, the main reactions are capture, fission, charged-particle emission, and neutron emission. Thus, the microscopic cross sections of the total, scattering, and absorption reactions are given by

$$\text{total cross section: } \sigma_t(E) = \sigma_s(E) + \sigma_a(E) \quad (2.10)$$

$$\text{scattering cross section: } \sigma_s(E) = \sigma_e(E) + \sigma_{in}(E) \quad (2.11)$$

absorption cross section:

$$\sigma_a(E) = \sigma_\gamma(E) + \sigma_f(E) + \sigma_p(E) + \sigma_\alpha(E) + \sigma_{(n,2n)}(E) \quad (2.12)$$

It is useful to discuss a general energy dependence of these microscopic cross sections. The neutron energy range to be considered in design of nuclear reactors is from the Maxwellian distribution of the thermal neutrons at room temperature to the fission spectrum of the prompt neutrons. Most nuclear design codes handle the range of 10^{-5} eV–10 MeV. In this energy range, the

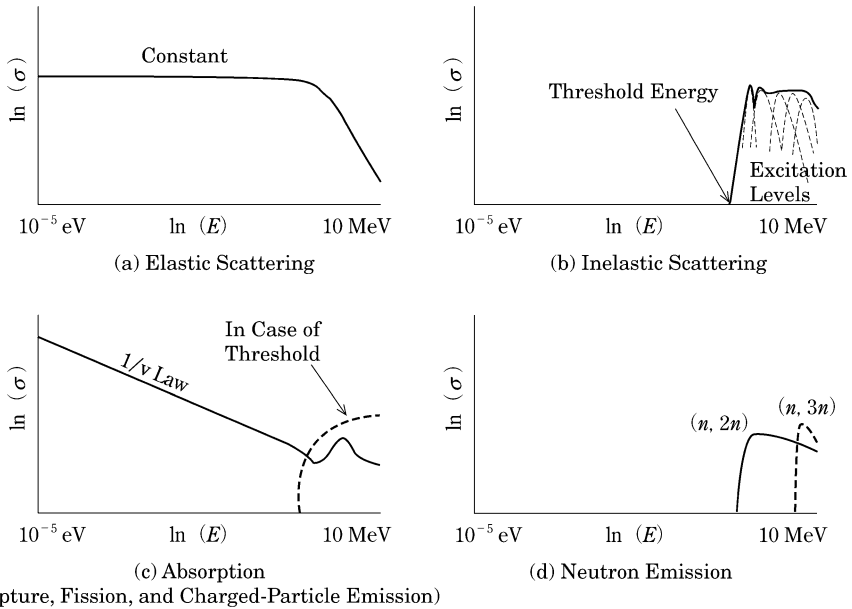


Fig. 2.2 Energy dependence of cross sections

microscopic cross sections introduced in Eqs. (2.10), (2.11), and (2.12) behave as shown in Fig. 2.2.

The elastic scattering cross section is mostly constant in all the energies except for the MeV region. Meanwhile, in inelastic scattering, the incident neutron should have sufficient kinetic energy to place the target nucleus in its excited state. Hence, the inelastic scattering cross section is zero up to some threshold energy of several MeV. Fast neutrons can be moderated by inelastic scattering with heavy nuclides, but by elastic scattering with light nuclides below threshold energies of the heavy nuclides.

Most absorption cross sections including the fission cross section appear as a straight line with a slope of $-1/2$ on a log–log scale. This means that the absorption cross sections are inversely proportional to the neutron speed ($1/v$ law) and therefore increase as the neutron energy decreases. Using such large fission cross sections at low neutron energies and thermal neutrons in the Maxwellian distribution make it possible that natural or low-enrichment uranium fueled reactors reach a critical state. The current thermal reactors, represented by LWRs, use the characteristics of the cross section.

For heavy nuclides such as fuel materials, many resonances are observed in elastic scattering and absorption cross section as shown in Fig. 2.3. The widths of the resonances broaden as fuel temperature increases. This is called the *Doppler effect*. The width broadening facilitates resonance absorption of neutrons under moderation. Most low-enrichment uranium fuel is composed of

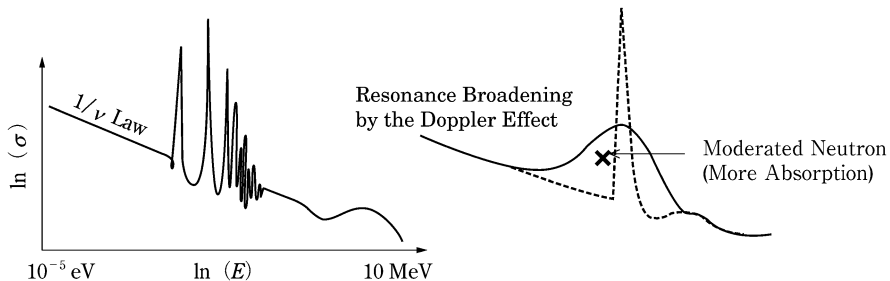


Fig. 2.3 Resonance absorption cross section and Doppler effect

fertile ^{238}U and thermal neutrons escaping from the resonance of capture reaction induce fissions for the next generation.

Hence, a rise in fuel temperature leads to a decrease in resonance escape probability of moderated neutrons and then fission events in the reactor decrease with thermal neutrons. Such a mechanism is called *negative temperature feedback*. The temperature dependence is not described in the Boltzmann equation of Eq. (2.1), but reflected in the cross sections of the equation.

[3] Evaluated nuclear data file

The primal data (microscopic cross sections, etc.) for the nuclear reactor calculation are stored in the evaluated nuclear data file which includes cross sections uniquely-determined in the whole range of neutron energy on the basis of fragmentally measured and/or theoretically calculated parameters. The cross sections are given for all possible nuclear reactions of more than 400 nuclides. JENDL [2], ENDF/B [3], and JEFF [4] are representative evaluated nuclear data files.

Extensive data are stored in 80-column text format in the evaluated nuclear data file as shown in Fig. 2.4 and complicated data such as resonance cross sections are also compactly-represented by mathematical formulas and their parameters.

The evaluated nuclear data, from anywhere in the world, are described based on the same format which might not make sense to beginners. The format has been changed according to advances in nuclear data and the current latest format is called ENDF-6 [5]. Various data of delayed neutron fractions, fission yields, half-lives, etc. as well as cross sections are available.

[4] Multi-group cross sections

The cross sections stored in the evaluated nuclear data file are continuous-energy data, which are converted to multi-group cross sections through energy discretization in formats suitable for most of nuclear design calculation codes, as shown in Fig. 2.5. The number of energy groups (N) is dependent on nuclear design codes and is generally within 50–200.

Multi-group cross sections are defined that integral reaction rates for reactions ($x = s, a, f, \dots$) of a target nuclide i) should be conserved within the range

9.223500+4	2.330250+2	0	0	0	0	09228	3	18	1
1.935800+8	1.935800+8	0	0	1	0	1409228	3	18	2
140	2	0	0	4	0	09228	3	18	3
1.000000+5	0.000000+0	2.530000+2	0.000000+0	3.000000+0	0.000000+4	0.000000+09228	3	18	4
3.000000+4	2.007500+0	3.250000+4	1.9672						
3.750000+4	1.886600+0	4.000000+4	1.8664						
5.000000+4	1.808200+0	5.500000+4	1.7930						
6.500000+4	1.757500+0	6.999990+4	1.7347						
7.999990+4	1.670400+0	8.499990+4	1.6361						
9.500000+4	1.572400+0	1.000000+5	1.5431						
1.250000+5	1.479300+0	1.375000+5	1.4721						
1.625000+5	1.445300+0	1.750000+5	1.4176						
2.000000+5	1.354000+0	2.250000+5	1.3039						
2.750000+5	1.250200+0	3.000000+5	1.2394						
3.500000+5	1.231800+0	3.750000+5	1.2280						
4.250000+5	1.203400+0	4.500000+5	1.1833						
5.000000+5	1.147100+0	5.250000+5	1.1383						
5.750000+5	1.135500+0	6.000000+5	1.1363						
6.500000+5	1.133440+0	6.750000+5	1.1294						

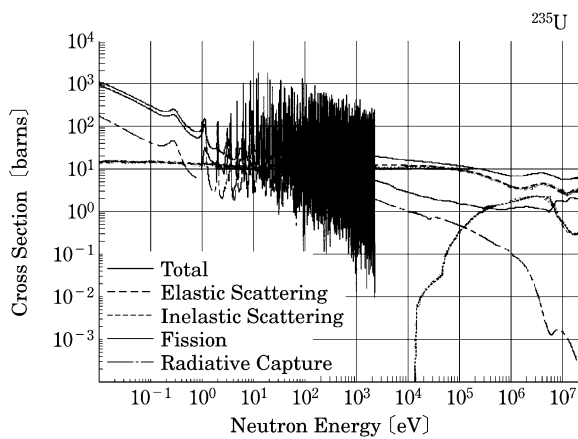


Fig. 2.4 Example of ^{235}U cross sections stored in JENDL (Right bottom figure: plot of the cross sections)

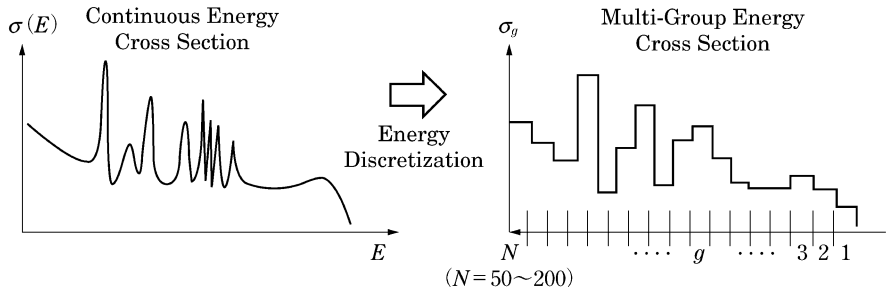


Fig. 2.5 Multi-group cross section by energy discretization

of energy group g (ΔE_g), as shown in Eq. (2.13). The neutron flux and cross section in group g are defined as Eqs. (2.14) and (2.15), respectively.

$$\int_{\Delta E_g} \sigma_x^i(E) \phi(E) dE = \sigma_{x,g}^i \phi_g \quad (2.13)$$

$$\phi_g \equiv \int_{\Delta E_g} \phi(E) dE \quad (2.14)$$

$$\sigma_{x,g}^i \equiv \frac{\int_{\Delta E_g} \sigma_x^i(E) \phi(E) dE}{\int_{\Delta E_g} \phi(E) dE} \quad (2.15)$$

The neutron spectrum of Fig. 2.1 can be used as $\phi(E)$ in Eq. (2.15) for thermal reactors. However, while those multi-group cross sections are introduced to calculate neutron flux in reactors, it is apparent that the neutron flux is necessary to define the multi-group cross sections. This is recursive and contradictory. For example, the depression of neutron flux due to resonance, shown in the $1/E$ region of Fig. 2.1, depends on fuel composition (concentrations of resonance nuclides) and temperature (the Doppler effect). It is hard to accurately estimate the neutron flux before design calculation. In actual practice, consideration is made for a representative neutron spectrum ($\phi_w(E)$: called the “weighting spectrum”) which is not affected by the resonance causing the depression and is also independent of position. Applying it to Eq. (2.15) gives Eq. (2.16).

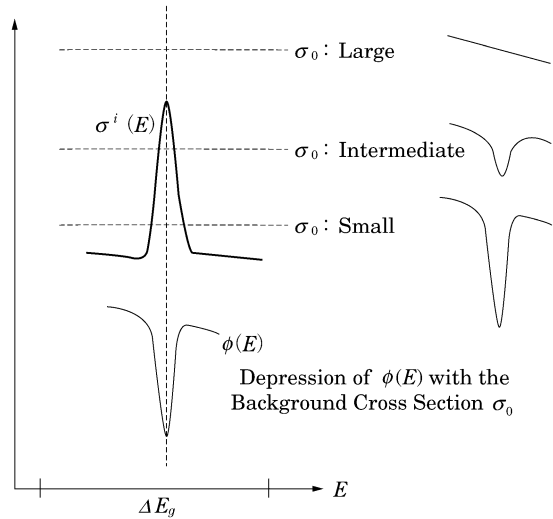
$$\sigma_{\infty, x, g}^i \equiv \frac{\int_{\Delta E_g} \sigma_x^i(E) \phi_w(E) dE}{\int_{\Delta E_g} \phi_w(E) dE} \quad (2.16)$$

Since these microscopic cross sections are not concerned with detailed design specifications of fuel and operating conditions of the reactor, it is possible to prepare them beforehand using the evaluated nuclear data file. The depression or distortion of neutron flux does not occur for resonance nuclides at sufficiently dilute concentrations and this is called the *infinite dilution cross section* ($\sigma_{\infty, x, g}^i$). On the other hand, the cross section prepared in Eq. (2.15) compensates for the neutron spectrum depression due to resonance in the $1/E$ region by some method, and is called the “effective (microscopic) cross section” ($\sigma_{eff, x, g}^i$). There are several approximation methods for the effective resonance cross section: NR approximation, WR approximation, NRIM approximation, and IR approximation. For more details, references [1, 6] on reactor physics should be consulted. The relationship between the effective cross section and infinite dilution cross section is simply discussed here.

Since neutron mean free path is long in the resonance energy region, a homogenized mixture of fuel and moderator nuclides, ignoring detailed structure of the materials, can be considered. If a target nuclide (i) in the mixture has a resonance, it leads to a depression in the neutron flux at the corresponding resonance energy as shown in Fig. 2.6. The reaction rate in the energy group including the resonance becomes smaller than that in the case of no flux depression (infinite dilution). Hence, the effective cross section is generally smaller than its infinite dilution cross section. The following definition is the ratio of the effective cross section to the infinite dilution cross section and called the *self-shielding factor*.

$$f_{x, g}^i \equiv \frac{\sigma_{eff, x, g}^i}{\sigma_{\infty, x, g}^i} \quad (2.17)$$

Fig. 2.6 Neutron flux depression in resonance



In Fig. 2.6, the neutron flux depression becomes large as the macroscopic cross section ($N_i\sigma_i$) of the target nuclide becomes large. On the other hand, if the macroscopic total cross section ($\sum_{j \neq i} N_j \sigma_j^i$) of other nuclides (assuming that they have no resonance at the same energy) becomes large, the resonance cross section of the target nuclide is buried in the total cross section of other nuclides and then the flux depression finally disappears when the total cross section is large enough. To treat this effect quantitatively, a virtual cross section (the *background cross section*) of the target nuclide, converted from the macroscopic total cross section, is defined as Eq. (2.18).

$$\sigma_0^i = \sum_{j \neq i} N_j \sigma_j^i / N_i \quad (2.18)$$

The self-shielding factor is dependent on the background cross section and the temperature of resonance material because the resonance width varies with the Doppler effect. In fact, the background cross section and material temperature are unknown before design specifications and operating conditions of a reactor are determined. Hence, self-shielding factors are calculated in advance and tabulated at combinations of representative background cross sections and temperatures. Figure 2.7 shows a part of the self-shielding factor table (*f* table) for the capture cross section of ^{238}U . The self-shielding factor in design calculation is interpolated from the *f* table at a practical background cross section (σ_0) and temperature (T). The effective microscopic cross section for neutron transport calculation can be obtained from the self-shielding factor as

$$\sigma_{eff, x, g}^i(\sigma_0, T) = f_{x, g}^i(\sigma_0, T_0 \rightarrow T) \cdot \sigma_{\infty, x, g}^i(T_0) \quad (2.19)$$

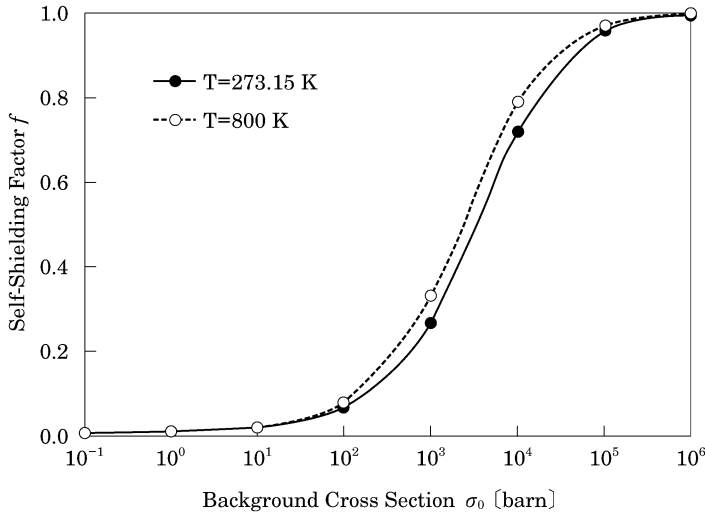


Fig. 2.7 Self-shielding factor of ^{238}U capture cross section ($\Delta E_g = 6.48 \sim 8.32\text{ eV}$)

where T_0 is normally 300 K as a reference temperature at which the multi-group infinite dilution cross sections are prepared from the evaluated nuclear data file.

Recent remarkable advances in computers have made it possible that continuous-energy data or their equivalent ultra-fine-groups (groups of several tens of thousands to several millions) are employed in solving the neutron slowing-down equation and the effective cross sections of resonance nuclides are directly calculated based on Eq. (2.15). Some open codes, SRAC [7] (using the PEACO option) and SLAROM-UF [8] for fast reactors, adopt this method. This method can result in a high accuracy for treating even interference effects of multiple resonances which cannot be considered by the interpolation method of a self-shielding factor table, though a long calculation time is required for a complicated system.

[5] Nuclear data processing and reactor constant library

Nuclear design codes do not use all the massive information contained in the evaluated nuclear data file and also cannot always effectively read out necessary data because of the data format putting weight on the compact storage. Therefore, nuclear design codes do not directly read out the evaluated nuclear data file, but (i) extract necessary data and (ii) prepare a preprocessed data set (reactor constant library) which is one processed suitably for each code. A series of tasks is done in order, for example, to select nuclides and cross section data required for nuclear design, to prepare their infinite dilution cross sections and self-shielding factor tables for a specified energy group structure of a nuclear design code, and to store the data in a quickly accessible form. As nuclear data processing code systems to perform such work, NJOY [9] of LANL and PREPRO [10] of IAEA have been used all over the world.

There are two different forms of the reactor constant library; a continuous-energy form and a multi-group energy form. The former is used in continuous-energy Monte Carlo codes such as MCNP [11] and MVP [12] and the latter in nuclear design codes.

Since most nuclear design codes are provided as a set with a multi-group reactor constant library, it is usually unnecessary to process the evaluated nuclear data file in the nuclear design. However, when introducing the latest evaluated nuclear data file or changing the energy group structure to meet advances in fuel and design specification of nuclear reactors, a new reactor constant library is prepared using the nuclear data processing code system. The reactor constant library, with which a nuclear design calculation begins, might be regarded as a general-purpose library. However, it should be noted that a weighting spectrum specified in part for a reactor type and resonance approximations are employed in preparing a multi-group form library.

Nuclear characteristic calculation methods depend on the type of reactor being targeted. The following discussions center on LWR (especially BWR) calculation methods which need the most considerations such as heterogeneity of the fuel assembly, effects of the nuclear and thermal-hydraulic coupled core calculation, and so on.

2.1.4 Lattice Calculation

[1] Purpose of lattice calculation

Even using a high performance computer, a direct core calculation with several tens of thousands of fuel pins is difficult to perform in its heterogeneous geometry model form, using fine-groups (e.g., 107 groups in SRAC) of a prepared reactor constant library. The Monte Carlo method can handle such a core calculation, but it is not easy to obtain enough accuracy for a local calculation or small reactivity because of accompanying statistical errors. Hence, the Monte Carlo method is not employed for nuclear design calculations requiring a fast calculation time. Instead, the nuclear design calculation is performed in two steps: lattice calculation in a two-dimensional (2D) infinite arrangement of fuel rods or assemblies and core calculation in a three-dimensional (3D) whole core. The lattice calculation prepares few-group homogenized cross sections which maintain the important energy dependence (neutron spectrum) of nuclear reactions, as shown in Fig. 2.8, and this reduces the core calculation cost in terms of time and memory. Since final design parameters in the core calculation are not concerned with the energy dependence, the spatial dependence such as for the power distribution is important.

[2] Multi-group neutron transport equation

The neutron transport equation in the lattice calculation is a steady-state equation without the time differential term in Eq. (2.1). Further, the neutron energy variable is discretized in the equation and therefore a multi-group form

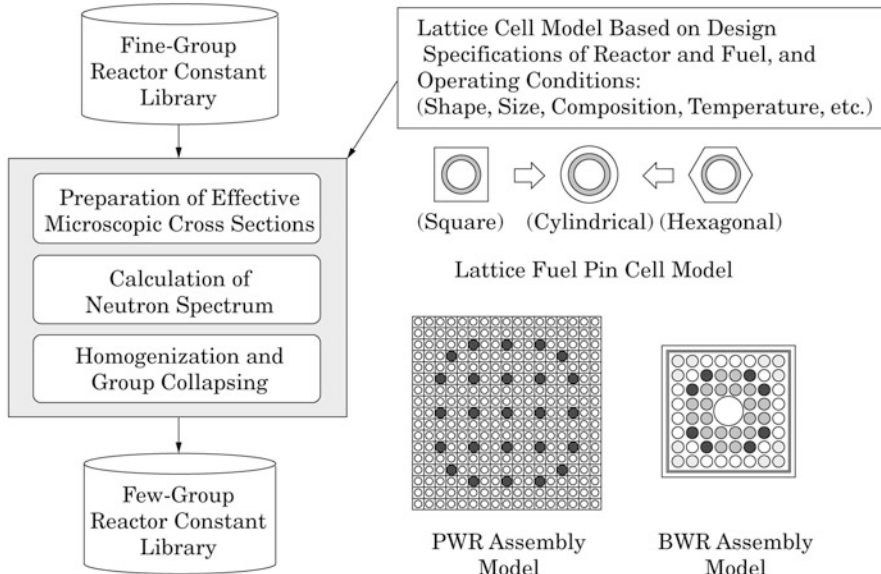


Fig. 2.8 Lattice calculation flow

is used in design codes as shown in Eq. (2.20). The neutron source of Eq. (2.21) is the multi-group form without the external neutron source of Eq. (2.2) at the critical condition.

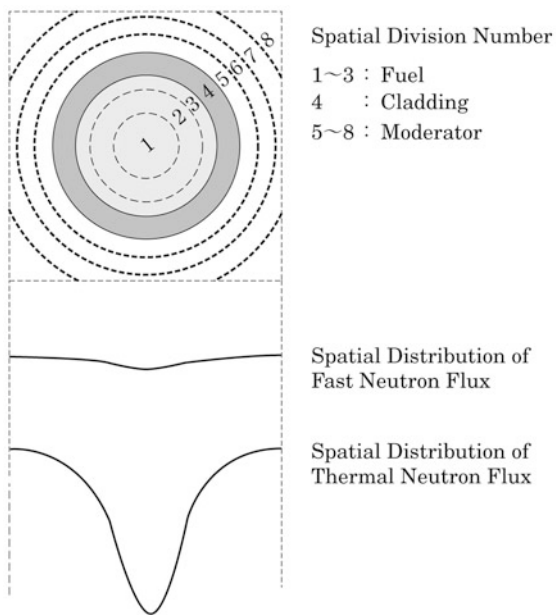
$$-\vec{\Omega} \cdot \nabla \phi_g(\vec{r}, \vec{\Omega}) - \Sigma_{t,g}(\vec{r}) \phi_g(\vec{r}, \vec{\Omega}) + S_g(\vec{r}, \vec{\Omega}) = 0 \quad (2.20)$$

$$\begin{aligned} S_g(\vec{r}, \vec{\Omega}) &= \int_{4\pi} d\vec{\Omega}' \sum_g \Sigma_{s,g' \rightarrow g}(\vec{r}, \vec{\Omega}' \rightarrow \vec{\Omega}) \phi_{g'}(\vec{r}, \vec{\Omega}') \\ &\quad + \frac{\chi_g}{4\pi} \sum_{g'} \nu \Sigma_{f,g'}(\vec{r}) \int_{4\pi} \phi_{g'}(\vec{r}, \vec{\Omega}') d\vec{\Omega}' \end{aligned} \quad (2.21)$$

The system to which the multi-group transport equation is applied is an infinite lattice system of a 2D fuel assembly (including assembly gap) with a reflective boundary condition. For a complicated geometry, two lattice calculations corresponding to a single fuel rod and a fuel assembly are often combined.

In practically solving Eq. (2.20) in the lattice model, the space variable (\vec{r}) is also discretized in the equation and each material region is divided into several sub-regions where neutron flux is regarded to be flat. In liquid metal-cooled fast reactors (LMFRs), neutron flux in each energy group has an almost flat spatial distribution within the fuel assembly because the mean free path of the fast neutrons is long. A simple hexagonal lattice model covering a single fuel rod or its equivalent cylindrical model simplified to one dimension is used in the

Fig. 2.9 Example of spatial division in rectangular lattice model of LWRs



design calculation of LMFRs. The spatial division can also be simplified by assigning the macroscopic cross section by material.

On the other hand, thermal reactors have a highly non-uniform distribution (called the *spatial self-shielding effect*) of neutron flux in a fuel assembly as thermal neutron flux rises in the moderator region or steeply falls in the fuel and absorber as shown in Fig. 2.9. Moreover, control rod guide tubes or water rods are situated within fuel assemblies and differently enriched fuels or burnable poison (Gd_2O_3) fuels are loaded. In such a lattice calculation, therefore, it is necessary to make an appropriate spatial division in the input data predicting spatial distribution of thermal neutron flux and its changes with burnup.

Numerical methods of Eq. (2.20) include the collision probability method (CPM), the current coupling collision probability (CCCP) method, and the method of characteristics (MOC) [13]. The SRAC code adopts the collision probability method and can treat the geometrical models as shown in Fig. 2.10. The collision probability method has been widely used in the lattice calculation, but it has a disadvantage that a large number of spatial regions considerably raise the computing cost. The current coupling collision probability method applies the collision probability method to the inside of fuel rod lattices constituting a fuel assembly and combines neighboring fuel rod lattices by neutron currents entering and leaving the lattices. This approach can substantially reduce the assembly calculation cost. Since the method of characteristics solves the neutron transport equation along neutron tracks, it provides computations at relatively low cost even for complicated geometrical shapes and it has become the mainstream in the recent assembly calculation [14].

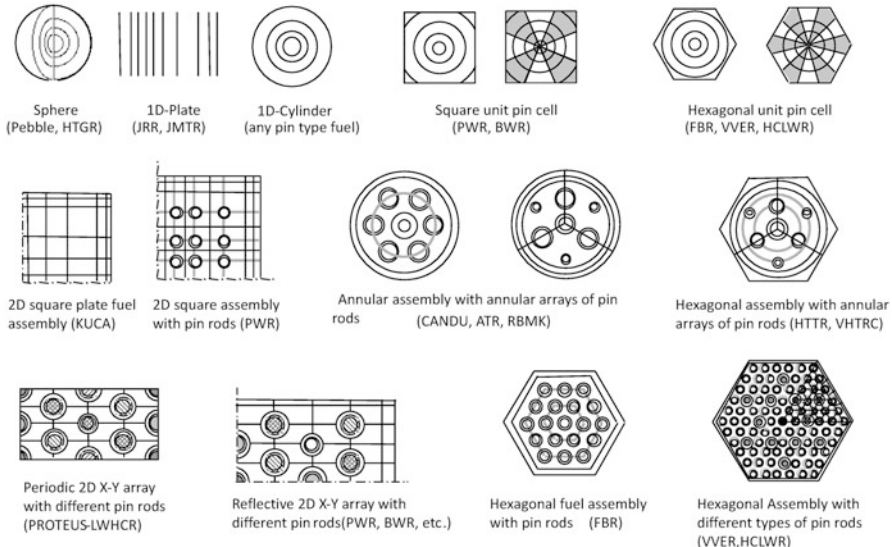


Fig. 2.10 Lattice models of SRAC [7]

In lattice calculation codes, effective microscopic cross sections are first prepared from fine-group infinite dilution cross sections based on input data such as material compositions, dimensions, temperatures, and so on. The effective cross sections are provided in solving Eqs. (2.20) and (2.21) by the use of the collision probability method, etc. and then multi-group neutron spectra are obtained in each divided region (neutron spectrum calculation).

[3] Homogenization and group collapsing

In the core calculations with a huge amount of space-dependent data (cross section and neutron flux), the effective cross sections are processed, with a little degradation in accuracy as possible, by using the results from the multi-group lattice calculation. There are two processing methods. One is homogenization to lessen the space-dependent information and the other is group-collapsing to reduce the energy-dependent information as shown in Fig. 2.11. The fundamental idea of both methods is to conserve neutron reaction rate. In the homogenization, a homogenized neutron flux ϕ_g^{homo} is first defined as averaged flux weighted by volume V_k of region (k). Next, a homogenized cross section $\Sigma_{x,g}^{homo}$ is determined as satisfying Eq. (2.23) to represent the reaction rate in the homogenized whole region of volume V^{homo} . The fine-group neutron flux $\phi_{g,k}$ is used to calculate the homogenized cross section in Eq. (2.24).

$$\phi_g^{homo} \equiv \sum_k \phi_{g,k} V_k / \sum_k V_k = \sum_k \phi_{g,k} V_k / V^{homo} \quad (2.22)$$

$$\Sigma_{x,g}^{homo} \phi_g^{homo} V^{homo} = \sum_k \Sigma_{x,g,k} \phi_{g,k} V_k \quad (2.23)$$

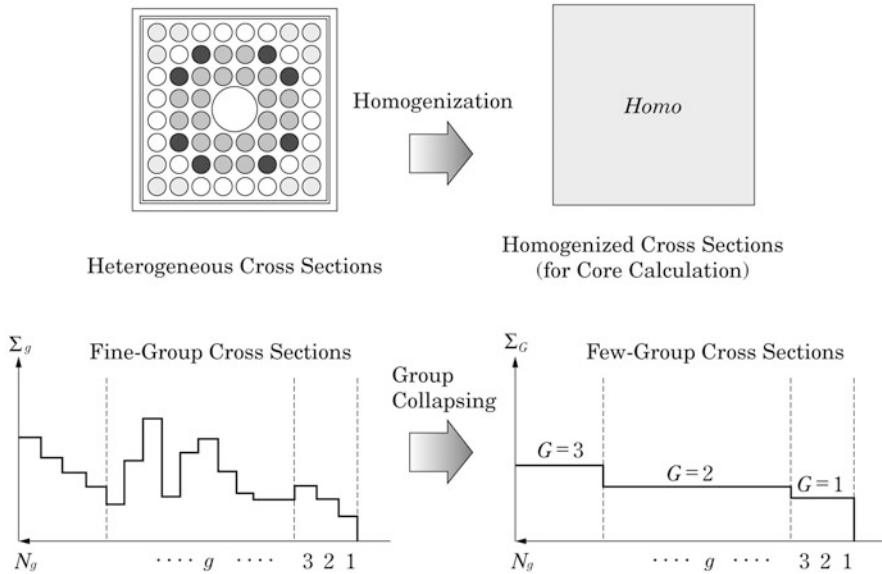


Fig. 2.11 Homogenization and group collapsing of cross section

$$\Sigma_{x,g}^{homo} \equiv \sum_k \Sigma_{x,g,k} \phi_{g,k} V_k / \phi_g^{homo} V^{homo} \equiv \sum_k \Sigma_{x,g,k} \phi_{g,k} V_k / \sum_k \phi_{g,k} V_k \quad (2.24)$$

Similarly, the homogenized microscopic cross section $\sigma_{x,g}^{i,homo}$ which represents the homogenized region is defined. First, the homogenized atomic number density $N^{i,homo}$ of nuclide i is defined from the following conservation of number of atoms

$$N^{i,homo} \equiv \sum_k N_k^i V_k / V^{homo} \quad (2.25)$$

The homogenized microscopic cross section is then given from the conservation of microscopic reaction rate of nuclide i as

$$\sigma_{x,g}^{i,homo} = \left(\sum_k N_k^i \sigma_{x,g,k}^i \phi_{g,k} V_k \right) / \left(N^{i,homo} \phi_g^{homo} V^{homo} \right) \quad (2.26)$$

Such homogenized neutron flux ϕ_g^{homo} and cross section $\Sigma_{x,g}^{homo}$ (or $\sigma_{x,g}^{i,homo}$) terms are used in performing the energy-group collapse. The fine-groups (g) are first apportioned to few-groups (G) for the core calculation as shown in Fig. 2.11. Since the multi-group neutron flux was obtained by the integration over its energy group, the few-group homogenized neutron flux can be represented by

$$\phi_G^{homo} \equiv \sum_{g \in G} \phi_g^{homo} \quad (2.27)$$

The next step is to consider the conservation of reaction rate in energy group G in the same manner as that in the homogenization.

The few-group homogenized macroscopic and microscopic cross sections are then given by

$$\Sigma_{x, G}^{homo} \equiv \sum_{g \in G} \Sigma_{x, g}^{homo} \phi_g^{homo} / \phi_G^{homo} = \sum_{g \in G} \Sigma_{x, g}^{homo} \phi_g^{homo} / \sum_{g \in G} \phi_g^{homo} \quad (2.28)$$

$$\sigma_{x, G}^{i, homo} \equiv \sum_{g \in G} \sigma_{x, g}^{i, homo} \phi_g^{homo} / \phi_G^{homo} = \sum_{g \in G} \sigma_{x, g}^{i, homo} \phi_g^{homo} / \sum_{g \in G} \phi_g^{homo} \quad (2.29)$$

The number of few-groups depends on reactor type and computation code. Two or three groups are adopted for the nuclear and thermal-hydraulic coupled core calculation of LWRs and about 18 groups are used for the core calculation of LMFRs. It should be noted that the conservation of reaction rate has been considered under the assumption that the lattice system can be represented as an infinite array of identical lattice cells. If the neutron spectrum in the actual core system is very different from the multi-group neutron spectrum calculated in the infinite lattice system, the applicability of such few-group homogenized cross sections to the core calculation is deteriorated. In this case, it is effective to increase the number of energy groups in the core calculation, but that gives a more costly computation.

[4] Lattice burnup calculation

The lattice burnup calculation prepares few-group homogenized cross sections with burnup on the infinite lattice system of fuel assembly. The series of lattice calculation procedures described in Fig. 2.8 are repeatedly done considering changes in fuel composition with burnup.

However, the lattice burnup calculation is not carried out in the design calculation of LMFRs which have a high homogeneity compared with LWRs and do not lead to a large change in neutron spectrum during burnup. Hence a macroscopic cross section at a position (\vec{r}) in the reactor core can be formed by Eq. (2.30) using the homogenized microscopic cross section prepared in the lattice calculation. At this time, the homogenized atomic number densities are calculated according to burnup of each region during the reactor core calculation.

$$\Sigma_{x, G}^{homo}(\vec{r}) = \sum_i N^{i, homo}(\vec{r}) \sigma_{x, G}^{i, homo} \quad (2.30)$$

By contrast, when considering ^{235}U in a fuel assembly of a LWR as an example, the constituents of UO_2 fuel, MOX fuel, or burnable poison fuel ($\text{UO}_2\text{-Gd}_2\text{O}_3$) each lead to different effective cross sections and composition variations with burnup. It is difficult to provide common few-group

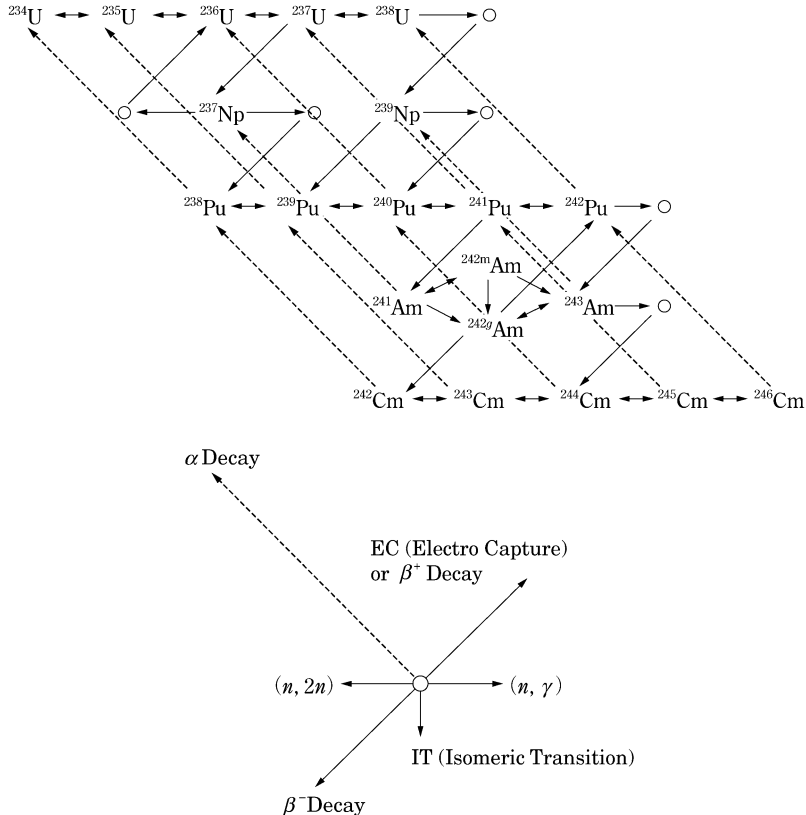


Fig. 2.12 An example burnup chain of heavy metals [7]

homogenized microscopic cross sections and homogenized atomic number densities suitable for all of them. Moreover, space-dependent lattice calculations by a fuel assembly model during the core calculation require an enormous computing time. In the design of reactors with this issue of fuel assembly homogenization, therefore, the lattice burnup calculation is performed in advance for the fuel assembly type of the core and then few-group homogenized macroscopic cross sections are tabulated with respect to burnup, etc. to be used for the core calculation. In the core calculation, macroscopic cross sections corresponding to burnup distribution in the core are prepared by interpolation of the table (the table interpolation method of macroscopic cross sections) [15].

Atomic number densities of heavy metals and fission products (FPs) are calculated along a burnup pathway as shown in Fig. 2.12, called the *burnup chain*.

The time variation in atomic number density (N^i) of a target nuclide (i) can be expressed as the following differential equation.

$$\frac{dN^i}{dt} = \sum_{j \neq i} f^{j \rightarrow i} \lambda^j N^j + \sum_{k \neq i} \sum_x g_x^{k \rightarrow i} N^k \langle \sigma_x^k \phi \rangle + \sum_l \gamma^{l \rightarrow i} F^l - (\lambda^i + \langle \sigma_a^i \phi \rangle) N^i \quad (2.31)$$

where the first term on the right-hand side expresses the production rate of nuclide i due to radioactive decay of another nuclide j on the burnup chain. λ^j is the decay constant of nuclide j and $f^{j \rightarrow i}$ is the probability (branching ratio) of decay to nuclide i . The second term is the production rate of nuclide i due to the nuclear reaction x of another nuclide k . The major nuclear reaction is the neutron capture reaction and other reactions such as the $(n,2n)$ reaction can be considered by necessity. $\langle \sigma_x^k \phi \rangle$, which is the microscopic reaction rate of nuclide k integrated over all neutron energies, is calculated from the fine-group effective cross section and neutron flux in the lattice calculation. $g_x^{k \rightarrow i}$ is the probability of transmutation into nuclide i for nuclear reaction x of nuclide k . The third term is for the production of FPs. F^l is the fission rate of heavy nuclide l and $\gamma^{l \rightarrow i}$ is the production probability (yield fraction) of nuclide i for the fission reaction. The last term is the loss rate of nuclide i due to radioactive decay and absorption reactions.

Applying Eq. (2.31) to all nuclides including FPs on the burnup chain gives simultaneous differential equations (burnup equations) corresponding to the number of nuclides. Ways to solve the burnup equations include the Bateman method [16] and the matrix exponential method [17]. This burnup calculation, called the *depletion calculation*, is performed for each burnup region in case of multiple burnup regions like a fuel assembly and it gives the variation in material composition with burnup in each region. The lattice calculation is carried out with the material composition repeatedly until reaching maximum burnup expected in the core.

The infinite multiplication factor calculated during the lattice calculation is described as the ratio between neutron production and absorption reactions in an infinite lattice system without neutron leakage.

$$\begin{aligned} k_\infty &= \text{Production Rate / Loss Rate} \\ &= \text{Production Rate / (Absorption Rate + Leakage Rate from System)} \\ &= \text{Production Rate / (Absorption Rate + 0.0)} \\ &= \sum_{g \in G} v \Sigma_{f,g}^{homo} \phi_g^{homo} / \sum_{g \in G} \Sigma_{a,g}^{homo} \phi_g^{homo} \end{aligned} \quad (2.32)$$

Figure 2.13 shows the infinite multiplication factor obtained from the lattice burnup calculation of a BWR fuel assembly. Since thermal reactors rapidly produce highly neutron absorbing FPs such as ^{135}Xe and ^{149}Sm in the beginning of burnup until their concentrations reach the equilibrium values, the infinite

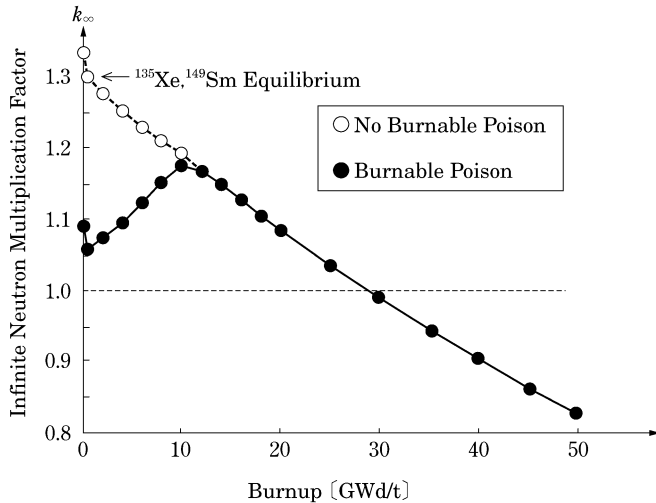


Fig. 2.13 Lattice burnup calculation of fuel assembly

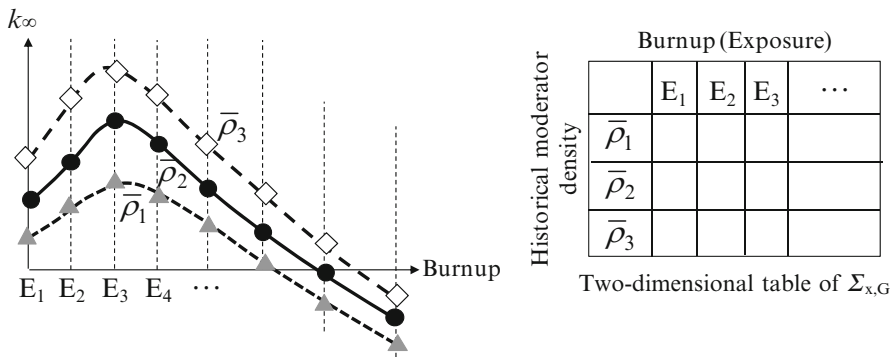
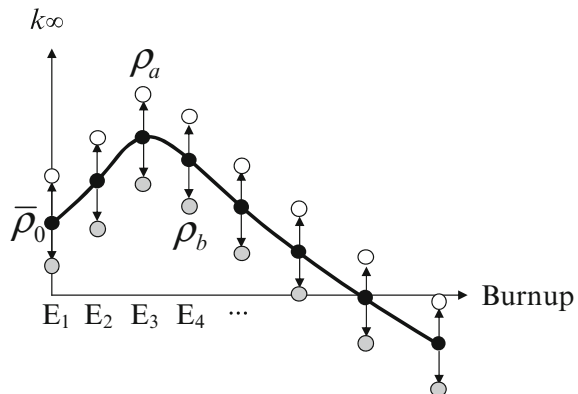


Fig. 2.14 Tabulation of few-group homogenized macroscopic cross sections in lattice burnup calculations

multiplication factor sharply drops during a short time. Then the infinite multiplication factor monotonously decreases in the case of no burnable poison fuel ($\text{UO}_2 + \text{Gd}_2\text{O}_3$). Meanwhile, it increases once in burnable poison fuel because burnable poisons burn out gradually with burnup, and then it decreases when the burnable poisons become ineffective.

The few-group homogenized macroscopic cross sections are tabulated at representative burnup steps (E_1, E_2, E_3, \dots) by the lattice burnup calculation and stored as a reactor constant library for the core calculation, as shown in Fig. 2.14. Three different moderator densities ($\bar{\rho}_1, \bar{\rho}_2, \bar{\rho}_3$) for one fuel type are assumed in the lattice burnup calculation of BWRs. Moderator density of BWRs

Fig. 2.15 Branch-off calculation of moderator density



is provided as a function of void fraction α for two densities ρ_l and ρ_g in liquid and vapor phases, respectively, in the steam table. That is, it is given by

$$\bar{\rho} = \rho_l(1 - \alpha) + \rho_g\alpha \quad (2.33)$$

where $\bar{\rho}_1$, $\bar{\rho}_2$, and $\bar{\rho}_3$ are the moderator densities corresponding to each void fraction at the core outlet ($\alpha = 0.7$), as an average ($\alpha = 0.4$), and at the inlet ($\alpha = 0.0$) of typical BWRs. Since this moderator density is assumed to be constant as an average value during each lattice burnup step, it is called a *historical moderator density*.

The few-group homogenized macroscopic cross sections are tabulated according to two historical parameters (burnup E and historical moderator density $\bar{\rho}$) by energy group (G) or cross section type (x). The cross section tables are prepared individually according to fuel type (F), control rod insertion or withdrawal, etc. Furthermore, homogenized microscopic cross sections and atomic number densities of ^{135}Xe , ^{149}Sm , ^{10}B , etc. can be tabulated by necessity.

[5] Branch-off calculation

In the lattice burnup calculation, a combination of parameters such as moderator density and temperature, and fuel temperature is made at representative values ($\bar{\rho}_0$, T_{m0} , T_{f0}) expected at normal operation of the reactor. In the core calculation, however, a different set (ρ , T_m , T_f) from the representative set is taken depending on position and time. Hence, a subsequent calculation called the *branch-off calculation* is performed after the lattice burnup calculation if necessary.

Figure 2.15 depicts an example branch-off calculation of moderator density. The calculation proceeds in the following order:

- (i) Perform the lattice burnup calculation at a reference condition ($\bar{\rho}_0$, T_{m0} , T_{f0}). Designate the few-group homogenized cross section prepared from the lattice burnup calculation as $\Sigma(\bar{\rho}_0, T_{m0}, T_{f0})$.

- (ii) Perform the lattice calculation at each burnup step on the condition that only the moderator density is changed from $\bar{\rho}_0$ to ρ_a , by using the same fuel composition at each burnup step. Designate the few-group homogenized cross section prepared from the lattice calculation (or the branch-off calculation) as $\Sigma(\bar{\rho}_0 \rightarrow \rho_a, T_{m0}, T_{f0})$.
- (iii) Carry out the branch-off calculation similar to (ii) at another moderator density of ρ_b and give $\Sigma(\bar{\rho}_0 \rightarrow \rho_b, T_{m0}, T_{f0})$.
- (iv) If the moderator density is instantaneously changed from $\bar{\rho}_0$ to an arbitrary ρ , calculate the corresponding cross section by the following approximation (quadratic fitting).

$$\Sigma(\bar{\rho}_0 \rightarrow \rho, T_{m0}, T_{f0}) \approx \Sigma(\bar{\rho}_0, T_{m0}, T_{f0}) + a(\rho - \bar{\rho}_0) + b(\rho - \bar{\rho}_0)^2 \quad (2.34)$$

- (v) Determine the fitting coefficients a and b from the approximation at $\rho = \rho_a$ and $\rho = \rho_b$.

Hence, the cross section at an arbitrary moderator density (an instantaneous moderator density) ρ away from the historical moderator density $\bar{\rho}_0$ can be expressed by the method mentioned above. If three moderator densities ($\bar{\rho}_1, \bar{\rho}_2, \bar{\rho}_3$) are employed as $\bar{\rho}_0$ as shown in Fig. 2.14, their branch-off calculations can give $\Sigma(\bar{\rho}_1 \rightarrow \rho, T_{m0}, T_{f0})$, $\Sigma(\bar{\rho}_2 \rightarrow \rho, T_{m0}, T_{f0})$, and $\Sigma(\bar{\rho}_3 \rightarrow \rho, T_{m0}, T_{f0})$. By interpolation of the three points, the cross section at ρ resulting from an instantaneous change from a historical moderator density $\bar{\rho}$ can be obtained as $\Sigma(\bar{\rho} \rightarrow \rho, T_{m0}, T_{f0})$.

The cross section at an instantaneous change in fuel or moderator temperature can also be described by the same function fitting as above. Since its change in cross section is not as large as a void fraction change (0–70 %), the following linear fittings are often used.

$$\Sigma(\bar{\rho}_0, T_{m0} \rightarrow T_{m0}, T_{f0}) = \Sigma(\bar{\rho}_0, T_{m0}, T_{f0}) + c(T_m - T_{m0}) \quad (2.35)$$

$$\Sigma(\bar{\rho}_0, T_{m0}, T_{f0} \rightarrow T_f) = \Sigma(\bar{\rho}_0, T_{m0}, T_{f0}) + d(\sqrt{T_f} - \sqrt{T_{f0}}) \quad (2.36)$$

Equation (2.36) has square roots of fuel temperature in order to express the cross section change due to the Doppler effect by a lower-order fitting equation. An employment of a higher-order fitting equation can lead to a higher expression capability and accuracy, but it gives rise to a substantial increase in the number of branch-off calculations and fitting coefficients and therefore results in an inefficient calculation. Thus, the reference cross sections and their fitting coefficients are stored into the few-group reactor constant library and used in the nuclear and thermal-hydraulic coupled core calculation.

2.1.5 Core Calculation

[1] Diffusion equation

In core calculations such as the nuclear and thermal-hydraulic coupled core calculation, core burnup calculation, or space-dependent kinetics calculation, high-speed calculation is the biggest need. Especially since large commercial reactors have a considerably larger core size compared with critical assemblies or experimental reactors, the neutron transport equation (2.1) has to take many unknowns and hence need a high computing cost.

For most core calculations, the angular dependence ($\vec{\Omega}$) of neutron flux is disregarded and the neutron transport equation is approximately simplified as Eq. (2.37).

$$\frac{1}{v} \frac{\partial \phi}{\partial t} = -\nabla \cdot \vec{J} - \Sigma_a \phi + S \quad (2.37)$$

Its physical meaning is simple. As an example, a space of unit volume (1 cm^3) like one die of a pair of dice is considered. The time variation in neutron population within the space [the LHS of Eq. (2.37)] is then given by the balanced relationship between neutron production rate (S), net neutron leakage rate through the surface ($\nabla \cdot \vec{J}$), and neutron loss rate by absorption ($\Sigma_a \phi$).

\vec{J} is referred to as the *net neutron current* and expressed by the following physical relation known as Fick's law

$$\vec{J} = -D \nabla \phi \quad (2.38)$$

where D is called the *diffusion coefficient*; it is tabulated together with few-group cross sections in the lattice calculation to be delivered to the core calculation. Inserting Eq. (2.38) into Eq. (2.37) gives the time-dependent diffusion equation.

$$\frac{1}{v} \frac{\partial \phi}{\partial t} = \nabla \cdot D \nabla \phi - \Sigma_a \phi + S \quad (2.39)$$

The time-independent form of Eq. (2.39) is the steady-state diffusion equation and all types of the core calculation to be mentioned thereafter are based on the equation

$$\nabla \cdot D \nabla \phi - \Sigma_a \phi + S = 0 \quad (2.40)$$

Thus, solving the diffusion equation in critical reactors is to regard the reactor core as an integration of subspaces like the dice cubes and then to find a neutron flux distribution to satisfy the neutron balance between production and loss in all the spaces (corresponding to mesh spaces to be described later).

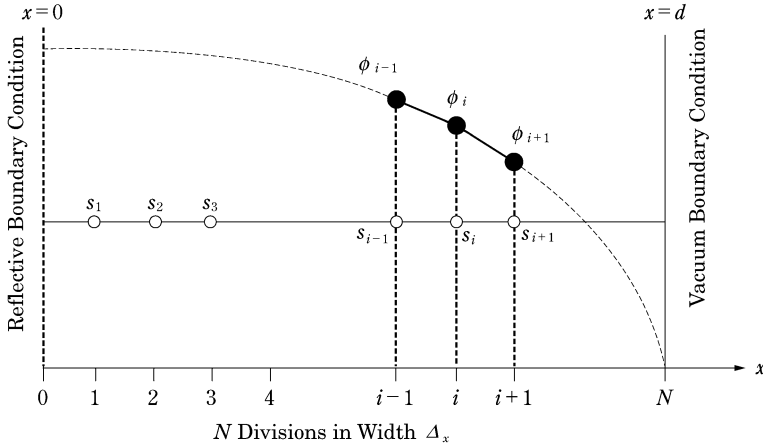


Fig. 2.16 Finite difference in 1D plane geometry

- [2] Solution to one-dimensional (1D) one-group diffusion equation by finite difference method

First a non-multiplying medium (e.g., water) is considered for simplicity of the equation, though practical systems are composed of various materials with different cross sections. In addition, it is assumed that all neutrons can be characterized by a single energy (one-group problem). Therefore, the cross section does not depend on location and in this case the diffusion equation is given by Eq. (2.41).

$$\nabla^2\phi - \Sigma_a\phi + S = 0 \quad (2.41)$$

∇^2 (the Laplacian operator) is dependent on the coordinate system and in the Cartesian coordinate system it is represented as Eq. (2.42).

$$\nabla^2 = \frac{\partial^2}{\partial x^2} + \frac{\partial^2}{\partial y^2} + \frac{\partial^2}{\partial z^2} \quad (2.42)$$

In an infinitely wide medium in y and z directions, the diffusion equation reduces to the 1D form.

$$-D \frac{d^2\phi(x)}{dx^2} + \Sigma_a\phi(x) = S(x) \quad (2.43)$$

Here a uniform neutron source ($s_1 = s_2 = s_3 \dots = s$) in a finite slab of width $2d$ is considered as shown in Fig. 2.16 and the finite difference method to solve for neutron flux distribution is discussed. The reflective boundary condition is applied to the center of the slab and one side of width d is divided into equal N regions (spatial meshes). The second-order derivative of Eq. (2.43) can be

approximated¹ by using neutron flux ϕ_i at a mesh boundary i and neutron fluxes at both adjacent sides as follows;

$$\frac{d^2\phi}{dx^2} \Big|_i \approx \frac{\left\{ \left(\frac{\phi_{i+1} - \phi_i}{\Delta_x} \right) - \left(\frac{\phi_i - \phi_{i-1}}{\Delta_x} \right) \right\}}{\Delta_x} = \frac{\phi_{i-1} - 2\phi_i + \phi_{i+1}}{\Delta_x^2} \quad (2.44)$$

Hence the diffusion equation at each mesh point can be given by

$$-D \left(\frac{\phi_{i-1} - 2\phi_i + \phi_{i+1}}{\Delta_x^2} \right) + \Sigma_a \phi_i = s_i \quad (i=1 \sim N-1) \quad (2.45)$$

It can be rewritten by

$$\left(\frac{1}{\Delta_x^2} \right) \phi_{i-1} + \left(\frac{-2}{\Delta_x^2} + \frac{-1}{D/\Sigma_a} \right) \phi_i + \left(\frac{1}{\Delta_x^2} \right) \phi_{i+1} = \left(-\frac{s_i}{D} \right) \quad (i=1 \sim N-1) \quad (2.46)$$

where

$$a \equiv \left(\frac{1}{\Delta_x^2} \right), \quad b \equiv \left(\frac{-2}{\Delta_x^2} + \frac{-1}{D/\Sigma_a} \right), \quad S_i \equiv \left(-\frac{s_i}{D} \right) \quad (2.47)$$

In the case of $N = 5$, the following simultaneous equations are gotten.

$$\begin{cases} a\phi_0 + b\phi_1 + a\phi_2 = S_1 \\ a\phi_1 + b\phi_2 + a\phi_3 = S_2 \\ a\phi_2 + b\phi_3 + a\phi_4 = S_3 \\ a\phi_3 + b\phi_4 + a\phi_5 = S_4 \end{cases} \quad (2.48)$$

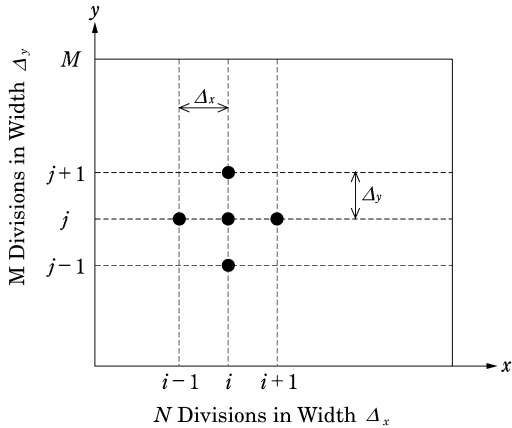
Since there are six unknowns (ϕ_0 to ϕ_5) among four equations in Eq. (2.48), another two conditions are needed to solve the simultaneous equations. Boundary conditions at both ends ($x = 0$ and $x = d$) of the slab are given by the following.

Vacuum boundary condition (an extrapolated distance is assumed zero):

$$\phi(x = d) = 0 \quad \rightarrow \quad \phi_5 = 0 \quad (2.49)$$

¹ Most practical codes of the finite difference method take neutron fluxes at the center points of divided meshes [13]. A simple and easy to understand method was employed here.

Fig. 2.17 Finite difference in 2D plane geometry



Reflective boundary condition:

$$\frac{d\phi}{dx} \Big|_{x=0} = 0 \rightarrow \frac{\phi_1 - \phi_0}{\Delta_x} = 0 \quad (2.50)$$

Equation (2.51) is obtained by inserting Eqs. (2.49) and (2.50) into Eq. (2.48) and rewriting in matrix form.

$$\begin{bmatrix} a+b & a & 0 & 0 \\ a & b & a & 0 \\ 0 & a & b & a \\ 0 & 0 & a & b \end{bmatrix} \begin{bmatrix} \phi_1 \\ \phi_2 \\ \phi_3 \\ \phi_4 \end{bmatrix} = \begin{bmatrix} S_1 \\ S_2 \\ S_3 \\ S_4 \end{bmatrix} \quad (2.51)$$

A 1D problem generally results in a tridiagonal matrix equation of $(N - 1) \times (N - 1)$ system which can be directly solved using numerical methods such as the Gaussian elimination method. Since the finite difference method introduces the approximation as Eq. (2.44), it is necessary to choose a sufficiently small mesh spacing. The spatial variation of neutron flux is essentially characterized by the extent of neutron diffusion such as the neutron mean free path. Hence the effect of the mesh size on nuclear characteristic evaluations of a target reactor core must be understood and then the mesh size is optimized relative to the computation cost.

[3] Solution of the multi-dimensional diffusion equation

The diffusion equation in a 2D homogeneous plane geometry is given by Eq. (2.52).

$$-D \left(\frac{\partial^2 \phi(x, y)}{\partial x^2} + \frac{\partial^2 \phi(x, y)}{\partial y^2} \right) + \Sigma_a \phi(x, y) = S(x, y) \quad (2.52)$$

The plane is divided into N and M meshes in x and y directions, respectively (Fig. 2.17). Similarly to the 1D problem, the second-order derivatives can be

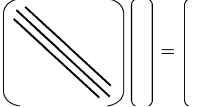
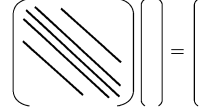
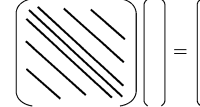
1D Problem	2D Problem	3D Problem
		
3-Point Difference Equations Tridiagonal Matrix of $(N-1) \times (N-1)$	5-Point Difference Equations 5-Diagonal Matrix of $(N-1)(M-1)^2$	7-Point Difference Equations 7-Diagonal Matrix of $(N-1)(M-1)(K-1)^2$

Fig. 2.18 Matrix equation forms of finite difference method

approximated by using neutron fluxes at a point (i, j) and its four adjacent ones as the following.

$$\frac{\partial^2 \phi}{\partial x^2} \Big|_{i,j} \approx \frac{\phi_{i-1,j} - 2\phi_{i,j} + \phi_{i+1,j}}{\Delta_x^2} \quad (2.53)$$

$$\frac{\partial^2 \phi}{\partial y^2} \Big|_{i,j} \approx \frac{\phi_{i,j-1} - 2\phi_{i,j} + \phi_{i,j+1}}{\Delta_y^2} \quad (2.54)$$

Hence the diffusion equation at each mesh point can be given by

$$-D \left(\frac{\phi_{i-1,j} - 2\phi_{i,j} + \phi_{i+1,j}}{\Delta_x^2} + \frac{\phi_{i,j-1} - 2\phi_{i,j} + \phi_{i,j+1}}{\Delta_y^2} \right) + \Sigma_a \phi_{i,j} = s_{i,j} \quad (2.55)$$

$(i = 1 \text{ to } N - 1, j = 1 \text{ to } M - 1)$

and it can be rewritten as Eq. (2.56).

$$\begin{aligned} \left(\frac{1}{\Delta_x^2} \right) \phi_{i-1,j} + \left(\frac{1}{\Delta_y^2} \right) \phi_{i,j-1} + \left(\frac{-2}{\Delta_x^2} + \frac{-2}{\Delta_y^2} + \frac{-1}{D/\Sigma_a} \right) \phi_{i,j} + \left(\frac{1}{\Delta_x^2} \right) \phi_{i+1,j} + \left(\frac{1}{\Delta_y^2} \right) \phi_{i,j+1} \\ = \left(-\frac{s_{i,j}}{D} \right) \quad (i = 1 \text{ to } N - 1, j = 1 \text{ to } M - 1) \end{aligned} \quad (2.56)$$

Next, the corresponding simultaneous equations are expressed in matrix form, similarly to the 1D problem except four boundary conditions are used: two conditions in each of the x and y directions.

A 3D problem even in a different coordinate system basically follows the same procedure and a matrix form of $([A]\phi = S)$ can be taken as shown in Fig. 2.18.

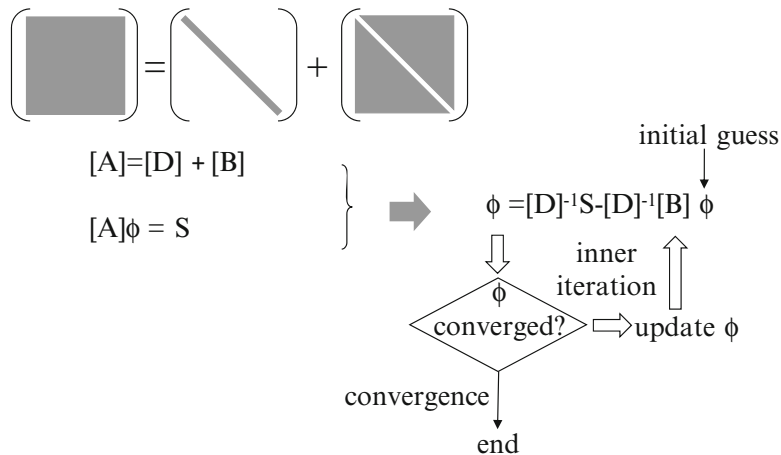


Fig. 2.19 Inner iteration to solve a system of equations

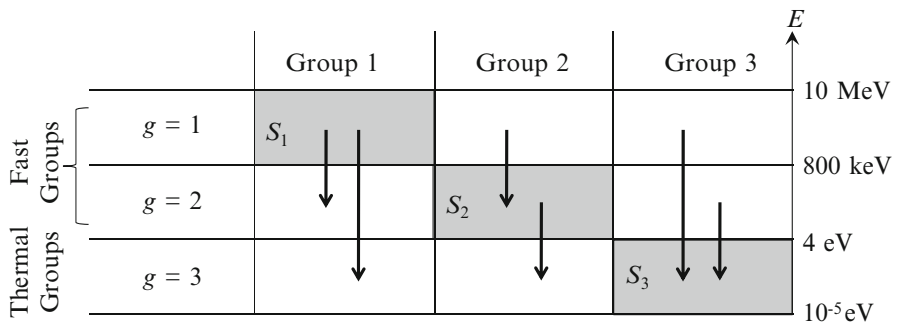


Fig. 2.20 Slowing-down neutron balance in three-group problem

In the case of a large-size matrix $[A]$, a direct method such as the Gaussian elimination leads to increased necessary memory size and it is liable to cause accumulation of numerical errors as well. Hence, generally first the matrix $[A]$ is composed into its diagonal element $[D]$ and off-diagonal element $[B]$. Then ϕ is guessed and new guesses are calculated iteratively to converge to the true solution (Fig. 2.19). This iterative algorithm, such as found in the Gauss-Seidel method or the successive overrelaxation (SOR) method, is frequently referred to as the *inner iteration*.

[4] Solution to multi-group diffusion equation

As already mentioned, the diffusion equation is a balanced equation between neutron production and loss. The multi-group diffusion theory is similarly considered except that the neutron energy is discretized into multi-groups. As shown in Fig. 2.20, subsequent treatment should be made for neutrons moving

to other groups through slowing down which is not considered in the one-group diffusion theory. In particular, there are two points:

- (i) Neutrons which move out of a target group to other groups by slowing down result in neutron loss in the neutron balance of the target group.
- (ii) Neutrons which move in a target group from other groups by slowing down result in neutron gain in the neutron balance of the target group.

Hence, the multi-group diffusion equation introduces the cross section $\Sigma_{g \rightarrow g'}$ (scattering matrix) characterizing neutrons which transfer from group g to group g' by elastic or inelastic scattering.

In the example of the three-group problem presented in Fig. 2.20, the neutron balance equation of each group can be given by

$$\text{Group 1: } D_1 \nabla^2 \phi_1 - (\Sigma_{a,1} \phi_1 + \Sigma_{1 \rightarrow 2} \phi_1 + \Sigma_{1 \rightarrow 3} \phi_1) + S_1 = 0 \quad (2.57)$$

$$\text{Group 2: } D_2 \nabla^2 \phi_2 - (\Sigma_{a,2} \phi_2 + \Sigma_{2 \rightarrow 3} \phi_2) + (S_2 + \Sigma_{1 \rightarrow 2} \phi_1) = 0 \quad (2.58)$$

$$\text{Group 3: } D_3 \nabla^2 \phi_3 - (\Sigma_{a,3} \phi_3) + (S_3 + \Sigma_{1 \rightarrow 3} \phi_1 + \Sigma_{2 \rightarrow 3} \phi_2) = 0 \quad (2.59)$$

It is seen that neutron loss due to slowing down in a group results in neutron gains in other groups. $\Sigma_{1 \rightarrow 2} \phi_1$ in Eq. (2.58) and $\Sigma_{1 \rightarrow 3} \phi_1 + \Sigma_{2 \rightarrow 3} \phi_2$ in Eq. (2.59) are referred to as the “slowing-down neutron source” since they represent the neutron source due to slowing down from other groups.

Equation (2.57) for group 1 can be rewritten as the following.

$$\nabla^2 \phi_1 - \Sigma_{r,1} \phi_1 + S_1 = 0 \quad (2.60)$$

$$\Sigma_{r,1} \equiv \Sigma_{a,1} + \Sigma_{1 \rightarrow 2} + \Sigma_{1 \rightarrow 3} \quad (2.61)$$

The sum of absorption cross section and group-transfer cross section, namely, the cross section which characterizes neutrons removed from the target group, is called the *removal cross section*. It is observed that Eq. (2.60) rewritten using the removal cross section is in the same form as the one-group diffusion equation and can be solved by the finite difference method mentioned before. Substituting the obtained ϕ_1 for the one in the slowing-down source of Eq. (2.58) makes it possible to calculate the neutron flux of group 2, ϕ_2 , in the same way. Further, the neutron flux of group 3, ϕ_3 , can be also obtained by substituting ϕ_1 and ϕ_2 into Eq. (2.59).

Thus, the multi-group diffusion equations can be solved in sequence from the highest energy group. However, the solution is not obtained by this method if the thermal energy region (up to about 4 eV) is divided into multi-groups. As an example, a four-group diffusion problem using two fast groups and two thermal groups is considered.

$$\text{Group 1: } D_1 \nabla^2 \phi_1 - (\Sigma_{a,1} \phi_1 + \Sigma_{1 \rightarrow 2} \phi_1 + \Sigma_{1 \rightarrow 3} \phi_1 + \Sigma_{1 \rightarrow 4} \phi_1) + S_1 = 0 \quad (2.62)$$

$$\text{Group 2: } D_2 \nabla^2 \phi_2 - (\Sigma_{a,2} \phi_2 + \Sigma_{2 \rightarrow 3} \phi_2 + \Sigma_{2 \rightarrow 4} \phi_2) + (S_2 + \Sigma_{1 \rightarrow 2} \phi_1) = 0 \quad (2.63)$$

$$\begin{aligned} \text{Group 3: } & D_3 \nabla^2 \phi_3 - (\Sigma_{a,3} \phi_3 + \Sigma_{3 \rightarrow 4} \phi_3) + (S_3 + \Sigma_{1 \rightarrow 3} \phi_1 + \Sigma_{2 \rightarrow 3} \phi_2 + \Sigma_{4 \rightarrow 3} \phi_4) \\ & = 0 \end{aligned} \quad (2.64)$$

$$\text{Group 4: } D_4 \nabla^2 \phi_4 - (\Sigma_{a,4} \phi_4) + (S_4 + \Sigma_{1 \rightarrow 4} \phi_1 + \Sigma_{2 \rightarrow 4} \phi_2 + \Sigma_{3 \rightarrow 4} \phi_3) = 0 \quad (2.65)$$

The fast-group neutron fluxes ϕ_1 and ϕ_2 can be derived by the same procedure as in the previous three-group problem. In the thermal groups, however, an event that a neutron gains kinetic energy in a collision with a moderator nuclide in thermal vibration, that is, the upscattering of thermal neutrons should be considered. The last term of Eq. (2.64) represents that. Thus, since the neutron source terms for group 3 include the unknown neutron flux of group 4, ϕ_4 , it is impossible to directly solve the equation. Here, a guess $\phi_4^{(0)}$ instead of ϕ_4 is taken at Eq. (2.64) and then a solution $\phi_3^{(1)}$ is given. Moreover, a solution $\phi_4^{(1)}$ is also acquired by the substitution of $\phi_3^{(1)}$ into Eq. (2.65). Since $\phi_3^{(1)}$ and $\phi_4^{(1)}$ are not correct solutions, another new guess $\phi_4^{(1)}$ is used in Eq. (2.64) to obtain $\phi_3^{(2)}$, which is substituted again into Eq. (2.65) to acquire $\phi_4^{(2)}$. Such calculations are iteratively performed until $\phi_3^{(n)}$ and $\phi_4^{(n)}$ come to an agreement with each previous $\phi_3^{(n-1)}$ and $\phi_4^{(n-1)}$. This calculation is referred to as the “thermal iteration” calculation.

The codes developed for core design of only fast reactors may have no such upscattering and iteration calculation function or may cut back the slowing-down groups by assuming collisions with only heavy metal elements such as sodium. Since such codes cannot correctly manage transport calculation of thermal neutrons, they should not be used carelessly in a thermal reactor calculation even though the codes solve the same fundamental equation.

[5] Eigenvalue problem with fission source

So far the diffusion equation has been discussed in a non-multiplying medium with an external neutron source. Here, fission neutron production (fission source) in a reactor core is applied to the diffusion equation. Assuming a volumetric fission reaction rate $\Sigma_f \phi$ and an average number of neutrons released per fission v in a unit cubic volume (1 cm^3) leads to a volumetric fission neutron production rate by multiplying both ones. Hence, substituting the fission source $v \Sigma_f \phi$ for the external source (S) in Eq. (2.41) gives the one-group diffusion equation at the steady-state reactor core as the following.

$$D\nabla^2\phi - \Sigma_a\phi + \nu\Sigma_f\phi = 0 \quad (2.66)$$

This equation represents a complete balance between the number of neutrons produced by fission and the number of neutrons lost due to leakage and absorption, in an arbitrary unit volume at the critical condition of the reactor. In actual practice, however, it is hard to completely meet such a balance in the design calculation step. A minor transformation of Eq. (2.66) can be made as

$$-D\nabla^2\phi + \Sigma_a\phi = \frac{\nu\Sigma_f}{k_{eff}}\phi \quad (2.67)$$

where k_{eff} is an inherent constant characterizing the system, called the *eigenvalue*. If $k_{eff} = 1.0$, Eq. (2.67) becomes identical to Eq. (2.66). The equation may be solved for the eigenvalue k_{eff} :

$$k_{eff} = \frac{(\nu\Sigma_f\phi)}{(-D\nabla^2\phi) + (\Sigma_a\phi)} = \frac{P}{L+A} \quad (2.68)$$

where L , A , and P denote neutron leakage, absorption, and production, respectively. If the space is extended to the whole reactor core (i.e., each term is integrated over the whole reactor core), k_{eff} can be interpreted as follows. The numerator is the number of neutrons that will be born in the reactor core in the next generation, whereas the denominator represents those that are lost from the current generation. Hence, the condition of the reactor core depends on the k_{eff} value as given next.

$$\begin{cases} k_{eff} > 1 : \text{Supercritical} \\ k_{eff} = 1 : \text{Critical} \\ k_{eff} < 1 : \text{Subcritical} \end{cases} \quad (2.69)$$

Another interpretation can be given for k_{eff} in Eq. (2.67). As mentioned above, it is highly unlikely to hit on the exact neutron balance of $L + A = P$ in a practical core design calculation. Neither the supercritical ($L + A < P$) nor subcritical ($L + A > P$) condition gives a steady-state solution to Eq. (2.66). Hence, if k_{eff} is introduced into the equation as an adjustment parameter like Eq. (2.67), the neutron balance can be forced to maintain ($P \rightarrow P/k_{eff}$) and the equation will always have a steady-state solution. In a supercritical condition ($k_{eff} > 1$), for example, the neutron balance can be kept by adjusting down the neutron production term ($\nu\Sigma_f\phi \rightarrow \nu\Sigma_f\phi/k_{eff}$).

A problem expressed as an equation in the form of Eq. (2.67) is referred to as an *eigenvalue problem*. By contrast, a problem with an external neutron source such as Eq. (2.41) is referred to as a *fixed-source problem*. The big difference between both equations is that the eigenvalue problem equation has an infinite set of solutions. For example, if ϕ is a solution of Eq. (2.67), it is self-evident

that 2ϕ and 3ϕ are also other solutions. Consequently, the solutions of the eigenvalue problem are not absolute values of ϕ but the eigenvalue k_{eff} and a relative spatial distribution of ϕ . Meanwhile, the fixed-source problem has a spatial distribution of absolute ϕ which is proportional to the intensity of the external neutron source.

[6] Solution to multi-group eigenvalue problem

The diffusion equation of the eigenvalue problem by the one-group theory [Eq. (2.67)] can be extended to an equation based on the multi-group theory and its numerical solutions are discussed here.

In the eigenvalue problem of the multi-group theory, it is necessary to describe the fission source term ($v\Sigma_f\phi$) in the multi-group form as well as the loss and production terms due to the neutron slowing-down. Since the fission reaction occurs in all energy groups, the total production rate of fission neutrons in the unit volume is given by Eq. (2.70).

$$P = v\Sigma_{f,1}\phi_1 + v\Sigma_{f,2}\phi_2 + v\Sigma_{f,3}\phi_3 \cdots = \sum_g v\Sigma_{f,g}\phi_g \quad (2.70)$$

The probability that a fission neutron will be born with an energy in group g is given by

$$\chi_g = \int_{AE_g} \chi(E) dE \quad (2.71)$$

where $\chi(E)$ is the fission neutron spectrum normalized to unity and therefore the sum of χ_g is the same unity.

$$\sum_g \chi_g = 1.0 \quad (2.72)$$

Hence, the fission source of group g can be expressed as Eq. (2.73).

$$\chi_g P = \chi_g \sum_{g'} v\Sigma_{f,g'}\phi_{g'} \quad (2.73)$$

For the three-group problem (fixed-source problem) of Fig. 2.20, replacement of the external source by the fission source is considered. If S_g is substituted by $\chi_g P/k_{eff}$ in Eqs. (2.57), (2.58), and (2.59), then the following diffusion equations are given for three-group eigenvalue problem:

$$\text{Group 1: } -D_1 \nabla^2 \phi_1 + (\Sigma_{a,1}\phi_1 + \Sigma_{1 \rightarrow 2}\phi_1 + \Sigma_{1 \rightarrow 3}\phi_1) = \frac{\chi_1 P}{k_{eff}} \quad (2.74)$$

$$\text{Group 2: } -D_2 \nabla^2 \phi_2 + (\Sigma_{a,2}\phi_2 + \Sigma_{2 \rightarrow 3}\phi_2) = \frac{\chi_2 P}{k_{eff}} + \Sigma_{1 \rightarrow 2}\phi_1 \quad (2.75)$$

$$\text{Group 3: } -D_3 \nabla^2 \phi_3 + (\Sigma_{a,3} \phi_3) = \frac{\chi_3 P}{k_{eff}} + (\Sigma_{1 \rightarrow 3} \phi_1 + \Sigma_{2 \rightarrow 3} \phi_2) \quad (2.76)$$

where

$$P = \nu \Sigma_{f,1} \phi_1 + \nu \Sigma_{f,2} \phi_2 + \nu \Sigma_{f,3} \phi_3 \quad (2.77)$$

In the three-group fixed-source problem, it was seen that the diffusion equations are solved in consecutive order from group 1. However, Eqs. (2.74), (2.75), and (2.76) have the fission source P which includes ϕ_1 , ϕ_2 , and ϕ_3 , and moreover k_{eff} is unknown. Hence, iterative calculations are performed as the next sequence.

- (i) Guess $k_{eff}^{(0)}$ for k_{eff} , and $\phi_1^{(0)}$, $\phi_2^{(0)}$, and $\phi_3^{(0)}$ for determining P . It is common to begin with an initial guess of $k_{eff}^{(0)} = 1.0$ and a flat distribution of the neutron fluxes (constant values).
- (ii) Since neutron fluxes are relative and arbitrary values in eigenvalue problems, normalize the initial neutron fluxes to satisfy Eq. (2.78).

$$k_{eff}^{(0)} = \int_{core} \nu \Sigma_{f,1} \phi_1^{(0)} + \nu \Sigma_{f,2} \phi_2^{(0)} + \nu \Sigma_{f,3} \phi_3^{(0)} dV \quad (2.78)$$

Since fission source terms are divided by k_{eff} in eigenvalue diffusion equations, Eq. (2.78) indicates that the total neutron source in the system is normalized to a value of 1 to fit into the next diffusion equation.

- (iii) Provide $P^{(0)}$ of Eq. (2.79) with the RHS of Eq. (2.80) and then solve this for $\phi_1^{(1)}$.

$$P^{(0)} = \nu \Sigma_{f,1} \phi_1^{(0)} + \nu \Sigma_{f,2} \phi_2^{(0)} + \nu \Sigma_{f,3} \phi_3^{(0)} \quad (2.79)$$

$$\text{Group 1: } -D_1 \nabla^2 \phi_1^{(1)} + (\Sigma_{a,1} + \Sigma_{1 \rightarrow 2} + \Sigma_{1 \rightarrow 3}) \phi_1^{(1)} = \frac{\chi_1 P^{(0)}}{k_{eff}^{(0)}} \quad (2.80)$$

- (iv) Substitute the solution of Eq. (2.80), $\phi_1^{(1)}$, for the second term in the RHS of Eq. (2.81) and then solve this for $\phi_2^{(1)}$.

$$\text{Group 2: } -D_2 \nabla^2 \phi_2^{(1)} + (\Sigma_{a,2} + \Sigma_{2 \rightarrow 3}) \phi_2^{(1)} = \frac{\chi_2 P^{(0)}}{k_{eff}^{(0)}} + \Sigma_{1 \rightarrow 2} \phi_1^{(1)} \quad (2.81)$$

- (v) Substitute again the solutions $\phi_1^{(1)}$ and $\phi_2^{(1)}$ from Eqs. (2.80) and (2.81) for the RHS of Eq. (2.82) and then solve this for $\phi_3^{(1)}$.

$$\text{Group 3: } -D_3 \nabla^2 \phi_3^{(1)} + \Sigma_{a,3} \phi_3^{(1)} = \frac{\chi_3 P^{(0)}}{k_{eff}^{(0)}} + (\Sigma_{1 \rightarrow 2} \phi_1^{(1)} + \Sigma_{2 \rightarrow 3} \phi_2^{(1)}) \quad (2.82)$$

(vi) Recalculate k_{eff} by $\phi_1^{(1)}$, $\phi_2^{(1)}$, and $\phi_3^{(1)}$ obtained in (iii) to (v) like Eq. (2.83)

$$k_{eff}^{(1)} = \int_{core} v \Sigma_{f,1} \phi_1^{(1)} + v \Sigma_{f,2} \phi_2^{(1)} + v \Sigma_{f,3} \phi_3^{(1)} dV \quad (2.83)$$

Here, k_{eff} is interpreted as the number of neutrons that will be born in the next generation finally, considering moderation and transport in the whole core, when assuming that one neutron is given as a fission source to the whole core. This is the definition of the effective multiplication factor.

Those solutions are not the correct ones yet because they are based on the initial guesses. The calculations from (iii) to (vi) are iteratively performed until k_{eff} and all of the group fluxes converge. This iterative calculation is known as the *outer iteration* calculation. The outer iteration test for convergence is done by comparing values at an iteration (n) with those at its previous iteration ($n - 1$):

$$\left| \frac{k_{eff}^{(n)} - k_{eff}^{(n-1)}}{k_{eff}^{(n)}} \right| \leq \epsilon_k \quad (2.84)$$

$$\max_{g, \vec{r}} \left| \frac{\phi_g^{(n)}(\vec{r}) - \phi_g^{(n-1)}(\vec{r})}{\phi_g^{(n)}(\vec{r})} \right| \leq \epsilon_\phi \quad (2.85)$$

where ϵ_k and ϵ_ϕ are the convergence criteria of the effective multiplication factor and neutron flux, respectively.

The relative neutron flux distribution $\phi_g(\vec{r})$ has absolute values due to the thermal power Q of the reactor. The normalization factor A of $\phi_g(\vec{r})$ to an absolute neutron flux distribution $\Phi_g(\vec{r})$ can be determined by

$$\Phi_g(\vec{r}) = A \phi_g(\vec{r}) \quad (2.86)$$

$$Q = \kappa \int_{Core} \Sigma_{f,g}(\vec{r}) \Phi_g(\vec{r}) dV = \kappa A \int_{Core} \Sigma_{f,g}(\vec{r}) \phi_g(\vec{r}) dV \quad (2.87)$$

where κ is the energy released per fission (about 200 MeV). Finally, the absolute neutron flux distribution for the thermal power can be given as the following.

$$\Phi_g(\vec{r}) = \left(\frac{Q}{\kappa \int_{Core} \Sigma_{f,g}(\vec{r}) \phi_g(\vec{r}) dV} \right) \phi_g(\vec{r}) \quad (2.88)$$

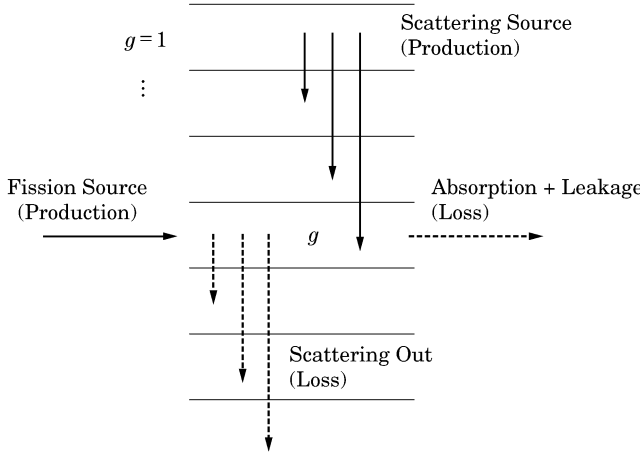


Fig. 2.21 Balance of neutron flux in group g

The distribution of the thermal power within the reactor core is

$$q'''(\vec{r}) = \kappa \sum_g \Sigma_{f,g}(\vec{r}) \Phi_g(\vec{r}) \quad (2.89)$$

which is used as a heat source for the thermal-hydraulic calculation.

A general form of the multi-group diffusion equation in the case of the eigenvalue problem is given by Eq. (2.90), which can be solved in the same way considering the balance between neutron production and loss in group g as shown in Fig. 2.21. It is seen that Eqs. (2.74), (2.75), and (2.76) are also represented by the general form.

$$-D_g V^2 \phi_g + \left(\Sigma_{a,g} + \sum_{g' \neq g} \Sigma_{g \rightarrow g'} \right) \phi_g = \frac{\chi_g}{k_{eff}} \sum_g \Sigma_{f,g} \phi_g + \sum_{g' \neq g} \Sigma_{g' \rightarrow g} \phi_{g'} \quad (2.90)$$

[7] Nodal diffusion method

The finite difference method is widely used in the design calculation of fast reactors, the analysis of critical assembly experiments, and so on. For fast reactors, convergence of the outer iteration is fast due to the long mean free paths of neutrons, and moreover, the nuclear and thermal-hydraulic coupled core calculation is not needed. Hence, the computation speed required for the design calculation can be achieved even with fine meshes in the finite difference method. For conventional LWRs as shown in Fig. 2.22, however, a fine meshing of 1–2 cm is necessary to obtain a high-accuracy solution because the neutron mean free path is short.

For example, a 3D fine meshing of a PWR core of over 30,000 liters leads to a formidable division of several tens of millions of meshes even though

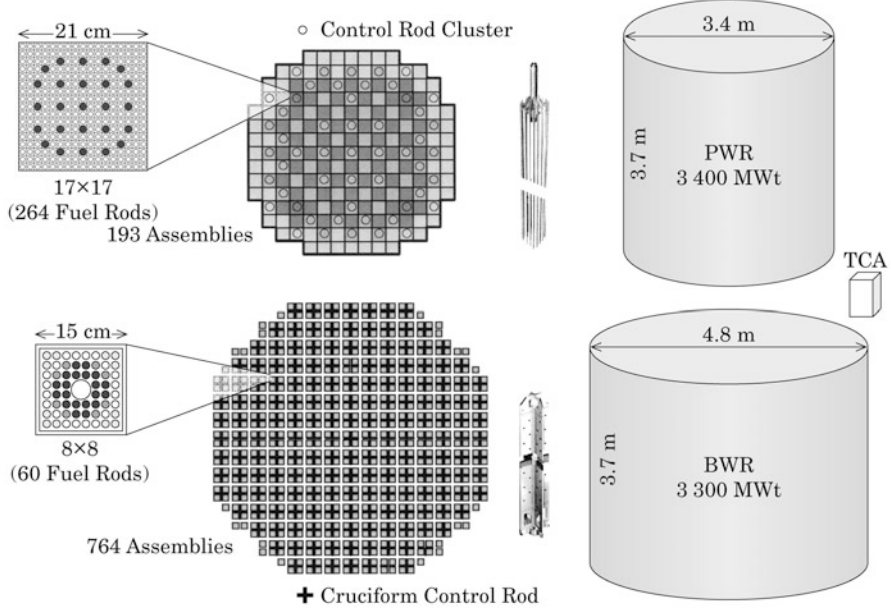


Fig. 2.22 Comparison of conventional LWRs and critical assembly (TCA) in size

excluding the reflector region. Furthermore, the neutron diffusion equation is repeatedly solved in the nuclear and thermal-hydraulic coupled core calculation, core burnup calculation, space-dependent kinetics calculation, and so on. Hence, a calculation using the 3D finite difference method with such a fine meshing is extremely expensive even on a current high-performance computer and therefore it is impractical. The nodal diffusion method [18] was, therefore, developed to enable a high-speed and high-accuracy calculation with a coarse meshing comparable to a fuel assembly pitch (about 20 cm). It is currently the mainstream approach among LWR core calculation methods [19].

The numerical solution of the nodal diffusion method is somewhat complicated and is not discussed here. The main features of the approach are briefly introduced instead.

- (i) Since the coarse spatial mesh (node) is as large as a fuel assembly pitch, the number of unknowns is drastically reduced compared with that of the finite difference method.
- (ii) The 3D diffusion equation in a parallelepiped node (k) is integrated over all directions except for the target direction and then is reduced to a 1D diffusion equation including neutron leakages in its transverse directions. For example, the diffusion equation in the x direction is expressed as

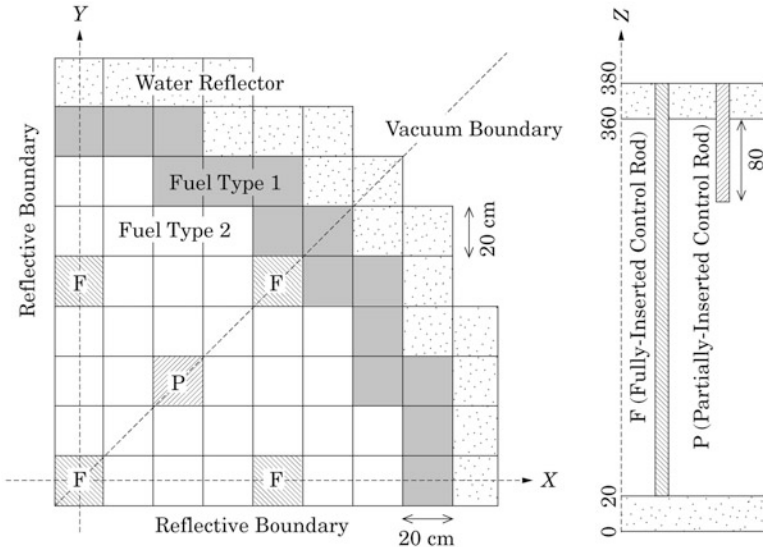


Fig. 2.23 3D benchmark problem of IAEA

$$-D \frac{d^2}{dx^2} \phi_x^k(x) + \sum_a \phi_x^k(x) = S_x^k(x) - \left\{ \frac{1}{\Delta_y^k} L_y^k(x) + \frac{1}{\Delta_z^k} L_z^k(x) \right\} \quad (2.91)$$

where Δ_y^k and Δ_z^k are the mesh widths in y and z directions, respectively. $L_y^k(x)$ and $L_z^k(x)$ represent the neutron leakage in each direction. These unknown functions are provided by a second-order polynomial expansion using the transverse leakages of two adjacent nodes.

- (iii) Typical solutions to the 1D diffusion equation of Eq. (2.91) are (a) the analytic nodal method [20] for two-group problems, (b) the polynomial expansion nodal method [18, 21] to expand $\phi_x^k(x)$ into a about fourth-order polynomial, and (c) the analytic polynomial nodal method [22, 23] to expand $S_x^k(x)$ into a second-order polynomial and to express $\phi_x^k(x)$ as an analytic function.

A 3D benchmark problem [24] given by the IAEA as shown in Fig. 2.23 is taken as a calculation example for the suitability of the nodal diffusion method. A PWR core model is composed of two types of fuels and control rods are inserted at five locations of the quadrant inner fuel region. At one location, control rods are partially inserted to 80 cm depth from the top of the core. The meshing effect on the power distribution is relatively large in this case and hence this benchmark problem has been widely employed to verify diffusion codes.

The calculation results using MOSRA-Light code [21] which is based on the fourth-order polynomial nodal expansion method are shown in Fig. 2.24 for two

Reference Values ($k_{\text{eff}} = 1.02903$)			F	0.597 - 1.31 0.51	
% Difference by MOSRA-Light ($\Delta = 20 \text{ cm}$, $k_{\text{eff}} = 1.02897$)			0.476 - 0.73 0.01	0.700 - 0.37 0.15	0.611 - 1.02 0.32
% Difference by MOSRA-Light ($\Delta = 10 \text{ cm}$, $k_{\text{eff}} = 1.02909$)			1.178 0.39 - 0.16	0.972 0.33 - 0.13	0.923 - 0.40 0.03
P					
 Control Rod Position			1.368 0.46 - 0.26	1.311 0.53 - 0.24	1.181 0.30 - 0.16
			1.397 0.47 - 0.32	1.432 0.50 - 0.34	1.291 0.39 - 0.29
			0.729 0.80 - 0.26	1.281 0.52 - 0.31	1.422 0.43 - 0.29
	F			1.193 0.54 - 0.22	0.610 0.18 - 0.07
		F		0.953 0.16 - 0.05	0.959 - 0.5 0.07
					0.777 - 0.5 0.13

Fig. 2.24 Comparison of effective multiplication factor and assembly power distribution by nodal diffusion method [21]

mesh sizes (20 and 10 cm). The reference solution has been taken by an extrapolation to zero size from the five calculations with different mesh sizes using a finite difference method code. For the effective multiplication factor, the discrepancy with the reference value is less than 0.006 % Δk in either case and thus the meshing effect can be almost ignored. For the assembly power, the discrepancy in the case of 20 cm mesh is as small as 0.6 % on average and 1.3 % at maximum. The discrepancy becomes smaller than 0.5 % on average in the case of a mesh size of 10 cm or less. It is noted that the finite difference method requires a mesh size smaller than 2 cm and more than 100 times longer computation time to achieve the same accuracy as that in the nodal diffusion method.

Thus the IAEA benchmark calculation indicates the high suitability of the nodal diffusion method to LWR cores which have fuel assemblies of about 14–21 cm size. An idea of the nodal diffusion method is its approach to decompose the reactor core into relatively large nodes and then to determine the neutron flux distribution within each node to maintain the calculation accuracy. For example, the polynomial nodal expansion method introduces the weighted residual method to obtain high-order expansion coefficients. It leads to an increased number of equations to be solved.

In other words, the high suitability of the nodal diffusion method to practical LWR calculation results is because the computation cost reduction due to a substantial decrease in the number of meshes surpasses the cost rise due to an increase in number of equations. Conversely, if it is possible to reach sufficient accuracy with the same meshing, the finite difference method will be effective

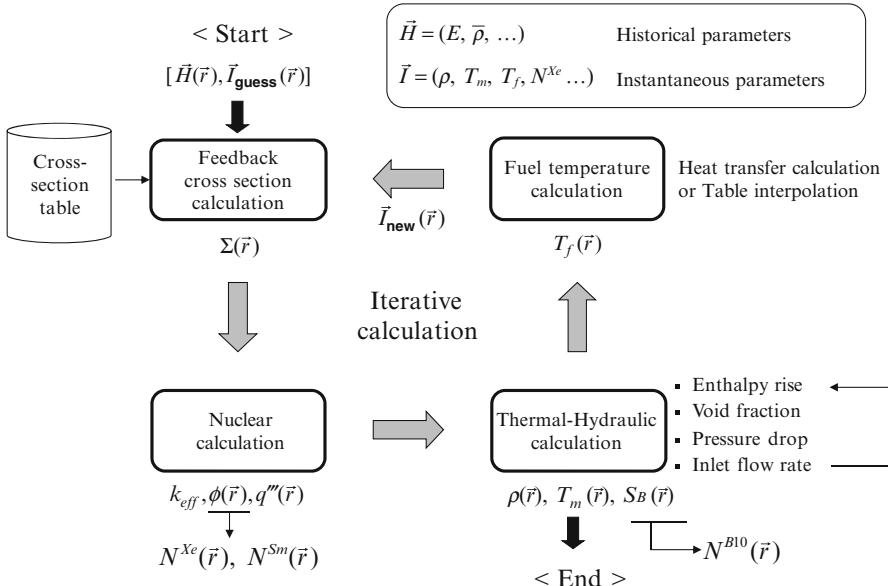


Fig. 2.25 Nuclear and thermal-hydraulic coupled core calculation of LWR

because it is not necessary to solve extra equations. Hence, the nodal diffusion method does not need to have an advantage over the finite difference method for the analysis of fast reactors or small reactors.

[8] Nuclear and thermal-hydraulic coupled core calculation

In the nuclear reactor design calculation, the thermal-hydraulic calculation is performed based on information on the heat generation distribution acquired from the nuclear calculation of the reactor core. In LWRs, the parameters such as moderator temperature, moderator density or void fraction, and fuel temperature obtained from the thermal-hydraulic calculation have a large effect on nuclear characteristics (nuclear and thermal-hydraulic feedback). The nuclear and thermal-hydraulic calculations should be mutually repeated until parameters of both calculations converge. This coupled calculation shown in Fig. 2.25 is referred to as the nuclear and thermal-hydraulic coupled core calculation (hereafter the N-TH coupled core calculation). The procedure of the N-TH coupled core calculation using the macroscopic cross section table prepared from lattice burnup calculations is discussed for a BWR example.

Two types of parameters are used in the coupled calculation. One is historical parameters related to the fuel burnup and the other is instantaneous parameters without a direct relation to it. The historical parameters such as burnup are obtained from the core burnup calculation discussed in the next section. Here it is assumed that all of the historical parameters are known. The macroscopic cross section is first required for the nuclear calculation of the

reactor core. The space and time-dependent macroscopic cross section of a LWR is, for example, represented as Eq. (2.92).

$$\Sigma_{x,g}(\vec{r}, t) = \Sigma_{x,g}(F, R, E, \bar{\rho}, \rho, T_f, T_m, N^{Xe}, N^{Sm}, S_B, f_{CR}, \dots) \quad (2.92)$$

- F*: fuel type (initial enrichment, Gd concentration, structure type, etc.)
R: control rod type (absorber, number of rods, concentration, structure type, etc.)
E: burnup (GWd/t)
 $\bar{\rho}$: historical moderator density (the burnup-weighted average moderator density)

$$\bar{\rho} = \int_0^E \rho dE / \int_0^E dE \quad (2.93)$$

ρ : moderator density (also called the instantaneous moderator density against $\bar{\rho}$) in which the void fraction α in BWRs is calculated from two densities ρ_l and ρ_g in liquid and vapor phases, respectively

$$\rho = \rho_l(1 - \alpha) + \rho_g\alpha \quad (2.94)$$

- T_f : fuel temperature (the average fuel temperature in the fuel assembly)
 T_m : moderator temperature (the average moderator temperature in the fuel assembly)
 N^i : homogenized atomic number density of nuclide *i* (e.g., ^{135}Xe or ^{149}Sm) for which the atomic number density changes independently of the burnup or the historical moderator density and which has an effect on the core reactivity depending on the operation condition such as reactor startup or shutdown
 S_B : concentration of soluble boron (e.g., boron in the chemical shim of PWRs)
 f_{CR} : control rod insertion fraction (the fraction of control rod insertion depth: $0 \leq f_{CR} \leq 1$)

These parameters are given as operation conditions, initial guess values, or iterative calculation values, and then the macroscopic cross section for the core calculation is prepared as follows.

- *E* and *R*: Use the corresponding macroscopic cross section table.
- *E* and $\bar{\rho}$: Interpolate the macroscopic cross section table in two dimensions.
- ρ , T_f , and T_m : Use the function fitting Eqs. (2.34), (2.35), and (2.36) based on the branch-off calculation.
- N^i and S_B : Correct the macroscopic cross section in the following equations, using the changes from the condition, in which the homogenized atomic number density was prepared, and the homogenized microscopic cross section:

$$\Sigma_{x,g}(\vec{r}, t) = \Sigma_{0,x,g}(\vec{r}, t) + \Delta N^i(\vec{r}, t) \sigma_{x,g}^i(\vec{r}, t) \quad (2.95)$$

$$\Delta N^i(\vec{r}, t) = N^i(\vec{r}, t) - N_0^i(E, \bar{\rho}) \quad (2.96)$$

where $\Sigma_{0,x,g}(\vec{r}, t)$ is the macroscopic cross section before the correction and $\sigma_{x,g}^i(\vec{r}, t)$ is the homogenized microscopic cross section prepared in the same way as Eq. (2.92). $N_0^i(E, \bar{\rho})$ is the atomic number density homogenized in the lattice burnup calculation and $N^i(\vec{r}, t)$ is the homogenized atomic number density in the core calculation. For example, the atomic number density of ^{135}Xe after a long shutdown is zero and it reaches an equilibrium concentration depending on the neutron flux level after startup. The concentration of soluble boron is similarly corrected changing the homogenized atomic number density of ^{10}B

- f_{CR} : Weight and average the macroscopic cross sections $\sum_{x,g}^{\text{In}}$ and $\sum_{x,g}^{\text{Out}}$ at control rod insertion and withdrawal respectively with the control rod insertion fraction.

$$\Sigma_{x,g}(\vec{r}, t) = f_{CR} \Sigma_{x,g}^{\text{In}}(\vec{r}, t) + (1-f_{CR}) \Sigma_{x,g}^{\text{Out}}(\vec{r}, t) \quad (2.97)$$

Since the cross section prepared in the iteration of the N-TH coupled core calculation reflects the feedback of instantaneous parameters, it is hereafter referred to as the *feedback cross section*. The nuclear calculation is performed with the feedback cross section by the nodal diffusion method or the finite difference method and it provides the effective multiplication factor, neutron flux distribution, power distribution, and so on. The distribution of homogenized atomic number density of nuclides such as ^{135}Xe is calculated from necessity. For example, since ^{135}Xe has an equilibrium concentration in a short time after startup as below, it is provided as a homogenized atomic number density used for the correction of microscopic cross section:

$$N^{xe}(\vec{r}, t) = \left(\gamma^{xe} \sum_g \Sigma_{f,g}(\vec{r}, t) \Phi_g(\vec{r}, t) \right) / \left(\lambda^{xe} + \sum_g \sigma_{a,g}^{xe}(\vec{r}, t) \Phi_g(\vec{r}, t) \right) \quad (2.98)$$

where γ^{xe} is the cumulative fission yield of ^{135}Xe and λ^{xe} is the decay constant of ^{135}Xe .

The thermal-hydraulic calculation is performed using the power distribution acquired from the nuclear calculation and gives the instantaneous moderator density ρ and the moderator temperature T_m . A BWR fuel assembly is enclosed in a channel box and the coolant flow inside the assembly is described as a 1D flow in a single channel with a hydraulic equivalent diameter (the “single channel model”). The core is modeled as a bundle of single channels, which are connected at the inlet and outlet, corresponding to each fuel assembly. This is referred to as the 1D multi-channel model. The calculation procedure for ρ and T_m in the 1D multi-channel model is as below.

- (i) The total flow rate at the inlet is constant and the inlet flow rate W_i for channel i is distributed (flow rate distribution). A guessed value is given to W_i if the flow rate distribution is unknown.
- (ii) The axial heat generation distribution $q'_i(z)$ (assembly linear power) of the fuel assembly from the nuclear calculation and the enthalpy at inlet h_i^{IN} are used to calculate the enthalpy rise in each channel.

$$h_i(z) = h_i^{IN} + \frac{1}{W_i} \int_0^z q'_i(z) dz \quad (2.99)$$

- (iii) The physical property values at an arbitrary position $\vec{r}(i, z)$ such as the fluid temperature $T_m(\vec{r})$ and $\rho_l(\vec{r})$ are obtained from the steam table.
- (iv) The void fraction distribution $\alpha(\vec{r})$ is acquired using $q'_i(z)$, $h_i(z)$, physical property values, and some correlations based on the subcooled boiling model. The distribution of the instantaneous moderator density $\rho(\vec{r})$ is calculated using the void fraction distribution.

$$\rho(\vec{r}) = \rho_l \{1 - \alpha(\vec{r})\} + \rho_g \alpha(\vec{r}) \quad (2.100)$$

- (v) The pressure drop ΔP_i by the channel is calculated using the information from (i) to (iv) including $\alpha(\vec{r})$ and correlations on pressure drop
- (vi) The inlet flow rate is determined so that the pressure drop in all channels is equal. A new flow rate distribution $W_i^{new}(z)$ is decided from the flow rate distribution W_i in (i) and the pressure drop ΔP_i in (v).
- (vii) The calculations from (i) to (vi) are repeated until the flow rate distribution is in agreement with the previously calculated one and the pressure drop of each channel is coincident (iterative calculation for flow rate adjustment). $\rho(\vec{r})$ and $T_m(\vec{r})$ at a convergence of the iterative calculation are taken and then the next fuel temperature calculation is done.

In a case such as the space-dependent kinetics calculation, the heat convection and conduction calculation is done using the same iteration approach of the N-TH coupled core calculation and then the temperature distribution in the fuel rod is calculated. In a case such as the steady-state calculation in which operation conditions are limited, it is common to calculate the fuel temperatures at representative linear power and fuel burnup in advance and then interpolate the linear power and burnup obtained from the core calculation into the fuel temperature table to simplify calculation of the fuel temperature $T_f(\vec{r})$.

The calculations mentioned above, the feedback cross section calculation, the nuclear calculation, the thermal-hydraulic calculation, and the fuel temperature calculation, are repeatedly performed until the effective multiplication factor and power distribution reach convergence.

[9] Core burnup calculation

Since the time variation of nuclear characteristics in the core is relatively slow with burnup, the normal N-TH coupled core calculation is carried out using the time-independent equation at each time step as shown in Fig. 2.26.

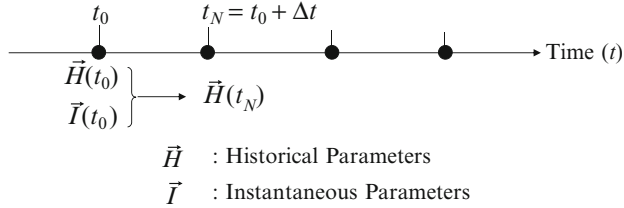


Fig. 2.26 Renewal of historical parameters in core burnup calculation

$\vec{H}(t_0)$ represents the distribution of historical parameters in the core at time t_0 . The burnup $E(\vec{r}, t_0)$ and the historical moderator density $\bar{\rho}(\vec{r}, t_0)$ are the typical historical parameters, and other ones can be used depending on reactor design code. The burnup in conventional LWRs is usually expressed in the unit of (MWd/t), which is measured as the energy (MWd) produced per metric ton of heavy metal initially contained in the fuel. That is, the burnup is the time-integrated quantity of the thermal power.

For the historical moderator density, a spatial distribution of burnup $E(\vec{r}, t_0)$ at time t_0 and a spatial distribution of thermal power density $q'''(\vec{r}, t_0)$ obtained from the N-TH coupled core calculation are considered next. The thermal power density is assumed not to change much through the interval to the next time step ($t_0 \leq t \leq t_0 + \Delta t$). Then, the burnup distribution at time $t_N (=t_0 + \Delta t)$ can be given by

$$E(\vec{r}, t_N) \approx E(\vec{r}, t_0) + C \cdot q'''(\vec{r}, t_0) \Delta t \quad (2.101)$$

where C is a constant for unit conversion.

Next, the distribution of the historical moderator density is recalculated. Since it is the burnup-weighted average value of the instantaneous moderator density, the historical moderator density at time t_N is given by

$$\bar{\rho}(\vec{r}, t_N) \equiv \frac{\int_0^{E_N} \rho(\vec{r}, t) dE}{\int_0^{E_N} dE} = \frac{\int_0^{E_0} \rho(\vec{r}, t) dE + \int_{E_0}^{E_N} \rho(\vec{r}, t) dE}{E(\vec{r}, t_N)} \quad (2.102)$$

where E_0 and E_N are abbreviations of $E(\vec{r}, t_0)$ and $E(\vec{r}, t_N)$, respectively. Here, if the distribution of instantaneous moderator density obtained from the N-TH coupled core calculation at time t_0 remains almost constant during the time interval ($t_0 \leq t \leq t_N$), $\bar{\rho}(\vec{r}, t_N)$ can be expressed as Eq. (2.103).

$$\begin{aligned}\bar{\rho}(\vec{r}, t_N) &\approx \frac{\int_0^{E_N} \rho(\vec{r}, t) dE + \rho(\vec{r}, t_0) \{E(\vec{r}, t_N) - E(\vec{r}, t_0)\}}{E(\vec{r}, t_N)} \\ &= \rho(\vec{r}, t_0) + \{\bar{\rho}(\vec{r}, t_0) - \rho(\vec{r}, t_0)\} \frac{E(\vec{r}, t_0)}{E(\vec{r}, t_N)}\end{aligned}\quad (2.103)$$

Hence, the historical moderator density at the next time step t_N can be calculated using the historical moderator density and the instantaneous moderator density obtained from the N-TH coupled core calculation, at time t_0 . Thus, the core burnup calculation can proceed until the target burnup by renewing the historical parameters with the burnup step.

[10] Space-dependent kinetics calculation

A space-dependent transient analysis for a short time is made using the time-dependent diffusion equation as

$$\begin{aligned}\frac{1}{v_g} \frac{\partial \phi_g(\vec{r}, t)}{\partial t} &= \nabla \cdot D_g(\vec{r}, t) \nabla \phi_g(\vec{r}, t) - \Sigma_{r,g}(\vec{r}, t) \phi_g(\vec{r}, t) \\ &\quad + \sum_{g' \neq g} \Sigma_{g' \rightarrow g}(\vec{r}, t) \phi_{g'}(\vec{r}, t) \\ &\quad + (1-\beta) \chi_g^p \sum_{g'} \frac{\Sigma_{f,g'} \phi_{g'}(\vec{r}, t)}{k_0} + \sum_i \chi_{i,g}^d \lambda_i C_i(\vec{r}, t)\end{aligned}\quad (2.104)$$

where β is the delayed neutron fraction, χ_g^p is the prompt neutron spectrum, and $\chi_{i,g}^d$ is the neutron spectrum of delayed neutron group i . C_i is the precursor concentration of delayed neutron group i and λ_i is its decay constant. Comparison with the normal multi-group diffusion equation [see Eq. (2.90)] shows that the time derivative term in the LHS is added and a different expression of the fission source is given by the fourth and fifth terms of the RHS. Both terms represent the prompt and delayed neutron sources which are classified by time behavior. The precursor concentration balance equation can be given by

$$\frac{\partial C_i(\vec{r}, t)}{\partial t} = \beta_i \sum_g \frac{\Sigma_{f,g'} \phi_{g'}(\vec{r}, t)}{k_0} - \lambda_i C_i(\vec{r}, t) \quad (2.105)$$

For an extremely short time difference of 10^{-4} to 10^{-3} ($t = t^{old} + \Delta t$), the following approximations are introduced.

$$\frac{1}{v_g} \frac{\partial \phi_g}{\partial t} \approx \frac{1}{v_g} \left(\frac{\phi_g - \phi_g^{old}}{\Delta t} \right) \quad (2.106)$$

$$\frac{\partial C_i}{\partial t} \approx \left(\frac{C_i - C_i^{old}}{\Delta t} \right) \quad (2.107)$$

The macroscopic cross section in Eq. (2.104) is the feedback cross section similar to that in the N-TH coupled core calculation. Since Δt is very short, the macroscopic cross section at time t can be substituted by the macroscopic cross section corresponding to the instantaneous parameters at $t = t^{old}$.

$$\Sigma_{x,g}(\vec{r}, t) \approx \Sigma_{x,g}(\rho(\vec{r}, t^{old}), T_m(\vec{r}, t^{old}), T_f(\vec{r}, t^{old}), \dots) \quad (2.108)$$

Substitution of Eqs. (2.106) and (2.107) into Eqs. (2.104) and (2.105) gives Eq. (2.109).²

$$\begin{aligned} & \nabla \cdot D_g \nabla \phi_g - \left(\Sigma_{r,g} + \frac{1}{v_g \Delta t} \right) \phi_g + \sum_{g' \neq g} \Sigma_{g' \rightarrow g} \phi_{g'} \\ & + \left\{ 1 - \sum_i \frac{\beta_i}{1 + \lambda_i \Delta t} \right\} \chi_g \sum_g \frac{\Sigma_{f,g'} \phi_{g'}}{k_0} + \left\{ \sum_i \frac{\chi_g \beta_i \lambda_i C_i^{old}}{1 + \lambda_i \Delta t} + \frac{\phi_g}{v_g \Delta t} \right\} \\ & = 0 \end{aligned} \quad (2.109)$$

This is in the same form as that of the steady-state multi-group diffusion equation for a fixed-source problem and it can be solved for $\phi_g(\vec{r}, t)$ by the numerical solutions mentioned until now. Then, the thermal-hydraulic calculation is performed and the instantaneous parameters are recalculated, similarly to the steady-state N-TH coupled calculation. The feedback cross section at the next time step is in turn prepared from Eq. (2.108) and the diffusion equation of Eq. (2.109) is solved again. These repeated calculations give the neutron flux distribution and its corresponding thermal power distribution at each time step.

Since it is hard to use a fine time interval less than 10^{-3} s in a practical code for the space-dependent kinetics calculation, a large number of considerations have been introduced for high-speed and high-accuracy calculation within a practical time [19]; two examples are the method to express the time variation in neutron flux as an exponential function and the method to describe the neutron flux distribution as the product of the amplitude component with fast time-variation and the space component with relatively smooth variation (the improved quasi-static method). The fast nodal diffusion method is a general solution in the analysis code for LWRs.

The point kinetics model widely used is in principle based on the first order perturbation theory where it is assumed that the spatial distribution of neutron flux does not change much even though the cross section varies by some external perturbation. Hence, when the neutron flux distribution is considerably distorted due to such an event as a control rod ejection accident, the space-dependent kinetics analysis must accurately predict the time behavior of the reactor.

²For simplicity, it is assumed that $\chi_{t,g}^d = \chi_g$ which is reasonable for the two-group problem.

2.2 Reactor Core, Plant Dynamics and Safety Calculations

Nuclear reactor design and analysis is done with knowledge and data from fundamental fields such as nuclear reactor physics, nuclear reactor kinetics and plant control, nuclear thermal-hydraulic engineering, nuclear mechanical engineering, and nuclear safety engineering. There are various calculation models from simple to detailed, and their selection depends on the purpose. Simple models have the advantage of giving a better understanding of calculation results and physical phenomena, and easy improvement of calculation codes. With today's high computational performance, it is common to use a calculation code based on detailed models from the viewpoint of generic programming. Since the accuracy and application range of calculation results depend on models and data, it is necessary to imagine the physical phenomena and comprehend the validity of the calculation results based on the fundamental knowledge concerning the calculation target.

The nuclear reactor calculation is classified broadly into the reactor core calculation and the nuclear plant characteristics calculation. The former is done to clarify nuclear, thermal, or their composite properties. The latter is done to clarify dynamic and control properties, startup and stability, and safety by modeling pipes and valves of the coolant system, coolant pump, their control system, steam turbine and condenser, etc. connected with the reactor pressure vessel as well as the reactor core.

2.2.1 Reactor Core Calculation

The reactor core calculation is carried out by the N-TH coupled core calculation, presented in the list [8] of Sect. 2.1.5, to evaluate properties in normal operation of the reactor. The concept of core design calculation and the calculation model are discussed here.

[1] Heat transfer calculation in single channel model

Figure 2.27 depicts a 1D cylindrical model to describe one fuel rod and its surrounding coolant with an equivalent flow path. It is called the *single channel model* and it is the basic model used in the core thermal-hydraulic calculation and the plant characteristics calculation. The thermal-hydraulic properties in the core can be calculated on the single channel model where the heat generated from fuel pellets is transferred to coolant which is transported with a temperature rise.

The radial heat transfer model is composed of fuel pellet, gap, cladding, and coolant. The radial heat conduction or convection between those components is considered in each axial region and then the axial heat transport by coolant or moderator is examined. The mass and energy conservation equations and the state equation are solved in each axial region in turn from the top of the upward coolant flow. The momentum conservation equation is also solved to evaluate the pressure drop. The axial heat conduction of the fuel pellet is ignored. This

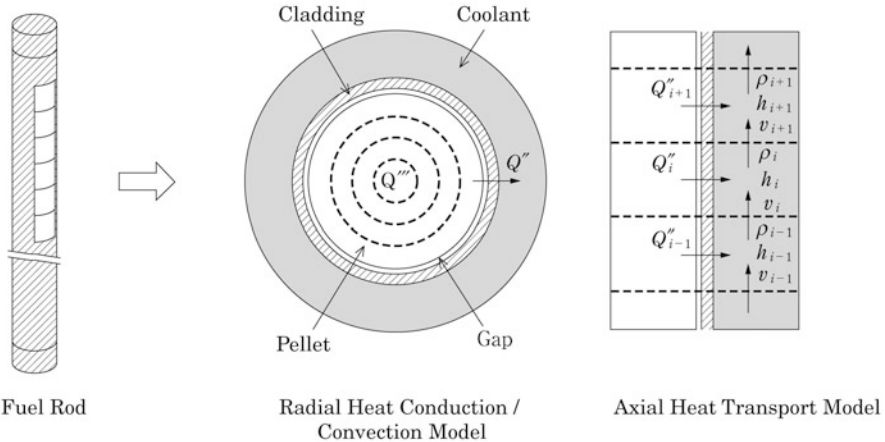


Fig. 2.27 Single-channel heat transfer calculation model

assumption is valid because the radial temperature gradient is several orders of magnitude larger than the axial one.

The difference between the fuel average temperature and the cladding surface temperature is expressed as

$$T_f^{ave} - T_s = \left(\frac{r_f + t_c}{r_f} \right) \left[\frac{r_f}{2k_f} + \frac{1}{h_g} + \frac{t_c}{k_c} \right] q'' \quad (2.110)$$

where,

k_f : average thermal conductivity of pellet (W/m-K)

h_g : gap conductance (W/m²-K)

k_c : thermal conductivity of cladding (W/m-K)

Q'' : heat flux from pellet (W/m²)

r_f : pellet radius (m)

t_c : cladding thickness (m)

T_f^{ave} : pellet average temperature (K)

T_s : cladding surface temperature (K).

The terms inside the RHS square brackets represent the temperature drop in fuel, gap, and cladding, respectively.

The heat transfer from cladding surface to coolant is described by *Newton's law of cooling*

$$q''(r_c) = h_c(T_s - T) \quad (2.111)$$

where,

h_c : heat transfer coefficient between cladding surface and coolant (W/m²-K)

r_c : cladding radius (m)

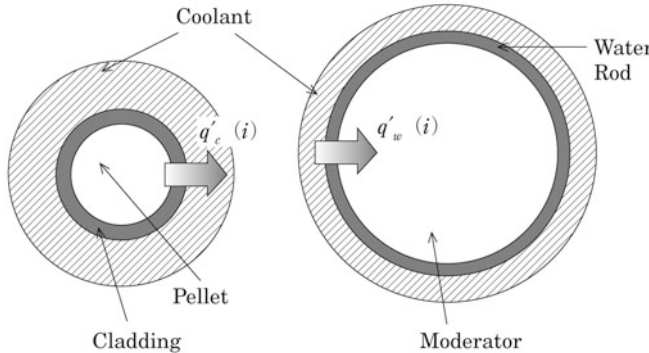


Fig. 2.28 Single-channel thermal-hydraulic calculation model

T_s : cladding surface temperature (K)

T : coolant bulk temperature (K).

The heat transfer coefficient h_c can be evaluated using the *Dittus-Boelter correlation* for single-phase flow and the *Thom correlation* or the *Jens-Lottes correlation* for nucleate boiling.

Water rods are often implemented into fuel assemblies, especially for BWRs. The heat transfer characteristics of the water rod can also be calculated using the single channel model. Figure 2.28 describes the heat transfer calculation model with two single channels of fuel rod and water rod. The heat from coolant is transferred through the water rod wall into the moderator.

The heat transfer of the water rod is also represented by Newton's law of cooling. The temperature difference between the coolant in the fuel rod channel and the moderator in the water rod channel is expressed as

$$T - T_w = \frac{N_f}{N_w} Q'_w \left[\frac{1}{\pi D_w h_{s1}} + \frac{1}{\pi (D_w - 2t_{ws}) h_{s2}} \right] \quad (2.112)$$

where,

T : coolant temperature in fuel rod channel (K)

T_w : moderator temperature in water rod channel (K)

D_w : hydraulic diameter of water rod

h_{s1} : heat transfer coefficient between coolant and outer surface of water rod (W/m²-K)

h_{s2} : heat transfer coefficient between inner surface of water rod and moderator (W/m²-K)

N_f : number of fuel rods per fuel assembly

N_w : number of water rods per fuel assembly

Q'_w : linear heat from coolant to water rod (W/m)

t_{ws} : thickness of water rod (m)

The terms inside of the RHS square brackets represent the heat transfer from the fuel rod channel to the water rod wall and back to the water rod, respectively. Temperature drop due to the water rod wall is ignored in this equation. It is also assumed that the water rod wall is an unheated wall, whereas the cladding is a heated wall. Hence, there is no boiling at the outer surface of the water rod although the outer surface of the water rod wall contacts with two phase coolant. It should be subsequently noted that the application condition of heat transfer correlations is not identical for such a water rod wall.

The thermal conductivity of the fuel pellet depends on temperature and in a BWR fuel, for example, it can be given by

$$k_f = \frac{3824}{402.4 + T_f^{ave}} + 6.1256 \times 10^{-11} (T_f^{ave} + 273)^3 \quad (2.113)$$

where T_f^{ave} and k_f are the average temperature (K) and thermal conductivity (W/m-K) of pellet, respectively. The thermal conductivity is actually a function of pellet density, plutonium containing fraction, burnup, etc. as well as temperature. Since the fission gas release during irradiation causes pellet swelling and hence it also changes the thermal gap conductance with cladding, the fuel behavior analysis code which includes irradiation experiments is required to precisely evaluate the fuel centerline temperature. However, since the fuel centerline temperature at normal operation is far lower than the fuel melting point, it does not need a highly accurately estimate in the reactor core design. In BWR fuel, the fuel centerline temperature at normal operation is limited to about 1,900 °C to prevent excessive fission gas release rate. The temperature drop in the pellet depends not on pellet radius, but linear power density and fuel thermal conductivity. Hence, the linear power density is restricted at normal operation of LWRs.

[2] 3D nuclear and thermal-hydraulic coupled core calculation

In nuclear reactors such as LWRs, in which the coolant serves as moderator, the moderator density varies with temperature change and boiling of coolant, and subsequently the reactivity and reactor power vary. The power distribution also varies with the moderator density change. The heat transfer calculation is performed to evaluate those core characteristics using the heat generation distribution in the core acquired from the nuclear calculation. The nuclear calculation is performed again using the macroscopic cross section changed by the coolant or moderator density distribution obtained in the heat transfer calculation. These calculations are repeated until a convergence. This is the nuclear and thermal-hydraulic coupled core calculation (the N-TH coupled core calculation) mentioned earlier.

A 2D core model cannot precisely handle power and burnup in each part of the core. This usually needs a 3D nuclear calculation, which is combined with the heat transfer calculation in the single channel model for each fuel assembly. Figure 2.29 shows a 3D N-TH coupled core calculation model which is a symmetric quadrant. Since the fuel assembly burnup differs with the power

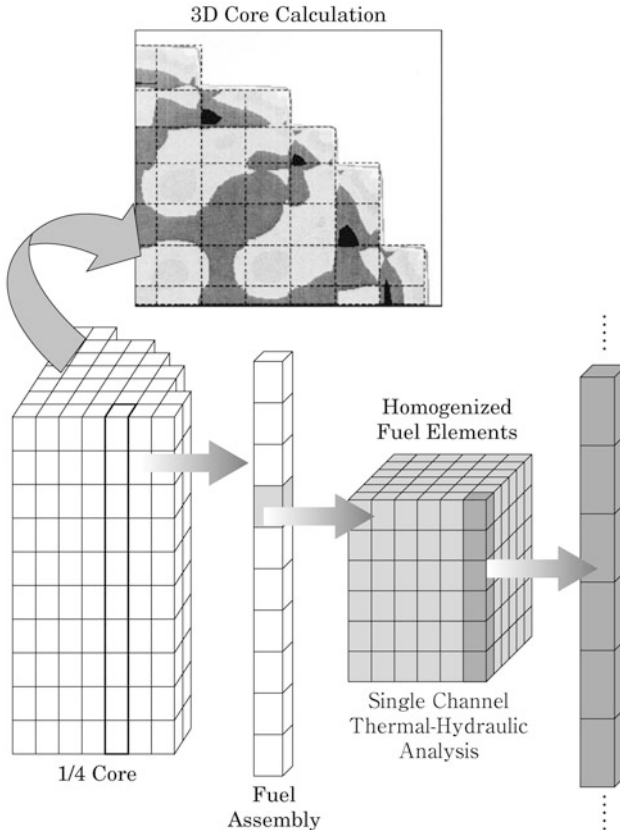


Fig. 2.29 3D nuclear and thermal-hydraulic coupled core calculation model

history at each position, the fuel assembly is axially segmented and the macroscopic cross section at each section is prepared for the core calculation. Each fuel assembly, which consists of a large number of fuel rods, is described as the single-channel thermal-hydraulic calculation model. The heat transfer calculation is carried out with the axial power distribution of each assembly obtained from the nuclear calculation and it provides an axial moderator density distribution.

The N-TH coupled core calculation above is repeatedly continued until it satisfies a convergence criterion and then it gives the macroscopic cross section which is used for calculations such as the core power distribution. This process is repeated at each burnup step and is referred to as the 3D nuclear and thermal-hydraulic coupled core calculation (3D N-TH coupled core calculation). In the practical calculation, as mentioned in Sect. 2.1, the macroscopic cross sections are tabulated in advance with respect to parameters such as fuel burnup and enrichment, moderator density, and so on. Each corresponding cross section is used in the N-TH coupled core calculation.

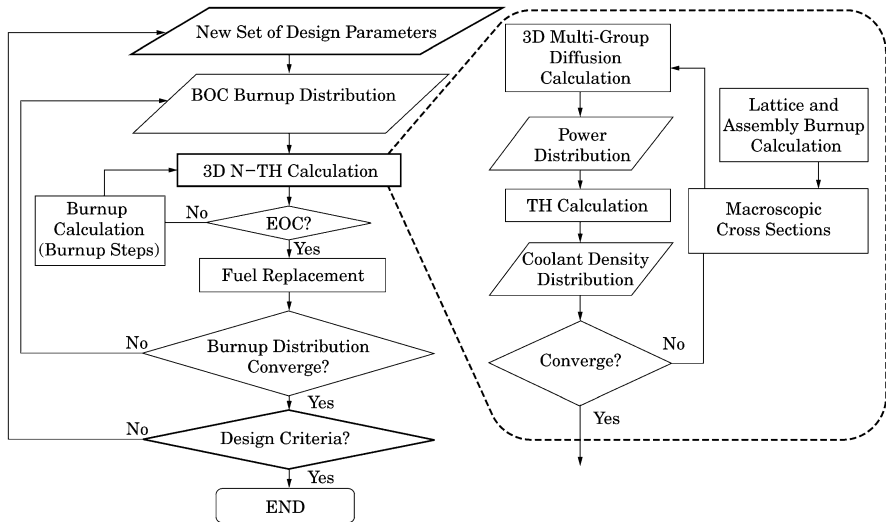


Fig. 2.30 Flow chart of equilibrium code design

Figure 2.30 shows a flow chart of an equilibrium core design using the 3D N-TH coupled core calculation [25]. Macroscopic cross section data are previously prepared from the lattice and/or assembly burnup calculation and then tabulated with fuel burnup and enrichment, moderator density, and so on. The macroscopic cross section is used in the 3D multi-group diffusion calculation to obtain the core power distribution, which is employed again in the thermal-hydraulic calculation.

Usually several different types of fuel assemblies are loaded into the core according to the purpose such as radial power distribution flattening or neutron leakage reduction. In the first operation of a reactor, all fresh fuel assemblies are loaded but they may have several different enrichments of fuel. This fresh core is called the *initial loading core*. After one cycle operation, low reactivity assemblies representing about 1/4 to 1/3 of the loaded assemblies are discharged from the reactor. The other assemblies are properly rearranged in the core considering the burnup distribution and other new fresh ones are loaded.

In the end of each cycle, the core is refueled as in the above way and then the reactor restarts in the next cycle. While such a cycle is being repeated, the characteristics of the core vary but gradually approach equilibrium quantities. When finally the characteristics at $N + 1$ the cycle have little change in comparison with those at the N cycle, the core is called the *equilibrium core*. In certain cases, it shows equilibrium characteristics at N and $N + 2$ cycles and these are also generally referred to as the equilibrium core. By contrast, the core at each cycle is called the “transition core” until it reaches the equilibrium core.

In the equilibrium core design, first a proper burnup distribution of the core is guessed at the beginning of the cycle (BOC), and a control rod and fuel loading pattern is assumed. Then, the N-TH coupled core calculation is performed for one cycle based on the assumed core design with the burnup distribution. After the core calculation, the refueling according to the fuel loading pattern is followed by evaluation of the new burnup distribution at BOC of the next cycle. Such evaluation after one cycle calculation is repeated until the burnup distribution at BOC converges, at which time it is regarded as attaining the equilibrium core.

The core design criteria, such as shutdown margin, moderator density coefficient, Doppler coefficient, fuel cladding temperature, and maximum linear power density, are applied to the equilibrium core. If the equilibrium core does not satisfy the core design criteria, the equilibrium core design is performed again after reviewing fuel enrichment zoning, concentration and number of burnable poison rods, fuel loading and control rod pattern, coolant flow rate distribution, and so on.

A 3D N-TH coupled core calculation is also performed for fuel management such as fuel loading and reloading. In this case, the equilibrium core is searched from an initial loading core. Some fuel assemblies are replaced with new fresh ones after the first cycle calculation and the new core configuration is considered in the next cycle calculation. The calculation procedure is also similar to Fig. 2.30.

It is noted again that operation management such as fuel loading pattern and reloading, and control rod insertion can be considered in the 3D N-TH coupled core calculation. Figure 2.31 shows an example of 3D core power distribution and coolant outlet temperature distribution.

In the core design and operation management, it is necessary to confirm that maximum linear power density (or maximum linear heat generation rate, MLHGR) is less than a limiting value. Figure 2.32 shows variation in MLHGR and maximum cladding surface temperature (MCST) with cycle burnup, which was from a 3D N-TH coupled core calculation for a supercritical water-cooled reactor (SCWR) as an example [26]. The limiting values at normal operation are 39 kW/m and 650 °C respectively in this example. The core calculation was performed according to the fuel loading and reloading pattern as described in Fig. 2.33. It is noted that the third cycle fuel assemblies are loaded in the core peripheral region to reduce neutron leakage (low leakage loading pattern). The control rod pattern is shown in Fig. 2.34.

The 3D N-TH coupled core calculation has been done for BWRs for many years. Since there are not many vapor bubbles in PWRs due to subcooled boiling, the N-TH coupled core calculation has not always been necessary, but it is being employed recently for accuracy improvement.

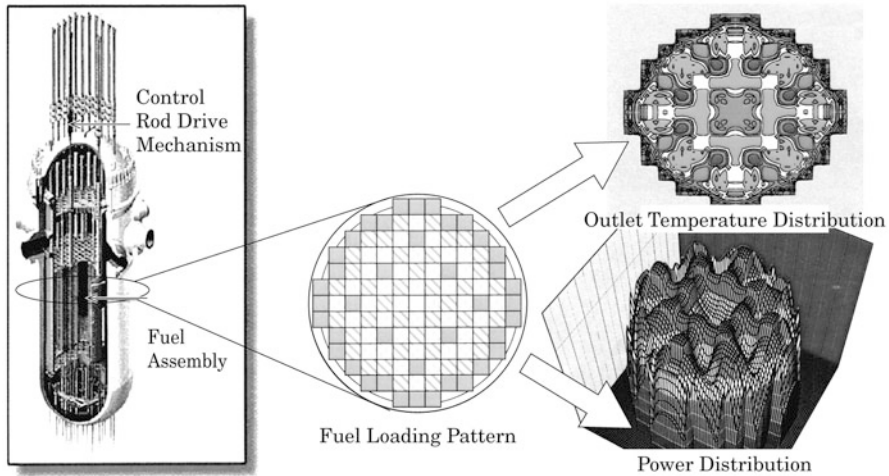


Fig. 2.31 3D core power distribution and coolant outlet temperature distribution

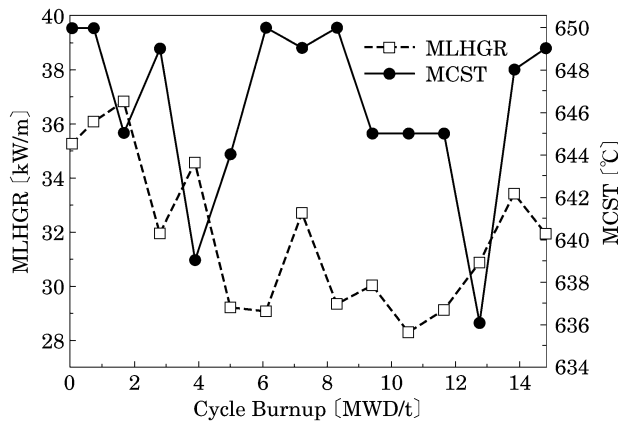


Fig. 2.32 Example of Variation in maximum linear power density and maximum cladding surface temperature with cycle burnup

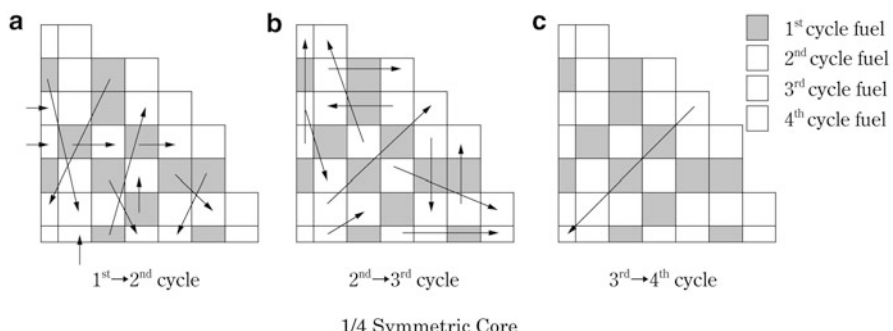


Fig. 2.33 Example of fuel loading and reloading pattern

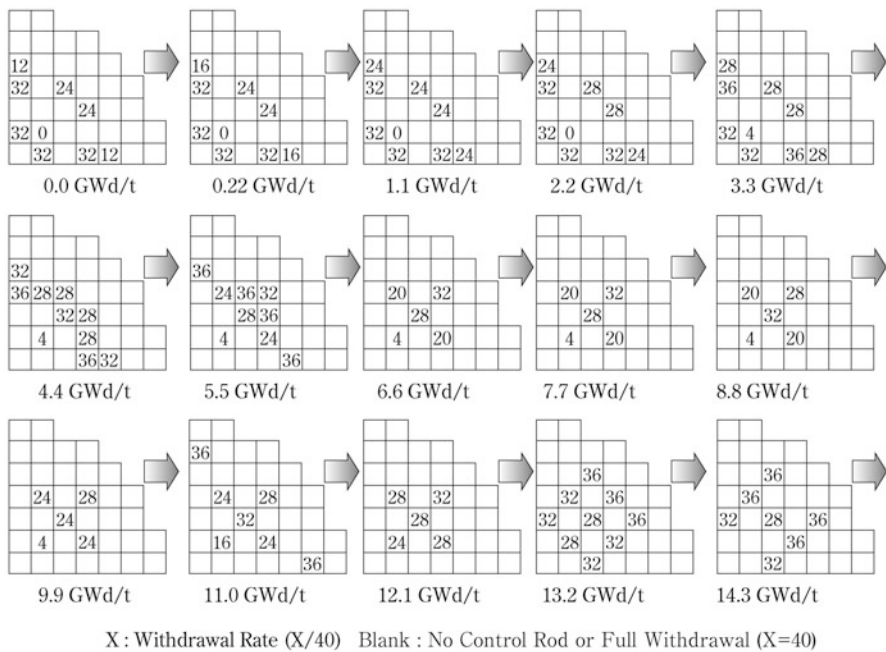


Fig. 2.34 Example of control rod pattern and insertion

In the core calculation, one fuel assembly is modeled not as a bundle of its constituent fuel rods but a homogenized assembly, which is represented as a single channel in the thermal-hydraulic calculation. However, the power of each fuel rod is actually a little different and hence it leads to a different coolant flow rate and a different coolant enthalpy in the flow path (subchannel) between fuel rods. This also causes a difference such as in cladding temperature which is particular to a single-phase flow cooled reactor. The heat transfer analysis for coolant flow paths formed by many fuel rods is called *subchannel analysis*, and it is used in evaluation of cladding temperature in liquid sodium-cooled fast reactors and so on.

In computational fluid dynamics (CFD), the behavior of fluid is evaluated through numerical analysis of the simultaneous equations: Navier–Stokes equations, continuity equation, and in some cases perhaps the energy conservation equation and state equation. It subsequently requires a huge computing time, but a detailed heat transfer analysis can be made. The CFD analysis can be used to calculate a circumferential distribution of fuel rod temperature in a single-phase flow cooled reactor or to analyze detailed fluid behavior inside the reactor vessel and pipes. Figure 2.35 depicts the three heat transfer analysis models mentioned above including the CFD analysis model.

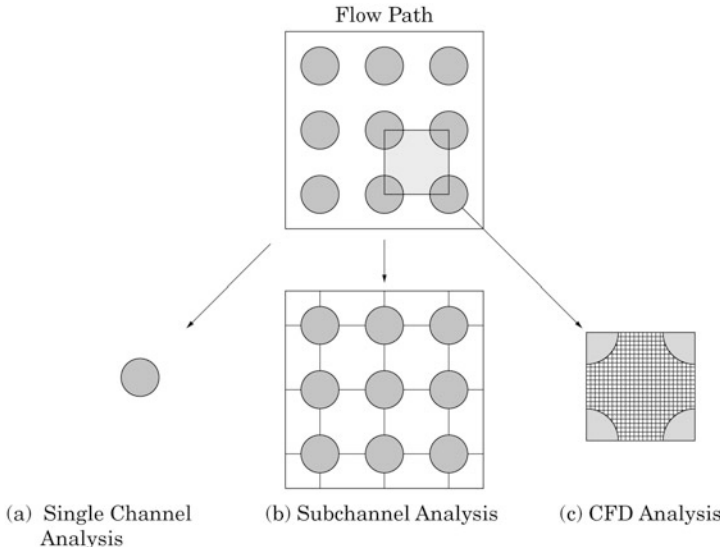


Fig. 2.35 Heat transfer analysis models

2.2.2 Plant Dynamics Calculation

[1] Plant dynamics calculation code

The plant dynamics calculation treats plant control, stability, and response at abnormal transients and accidents. A simple model for heat transfer calculation in a plant is the node junction model as shown in Fig. 2.36 [27]. In the node junction model, reactor components are represented as 1D nodes and connected; the connected items include core, upper and lower plena, downcomer (inlet coolant flows down the downcomer region which is placed between the core and reactor pressure vessel), main feedwater and main steam lines, valves, etc. The node junction calculation begins from an upstream node based on mass and energy conservation laws. The momentum conservation law is also considered for pressure drop and flow rate distribution calculations. In the case of Fig. 2.36, for example, the core is described with two single channel models at average and maximum power. The core design calculation is performed at steady state as mentioned before, but a transient single channel model is used in the plant dynamics calculation.

A transient radial heat conduction in fuel can be expressed as

$$\frac{\partial}{\partial t} (\rho_f C_p T_f) = \frac{1}{r} \frac{\partial}{\partial r} \left(r k_f \frac{\partial T_f}{\partial r} \right) + q''' \quad (2.114)$$

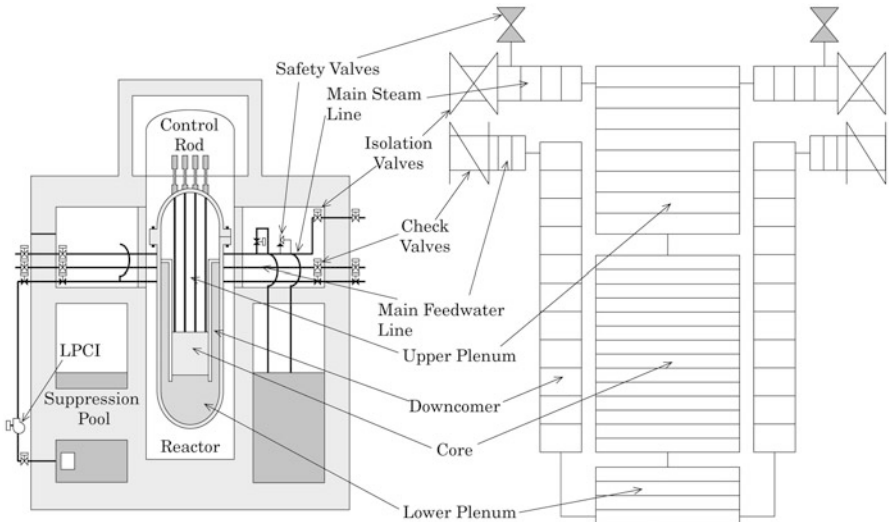


Fig. 2.36 Node junction model

where,

- C_p : specific heat of pellet (J/kg-K)
- k_f : thermal conductivity of pellet (W/m-K)
- q^m : power density (W/m³)
- r : radial distance (m)
- T_f : pellet temperature (K)
- ρ_f : pellet density (kg/m³).

The heat transfer from cladding outer surface to coolant is evaluated by Newton's law of cooling. A proper heat transfer coefficient should be used considering flow regime and temperature, pressure, etc.

Plant dynamics analysis codes are constructed with the node junction model and the following reactor kinetics model. The simplest kinetics model is the point reactor kinetics model (point reactor approximation) as

$$\frac{\partial n(t)}{\partial t} = \frac{\Delta\rho - \beta}{\Lambda} n(t) + \sum_{i=1}^6 \lambda_i C_i(t) \quad (2.115)$$

$$\frac{\partial C_i(t)}{\partial t} = \frac{\beta_i}{\Lambda} n(t) - \lambda_i C_i(t) \quad (i=1 \sim 6)$$

$$\Delta\rho = \Delta\rho(T_f^{ave}, \rho_{mod})$$

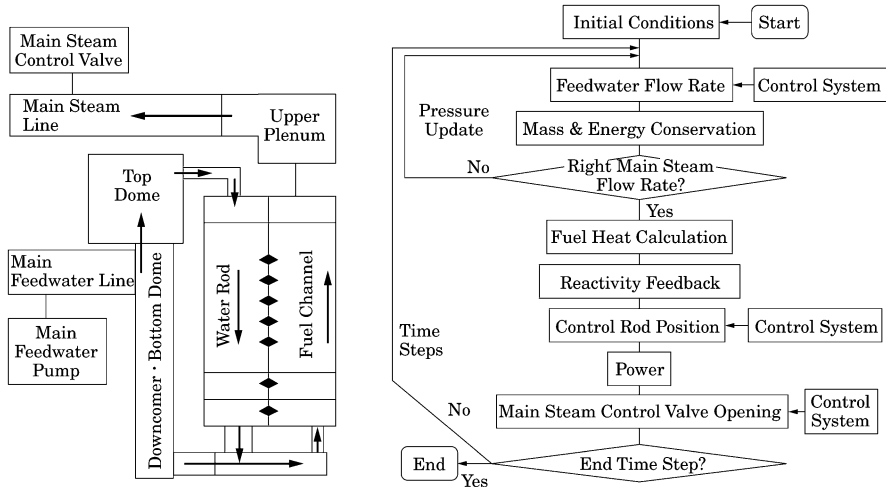


Fig. 2.37 Plant dynamics analysis model and calculation flow chart

where,

$n(t)$: number of neutrons

$C_i(t)$: number of delayed neutron precursor for group i

t : time

β_i : fraction of delayed neutron group i

$$\beta = \sum_{i=1}^6 \beta_i$$

$\Delta\rho$: reactivity

Λ : prompt neutron generation time (s)

λ_i : decay constant of precursor of delayed neutron group i (s^{-1})

$T_f^{ave}(t)$: average fuel temperature (K)

$\rho_{mod}(t)$: moderator density (g/cm^3).

The reactivity feedback of fuel temperature (Doppler effect) and moderator density is applied to the point reactor kinetics equations. Even though large power reactors such as LWRs show space-dependent kinetic characteristics, the reactivity feedback effect can be expressed with the point reactor approximation using a space-dependent weight function (adjoint neutron flux).

Figure 2.37 shows an example of a node junction model in a plant dynamics analysis code and its calculation flow chart. This model describes coolant flow which is fed to the water moderation rods through the top dome of the reactor vessel for a supercritical water-cooled thermal reactor (Super LWR) [28, 29].

The mass, energy, and momentum conservation equations used in the node junction model are a time-dependent form of the single-channel

thermal-hydraulic model in the core design. In the case of single channel, single phase, and one dimension, the mass conservation equation is given by Eq. (2.116)

$$\frac{\partial \rho}{\partial t} + \frac{\partial(\rho u)}{\partial z} = 0 \quad (2.116)$$

and the energy conservation equation is given by Eq. (2.117).

$$\frac{\partial(\rho h)}{\partial t} + \frac{\partial(\rho uh)}{\partial z} = \frac{P_e}{A} q'' \quad (2.117)$$

The momentum conservation equation is expressed as

$$-\frac{\partial P}{\partial z} = \frac{\partial(\rho u)}{\partial t} + \frac{\partial(\rho u^2)}{\partial z} + \rho g \cos \theta + \frac{2f}{D_h} \rho u^2 \quad (2.118)$$

and the state equation is

$$\rho = \rho(P, h) \quad (2.119)$$

where,

t: time (s)

z: position (m)

ρ : coolant density (kg/m^3)

u: fluid velocity (m/s)

h: specific enthalpy (J/kg)

q'' : heat flux at fuel rod surface (W/m^2)

A: flow area of fuel channel (m^2)

P_e : wetted perimeter of fuel rod (m)

P: pressure (Pa)

g: gravitational acceleration

D_h : hydraulic equivalent diameter of fuel channel (m)

Re: Reynolds number

θ : vertical angle of fuel channel

f: frictional coefficient

for example, $f = 0.0791 \times \text{Re}^{-0.25}$ (Blasius equation).

In the case of a water rod, the energy transferred to the water rod should be considered in the energy conservation equation of the fuel rod cooling channel. In the case of light water, the steam tables of the Japan Society of Mechanical Engineers (JSME) or the American Society of Mechanical Engineers (ASME) can be used in the state equation of the coolant.

The following introduce heat transfer coefficients for water-cooled reactors. In a single-phase turbulent flow, for example, the heat transfer coefficient can be obtained from the Dittus-Boelter correlation

$$h = 0.023 \left(\frac{k}{D_e} \right) (Pr)^{0.4} \left(\frac{GD_e}{\mu} \right)^{0.8} \quad (2.120)$$

where,

D_e : hydraulic equivalent diameter (m)

G : mass flux ($\text{kg}/\text{m}^2\text{-s}$)

h : heat transfer coefficient ($\text{W}/\text{m}^2\text{-K}$)

k : thermal conductivity ($\text{W}/\text{m}\text{-K}$)

Pr : Prandtl number

μ : viscosity coefficient ($\text{Pa}\cdot\text{s}$).

If nucleate boiling occurs, the heat transfer for PWR can be described by the Thom correlation

$$h = \frac{1}{dT} \left(\frac{\Delta T_{sat} e^{p/8.6}}{0.022} \right)^2 \quad (2.121)$$

where,

h : heat transfer coefficient ($\text{W}/\text{m}^2\text{-K}$)

P : pressure (MPa)

dT : temperature difference between wall surface and fluid (K)

ΔT_{sat} : wall temperature elevation above saturation temperature (K)

and it is applied for the range of

pressure: 5.2–14.0 MPa

mass flux: 1,000–3,800 $\text{kg}/\text{m}^2\text{-s}$

heat flux: 0–1600 kW/m^2 .

The Jens-Lottes correlation can be used for BWRs.

If there is a thin liquid film in annular flow with a high steam quality, for example, the heat transfer to a vertical upward water flow can be represented by the *Schrock-Grossman correlation*

$$h = (2.50)(0.023) \left(\frac{k_f}{D_e} \right) (Pr_f)^{0.4} \left[\frac{GD_e(1-X)}{\mu_f} \right]^{0.8} \left(\frac{1}{X_{tt}} \right)^{0.75} \quad (2.122)$$

$$\frac{1}{X_{tt}} = \left(\frac{X}{1-X} \right)^{0.9} \left(\frac{\rho_f}{\rho_g} \right)^{0.5} \left(\frac{\mu_g}{\mu_f} \right)^{0.1}$$

where,

D_e : hydraulic equivalent diameter (m)

G : mass flux ($\text{kg}/\text{m}^2\text{-s}$)

h : heat transfer coefficient ($\text{W}/\text{m}^2\text{-K}$)
 k_f : thermal conductivity of water ($\text{W}/\text{m}\text{-K}$)
 Pr_f : Prandtl number of water
 X : steam quality
 ρ_f : water density (kg/m^3)
 ρ_g : steam density (kg/m^3)
 μ_f : viscosity coefficient of water ($\text{Pa}\cdot\text{s}$)
 μ_g : viscosity coefficient of steam ($\text{Pa}\cdot\text{s}$)

and it is applied for the range of

pressure: 0.3–3.5 MPa
 mass flux: 240–4,500 $\text{kg}/\text{m}^2\text{-s}$
 heat flux: 190–4,600 kW/m^2 .

In the post-dryout region of BWRs, namely, the steady-state film boiling state of mist flow where steam flow is accompanied with liquid droplets, for example, the heat transfer can be described by the *Groeneveld correlation*.

$$h = 0.00327 \left(\frac{k_g}{D_e} \right) (Pr_{v,w})^{1.32} \left[\left(\frac{GD_e}{\mu_g} \right) \left(X + \frac{\rho_g}{\rho_f} (1-X) \right) \right]^{0.901} Y^{-1.50} \quad (2.123)$$

$$Y = \max \left[1 - 0.1(1-X)^{0.4} \left(\frac{\rho_f}{\rho_g} - 1 \right)^{0.4}, \ 0.1 \right]$$

where,

h : heat transfer coefficient ($\text{W}/\text{m}^2\text{-K}$)
 k_g : thermal conductivity of saturated steam ($\text{W}/\text{m}\text{-K}$)
 $\text{Pr}_{v,w}$: Prandtl number of steam at wall surface
 D_e : hydraulic equivalent diameter (m)
 G : mass flux ($\text{kg}/\text{m}^2\text{-s}$)
 μ_g : viscosity coefficient of steam ($\text{Pa}\cdot\text{s}$)
 X : steam quality
 ρ_f : water density (kg/m^3)
 ρ_g : steam density (kg/m^3)

[2] Plant control

The plant dynamics analysis covers the plant control system. Figure 2.38 presents the plant control system of a SCWR as an example [27]. Typical control systems of LWRs are actually more complex, but they are based on the concept below. The plant control system of nuclear power plants uses *proportional-integral-derivative (PID) control* which is widely used in the control system of other types of practical plants as well.

Composition of the plant control system is based on similar existing plant control systems and its parameters are determined using plant dynamics analysis codes using the procedure below.

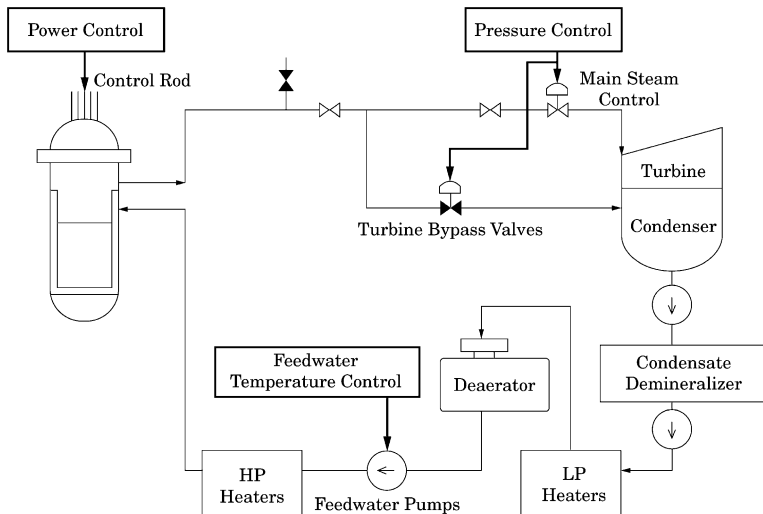


Fig. 2.38 Plant control system (supercritical water-cooled reactor)

- ① Investigate responses to external disturbances without control system, and decide what state variables (e.g., power) to control and how to control them (e.g., by control rod) according to their sensitivities.
- ② Design a control system.
- ③ Confirm responses to the external disturbances under the control system.

For example, in the case of reducing feedwater flow rate, changing control rod position, inserting a reactivity, or closing main steam control valves, variations in main steam temperature, power, or pressure are investigated for each case using plant dynamics analysis codes. In Fig. 2.38, the main steam temperature is controlled by regulating feedwater flow rate, the reactor power by control rods, and the main steam pressure by main steam control valves considering highly sensitive parameters.

Figure 2.39 shows the power control system by control rods. This control system is governed by a proportional controller which decides a control rod drive speed in proportion to the deviation between actual power and power setpoint. Control rods are driven at a maximum speed for a deviation larger than a constant value b .

Figure 2.40 represents the main steam temperature control system which is driven by a proportional-integral (PI) controller after a lead compensation for time-lag of a temperature sensor. The PI control parameter values are determined for stable and fast-convergence responses through fine tuning of the integral gain with a little change of the proportional gain.

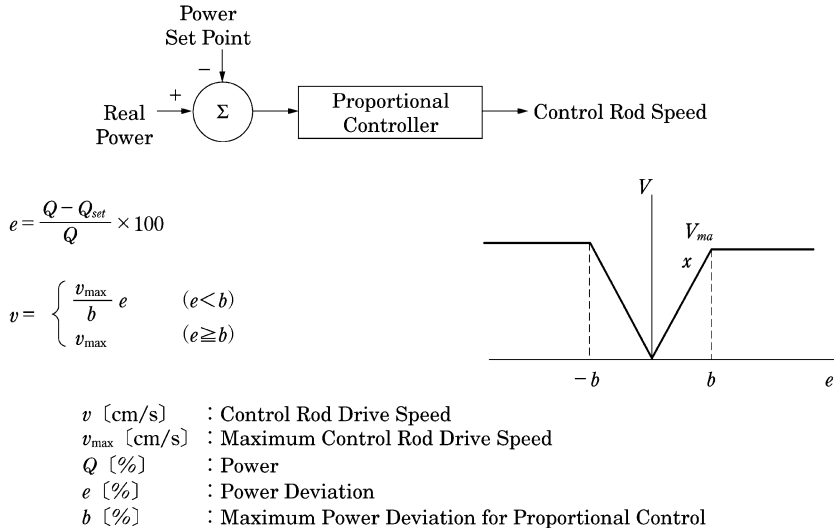
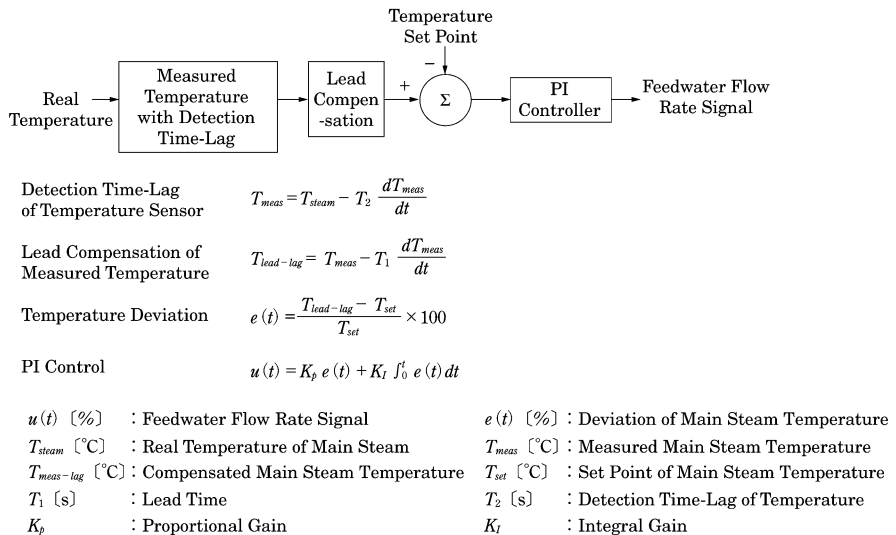
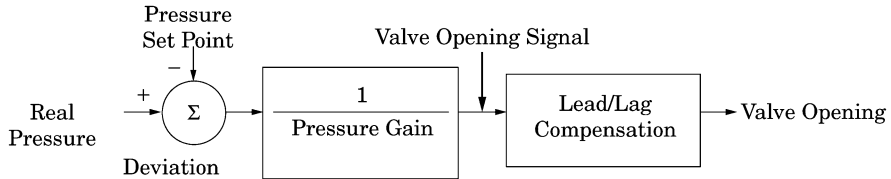
**Fig. 2.39** Power control system**Fig. 2.40** Main steam temperature control system

Figure 2.41 shows the pressure control system which controls valve opening by converting the deviation from the pressure setpoint into a valve opening signal with lead/lag compensation. The control parameter value is determined for a stable convergence response from investigation of a time variation in the main steam pressure with a little change of the pressure gain.



$$V_{\text{demand}}(t) = 100 - \frac{P - P_{\text{set}}}{K}$$

$$V(t) = T_1 \frac{dV_d}{dt} - T_2 \frac{dV}{dt}$$

P [MPa] : Turbine Inlet Pressure

P_{set} [MPa] : Set Point of Turbine Inlet Pressure

V [%] : Opening of Main Steam Control Valve

T_1 [s] : Lead Time

T_2 [s] : Lag Time

K [MPa] : Pressure Gain

V_{demand} [%] : Opening Signal of Main Steam Control Valve

Fig. 2.41 Pressure control system

After all control systems are set up, the plant behavior with external disturbances of power, pressure, and flow rate is analyzed using the plant dynamics analysis code until finally stable and fast convergence is confirmed.

[3] Plant startup

Since the plant startup and stability show a slow behavior change over a long time, the balance of plant (BOP) such as the turbine system is included in the calculation model of plant dynamics calculation codes. Figure 2.42 shows an example of the calculation model for a SCWR [28]. The BOP can be modeled as properly describing mass and energy conservation and plant time behavior without a detailed embodiment. The reactor core is represented as a single channel model in the figure, but it can be described by two single channels, i.e. average and hot channels.

The following are models for pressure change in inlet orifice, feedwater pump, feedwater pipe, and outlet valve used in the ex-core circulation system.

$$\text{Orifice Model: } \Delta P = \zeta \frac{\rho u^2}{2}$$

$$\text{Feedwater pump model: } \delta P = C_{\text{pump}} \delta u$$

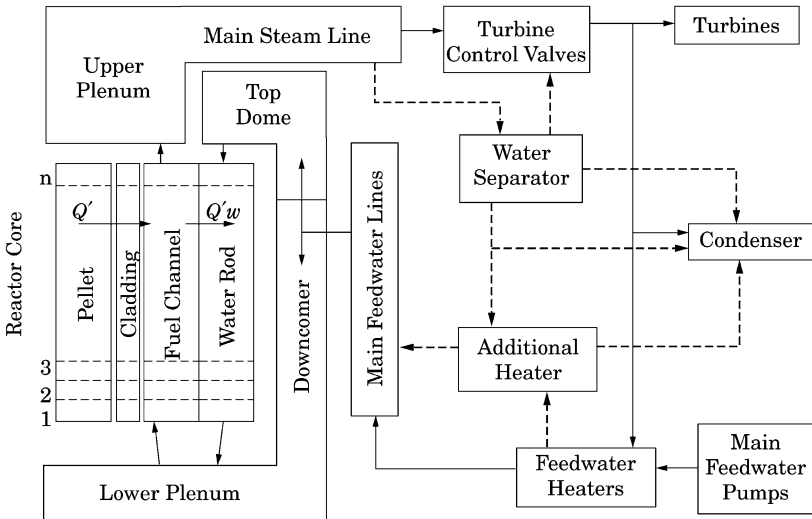


Fig. 2.42 Calculation model for plant startup and stability analysis

$$\text{Feedwater line model: } -\frac{dP}{dz} = \frac{d}{dt} \rho u + \frac{d}{dz} \rho u^2 + \frac{2f}{D} \rho u^2$$

$$\text{Valve model: } \Delta P = \zeta \frac{\rho u^2}{2}$$

P : pressure (Pa)

ΔP : pressure drop (Pa)

δP : pressure change in pump (Pa)

ζ : orifice or valve pressure drop coefficient

ρ : coolant density (kg/cm^3)

u : fluid velocity (m/s)

δu : fluid velocity change in pump

C_{pump} : pressure drop coefficient of pump

z : position (m)

t : time (s)

f : friction pressure drop coefficient

D : diameter of feedwater pipe (m)

The plant startup procedure is established to satisfy constraints at startup using the calculation models above. The constraints at startup depend on reactor type: for example, maximum cladding surface temperature for SCWRs; restrictions in heat flux, various safety parameters, and pump cavitation for LWRs; restrictions of vapor fraction in main steam for direct-cycle reactors. There are also restrictions from thermal stress to temperature rise of the reactor vessel.

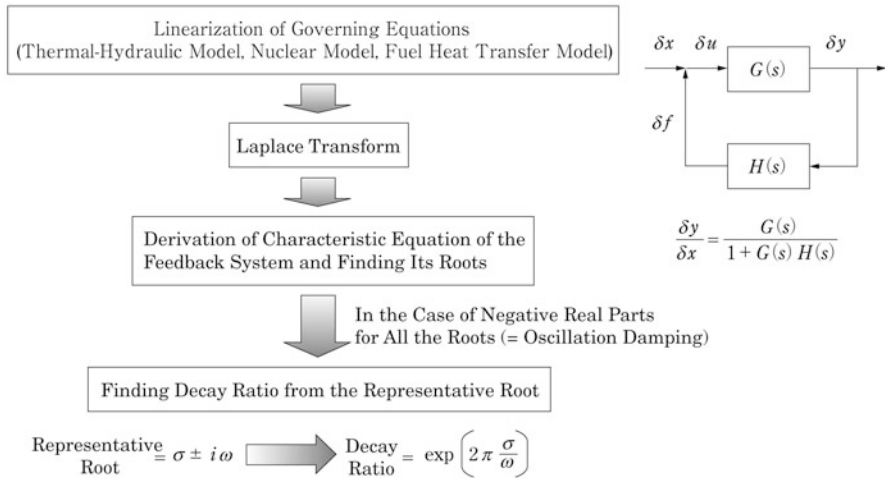


Fig. 2.43 Procedure of linear stability analysis

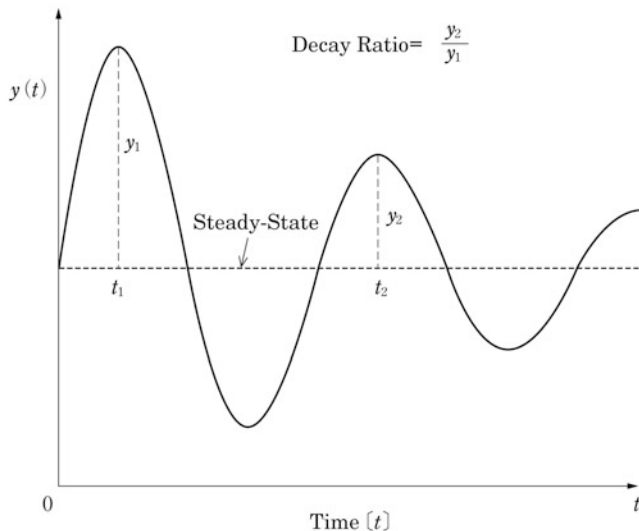
[4] Reactor stability analysis

In the reactor stability analysis, first governing equations are established for normal and perturbed values of state variables from the plant dynamics codes and then the governing equations are linearized for the perturbed one. The equations are converted into a frequency domain by the Laplace transform and analyzed there. This is referred to as *linear stability analysis* and the procedure for it in the frequency domain is shown in Fig. 2.43.

In the figure, the system transfer function (closed-loop transfer function) is defined with the open-loop transfer functions, $G(s)$ and $H(s)$. The system stability is characterized by the poles of the transfer function (the roots of the characteristic equation in its denominator) and described by the decay ratio. The concept and the stability criteria are given in Fig. 2.44. For the system to be stable with damping, all the roots of the characteristic equation must have negative real parts. The decay ratio, which is defined as the ratio of two consecutive peaks of the impulse response of the oscillation for the representative root (the root nearest to the pole axis), depends on the calculation mesh size. The decay ratio is determined by extrapolation to zero mesh size following calculations with different mesh size.

The following should be considered in the stability analysis of nuclear reactor design.

- (i) Channel stability: This is thermal-hydraulic stability of the fuel cooling channel.
- (ii) Core stability: This is the nuclear and thermal-hydraulic coupled stability where the whole core power (neutron flux) regularly oscillates as a fundamental mode due to the moderator density feedback



Examples of Stability Criteria

	Normal Operation	All Operations
Thermal-Hydraulic Stability	Decay Ratio ≤ 0.5	Decay Ratio < 1.0
Core Stability	Decay Ratio ≤ 0.25	Decay Ratio < 1.0

Fig. 2.44 Decay ratio and stability criteria

- (iii) Regional stability: This is a kind of core stability and the neutron flux of each region oscillates as a high-order mode by reciprocally going up and down.
- (iv) Plant stability
- (v) Xenon stability (Xe spatial oscillation): This is a function of accumulation and destruction of FP Xe, and spatial change of neutron flux

The channel stability is thermal-hydraulic stability of single coolant channel in the core. The core stability is the nuclear and thermal-hydraulic coupled stability where the whole core power (neutron flux) regularly oscillates as a fundamental mode due to the moderator density feedback. The regional stability is a kind of core stability and the neutron flux of each region oscillates as a high-order mode by reciprocally going up and down. These three stabilities are inherent characteristics of nuclear reactors with a large change in moderator density in the core such as BWRs, and hence they are evaluated by the frequency-domain stability analysis. The plant stability is the stability of plant system including its control system and is evaluated by time-domain analysis using a plant dynamics analysis code. Xenon spatial oscillation is caused by accumulation and destruction of Xenon-135, and spatial change of neutron flux. The xenon stability is analyzed by the production and destruction equation of Xenon-135.

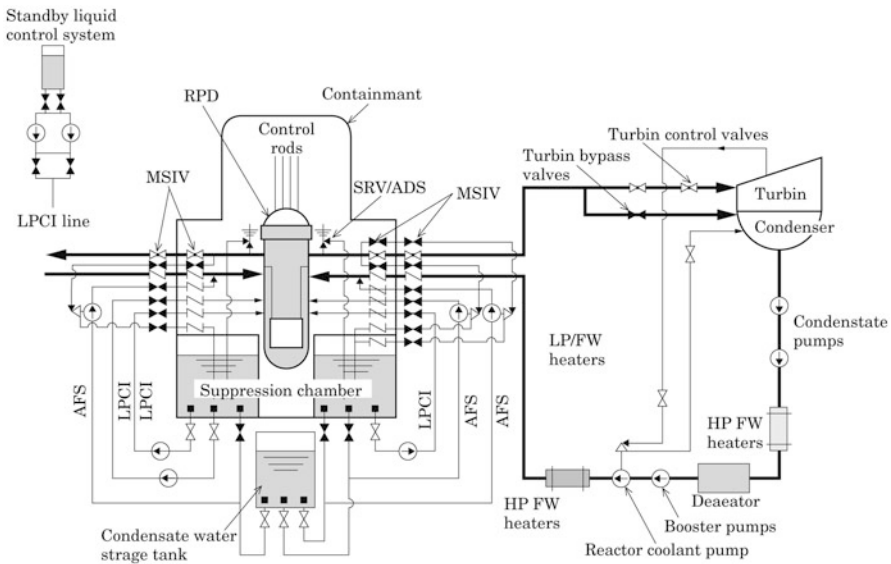


Fig. 2.45 Plant and safety system (SCWR)

2.2.3 Safety Analysis

[1] Analysis of abnormal transients and design based accidents

In the safety analysis of nuclear power plants, safety system models and scenarios of abnormalities are implemented into the plant dynamics calculation code. Abnormal events are classified into abnormal transients and design basis accidents depending on the initial event frequency, namely, high and low frequencies respectively.

For examples, Fig. 2.45 describes the plant system of a SCWR with the safety system and Fig. 2.46 shows the calculation model of its safety analysis code [27, 29].

The SCWR is a direct steam cycle system and its safety system is similar to that of BWRs. Safety relief valves (SRVs) and an automatic depressurization system (ADS) are installed into the main steam lines. Turbine bypass valves are used to dump the main steam to the condenser at a sudden closure of the main steam control valves. This is made in a manner to prevent damage to the turbine from over-rotation by a turbine load loss due to a breakdown of the electric transmission system. The high-pressure auxiliary feedwater system (AFS, high-pressure coolant injection system) is equipped to maintain coolant supply at an abnormal event of the main feedwater system. The low pressure coolant injection (LPCI) system is prepared to flood and cool the core after reactor depressurization at a loss of coolant accident (LOCA). The water is fed from the suppression chamber or condensate water storage tank. The LPCI system also

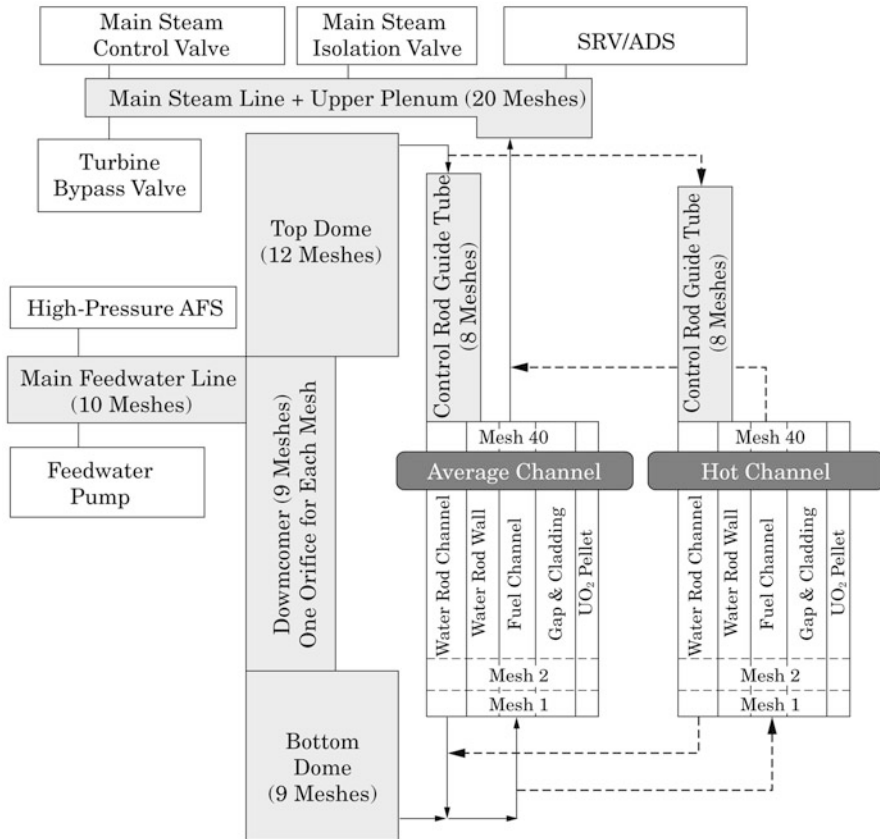


Fig. 2.46 Calculation model for abnormal transient and accident analysis

has the function of residual heat removal (RHR) after reactor shutdown. The boric acid injection system (standby liquid control system, SLC system) is provided for backup shutdown.

Figure 2.46 models main steam control valves (turbine control valves), SRVs, turbine bypass valves, AFS, reactor coolant pump (RCP), and so on. The core is modeled by average and hot channels. Since abnormal events for safety analysis are often relatively short-term ones, heat removal models including the turbine system are not always necessary. The calculation model in the figure does not comprise safety systems for LOCA analysis such as the LPCI. General-purpose safety analysis codes have models to handle those systems.

[2] Loss of coolant accident

LOCA analysis is composed of two parts: blowdown phase and reflood phase. As an example of SCWR, the blowdown analysis model is shown in Fig. 2.47 in which valves and systems able to simulate cold-leg break and hot-leg break are implemented into the abnormal transient and accident analysis model of Fig. 2.46.

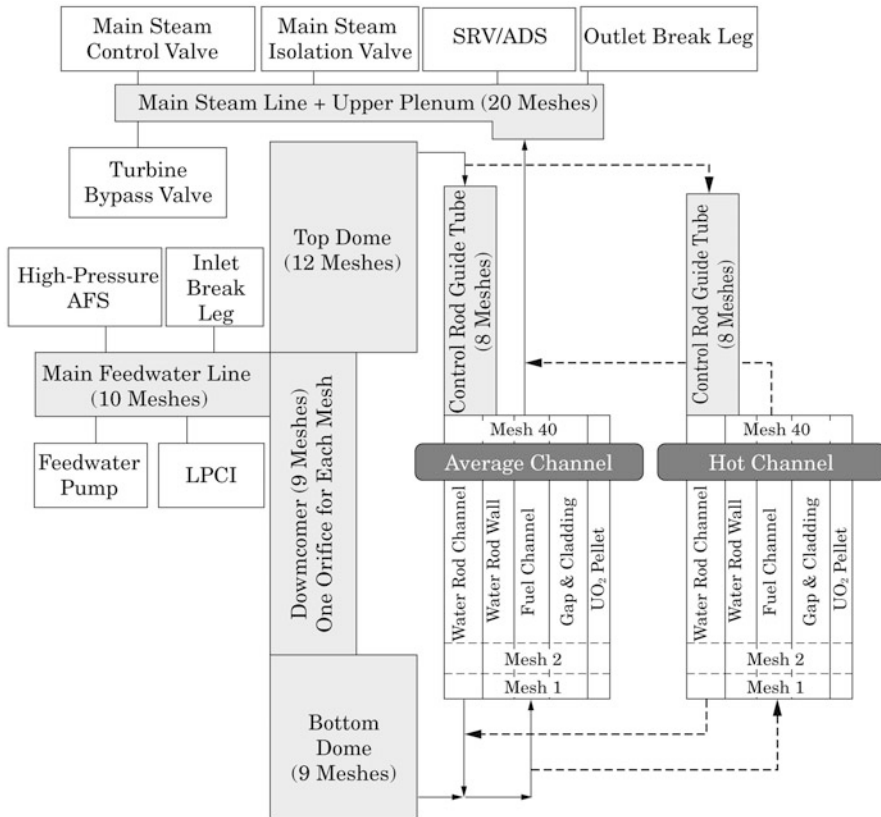


Fig. 2.47 Calculation model for LOCA blowdown analysis

The reflood phase can be analyzed by modeling the LPCI in the calculation code as shown in Fig. 2.48. In the practical analysis of plant safety, general-purpose codes are used to describe more detailed models and to calculate the blowdown and reflood phases as one body.

2.2.4 Fuel Rod Analysis

[1] Fuel rod integrity

The principle role of fuel rod cladding is to confine radioactive FPs and to prevent contamination of the coolant system; therefore an assurance of fuel rod integrity is important for reactor design and safety.

When an abnormal transient event occurs in a nuclear plant with a frequency of more than once during the plant life time, the safety criterion is associated with whether the core can return to the normal operation without core damage

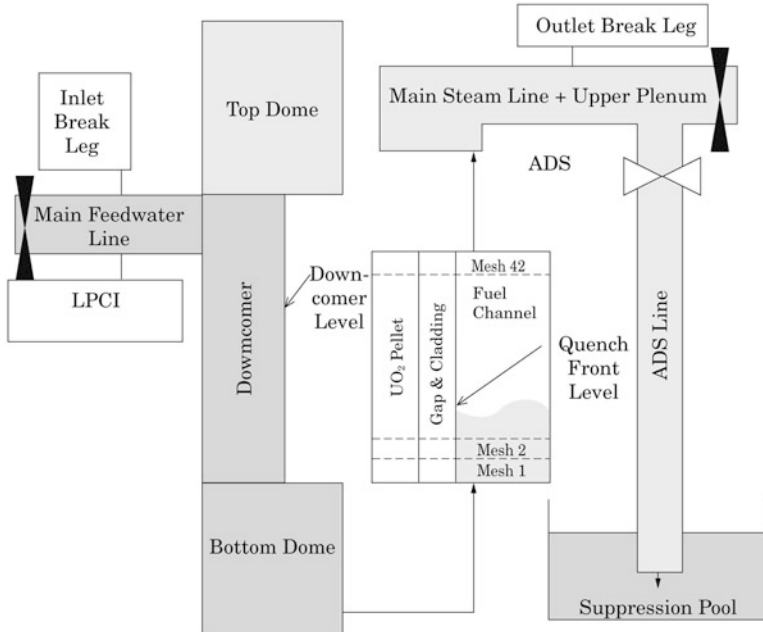


Fig. 2.48 Calculation model for LOCA reflooding analysis

after the plant is stabilized. Thus, fuel rods are required to keep their integrity during abnormal transients (anticipated operational occurrences) as well as normal operation.

The criteria for fuel rod integrity differ somewhat between BWRs and PWRs because of different operating conditions. Fuel rods are designed generally based on the following criteria [25, 27].

- (i) Average circumferential plastic deformation of fuel cladding $< 1\%$
- (ii) Fuel centerline temperature $<$ Pellet melting point (PWR)
- (iii) No overpressure within fuel rod
- (iv) Allowable stress of fuel rod cladding
- (v) Cumulative damage fraction < 1

The overall fuel rod integrity is evaluated further in cladding corrosion and hydriding, pellet cladding interaction (PCI), cladding creep rupture, rod fretting wear, cladding bending, and irradiation growth of the fuel rod and assembly.

The fuel damage criteria and allowable limits of BWRs and PWRs are given in Table 2.2. Based on the system of fuel damage occurrence in BWRs or PWRs, restrictions at normal operation and allowable limits at abnormal transient are determined in the fuel design considering the each following;

- (i) Cladding damage due to overheating resulting from insufficient cooling
- (ii) Cladding damage due to deformation resulting from a relative expansion between pellet and cladding

Table 2.2 Criteria and allowable limits of fuel damage in BWR and PWR

Damage		BWR	PWR
(i) Cladding overheating	Criteria	The fuel cladding integrity ensures that during normal operation and abnormal transients, at least 99.9 % of the fuel rods in the core do not experience transition boiling	The DNB design basis requires at least a 95 % probability, at a 95 % confidence level, that the limiting fuel rods in the core will not experience DNB during normal operation or any transient conditions
	Allowable limits at transient	MCPR: 1.07	MDNBR: 1.30
	Restrictions at normal	MCPR: 1.2–1.3	MDNBR: 1.72
(ii) Cladding deformation	Criteria	The fuel cladding integrity ensures that during normal operation and abnormal transients, the fuel rods in the core do not experience circumferential plastic deformation over 1 % by PCI	The fuel cladding integrity ensures that during normal operation and abnormal transients, the fuel rods in the core do not experience circumferential deformation (elastic, plastic, and creep) over 1 % by PCI
	Allowable limits at transient	Direct evaluation of criteria by experiments	MLHGR: 59.1 kW/m (2,300 °C fuel centerline temperature)
	Restrictions at normal	MLHGR: 44 kW/m	MLHGR: 43.1 kW/m (1,870 °C fuel centerline temperature)

For damage mechanism (i), the BWR criterion is that “the fuel cladding integrity ensures that during normal operation and abnormal transients, at least 99.9 % of the fuel rods in the core do not experience transition boiling”. In PWRs, similarly, the criterion is that “the DNB design basis requires at least a 95 % probability, at a 95 % confidence level, that the limiting fuel rods in the core will not experience DNB during normal operation or any transient conditions”. (DNB means the departure from nucleate boiling.)

Based on those criteria, the BWR design requires the allowable limit of the minimum critical power ratio (MCPR) to be 1.07 at abnormal transients and the restriction to be 1.2–1.3 at normal operation. Similarly, the PWR design has the allowable limit of minimum heat flux ratio (minimum departure from nucleate boiling ratio, MDNBR) to be 1.30 at abnormal transients and the restriction to be 1.72 at normal operation.

For the damage mechanism (ii), the BWR criterion is that “During normal operation and abnormal transients, the fuel rods in the core do not experience circumferential plastic deformation over 1 % by PCI”. In PWRs, similarly, the criterion is that “During normal operation and abnormal transients, the fuel rods

Table 2.3 Fuel rod behavior in FEMAXI-6

	Thermal behavior (temperature dependent)	Mechanical behavior
Pellet	Thermal conduction (radial heat flux distribution)	Thermal expansion, elasticity and plasticity, creep, cracking, initial relocation, densification,
	Fission gas release (temperature and burnup dependent)	swelling (solid FPs and gas bubbles), hot-press
Cladding	Thermal conduction Oxidation film growth	Thermal expansion, elasticity and plasticity, creep, irradiation growth, oxidation film growth
Fuel Rod	Gap thermal conduction (mixed gas, contact, radiation)	PCMI (pellet cladding mechanical interaction), friction, bonding
	Cladding surface heat transfer	
	Gap gas flow	

in the core do not experience circumferential deformation (elastic, plastic, and creep) over 1 % by PCI”.

Central melting of pellets in LWR fuel causes a phase change and a volume increase, and the fuel cladding may be substantially deformed mainly due to pellet cladding mechanical interaction (PCMI). The fuel rod design criteria of PWRs require that the fuel centerline temperature will be lower than the pellet melting point. Hence, the allowable limit of the fuel centerline temperature is determined to be 2,300 °C at abnormal transients and its corresponding maximum linear power density is 59.1 kW/m. The restrictions at normal operation are 1,870 °C for the fuel centerline temperature and 43.1 kW/m of the maximum linear power density.

For internal pressure of fuel rods, the BWR design requires that the cladding stress due to the internal pressure will be less than the allowable strength limit. The PWR design restricts the internal pressure of fuel rods to less than the rated pressure of primary coolant (157 kg/cm²-g) in order to avoid expansion of the gap between pellet and cladding due to creep deformation of cladding outside at normal operation. This phenomenon is called “lift-off”. The criteria of “ASME B&PV Code Sec III” are used as allowable stress limits for LWRs.

[2] Fuel rod behavior calculation

The fuel rod behavior caused by irradiation of fuel pellets and cladding is complicated for investigation in an analytical method. Fuel rod behavior calculation codes were developed from various experiments and operational experiences. FEMAXI-6 [30] as an open code developed in Japan is a general analysis code for fuel rod behavior at normal operation or abnormal transients in LWRs. It constructs a model composed of one fuel pellet, cladding, and internal gas, and then analyzes thermal, mechanical, and chemical behavior and reciprocal action at normal operation or abnormal transients from overall power history data. Table 2.3 shows fuel rod behavior analyzed in FEMAXI-6.

The overall structure of FEMAXI-6 consists of two parts, thermal analysis and mechanical analysis, as shown in Fig. 2.49. The thermal analysis part evaluates radial and axial temperature distributions considering a change in gap size between pellet and cladding, FP gas release models, axial gas flow and

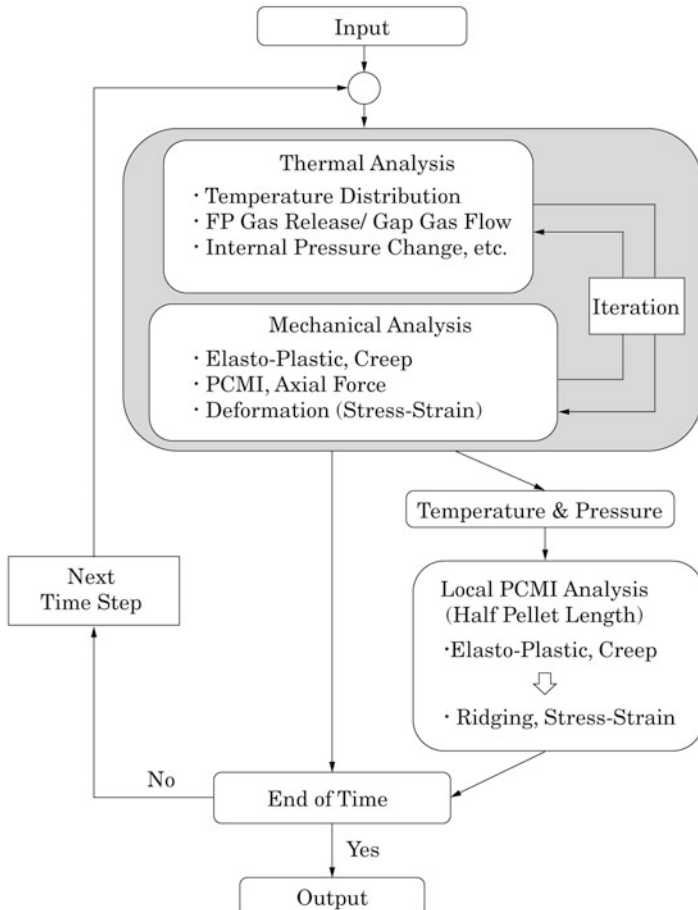


Fig. 2.49 Overview of FEMAXI-6 structure

its feedback to heat transfer in gap, and so on. The mechanical analysis part applies the finite element method (FEM) to the whole fuel rod and analyzes mechanical behavior of fuel pellet and cladding as well as PCMI. It also calculates an initial deformation due to thermal expansion, fuel densification, swelling, and pellet relocation, and then calculates stress and deformation of pellet and cladding considering cracking, elasticity/plasticity, and pellet creep. The thermal and mechanical analysis is iteratively performed to consider the thermal feedback effect on the fuel rod mechanical behavior. Further, the local PCMI can be analyzed by the 2D FEM, based on the calculation results from both analysis parts such as temperature distribution and internal pressure.

Figure 2.50 describes the calculation model of FEMAXI-6. The entire fuel rod is divided axially into several tens of segments and radially into ring elements. For example, the figure shows ten axial and radial divisions in the fuel pellet.

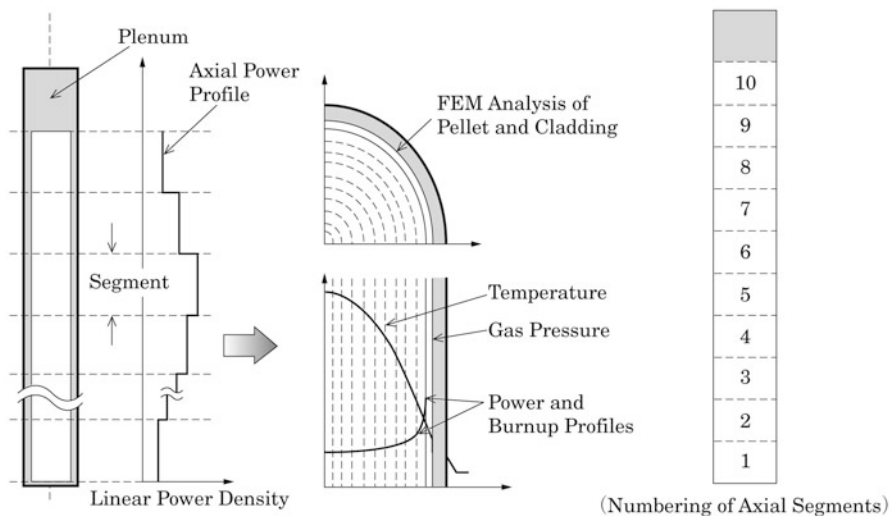


Fig. 2.50 FEMAXI-6 calculation model

FEMAXI-6 contains various calculation models and experimental correlations that users can specify. Details of models, physical properties, or correlations are described in the code manual [30] of FEMAXI-6.

Exercises of Chapter 2

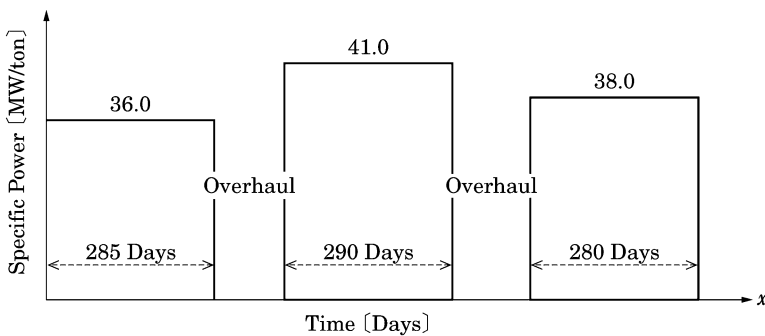
- [1] Consider a PWR UO_2 pellet 0.81 cm in diameter, 1.0 cm in height, and 10.4 g/cm^3 in density in which the uranium is enriched to 3.2 wt. % ^{235}U . Answer the following questions.
- Calculate the atomic number densities of ^{235}U , ^{238}U , and O in the pellet. UO_2 contains only ^{235}U , ^{238}U , and O. Their atomic masses are $M(^{235}\text{U}) = 235.04$, $M(^{238}\text{U}) = 238.05$, and $M(\text{O}) = 16.0$, and Avogadro's number is 0.6022×10^{24} .
 - One-group microscopic cross sections of ^{235}U , ^{238}U , and O are given in the following table.

Nuclide	Absorption σ_a (barn)	Fission σ_f (barn)
^{235}U	50	41
^{238}U	1.00	0.10
O	0.0025	0.00

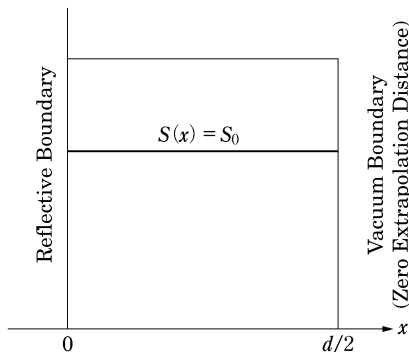
(1 barn = 10^{-24} cm^2)

Compute the macroscopic absorption and fission cross sections of the pellet. What is the probability that a neutron will cause a fission on being absorbed into the pellet?

- (c) Compute the mass (in tons) of metal uranium in one pellet 1.0 cm in height. A PWR fuel assembly consists of 265 fuel rods bundled into a 17×17 array (including 24 guide tubes) with an active height of 366 cm. Compute the initial mass of uranium in one fuel assembly and compute the total loading amount of uranium (the mass of metal uranium) in the core which contains the 193 fuel assemblies.
- (d) Calculate the linear power density (W/cm) of the fuel rod when one-group neutron flux in the pellet is $3.2 \times 10^{14} \text{ n/cm}^2\text{-s}$. The energy released per fission is 200 MeV ($1 \text{ MeV} = 1.602 \times 10^{-13} \text{ J}$). What is the specific power [power per initial mass of metal uranium (MW/ton)]?
- (e) Compute the burnup (MWd/ton) of the pellet consumed along the specific powers as shown in the figure



- (f) Compute the consumed amount of ^{235}U in the pellet from the burnup of (e). Two-thirds of the total power is generated by the uranium (^{235}U and ^{238}U) fission and the rest by the fission of plutonium produced from the conversion of ^{238}U .
- [2] An infinite slab of non-multiplying uniform medium of thickness d ($= 400 \text{ cm}$) contains a uniformly distributed neutron source S_0 as shown in the following figure.



The neutron flux distribution in the slab can be determined by solving the one-group diffusion equation

$$-D \frac{d^2\phi(x)}{dx^2} + \Sigma_a \phi(x) = S_0$$

where $D = 1.0$ cm, $\Sigma_a = 2.5 \times 10^{-4}$ cm $^{-1}$, and $S_0 = 1.0 \times 10^{-3}$ n/cm 2 -s. Discretize one side to the reflective boundary in the middle into four meshes ($N = 4$) and calculate the neutron flux distribution using the finite difference method. Plot the distribution and compare it with the analytical solution

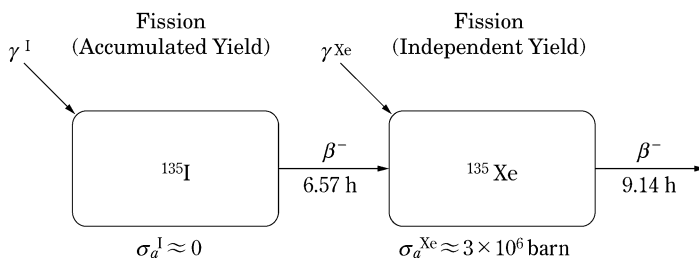
$$\phi(x) = \frac{S_0}{\Sigma_a} \left(1 - \frac{\cosh(\frac{x}{L})}{\cosh(\frac{d}{2L})} \right) \quad \text{where, } L = \sqrt{D/\Sigma_a}$$

Calculate for $N = 8$ and 16 if programming is available.

- [3] (a) Consider a multiplying system with an effective multiplication factor k_{eff} . Develop the diffusion equations for fast and thermal groups in terms of the two-group constant symbols in the following table.

Fast group	Thermal group
χ_1	1.00
ν_1	2.55
$\Sigma_{f, 1}$	2.76×10^{-3}
$\Sigma_{a, 1}$	9.89×10^{-3}
$\Sigma_{1 \rightarrow 2}$	1.97×10^{-2}
D_1	1.42
χ_2	0.00
ν_2	2.44
$\Sigma_{f, 2}$	5.45×10^{-2}
$\Sigma_{a, 2}$	8.20×10^{-2}
$\Sigma_{2 \rightarrow 1}$	0.00
D_2	0.483

- (b) Calculate the infinite multiplication factor k_∞ using the two-group constants.
[4] The burnup chain of ^{135}I and ^{135}Xe is given by the following figure

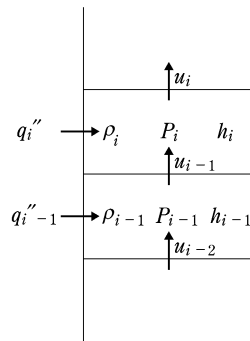


Show that the equilibrium concentration of ^{135}Xe (N_∞^{Xe}) in the reactor operating at a sufficiently high neutron flux is given approximately by

$$N_{\infty}^{Xe} = \frac{(\gamma^I + \gamma^{Xe}) \Sigma_f}{\sigma_a^{Xe}}$$

where γ^I and γ^{Xe} are the fission yields of ^{135}I and ^{135}Xe respectively, and σ_a^{Xe} is the one-group microscopic absorption cross section of ^{135}Xe and Σ_f is the one-group macroscopic fission cross section.

- [5] The energy conservation equation is given by Eq. (2.117) for no water moderation rod. Develop the energy conservation equation when introducing the water moderation rod.
- [6] Develop equations for single-phase transient analysis at the 1D axial node i of a single coolant channel, based on the mass conservation equation [Eq. (2.116)], the energy conservation equation [Eq. (2.117)], the momentum conservation equation [Eq. (2.118)], and the state equation [Eq. (2.119)], referring to the figure.



References

1. Lamarche JR (1966) Introduction to Nuclear Reactor Theory. Addison-Wesley, Reading
2. Shibata K et al (2011) JENDL-4.0: a new library for nuclear science and engineering. J Nucl Sci Tech 48:1
3. Chadwick MB et al (2011) ENDF/B-VII.1 nuclear data for science and technology: cross sections, covariances, fission product yields and decay data. Nucl Data Sheets 112:2887
4. Koning A et al (ed) (2006) The JEFF-3.1 nuclear data library. JEFF report 21, NEA Data Bank
5. Trkov A, Herman M, Brown DA (eds) (2012) ENDF-6 Formats manual, data formats and procedures for the evaluated nuclear data files ENDF/B-VI and ENDF/B-VII. CSEWG Document ENDF-102, BNL-90365-2009 Rev. 2
6. Kobayashi K (1996) Nuclear reactor physics. Korona Press, Tokyo (in Japanese)
7. Okumura K, Kugo T, Kaneko K, Tsuchihashi K (2007) SRAC2006: a comprehensive neutronics calculation code system, JAEA-Data/Code 2007-004. Japan Atomic Energy Agency, Tokai-mura
8. Hazama T, Chiba G, Sato W, Numata K (2009) SLAROM-UF: ultra fine group cell calculation code, JAEA-Review 2009-003. Japan Atomic Energy Agency, Tokai-mura
9. MacFarlane RE, Kahler AC (2010) Methods for processing ENDF/B-VII with NJOY. Nucl Data Sheets 111:2739
10. Cullen DE (2012) PREPRO 2012 2012 ENDF/B pre-processing codes, IAEA-NDS-39. IAEA Nuclear Data Section, Vienna

11. X-5 Monte Carlo Team (2003) MCNP: a general Monte Carlo N-particle transport code, version 5, LA-UR-03-1987
12. Nagaya Y, Okumura K, Mori T, Nakagawa M (2005) MVP/GMVP II: general purpose Monte Carlo codes for neutron and photon transport calculations based on continuous energy and multigroup methods. JAERI 1348. Japan Atomic Energy Research Institute, Tokai-mura
13. Knott D, Yamamoto A (2010) Lattice physics computation. In: Handbook of nuclear engineering, vol 2. Springer, New York, p 913
14. Nuclear Handbook Editorial Committee (2007) Nuclear handbook. Ohmsha Press, Tokyo (in Japanese)
15. Okumura K (2007) COREBN: a core burn-up calculation module for SRAC2006, JAEA-Data/Code 2007-003. Japan Atomic Energy Agency, Tokai-mura
16. Tasaka K (1997) DCHAIN: code for analysis of build-up and decay of nuclides, JAERI 1250. Japan Atomic Energy Research Institute, Tokai-mura (in Japanese)
17. Croff AG (1983) ORIGEN2: a versatile computer code for calculating the nuclide compositions and characteristics of nuclear materials. Nucl Tech 62:335
18. Lawrence RD (1986) Progress in nodal methods for the solution of the neutron diffusion and transport equations. Prog Nucl Energy 17(3):271
19. Expert Research Committee on Improvement in Neutronics Calculation (2001) Status and prospect of improvement in neutronics calculation. Atomic Energy Society of Japan, Tokyo (in Japanese)
20. Greenman G, Smith KS, Henry AF (1979) Recent advances in an analytic nodal method for static and transient reactor analysis. In: Proceedings of the computational methods in nuclear engineering. ANS, Williamsburg, VA, pp 3–49, 23–25 Apr 1979
21. Okumura K (1998) MOSRA-light: high speed three-dimensional nodal diffusion code for vector computers, JAERI-Data/Code 98-025. Japan Atomic Energy Research Institute, Tokai-mura (in Japanese)
22. Ito N, Takeda T (1990) Three-dimensional multigroup diffusion code ANDEX based on nodal method for cartesian geometry. J Nucl Sci Tech 27:350
23. Iwamoto T, Yamamoto M (1999) Advanced nodal methods of the few-group BWR core simulator NEREUS. J Nucl Sci Tech 36:996
24. Argonne Code Center (1977) Benchmark problem book (11. Multi-dimensional (x-y-z) LWR model), ANL-7416, Suppl. 2. Argonne National Laboratory, Illinois
25. Yamaji A (2005) Core and fuel design of the super LWR. Ph.D. Thesis, University of Tokyo (in Japanese)
26. Oka Y et al (2009) Nuclear plant engineering, section 6–2: supercritical water-cooled reactor. Ohmsha Press, Tokyo (in Japanese)
27. Oka Y, Koshizuka S, Ishiwatari Y, Yamaji A (2010) Super light water reactor and super fast reactor. Springer, New York
28. Yi TT (2004) Startup and stability of a high temperature supercritical-pressure light water reactor. Ph.D. Thesis, University of Tokyo
29. Ishiwatari Y (2006) Safety of the super LWR. Ph.D. Thesis, University of Tokyo (in Japanese)
30. Suzuki M, Saitou H (2006) Light water reactor fuel analysis code FEMAXI-6(Ver.1) – Detailed Structure and User's Manual JAEA-Data/Code 2005-003). Japan Atomic Energy Agency, Tokai-mura
31. Oka Y, Suzuki K (2008) Nuclear reactor dynamics and plant control. Ohmsha Press, Tokyo (in Japanese)
32. The Japan Society of Mechanical Engineers (1986) Heat transfer, Rev. 4. The Japan Society of Mechanical Engineers (in Japanese)

Chapter 3

Light Water Reactor Design

Yoshiaki Oka, Sadao Uchikawa, and Katsuo Suzuki

Abstract Summary of development and improvement of light water reactors is described in Sect. 3.1. It is written by Yoshiaki Oka.

Design and management of a boiling water reactor (BWR) core is described in Sect. 3.2. It includes design criteria, design of fuel lattice and assembly, reactivity change with burn-up, control of power distribution and history, future trends in core design, core and fuel management. The author of the section is Sadao Uchikawa.

The core nuclear design of PWR is written in Sect. 3.3. The features of PWR core and basic criteria of PWR core design are presented. The design setup of core, fuel lattice, and fuel assembly follows. Control rods and chemical shim are described in the reactivity characteristics. Power distribution control is explained. In addition, evolution and future trend, core management, and fuel management are shown briefly. This section is written by Katsuo Suzuki.

3.1 Development and Improvement of Light Water Reactors

3.1.1 Pressurized Water Reactors

Pressurized water reactors (PWRs) were originally designed to serve as nuclear submarine power plants and were commercialized to large-sized ones currently in operation. The nuclear propulsion allowed submarines to remain submerged without refueling for far longer than oil-fueled vessels. The Argonne National Laboratory (ANL) of the USA found out in the early research that a small reactor with enriched uranium and pressurized water was available to submarines. The development of a nuclear submarine was triggered by the Westinghouse Corporation (WH) as the contractor of the United States navy in 1949. A land-based prototype nuclear propulsion reactor reached criticality at the National Reactor

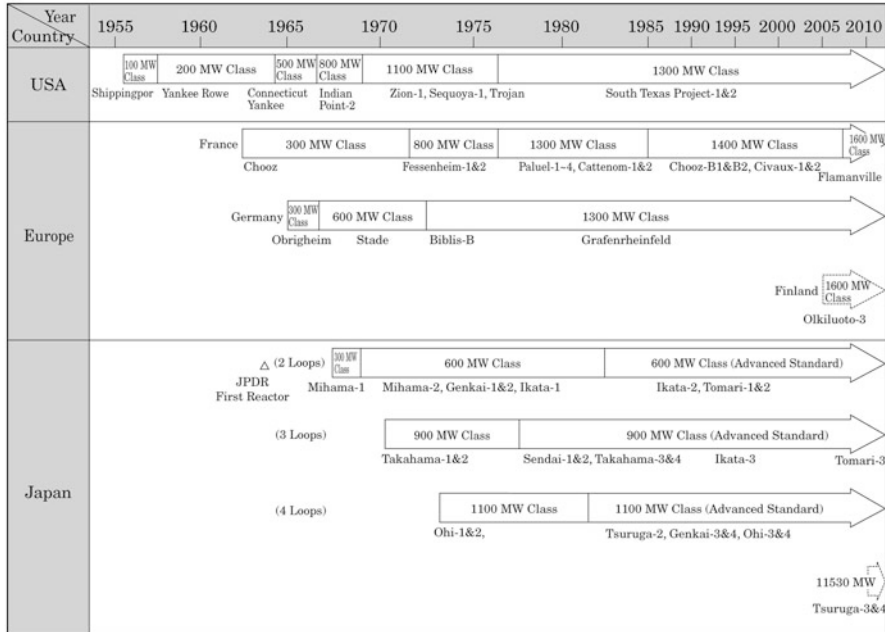


Fig. 3.1 History of PWR [1, 2]

Testing Station (NRTS) in the Idaho desert in 1953. The world's first nuclear-powered submarine, the USS *Nautilus*, was launched in 1955 and accomplished the first undersea voyage to the North Pole in summer, 1958.

The first prototype PWR for electric power generation was *Shippingport Atomic Power Station* built by the Atomic Energy Commission (AEC) and the WH, located near Pittsburgh, USA and operated from December 1957. The electric power was 60 MWe and supplied to the Pittsburgh city.

The first commercial PWR based on the technology, *Yankee Rowe* (185 MWe), began commercial operation in 1961. *Connecticut Yankee* (575 MWe) was ordered in 1963 and *San Onofre* (600 MWe) followed. In Japan, *Mihama* Unit 1 of the Kansai Electric Power Company started operation as the first Japanese PWR in 1970. The WH also developed a 20 MW-Saxton test reactor and applied to improvement in PWR.

The history of PWR technology is summarized in Fig. 3.1 and Table 3.1. For a higher power PWR, a scheme was devised in which the number of primary coolant loops increases as the power class was upgraded without increasing the capacity of the primary coolant pumps or steam generators: two loops for 600 MWe class, three loops for 800–900 MWe class, and four loops for 1,100 MWe class. Yankee Rowe reactor had a cruciform type control rod design which was inserted between fuel assemblies. Since Connecticut Yankee reactor, however, the current cluster type design for control rods has been employed in PWRs worldwide. Stainless steel was

Table 3.1 History of PWR specifications [1, 2]

Plant class	100–400 MW class			500–600 MW class			800–900 MW class			1,100–1,200 MW class			1,300 MW class			1,600 MW class		
	Yankee	Mihama-1	Connecticut Yankee	Mihama-2	Indian Point-2	Takahama-1	Sendai-1 Advanced Standard	Zion-1	Ohi-1	Tsung-a-2 Advanced Standard	South Texas project-1	APWR	EPR					
Construction/operation start year	1958/ 1961	1967/ 1970	1964/ 1968	1968/ 1972	1966/ 1974	1970/ 1974	1979/ 1984	1972/ 1973	1982/ 1987	1975/ 1987	(2010)/ (2016)	2005/ (2012)						
Power (MW)	186	340	606	500	906	826	890	1,085	1,175	1,160	1,312	1,530	1,600					
Fuel assembly type	(6 × 6) × 9	14 × 14	15 × 15	14 × 14	15 × 15	15 × 15	17 × 17	15 × 15	17 × 17	17 × 17	17 × 17	17 × 17	17 × 17					
Average core power density (kW/l)	93	71	82	84	85	92	100	105	105	105	99	103						
Primary coolant pump [gpm]	Canned type 63 Capacity 23,700	Canned type 93A Capacity 70,000	67,200	89,000	93A 89,000	93A 89,000	93A 89,000	93A 89,000	93A 89,000	93A-1 89,000	93A-1 89,000	100	100A					
Steam generator heat transfer area [ft ²]	CE 35,870	CE 27,700	44	44	51	51F 51,500	51	51	51FA 51,500	E 51,500	E 51,500	70F-1 67,000	70F-1 65,000					
No. of loops	4	2	4	2	4	3	3	4	4	4	4	4	4					
Containment vessel steel	Spherical steel	Dry steel self-supported type	PCCV	Dry steel self-supported type	RCCV	Dry steel self-supported type	PCCV	Dry steel self-supported type	PCCV	Ice-condenser type	PCCV	RCCV	PCCV					

PCCV prestressed concrete containment vessel, RCCV reinforced concrete containment vessel

used as fuel cladding material in the beginning and then zirconium alloy was developed and it is still used today. Fuel rods were made thinner in diameter and subsequently a larger number of fuel rods can be loaded into fuel assemblies. Improvements for achieving high burnup are still in progress by further decreasing the fuel rod load.

The PWRs developed by the WH were introduced and improved in France and Germany (former West Germany). In the USA, the Babcock & Wilcox Corporation (B&W) and the Combustion Engineering Corporation (CE) also developed and built PWR design power plants. The CE-PWR design is similar to the WH-PWR one, but it has two steam generators even in a large class reactor. PWRs in Korea were based on the CE-PWR design. The PWR design developed in Russia, referred to as the *VVER*, features a hexagonal lattice fuel assembly, a hollow fuel, and a horizontal steam generator, and so on. China proceeds in parallel to independent PWR development based on the WH-PWR design and PWR construction by foreign companies from France and Russia.

3.1.2 Boiling Water Reactors

The *Boiling water reactor* (BWR) concept was originally developed based on an early collaborative research between the General Electric Company (GE) and the ANL, and a series of the nuclear reactor experiments called the BORAX experiments. The first prototype BWR for electric power generation was *Dresden* Unit 1 (180 MWe) constructed near Chicago in 1960. The reactor was characterized by a dual cycle design of both direct and indirect cycles. After that, a forced circulation type of a single direct cycle has been used as a standard BWR design. The full-scale commercial BWR power plants began with *Oyster Creek* (650 MWe) which started operation in 1963. The GE also built a test reactor, *Vallectios* BWR (VBWR), in 1957 and used it in various improvements of BWR.

The first electricity from nuclear energy in Japan was generated by a 12.5 MWe-BWR, *Japan Power Demonstration Reactor* (JPDR), at the Japan Atomic Energy Institute (JAERI) in 1963. Later, the commercial BWRs started operation with *Tsuruga* Unit 1 (357 MWe) of the Japan Atomic Power Company in 1969 and *Fukushima Daiichi* Unit 1 (460 MWe) of the Tokyo Electric Power Company in 1970.

The history of BWR technology is summarized in Fig. 3.2 and Table 3.2. The main research and development of the BORAX series is shown in Table 3.3. In addition to USA and Japan, commercial BWRs are operated in Sweden, Germany, Mexico, India, etc.

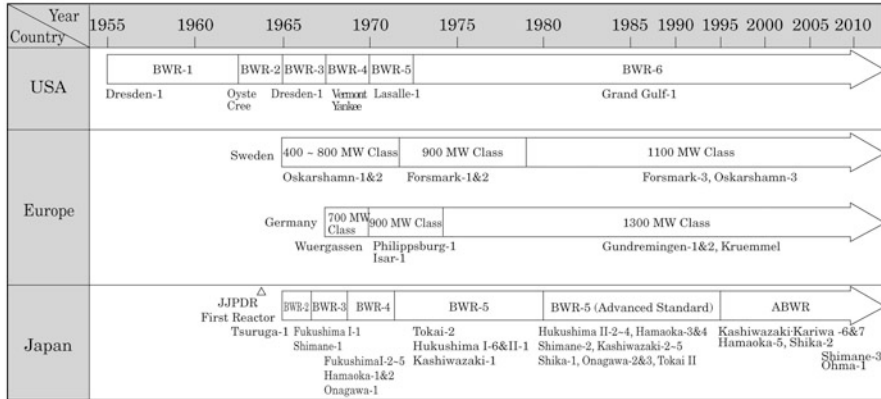


Fig. 3.2 History of BWR [1, 2]

3.2 BWR Core Design and Core and Fuel Management

3.2.1 General Core Design

[1] Features of BWR core [3]

BWRs operate in a *direct cycle* in which the steam formed in the core goes directly to turbines to generate electricity. A big difference from other type reactor cores is that there is a distribution of moderator density within the BWR core because the neutron moderator, as coolant, is boiling as it flows through the core which leads to two-phase flow.

Figure 3.3 shows a BWR core cross-sectional view and structures. There are some distinctive features to BWR core structures. One is the set of a cruciform control rod and four surrounding assemblies; the sets are regularly arranged in the core. Another feature is that the control rod and fuel assemblies are mutually separated by channel boxes wrapping each fuel assembly, in which fuel rods and water rods are tied in an array of, for example, 8×8 or 9×9 , by spacers. A third feature is that the coolant flow path in the core is divided by the channel boxes and each fuel assembly makes a coolant flow path. There is a water gap region, in which water does not boil, between adjacent fuel assemblies. The coolant flowing in from the core bottom comes to boiling and then a two-phase flow of water and steam is produced due to heat from the fuel rods within the fuel assemblies isolated by the channel boxes, but coolant is maintained in the non-boiling state outside the assemblies.

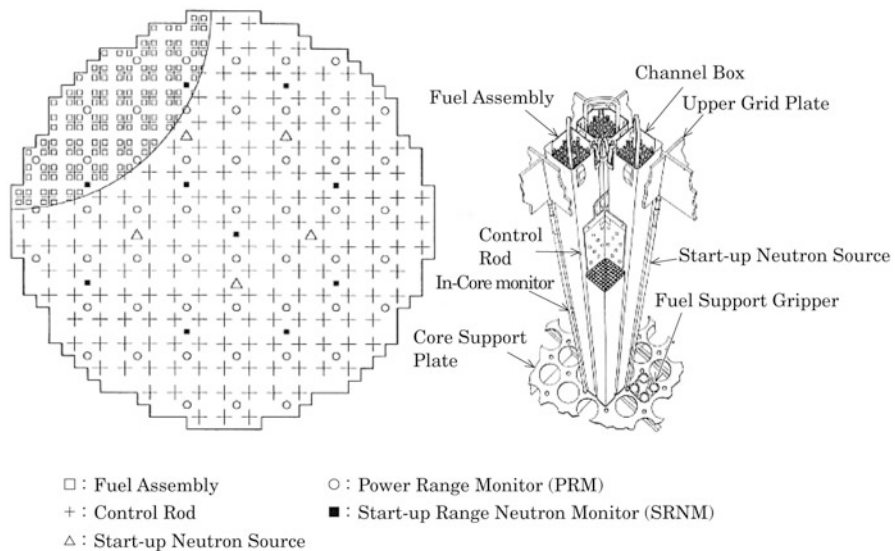
Those features of BWR core structures make it possible to improve or modify the intra-assembly design such as fuel rod size and array without changing specifications concerning the whole core construction such as control rod arrangement and fuel assembly shape.

Table 3.2 History of BWR Specifications [1, 2]

Type	BWR-1	BWR-2	BWR-3	BWR-4	BWR-5	BWR-6	ABWR
Construction/ operation start year	USA 1956/1960 Japan □	1964/1969 1966/1970	1966/1970 1966/1971	1967/1974 1969/1974	1973/1982 1973/1978	□ 1979/1984	1974/1985 1991/1996
Plant example [Power, MWe]	USA Dresden-1 (180) Japan □	Oyster Creek (636) Tsuruga-1 (350)	Dresden-2 (850) Fukushima I-2 I-1 (460)	Browns Ferry-1 (1155) Lasalle-1 (1138) Tokai-2 (1100) (780)	□ Fukushima II-2 (110)	Grand Gulf-1 (1266)	Kashiwazaki Kariwa-6 (1350)
Features	First commer- cial power plant	Forced circulation Type of single direct cycle	Improvement in power density	Recirculation flow rate control by valves or M.G. set	Improvement in operation per- formance	Improvement in power	Internal pumps Advanced control ele- ment drive mecha- nism RCCV
Fuel assembly type	6 × 6	7 × 7	7 × 7	7 × 7	8 × 8	8 × 8	9 × 9
Average core power density [kW/l]	31	34	41	51	51	~54	51
Forced circulation type of core coolant	External loops(3~5 loops) External recirculation pump	External loops (2 loops) External recirculation pump + jet pump	External recirculation pump	External recirculation pump + 5-nozzle jet pump	External recirculation pump	MARK-II advanced (Cone type) MARK-II (Cone type) MARK-II	MARK-II (Cylinder type)
Containment vessel	Dry spherical type						RCCV MARK-II

Table 3.3 BORAX and early test BWRs

Test reactor	Research and development
BORAX-I	Verification of inherent safety and power excursion
BORAX-II	Research on pressurization and instability
BORAX-III	Electricity generation test
BORAX-IV	Examination on UO_2 fuel use, stability, water radiolysis, and turbine radioactivity
BORAX-V	Examination on high power density core and nuclear superheat
EBWR (ANL, 5 MWe)	Power test and trouble experience
VWBR (GE)	Economical improvement test, natural/forced circulation, direct/indirect cycle, material test, etc.

**Fig. 3.3** BWR core cross-sectional view and structures

[2] Basic criteria of core design

The main targets of the reactor core design are to reduce electricity generation costs and secure reactor safety. Core performance targets are established to realize the main targets. Improvement in power density and fuel burnup, reduction in necessary uranium resources, and extension of continuous operating period are all related to the reduction in electricity generation costs. Security of negative power coefficient and reactor shutdown capability, and prevention of fuel failure are required from the viewpoint of reactor safety. Table 3.4 introduces the basic criteria [4, 5] to be considered in the BWR core design based on its features.

Table 3.4 Main criteria of BWR core design [4, 5]

Design criteria		Allowable limits or operation criteria
Self-controllability	Designed to assure the inherent negative reactivity feedback characteristics (negative power coefficients) in the power operating range	Negative void reactivity coefficients
Reactor shutdown	Designed to assure the complete core shutdown capability even with the most reactive rod stuck in the fully withdrawn position	One stuck rod margin: $\geq 0.01 \Delta k$
	Designed with appropriate limits of any single-control rod worth and of the control rod speed to secure the core safety against accidental withdrawal of control rods	Maximum control rod worth: $\leq \sim 0.015 \Delta k$
Fuel failure prevention	Designed to assure that at least 99.9 % of the fuel rods in the core would not be expected to experience boiling transition	MCPR: ≥ 1.07 at transient 1.2–1.3 at normal
	Designed to assure that the plastic circumferential deformation of fuel rod cladding due to pellet cladding interaction (PCI) would not be expected to exceed 1 %	Allowable limit at transient: design criteria Restriction at normal: $MLHGR \leq 44.0 \text{ kW/m}$
Stability	Designed to secure the stability without the flow-induced vibration (thermal-hydraulic stability of channel)	Allowable limit: decay ratio < 1.0
	Designed to secure the stability without the power oscillation. (core stability and regional stability)	Allowable limit: decay ratio < 1.0 Design criterion at normal: decay ratio < 0.25
	Designed to secure the stability with enough plant controllability (plant stability)	Allowable limit: decay ratio < 0.25
	Designed to secure the stability without the spatial oscillation of power distribution due to Xe accumulation (Xe stability)	Sufficient power coefficients

(1) Sufficient negative power coefficients

The inherent safety by which an increase in reactor power leads to a decrease in reactivity is required to work automatically against a reactor power rise. As reactivity feedback characteristics to determine self-controllability of the reactor core, there are: Doppler feedback which is concerned with an increase in neutron resonance absorption due to fuel temperature rise; void feedback which is concerned with a reduction in neutron moderation effect due to coolant boiling; and moderator temperature feedback which is concerned with a decrease in moderator density due to moderator temperature rise. BWRs, in which water (serving both as moderator and coolant) boils to become steam to drive the turbines, are designed to have a negative void reactivity coefficient which indicates the reactivity change due to a change in void fraction (volume fraction of steam in coolant). In other words, the reactivity decreases and the power falls when the void fraction increases due to increase of reactor power and

decrease of core flow rate. It is the most important essential characteristic for the reactivity control of BWR. The negative void reactivity coefficient is also utilized to control the reactor power by adjusting the core flow rate.

(2) Proper reactor shutdown margin

To shutdown a nuclear reactor by insertion of control rods, it is necessary to have a reactor shutdown margin which leads to subcriticality (e.g., $\geq 1.0\% \Delta k/k$) with the exception of the most reactive control rod being stuck in the full-out position from the core (one rod stuck). For the reactor shutdown margin, burnable poison is partially mixed with fuel pellets to suppress the initial reactivity of fuel, and as well, a sufficient control rod worth is secured. The excess reactivity of core is restrained and controlled by both the control rods and burnable poison.

The worth per control rod is restricted below a constant value to secure safety against accidental withdrawal of control rods. The maximum reactivity insertion rate due to withdrawal of control rods is also limited to supervise and control the withdrawal safely.

(3) Fuel failure prevention

From the viewpoint of fuel integrity during reactor operation, the following two mechanisms are considered in fuel rod design as a mechanism of fuel failure and the design criteria and limit values are set for each.

(i) Cladding damage due to overheating resulting from insufficient cooling

For fuel failure prevention, BWRs are designed to assure that at least 99.9 % of the fuel rods in the core would not be expected to experience boiling transition during normal operation and abnormal transients. As a performance indicator of the design criterion, *critical power ratio* (CPR) is defined as the ratio between the critical power at a boiling transition in the thermally severest location of a fuel assembly, and the assembly power at normal operation. Fuel rods are designed to have a larger CPR than the *minimum critical power ratio* (MCPR) even at abnormal transients causing a change in coolant flow rate and reactor power (e.g., $MCPR \geq 1.07$). In normal operation, MCPR is restricted to a higher value (e.g., 1.2–1.3), so that it does not reach the limit in abnormal transients considering that MCPR falls in the abnormal transients. Since MCPR strongly depends on the radial power peaking of core, the radial power distribution should be flattened to place MCPR beyond the restriction.

(ii) Cladding damage due to deformation resulting from a relative expansion between pellet and cladding

Gaseous FPs are released into the gap between pellet and cladding with fuel burnup, and then accumulated in the gas plenum, which causes an internal pressure rise of the cladding. Pellet swelling causes pellet-cladding contact, and stress to the cladding. In abnormal transients, the

stress will increase with a temperature rise since the thermal expansion rate of zircaloy in cladding is smaller than that of UO₂ pellets.

Based on these phenomena, BWRs are designed to assure that the plastic circumferential deformation of cladding due to *pellet-clad interaction* (PCI) will not be expected to exceed 1 % at abnormal transients. In normal operation, there is a restriction on maximum linear heat generation rate (e.g., 44 kW/m) to restrain PCI.

In addition, an allowable maximum burnup of fuel assemblies is set based on operating experiences and irradiation tests. The core and fuel rod design and the core management are done so that the burnup limit is not exceeded.

(4) Stability against perturbations

Nuclear reactors and their related systems have to be operated stably against various perturbations. Fluctuations in reactor power due to fluid flow characteristics and reactivity feedback, or some factors related to characteristics of reactor control systems can obstruct stable operation of the reactors. Returning to the original stable state is essential against those perturbations. As kinds of stability required in BWR core design, there are channel stability (thermal-hydraulic stability) against flow vibration caused by a pressure drop feedback in the flow path, core and regional stability against power oscillation caused by the nuclear feedback of thermal-hydraulic properties and void reactivity, plant stability for sufficiently stable control of plants, and Xe stability (Xe spatial oscillation stability) against power oscillation caused by the accumulation and destruction of FP Xe. The channel stability, core stability, and regional stability are particularly important for BWRs with a large variation in coolant density in the core.

As an indicator of stability evaluation, the *decay ratio*, which is defined as the ratio between the initial and the next oscillation amplitudes, characterizes the extent of oscillation amplitude of a watched parameter by a perturbation. The fundamental design criterion is decay ratio <1 for channel stability, core stability, regional stability, and plant stability in all reactor operating conditions. A decay ratio less than 1 (e.g., 0.25) is set for core stability and plant stability during normal operation for a margin to the design criterion.

Characteristics such as pressure drop in the core flow path and void reactivity feedback have a large effect on the above stabilities. Overall, the stability against perturbations can be secured by setting these characteristics as a fixed range. The Xe spatial oscillation can be suppressed by designing a negative power coefficient less than a fixed value.

In relation to the mechanical design of reactor core elements other than the main criteria of the BWR core design mentioned above, the endurance of core structure materials is necessary against high-level radiation doses and high temperatures and pressures. The reactor pressure vessel should

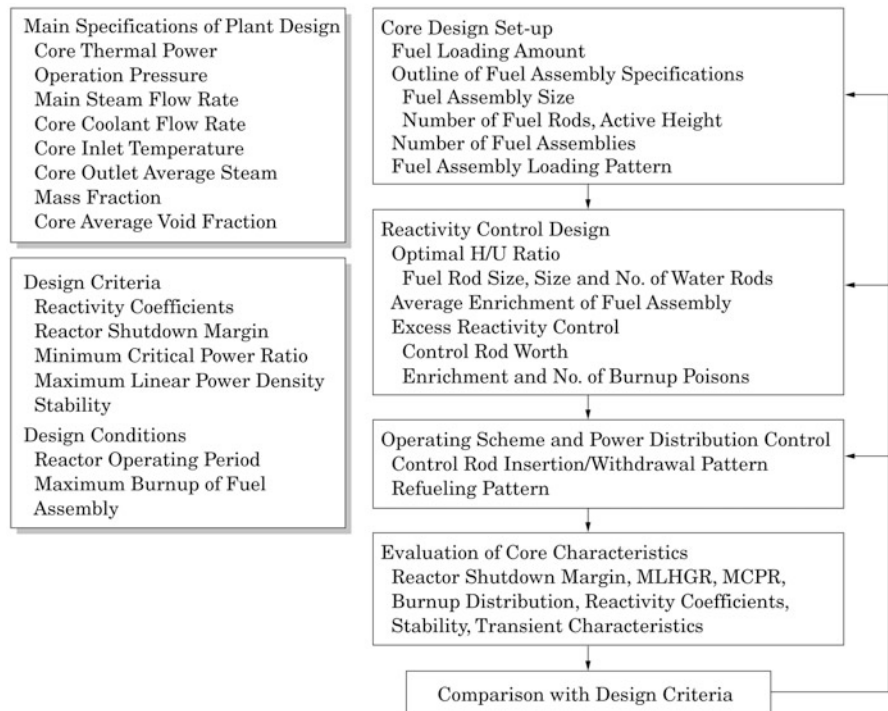


Fig. 3.4 Procedure of BWR core design

also be able to withstand high pressures, high temperatures and radiation doses during the reactor operating period (e.g., 30–60 years). Mechanical design criteria are set for the reactor core elements.

[3] Core design procedure

Figure 3.4 shows the procedure followed in BWR core design. The fundamental specifications of a power plant such as reactor thermal power and operating pressure, and the main specifications of the core design such as shapes and numbers of fuel assemblies are established in the first step of the core design (Table 3.5). Next, the fuel rod design for a reactor operating period and a target fuel burnup is performed regarding fuel rod size and fuel enrichment, and the scheme of excess reactivity control is specified. The detailed design of fuel assemblies is determined based on the fuel rod design and the excess reactivity control scheme. Then, the fuel loading and refueling pattern is treated considering power and burnup distributions, and an outline of the control rod insertion and withdrawal pattern during reactor operation is framed for reactivity and power distribution control. Core characteristics are evaluated for the reactor core, fuel assembly, and operating scheme mentioned above by using various nuclear and thermal-hydraulic coupled core analyses. This sequence of steps is repeated to determine core specifications which meet the core design criteria and target.

Table 3.5 Main design specifications of BWR (1,350 MWe-class ABWR)

Reactor thermal power	3,926 MWth	
Reactor pressure (at RPV dome)	7.17 MPa (73.1 kg/cm ² a)	
Steam flow rate	7.64 × 10 ³ t/h	
Steam pressure	7.17 MPa (73.1 kg/cm ² a)	
Steam temperature	287 °C	
Core	Active height	3.71 m
	Equivalent diameter	5.16 m
	Core flow rate	~52.2 × 10 ³ t/h
	Core inlet subcooling	~54.2 kJ/kg
	Core outlet average steam mass	~14.5 %
	Core power density	~50.6 kW/l
Fuel	Specific power	~26.2 MWth/tU
	Fuel loading amount	~150 tU
	No. of fuel assemblies	872

3.2.2 Core Design Set-Up [3]

As mentioned before, BWRs have the feature that the sets of a cruciform control rod and four surrounding assemblies are regularly arranged in the core. In the case of no large change in dimensions of fuel assemblies and fuel rods, the main investigation point in core design set-up is to determine how many fuel assemblies to load. When altering the dimensions of fuel assemblies or fuel rods in order to improve the core performance, it is important to investigate the relationships of each design parameter to the core performance and to other design parameters.

[1] Fuel inventory

Technical terms and their definitions [7] concerning fuel loading amount in core are as follows.

- (i) *Fuel inventory (W)*: total mass amount of fissionable materials in reactor core [kg or ton].
- (ii) *Specific power (P_s)*: the thermal power produced per unit fuel inventory [kW/kg or MW/t].
- (iii) *Fuel discharge burnup (B_d)*: the total energy produced per unit mass of initial fuel until the fuel materials are discharged from the core [MWd/t]; there is a restriction from the viewpoint of mechanical design of fuel.
- (iv) *Operating cycle length (D)*: the length of the cycle of continuous operation after refueling [days or months].
- (v) *Fuel batch size (n)*: the reciprocal of the discharged fuel fraction in one refueling.

For a reactor thermal power of Q , the fuel batch size n and the specific power P_s are given by Eqs. (3.1) and (3.2).

$$n = B_d / (Q \times D / W) = B_d / (P_s \times D) \quad (3.1)$$

$$P_s = Q/W = B_d / (n \times D) \quad (3.2)$$

The fuel batch size is deeply related to the fuel economy. A large batch size leads to a small number of fuel assemblies to be discharged in refueling. The fuel assemblies remain in the core for a long period and reach a high burnup. Therefore, the fuel cycle cost is reduced. On the other hand, a small batch size shortens the burning period of fuel assemblies in the core and leads to a low burnup. Hence, the fuel cycle cost is increased. The typical batch size of BWRs is about 4, namely, about one of four fuel assemblies is discharged and replaced in one refueling.

If a small amount of fuel is loaded in the core, that is, if a high specific power is intended, the fuel batch size becomes small. For a given fuel discharge burnup and operating cycle length, it is necessary to set the specific power so that the fuel batch size does not become extremely small. Since the specific power is equivalent to the measure of energy produced per unit volume of pellets, it is related to the linear heat generation rate of fuel rods and the heat flux density on the fuel rod surface as well. Therefore, the specific power is designed considering fuel integrity and coolant heat removal.

Based on the discussions above, the specific power of a BWR is set roughly as 25 kW/kgU as a criterion. The specific power and fuel batch size are important indicators in estimating the fuel inventory for a given reactor power or in evaluating the validity of the fuel inventory estimated from the specifications of fuel rods and assemblies.

[2] Specifications of fuel assembly and rod (number and size)

The fuel inventory (W) can be given by

$$W = \rho_p \times N_B \times N_{rod} \times L_{rod} \times \pi (D_p/2)^2 \quad (3.3)$$

where N_B is the number of fuel assemblies, N_{rod} is the number of fuel rods per fuel assembly, L_{rod} is the active height of fuel rod (= active core height), and D_p and ρ_p are diameter and density of the fuel pellet, respectively. The fuel rod diameter D_{rod} is determined from the pellet diameter D_p , cladding thickness, and gap between cladding and pellet. The core volume V_{core} and the equivalent core diameter D_{core} can be calculated by

$$V_{core} = N_B \times L_B \times L_B \times L_{rod} \quad (3.4)$$

$$D_{core} = 2 \times (N_B \times L_B \times L_B / \pi)^{1/2} \quad (3.5)$$

where L_B is the fuel assembly pitch.

For a constant fuel inventory in the core, a long active core height L_{rod} reduces the number of fuel assemblies N_B . This is desirable from the viewpoint of fuel management, but not from the viewpoints of nuclear and thermal-hydraulic design and mechanical design of fuel. A low neutron leakage leads to an effective usage of neutrons and enhances the efficiency from the

viewpoint of nuclear design. It is desirable that the surface area of the core is small, namely, the ratio between the active height and equivalent diameter of the core L_{rod}/D_{core} is close to 1.0. From the viewpoint of thermal-hydraulic design, a long fuel rod causes a high pressure drop in the fuel assembly and has an effect on the primary coolant pump design. Since it also increases the buoyancy of the fuel assembly, a design consideration is needed so that it does not rise. From the viewpoint of mechanical design, a long fuel rod is easily bent and therefore that influences the fuel loading characteristics. The typical design has about 4 m core height and about 3.6–3.7 m active height of the fuel assembly including fissionable materials.

A large-sized fuel assembly reduces the number of fuel assemblies to be replaced in refueling and that leads to an improvement in reactor capacity factor. It is desirable to make the factor large to the extent possible. From the safety viewpoint for handling fuel assemblies outside the core, however, the fuel assembly cannot be sized too large. The fuel assembly is required to maintain subcriticality, even if it is flooded in fresh water, for which the fuel enrichment is an important parameter. The fuel enrichment of 5 % is considered as an upper limit and its corresponding fuel assembly size is limited to about 220 mm when not considering the burnable poison effect on reactivity control. The practical size of fuel assembly is about 135 mm.

[3] Power peaking factor

To set the main specifications such as numbers of fuel assemblies and rods, and fuel rod size, the design parameters referred to as *power peaking factors* are defined, and roughly investigation is made that the maximum linear heat generation rate and assembly power which fuel rods experience during reactor operation satisfy the thermal design conditions.

(i) *Radial power peaking factor* F_R = ratio between the maximum and average values of fuel assembly - averaged power in the core (3.6)

(ii) *Axial power peaking factor* F_Z = ratio between the maximum and average values of fuel assembly cross section - averaged power in the axial direction (3.7)

(iii) *Local power peaking factor* F_L = ratio between the maximum and average values of fuel rod - averaged power in the fuel assembly (3.8)

(iv) *Total power peaking factor* F_P = ratio between the maximum and average values of local power in the core

$$\doteq F_R \times F_Z \times F_L \quad (3.9)$$

Table 3.6 shows examples of the power peaking factors which are evaluated by detailed design calculations in the step when reactor specifications and operating conditions are determined. However, generally the factors are set based on the design and operating experiences and then investigate them.

Table 3.6 Examples of power peaking factors in design of power distribution

	1,100 MWe-Class BWR [6]	1,350 MWe-Class BWR [5]
Radial power peaking factor	1.40	1.40
Axial power peaking factor	1.40	1.40
Local power peaking factor	1.24	(1.19) ^a
Total power peaking factor	(2.43) ^a	2.33

^aPresumption values from the references

Using the power peaking factors above, the average fuel rod linear heat generation rate (power per unit length of fuel rod) q_{ave} , the maximum linear heat generation rate q_{max} , the average fuel assembly power P_{Bave} , and the maximum power P_{Bmax} can be given by the following equations.

$$q_{ave} = Q / (N_B \times N_{rod} \times L_{rod}) \quad (3.10)$$

$$q_{max} = F_p \times q_{ave} \quad (3.11)$$

$$P_{Bave} = Q / N_B \quad (3.12)$$

$$P_{Bmax} = F_R \times P_{Bave} \quad (3.13)$$

The maximum linear heat generation rate q_{max} is the dominant factor in the thermal and mechanical integrity of fuel such as the maximum fuel temperature and the maximum heat flux on the fuel rod surface. A low value of q_{max} is desirable to secure the reactor safety. In order to decrease q_{max} , the following measures can be considered.

- (i) Flatten the power distribution in consideration of enrichment zoning in the fuel assembly or fuel loading pattern so as to reduce the power peaking factor.
- (ii) Reduce the fuel rod diameter D_{rod} and change the fuel rod array (8×8 , 9×9 , or 10×10) so as to increase the number of fuel rods per fuel assembly.
- (iii) Increase the number of fuel assemblies.
- (iv) Lengthen the active height of fuel rods.

Since (iii) and (iv) increase the core size, (i) and (ii) are usually investigated first. Too thin a fuel rod gives rise to difficulties such as its bending and an increase in fuel processing cost. Therefore, the fuel rod size is naturally limited. The main specifications of BWR fuel rod design are shown in Table 3.7. The diameter of the fuel rods was as large as about 14 mm early in BWR development. The number of fuel rods in the same-sized fuel assembly was then increased from the viewpoint of increasing volumetric power and improved safety margins. A thinner fuel rod of about 10 mm is currently used.

Table 3.7 Examples of main specifications of BWR fuel design

Outer diameter (mm)	14.3	14.3	12.5	12.3	12.3	(Zirconium liner)	(Zirconium liner)	(Zirconium liner)
Thickness (mm)	0.81	0.94	0.86	0.86	0.86	0.86	0.71	0.70
Zirconium liner thickness (mm)	—	—	—	—	~0.1	~0.1	~0.1	~0.1
No. of fuel rods per assembly	49	49	63	62	62	60	74	72
No. of water rods	0	0	1	2	2	1 (large diameter)	2 (large diameter)	—
No. of water channels	—	—	—	—	—	—	—	1 (Square)
Spacer type	Grid type Helium	Circular cell type Helium	Circular cell type Helium	Ring type Helium				
Gas filled in rod gap (pressure)	(0.1 MPa)	(0.1 MPa)	(0.1 MPa)	(0.1 MPa)	(0.3 MPa)	(0.5 MPa)	(1.0 MPa)	(1.0 MPa)

The maximum fuel assembly power P_{Bmax} must be below the assembly power which meets the limit of MCPR to avoid boiling transition. P_{Bmax} can be reduced through the following measures.

- (i) Improve the radial power peaking factor considering fuel loading pattern and control rod pattern.
- (ii) Increase the number of fuel assemblies N_B .

[4] Power density

The power density, which is defined as the power produced per unit volume of the reactor core, is an important indicator to determine core size. It is usually provided in the unit of kW/l and the average power density of BWR is given by

$$\text{Average power density} = Q/V_{core} = q_{ave} \times N_{rod} / (L_B \times L_B) \quad (3.14)$$

The average power density can be raised by increasing the average linear heat generation rate of the fuel rods or by increasing the number of fuel rods per unit cross section. The number of fuel rods should be set as the most optimal value with a consideration on the nuclear design such as the volume ratio of coolant and fuel which is mentioned later, and on the thermal-hydraulic design such as the heat removal capability related to the heat transfer areas of fuel rods and coolant flow path. The average power density of BWRs operated until the present is in the range of about 40–60 kW/l .

3.2.3 Design of Fuel Lattice and Assembly

As shown in Fig. 3.5, the set of a fuel assembly, water gap outside channel box, and a quarter of cruciform control rod form a unit lattice and unit lattices are regularly arranged radially in the BWR core.

As main parameters of the unit lattice, there are the size and shape of the channel boxes wrapping the fuel assemblies, the number and diameter of fuel rods, the fuel rod pitch and pellet size, the size and location of the water rods, specifications of control rods, and so on. The amount of fissionable materials in each fuel rod, namely, the enrichment and density of U^{235} in the case of uranium fuel and the amount of gadolinia in case of burnable poison-mixed fuel are the basic nuclear design parameters.

Figure 3.6 [3] shows the procedure flow in the fuel assembly design. An optimal ratio of fuel to moderator is established from the viewpoint of the reactor nuclear performance, and the fractions of coolant and fuel regions are selected. The fuel assembly design proceeds with the fuel rod pitch and water rod size maintaining consistency with the design requirements to the number and diameter of fuel rods from the viewpoints of fuel inventory and fuel integrity. In the actual work, the final design of fuel assemblies is determined by repeating this sequence.

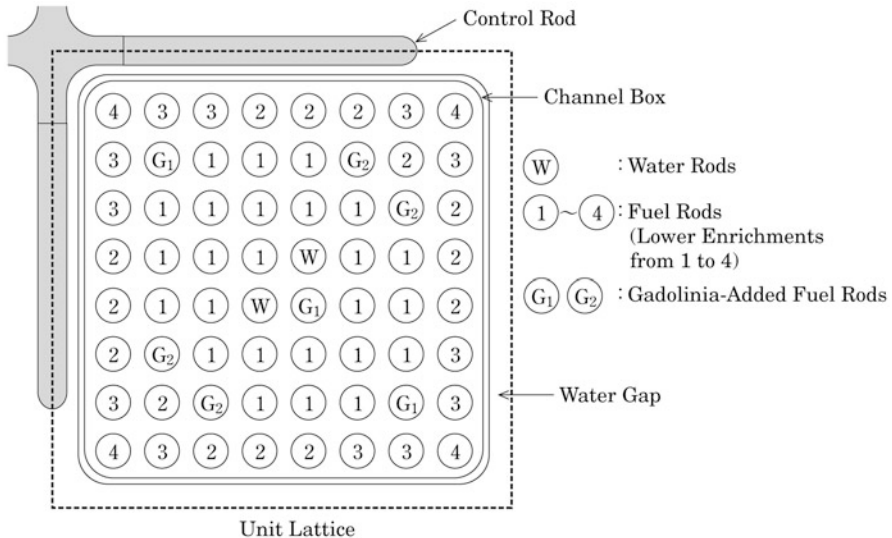


Fig. 3.5 Fuel lattice of BWR fuel assembly

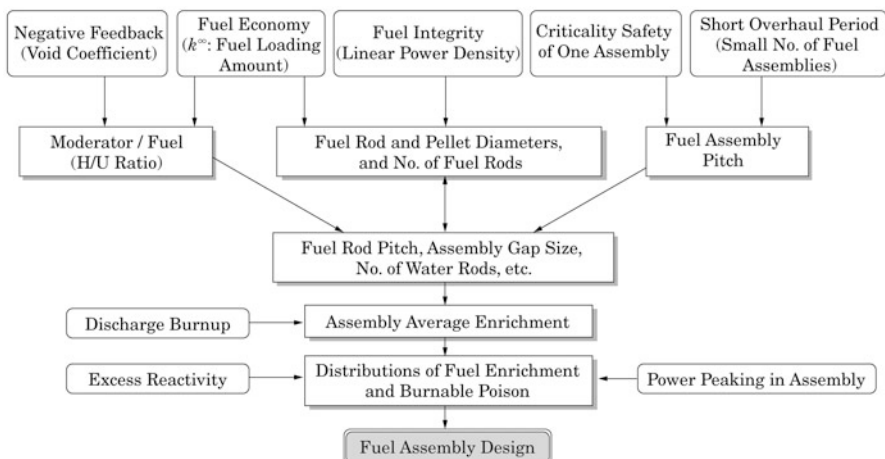


Fig. 3.6 Fuel assembly design flow

In determining the fuel assembly design, it is especially important to consider the relation between the moderator-to-fuel ratio in the unit lattice, which has a large effect on the nuclear performance, and the parameters mentioned above.

[1] H/U ratio

The moderator-to-fuel ratio in the unit lattice relates to the size and shape of fuel rods and water rods, and the void fraction, and is derived from the

Table 3.8 Moderator-to-fuel ratio in BWR 8 × 8 fuel assembly

	Unit	8 × 8 step I fuel	8 × 8 step II fuel
No. of fuel rods	No.	62	60
No. of water rods	No.	2	1 (Large Diameter)
Pellet region	cm ²	~52	~50
<i>Non-boiling region</i>			
Water rod	cm ²	~3	~8
Water gap (outside channel box)	cm ²	~48	~48
Boiling region (inside channel box)	cm ²	~102	~99
V_m/V_f ratio (void fraction 0 %)	–	2.9	3.1
<i>H/R ratio</i>			
Void fraction 0 %	–	6.2	6.5
Void fraction 40 %	–	4.6	4.9
Void fraction 70 %	–	3.4	3.7

structural feature of the BWR core where the coolant in the flow path of the channel box boils, but the water in the water rod and the assembly gap outside the channel box do not boil. The H/U ratio, which is defined as the ratio of hydrogen atoms in moderator to uranium atoms ($^{235}\text{U} + ^{238}\text{U}$) in fuel, rather than the moderator-to-fuel volume ratio (V_m/V_f) is used as the moderator-to-fuel ratio in the unit lattice. The evaluation of the effect of lattice shape and void fraction based on the H/U ratio is suitable for a consistent investigation into the effect of each parameter.

The H/U ratio is given by

$$\text{H/U ratio} = (\text{No.of hydrogen atoms in unit lattice}) / (\text{No.of fuel atoms in unit lattice}) \quad (3.15)$$

$$\begin{aligned} \text{No of hydrogen atoms in unit lattice} &= \{n_H^0 \times (1 - \alpha) + n_H^S \times \alpha\} \times \\ &(\text{Cross-sectional area of boiling region inside channel box}) + n_H^0 \times \\ &(\text{Cross-sectional area of non-boiling region inside} \\ &\text{channel box (water rod region)}) + n_H^0 \times \\ &(\text{Cross-sectional area of non-boiling region outside channel box} \\ &(\text{Water gap region})) \end{aligned} \quad (3.16)$$

$$\text{No.of fuel atoms in unit lattice} = n_u \times N_{rod} \times \pi(D_{p/2})^2 \quad (3.17)$$

Here α is the void fraction inside the channel box, n_H^0 is the atomic density of hydrogen in the saturated water, n_H^S is the atomic density of hydrogen in the steam, and n_u is the atomic density of uranium in the pellet. It is necessary to remark that the hydrogen atoms in the water gap and water rods (non-boiling region) are considered in the H/U ratio and moreover the H/U ratio depends on the void fraction inside the channel box. The H/U ratios of typical BWR fuel assemblies are shown in Table 3.8.

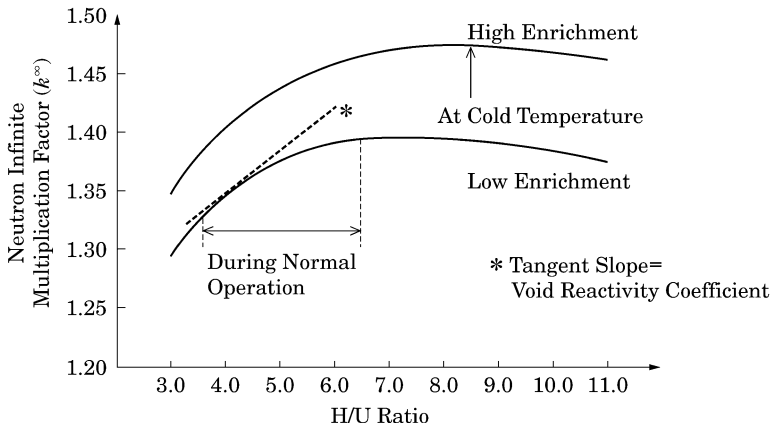


Fig. 3.7 Infinite multiplication factor as a function of moderator-to-fuel ratio (H/U ratio)

[2] H/U ratio and nuclear characteristics [8, 9]

Figure 3.7 shows a typical relation between H/U ratio and neutron infinite multiplication factor (k_{∞}). The k_{∞} increases as H/U ratio increases in the beginning because large numbers of neutrons are moderated to thermal neutrons by the moderation effect of water (specifically, its hydrogen atoms). However, a further increase in H/U ratio beyond the turning point contrarily leads to a decrease in k_{∞} because the neutron absorption by hydrogen atoms becomes dominant. Therefore, k_{∞} has a maximum value with respect to H/U ratio. The region on the left side of the maximum indicates an undermoderation region. If an H/U ratio which is a little smaller than the maximum is given at the cold temperature, the H/U ratio is decreased by the moderator density decrease and coolant voiding during reactor operation and then k_{∞} decreases. The void coefficient and moderator temperature coefficient become negative. As shown in Fig. 3.8, an increase in H/U ratio leads to a less negative void reactivity coefficient and a large control rod worth because of neutron spectrum softening. In general, BWRs are designed to have an H/U ratio of 4 to 5 for the average void fraction of about 40 % at normal operation.

An increase in fuel enrichment for high burnup leads to a large amount of fissile materials in the fuel, and then the neutron absorption of hydrogen atoms in the moderator is lowered and the maximum value of k_{∞} shifts to a higher H/U ratio as shown in Fig. 3.7. Figure 3.9 shows an example of the dependence of void reactivity coefficient and control rod worth on fuel enrichment. If the H/U ratio is set for low fuel enrichment at the reference core design, the void reactivity coefficient becomes more negative and the control rod worth becomes smaller as the fuel enrichment increases. It is, therefore, necessary to properly adjust the H/U ratio for high fuel enrichment.

As a way to increase H/U ratio, a more slender fuel rod can be made to reduce the fuel inventory, but that is not generally desirable from the viewpoint of fuel

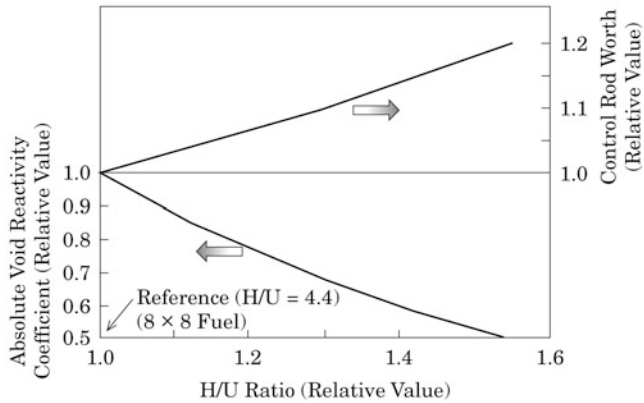


Fig. 3.8 Void reactivity coefficient and control rod worth as a function of H/U ratio

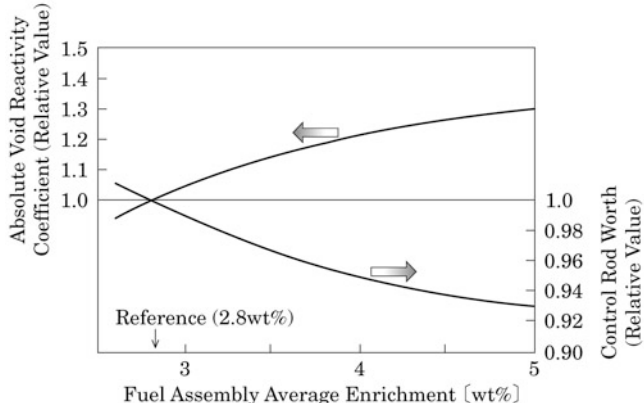


Fig. 3.9 Dependence of void reactivity coefficient and control rod worth on fuel enrichment

economy. The position and amount of the non-boiling regions inside and outside the channel box are optimized instead as a feature of BWR core structures. The H/U ratio can be increased without changing the fuel inventory by the following measures.

- (i) Increase the non-boiling region inside the channel box (water rod region).
- (ii) Increase the non-boiling region outside the channel box (water gap region).

Figure 3.10 shows the effect [9] of such a non-boiling region increase on reactivity increase at the cold temperature under a constant fuel inventory; reactivity changes with the change from the normal to cold temperature condition. Figures 3.11 and 3.12 show effects of the non-boiling region increase on void reactivity coefficient and infinite multiplication factor, respectively. To achieve measure (i), the central fuel rods in the fuel assemblies are replaced

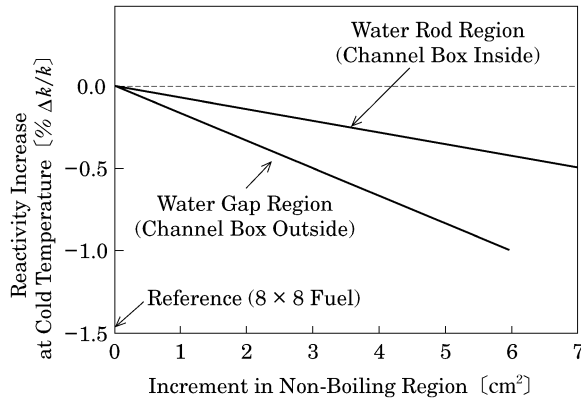


Fig. 3.10 Effect of non-boiling region on reactivity increase at cold temperature

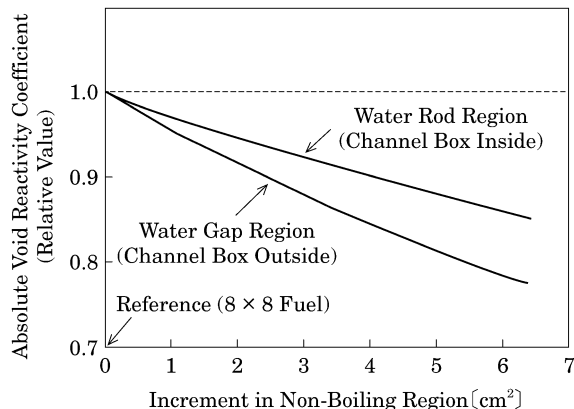
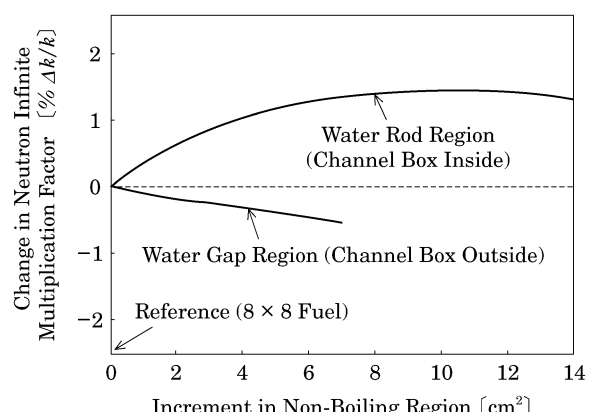


Fig. 3.11 Effect of non-boiling region on void reactivity coefficient

Fig. 3.12 Effect of non-boiling region on infinite multiplication factor



with water rods and the fuel rod diameter is increased to maintain the same fuel inventory. The width of the channel box is reduced and the fuel rod pitch is adjusted to use measure (ii).

The suppression of the reactivity increase at the cold temperature and the improvement in the void reactivity depend more highly on the water gap region outside the channel box. It is because the neutrons can be effectively moderated before they are absorbed in the fuel since the water gap region is located relatively far from the fuel rods. On the other hand, the increase of the water gap region leads to a maldistribution of moderator and then it causes a large distortion of thermal neutron flux in the fuel assemblies. Therefore, the neutron absorption rate increases in the water gap region where the peak thermal neutron flux is seen, and the neutron infinite multiplication factor decreases. Fuel assembly design specifications suitable for target characteristics are determined through control and adjustment of reactivity and reactivity coefficients by size and location of the non-boiling water region. Improvement of fuel assembly design for higher burnup can be achieved by increasing the water rod region with a proper H/U ratio to make reactivity high.

3.2.4 Characteristics of Reactivity

[1] Reactivity for reactor operation

The reactivity of nuclear reactors is defined in terms of the effective multiplication factor k_{eff} as follows.

$$\rho = (k_{eff} - 1) / k_{eff} \quad (3.18)$$

Figure 3.13 shows a typical variation in reactivity with nuclear reactor operation. Nuclear reactors operate at the critical state of $k_{eff} = 1$, namely, $\rho = 0$. The effective multiplication factor and reactivity change with variations in conditions such as reactor pressure, fuel temperature, coolant temperature, and void fraction. As mentioned in Sect. 3.2.1, LWRs are designed so that the reactivity decreases when fuel and coolant temperatures rise and coolant void occurs or enlarges. Since neutron absorbers such as the FPs Xe and Sm are accumulated immediately after reactor startup, the reactivity is also reduced. It is, therefore, essential to give an excess reactivity corresponding to the expected reactivity decrease before reactor startup in order to maintain the critical state at a rated power operation. Moreover, it is also necessary to provide an excess reactivity compensating for the reactivity decrease with burnup after reactor startup in order to operate the reactor at the rated power during the operation period because the accumulation of FPs as neutron absorbers leads to a reactivity decrease while the amount of fissile nuclides in fuel decrease with reactor operation.

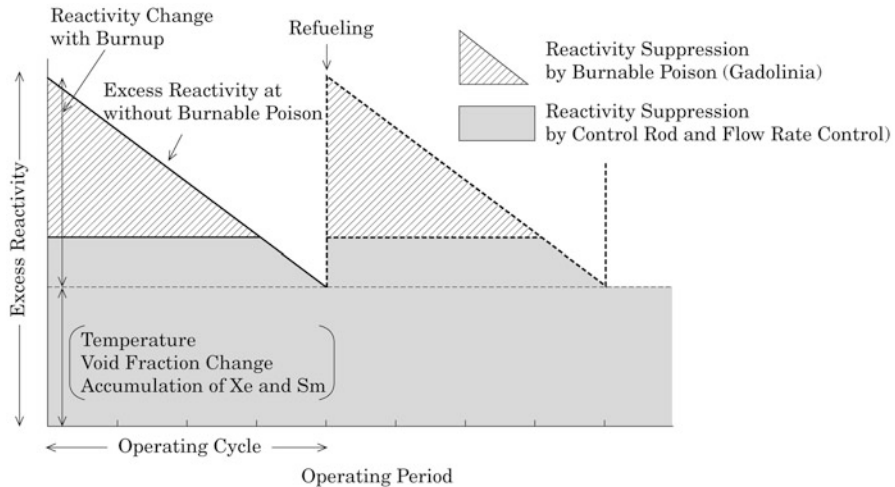


Fig. 3.13 Long-term variations in reactivity with nuclear reactor operation

Table 3.9 Excess reactivity and reactivity worth of control elements for BWR operation

Total excess reactivity	$\sim 20\% \Delta k/k$
Temperature change (with Doppler effect)	$\sim 4\% \Delta k/k$
Void fraction change	$\sim 3\% \Delta k/k$
Xe and Sm	$\sim 3\% \Delta k/k$
Burnup	$\sim 8\% \Delta k/k$
Others operating margin	$\sim 2\% \Delta k/k$
Total control reactivity worth	$\sim 25\% \Delta k/k$
Control rod worth	$\sim 18\% \Delta k/k$
Burnable poison	$\sim 7\% \Delta k/k$
k_{eff} at all control rod insertion	~0.95
k_{eff} at the most reactive control rod stuck	<0.99

Hence, a larger fuel amount than a critical one is loaded into the reactor and an excess reactivity necessary for reactor operation is provided considering variation in temperature, boiling effect, decrease in fissionable material with burnup, accumulation of FPs, and so on. The reactor should be designed to safely operate with proper control of the excess reactivity during the reactor operation period. Table 3.9 presents an example of the excess reactivity and reactivity worth of control elements for BWRs, which are designed to have a capability for reactivity control larger than the total excess reactivity for core shutdown even with one control rod stuck in the fully withdrawn position, including a calculation error.

The long-term variations in reactivity with burnup are controlled by control rods, coolant flow rate in core, and burnable poisons added to fuel pellets as shown in Fig. 3.13. Since the amount of burnable poisons cannot be adjusted during reactor operation, the reactor startup and shutdown are performed by

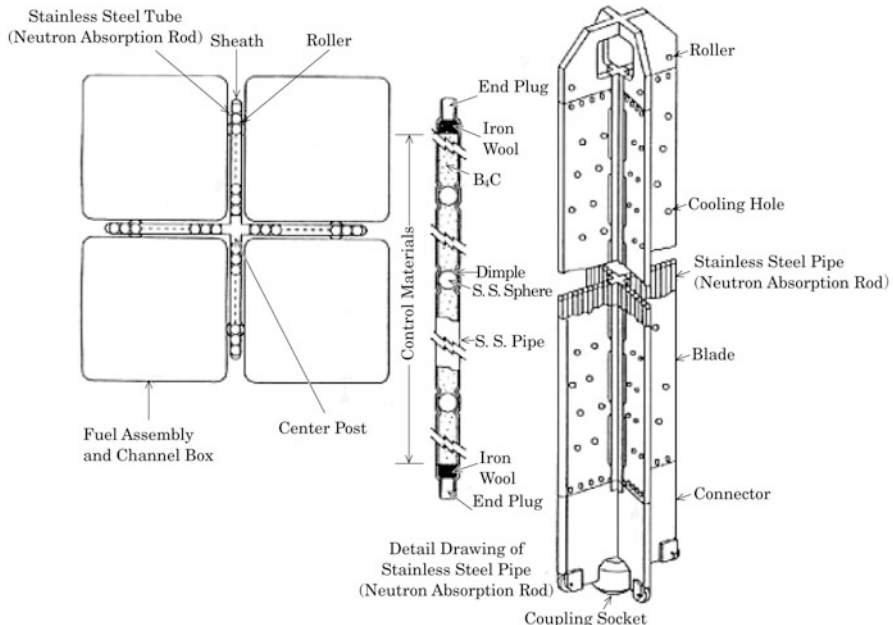


Fig. 3.14 BWR control rod (B₄C type of ABWR)

controlling control rods and coolant flow rate. A control rod scram is activated to shut down the reactor at an emergency and a boric acid solution injection system is provided as a control element for backup shutdown.

[2] Reactivity control by control rods and coolant flow rate [3]

Cruciform control rods are employed for BWRs as shown in Fig. 3.14, and boron carbide (B₄C) or hafnium is usually used as a neutron absorber. The control rods are inserted from the bottom of the reactor pressure vessel into the cruciform region formed between four fuel assemblies. There are two types of control rod drive mechanisms: hydraulic pressure piston drive and electric motor drive. Most of BWRs use the hydraulic pressure-driven system to move the control rods in 15.2 cm increments (one notch). The control rods in the advanced BWR (ABWR) design are driven in 1.8 cm increments (one step) by electric fine motion motors which make it possible to simultaneously move the maximum 26 control rod groups. For B₄C control rods, stainless steel tubes, which are arranged in a blade sheath, are filled with B₄C powder. For hafnium control rods, metal hafnium plates or rods are inserted into the sheath.

All control rods are inserted at reactor shutdown and control rods of about 5–10 % are inserted to control the excess reactivity during reactor operation at the rated power.

An inherent feature of power and reactivity control of BWRs is to control reactivity by changing the coolant flow rate in the core, which can be controlled by changing the pumping speed of the coolant recirculation pumps. BWR cores

have a coolant void and its value decreases as the coolant flow rate increases from the normal condition. Since the coolant also serves as a moderator in the core, the reduction in void fraction leads to a large effect on neutron moderation and results in progression of neutron spectrum softening. Therefore, the reactivity and reactor power increase. This leads to an increase in the void fraction again and results in an equilibrium state of the reactor power level corresponding to the void fraction at reactivity balance. On the other hand, a decrease in the coolant flow rate leads to a reactivity decrease and then the reactor power equilibrates at a lower level. Another feature of BWR cores is that the core power distribution hardly changes before and after a variation in core coolant flow rate.

This capability for reactivity control by coolant flow rate can be applied to compensate for the reactivity variation during reactor operation; fissile materials are consumed and reactor power gradually drops with reactor operation. Control rods can be withdrawn little by little to maintain the reactor power and to control the reactivity, but it gives rise to a distortion of the core power distribution. The change in coolant flow rate makes it possible to control the reactivity without distorting the core power distribution and moreover change in coolant flow rate is relatively easy to implement.

[3] Reactivity control by burnable poisons

As shown in Fig. 3.13, reactors in the beginning of the operation cycle are required to have an excess reactivity compensating for the reactivity variation due to consumption of fissile materials and accumulation of FPs with burnup. Since some fuel rods of fresh fuel assemblies include pellets containing several weight percent of burnable poisons (neutron absorbers), the excess reactivity necessary at the beginning of the operation cycle is mitigated and the reactivity variation during reactor operation is lessened. In other words, the effect of burnable poisons on reactivity control is large at the beginning of the operation cycle because of the large amount of burnable poisons and neutron absorption. The reactivity variation with burnup becomes small through the balance between the reactivity decrease with burnup and the reactivity recovery due to the neutron absorption decrease with burning of burnable poisons.

Burnable poisons, with the functions noted above, are required to have a large neutron absorption cross section and gadolinia (Gd_2O_3) is used as a burnable poison material for BWRs. Several weight percent of gadolinia are mixed with uranium oxide (UO_2) powder and processed into pellets which are inserted into several fuel rods. Since gadolinia is solid-soluble in uranium dioxide, it can be uniformly distributed in the pellets [3]. In the BWR fuel assembly design shown in Fig. 3.5, seven of 62 fuel rods are gadolinia-added fuel rods to control the excess reactivity.

Figure 3.15 shows the typical burnup characteristic of a fuel assembly containing the burnable poison gadolinia. The burnable poison-containing rods make the infinite multiplication factor small (suppression of excess reactivity) at the beginning of burnup when the concentrations of ^{155}Gd and ^{157}Gd are high. ^{155}Gd and ^{157}Gd are converted with burnup into ^{156}Gd and ^{158}Gd .

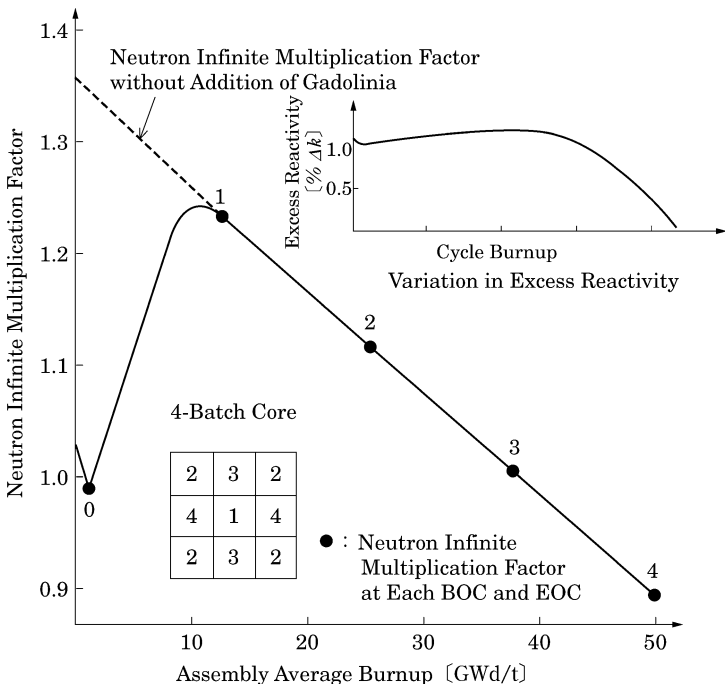


Fig. 3.15 Burnup characteristics of fuel assembly with burnable poison (Gadolinia)

respectively, which have small absorption cross sections, and their concentrations decrease. The suppression effect on the excess reactivity therefore, becomes small and the infinite multiplication factor is recovered almost to the value when not including the gadolinia-added fuel rods. Any remaining gadolinia at the end of the operation cycle will cause a reactivity loss as a useless neutron absorber, so the concentration of gadolinia is set to be burned out at the end of the operation cycle.

The number of gadolinia-added fuel rods can be increased for high suppression of the excess reactivity at the initial burnup and the gadolinia concentration can be increased for long-term suppression of the excess reactivity. Figure 3.15 shows variation of the infinite multiplication factor with the average fuel assembly burnup for a 4-batch refueling; numbering corresponds to each BOC and EOC. In a core loaded with the fuel assemblies having the burnup characteristics shown in Fig. 3.15, the infinite multiplication factor of fresh fuel assemblies increases with reactor operation (0–1) and those of other fuel assemblies decrease (1–2, 2–3, and 3–4). Both characteristics compensate each other and therefore the variation in excess reactivity during an operating cycle becomes small as shown in the insert figure of Fig. 3.15. Such a proper usage of burnable poisons mitigates the work burden of control rod operation and coolant flow rate change, and considerably improves the controllability of reactor operation.

3.2.5 Control of Power Distribution

Along with the reactivity control, control of the power distribution in core is one of the important challenges in core design. Technologies for power distribution control have been developed and applied to the pin power distribution in a fuel assembly, the core axial power distribution, and the core radial power distribution.

[1] Power distribution in a fuel assembly

The relative power density of each fuel rod to the average power density of fuel rods in the fuel assembly is referred to as the *local power peaking*. Areas inside and outside of the channel box of the fuel assembly are completely separated in BWRs. When a void occurs inside the channel box, it does not occur in the water gap region outside the channel box. This, therefore, leads to high power of the outermost fuel rods neighboring the water gap which increases the neutron moderation effect; in other words, a high local power peaking is caused. The water rods, which are arranged in the central region to optimize the H/U ratio, increase the power of the central fuel rods by increasing the moderation effect, therefore contributing to a flat power distribution.

To flatten the pin power distribution and suppress the local power peaking, different enrichments of fuel rods are properly arranged as shown in Fig. 3.5; low enrichment fuel rods are near the channel fox and high enrichment fuel rods are in the central region.

The pin power distribution in a fuel assembly varies with burnup. Generally higher power fuel rods at initial burnup lead to a larger power decrease with burnup, and therefore the high local power peaking at the initial burnup is mitigated with burnup. The enrichment zoning of fuel rods and the arrangement and concentrations of burnable poison rods are determined so as to maintain a flat power distribution during burnup until the fuels are discharged. Since the gadolinia-added fuel rods suppress pin powers at initial burnup, the burning speed of fissile materials in the fuel rods is slower than that of neighboring fuel rods. The gadolinia-added fuel rods are designed to have a relatively low enrichment compared with the neighboring fuel rods in order to avoid a high local power peaking caused by the remaining fissile materials after burning out of gadolinia. Since the variation in gadolinia concentration with burnup depends on the thermal flux near the gadolinia-added fuel rods, the concentration is properly determined to optimize the fuel burnup and gadolinia burning, corresponding to the location of the gadolinia-added fuel rods.

[2] Core axial power distribution

Since the BWR core has a low void fraction in the lower part and a high void fraction in the upper part due to steam being directly generated in the core, this leads to an axial distribution of void fraction in the core. The axial void distribution causes a difference in the moderation effect between the core lower and upper parts and the lower part, with the large moderation effect, has a relatively high multiplication factor compared with the upper part. This, therefore, gives rise to power peaking in the lower part. The mitigation of the axial power peaking is an important challenge to improve the plant capacity

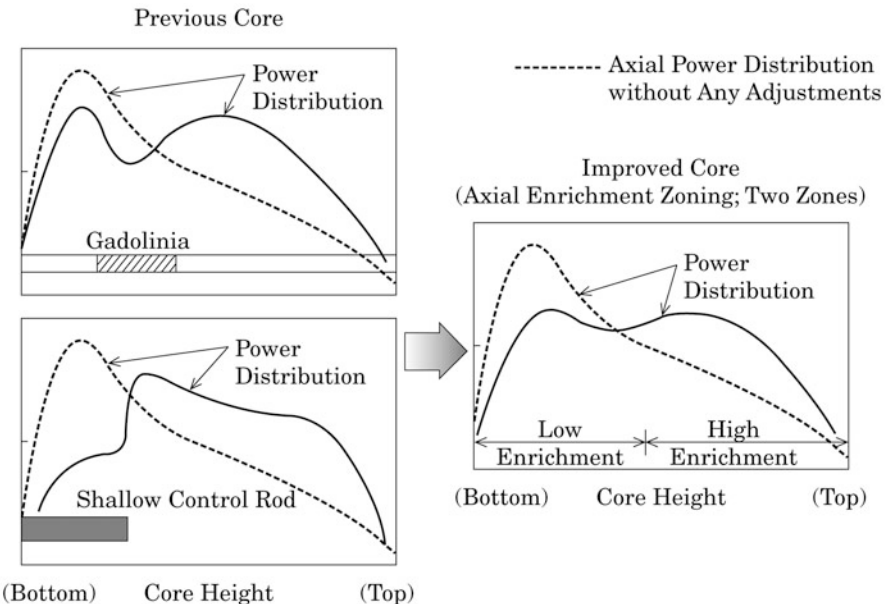


Fig. 3.16 Improvement in flattening of axial power distribution

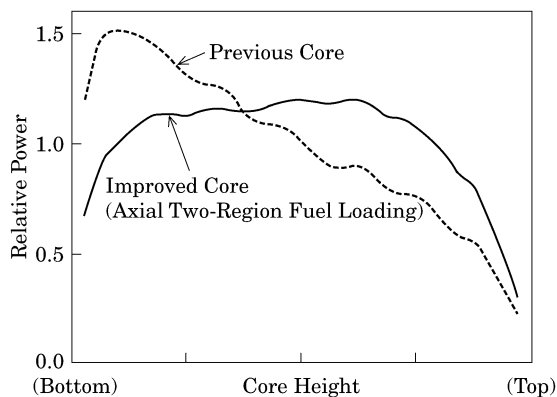


Fig. 3.17 Improvement in axial power distribution at EOC

factor in considering an increase of operating easiness as well as maintaining the core thermal margin.

As shown in Fig. 3.16, control rods were shallowly inserted from the core bottom and gadolinia was added to the lower part of the fuel rods to suppress the distortion of axial power distribution in early BWR designs. However, this strategy caused high power peaking in the lower part of the core, as shown in Fig. 3.17, because the core excess reactivity decreases with burnup and control

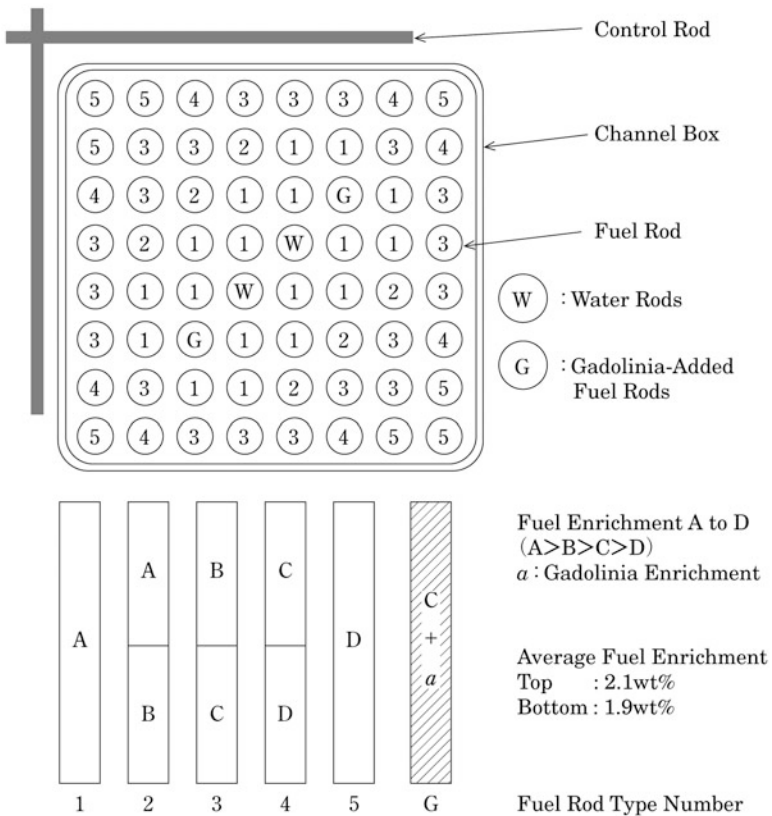


Fig. 3.18 Example of axial two-region fuel (initial core)

rods are withdrawn to compensate for the decrement near the end of the operating cycle.

As a solution of this problem, the uranium enrichment in the core upper part can be increased a little more than that in the lower part to compensate for the decrease of the infinite multiplication factor due to the void in the core upper part. This strategy balances the infinite multiplication factor between the core upper and lower parts, and is practically employed to flatten the core axial power distribution; it is referred to as the *axially two-zoned fuel* concept [10, 11]. Figure 3.18 shows an example of an axially two-zoned fuel core design [10]. The enrichment of upper pellets of some fuel rods is higher by about 0.2–0.5 wt% than that of lower ones and the cross-sectional average enrichment of the fuel assembly upper part is higher by about 0.2 wt% to give a balance of infinite multiplication factors between the upper and lower parts. While control rods are withdrawn and the effect of burnable poisons is decreasing with burnup, the effect of the axially two-zoned fuel on the flat axial power distribution can be maintained with burnup even at the end of the operating

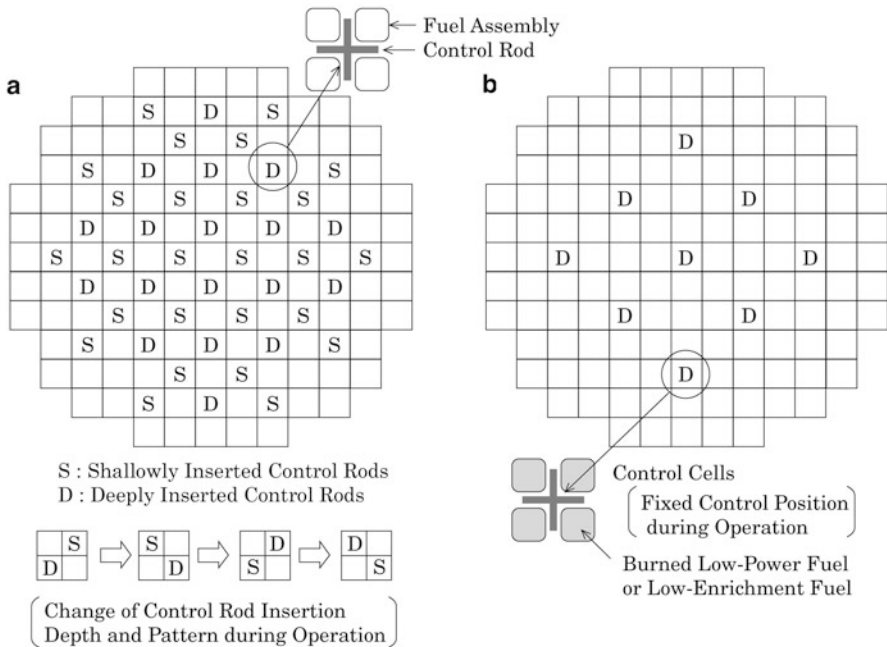


Fig. 3.19 Comparison of control rod pattern between (a) Previous core and (b) Control cell core

cycle [14] as shown in Fig. 3.17. The axially two-zoned BWR core considerably improves the plant capacity factor by decreasing the maximum linear heat generation rate by 20 % compared with the previous core and by simplifying the control rod operation [12–14].

Thus, different axial enrichments, independent of the core reactivity control, are applied to control of the axial power distribution in the axially two-zoned BWR core. This makes it easy to optimize the axial power distribution and makes it possible to use burnable poisons in core reactivity control separately from control of the axial power distribution.

[3] Core radial power distribution

The core radial power distribution can be flattened by properly designing the control rod insertion positions (the control rod pattern) and the fuel loading pattern.

Figure 3.19 compares two examples of control rod patterns in BWRs. While control rods are shallowly inserted for control of the axial power distribution, they are generally deeply inserted for control of the radial power distribution. Neutron absorption by control rods suppresses the power of adjacent fuel assemblies and has an effect on the power of surrounding fuel assemblies through a change in the neutron flux distribution. Thus, the control rods control the radial power distribution of the whole core. In the previous design which lacked the axially two-zoned fuel concept, the same control rod is not inserted

for a long period of time to avoid slow burning of the adjacent fuel and all control rods are alternatively inserted to give uniform fuel burning in the core. The insertion positions of the control rods (control rod pattern) are changed during the operation cycle.

Such a change in control rod pattern during reactor operation is performed generally at a power level lower than the rated one to avoid a rapid variation in fuel rod power due to the control rod operation. This was a factor which interfered with improvement in the reactor capacity factor. A *control cell core* [15] has been developed as a core in which such a change in the control rod pattern is unnecessary and the reactor operation is simple. Figure 3.19 compares [16] the control rod pattern of the control cell core with that of the previous core. In the control cell core [17], there are several control cell regions in which low enrichment or high burnup low reactivity fuel assemblies are arranged near control rods. The control rods in the control cells are deeply inserted during reactor operation, while the other control rods are fully withdrawn. Although the control rods in the control cells are withdrawn to compensate for a reactivity loss with burnup, it does not cause a large power peaking because the neighboring fuel assemblies also have a low reactivity. The effect on fuel integrity is therefore small. Thus, the elimination of shallow insertion of control rods by adoption of the axially two-zoned core, the small excess reactivity by a proper addition of burnable poisons into fuel rods, and the reduction of necessary control rods by the control cells lead to a simple reactor operation without a change in control rod pattern.

In addition to the control of core radial power distribution by control rods, an exchange of fuel loading location (*fuel shuffling*) can be carried out to flatten the core radial power distribution, considering proper loading location of fresh fuel assemblies and the number and burnup of burned fuel assemblies.

BWRs are generally designed to have a scatter-loading pattern in which fuel assemblies are regularly dispersed in the core depending on the burned cycle. Another choice is a low leakage loading pattern in which high burnup fuel assemblies are loaded in the outermost region of the core to reduce the neutron leakage and increase the core reactivity. Figure 3.20 shows an example of the fuel loading pattern at the equilibrium cycle of the 1,100 MWe BWR core. In the 4-batch equilibrium core, fuel assemblies are kept in almost the same location until the third cycle after being loaded, and then moved to the outermost region of the core or the control cell region. This scatter-loading pattern can produce a self-flattening effect of the power distribution with burnup and minimize the fuel shuffling for flattening of the power distribution.

In early BWR designs, generally, one type of fuel assembly was loaded in the initial core and the core radial power distribution was mainly controlled by control rods. In recent designs, an equilibrium core is simulated and different enrichments of fuel assemblies are employed [18]. The low leakage loading pattern mentioned above is usually used for improvement in economy. The control cell consists of four low enrichment fuel assemblies and other fuel assemblies with different enrichments are dispersed in other regions. In some of

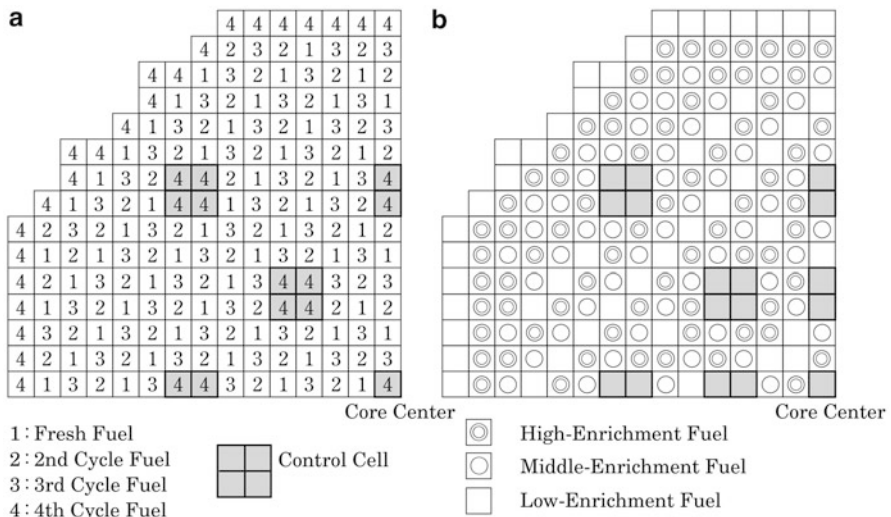


Fig. 3.20 Example of BWR fuel loading pattern (1,100 MWe plant core). (a) Equilibrium core (b), initial core

the practical intial core designs, high enrichment fuel assemblies are loaded into the outermost region of the core.

[4] Haling distribution [7]

As a reference power distribution for investigating power distribution flattening by a burnable poison design, and fuel loading and control rod patterns, the *Haling distribution* [19] may be used. It is based on the principle that *if a power distribution can be kept constant through the operating cycle by proper management of burnable poison and movable control rods, the peak-to-average value will be at a minimum*. In derivation of the principle, it was assumed that the infinite multiplication factor of a fuel assembly is a decreasing function of burnup and variation in the flux-to-power ratio with burnup is small or a decreasing function of burnup. This assumption leads to a conclusion that *in comparison with the case of a constant power distribution through the operating cycle, a slightly smaller power peaking for a period of the operating cycle will require fuel burning by reactor operation under a high power peaking for another period*.

In a given fuel design, the Haling distribution of the fuel arrangement can be obtained from calculation of an initial power distribution shape and repeated calculations between the power distribution shape and burnup distribution. The repeated calculations finally give a consistent distribution between power and burnup. If this power distribution shape can be realized during the operating cycle by adjusting the burnable poison distribution in fresh fuel and the insertion amount and position of control rods, namely, the neutron absorber distribution, it will give a minimum power peaking.

This principle is useful in designing the control rod pattern during the operating cycle. For a given fuel arrangement, cycle length, and effective multiplication factor at EOC, a corresponding Haling distribution and the necessary infinite multiplication factor in each location of the core are obtained. The reactivity worth to be controlled by control rods and burnable poisons is found by taking the difference between the infinite multiplication factor distribution at BOC and the one necessary for the Haling distribution. The insertion location and depth of control rods are determined based on the difference. The insertion and withdrawn of control rods are actually discrete and the Haling distribution cannot be achieved strictly. The Haling distribution is, however, useful as a target plan for control rod operation.

A big advantage in using the Haling distribution for setting the control rod pattern is to be able to separately handle the fuel loading patterns over several cycles and the control rod pattern in the cycle of interest when the reactor is operated. In other words, when the fuel loading pattern is planned, the power distribution during reactor operation dose not need to be predicted based on a detailed control rod pattern, but is assumed to have a Haling distribution, in which the number of fresh fuel assemblies and the location change of reloading fuel assemblies are determined by evaluating the fuel burnup.

The nuclear design of the fuel assembly, namely, the design of the fuel enrichment zoning and burnable poison distribution in the fuel assembly, is optimized generally based on the fuel burnup distribution at an equilibrium cycle to exclude the singularity of a specific operating cycle. The Haling distribution has been used in design of the equilibrium cycle core and evaluation of fuel discharge burnup and required enrichment.

3.2.6 *History and Future Trends in Core Design*

Commercial BWRs in Japan have had an operating experience of over 40 years since the Tsuruga Nuclear Power Plant Unit 1 was started in 1970. The core and fuel have been improved on the basis of accumulated operating experiences and technological progress and Fig. 3.21 shows the history [20] of improvements in it.

In the beginning, there were various improvements related to security and reliability of fuel safety; these included enhanced moisture management in fuel fabrication, application of the *Pre-Conditioning Interim Operating Management Recommendation* (PCIOMR) [21], and reduction in the average linear heat generation rate by using a larger number of fuel rods (changing from the 7×7 type to the 8×8 type lattice). The PCIOMR sets restrictions on reactor operation. These include limits on the linear heat generation rate for free operation of control rods to mitigate pellet clad interaction (PCI); a mild power increase by coolant flow rate control when the power is increased over the allowable linear heat generation rate; and keeping the power at a level for a fixed period after which the power may be freely changed within the level. It is very effective as a measure of the PCI, while it

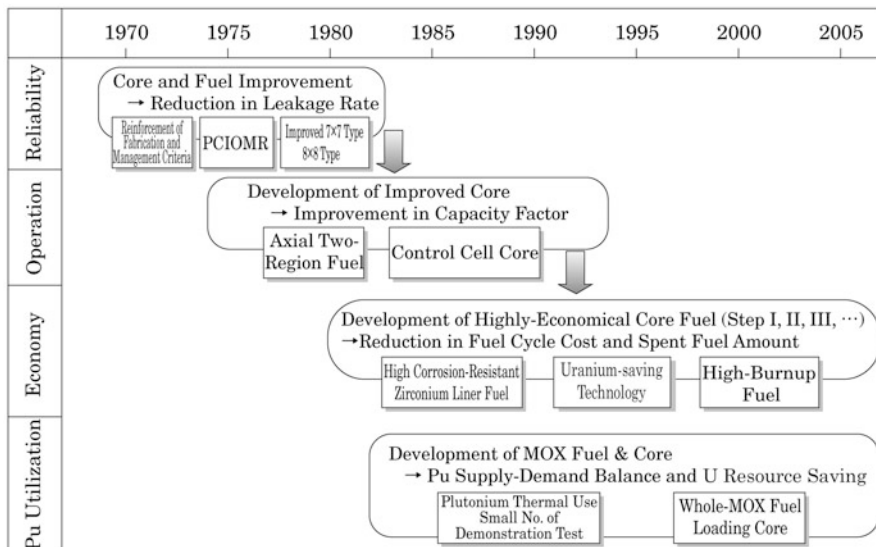


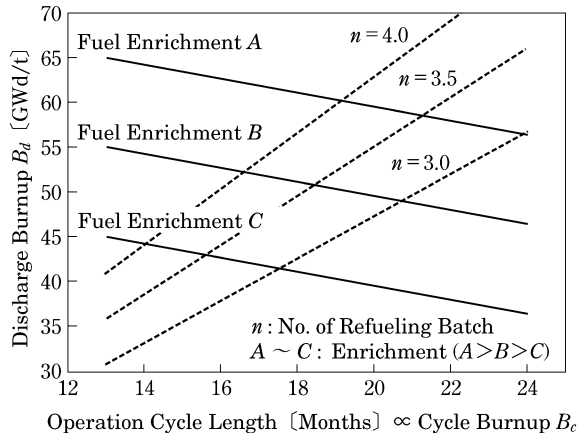
Fig. 3.21 Improvement of BWR core and fuel in Japan

leads to a decrease in the reactor capacity factor. Core improvement was undertaken to actualize flattening of the core power distribution for the purposes of improving the capacity factor under the PCIOMR application and simplifying the reactor operation, thus securing fuel integrity. The development of improved cores such as the axially two-zoned core and control cell core considerably enlarged the core thermal margin, and improved the reactor operation and capacity factor by reducing the PCI load. Since the 1980s, high burnup and high economy cores have been developed to further raise the economy of nuclear power and to lighten the burden of fuel cycle, such as by lowering the amount of spent fuel and high level wastes. The development of the *Pu-thermal core* (MOX-fueled core) and its fuel have also proceeded to establish a fuel recycling by using plutonium in LWRs. Moreover, the operation cycle length has been prolonged to improve the capacity factor and an increase in the rated reactor power has been planned from the viewpoint of advanced use of existing power plants. It is important to continue to develop core and fuel corresponding to those improvements.

[1] High burnup and long operation cycle length

High burnup increases the total energy (discharge burnup × fuel inventory) produced from fuel assemblies from the time they are loaded into core until they are discharged. It can significantly extend the operating cycle length without increasing the number of fuel assemblies to be exchanged in refueling, and then improve the capacity factor, which helps to reduce power generation costs. Since high burnup also increases the total energy per fuel inventory and reduces the spent fuel amount per unit energy generation, it is possible to reduce

Fig. 3.22 Discharge burnup with operation cycle length



the reprocessing and waste disposal costs in the fuel cycle cost. The natural uranium and enrichment conversion cost in the fuel cycle cost can be reduced by decreasing natural uranium resources necessary for unit energy generation, namely, by improving fuel economy. The following describes the effect on fuel economy of the high burnup and long operation cycle length.

In the *linear reactivity model* based on the assumption that the reactivity decreases linearly with burnup, when it is considered that enriched fuel assemblies loaded into core stay during n operation cycles and $1/n$ fuel assemblies are replaced in refueling, namely, the batch size is n , the cycle burnup $B_c(n)$ and the discharge burnup $B_d(n)$ can be given by [7]

$$B_c(n) = 2 \times B_0 / (n + 1) \quad (3.19)$$

$$B_d(n) = n \times B_c(n) = 2n \times B_0 / (n + 1) \quad (3.20)$$

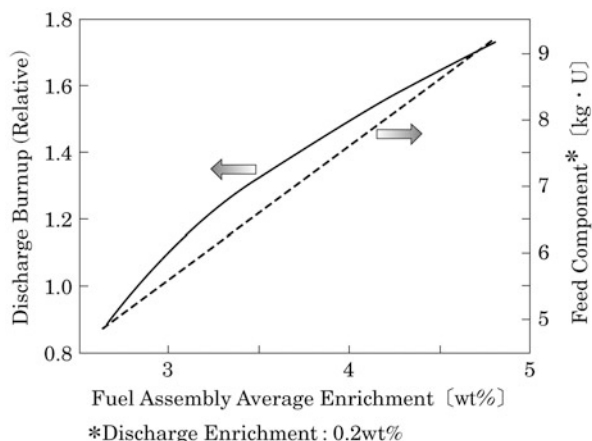
$$B_d(n) + B_c(n) = 2B_0 \quad (3.21)$$

where B_0 is the achievable discharge burnup of fresh fuel when it burns without replacement and it is a constant depending on fuel enrichment. In the case of a change in the refueling batch size from n_1 to n_2 to extend the operation cycle length, the discharge burnup change can be written by

$$\Delta B_d(n) = B_d(n_2) - B_d(n_1) = 2B_0(n_2 - n_1) / (n_2 + 1)(n_1 + 1) \quad (3.22)$$

When the operation cycle length is extended by increasing the number of refueling fuel assemblies ($n_1 > n_2$) without changing the average enrichment (B_0 is constant), the discharge burnup decreases and the fuel economy is compromised as shown in Fig. 3.22. A large B_0 , namely, a high average enrichment is required to prolong the operation cycle length [large $B_c(n)$] by

Fig. 3.23 Discharge burnup and feed component with enrichment



increasing the number of refueling fuel assemblies while maintaining the discharge burnup (B_d) is constant).

Figure 3.23 shows the relation [8] between the average enrichment of a fuel assembly and the discharge burnup or the feed component which is the natural uranium resources necessary for fabrication of 1 kg of enriched uranium. The increment of the feed component by increasing the average enrichment is smaller than that of the discharge burnup. The increase of the average enrichment leads to a higher infinite multiplication factor of the fuel assembly, which can meet the critical condition in the core even after burning to a low infinite multiplication factor. In other words, the high burnup obtained by increasing the average enrichment can reduce the necessary natural uranium resources per unit energy generation.

[2] Uranium-saving technology [3, 16, 20]

Uranium-saving technology is intended to attain a high burnup with the least increment of fuel enrichment by effectively burning the uranium loaded in the core. Only a simple increase in fuel enrichment raises the uranium and enrichment cost. For an economic high burnup, therefore, it is important to save the uranium simultaneously. The basis of uranium-saving technologies used practically in BWRs is the development of *zirconium liner fuel* in which the inside of the zircaloy-2 cladding is lined with soft and pure zirconium. The zirconium liner fuel mitigates the pellet-clad mechanical interaction (PCMI) and increases fuel integrity against a rapid power rise. Hence, it eliminates restrictions on the PCIMR and makes it unnecessary to take an excessive design margin for the linear heat generation rate. The thermal margin obtained from the power distribution flattening for improvement of the capacity factor can be applied to the uranium saving.

(1) Utilization of power peaking

Arrangement of the high enrichment fuel in the proper locations with high thermal neutron fluxes can increase the core reactivity. High enrichment

zoning in the peripheral region of a fuel assembly causes bias of the pin power distribution and large local power peaking. In the early core design, low enrichment zoning in the peripheral region was employed to improve the thermal margin and to mitigate the restrictions on the PCIOMR. However, since the zirconium liner fuel has been employed and the axially two-zoned core has reduced the axial power peaking as mentioned, the core reactivity can be improved by allowing a larger local power peaking. The installation of natural uranium blankets on the upper and lower end parts and the arrangement of low enrichment fuel assemblies in the core periphery region cause a large axial and radial power peaking of the core. However, the power peaking margin from the axially two-zoned core can give a reactivity gain.

(2) Reduction in gadolinia residual

The *reduction in gadolinia residual* is the technology to minimize gadolinia embers in the core upper and periphery parts and to increase the core reactivity. The placement of natural uranium blankets on the upper and lower end parts also contributes to the reactivity gain by replacing the corresponding gadolinia.

(3) Spectral shift operation

The *spectral shift operation* is the technology to get a reactivity gain by changing the neutron spectrum through a change in the void fraction and distribution which are features of the BWR core. The void fraction change can be accomplished by the coolant flow rate control to decrease the core coolant flow rate during the first half of the operating cycle, which leads to a high void fraction in the core, less neutron moderation, and acceleration of ^{238}U conversion to plutonium, and then to increase the core coolant flow rate during the latter half of the operating cycle, which leads to a burning of the plutonium accumulated in the first half. The void distribution change can be performed by the axial power distribution control to distort the axial power distribution downward, which leads to a downward shift of the void generation point and an increase of the void fraction in the core, and then oppositely to extend the axial power distribution upward, which leads to a decrease of the void fraction.

(4) Optimization of H/U ratio

High enrichment of uranium for high burnup decreases the ratio between H and ^{235}U atoms, and hardens the neutron spectrum. It is, therefore, necessary to set the proper H/U ratio in order to effectively use fuel and to efficiently utilize thermal neutrons. The H/U ratio can be raised by increasing the number of water rods in the fuel assemblies or by enlarging their cross-sectional area as mentioned in Sect. 3.2.3.

[3] High burnup fuel [22]

Japan's development of high burnup BWR fuel has been advanced by stages, Step I, Step II, and Step III, as shown in Fig. 3.24, with each step confirming the usage results.

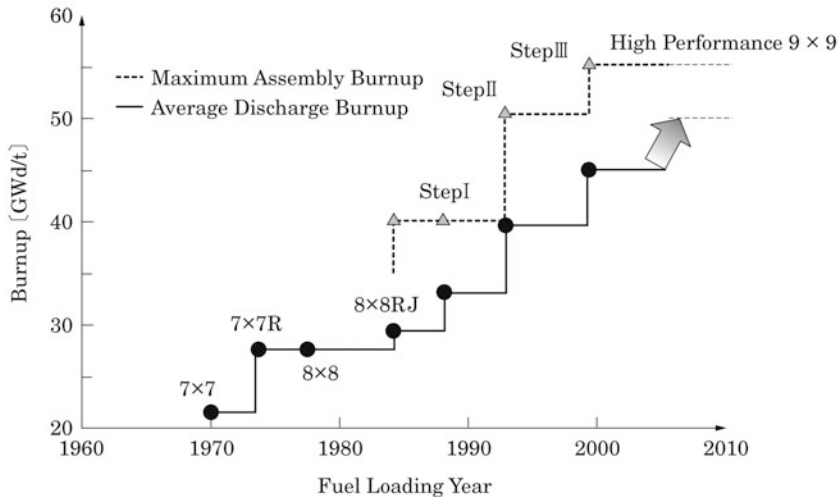


Fig. 3.24 Development of high burnup BWR fuel [22]

Step I fuel has been used practically since 1987. It employs the zirconium liner fuel, while having the same structure as the previous 8×8 type lattice (8×8 RJ). By applying the uranium-saving technology using power peaking such as the installation of natural uranium blankets on the core upper and lower end parts, the discharge burnup for the same average enrichment was increased by about 10 % from about 29.5 GWd/t to 33.0 GWd/t and the fuel cycle cost was also reduced by about 10 %.

The high burnup 8×8 fuel of Step II has been used as a reload fuel since 1991. It has a higher enrichment for high burnup and economy. The average discharge burnup is 39.5 GWd/t and the maximum burnup of fuel assembly was increased to 50 GWd/t from 40 GWd/t of the Step I fuel. To suppress fuel temperature and rod internal pressure rise during reactor operation, the initial pressure of helium gas was increased from about 0.3 MPa to 0.5 MPa and the theoretical density of pellets was raised from about 95 % to 97 %. Four fuel rods in the center of the fuel assemblies were replaced with a large diameter water rod and the H/U ratio was increased to enhance neutron moderation efficiency. Ring-type spacers were used to improve the thermal margin (power limit) of fuel rods and upper tie plates were designed as a low pressure drop type with a small resistance against water flow.

The 9×9 fuel of Step III, which has been used on a full scale since 1999, gives a higher discharge burnup of 45 GWd/t by increasing fuel enrichment and a higher maximum burnup of fuel assemblies of 55 GWd/t. The change to the 9×9 arrangement of fuel rods, which increases the number of fuel rods per fuel assembly, reduces the average linear heat generation rate and increases the nuclear design flexibility. There are two design types for Step III fuel assemblies; types A and B. The type A assembly consists of 74 fuel rods and two large

diameter water rods. A high pressure drop at the non-boiling fuel assembly inlet and a low pressure drop in the boiling region can stabilize the coolant flow in the fuel assemblies. The assembly adopts a high pressure drop type lower tie plate and partial length fuel rods (about 2/3 the usual length). The type B assembly is composed of 72 fuel rods and a square water channel to increase the H/U ratio and to optimize neutron moderation. It improves the nuclear and thermal-hydraulic characteristics such as core safety. Both fuel assembly types have a higher initial pressure of helium gas, 1.0 MPa, to improve the heat transfer between pellet and cladding and to mitigate the internal pressure rise of fuel rods with neutron irradiation.

The BWR fuel assembly has been improved with respect to intra-assembly design points such as fuel rod size and arrangement without considerably changing the fuel assembly size and therefore it can be applied to existing reactors. Application of high burnup fuel through those three phases has extended the average discharge burnup to about 1.5 times than that of the early 8×8 fuel and reduced the fuel cycle cost by about 30 %. The spent fuel amount is also reduced in inverse proportion to the discharge burnup increase.

As a restriction in the fuel cycle for high burnup, there are limited acceptances to reprocessing facilities (maximum burnup of fuel assembly < 55 GWD/t at Rokkasho, Japan) and transport and processing facilities (maximum uranium enrichment < 5 wt%). Since Step III, the development of high burnup fuel has been continued within the restriction to increase the burnup and reduce the fuel cycle cost and spent fuel amount.

[4] MOX-fueled core

Fresh uranium fuel is usually enriched to about 3–4 wt% of ^{235}U on average for a fuel assembly. ^{235}U decreases with burnup and part of the ^{238}U is converted to plutonium through neutron capture. Typical spent fuel contains about 1 wt% of ^{235}U and about 1 wt% of plutonium converted from ^{238}U . ^{239}Pu and ^{241}Pu account for about 60–70 % of the plutonium. MOX fuel is an oxide mixture of plutonium recovered from spent fuel and natural or depleted uranium, containing about 3–5 wt% of plutonium per fuel assembly. The difference between MOX fuel and uranium fuel is that plutonium is blended into the fresh fuel and its amount is larger than that in uranium fuel. This brings about a change in core characteristics due to the different nuclear characteristics of plutonium. As shown in Fig. 3.25, plutonium has a larger neutron absorption cross section in thermal and resonance regions than uranium, and a smaller delay neutron fraction. The different characteristics have the following effects on core characteristics.

- (i) MOX fuel reduces the number of thermal neutrons and the neutron spectrum is hardened, and therefore it causes a decrease in neutron absorption of the control rods and boric acid water. It is necessary to assure the core shutdown capability even with one control rod stuck in the fully withdrawn position or with boric acid water injection under the condition of all control rods stuck.

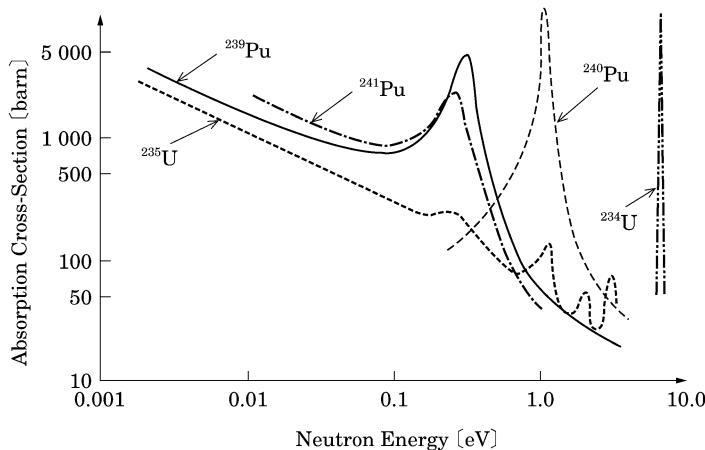


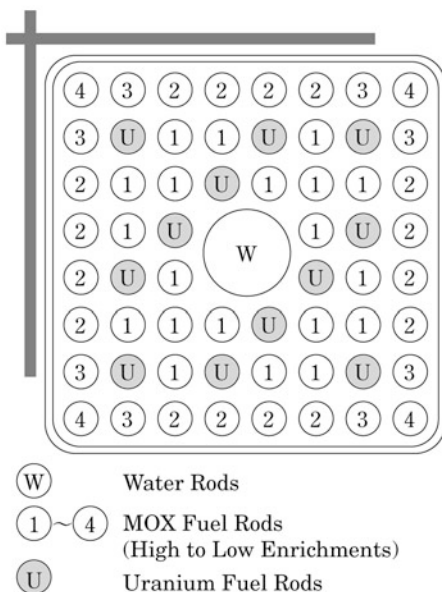
Fig. 3.25 Neutron absorption cross-sections

- (ii) In connection with the large resonance absorption cross section of ^{240}Pu , MOX-fueled BWR cores have a larger reactivity change relative to a change in void fraction than uranium-fueled cores. This tends to give a more negative void reactivity coefficient. It is, therefore, necessary to check the impact on core characteristics and stability at transients.
- (iii) Since MOX fuel rods tend to generate a relatively higher power when loaded together with uranium fuel rods in the fuel assembly, it is necessary to assume that the maximum linear heat generation rate and MCPR at normal operation meet the operation criteria. Especially, fuel rods facing the water gap region generate a large power and therefore particular attention should be given to the fuel rod arrangement in the fuel assembly.

In use of MOX fuel, the plutonium enrichment and MOX fuel inventory are adjusted based on the effects mentioned above. Actually, MOX-fueled cores are designed to have a margin to meet changes of the characteristics, considering the range of variation in various factors due to nuclear calculation error and future fuel design changes. Existing reactors have been evaluated as able to operate with MOX fuel replacing about 1/3 of the core fuel [23].

The BWR MOX fuel used in the initial step of the Japanese plan for Pu-thermal utilization has the same structure as that of Step II fuel because of the rich operating experiences already available for uranium fuel. The discharge burnup of the MOX fuel is about 33 GWd/t, which is just slightly lower than the 39.5 GWd/t discharge burnup of Step II uranium fuel. The MOX fuel is being introduced with repeated usage experience. The Step II fuel assembly developed for high burnup has a large diameter water rod to improve the neutron moderation effect. The water rod has the effect of getting a less negative void reactivity coefficient. In design of the MOX fuel rod, the active height of the fuel rod is shorter considering that the FP gas release rate is

Fig. 3.26 Example of fuel rod arrangement in MOX-fueled assembly



slightly higher than that of uranium fuel. Figure 3.26 shows a fuel rod arrangement in an MOX-fueled assembly. Low enrichment plutonium fuel rods are arranged on the periphery as a measure to get local power peaking like done for use of uranium fuel. Experienced gadolinia-added uranium fuel rods are arranged among MOX fuel rods in the assembly as burnable poison rods for excess reactivity control.

In ABWRs, the fuel assembly size is the same as that of BWRs, but the fuel assembly gap was expanded to enlarge the non-boiling region outside the channel box, which increases the water-to-fuel volume ratio. This mitigates an increase in negative void reactivity coefficient by MOX fuel loading and a reduction in reactivity worth by control rods and boric acid water. Sufficient thermal margin and reactor shutdown capability were obtained from a 100 % MOX-fueled ABWR core and the MOX fuel loading has been confirmed to have a high flexibility [24].

Differently from uranium fuel, MOX fuel does not need an enrichment process, and the fraction of plutonium oxide to be mixed with depleted uranium oxide is only increased for high burnup. Such a high burnup with no enrichment cost increase has a large effect on the fuel cycle cost. A high burnup MOX fuel is being developed through irradiation tests in experimental reactors the same approach as taken for developing the high burnup uranium fuel.

Plutonium is an α emitter. Secondary reactions of the released α particles and the self-fission of ^{240}Pu release neutrons. MOX fuel treatment must pay more attention to radiation protection and heat generation than uranium fuel treatment. Features and measures of radiation and decay heat in MOX fuel are mentioned in Sect. 3.3.6.

[5] Reactor power uprates [25]

Reactor power uprates are intended to raise the reactor electric power by about several to 20 % as thermal power rise without compromising reactor safety in existing nuclear power plants. For example, a reactor power uprate by 5 % in 20 power plants has the same effect as the construction of a new power plant. European and USA regulatory authorities have given about 160 approvals for these uprates and extensive experience has been gained since the 1970s.

Classifications of reactor power uprates are described below.

(1) Measurement-Uncertainty-Recapture type

MUR types of power uprates are based on improved measurement of feedwater flow rate through use of ultrasonic flow metering to significantly reduce the uncertainty in thermal power calculations for safety analysis. Reduction of the uncertainty can result in uprates of up to 1.5 % in reactor thermal power (steam flow rate) within the allowable range of safety analysis.

(2) Stretch type

Stretch types of power uprates can be typically introduced up to around 7 % of the original licensed power levels without major plant modification by using conservative measures built into the plant.

(3) Extended type

Extended types of power uprates can increase the original rated thermal power by up to 20 % with high performance fuel, but require significant modifications to major plant machinery such as the steam turbine and main electric generator.

The following effects are expected in BWR power uprates.

- Nuclear and thermal margin (core and fuel)
- Neutron flux increase (reactor vessel)
- Decay heat increase (containment vessel)
- Steam flow rate increase (turbine system)
- Load factor increase (turbine system and electric generator)
- Turbine exhaust heat increase (condenser)
- Condenser flow rate increase (feedwater pipe and feedwater heater)

Those effects of power uprates have been evaluated as to whether they are allowable within the design criteria or not, considering reactor operation and maintenance experience and operation data. The range of improvements and facility modifications are determined based on the evaluation results.

As discussed before, the fuel lattice design of BWRs is easily changed. An increase in the number of fuel rods is one of the leading core and fuel technologies to secure the nuclear and thermal margin in uprating reactor power and to improve plant economy. As using a large number of fuel rods improves critical power characteristics and reduces average linear heat generation rate of fuel rods, therefore a lattice design with more rods can be applied to a high burnup long-operating cycle core and a high power density core.

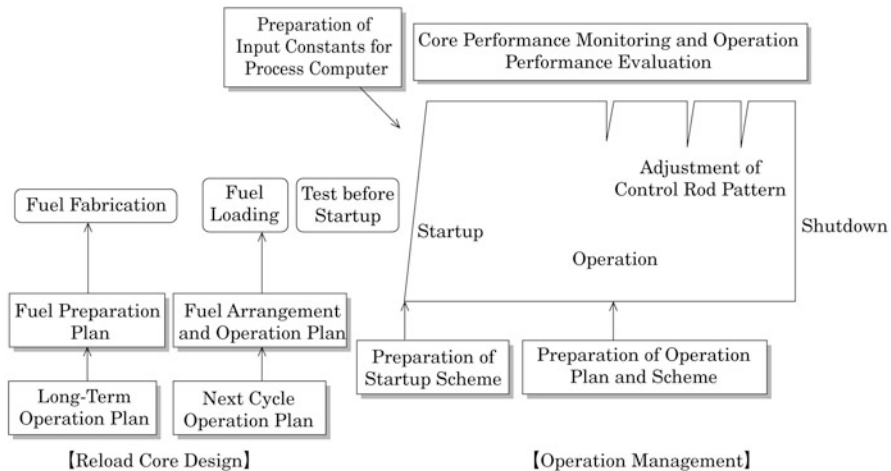


Fig. 3.27 Flow of core management

On the other hand, it causes an increase in pressure drop within a fuel assembly and reduces thermal-hydraulic stability. Hence, a practical 10×10 type fuel has been introduced coupled with measures against the pressure drop such as partial length fuel rod.

3.2.7 Core Management [3, 26, 27]

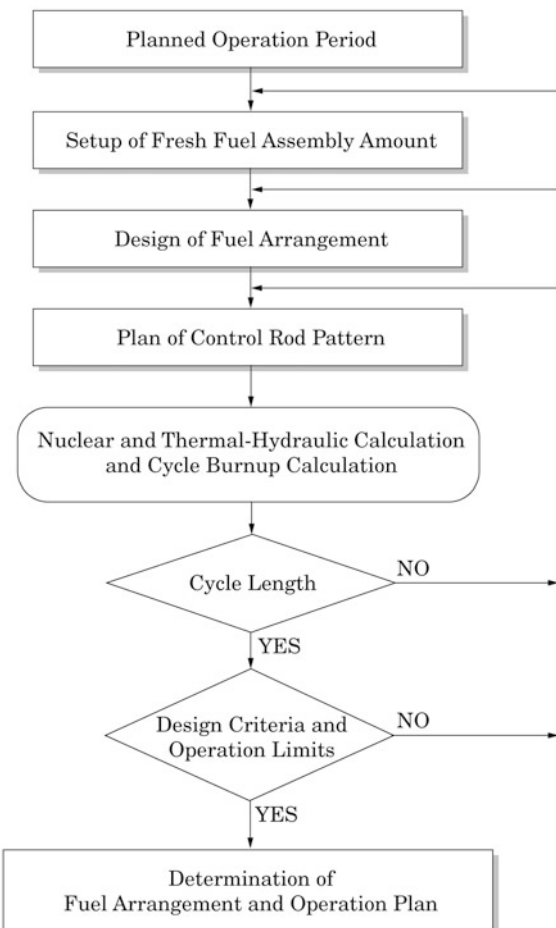
[1] Summary of core management

Core management technology is intended to secure reactor safety and to realize efficient and economic fuel burning. BWR core management can be divided into reload core design and operation management as shown in Fig. 3.27. In the reload core design, middle- and long-term fuel preparation plans are made and the fuel assembly arrangement and basic operation plan are determined for each reload core. The operation management determines a detailed operation scheme at startup and normal operation and supports safe operation by monitoring core performance using process computers.

[2] Reload core design

Nuclear reactor operation management is based on a long-term operation plan of 3–5 years. The plan includes startup date of each operating cycle, shutdown period for periodic inspection, and load factor in operation. It also includes intermediate shutdown planned in each operating cycle. After the long-term operation plan, the cycle burnup is obtained from reactor operating days and load factor of each cycle, and the plan of fuel exchange to be performed during the periodic inspection period is investigated. Core analysis is done for each cycle to evaluate the plan. Proper fuel loading pattern of each cycle is investigated and fresh fuel amount and types are determined.

Fig. 3.28 Typical flow of reload core design



This long-term burnup plan is used to systematically procure fuel which is ordered from the supplier at the very latest 2 years before delivery to the plant; this is based on considerations of procurement of enriched uranium and cladding and fuel fabrication times from pellet to fuel assembly.

Main tasks in the reload core design are to determine fresh fuel amount necessary for the planned operating cycle and its arrangement in the core and to make a basic operation plan.

Figure 3.28 shows a typical process flow for the reload core design in which an optimal reload core is designed by repeated investigations with combinations of available fuel assemblies after the number and arrangement of fuel assemblies loaded into the core and control rod pattern are guessed first.

Safety parameters for the BWR reload core include the reactivity shutdown margin, maximum linear heat generation rate, MCPR, maximum fuel assembly

burnup, channel stability, core stability, and control rod irradiation lifetime, as discussed in the beginning of this section.

During the periodic inspection period, fuel exchange is performed based on the prepared fuel loading pattern. Usually, about 1/4 of the core fuel assemblies are replaced with fresh ones and the other fuel assemblies are, if necessary, moved to different locations in the core (fuel shuffling). This refueling operation is a major step to determine the periodic inspection period and therefore a plan with less movement of fuel assemblies, namely, a plan with less fuel shuffling is important from the viewpoint of an improved capacity factor by shortening the periodic inspection period. In the fuel loading pattern of the equilibrium cycle core shown in Fig. 3.20, fuel assemblies stay in almost the same location until the third cycle since they were first loaded, and then they are moved to the outermost region of the core or the control cell region for the fourth cycle. This results in the flat power distribution as well as less fuel shuffling.

Possible fuel loading patterns are innumerable, even considering core symmetry, and search for an optimized loading pattern in combination with control rod patterns is inevitably limited by limited computational resources. Recently, a tool based on accumulated operation knowledge was developed to automatically plan and optimize the fuel loading and control rod pattern [28].

After the periodic inspection, various performance factors are tested before startup, including the reactor shutdown margin in core and safety in fuel reloading.

[3] Operation management

As mentioned, the reactor power of BWRs can be controlled by control rods and core flow rate. BWR operation management must accurately calculate power distribution in each part of the core and achieve efficient fuel burnup by control of control rods and core flow rate. A reactor operation scheme is prepared by using computational codes to simulate the reactor operation state; a time variation in Xe concentration as power is evaluated and 3D nuclear and thermal-hydraulic coupled core calculations are performed.

In the early BWR startup, core power was slowly increased while applying the PCIOMR, accumulating Xe. It took 3–4 days to reach the rated power from start of the electric generator. The startup period was reduced to about 1 day by improvement in fuel performance and power rise speed and by effective combination of control rod operation and core flow rate adjustment.

After startup, the long term reactivity is controlled by changing the control rod location and depth (control rod pattern) and the short term reactivity by core flow rate. Reactor operation management during operation involves preparing the period and scheme for control rod pattern adjustment. In the past the control rod pattern was adjusted mainly at low core power, but recently it is conducted at nearly the rated core power because of improved fuel performance.

[4] Core performance monitoring

Startup range neutron monitor (SRNM) and power range monitor (PRM) systems are separately used from startup to the full power condition in nuclear measurement of BWRs. Since neutron flux level varies by about nine orders of magnitude from startup to full power, two different types of monitors are employed corresponding to each detectable neutron flux level. Both types of monitors are installed in the core as shown in Fig. 3.3. Fission ionization chamber type monitors are used in the SRNM system as a fixed arrangement type one. In a 1,300 MWe-class ABWR plant, the PRM system consists of 208 local power range monitors (LPRMs) and traversing in-core probes (TIPs) for LPRM calibration. LPRMs are inserted into the neutron flux instrumentation tubes in the gap between channel boxes at the corner of the fuel assemblies and four LPRMs are axially installed in one instrumentation tube. LPRMs are components of the average power range monitor (APRM) system and they average the power signals as well as detect the usual neutron flux distribution in the core at normal operation [3].

One PRM or LPRM is usually used for every 16 fuel assemblies as shown in Fig. 3.3 and it corresponds to one for four fuel assemblies in considering a quarter-symmetric core. LPRM measurements are spatially discrete information which is not intended to directly measure the fuel assembly and fuel rod power. The assembly power distribution in the entire core is evaluated in combination with the relation between measured values and adjacent fuel assembly powers and the 3D computational model. Operation parameters such as maximum linear heat generation rate and MCPR are regularly monitored. Such power monitoring is implemented by a process computer referred to as *core performance calculation system*. It is necessary to prepare input constants of the process computer for the power distribution calculation using LPRM measurements before reactor startup; this is an important core management task.

Because of recent improvements in computer performance, a 3D nuclear and thermal-hydraulic coupled calculation model in a core design code is generally used in the core performance calculation of the process computer. Results of the core performance calculations are corrected by measurements from LPRMs and TIPs in each location to more accurately monitor and predict the core power distribution. The variation in burnup and fuel materials of each fuel assembly is also calculated in the process computer.

Alternatively, follow-up calculations of reactor operation are usually performed every month by off-line computers in which the same core design codes are installed. In the computers, calculations from the core design and measurements during operation, and results from the follow-up calculations and operation data are compared to evaluate and confirm the reproducibility of core design codes in the actual operation. The off-line computers are also used to calculate predicted operation in the next cycle and if necessary to re-investigate the control rod patterns. Thus, highly accurate and quick operation management based on the real operation data is possible.

3.2.8 Fuel Management

[1] Fresh and spent fuel management [3]

Fuel management of nuclear power plants includes the tasks described next.

(1) Fresh fuel acquisition

Fuel assemblies manufactured in a nuclear fuel factory are transported to the power plant 3–4 months before the periodic inspection and then the acceptance inspection of fresh fuel is made to ensure there was no abnormality caused during the transport, and to confirm the fuel assembly appearance and size are as specified.

(2) Refueling during overhaul

Fresh fuel assemblies are stored in the fresh fuel storage after the acceptance inspection and then moved to spent fuel storage pool before the periodic inspection. Alternatively, fresh fuel assemblies may be directly moved to the spent fuel storage pool after the acceptance inspection without being stored in fresh fuel storage.

In BWR refueling, usually not all fuel assemblies are moved to spent fuel storage pool as long as there is no large-scale construction in the core and reload fuel assemblies are shuffled in the core. Spent fuel assemblies are discharged to the spent fuel storage pool, and fresh fuel assemblies are loaded and shuffled in the core. After fuel loading, underwater TV cameras are used to confirm that the fuel assemblies are correctly loaded according to the fuel loading pattern.

(3) Fuel inspection during overhaul

Overview inspection of fuel assemblies is made to confirm integrity of fuel was kept during irradiation. Two fuel assemblies with maximum burnup in each assembly type are inspected for fuel rod damage, deformation, and gap clearance change through visual observation.

Shipping inspection is made to check for leakage of radioactive materials from fuel assemblies. Fuel assemblies are covered by channel boxes. Shipping caps are placed on the channel boxes in the core and they collect water inside each channel box. The presence of radioactive material leakage is evaluated by ^{131}I concentration in the water sample.

(4) Spent fuel storage and carry-out

Spent fuel discharged from the reactor core is stored in the spent fuel storage pool and cooled over a period, and then taken to the reprocessing factory. Recently, dense storage using boron-containing fuel storage racks, establishment of an independent storage pool in the power plant site, and use of dry storage casks are employed to enhance the storage capacity of spent fuel.

(5) Nuclear material accounting and safeguards

Fuel contains nuclear materials such as uranium and plutonium. A record of change and inventory of nuclear materials is prepared and regularly reported to the government and the International Atomic Energy Agency (IAEA). Inspectors from the government and IAEA also regularly inspect it to prevent unauthorized use of nuclear materials (safeguards activity).

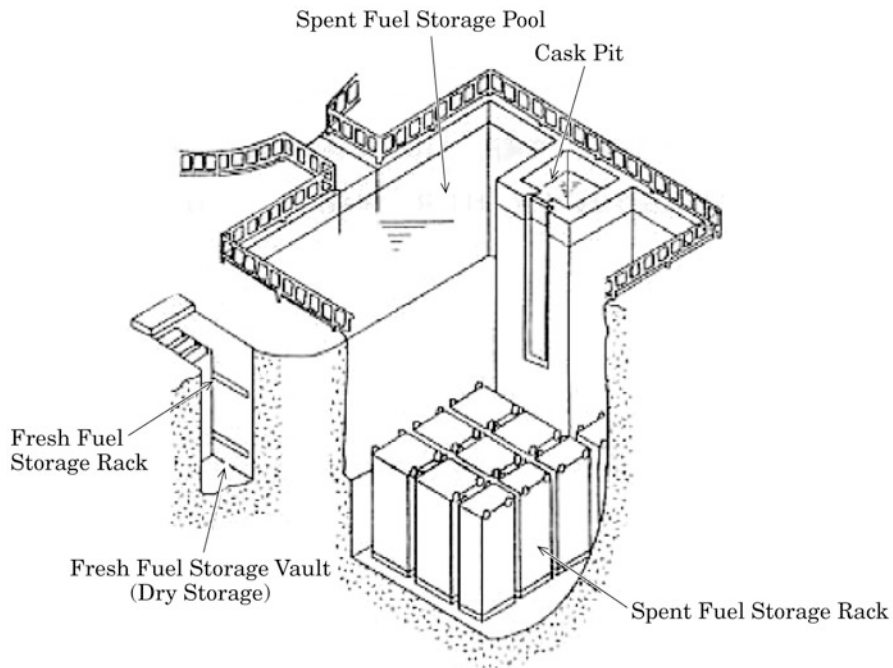


Fig. 3.29 Schematic view of spent fuel storage and handling facilities in nuclear reactor area

Table 3.10 Example of main specifications of spent fuel storage facilities [4]

Spent fuel storage pool	Type	Stainless steel lining pool type (rack storage)
	Capacity	~430 % of whole core
Spent fuel storage rack	Type	Stand rack type
	Material	Boron-added (1.0–1.75 wt%) stainless steel

[2] Fuel storage and handling facilities [4]

Fuel storage and handling facilities are for storage and handling of fresh fuel from the carry-in to the power plant to loading, and of spent fuel from discharge from core to the carry-out from power plant. They include the fresh fuel storage, spent fuel storage pool, cask pit, refueling machine, reactor building crane, and fuel pool cooling cleanup system. Figure 3.29 shows a schematic view of the spent fuel storage and handling facilities in an ABWR and Table 3.10 presents the main specifications of spent fuel storage facilities.

Fuel storage and handling facilities are designed according to the “Review Guide for Safety Design” to secure safety in storing and handling fuel. For criticality safety, it is required that *fuel storage and handling facilities must be designed to prevent criticality in any cases to be expected by geometrical safe arrangement or other suitable means*. An outline and the design points of the main facilities follow below.

(1) Fresh fuel storage facilities

Fresh fuel storage consists of reinforced concrete facilities to store fresh fuel carried into the power plant until fuel loading after acceptance inspection. Fuel is stored vertically in metal racks in a dry condition. Fresh fuel storage is constructed to prevent water flooding and is able to drain water which may have entered the storage.

The capacity for fresh fuel storage is designed considering that spent fuel storage pool accommodates fresh and reloading fuel assemblies in one refueling. The fresh fuel storage of ABWRs is designed to be able to accommodate 5 % of the fuel assemblies of the entire core.

Fresh fuel storage racks are designed to assure that the effective multiplication factor is maintained at less than 0.95 even in a severe condition such as water flooding when the maximum amount of fresh fuel is being stored; this is done by holding a proper fuel assembly spacing to prevent criticality of storage fuel. In the analysis of subcriticality in fresh fuel storage, the infinite multiplication factor of fresh fuel in being loaded into the core is assumed to be 1.30 for a sufficient safety evaluation.

(2) Spent fuel storage pool

The spent fuel storage pool is connected to the reactor well through the pool gate installed on the top floor in the reactor building and fuel is stored in spent fuel storage racks which are fixed to the bottom of the pool. The spent fuel storage pool is designed with a capacity that all fuel assemblies in the core can be moved to the pool even after spent fuel is stored as planned. The spent fuel storage pool of ABWRs, as shown in Table 3.10, can accommodate a fuel amount to as much as about 430 % of the whole core.

Spent fuel storage racks are designed to assure that the effective multiplication factor is maintained at less than 0.95 in any cases to be expected for water temperature in the pool and fuel location in the racks under the maximum fuel storage, by holding a proper fuel assembly spacing to prevent criticality of storage fuel. In the analysis of subcriticality in spent fuel storage, the infinite multiplication factor of stored fuel to be loaded into the core is assumed to be 1.30, the same as for the fresh fuel storage. Recently, stainless steel containing boron as a neutron absorber is used in spent fuel storage racks to increase storage density.

The wall and bottom of the spent fuel storage pool and cask pit are shielded by a concrete wall and the top of spent fuel is secured by a water depth to ensure a sufficient shielding effect. The internal surface of the pool and cask pit is lined with stainless steel to prevent leaks. In addition, the spent fuel storage pool and cask pit are designed to have no drains and check valves are established in pipes connected to the pool, to prevent outflow from the pool by siphon effect even if the pipes break.

Fuel handling facilities are designed to have a structure in which fuel assemblies can be handled independently to prevent criticality of fuel, and in which the transportation (from core to the spent fuel storage pool) and storage (to cask) of spent fuel can be performed under water.

(3) Fuel pool cooling cleanup system

The fuel pool cooling cleanup system has a function to remove decay heat from spent fuel in the heat exchanger and the fuel cooling pool, and to desalt/filter pool water and maintain water purity and transparency. The fuel pool cooling cleanup system is designed to keep pool water temperature below 52 °C in the case of the usual maximum heat load which is defined as the sum of two different decay heats: one is from the discharged spent fuel in one refueling when closing the pool gate which separates the reactor well and fuel pool and the other is from the previously discharged spent fuel. Also, the system should have sufficient cooling performance to maintain the pool water temperature below 65 °C, in combination with residual heat removal system, in the case of maximum heat load which is defined as the sum of two different decay heats: one is from the whole core at the end of cycle and the other is from the previously discharged spent fuel.

3.3 PWR Core Design and Core·Fuel Management

3.3.1 General Core Design

[1] Features of PWR Core

PWRs operate in an *indirect cycle* in which the primary coolant heated and pressurized in the reactor core is cooled through steam generators and pumped under high pressure into the reactor core again. The steam generated in the secondary loop is fed through a turbine which drives an electrical generator. The coolant as a neutron moderator is pressurized to about 15.5 MPa in the pressurizer and forced to circulate to cool the core with a single-phase flow with hardly any occurrence of boiling. Therefore, the moderator density variation in the core is small. The boric acid as a neutron absorber is dissolved into the moderator.

Figure 3.30 shows a cross-sectional view and structures of a PWR core which has an arrangement of 193 fuel assemblies with fuel rods of 17 × 17 type array. Each fuel assembly consists of 264 fuel rods, 24 control rod guide tubes (guide thimbles), and 1 core instrumentation tube (guide thimble). The control rod guide tubes are used for insertion of control rod clusters and burnable poison rods.

[2] Basic Criteria of Core Design

The main target of the reactor core design is same as that of BWR core design, to improve cost performance while securing reactor safety. The security of reactor shutdown capability, reactivity insertion limit, self-controllability, fuel failure prevention, power distribution restriction, and stability are all required for safety. Table 3.11 introduces the basic criteria to be considered in the PWR core design.

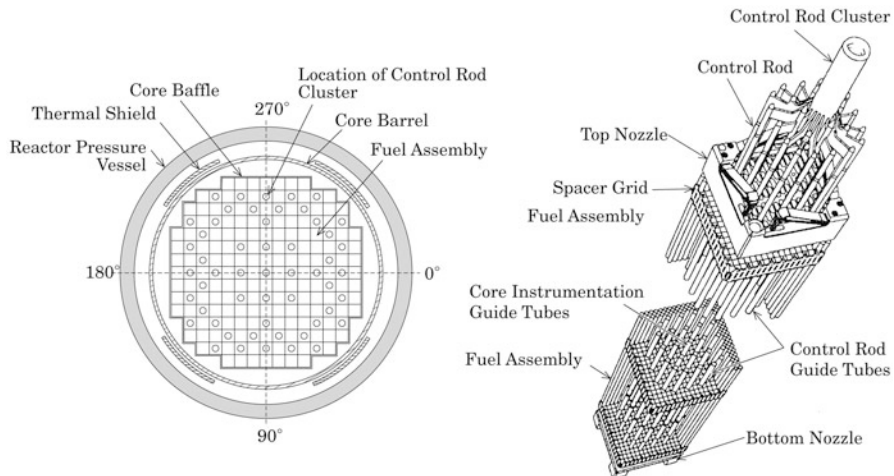


Fig. 3.30 Cross-sectional view and fuel assembly of a PWR core (Copyright Mitsubishi Heavy Industries, Ltd., 2014 all rights reserved)

(1) Reactor Shutdown Margin

PWR cores are designed to assure complete core shutdown capability at the hot temperature condition even with the most reactive rod cluster control assembly (RCCA) stuck in the fully withdrawn position. They are also designed to maintain the core shutdown capability even at the cold temperature condition by boric acid injection using the chemical and volume control system.

(2) Reactivity Insertion Limit

The rod cluster control assembly (RCCA) is designed with appropriate limits on the maximum worth so that the core internal structures can provide core cooling without damage to the integrity of the coolant pressure boundary at an ejection of a RCCA. Secondly, it is designed with appropriate limits on the maximum reactivity insertion rate so that the fuel integrity is secured at a simultaneous withdrawal of two banks of RCCAs at the maximum speed. Thirdly, it is also designed with appropriate limits on the maximum worth so that the fuel integrity is secured at a drop of a fully-withdrawn RCCA at the hot full power condition.

(3) Self Controllability

Cores are designed to assure the inherent negative reactivity feedback characteristics. The fuel temperature coefficient (Doppler temperature coefficient) is always negative and it is designed so that the moderator temperature coefficient is negative at hot power operation. Getting the negative power coefficient by the combination of fuel and moderator coefficients suppresses the power rise in abnormal transients.

Table 3.11 Main criteria of PWR core design [29]

Items	Design principles	Examples of limits
Reactor shutdown	Designed to assure the complete core shutdown capability at hot temperature condition even with the most reactive rod cluster control assembly (RCCA) stuck in the fully withdrawn position. Designed to maintain the core shutdown capability even at cold temperature condition by boric acid injection of chemical and volume control system	Reactivity shutdown margin $>0.016 \Delta k/k$ at hot temperature $>0.01 \Delta k/k$ at cold temperature
Reactivity insertion limit	Designed with appropriate limits of the maximum rod cluster control assembly (RCCA) worth so that the core internal structures function for a core cooling without damage to integrity of coolant pressure boundary at the ejection of a rod cluster control assembly	Ejected RCCA worth $<1.2 \times 10^{-3} \Delta k/k$ at hot full power
	Designed with appropriate limits of the maximum reactivity insertion rate so that the fuel integrity is secured at a withdrawal of two banks of RCCAs at the maximum speed	Maximum reactivity insertion rate $<7.5 \times 10^{-4} \Delta k/k/s$
	Designed with appropriate limits of the maximum RCCA worth so that the fuel integrity is secured at a sudden drop of a fully-withdrawn RCCA at hot full power condition	Dropped RCCA worth $<2.5 \times 10^{-3} \Delta k/k$
Self controllability	Designed to assure the inherent negative reactivity feedback characteristics where the Doppler coefficient is always negative and the moderator temperature coefficient is negative at hot power operation	Doppler coefficient $-5.2 \sim -1.8 \times 10^{-5} \Delta k/k^{\circ}\text{C}$ Moderator temperature coefficient $<0 \Delta k/k^{\circ}\text{C}$ at hot power operation
Fuel integrity	Designed to assure that the minimum DNBR is larger than the allowable limit	Minimum DNBR >1.42 at abnormal transients
	Designed to assure that the maximum fuel centerline temperature is lower than the fuel melting point	Maximum fuel centerline temperature $<2,580^{\circ}\text{C}$ for fresh fuel
	Designed to assure that the maximum burnup is lower than the design limit	Maximum fuel assembly burnup $<55,000 \text{ MWd/t}$
Power distribution restriction	Designed to assure that the nuclear enthalpy rise hot channel factor ($F_{\Delta H}^N$) is lower than the design limit at normal operation	Nuclear enthalpy rise hot channel factor $F_{\Delta H}^N \leq 1.64 \times \{1 + 0.3(1 - P)\}$ P : rated core power to 1.0 Heat flux hot channel factor $F_Q \leq 2.32/P$
	Designed to assure that the heat flux hot channel factor (F_Q) is lower than the design limit at normal operation	
	Designed to assure that the maximum linear power density does not exceed the design limit at abnormal transients	Maximum linear power density $<59.1 \text{ kW/m}$
Stability	Designed to assure no abnormal oscillation of power distribution where the oscillation decay characteristics are sufficient or any oscillation is detected and easily suppressed	Radial oscillation Decay characteristics Axial oscillation Suppression capability

(4) Fuel integrity

The minimum *departure from nucleate boiling ratio* (DNBR) and maximum fuel centerline temperature are limited to secure fuel integrity at normal operation and abnormal transients. DNBR is defined as the ratio of predicted *critical heat flux* (heat flux at the time when a departure from nucleate boiling occurs in boiling heat transfer, referred to as *DNB heat flux*) to actual heat flux. Cores are designed to have a minimum DNBR larger than the allowable limit and a fuel centerline temperature lower than the fuel melting point.

In addition, the cores are designed to assure that maximum burnup is lower than the design limit confirmed for fuel integrity. There is also another maximum burnup limit obtained from fuel cycle considerations such as the acceptance limit set by reprocessing facilities.

(5) Power Distribution Restriction

To meet the minimum DNBR limit at normal operation and abnormal transients, cores are designed to assure that the nuclear enthalpy rise hot channel factor ($F_{\Delta H}^N$) is lower than the design limit at normal operation. The heat flux hot channel factor (F_Q) must be lower than the design limit at normal operation to satisfy safety analysis (LOCA analysis) initial conditions, and moreover, maximum linear power density must not exceed the design limit at abnormal transients due to the limits of minimum DNBR and maximum fuel centerline temperature at abnormal transients.

(6) Stability

Cores are designed to assure no abnormal oscillation of the power distribution where oscillation decay characteristics are sufficient or if there are any oscillations, that they can be easily detected and suppressed.

[3] Core Design Procedure

The flow diagram in a new core design is shown in Fig. 3.31. Core thermal power and cycle length are given as the basic core design goals. Maximum fuel assembly burnup and maximum linear power density are determined according to core design principles.

First, the fuel loading amount is determined to satisfy the core thermal power, cycle length, and maximum fuel assembly burnup limit. Core volume is determined from the fuel loading weight and the moderator-to-fuel volume ratio (V_m/V_f) set by considering the core nuclear characteristics. Fuel rods and assemblies are designed to meet fuel integrity requirements such as maximum linear power density, considering control rod arrangement. The number of fuel assemblies and the core configuration are determined to meet the determined core volume. Core characteristics are evaluated with those core design parameters. The loops of this core design procedure are repeated until the values satisfy the core design principles.

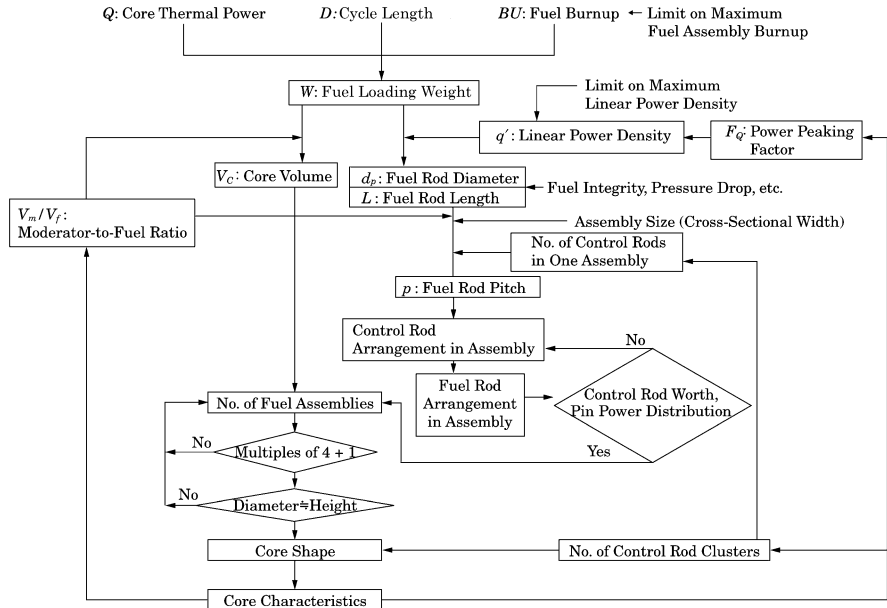


Fig. 3.31 PWR core design flow

3.3.2 Core Size and Figure Set-up

[1] Fuel loading weight

As mentioned above, the fuel loading weight is first determined in the core design based on the cycle length and rated core thermal power as given by the next equation.

$$W = Q \times D \times N_b / BU \quad (3.23)$$

W : fuel loading weight (t)

Q : core thermal power (MW)

D : operation cycle length (day)

N_b : refueling batch number (the reciprocal of the discharged fuel fraction in one refueling = the reciprocal of the new fuel fraction)

BU : region or batch averaged fuel assembly burnup (MWd/t)

The operation cycle length is fixed by considering refueling and periodic inspection intervals. Since generally a longer cycle length leads to a higher capacity factor and a lower operating cost of the plant, there is a tendency to set the cycle length as long as possible.

Fuel economy is strongly dependent on the fuel batch size. With a larger batch size, fuel assemblies can stay longer in core and achieve higher burnup,

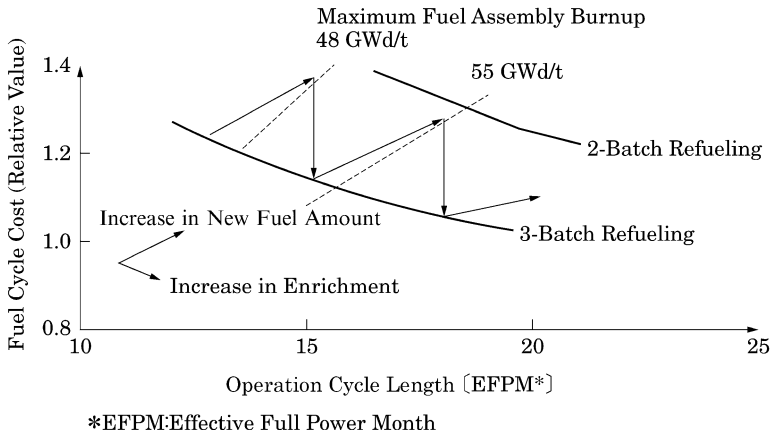


Fig. 3.32 Example of fuel cycle cost variation for operating cycle length, with batch size and maximum fuel assembly burnup as parameters (Copyright Mitsubishi Heavy Industries, Ltd., 2014 all rights reserved)

and therefore that results in a reduction in fuel cycle cost. The fuel batch size is, however, restricted by the design limit of the maximum fuel assembly burnup. For a given operating cycle length, the largest batch size is taken in the range of possible maximum fuel assembly burnups. The average fuel assembly burnup becomes higher as the variation in discharge burnup of each fuel assembly is smaller. Usually, the average fuel assembly burnup is supposed assuming a certain ratio of the maximum to average fuel assembly burnups (for example, about 1.1). Hence, the fuel loading weight in Eq. (3.23) is determined with these considerations.

Figure 3.32 shows the relationships for cycle length, batch size, maximum fuel assembly burnup, and fuel cycle cost.

- (i) For a longer operating cycle length, fuel enrichment can be increased for higher burnup under a constant batch size or the number of new fuel assemblies can be increased; namely, fuel batch size is decreased under a constant fuel enrichment. Fuel enrichment is usually standardized and fixed, and therefore it is usual to increase the number of new fuel assemblies. Maximum fuel enrichment is currently limited to 5 % by restrictions on fuel fabrication facilities and transportation.
- (ii) An increase in the number of new fuel assemblies and then a decrease in batch size lead to a lower average fuel assembly burnup and a higher fuel cycle cost. Since fuel cycle cost occupies a small fraction of total plant operating cost, a longer operating cycle length reduces the total plant operating cost even for a smaller batch size.
- (iii) For a long cycle length and low fuel cycle cost, it is also necessary to advance the limit of the maximum fuel assembly burnup. This can be

achieved by loading an improved type of fuel such as with new alloy cladding. A higher limit for the maximum fuel assembly burnup increases the fuel batch size and reduces the fuel cycle cost even for the same cycle length.

[2] Core size and figure

The fuel loading weight per unit core volume is determined by considering the moderator-to-fuel volume ratio (V_m/V_f) (which is discussed in the next section) and fuel density. Then the total core volume is calculated from the weight per volume and the total fuel loading weight W determined by Eq. (3.23). Core height and equivalent diameter are determined according to the following conditions.

- (i) Equivalent core diameter should be suitable for reactor vessel design and manufacture.
- (ii) Core height and equivalent diameter should be as close to each other in value as possible to reduce neutron leakage to the core outside from the viewpoint of neutron economy.
- (iii) The number of fuel assemblies should be a multiple of four + one; quarter-symmetry fuel loading pattern and one rod cluster control assembly located in the core center.

Current plants have small variations regarding the second condition which was considered in the early core designs. In the process of sizing up the core, a large equivalent diameter has come to be used since fuel active height was standardized (namely, the core height was fixed).

An example of core configuration with fuel assemblies can be seen in Fig. 3.30. The core is a four-loop core with 193 fuel assemblies.

3.3.3 Design of Fuel Lattice and Assembly

[1] Optimization of Fuel Lattice

A change in the ratio of moderator to fuel causes a variation in the neutron spectrum and leads to different core nuclear characteristics. The variation in nuclear characteristics can be evaluated as a function of the moderator-to-fuel volume ratio (V_m/V_f) or H/U atomic ratio. The following parameters change the H/U ratio in the fuel lattice, beginning from the reference design of the fuel assembly:

- (i) fuel rod diameter
- (ii) fuel rod pitch
- (iii) moderator density
- (iv) pellet density

Figure 3.33 shows an example of the variation in infinite multiplication factor (k_∞) with the H/U ratio changed by fuel rod pitch. k_∞ increases with the H/U ratio, which indicates that the excess reactivity to be controlled also

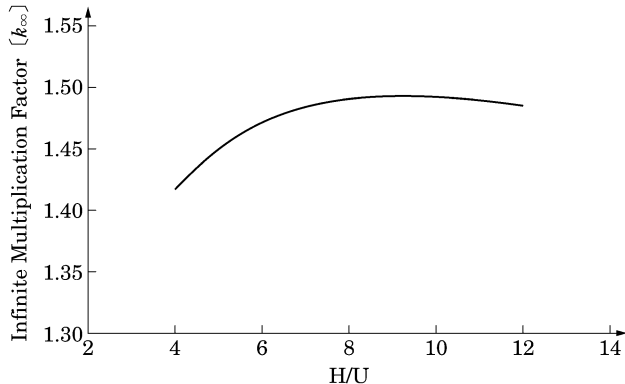


Fig. 3.33 Typical infinite multiplication factor as a function of H/U ratio (Copyright Mitsubishi Heavy Industries, Ltd., 2014 all rights reserved)

increases. The H/U ratio at the maximum k_{∞} is about 9 which is larger than the H/U ratio of current PWRs which is about 4. An increase in H/U ratio leads to a larger thermal neutron flux by the moderation effect of the increased number of hydrogen atoms and therefore a k_{∞} rise. If H/U exceeds about 9, however, neutron absorption in water becomes dominant and k_{∞} oppositely decreases.

The sign (positive or negative) of the moderator temperature coefficient can also be explained using this figure. A moderator temperature rise decreases the H/U ratio and the moderator temperature coefficient becomes negative if k_{∞} decreases as the H/U ratio decreases. Therefore, the H/U ratio should be to the left of the maximum k_{∞} . The H/U atomic ratio of 4 approximately corresponds to the moderator-to-fuel volume ratio of 2. The core nuclear characteristics with H/U ratio as a parameter have been extensively surveyed by the researchers [30].

[2] Fuel Assembly Design

(1) Fuel Assembly Size

Large-size fuel assemblies can reduce the number of fuel assemblies to be loaded in core and to be handled in refueling, and therefore they result in an improved capacity factor of a plant. However, a larger size leads to an increase in effective multiplication factor and even one fuel assembly may result in criticality. It is necessary to ensure that one fuel assembly to be handled outside the core should be subcritical in unborated water. For 5 % fuel enrichment, the maximum fuel assembly size to satisfy this condition is a cross-sectional width of about 22 cm.

(2) Fuel Rod Pitch

Fuel rod pitch can be determined by fuel rod diameter and moderator-to-fuel volume ratio V_m/V_f (H/U atomic ratio). Since control rods as well as fuel rods are placed in fuel assemblies, the number and arrangement of fuel rods are determined according to the following items. Control rods are usually withdrawn in normal operation. Therefore, the control rod volume

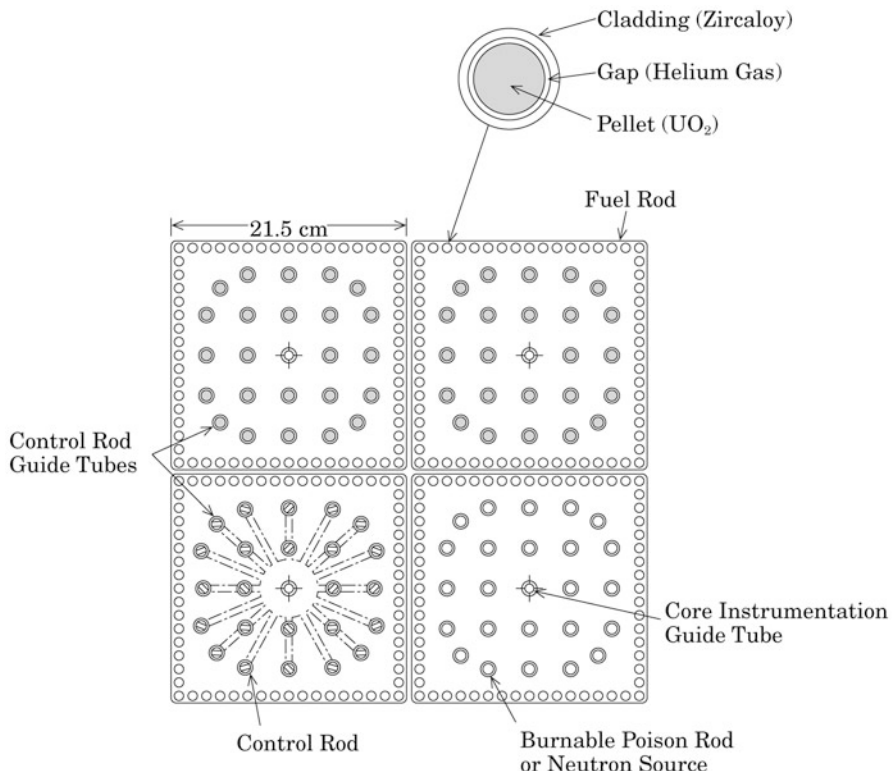


Fig. 3.34 Cross-sectional view of PWR fuel assembly (17 × 17 type) [31] (Copyright Mitsubishi Heavy Industries, Ltd., 2014 all rights reserved)

in fuel assembly is also regarded as the moderator volume in evaluating the moderator-to-fuel volume ratio.

(3) Control Rod and Fuel Rod Arrangement in Fuel Assembly

The numbers of rod cluster control assemblies (RCCAs) and rods per assembly are determined to secure necessary reactivity. RCCAs are inserted into some of the fuel assemblies (e.g., Fig. 3.30). In addition to securing the reactivity, the control rod arrangement is determined so that it flattens the pin power distribution in the fuel assembly when control rods are withdrawn, considering also mechanical integrity of RCCAs. After that arrangement is determined, a nuclear instrumentation guide tube is placed near the center of the fuel assembly and then fuel rods are arranged in the remaining locations. The 17 × 17 square lattice arrangement for a fuel assembly is shown in Figs. 3.30 and 3.34. This arrangement is composed of 24 control rod guide tubes (guide thimbles), one nuclear instrumentation guide tube (guide thimble), and the rest are fuel rods. Fuel assemblies of 14 × 14 and 15 × 15 types are also used in Japan.

(4) Fuel Assembly Height

A higher fuel assembly height can reduce the number of fuel assemblies and therefore improve the capacity factor of a plant. There is, however, a limitation in fuel assembly height. A higher assembly height causes an increased pressure drop in the thermal-hydraulic design and therefore requires a higher capacity primary coolant pump. It also gives rise to an increase in fuel assembly bowing in fuel mechanical design and therefore has an adverse effect on fuel loading operation into core. From the viewpoint of nuclear design, as discussed before, the core for which the ratio of the core height to the equivalent diameter is 1.0 gives a good neutron economy because of low neutron leakage. However, the fuel assembly active height was standardized as about 3.7 m for economy in fuel assembly fabrication.

3.3.4 Reactivity Characteristics

Nuclear reactors are designed to have inherent characteristics of power suppression, namely, to have negative reactivity coefficients for temperature variation. Therefore, an excess reactivity to accommodate temperature variation is required to operate the reactor during a given cycle length. Reactors are designed to be shut down safely by properly controlling the excess reactivity.

[1] Reactivity Coefficients

PWR cores have almost no voids and therefore the void coefficient is not significant (only a small void fraction is assumed in evaluating shutdown margin in core design). Important reactivity coefficients in self-controllability of the reactor core are moderator temperature coefficient and Doppler coefficient.

(1) Moderator Temperature Coefficient

The *moderator temperature coefficient* is defined as a reactivity variation by the moderator temperature rise of 1 °C. In PWRs, water density decreases as moderator temperature increases, and reactivity varies correspondingly.

Boron in the moderator, used as a means of reactivity control, makes the moderator temperature coefficient less negative because the moderator temperature rise results in a decrease in boron concentration as well as water density. Figure 3.35 shows the dependence of the moderator temperature coefficient on boron concentration. A high boron concentration can cause a positive moderator temperature coefficient. Burnable poison rods and gadolinia-added fuel rods can be employed to lower boron concentration and maintain a negative moderator temperature coefficient. Thus, reactor cores are designed to have a negative moderator coefficient during power operation and therefore a moderator temperature rise leads to the nuclear feedback to decrease reactivity.

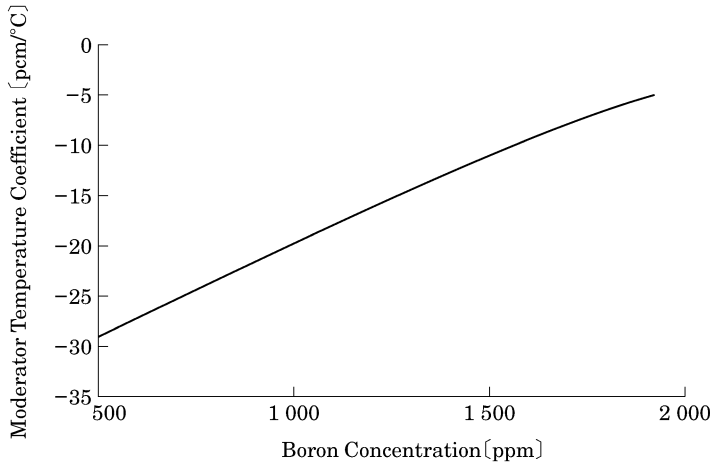


Fig. 3.35 Typical dependence of moderator temperature coefficient on boron concentration (BOC) (Copyright Mitsubishi Heavy Industries, Ltd., 2014 all rights reserved)

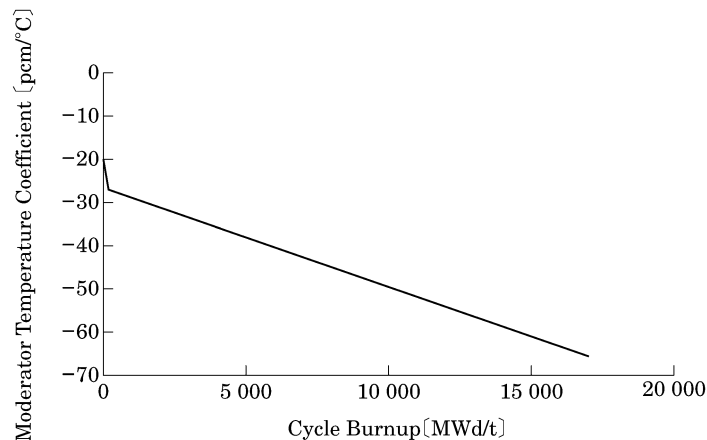


Fig. 3.36 Typical dependence of moderator temperature coefficient on cycle burnup (Copyright Mitsubishi Heavy Industries, Ltd., 2014 all rights reserved)

Rod Cluster Control Assemblies insertion gives a more negative moderator temperature coefficient because neutrons with a longer mean free path due to the moderator temperature rise are more easily absorbed in control rods.

The moderator temperature coefficient shifts to more negative values with increasing burnup, as shown in Fig. 3.36. The main reason is the decline of critical boron concentration as burnup proceeds and the production of plutonium and FPs also contribute to the more negative moderator temperature coefficient as burnup proceeds.

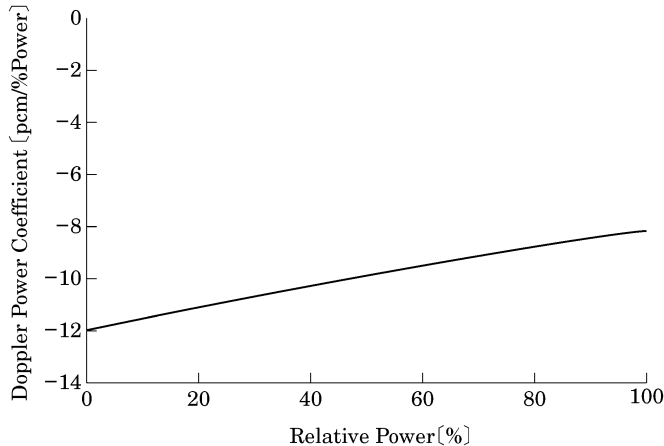


Fig. 3.37 Typical Doppler power coefficient (Copyright Mitsubishi Heavy Industries, Ltd., 2014 all rights reserved)

(2) Doppler coefficient

The Doppler coefficient represents that reactivity is decreased by an increase in neutron resonance absorption (mainly by ^{238}U and ^{240}Pu) resulting from power and then fuel temperature rises. A reactivity variation to a 1 % power rise is referred to as the *Doppler power coefficient*, and a reactivity variation to a 1 $^{\circ}\text{C}$ fuel temperature rise is referred to as the *Doppler temperature coefficient*. As units of reactivity change, pcm and $\%\Delta k/k$ are used where $1 \text{ pcm} = 10^{-5} \Delta k/k$ and $1 \% \Delta k/k = 10^{-2} \Delta k/k$. The former unit is mainly used for a relatively small reactivity change such as with reactivity coefficients and the latter is used for a relatively large reactivity change. Production of ^{240}Pu as burnup proceeds makes the Doppler temperature coefficient more negative, while the fuel temperature increment by the power rise becomes smaller. Therefore, the Doppler power coefficient becomes slightly less negative as burnup increases. Typical Doppler power coefficient as a function of power is shown in Fig. 3.37.

The Doppler temperature coefficient is about -3 to -5 pcm/ $^{\circ}\text{C}$. LWRs have negative Doppler coefficient and reactivity is decreased by the feedback when power increases.

[2] Reactivity Control

The reactivity control in PWRs is done by control rod operation, adjustment of boron concentration in primary coolant (referred to as *chemical shim*) and if necessary using burnable poison rods.

(1) Design Principles for Reactivity Control

- (i) The reactor core should be made subcritical without exceeding the allowable design limit of fuel from the hot standby or hot operation

condition. Core reactivity should be controlled at the hot condition by at least two independent control systems: the *control rod control system* and the *chemical and volume control system*. The latter adjusts the boron concentration in primary coolant.

- (ii) Core reactivity is controlled usually through role sharing of the reactivity control equipment as follows.

- *Rod Cluster Control Assemblies*: Rod cluster control assemblies are used to control the reactivity variation (*power defect*) by the power variation from hot zero power to hot full power; i.e. they provide control of relatively fast reactivity variations.
- *Boron concentration*: Boron concentration is adjusted to control reactivity variations due to the primary coolant temperature variation from cold temperature to hot zero power temperature, FP (Xe and Sm) concentration variation, and fuel burnup; i.e. they provide control of relatively slow reactivity variations.
- *Burnable poisons*: Burnable poisons are employed to partially control the excess reactivity necessary for fuel burnup, which makes the moderator temperature coefficient negative at hot power operation by being able to reduce the boron concentration in the primary coolant.

Figure 3.38 shows a typical reactivity control scheme by the listed reactivity control equipment. The left part (i.e. time before shutdown) indicates the necessary excess reactivity for fuel burnup, being controlled by soluble boron and burnable poison, and the reactivity decline as burnup, being compensated by boron dilution, where the reactivity is set as zero at hot full power. Control rods are inserted to shut down the core (from hot full power to hot zero power) at time zero and to secure subcriticality. The Xe decay following Xe accumulation is compensated by increasing the boron concentration (boration) and the coolant temperature decrease from hot to cold is also compensated in a similar way.

Figure 3.38 indicates that the boron concentration changes during the period of the Xe decay and the coolant temperature decrease. In actual reactor operation, however, the operation of changing the boron concentration can be activated before that period and the reactivity control scheme does not necessarily correspond to the period.

(2) Rod Cluster Control Assembly

(i) Structure of Rod Cluster Control Assembly (RCCA)

A RCCA consists of a set of control rods arranged by spider connecting fingers as shown in Fig. 3.39. Each RCCA moves up and down through inside the control rod guide tube (thimble).

Control rods are made of an alloy (Ag 80 %-In 15 %-Cd 5 %) as a neutron absorbing material enclosed by stainless steel cladding and end plugs are welded at both ends. This alloy is widely used because of its excellent properties regarding neutron absorption, metallurgy,

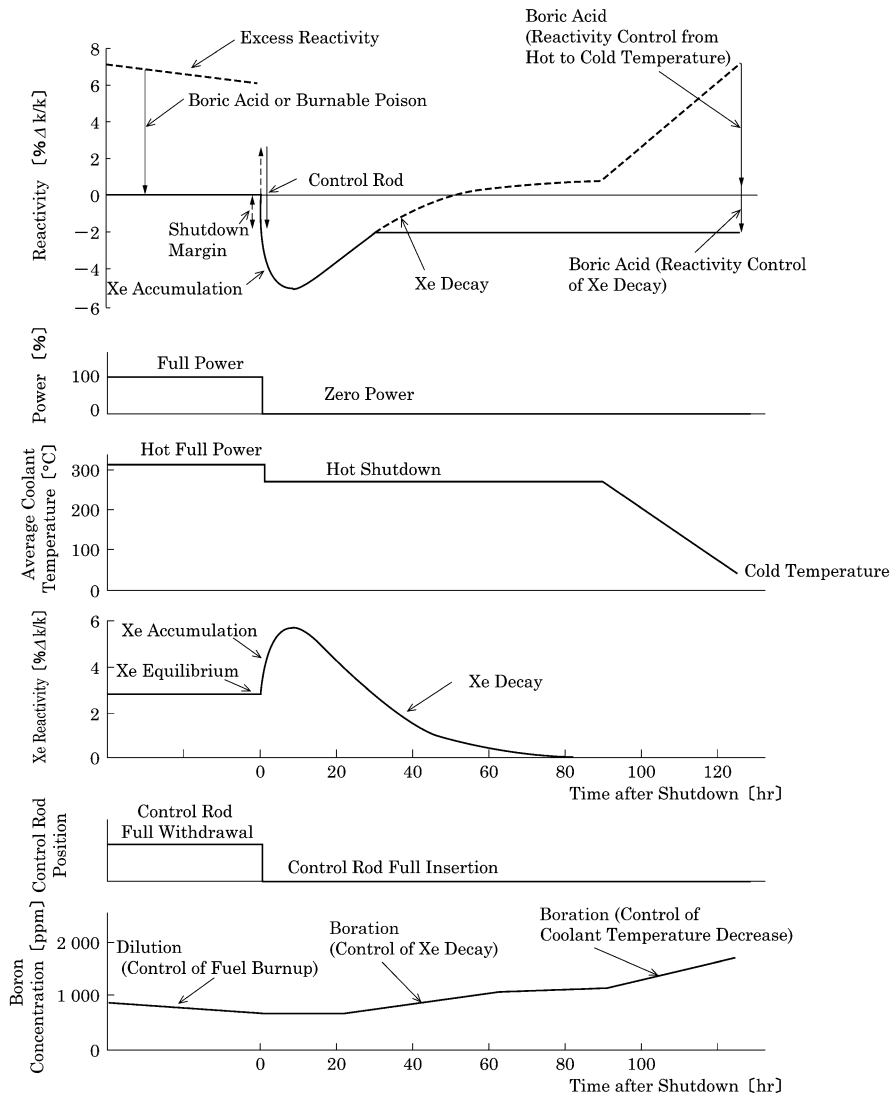
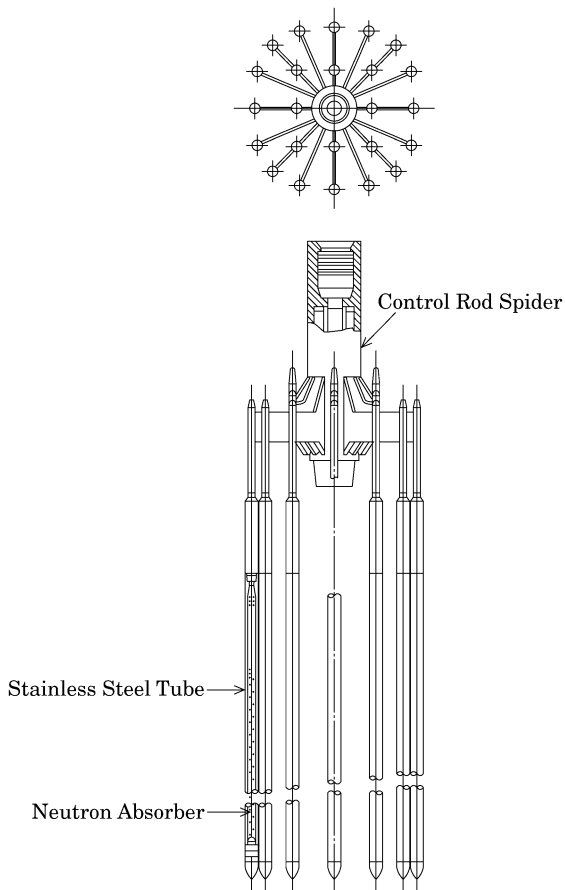


Fig. 3.38 Reactivity control scheme (Copyright Mitsubishi Heavy Industries, Ltd., 2014 all rights reserved)

and ease of manufacture. Cd has a large thermal neutron absorption cross section and Ag and In have suitable thermal neutron absorption cross sections and resonance absorption cross sections as well. Thus, the alloy has overall good neutron absorption properties. Also, from the viewpoint of metallurgy, it has excellent stability as a single-phase solid solution and excellent corrosion resistance. Finally, the alloy produces no gaseous element, i.e. helium gas through the (n, α) reaction

Fig. 3.39 Rod cluster control assembly (RCCA) of PWR (17×17 Type) [31] (Copyright Mitsubishi Heavy Industries, Ltd., 2014 all rights reserved)



as is the case with B_4C . A hybrid type of Ag-In-Cd alloy and B_4C , or Hf is used as a neutron absorber for control rods in some PWRs.

The control rod drive mechanism is mounted on the reactor vessel head and drives RCCAs which are inserted from the core top and moved in about 1.6 cm increments (one step) in the magnetic jack type mechanism. At a reactor trip, all RCCAs are inserted at once by free fall by a power cutoff.

(ii) Pattern and control of Rod Cluster Control Assemblies (RCCAs)

The number and pattern of RCCAs are determined to control the following three reactivities.

- Power defect: The power defect is the reactivity difference from full power to zero power. This is the sum of reactivity changes by fuel temperature variation (Doppler defect), moderator temperature variation (moderator temperature detect), and neutron flux distribution variation (neutron flux redistribution effect), from full power to zero power.

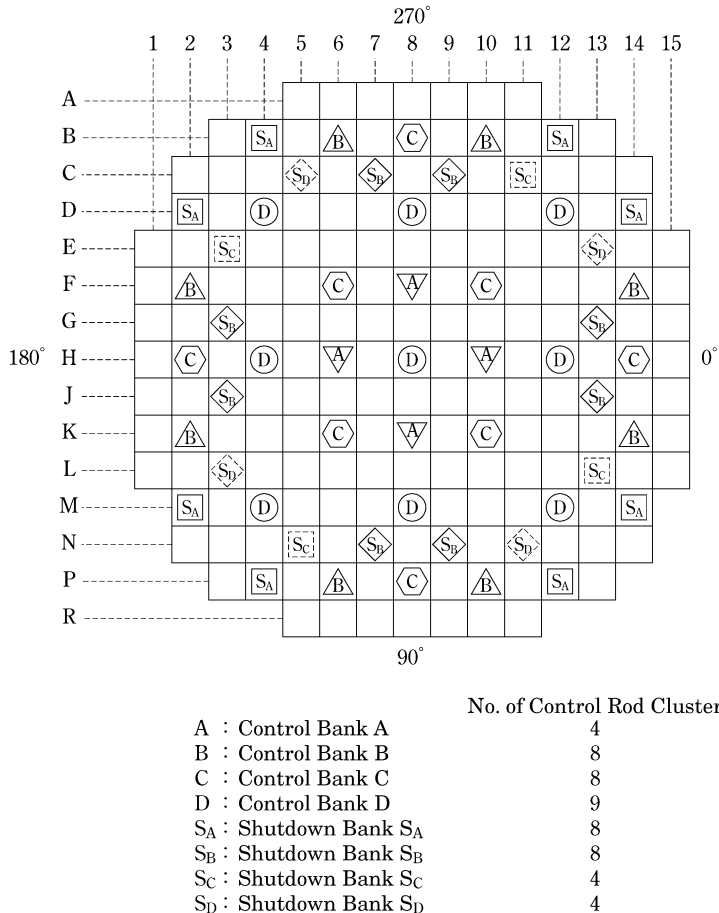


Fig. 3.40 Arrangement of control rod cluster (4-Loop PWR) [32] (Copyright Mitsubishi Heavy Industries, Ltd., 2014 all rights reserved)

- Void disappearance: Voids assumed in a small fraction of core disappear with power decrease and then the corresponding reactivity is inserted.
- Shutdown margin: A negative reactivity margin should be secured at shutdown. This is set based on the evaluation of overcooling transients and accidents (abnormal depressurization of the secondary system or main steam line break, etc.). In other words, overcooling transients and accident may lead to a decrease in moderator temperature, a reduction in reactivity shutdown margin, and re-criticality of core. The reactivity shutdown margin is assumed as the initial condition of the analysis in evaluating such a transient and accident.

Rod Cluster Control Assemblies (RCCAs) are uniformly located in the core as shown in Fig. 3.40. RCCAs are divided into two groups according to

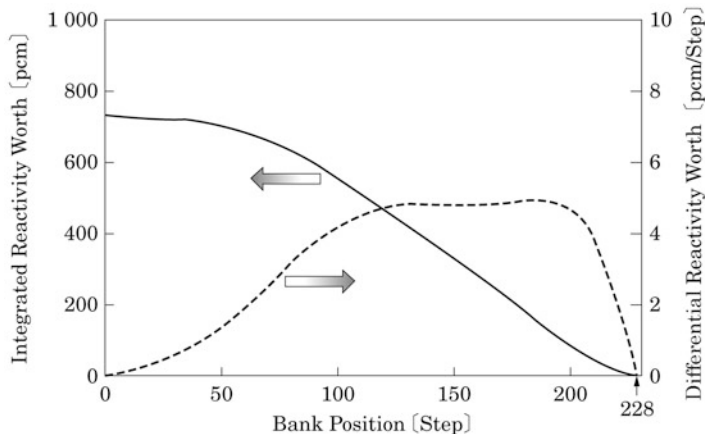


Fig. 3.41 Typical control rod worth curve of control bank D (Copyright Mitsubishi Heavy Industries, Ltd., 2014 all rights reserved)

their main purpose: the control group for power control and the shutdown group for shutdown margin. The groups are divided again into smaller groups, called *banks*, to reduce the effect on the power distribution and to avoid the too large reactivity change in control rod insertion. In particular, the control group is usually divided into four banks, considering control characteristics during reactor operation. In Fig. 3.40, both control and shutdown groups have four banks each which are withdrawn in the order of S_A , S_B , S_C , S_D , A, B, C, D and inserted in the reverse order. This order of withdrawal and insertion is not changed during an operating cycle.

Figure 3.41 presents differential control rod worth (reactivity change per one step) of a single bank. The differential control rod worth is zero at core top and bottom. In actual operation, however, control bank D is positioned not at full withdrawal but at about 5 % insertion and it correspondingly provides an appropriate differential control rod worth. An overlapping method, in which insertion of control bank C begins when control bank D is inserted about 60 % (usually at 100-step position), is employed to avoid zero differential control rod worth at the core bottom. This method reduces the fluctuation of differential control rod worth as shown in Fig. 3.42.

If RCCAs are deeply inserted during reactor operation, the remaining reactivity worth of RCCAs for shutdown becomes small. Control rod insertion depth is limited, as shown in Fig. 3.43, to reduce the decrement of reactivity worth and to secure shutdown margin. This is referred to as the control rod insertion limit and it is monitored by the shutdown margin monitoring system during reactor operation. An evaluation of reactivity shutdown margin is given in Table 3.12.

Since control rods are almost completely withdrawn during reactor power operation, there is almost no decline in control rod worth by

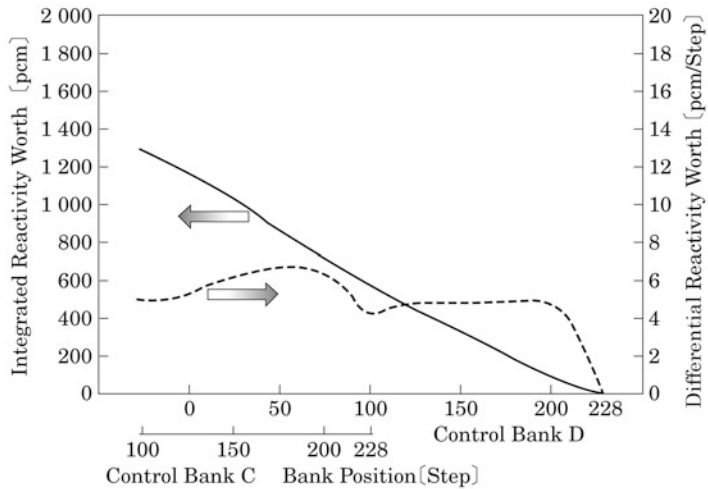


Fig. 3.42 Typical control rod worth curve of control banks with overlapping (Copyright Mitsubishi Heavy Industries, Ltd., 2014 all rights reserved)

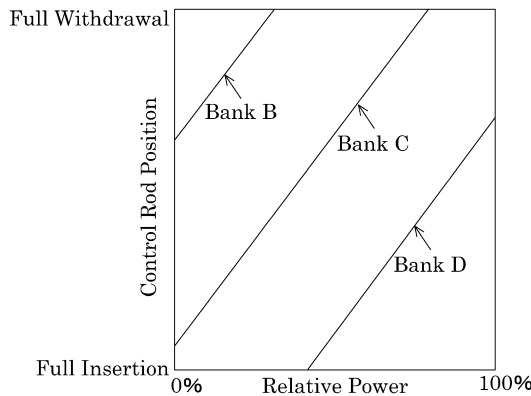


Fig. 3.43 Typical control rod insertion limit (Copyright Mitsubishi Heavy Industries, Ltd., 2014 all rights reserved)

depletion of neutron absorbing nuclides. Control rod lifetime depends on mechanical integrity such as wear of control rod cladding rather than nuclear depletion.

(3) Adjustment of soluble boron concentration

The reactivity controlled by soluble boron concentration adjustment is relatively slow temperature change from cold to hot, excess reactivity decline during an operating cycle, and FP concentration variation. The reactivity variations can be approximated as the following three items.

Table 3.12 Example of Evaluation of Reactivity Shutdown Margin [29]

	End of equilibrium cycle (% $\Delta k/k$)
Required control reactivity (1)	~2.82
Power defect ^a	~2.77
Void decrease	~0.05
Control rod worth (2) ^b	~4.62
Reactivity shutdown margin = (2)–(1)	~1.80
Shutdown margin limit	>1.6

^aThe power defect includes the Doppler effect and the change in reactivity by variation in moderator temperature and neutron flux distribution

^bThe initial condition is set that the control bank D is inserted to the insertion limit and it is assumed that the most reactive RCCA is stuck at the fully withdrawn position and the other RCCAs are fully inserted, and the design margin of 10 % is considered

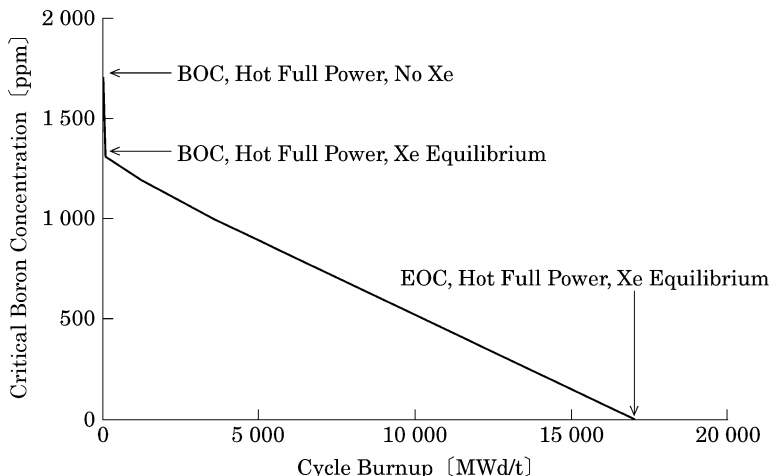


Fig. 3.44 Typical critical boron concentration with cycle burnup (100 % power) (Copyright Mitsubishi Heavy Industries, Ltd., 2014 all rights reserved)

- Reactivity change from cold to hot temperature: about 6 % $\Delta k/k$
- Reactivity decline during operating cycle: about 10 % $\Delta k/k$ (depends on cycle length)
- Xe reactivity: about 3 % $\Delta k/k$ at equilibrium full power and maximum about 6 % $\Delta k/k$ after shutdown.

Figure 3.44 shows dependence of critical boron concentration on cycle burnup at hot full power operation, which is monotonous, and therefore it is easy to manage the excess reactivity.

The Xe reactivity is important in core management. A reactivity variation from the equilibrium Xe condition to after reactor shutdown is

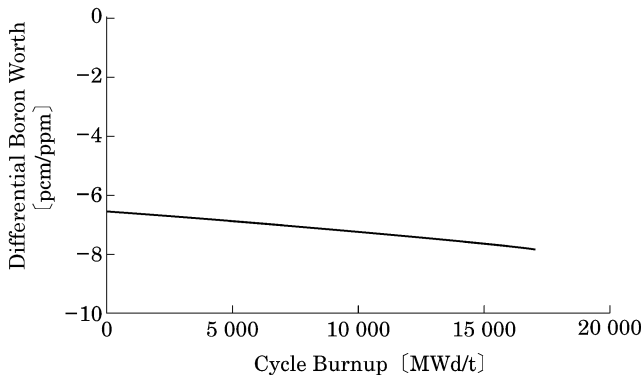


Fig. 3.45 Typical differential boron worth with cycle burnup (Copyright Mitsubishi Heavy Industries, Ltd., 2014 all rights reserved)

described in the fourth graph of Fig. 3.38. ^{135}Xe , which has a very large neutron absorption cross section, is produced mainly through fission $\rightarrow ^{135}\text{I}$ (half-life 6.7 h) $\rightarrow ^{135}\text{Xe}$ (half-life 9.2 h) $\rightarrow ^{135}\text{Cs}$ (half-life 2.6×10^6 years). The Xe reactivity temporarily increases by decay of ^{135}I after reactor shutdown, and monotonously decreases after a peak at about 8 h and becomes almost zero after about 3 days. When the reactor re-starts up within 3 days after shutdown, it is necessary to evaluate such Xe reactivity and to predict a critical point, and then to adjust the soluble boron concentration.

The differential boron worth is shown in Fig. 3.45.

(4) Burnable poison (burnable absorber)

Burnable poison (burnable absorber) assemblies are constructed of boron-added absorber (borosilicate glass tube or $\text{Al}_2\text{O}_3\text{-B}_4\text{C}$ pellet) and corrosion-resistant cladding (stainless steel or zircaloy-4), as shown in Fig. 3.46.

Burnable poison rods are used to maintain a negative moderator temperature coefficient during reactor operation. As mentioned in the list 1 of Sect. 3.3.4, moderator temperature coefficients become less negative as soluble boron concentration increases. For a long cycle length, therefore, a high concentration of soluble boron to compensate for the excess reactivity may lead to a positive moderator temperature coefficient. Such an increase in soluble boron concentration should be restrained by using burnable poisons. From the viewpoint of reactivity control, thus, burnable poisons are used to compensate for a part of the excess reactivity corresponding to operating cycle length. The compensating reactivity amount depends on the operating cycle length and varies from 0 to 8 % $\Delta k/k$ in the current operation. For a long cycle length, PWRs also adopt gadolinia-added fuel and the use of conventional burnable poisons is decreasing. Burnable poisons also play a role in flattening core radial power distribution by adjusting their location in the core.

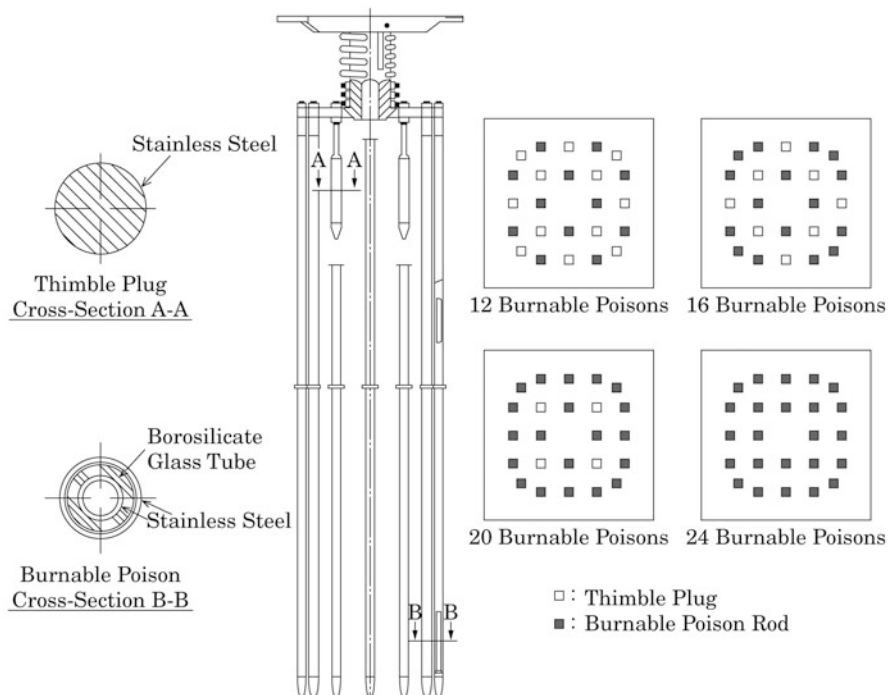


Fig. 3.46 Burnable poison (burnable absorber) assembly of PWR (17 × 17 Type) [31] (Copyright Mitsubishi Heavy Industries, Ltd., 2014 all rights reserved)

3.3.5 Power Distribution Control

[1] Characteristics of Power Distribution

PWR cores have the following features in power distribution;

- Enrichment zoning in fuel assembly is not necessary and enrichment is uniform, but there are some designs employing the enrichment zoning.
- The core radial power distribution can be flattened in the core design phase and no special adjustment is necessary during reactor operation.
- Only the core axial power distribution need to be adjusted during reactor operation.

These characteristics are attributed to the basic features of PWR core design which are no boiling in core, a canning-less fuel assembly (no channel box), cluster type control rods, and reactivity control by soluble boron concentration adjustment.

[2] Power Peaking Factor

The heat flux hot channel factor (F_Q) and the nuclear enthalpy rise hot channel factor ($F_{\Delta H}^N$) are the basic design parameters concerned with the core power

distribution. Core radial and axial power distributions are flattened to meet the design limits of the parameters.

(i) Nuclear Heat Flux Hot Channel Factor (F_Q^N)

Nuclear heat flux hot channel factor is defined as the ratio of core maximum to average linear power density based on core design specifications and given by the following factors

$$F_Q^N = \text{Max}\{P(X, Y, Z)\} \times F_U^N \quad (3.24)$$

$P(X, Y, Z)$: the relative local power at position (X, Y, Z)

F_U^N : the factor concerned with nuclear uncertainty (evaluated by a statistical difference between calculations and measurements, usually about 1.05)

(ii) The Engineering Heat Flux Hot Channel Factor (F_Q^E)

The *engineering heat flux hot channel factor* is the factor to consider the effect of tolerances in fuel fabrication on the heat flux hot channel factor. Tolerances of pellet diameter, pellet density, enrichment, cladding thickness, etc are statistically combined to evaluate this factor. For example, it is 1.03 for uranium fuel and 1.04 for MOX fuel.

(iii) Heat Flux Hot Channel Factor (F_Q)

The *heat flux hot channel factor* is defined as the ratio of the core maximum to average linear power density and given by Eq. (3.25).

$$F_Q = F_Q^N \times F_Q^E \quad (3.25)$$

(iv) Heat Flux Hot Channel Factor ($F_Q(Z)$) at Core Height Z

The *heat flux hot channel factor at core height Z* is expressed as Eq. (3.26).

$$F_Q(Z) = \text{Max}_{X, Y}\{P(X, Y, Z)\} \times F_U^N \times F_Q^E \quad (3.26)$$

(v) Limits of Heat Flux Hot Channel Factor

Equation (3.27) is comprehensively used during normal operation and Eq. (3.28) is used for the limit of core detailed design and management.

$$F_Q \times P \leq 2.32 \quad (3.27)$$

$$F_Q(Z) \times P \leq 2.32 \times K(Z) \quad (3.28)$$

where P : The relative power

$K(Z)$: the envelope curve function, for example, $2.32 \times K(Z)$ in Fig. 3.54.

(vi) Definition and Limits of Nuclear Enthalpy Rise Hot Channel Factor

The nuclear enthalpy rise hot channel factor is defined as the ratio of the maximum to average fuel rod power. It is limited in core design, for example, by relationships such as Eq. (3.29) which is used in evaluating DNB.

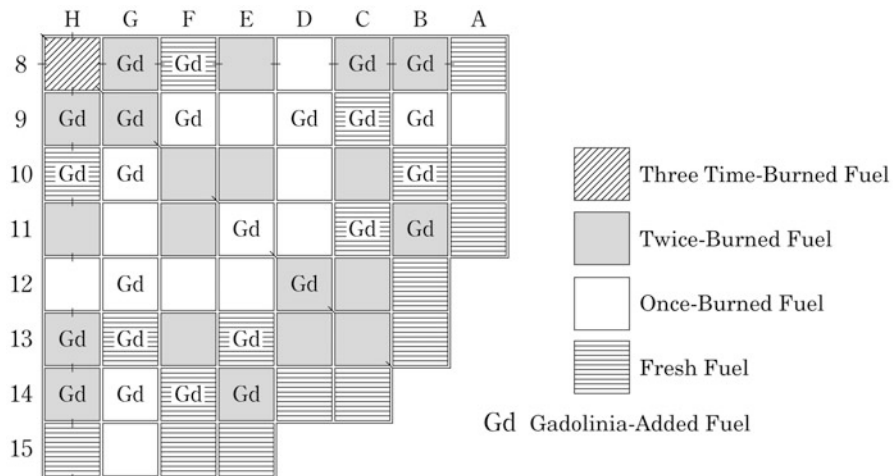


Fig. 3.47 Example of reload core fuel loading pattern with gadolinia-added fuel (Copyright Mitsubishi Heavy Industries, Ltd., 2014 all rights reserved)

$$F_{\Delta H}^N \leq 1.64 \{ 1 + 0.3(1 - P) \} \quad (3.29)$$

[3] Control of Core Radial Power Distribution

Radial power distribution of PWR cores is less dependent on relative power. The number and depth of inserted rod cluster control assemblies are small and therefore the effect of control rods is small and the burnup effect is also mild. For flattening of the core radial power distribution, it is, therefore, sufficient only to properly locate fuel assemblies and burnable poisons in the core design. The core radial power distribution is just monitored during reactor operation and adjustment by control rods is not needed. A specific arrangement of fuel assemblies is shown in Fig. 3.47 (gadolinia-added fuel assemblies are used, and no burnable poison rods in this example) and its corresponding radial power distributions are shown in Fig. 3.48 (BOC) and Fig. 3.49 (EOC). The radial power distribution is represented as the relative value of fuel assembly power to core-averaged fuel assembly power for the symmetric octant core. Comparison between the radial power distributions at BOC and EOC indicates that gadolinia-added fresh fuel assemblies and neighboring fuel assemblies give a relatively large increase in power, but the variation in power is mild as burnup progresses.

[4] Control of Core Axial Power Distribution

The core axial power distribution is important in PWR cores because the temperature variations with power and control rod operations have a large effect on this distribution. Figure 3.50 illustrates basic behavior of the core axial power distribution in PWRs.

Fig. 3.48 Radial power distribution (BOC, hot full power, control rod fully withdrawn) (Copyright Mitsubishi Heavy Industries, Ltd., 2014 all rights reserved)

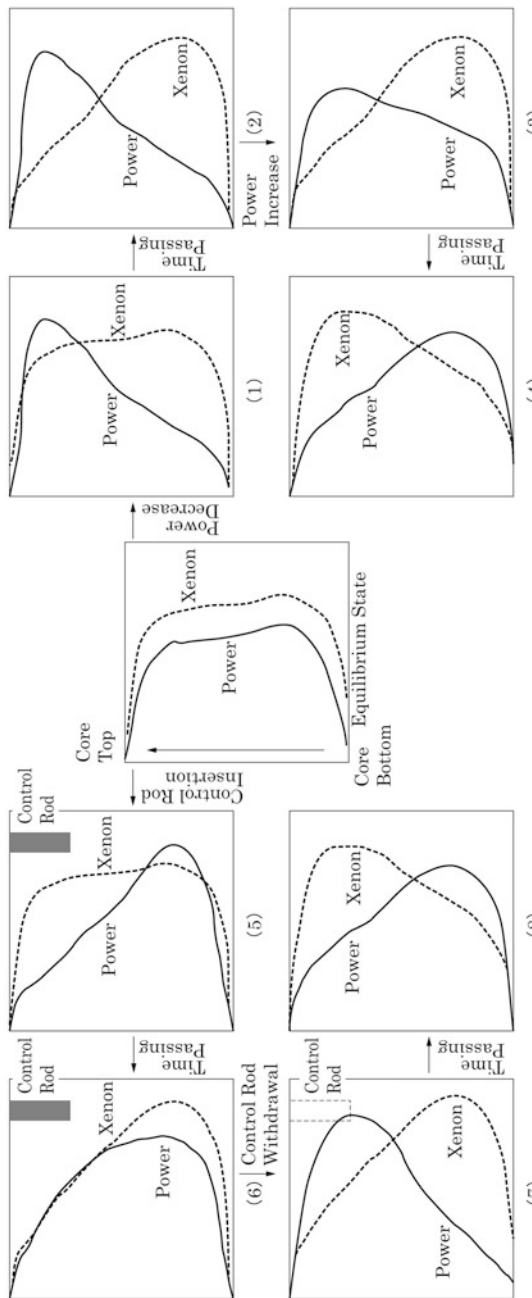
	H	G	F	E	D	C	B	A
8	0.45							
9	0.57	0.64						
10	1.00	1.01	0.90					
11	1.11	1.34	1.02	1.20				
12	1.31	1.27	1.29	1.24	0.89			
13	0.94	1.16	0.96	1.06	0.92	0.75		
14	0.87	1.04	1.06	0.77	0.98	0.69		
15	1.01	0.92	1.01	0.74				

Fig. 3.49 Radial power distribution (EOC, hot full power, control rod fully withdrawn) (Copyright Mitsubishi Heavy Industries, Ltd., 2014 all rights reserved)

	H	G	F	E	D	C	B	A
8	0.60							
9	0.69	0.73						
10	1.14	0.96	0.83					
11	0.96	1.09	0.86	1.00				
12	1.09	1.08	1.11	1.10	0.86			
13	0.96	1.32	1.02	1.27	0.94	0.78		
14	0.92	1.10	1.31	0.98	0.98	0.73		
15	0.96	0.91	1.02	0.81				

The *constant axial offset control* (CAOC) method is adopted to suppress the heat flux hot channel factor for the basic behavior of core axial power distribution. It suppresses the imbalance (referred to as axial offset, A.O., for which Axial Flux Difference $\Delta I = \text{A.O.} \times P$ is used as the index during reactor operation) in the axial power distribution to an as narrow range as possible (typical range = $\pm 5\% \Delta I$ from the ΔI at the Xe equilibrium state) and to reduce the imbalance of ^{135}Xe and ^{135}I distributions. The basic concept of CAOC operation is shown in Fig. 3.51. A large A.O. or ΔI (in absolute value) leads to a large F_Q . If A.O. or ΔI is not restricted as shown in the top figure, $F_Q \times$ core relative power can exceed the allowable design limit. As shown in the middle figure, if A.O. or ΔI is restricted within the narrow range which is set as $\pm 5\% \Delta I$ along the line to link two ΔI values at core relative powers of 1.0 (at Xe equilibrium) and 0.0, it is possible to suppress $F_Q \times$ core relative power and to maintain it at less than the allowable design limit as shown in the bottom figure.

Power distribution is controlled by a control rod bank (usually bank D) of the control group control rods. Figure 3.52 shows the variation in core parameters in CAOC operation. The load following operation during the change from 100 % to 50 % in core power as shown in the top figure can be performed by adjusting rod cluster control assemblies and soluble boron concentration.



- (5) The power in the core upper part decreases due to the control rod insertion.
- (6) The Xe concentration in the upper part temporarily increases and then decreases with time.
- (7) Since the Xe concentration in the upper part was decreased, the power in the upper part increases when the control rod is withdrawn.
- (8) The Xe concentration in the upper part temporarily decreases, and then increases with time and the power in the upper part decreases.
- (1) Since the moderator temperature is high in the core upper part at equilibrium state, the power in the core upper part is suppressed by the effect of the moderator temperature coefficient. The power increases by the less effect when the core power decreases.
- (2) Since the power in the core upper part is large, Xe is reduced due to neutron absorption.
- (3) Since the power in the core lower part is small, however, the Xe reduction is mitigated in the core lower part and moreover Xe is increased by the decay of $\text{^{131}I}$.
- (4) The power in the high-temperature upper part is a little suppressed due to the effect of the moderator temperature coefficient by the power increase.

Fig. 3.50 Fundamental characteristics of axial power distribution (Copyright Mitsubishi Heavy Industries, Ltd., 2014 all rights reserved)

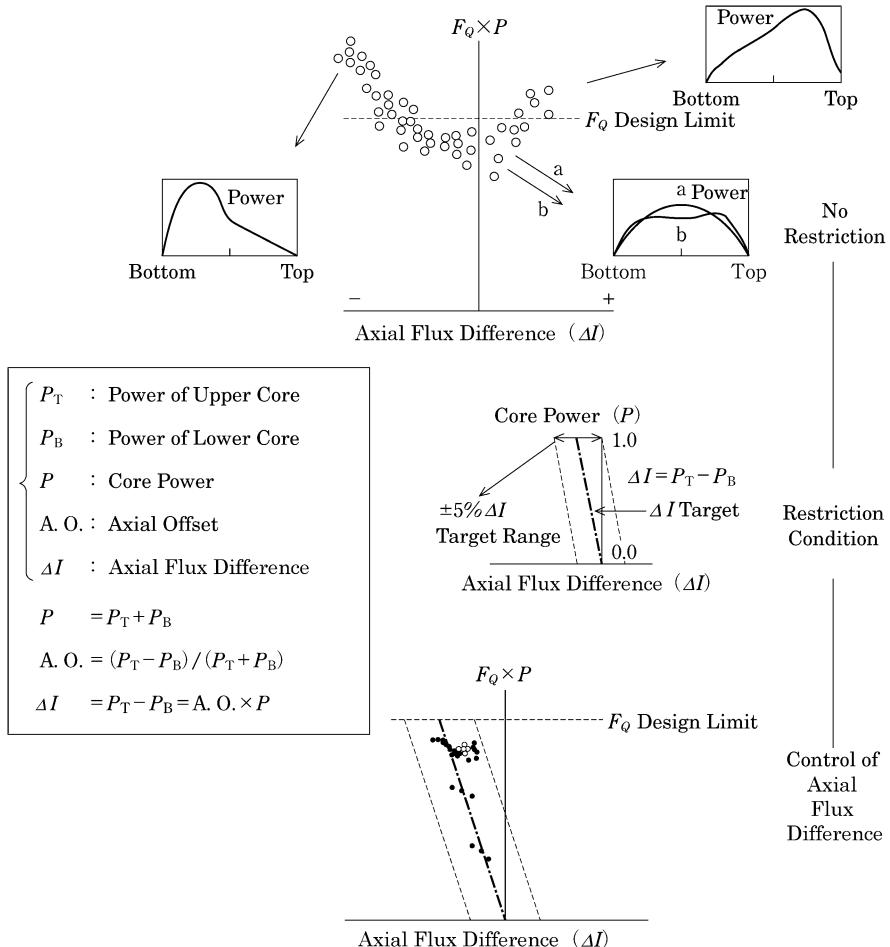


Fig. 3.51 Basic concept of CAOC operation [31] (Copyright Mitsubishi Heavy Industries, Ltd., 2014 all rights reserved)

F_Q at normal operation is evaluated for such a load following operation. Figure 3.53 shows an example of the F_Q evaluation at normal operation and a typical $F_Q(Z) \times$ relative power is given as a function of core axial height Z in Fig. 3.54. Positive and Negative A.O. at BOC and EOC shows the $F_Q(Z) \times$ Relative Power at the most positive and negative A.O. in the range of the limit, respectively. They are below the *envelope curve* in Fig. 3.54. The maximum $F_Q(Z) \times$ relative power over all points of time is also below the envelope curve as well as at representative points introduced here. The envelope curve is used as the heat generation distribution at normal operation for the initial condition of LOCA analysis.

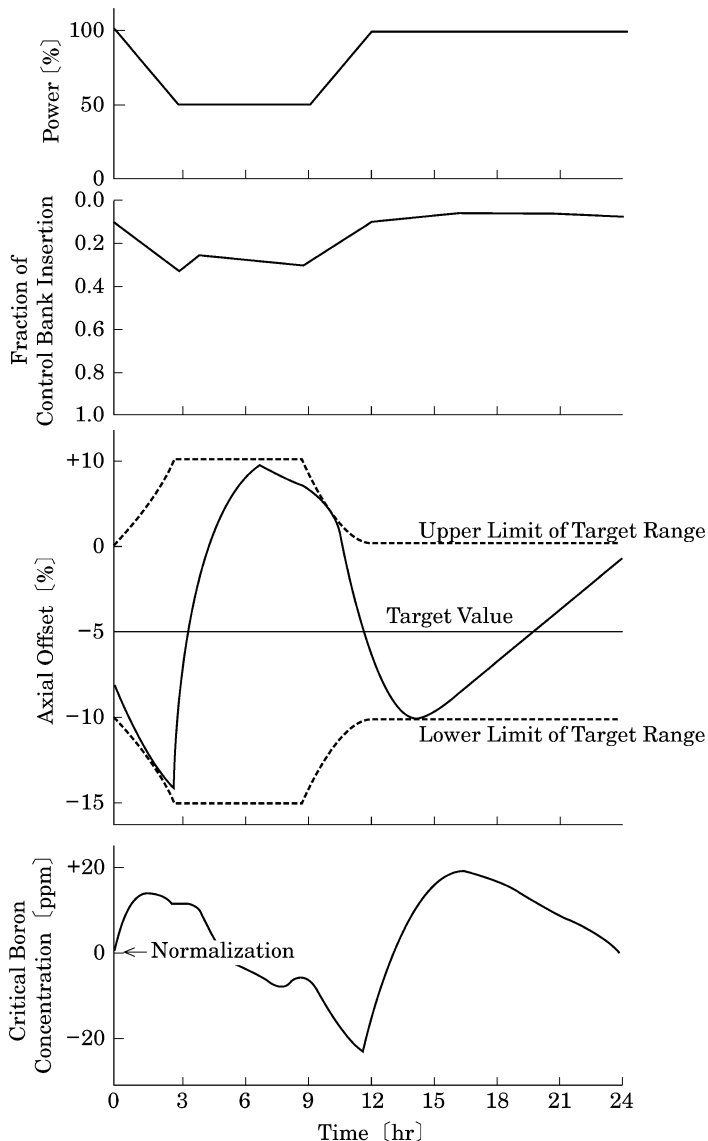


Fig. 3.52 Typical variation of core parameters in load following operation [31] (Copyright Mitsubishi Heavy Industries, Ltd., 2014 all rights reserved)

Evaluations and limits for gadolinia-added fuel are also given in Fig. 3.53 here and Figs. 3.55 and 3.56 introduced later. The limits for gadolinia-added fuel are set lower than those of uranium fuel, considering the different physical properties.

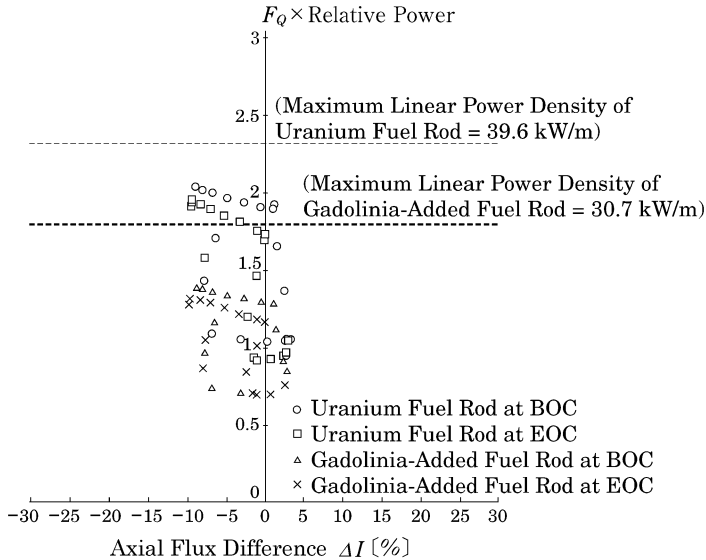


Fig. 3.53 Typical $F_Q \times$ relative power versus axial flux difference [32] (17 × 17 type, 3-loop core, and normal operation) (Copyright Mitsubishi Heavy Industries, Ltd., 2014 all rights reserved)

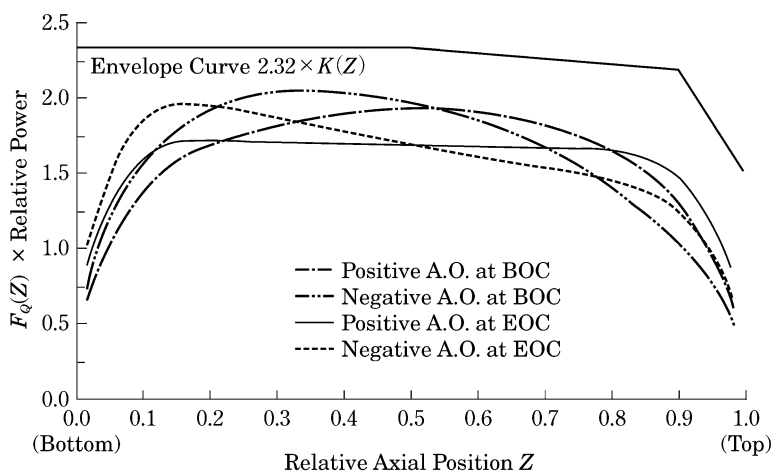


Fig. 3.54 Typical $F_Q(Z) \times$ relative power versus axial position [32] (17 × 17 type, 3-loop core, and normal operation) (Copyright Mitsubishi Heavy Industries, Ltd., 2014 all rights reserved)

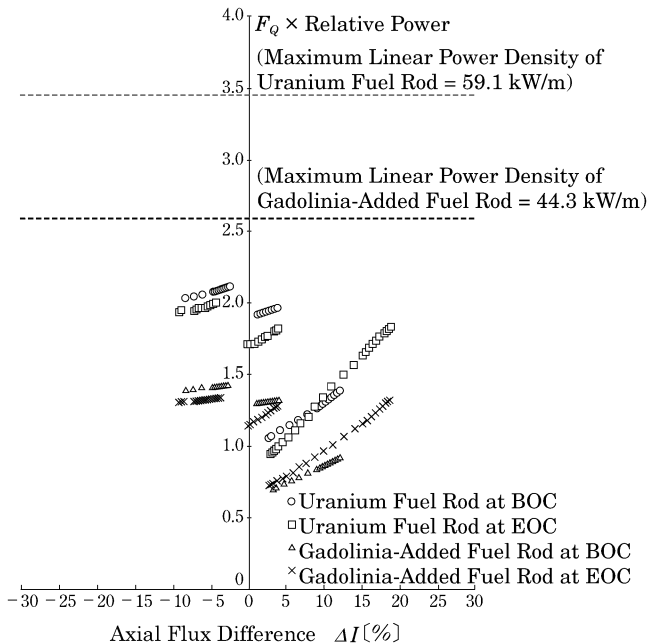


Fig. 3.55 Typical $F_Q \times$ relative power versus axial flux difference [32] (17 × 17 type, 3-loop core, and abnormal control rod withdrawal at power) (Copyright Mitsubishi Heavy Industries, Ltd., 2014 all rights reserved)

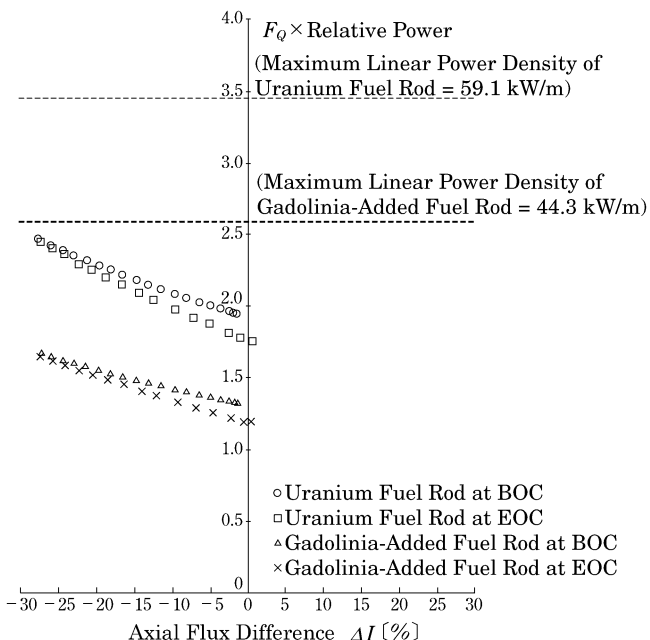


Fig. 3.56 Typical $F_Q \times$ relative power versus axial flux difference [32] (17 × 17 type, 3-loop core, and abnormal dilution or boration in the primary coolant) (Copyright Mitsubishi Heavy Industries, Ltd., 2014 all rights reserved)

[5] Maximum Linear Power Density at Abnormal Transients

In normal operation, a failure of the system or an operator's error causes an abnormal transient state for which maximum linear power density is evaluated to assure that fuel rods do not exceed the allowable design limits (no melting of fuel, no occurrence of DNB, etc.). Two typical transients are evaluated here as an abnormal transient in operation.

(1) Abnormal withdrawal of control rods at power

An abnormal withdrawal of control rods by a malfunction of the control rod control system or an operator's error causes an increase in power and a change in power distribution. However, the withdrawal of rod cluster control assemblies is stopped or the reactor is shutdown by the reactor protection systems, such as the high neutron flux, the over-temperature ΔT and over-power ΔT . Control rods could be withdrawn from an arbitrary position to the fully withdrawn.

(2) Abnormal dilution or boration in the primary coolant

A malfunction of the chemical and volume control system or an operator's error can cause an unplanned abnormal dilution or boration in the primary coolant. In the automatic control mode of control rods, reactor power is kept constant and control rods are withdrawn or inserted depending on the boration or dilution, and the power distribution is varied.

Such an abnormal transient arising from normal operation such as load following operation can be analyzed and evaluated as the maximum linear power density by a core nuclear calculation. $F_Q \times$ relative power, namely, maximum linear power density is evaluated for *abnormal withdrawal of control rods at power* in Fig. 3.55 and for *abnormal dilution or boration in the primary coolant* in Fig. 3.56.

It is seen that both maximum linear power densities are lower than the design limit of 59.1 kW/m for the 17×17 fuel assembly. In the case of abnormal dilution or boration in the primary coolant, the linear power density can be maintained below 59.1 kW/m, even for the large (absolute value) Axial Flux Difference for the following two reasons.

- Corrective action of operator can be expected, since the transient is relatively slow
- Even if the corrective action of operator is not taken, the power is reduced or the reactor is tripped by the over-temperature ΔT or over-power ΔT with large absolute value of ΔI .

[6] Stability of power distribution

Negative power coefficients keep the PWR cores stable against core power oscillation. The stability of PWR cores is focused on the core power spatial oscillation induced by xenon, which tends to become larger and gives a less convergence for a larger core and a flatter power distribution.

(1) Radial Power Distribution Oscillation

A radial power distribution oscillation may occur by abnormal operation of rod cluster control assemblies (for example, only one rod cluster control

assembly works in an abnormality). Core equivalent diameter is smaller than one causing an oscillation divergence and the radial power distribution oscillation has an inherent convergence feature due to the feedback effect of moderator temperature coefficient. Therefore, it is not necessary to suppress the radial power distribution oscillation which can be continuously monitored and detected by quadrant core power tilt (a symmetry index of core four-quadrant powers) through the coolant outlet temperature distribution and ex-core neutron detectors.

(2) Axial Power Distribution Oscillation

For a constant core power, the difference in average moderator temperature between upper and lower core region is constant and independent of axial power distribution. Hence, axial power distribution oscillation cannot be expected to be suppressed by the moderator temperature coefficient and the Doppler effect will be expected instead. Since the axial power distribution becomes flatter with burnup from an initial cosine distribution at BOC, the stability of the axial power distribution oscillation becomes lower and it may cause a little divergence near EOC. In this case, the axial power distribution can be controlled by the CAOC operation mentioned before and the axial power distribution oscillation can be sufficiently suppressed. The axial power distribution oscillation induced by axial Xe oscillation can also be suppressed as shown in Fig. 3.57. The axial power distribution can be continuously monitored by upper and lower separate ex-core neutron detectors and the oscillation can be detected and suppressed.

3.3.6 Evolution and Future Trends of Core Design

[1] Development history and future trends

The history of PWR power plants in Japan started from the Mihama Unit 1 built with technology introduced from the United States in the late 1960s [33]. Since then, the plants have been improved and standardized [34] toward high power density and large size without a significant change in the basic design specifications. Economy and reliability in core and fuel utilization technology have also been improved as follows.

- (i) High fuel burnup (maximum fuel assembly burnup: 39 GWd/t → 48 GWd/t → 55 GWd/t)
 - High enrichment (3.1 wt% → 4.1 wt% → 4.8 wt%)
- (ii) Long cycle length (9 EFPM → 12 EFPM → 13.5 EFPM → 18 EFPM (planned) → 24 EFPM (planned))
- (iii) Low leakage core
- (iv) Gadolinia-added fuel
- (v) MOX fuel

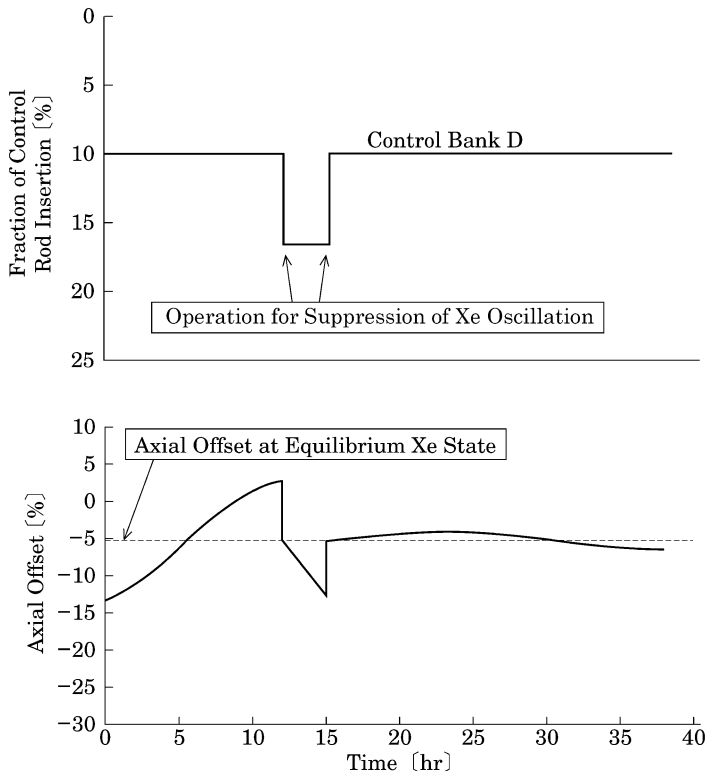


Fig. 3.57 Typical suppression of axial power distribution oscillation [32] (17 × 17 Type, 3-loop core, and EOC) (Copyright Mitsubishi Heavy Industries, Ltd., 2014 all rights reserved)

- (vi) Measure of load following operation
- (vii) Advanced PWR (APWR) (adoption of neutron reflector)

The implementation of the low leakage core and gadolinia-added fuel is discussed next, and the APWR (neutron reflector), high burnup, MOX-fueled core, and power up-rating issues are mentioned following that. The long cycle length and load following operation were touched in the list [1] of Sect. 3.3.2 and [4] of Sect. 3.3.5 respectively.

(1) Low Leakage Core

Originally the PWR fuel loading pattern was generally an *out-in* pattern (fresh fuel is loaded in the outermost core region and burned fuel in the core inside region). This pattern can flatten the core radial power distribution and reduce the power peaking factor. However, the loading of fresh fuel in the outermost core region leads to a high power in the core periphery and large neutron leakage to the core outside, and therefore it gives a disadvantage in reactivity. Hence, since the late 1980s, a new fuel loading

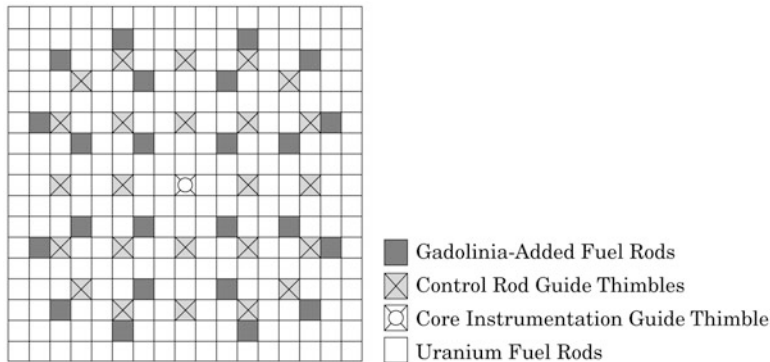


Fig. 3.58 Arrangement of gadolinia-added fuel rods in fuel assembly [36] (17 × 17 type and 24 gadolinia-added fuel rods) (Copyright Mitsubishi Heavy Industries, Ltd., 2014 all rights reserved)

pattern, in which burned fuel assemblies are loaded in the core periphery within the design limit such as power peaking, has been implemented in refueling instead of the out-in pattern. The new fuel loading pattern is advantageous regarding reactivity because of small neutron leakage to the core outside. The higher burnup and larger number of burned fuel assemblies loaded in the outermost core region can lead to higher reactivity and a smaller number of discharged fuel assemblies (i.e. smaller number of fresh fuel assemblies). For example, number of fresh fuel assemblies needed can be reduced by two applying such a low leakage loading pattern. Various fuel loading patterns are investigated for advantageous reactivity within the basic criteria of core design [35].

(2) Gadolinia-Added Fuel

For a long cycle length, burnable poison rods are used to maintain moderator temperature coefficient negative as mentioned in the list 1 of Sect. 3.3.4. However, a large amount of burnable poisons causes a reactivity penalty at EOC that cannot be ignored (even if burnable poison were depleted, the effect of a structure such as the cladding remains) and it gives rise to a problem in spent burnable poison as a solid waste. Gadolinia-added fuel for PWRs was developed and employed to solve these problems.

In the design of the gadolinia-added fuel assembly, gadolinia content and the number and location of gadolinia-added fuel rods are investigated for required performance. Having a large number of gadolinia-added fuel rods gives a high reactivity suppression effect (reactivity reduction at BOC). The location of the gadolinia-added fuel rods in a fuel assembly can be determined to reduce power peaking through the fuel burnup. Figure 3.58 depicts an arrangement of 24 gadolinia-added fuel rods in the 17 × 17 type fuel assembly and Fig. 3.59 shows the variation in infinite multiplication

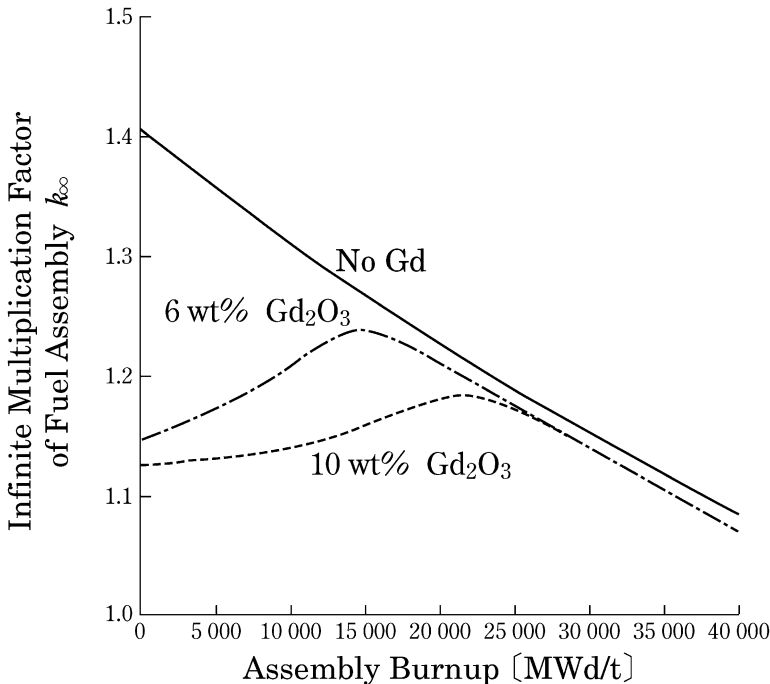


Fig. 3.59 Typical variation in infinite multiplication factor with burnup [36] (17 × 17 type, 4.8 wt% Uranium enrichment, and 24 gadolinia-added fuel rods with 3.2 wt% enriched Uranium) (Copyright Mitsubishi Heavy Industries, Ltd., 2014 all rights reserved)

factor k_{∞} with burnup. k_{∞} is suppressed by the gadolinia-added fuel rods at the beginning of burnup, but increases with burning of the gadolinia and reaches a peak when the gadolinia is almost depleted, and then decreases as fuel burnup continues.

The larger content of gadolinia (wt% Gd_2O_3) leads to its slower depletion and a longer reactivity suppression effect. This is because the self-shielding effect of gadolinia becomes stronger. Figure 3.60 compares the nuclear enthalpy rise hot channel factor ($F_{\Delta H}^N$), which usually occurs at a gadolinia-added fuel assembly or a neighboring fuel assembly. In considering the behavior of reactivity variation, the power peaking factor in the case of low-content gadolinia tends to increase with gadolinia depletion and it becomes a maximum in the late of the cycle. High-content gadolinia oppositely leads to a mild variation and no peak in the nuclear enthalpy rise hot channel factor. Thus, higher content of gadolinia is suitable for a longer cycle length.

The addition of gadolinia to uranium fuel causes deterioration of thermal conductivity and lowering of melting point, and reduces the margin of fuel centerline temperature against melting. To secure the same mechanical

Fig. 3.60 Typical variation in nuclear enthalpy rise hot channel factor with burnup [36] (17 × 17 type, 4-loop core, 4.8 wt% Uranium enrichment, and 24 gadolinia-added fuel rods with 3.2 wt% enriched Uranium) (Copyright Mitsubishi Heavy Industries, Ltd., 2014 all rights reserved)

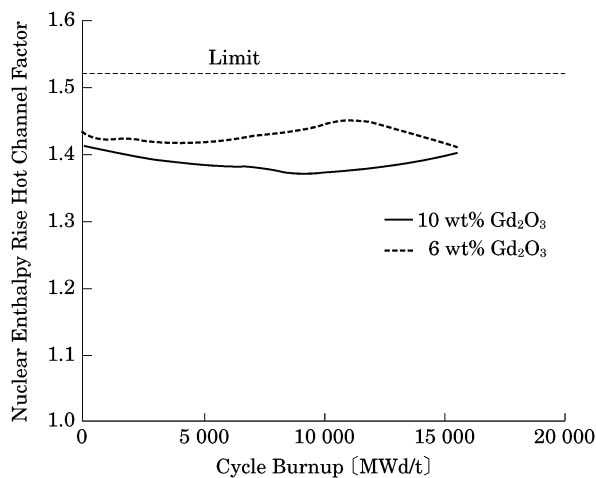


Table 3.13 Reactor and core specifications of advanced PWRs [38]

	Unit	Advanced PWR	Conventional 4-loop PWR
Core thermal power	MW	~4,451	~3,411
Primary coolant flow rate	kg/h	~77.3 × 10 ⁶	~60.1 × 10 ⁶
RPV inlet coolant temperature	°C	~289	←
RPV outlet coolant temperature	°C	~325	←
Reactor pressure	—	~15.4 MPa(gage)	←
Active core height	m	~3.7	←
Equivalent core diameter	m	~3.9	~3.4
Core Uranium amount	ton	~121	~89
No. of coolant loops	—	4	←
Reflector material	—	Light water and stainless steel	Light water

integrity as that of conventional uranium fuel, the gadolinia-added fuel rod is designed to have low uranium enrichment to suppress an increase in linear power density.

In 10 wt% Gd₂O₃ gadolinia-added fuel, for example, the gadolinia-added fuel with 3.2 w% enriched uranium is used instead of the conventional 4.8 w% enriched uranium.

[2] Core Improvement Technology (Advanced PWR)

The major features [37] of the Advanced PWR core design are the large-size core and introduction of neutron reflector in comparison with conventional PWRs. Table 3.13 summarizes the main core parameters of the Advanced PWR in comparison with the conventional 4-loop core. The core became large-sized, with 257 fuel assemblies. The radial power distribution oscillation by xenon should be noted with the enlargement of core, but such a large-size core still maintains the oscillation convergent.

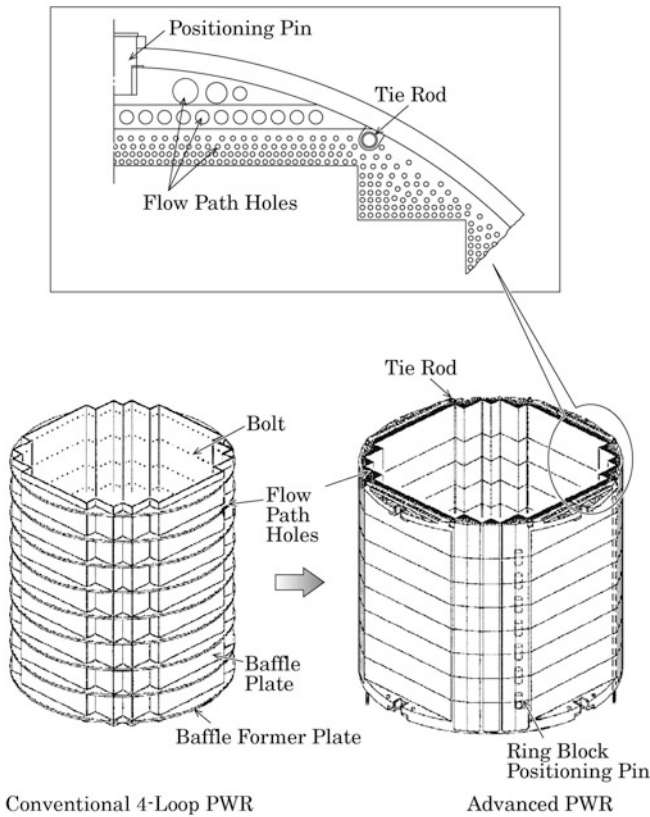
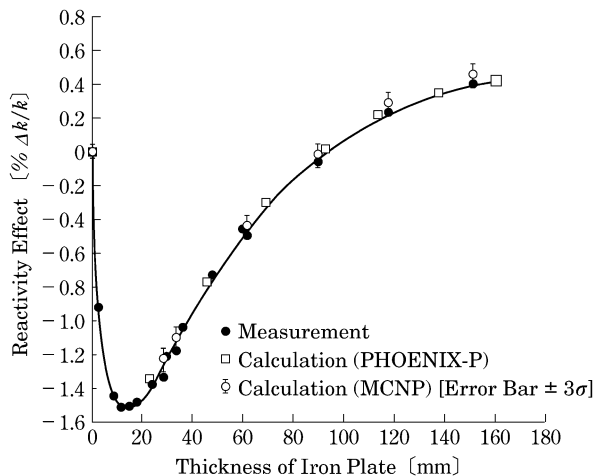


Fig. 3.61 Structures of PWR reflector [38] (Copyright Mitsubishi Heavy Industries, Ltd., 2014 all rights reserved)

Another feature of the Advanced PWR core is the stainless steel neutron reflector installed around outmost fuel assemblies for improvement in neutron economy, reduction of neutron irradiation on the reactor vessel, and reduction in the number of parts by simplification of structures. The neutron reflector is constructed of stainless steel ring blocks piled up to eight stages, enclosing the fuel assemblies. Figure 3.61 depicts the neutron reflector structure in comparison with that of the conventional 4-loop core. While the conventional PWR had a stainless steel baffle and water in the reflector region outside core, the Advanced PWR introduces the stainless steel reflector and its cooling water which reduces the size of the water region and effectively reflects fast neutrons to the core inside without slowing down the neutrons.

Experiments in Japan using TCA, the light water critical assembly, have also confirmed that the steel reflector with the smaller sized water region gives excellent reactivity characteristics. In that experiment, the effect of the stainless steel reflector was estimated using iron reflector. The contribution of the iron

Fig. 3.62 Reactivity effect of reflector [38]
 (Copyright Mitsubishi Heavy Industries, Ltd., 2014 all rights reserved)



reflector to reactivity was investigated with different thicknesses of the iron reflector installed at both ends of the fuel region with the 15×15 fuel rod arrangement. Figures 3.62 shows the result. It is seen that there is a reactivity gain of about 0.38 % $\Delta k/k$ for the iron reflector thickness of about 150 mm. It is also noted that this gives a reactivity gain of about +1.8 % $\Delta k/k$ from -1.4 % $\Delta k/k$ at 22 mm in thickness. The 22 mm corresponds to the thickness of the stainless steel baffle. Thus, the experiments confirmed that the steel reflector reduces neutron leakage from core and significantly increases core reactivity.

[3] High burnup core

PWR fuel has been improved for high burnup from the viewpoint of high economy in fuel cost and lowered amount of spent fuel to be handled and stored. The limit of the maximum fuel assembly burnup was 39,000 MWd/t in the beginning, and increased to 48,000 MWd/t in Step I and 55,000 MWd/t in Step II fuels. Further high burnup is planned [39]. Such a high fuel burnup has the following effects on core and plant facilities and measures against them are discussed below.

- (i) Neutron spectrum hardening
- (ii) Enrichment increase (increase in ^{235}U)
- (iii) Fission product accumulation increase

(1) Impact of high enrichment and burnup

A high enrichment and burnup leads to an increase in thermal neutron absorbing materials such as ^{235}U , plutonium and FPs and a decrease in thermal neutron flux. Therefore, the thermal neutron absorption by the rod cluster control assemblies (RCCAs) and soluble boron in primary coolant is reduced and their reactivity worth is decreased slightly.

As a measure of the reactivity worth reduction of RCCAs, a proper arrangement of fuel assemblies loading pattern in the core can secure the

reactivity shutdown margin. The number of RCCAs should be increased if insufficient.

As a measure of the reactivity worth reduction of soluble boron, the boron concentration can be increased for reactor shutdown if necessary. The boron concentration in the refueling water storage tank (the boric acid water stored in the refueling water storage tank could be injected into the reactor at abnormal transients or accidents in which the boron injection function of the *emergency core cooling system* is expected to work) can also be increased.

The increase of enrichment also leads to lower subcriticality margin of fuel storage facilities. Since the subcriticality evaluation of fuel storage facilities has been performed for fresh fuel with initial enrichment of 5.05 wt%, a new measure is not necessary if the enrichment is lower than 5 wt%.

(2) Impact of high burnup

A high burnup increases the amount of fission products and therefore increases the decay heat of spent fuel. Spent fuel storage cooling system are enhanced in case of insufficient cooling capability, considering heat load to spent fuel pit.

[4] MOX-Fueled Core

MOX fuel assemblies loaded in PWR cores have basically the same structure as those of uranium fuel assemblies; uranium fuel pellets are just replaced with MOX fuel pellets. The fraction of MOX fuel in the core reaches approximately 1/4–1/3. MOX fuel has different features from uranium fuel in terms of its nuclear characteristics, physical properties and irradiation behavior, and radiation and decay heat. The different features in nuclear characteristics, and radiation and decay heat, and their effects are discussed here.

(1) Nuclear Characteristics

In comparison with uranium, plutonium is characterized by the following nuclear characteristics.

- (i) Plutonium has a large thermal neutron absorption cross section (capture and fission) and it hardens the neutron spectrum as shown in Fig. 3.63.
- (ii) Plutonium also has a large resonance absorption cross section (for example, ^{240}Pu has resonance peaks at relatively low neutron energies such as 1 eV).
- (iii) Plutonium has a small delayed neutron fraction (^{239}Pu : ~ 0.2 %, ^{241}Pu : ~ 0.5 %, and ^{235}U : ~ 0.6 %).

From these nuclear characteristics of plutonium, the effects of MOX fuel on the core and necessary countermeasures are discussed.

- (i) Plutonium has a larger thermal neutron absorption cross section than uranium and it hardens the neutron spectrum. Therefore, it decreases the reactivity worth of control rods and soluble boron in

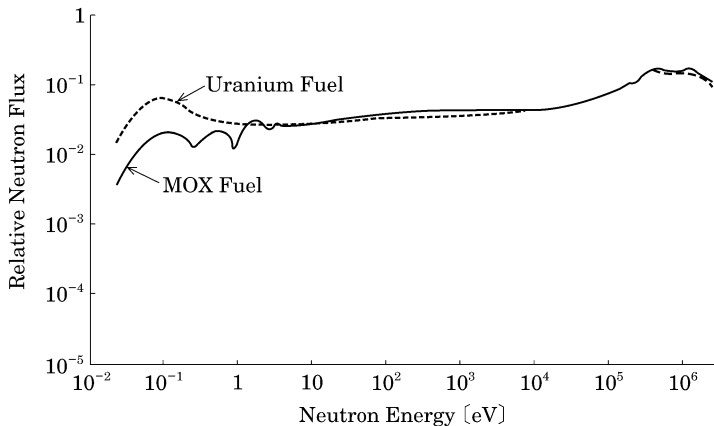


Fig. 3.63 Neutron spectrum comparison of Uranium and MOX fuels [40] (Copyright Mitsubishi Heavy Industries, Ltd., 2014 all rights reserved)

coolant. This effect is generally larger than that of the high burnup mentioned before and similar countermeasures of larger scale are necessary. As a measure of the reduction in control rod worth, if the fraction of MOX fuel assemblies is less than 1/3, the fuel assemblies loading pattern can be properly arranged in the core, such as loading the MOX fuel assembly avoiding control rods locations, to secure the reactivity shutdown margin. The number of rod cluster control assemblies can be increased in the case of insufficient reactivity shutdown margin due to such as higher burnup. As a measure of the reduction in boron reactivity worth, the boron concentration necessary for shutdown can be increased and the boron concentration in the refueling water storage tank can be increased.

- (ii) Thermal neutrons coming from uranium fuel are absorbed in the neighboring MOX fuel and they increase power of periphery fuel rods in MOX fuel assemblies. Three different fissile plutonium contents (Pu^f contents) of fuel rods are arranged in a MOX fuel assembly to suppress pin power peaking in a fuel assembly. Figure 3.64 depicts an arrangement of fuel rods in a MOX fuel assembly.
- (iii) In addition to the neutron spectrum hardening, plutonium gives more negative moderator temperature and Doppler coefficients because of the large resonance absorption. However, the effect is not so large and the magnitude is usually in the range considered in safety analysis of uranium fuel.
- (iv) Plutonium has a larger thermal neutron cross section than uranium and it results in a shorter prompt neutron lifetime in

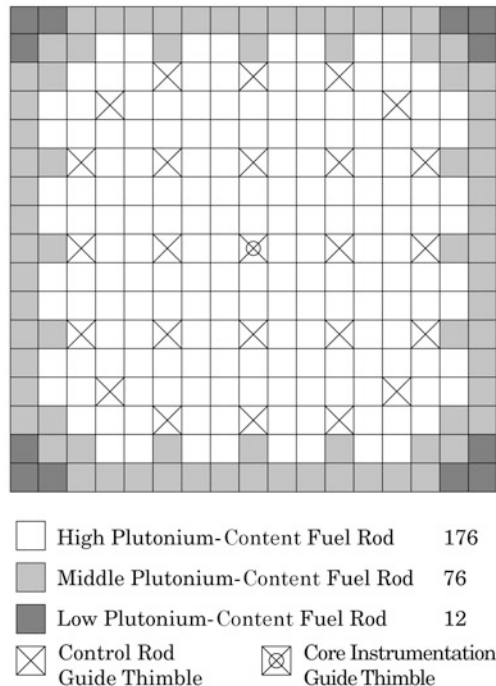


Fig. 3.64 Example of fuel rod arrangement in MOX fuel assembly [40] (Copyright Mitsubishi Heavy Industries, Ltd., 2014 all rights reserved)

MOX-fueled cores. As well, plutonium has a smaller delayed neutron fraction than uranium and it reduces the effective delayed neutron fraction of MOX-fueled cores. Therefore, the core safety analysis is done based on properly established safety analysis parameters considering these effects.

(2) Features in Radiation and Decay Heat

MOX fuel has different features from uranium fuel. The features and countermeasures are discussed next.

(i) Source Strength of MOX Fresh Fuel

MOX fresh fuel releases neutrons by self-fission of ^{240}Pu and (α, n) reaction of ^{238}Pu , and gamma rays by ^{241}Am and its source strength becomes high. Therefore, MOX fresh fuel provides a high surface dose rate in comparison with uranium fresh fuel. Dedicated MOX fresh fuel handling equipments with sufficient shield are used to reduce the exposure of workers and proper handling management is necessary.

(ii) Source Strength of MOX Spent Fuel

In comparison with uranium spent fuel, MOX spent fuel contains a large amount of high-order actinides, such as Am and Cm, produced

by neutron absorption of plutonium isotopes and it leads to high neutron source strength. Gamma source strength of MOX spent fuel is relatively small because plutonium has a larger fission energy and a smaller number of fission events, resulting in a smaller FP amount compared to uranium fuel for the same burnup. The different FP yield of Plutonium is another reason for the difference of the gamma source strength. Since the neutron shielding effect of water in the spent fuel pit is sufficient, there is no limitation in handling MOX spent fuel in uranium fuel storage facilities even though MOX spent fuel has high neutron source strength.

(iii) Decay Heat of MOX Spent Fuel

FPs are the dominant source of decay heat for a short cooling period, but high-order actinides such as Am and Cm are dominant for a long cooling period. MOX spent fuel contains a large amount of high-order actinides, as mentioned above, and it gives a larger decay heat than uranium fuel at a long cooling time. Spent fuel storage cooling systems are enhanced in case of insufficient cooling capability, considering the heat load to the spent fuel pit. MOX fuel produces a slightly smaller decay heat than uranium fuel for a short cooling period.

(3) Pu^f content of MOX fuel

MOX fuel assemblies have a zoning configuration with three different contents of plutonium as shown in Fig. 3.64. The reactivity of MOX fuel assembly is determined by the assembly-averaged Pu^f content. Plutonium used in MOX fuel has been reprocessed and recovered from spent fuel of various types of reactors and therefore it has various isotope compositions. The assembly-averaged Pu^f content is set to give a proper reactivity corresponding to plutonium isotope composition. As a currently implemented method to set the assembly-averaged Pu^f content, the *MOX fuel assembly to give the same reactivity as ^{235}U 4.1 wt% uranium fuel at 28,100 MWd/t* is used as a criterion for the appropriate reactivity [41]. The enrichment of 4.1 wt% and burnup of 28,100 MWd/t are the enrichment and the core average burnup at EOC for the typical uranium fuel in the standard 3-loop PWR (See Problem 6 at the end of this chapter). To match reactivity at the core average burnup of EOC means that MOX-fueled core has the same operating cycle length as the uranium-fueled core.

Figure 3.65 compares variation in the infinite multiplication factor between typical MOX fuel and ^{235}U 4.1 wt% uranium fuel. The MOX fuel shows a milder variation in infinite multiplication factor with burnup than the uranium fuel and the line intersects that of the uranium fuel at a point. The infinite multiplication factor line of MOX fuel moves up and down with almost the same slope as Pu^f content increases and decreases. Therefore, a proper reactivity of MOX fuel can be obtained by adjusting Pu^f content responding to plutonium isotope compositions in MOX fuel

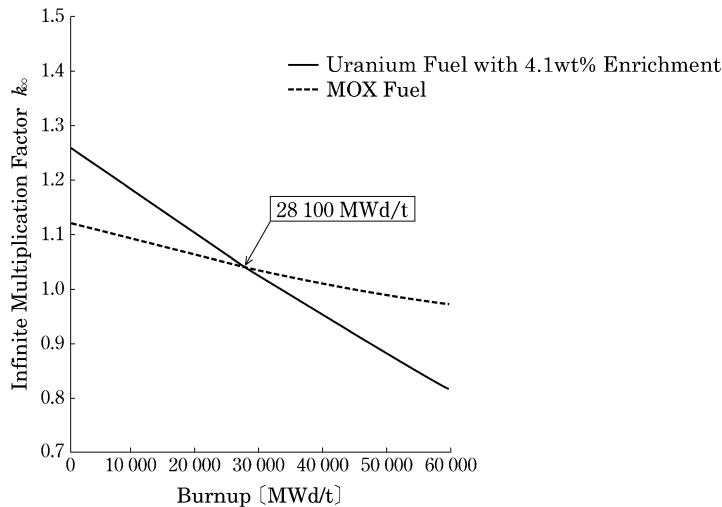


Fig. 3.65 Comparison of infinite multiplication factor between MOX and Uranium fuels [41] (Copyright Mitsubishi Heavy Industries, Ltd., 2014 all rights reserved)

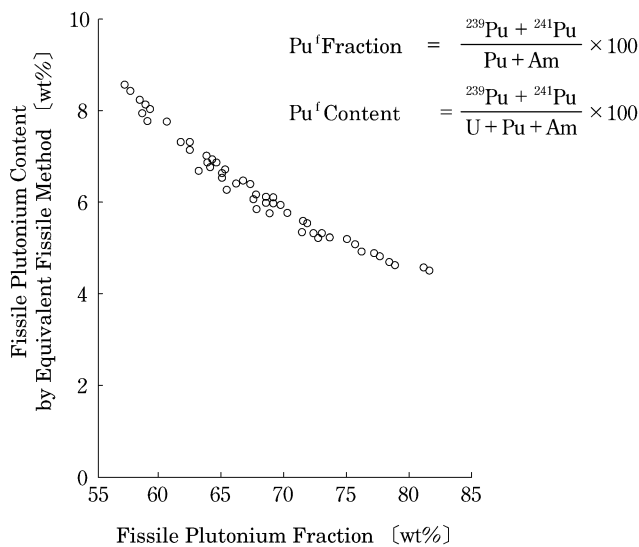


Fig. 3.66 Relation between fissile (Pu^f) content and fissile (Pu^f) fraction [41] (Copyright Mitsubishi Heavy Industries, Ltd., 2014 all rights reserved)

fabrication. Practically, the reactivity worth of each plutonium isotope is replaced with an equivalent reactivity worth of ^{239}Pu , referred to as the *equivalent fissile method* [41]. Figure 3.66 shows the relation between Pu^f content and Pu^f fraction set by the equivalent fissile method.

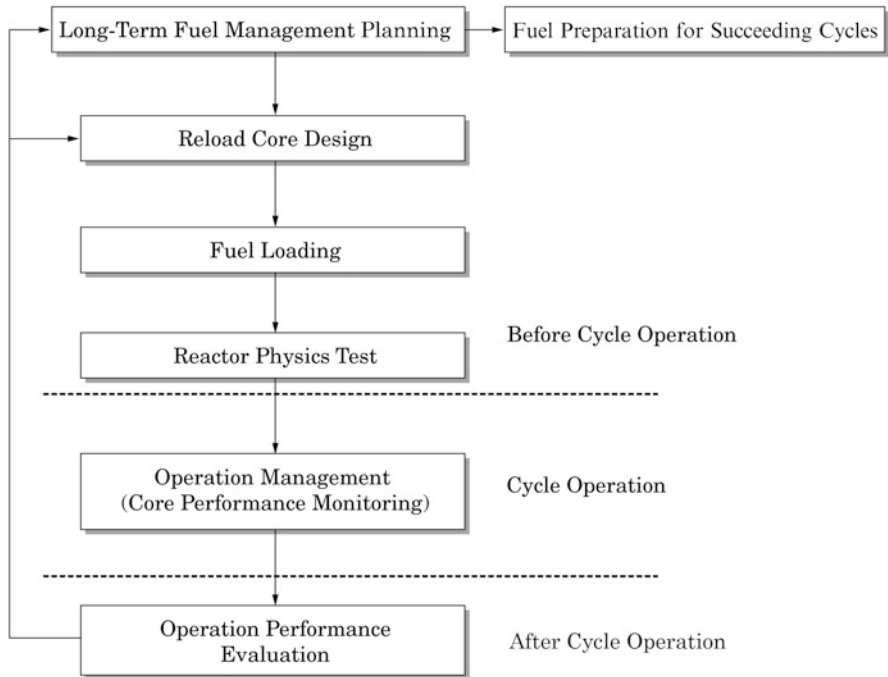


Fig. 3.67 Outline flow of PWR core management

[5] Reactor Power Uprating

Reactor Power Uprating for PWRs are evaluated considering the same effects as for BWRs mentioned in the list [5] of Sect. 3.2.6 and the range of facility modification is determined. It has been reported that advanced safety analysis methods and development and introduction of advanced fuel are important for significant power uprating [42].

3.3.7 Core Management

[1] Summary of Core Management

The flow chart of PWR core management is shown in Fig. 3.67. Since it takes a considerable time from placement of a fuel order to its shipment, the required fuel assemblies are ordered several years ahead based on the operation plan. This is referred to as the *long-term fuel management planning* in which core characteristics such as core reactivity, power distribution, and burnup of each fuel assembly are evaluated for multiple cycles.

Then, in the present cycle design referred to as the *reload core design*, the number of fresh fuel assemblies and fuel assemblies loading pattern in the core

are determined for getting a safe and economic core during the planned cycle length. Core characteristics are evaluated using nuclear design codes [40, 43] in both the long-term fuel management planning and the reload core design.

Fuel assemblies are loaded in the core based on the fuel loading pattern determined in the reload core design. Core physics tests are performed to measure core characteristics such as critical boron concentration, moderator temperature coefficient, control rod worth, and power distribution, and to confirm the core safety by comparing with the design values. Operation management such as core performance monitoring is carried out during the reactor operating cycle, and operation data are evaluated and reflected on the long-term fuel management or the next reload core design after the cycle.

[2] Long-Term Fuel Management Planning

The main purpose of the long-term fuel management planning is to predict the number of fresh fuel assemblies necessary for the operating cycle length in multiple cycles. The fuel loading pattern of each cycle to meet the design criteria is determined continuously over several cycles. The investigation contents of the long-term fuel management planning are similar to those of the reload core design to be discussed in the next item. Investigation of some core characteristics may be omitted.

[3] Reload Core Design

As shown in Fig. 3.68, the number of fresh fuel assemblies to be loaded and fuel assemblies loading pattern in the core are determined for getting a safe and economic core during the planned cycle length. Since control rods are almost completely withdrawn during reactor operation, core characteristics concerning safety and economy are determined mainly by fuel loading pattern in the core. The number of fresh fuel assemblies to be loaded is set to achieve the required operating cycle length and the fuel loading pattern is designed in combination of reloaded and fresh fuel assemblies. Core characteristics (nuclear design parameters) such as reactivity shutdown margin and power distribution are evaluated to meet the design criteria, considering the limiting conditions for operation (e.g., control rod insertion limit) and reactor protection system set-point (e.g., over-power ΔT reactor trip). The fuel loading pattern is repeatedly changed and investigated until the core characteristics satisfy all the design criteria or the number of fresh fuel assemblies to be loaded would be changed if necessary. Various optimization methods [35] are adopted for an economic fuel loading pattern (a small number of fresh assemblies) under the design criteria. For a determined fuel loading pattern, various characteristics such as critical boron concentration for excess reactivity control and control rod worth are evaluated and the results are given to the reload core design data set necessary for operation.

[4] Core Performance Monitoring

Control rods are almost completely withdrawn during reactor operation and the variation in core characteristics as burnup progresses is mild. Regular tracking of the critical boron concentration and in-core power distribution measurements once a month are mainly carried out in the core management. The measurements

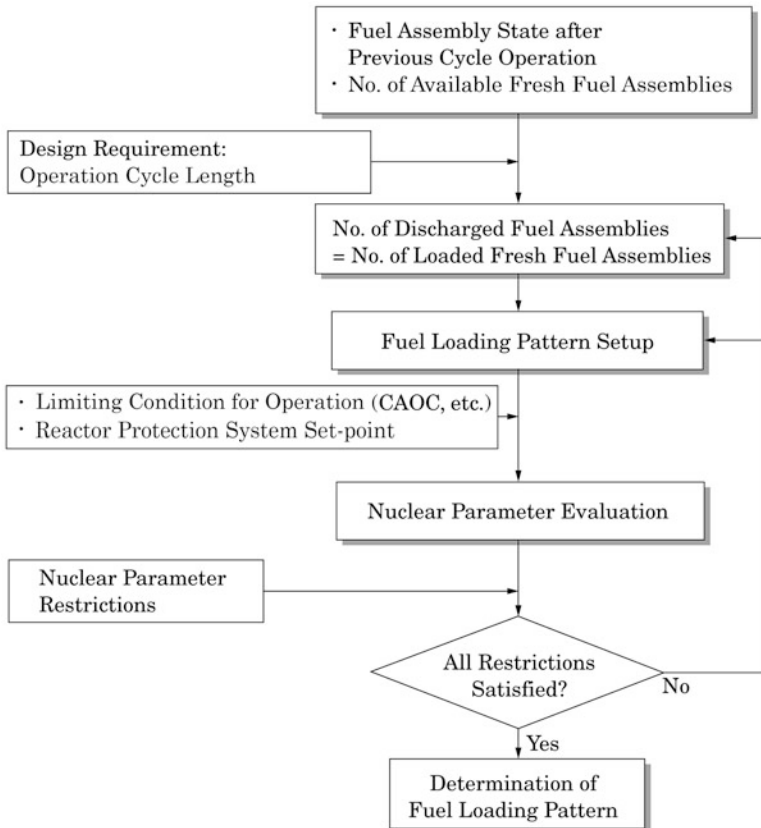


Fig. 3.68 Reload core design flow of PWR

are compared with the design values, and the differences are verified to be within the allowed ranges to assure the core safety. The power distribution is measured by in-core neutron detectors which are placed in about 1/3 of the fuel assemblies in the core as shown in Fig. 3.69. Power of each fuel assembly and peaking factors such as heat flux hot channel factor (F_Q) and nuclear enthalpy rise hot channel factor ($F_{\Delta H}^N$) are evaluated by processing the measured reaction rate distribution and the core design power distribution [44].

As mentioned in Sect 3.3.5, power distribution is continuously monitored by ex-core neutron detectors which are calibrated by the in-core detector measurement. Thus, the A.O. monitored by the ex-core neutron detectors can properly express the in-core power distribution.

Recently, core design codes are used in continuous on-site monitoring of three-dimensional power distribution and re-startup prediction (operation support) in combination with ex-core neutron detector and thermocouple signals of core outlet temperature.

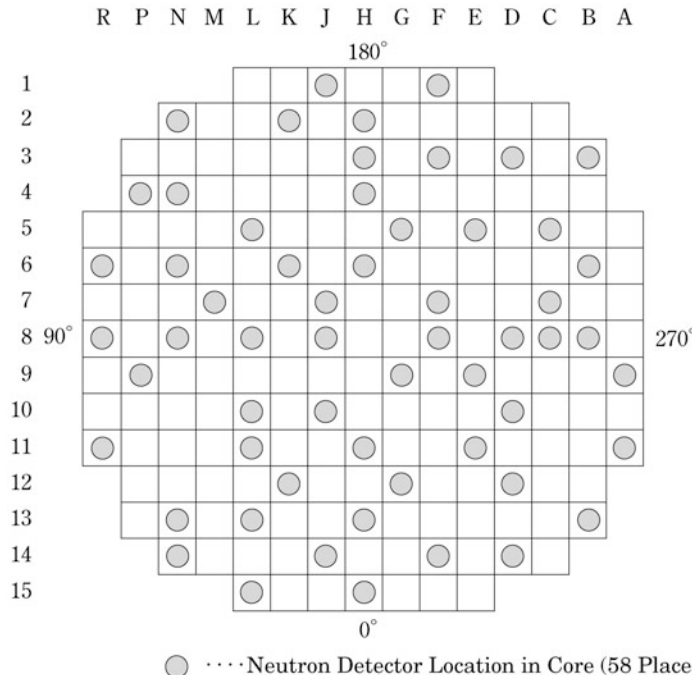


Fig. 3.69 Location of in-core neutron detectors (4-loop core) [32] (Copyright Mitsubishi Heavy Industries, Ltd., 2014 all rights reserved)

3.3.8 Fuel Management

[1] Fresh and Spent Fuel Management

Fuel management items of PWR plants are similar to that of BWR plants as listed below, and only the major different items are complemented [3].

(1) Fresh fuel acquisition

(2) Refueling during overhaul

In PWRs, all fuel assemblies are moved to the spent fuel pit. Since rod cluster control assemblies, burnable poison rods, and neutron sources or thimble plugs are to be inserted into the fuel assemblies, their shuffling and insertions are carried out in the spent fuel pit according to the fuel loading pattern and checked by using underwater TV cameras.

(3) Fuel inspection during overhaul

In PWRs, a part of the reloaded fuels are inspected for fuel rod damage, deformation, and gap clearance change (fuel rod bowing) through visual observation. Sipping inspection is made to check for leakage of radioactive materials from fuel assemblies by using a dedicated inspection container outside the reactor.

(4) Spent Fuel Storage and Carry-out

(5) Accounting of fissile material and safeguards

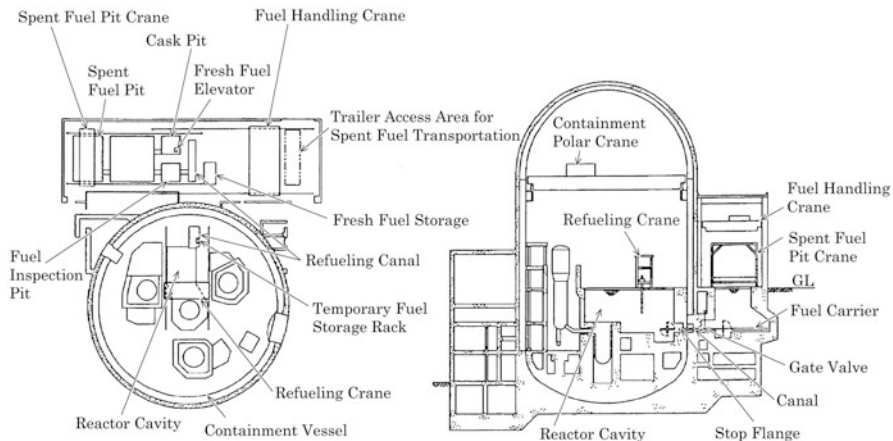


Fig. 3.70 Schematic view of fuel storage and handling facility [45] (Copyright Mitsubishi Heavy Industries, Ltd., 2014 all rights reserved)

Table 3.14 Example of main specifications of fuel storage facility [45]

	Fresh fuel storage	Spent fuel storage
No. of units	1	2
Storage capacity	As much as ~23 % of whole core	As much as ~920 % of whole core
Rack material	Stainless steel	Boron-added (0.95–1.05 wt%) stainless steel
Lining material	—	Stainless steel

[2] Fuel Storage and Handling Facilities

Fuel storage and handling facilities of PWRs consist of fresh fuel storage facilities, spent fuel storage facilities, spent fuel pit water cleanup system, refueling crane, spent fuel pit crane, fuel handling crane, and fuel-carrying facilities [45]. Figure 3.70 illustrates a schematic view of fuel storage and handling facilities and Table 3.14 gives the main specifications of the fuel storage facilities.

Fuel storage and handling facilities are designed to prevent criticality in any cases to be expected by using a geometrically safe arrangement or other suitable means. Therefore, fuel storage facilities are designed to secure subcriticality even when fully loaded and flooded with full-density unborated water. Fuel handling facilities are designed to have a structure in which only one fuel assembly can be handled independently to prevent criticality.

(1) Fresh Fuel Storage Facilities

Fresh fuel storage is constructed of reinforced concrete, established in an independent area of the fuel handling building. Fresh fuel assemblies are stored one by one in stainless steel racks in a dry condition. The fresh fuel storage is constructed to prevent water flooding and to be able to drain water when it enters the storage.

The storage capacity of the fresh fuel storage is usually set considering the number of fresh fuel assemblies to be loaded and alternative storage of fresh fuel in the spent fuel pit. In Table 3.14, the storage capacity corresponds to about 23 % of the whole core fuel. Fresh fuel storage racks are designed to assure that the effective multiplication factor of less than 0.95 must be maintained even in a severe condition such as unborated water flooding for the maximum storage amount of fresh fuel, by holding a proper fuel assembly spacing to prevent criticality of storage fuel. Moreover, the fresh fuel storage racks are designed to prevent criticality even filled with unborated water of the optimum moderating density.

(2) Spent Fuel Storage Facilities

The spent fuel pit, established in the fuel handling building, uses reinforced concrete facilities. The wall and bottom of the spent fuel pit are shielded by a sufficiently thick concrete wall and the top of the spent fuel is secured by a water depth to ensure a sufficient shielding effect. The internal surface of the spent fuel pit is lined with stainless steel to prevent water leakage from the spent fuel pit even if a fuel assembly is dropped. In addition, spent fuel is stored under borated water in the spent fuel pit which is designed to remove decay heat by the spent fuel cooling system.

Spent fuel racks to vertically store fuel assemblies are arranged in the spent fuel pit. The spent fuel racks have a structure in which fuel assemblies are inserted one by one in each rack. In a recent design, spent fuel racks are designed which use boron-added stainless steel, and to assure that the effective multiplication factor of less than 0.98 is maintained even in a severe condition such as unborated water flooding under the maximum storage amount of fresh fuel, a proper fuel assembly spacing is held to prevent criticality of storage fuel. Table 3.14 shows that the storage capability reaches about 920 % of the whole core fuel in this example.

Fresh fuel assemblies as well as spent rod cluster control assemblies and burnable poison assemblies are temporarily stored in the spent fuel racks.

A cask pit is also established near the spent fuel pit to accommodate spent fuel into a spent fuel transport cask.

(3) Spent Fuel Pit Cooling and Purification System

The spent fuel pit cooling and purification system has a function to remove decay heat from spent fuel stored in the spent fuel pit and to remove solid and ion impurities in the spent fuel pit water, purifying it. Spent fuel pit pump, spent fuel pit cooler, and spent fuel pit demineralizer and filter are installed as well. Two spent fuel pit coolers operate to maintain the average temperature of the spent fuel pit water below 52 °C in the case that all fuel assemblies in the core are discharged and stored in the spent fuel pit in which spent fuel assemblies discharged from the previous cycles are already stored. Even operation with one spent fuel pit pump can maintain the average temperature of spent fuel pit water below 65 °C.

Exercises of Chapter 3

1. Give an overview of improvements for advanced standardization of LWRs from 1975 to 1985 in Japan.
2. Refer to the specifications (Tables 3.7 and 3.8) of high burnup 8×8 fuel (Step II). Determine size specifications of the fuel and water rods in the 10×10 fuel assembly to meet the conditions below.
 - No change in channel box size
 - The same fuel loading weight as Step II fuel
 - Non-boiling region area inside the water rod is equal to or larger than Step II fuel.

Main specifications of high burnup 8×8 fuel (Step II): channel box inner width, 134 mm; number of fuel rods, 60; cladding outer diameter, 12.3 mm; cladding thickness, 0.86 mm; cladding inner diameter, 10.58 mm; pellet diameter, 10.4 mm; water rod inner diameter, 32 mm; inner cross-sectional area of channel box, about 179.3 cm^2 .

3. Calculate the following items for a BWR of 26.2 MWth/tU specific power.
 - (a) Cycle burnup at a cycle length of 12 months and load factor of 100 %.
 - (b) Core average burnup at the end of the equilibrium cycle for a discharge burnup of 45 GWd/t under the above fuel conditions.
 - (c) Achievable discharge burnup within the linear reactivity model for an extended cycle length to 15 months under the above fuel conditions.
4. Answer the following questions on reactivity control of a BWR in normal operation.
 - (a) Explain burnup reactivity control of the BWR.
 - (b) Set a typical void reactivity coefficient for the BWR and calculate the amount of reactivity control when the void fraction of the core is changed by 5 % using core flow rate control.
 - (c) Explain the control rod position adjustment and core flow rate control during the cycle operation for the excess reactivity with cycle burnup as given in the figure below.

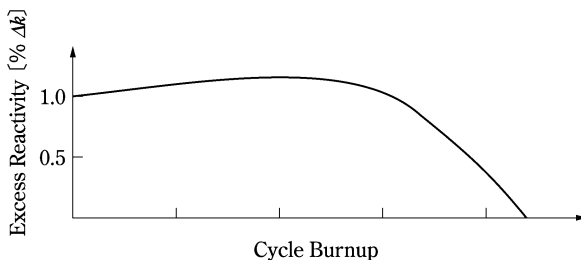


Figure variation in excess reactivity with cycle burnup

5. Explain challenges and measures in core design for high burnup based on the transition of design specifications of BWR fuel assembly.
6. Calculate the core average burnup at the end of the equilibrium cycle of the standard 3-loop PWR assuming a constant power with burnup under the following conditions.

Core thermal power: 2,652 MW

Number of fuel assemblies in the core: 157

Initial uranium weight per assembly: 460 kg

Number of fresh fuel assemblies: 60

Equilibrium cycle length: 413 days (full power)

7. Discuss design feasibility of a PWR core without soluble boron in the primary coolant for reactivity control.
8. Consider a PWR in hot full power normal operation with 700 ppm boron concentration in the primary coolant as shown in Fig. 3.38. The PWR was instantly put into hot shutdown. Calculate the boron concentration necessary for achieving criticality at the following times after shutdown, while maintaining the hot temperature.
 - (a) 8 h
 - (b) 20 h
 - (c) 90 h
9. Discuss measures against positive moderator temperature coefficients for the following two cases.
 - (a) In the process of reload core design, the moderator temperature coefficient for a fuel loading pattern was +2 pcm/ $^{\circ}\text{C}$ at BOC and hot zero power. How many burnable poison rods are necessary to make the moderator temperature coefficient negative? Assume that the dependence of moderator temperature coefficient on boron concentration is the same as that in Fig. 3.35 and a burnable poison rod can reduce the critical boron concentration by about 0.5 ppm.
 - (b) For startup after refueling, the moderator temperature coefficient was measured as +2 pcm/ $^{\circ}\text{C}$ at hot zero power. What operational limitations are available to make the moderator temperature coefficient negative at hot zero power? Refer to Figs. 3.45 and 3.42 for boron worth and control rod worth, respectively.

References

1. Aasada T et al (1989) Nuclear handbook, Newth edn. Ohmsha Press, Amsterdam (in Japanese)
2. Nuclear Handbook Editorial Committee (2007) Nuclear handbook. Ohmsha Press, Amsterdam (in Japanese)
3. Nuclear Safety Research Association (1998) The behavior of LWR fuel. Nuclear Safety Research Association, Tokyo (in Japanese)

4. Electric Power Development Corporation Ltd. (1999) Application for reactor establishment permit of Ohma nuclear power station. Electric Power Development Corporation Ltd, Tokyo (in Japanese)
5. Tokyo Electric Power Corporation Inc. (1988) Application for reactor establishment alteration permit of Kashiwazaki-Kariwa nuclear power station (Units 6 and 7). Tokyo Electric Power Corporation Inc., Tokyo (in Japanese)
6. Chubu Electric Power Corporation Inc. (1986) Application for reactor establishment alteration permit of Hamaoka nuclear power station (Unit 4). Chubu Electric Power Corporation Inc., Nagoya (in Japanese)
7. Graves HW Jr (1979) Nuclear fuel management. Wiley, New York
8. Aoyama M et al (1984) A conceptual design of a fuel bundle for extended burnup in boiling water reactors. *Nucl Technol* 64:19
9. Aoyama M et al (1989) Reactivity control method for extended burnup of boiling water reactor fuel bundles. *J Nucl Sci Technol* 26(4):403
10. Takeda R et al (1978) New BWR core concept of improved performance summary of WNS core. *Trans Am Nucl Soc* 28:558
11. Kurihara K et al (1981) Power flattening method for boiling water reactor. *J Nucl Sci Technol* 18(2):116–124
12. Sugimoto O et al (1981) Operating experience at Shimane-1 with WNS-type initial fuel. *Trans Am Nucl Soc* 39:912
13. Shimoshige T et al (1985) Operating experience with axially two-zoned initial fuel core. *Trans Am Nucl Soc* 50:565
14. Nishimura A et al (1985) Experience with shingle control rod pattern operation in axially two-zoned fuel cores. *Trans Am Nucl Soc* 50:567
15. Kobayashi Y et al (1979) New BWR core concept with WNS-type fuel and 9 control cells. *Trans Am Nucl Soc* 33:641
16. Yamashita J et al (1986) Development of highly-economical BWR fuel. *Hitachi Rev* 68(4):47–52 (in Japanese)
17. Fennern L et al (1979) Improved control cell core design concept. *Trans Am Nucl Soc* 33:642
18. Nishimura S et al (1990) Development and application of high burnup BWR core and fuel. *Hitachi Rev* 72(10):47–54 (in Japanese)
19. Haling RK (1964) Operating strategy for maintaining optimum power distribution throughout life. Proc. topl. mtg. nuclear performance of power reactor core, TID-7672, U.S. Atomic Energy Commission, Washington
20. Yamashita J et al (1988) Application and development of improved BWR core and fuel technology. *Hitachi Rev* 70(4):61–67 (in Japanese)
21. Kawahara A et al (1980) Improvement in PCIOMR for fuel integrity security. *Hitachi Rev* 62(9):23–26 (in Japanese)
22. Tanabe A et al (2004) Introduction to nuclear fuel engineering: focused on LWR fuel: (3) LWR fuel: 1. *J At Energy Soc Jpn* 46(7):31–37 (in Japanese)
23. Nuclear Safety Commission of Japan (1999) Full core loading of MOX fuel in advanced BWR. Nuclear Safety Commission of Japan (in Japanese)
24. Aoyama M et al (1995) Development of full MOX-ABWR core. *Hitachi Rev* 77(10):63–66
25. Atomic Energy Society of Japan (2008) Expert research committee report on technical evaluation of reactor power improvement. Atomic Energy Society of Japan, Tokyo (in Japanese)
26. Shinohara Y (1994) Core management technology of a light water reactor, BWR. *Nucl Ind* 40(4):49–55 (in Japanese)
27. Mochida T et al (1997) Research results of nuclear calculation methods and advancement of core design methods: core designs and control of light water reactor. *J At Energy Soc Jpn* 39(1):15–18 (in Japanese)
28. Yamamoto A et al (2006) Design the fuel loading pattern: loading pattern optimization methods in commercial light water reactors. *J At Energy Soc Jpn* 48(12):22–46 (in Japanese)

29. Kansai Electric Power Corporation Inc. (2002) Application for reactor establishment alteration permit of Ohi nuclear power station. Kansai Electric Power Corporation Inc., Osaka (in Japanese)
30. Xu Z, Driscoil MJ, Kazimi MS (2002) Neutron spectrum effects on burnup, reactivity, and isotopes in UO₂/H₂O lattices. *Nucl Sci Eng* 141:175–189
31. Kondo Y, Teranish T, Watarumi C (1982) Improvement and development of PWR core and fuel. Mitsubishi Heavy Ind Technical Rev 19(6):652–670 (in Japanese)
32. Mitsubishi Heavy Industries, Ltd. (2004) Power distribution control of mitsubishi PWR, MHI-NES-1027 Rev. 2 (in Japanese)
33. Shimada S (2008) LWR-plants: development for the PWR type light water reactor in Japan and USA: from shipping port to MIHAMA unit 1 plant. *J At Energy Soc Jpn* 50(2):109–113 (in Japanese)
34. Kitamura T, Suzuki S (2008) LWR-plants: light water reactor's development in Japan (3) – improvement standardization program for light water reactors: PWR 1. *J At Energy Soc Jpn* 50(6):384–388 (in Japanese)
35. Yamamoto A, Jagawa H, Sato D, Sato H, Yamasaki M (2006) Design the fuel loading pattern: loading pattern optimization methods in commercial light water reactors. *J At Energy Soc Jpn* 48(12):924–954 (in Japanese)
36. Mitsubishi Heavy Industries, Ltd. (2005) Nuclear design of gadolinia-containing fuel, MAPI-1066 Rev. 6 (in Japanese)
37. Mukai S, Suzuki S (2008) LWR-plants: light water reactor's development in Japan (7): improvement standardization program for light water reactors: PWR 3. *J At Energy Soc Jpn* 50(10):654–658 (in Japanese)
38. Mitsubishi Heavy Industries, Ltd. (2003) Nuclear design of mitsubishi advanced PWR, MHI-NES-1026 Rev. 1 (in Japanese)
39. Tsukuda Y, Kamimura S, Kohno N, Hattori T, Ito K, Mozumi Y (2003) Irradiation behavior of LWR high burnup fuel. *J At Energy Soc Jpn* 45(11):682–710 (in Japanese)
40. Heavy Industries, Ltd. (2004) Improved nuclear design method and reliability of mitsubishi PWR, MAPI-1087 Rev. 6 (in Japanese)
41. Mitsubishi Heavy Industries, Ltd. (1998) Plutonium content of MOX fuel for PWR, MHI-NES-1001 Rev. 1 (in Japanese)
42. Atomic Energy Society of Japan (2007) Expert research committee report on technical study on nuclear reactor safety assessment for power uprates (in Japanese)
43. Nuclear Fuel Industries, Ltd. (1995) PWR Nuclear design method and reliability (Improved NULIF system), NFK-8102 (in Japanese)
44. Mitsubishi Heavy Industries, Ltd (1988) Mitsubishi PWR core management code, MAPI-1084 (in Japanese)
45. Hokkaido Electric Power Corporation Inc. (2000) Application for reactor establishment alteration permit of Tomari nuclear power station (Expansion of unit 3) (in Japanese)

Chapter 4

Design of Advanced Reactors

Hiroo Osada and Kiyonobu Yamashita

Abstract Section 4.1 describes features of a fast reactor core and the procedure of the core design. The characteristics of reactivity and power distributions are explained in the nuclear design section and the reactivity control requirements are also explained in this section. The section of core thermal-hydraulic design explains the outline of the coolant flow allocation procedure and the evaluation methods of temperature distributions in a fuel subassembly. The author of Sect. 4.1 is Hiroo Osada.

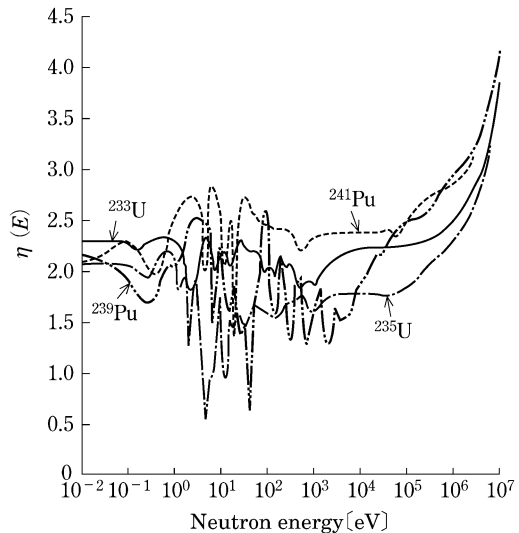
Section 4.2 describes design of high temperature gas-cooled reactor (HTGR). HTGR's cores consist of graphite internals and coated particle fuels that possess high temperature resistant. Helium gas is used as coolant that has high chemical stability in any temperature. High reactor outlet coolant temperature around 1,000 °C is possible for HTGRs with the high stable characteristics of graphite, fuel and coolant. High outlet coolant temperature enables high efficiency of electricity generation and broad utilization of HTGRs not only as electricity generation but also as a heat source for chemical industry. In comparison to LWRs, the outlet coolant temperature is high and difference between inlet and outlet coolant temperature is large for HTGRs. It results in different core design philosophy for HTGRs from LWRs. The core design of the High Temperature Engineering Test Reactor (HTTR) is presented as an example of HTGRs core design. The author of Sect. 4.2 is Kiyonobu Yamashita.

4.1 Design of Fast Reactors

Natural uranium contains only 0.7 % ^{235}U . The remaining 99.3 % is non-fissile material. Light water reactors (LWRs), operated under the thermal spectrum, mainly utilize ^{235}U as nuclear fuel.

A ^{238}U nuclide is converted to a ^{239}Pu nuclide by capturing a neutron. ^{239}Pu is a new nuclear fuel. The ^{239}Pu nuclide is further converted to ^{241}Pu through ^{240}Pu by capturing a neutron twice. ^{241}Pu is also a new nuclear fuel. By utilizing those

Fig. 4.1 Neutron yields per absorption (η) [1]



conversions, breeder reactors where production of ^{239}Pu and ^{241}Pu is larger than their consumption have been developed.

The configuration of a nuclear reactor, which pursues breeding of nuclear fuel, is determined by fundamental phenomena: nuclear reactions. The neutron yield per absorption η becomes

$$\eta = \frac{\nu \sigma_f}{\sigma_f + \sigma_c} = \frac{\nu}{1 + \alpha} \quad (4.1)$$

where ν , σ_c , σ_f , α are neutron yield per fission, capture cross section, fission cross section and the ratio σ_c/σ_f . Among η neutrons, one neutron is absorbed by a fissile nuclide to keep the fission chain reaction going. L neutrons are consumed by being absorbed by structures and coolant or leaking to the outside of the reactor. The remaining $\eta - (1 + L)$ neutrons are captured by fertile materials (^{238}U , ^{240}Pu) and produce new fissile materials (^{239}Pu , ^{241}Pu). For breeding the fissile materials, condition (4.2) is necessary.

$$\eta - (1 + L) \geq 1 \quad (4.2)$$

As L cannot be zero, breeding is fundamentally impossible unless η is over 2. Figure 4.1 shows η . It depends on neutron energy. Among fissile materials, ^{239}Pu gives the highest η for fast neutrons and hence the highest breeding performance. A nuclear reactor that breeds nuclear fuel by utilizing fast neutrons is called a *fast breeder reactor* (FBR) [2, 3]. On the other hand, a nuclear reactor where fission reactions are mainly caused by thermal neutrons is called a *thermal reactor* such as a LWR. Figure 4.2 shows neutron spectra of typical fast and thermal reactors.

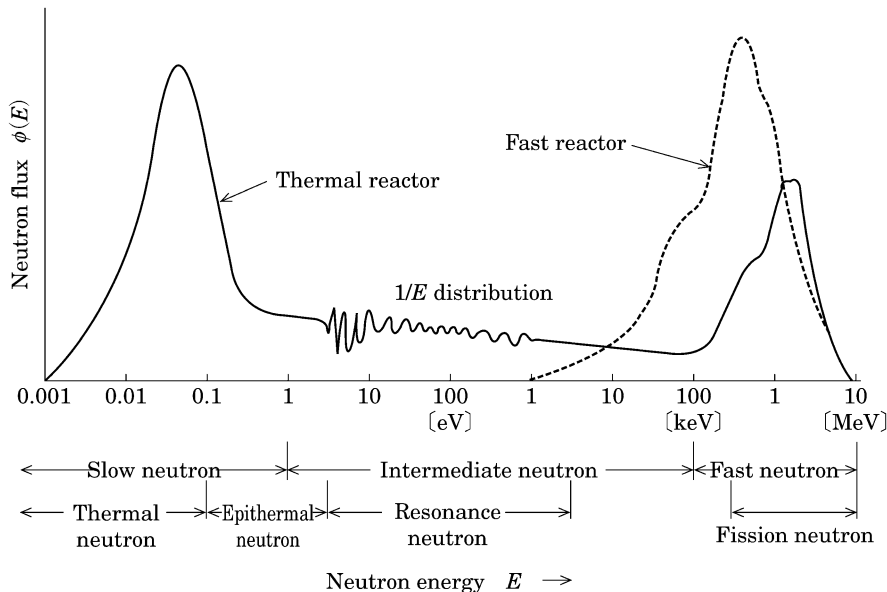


Fig. 4.2 Comparison of neutron spectra of fast and thermal reactors [4]

For the reactor core concept of a fast reactor, the following conditions are essential.

- Remove materials that moderate fast neutrons.
- Make the fraction of fissile fuel and fertile materials in the core as large as possible in order to efficiently utilize neutrons for breeding.

The breeding ratio (BR) and doubling time (DT) indicate the characteristics of a fast reactor.

$$BR = \frac{\text{Fissile materials produced per unit time}}{\text{Fissile material destroyed per unit time}} \quad (4.3)$$

$$DT = \text{Time for doubling mass of fissile materials} \\ \propto \frac{\text{Initial loading mass of fissile materials}}{(BR - 1) \times (\text{Reactor power})} \quad (4.4)$$

As BR becomes higher or the specific power, which is the ratio of the reactor power and the initial loading mass of fissile materials, becomes higher, DT is shorter [3, 5].

Liquid metal fast breeder reactors (LMFBRs) have been developed by giving shape to the fast reactor concept described above. The liquid metal (mainly sodium) was selected in consideration of the following conditions.

- (a) Moderation of neutrons is as little as possible.
- (b) The breeding ratio is kept as high as possible.
- (c) Cooling performance is very high in order to realize a high power density.

Despite not satisfying(c), gas cooled fast reactors have also been researched because their characteristics associated with (a) and (b) are good [3].

In the following subsections, core design mainly for the LMFBR is introduced.

4.1.1 Basic Procedure of Core Design

[1] Characteristics of fast reactor core

In the primary cooling system of the LMFBR, the high-temperature and low-pressure sodium heated in the core is cooled by the intermediate heat exchangers and then sent back to the core. In the secondary cooling system, the sodium receives heat from the primary cooling system through the intermediate heat exchangers and gives heat to water and steam through the steam generators. The energy of the generated steam is converted to electricity through the steam turbines and generators. The secondary cooling system in the LMFBR is necessary for two reasons: the high radioactivity of the primary coolant; and preventing the core from being directly affected by the accidental sodium-water reaction in the steam generator. Sodium as the primary coolant provides forced cooling of the core by single-phase flow under low pressure. It does not evaporate in the core due to its high boiling point.

Figure 4.3 illustrates the cross section of a fast reactor core. In this example, the core consists of 198 core fuel assemblies, 19 control rod assemblies, surrounding blanket fuel assemblies and neutron shieldings. The shape of the whole core is almost hexagonal. Each core fuel assembly contains 169 fuel elements in a hexagonal wrapper tube.

[2] Basic design conditions [6–8]

Just as it is in LWRs, the main objective of reactor core design is to improve economy while ensuring safety. The requirements for safety are ensuring shutdown capability, limiting reactivity insertion rate, getting self controllability, preventing fuel failure, limiting the power distribution, and ensuring stability. The main requirements for economy are getting adequate burnup and breeding performance. The basic design principles are summarized in Table 4.1.

(1) Reactor shutdown

The design conditions of the reactor shutdown system are determined in order to shut down the reactor safely and surely at abnormal incidences. For that purpose, the following criteria are adopted.

- Provide two independent shutdown systems.
- Design at least one system able to shut down the reactor at low temperature with the required shutdown margin even if the control rod with the highest reactivity worth is fully withdrawn and stuck.

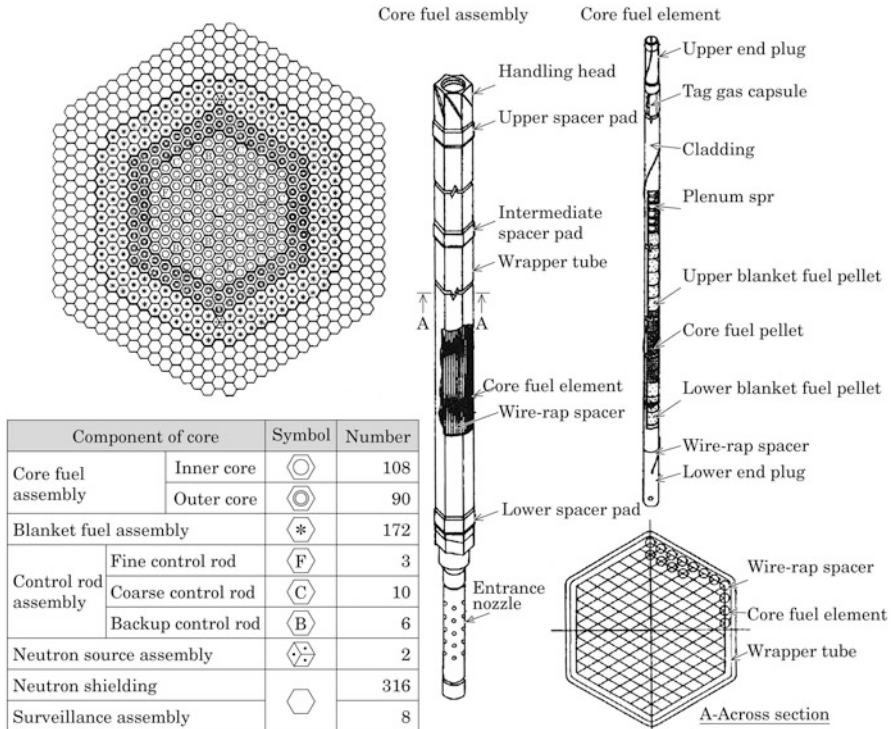


Fig. 4.3 Driver fuel assembly and core configuration of Japanese prototype reactor monju [6]

- Design the shutdown systems so that, even if one shutdown system completely fails, another system can keep the reactor subcritical at low temperature.

(2) Limitation of reactivity insertion rate

The maximum reactivity insertion rate of the control rod is limited so as to prevent loss of coolant boundary integrity or core internal integrity. For that purpose, the following measures are taken.

- Limit the number of control rods that can be simultaneously withdrawn.
- Limit the maximum withdrawal velocity.

(3) Self controllability

The core has an instantaneous negative feedback characteristic. That means the following.

- Mixed oxide (MOX) fuel itself has negative temperature coefficients based on the Doppler effect and thermal expansion.
- By combining the temperature coefficients of fuel, structure, coolant and core support plate, the power reactivity coefficient is negative.

Table 4.1 Major design principles of LMFBR Core [6]

Item	Design principle	Example of criteria
Reactor shutdown	(a) Two independent shutdown systems are provided (b) At least one system can shut down the reactor at low temperature with the required shutdown margin even if the control rod with the highest reactivity worth is fully withdrawn and stuck (c) Reactor is kept subcritical at low temperature even if one shutdown system is assumed to fail	Reactor shutdown margin Over 0.001 $\Delta k/k$ at low temperature
Limitation of reactivity insertion rate	(a) Maximum reactivity insertion rate of control rod is limited so that rod withdrawal at maximum possible velocity leads to neither loss of coolant boundary integrity nor failure of core, reactor internals etc which deteriorate core cooling	Maximum reactivity insertion rate Below $8.5 \times 10^{-5} (\Delta k/k)/s$
Self controllability	(a) Doppler coefficient and power reactivity coefficient, which is obtained by combining all kinds of reactivity coefficients such as temperature coefficients of fuel, structure, coolant and core support plate, is kept negative under all operating conditions in order to provide negative feedback characteristic	Doppler coefficient $-5.7 \text{ to } -7.6 \times 10^{-3} T \frac{dk}{dT}$
Fuel integrity	(a) Maximum temperature of fuel cladding is limited (b) Maximum fuel centerline temperature is kept below melting point of fuel pellets (c) Maximum burnup of fuel assembly is limited.	(a) Below 675 °C at normal operation and 830 °C at abnormal operational occurrences (center of wall thickness) (b) Below 2 650 °C for unirradiated fuel (c) Below 93,000 MWd/t
Limitation of power distribution	(a) At normal operation and anticipated operational occurrences, adequate power distribution is kept so that allowable design limit of fuel is not exceeded (b) Power distribution is flattened in order to efficiently take out thermal power. Core is divided into two regions with different plutonium enrichments. Outer core has higher plutonium enrichment (c) Maximum linear heat rate is limited.	Maximum linear heat rate Below 360 W/cm
Stability	(a) Throughout the operation period, power oscillation which leads to an	Abnormal oscillation of power distribution does not occur because

(continued)

Table 4.1 (continued)

Item	Design principle	Example of criteria
	excess of allowable design limit of fuel is prevented at normal operation and anticipated operational occurrences	no fission products have large absorption cross section in the fast reactor energy range
Limitation of coolant temperature	(a) Coolant temperature is kept below boiling point at normal operation, anticipated operational occurrences and design basis accidents	
Breeding performance	(a) Adequate breeding ratio is achieved	About 1.2 as target

- Increase in the power is suppressed by the negative reactivity feedback even at anticipated operational occurrences.

(4) Fuel integrity

The maximum fuel centerline temperature and the maximum cladding temperature are limited in order to ensure fuel integrity at normal operation and anticipated operational occurrences.

- The fuel centerline temperature must not reach the melting point of the oxide fuel pellet.
- The cumulative fatigue cycle of fuel cladding must not reach the design fatigue life.
- The burnup is designed below the limit for which fuel integrity has been ensured by irradiation tests.

(5) Limitation of power distribution

At normal operation and anticipated operational occurrences, the power distribution is suitably designed so that the allowable design limit of fuel is not exceeded.

- The maximum linear heat rate at normal operation is limited.
- Power distribution is flattened in order to efficiently take out thermal power.

To do that, the core is divided into two regions with different plutonium enrichments.

The outer core has higher plutonium enrichment.

(6) Stability

Power oscillation which leads to an excess of the allowable design limit of fuel must not occur.

(7) Limitation of coolant temperature

Boiling of coolant must not occur at normal operation, anticipated operational occurrences and design basis accidents. Even if a void is generated in the primary coolant, the inserted reactivity largely depends on the core size and core shape. Generally, the inserted positive reactivity becomes larger with larger core size. Although such an incident is beyond design basis and cannot occur from a technical viewpoint, an adequate safety level is ensured by the core design.

(8) Breeding performance

The required breeding performance for a fast reactor is determined based upon balance between the demand and supply of plutonium at the time of construction to avoid an excessive plutonium accumulation from the viewpoint of non proliferation.

[3] Design procedure

The procedure for designing a fast reactor core is schematically shown in Fig. 4.4. The core thermal power and the operation period per cycle are determined as the basic specifications of the core design. The fuel assembly maximum burnup (or discharged burnup), the maximum allowable linear heat rate and the breeding ratio are given from the design principles.

First, the total length of the fuel elements and the number of fuel assemblies are preliminarily determined according to the core thermal power, the linear heat rate of fuel and the core height. The fuel loading amount is obtained by determining diameter of the fuel element. Then, the control rods are arranged based on the functions. The core configuration is determined. The core characteristics are iteratively evaluated until the design principles are satisfied by adjusting the trade-off conditions as illustrated below.

- If the burnup is lower than the target, the fuel element is made thinner to reduce the fuel loading or the number of fuel exchange batches is increased.
- If the breeding ratio is lower than the target, the fuel element is made thicker or the core height is increased.
- If the void reactivity is too large, the core height is reduced.

When all the design targets and criteria are satisfied, the core design is fixed.

4.1.2 Core Geometry, Operation and Management

[1] Setting of core geometry

The fast reactor core consists of the core fuel assemblies, the control rod assemblies, and the surrounding blanket fuel assemblies and reflectors (cf. Fig. 4.3). The core fuel is MOX. The blanket fuel is depleted UO₂. The core fuel region consists of two types of core fuel assemblies with different plutonium enrichments. The outer core has higher plutonium enrichment to flatten the power distribution. The core fuel assembly consists of the fuel

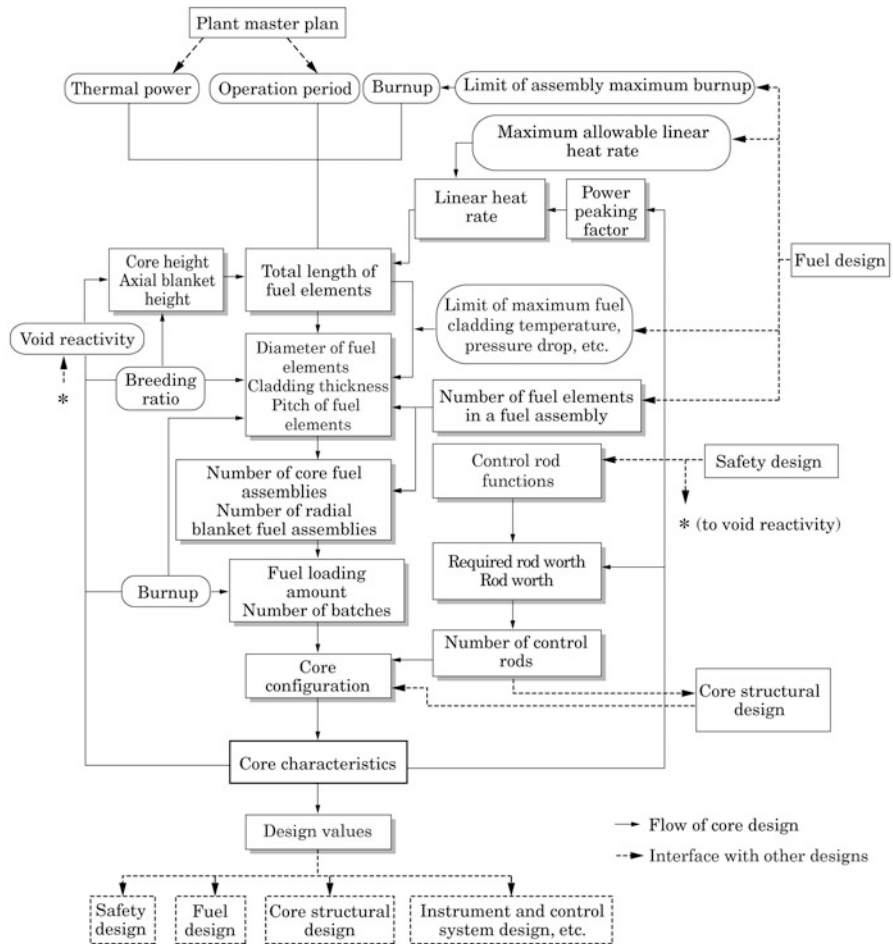


Fig. 4.4 Procedure of fast reactor core design

elements containing upper and lower axial blanket fuels as well as the core fuel. The blanket fuel assemblies surround the core region. They contribute to breeding by efficiently capturing leaking neutrons from the core region and also by reducing neutron leakage to the outside. The blanket region is surrounded by the reflectors in order to further reduce the neutron exposure of the structures.

In the core design, the total length of core fuel elements for target thermal power is calculated first from the linear heat rate. The total number of core fuel elements is calculated from the core height. The number of core fuel elements in a core fuel assembly is determined by selecting the diameter of the core fuel element. Then, the number of core fuel assemblies is determined. The relation between the core thermal power and the number of core fuel assemblies is

$$N_A = \frac{Q}{q \times H_c \times N_e} \quad (4.5)$$

N_A : Number of core fuel assemblies

Q : Core thermal power (MW)

q : Average linear heat rate (MW/m)

H_c : Core height (m)

N_c : Number of core fuel elements in a core fuel assembly

The amount of fuel loading is determined from the diameter of the core fuel element. The relationship among the core thermal power, the operation period per cycle, the fuel loading amount, and the number of batches is given by Eq. (4.6).

$$W = Q \times D \times N_b / BU \quad (4.6)$$

W : Fuel loading amount (t)

Q : Core thermal power (MW)

D : Operation period per cycle (d)

N_b : Number of batches (reciprocal of the fraction of refueled assemblies at a refueling)

BU : Average discharge burnup (MWd/t).

The core thermal power and the burnup are set as the design conditions. After selecting the operation period, the variables are the fuel loading amount and the number of batches. The fuel loading amount (diameter of the fuel element) strongly relates to the breeding ratio.

The breeding ratio is one of the important indices for the core characteristics of a fast reactor. On the other hand, the core size is limited from the viewpoint of safety because a larger core has a more positive coolant void reactivity. The breeding ratio increases with the fuel volume fraction by making the fuel element thicker and reducing the fuel element pitch. The breeding ratio also increases by making the ratio of core height and diameter closer to unity due to smaller leakage of neutrons. However, those changes lead to more positive void reactivity. Therefore, the following procedures are carried out.

- (a) The core height and the thickness of blanket region etc. are preliminarily determined. Then, the possible ranges of the fuel element diameter and the fuel element pitch etc. for achieving the target breeding ratio are identified through parametric surveys.
- (b) The possible ranges of the core height for achieving the target breeding ratio and the coolant void reactivity below the limit are identified through a parametric survey. Generally, the ratio of the core height and diameter is set small to reduce the void reactivity and coolant pressure drop. Designs so far have adopted ratios of 0.3–0.5 [9].

- (c) The possible range of the thickness of the blanket region for achieving the target breeding ratio is identified through a parametric survey.
- (d) The number of batches to achieve the target fuel burn-up with the designed operation period is considered.

As described above, the core characteristics are iteratively evaluated by changing the design parameters and finally the design specifications for achieving the design targets are determined.

The core configuration is generally made as symmetric as possible from the viewpoint of flattening the power distribution [9]. The total number of the core fuel assemblies and control rod assemblies is set as a multiple of 6 plus 1. The core fuel region including the control rod assemblies is divided into two regions: inner core and outer core.

The heights of the upper and lower axial blanket fuels are determined so as to achieve the designed breeding ratio. The number of radial blanket layers is determined in the same manner.

The number of control rods is determined so as to ensure the necessary reactivity worth. In the designs so far, 7–10 % of the core fuel region was occupied by the control rod assemblies [9]. The control rod assemblies are symmetrically arranged for flattening the power distribution, and the influences of the inserted rods and fully withdrawn rods at normal operation on the power distribution are also considered.

[2] Operation and management of core

(1) Refueling and operation cycle

Refueling is carried out in every operation cycle. After a cycle, the necessary number of discharged and loaded assemblies and their positions for achieving criticality throughout the next cycle are determined in consideration of the operation conditions. The scattered batch refueling method is adopted. In this method, the fraction of discharged fuel assemblies in a particular region (inner core, outer core or blanket) over the total fuel assemblies within that region is kept equal among the three regions. In that way, the power distribution and other neutronic characteristics are kept virtually unchanged between operation cycles.

In design of the refueling core, the refueling plan (i.e. the number and position of discharged fuel assemblies) is made for ensuring designed cycle length and achieving a safe and economical core configuration. By assuming the range of the content of available plutonium, the core reactivity and the core characteristics (such as power distribution, reactivity coefficients, and burnup) are evaluated. According to the evaluations, the core characteristics and safety in the target cycle are confirmed based on the plutonium content used in the detailed design and the refueling plan. The designed core characteristics are confirmed again by the reactor physics tests at actual reactor startup.

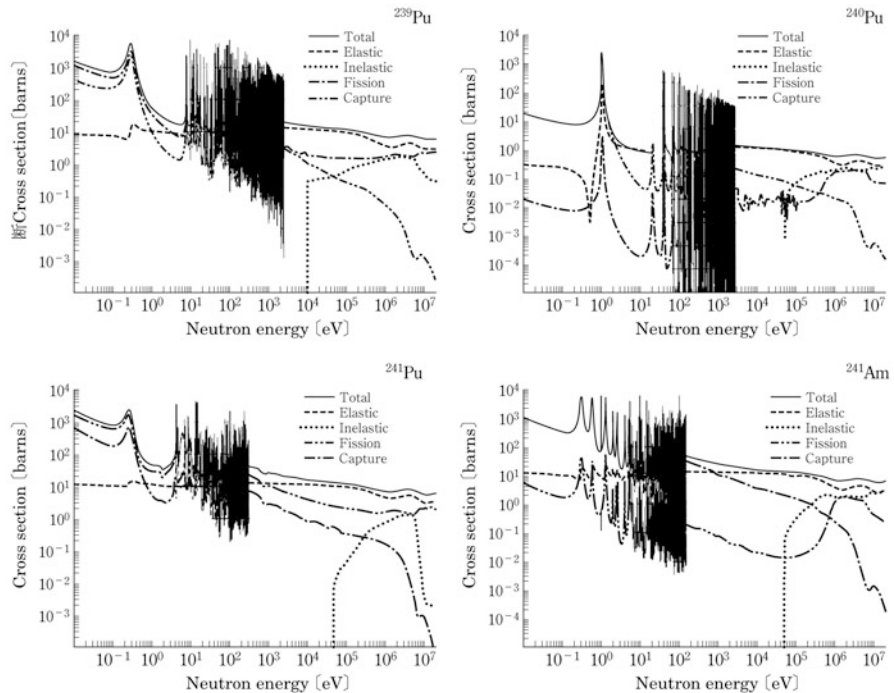


Fig. 4.5 Cross Sections of Plutonium and Americium [11]

(2) Variation of plutonium content and the equivalent fissile content method [10]

(a) Variation of plutonium content

Before being used as nuclear fuel, plutonium was irradiated in various reactors and reprocessed. The plutonium content of MOX fuel depends on the burnup of the original spent fuel, cooling time etc. The higher the burnup of the original spent fuel, the larger the fraction of higher order isotopes such as ^{240}Pu , ^{241}Pu and ^{242}Pu becomes. ^{241}Pu in the reprocessed plutonium decays into ^{241}Am with a half-life of 14.2 years. The decay of the fissile ^{241}Pu reduces the reactivity of MOX fuel. ^{241}Am has larger capture cross section than ^{240}Pu and ^{242}Pu , and it has a much smaller fission cross section than fissile materials like ^{239}Pu . Accumulation of ^{241}Am decreases the reactivity of MOX fuel. Figure 4.5 shows the cross sections of plutonium isotopes and ^{241}Am . As the decay of ^{241}Pu and production of ^{241}Am continue after fabricating the fuel elements, the designed plutonium enrichment in the fabricating process must be determined by considering the duration to the loading in the core.

(b) The equivalent fissile content method

Since the contribution of plutonium to the core reactivity largely depends on the plutonium content, the necessary plutonium enrichment

Table 4.2 Plutonium Equivalent Worths in FBR [10]

Nuclide	Inner core	Outer core
^{235}U	0.84	0.80
^{238}U	-0.02	-0.01
^{238}Pu	0.59	0.65
^{239}Pu	1.0	1.0
^{240}Pu	0.18	0.20
^{241}Pu	1.40	1.37
^{242}Pu	0.14	0.17

also depends on the plutonium content. However, the core reactivity can be accurately estimated by equivalently treating the fissile enrichment in the fuel. This method is called the *The Equivalent Fissile Content Method*.

In this method, the contribution of ^{239}Pu , which has the highest fraction among plutonium isotopes, is set as the reference (1.0). The relative contributions by other plutonium isotopes including ^{241}Am (treated as one of the plutonium isotopes) are defined as the *plutonium equivalent worths* (η_i^{PU} , η_L^{U}). Examples of the plutonium equivalent worths are listed in Table 4.2. By using them, the adjusted fissile enrichments corresponding to the plutonium enrichments of the inner core and outer core are calculated as Eq. (4.7).

$$E_{239} = \varepsilon_{\text{Pu}} \sum_i \alpha_i \eta_i^{\text{Pu}} + (1 - \varepsilon_{\text{Pu}}) \sum_j \beta_j \eta_j^{\text{U}} \quad (4.7)$$

ε_{pu} : Plutonium enrichment

α_i : Fraction of plutonium isotopes i

β_j : Fraction of uranium isotopes j

η_i^{PU} : Plutonium equivalent worth of plutonium isotope i

η_L^{U} : Plutonium equivalent worth of uranium isotope i

Although the content of the obtained plutonium at the moment of fuel fabrication is different from the plutonium content at the moment of design, equal core reactivity can be achieved by adjusting the plutonium enrichment during the fabrication so that the equivalent fissile enrichment is equal to the design value.

4.1.3 Design of Fuel Element and Fuel Assembly

[1] Design of fuel element

(1) Operating environment features for fast reactor fuel

Fast reactor fuel has a different operating environment from LWR fuel has. That difference needs to be considered in fuel design. As an example, general features and special points to note for consideration are summarized below for MOX fuel, which has acquired much operating experience as fast reactor fuel.

- (a) High fast neutron flux and fast neutron exposure enhance swelling and creep deformation of the fuel clad and wrapper tube. Measures should be taken for them.
 - (b) High operating temperatures of coolant and materials lead to changes of the materials, and care should be taken for them, including especially corrosion-caused changes.
 - (c) The high pellet temperature of MOX fuel leads to significant restructuring of the pellet and increases the FP gas release rate.
 - (d) The temperature gradients in the radial and axial directions of the pellet are large causing cracking and relocation (slipping of the cracked pellet fragment), and also causing redistribution of the O/M (oxygen-metal ratio) and migration (movement inside the pellet) of plutonium and FPs such as cesium. Those pellet behaviors during irradiation should be taken into account in the design.
 - (e) High burnup enhances pellet swelling and FP gas release.
 - (f) Due to the high burnup and low coolant pressure compared to LWRs (especially PWRs), the fuel cladding internal pressure is higher than its external pressure. Thus, creep rupture of the fuel cladding by the high internal pressure is selected as the major failure mode of fast reactor fuel to be considered.
- (2) Major design principles of fast reactor fuel element
- Based on the above operating environment features, the major design principles of the fast reactor fuel element are summarized as the following.
- (a) The fuel element must not fail at normal operation and anticipated operational occurrences. Concretely, creep rupture by internal pressure is avoided and pellet cladding mechanical interaction (PCMI) is mitigated. To avoid creep rupture by internal pressure, an adequate length of the gas plenum, optimization of the cladding thickness and limitation of the cladding temperature must be provided. For mitigating PCMI, optimization of the fuel density and adequate initial pellet-cladding gap must be provided.
 - (b) Cladding deformation must not be excessive. Since excess deformation of the cladding blocks the coolant flow path, deteriorating the cooling performance, the cladding deformation by swelling and creep needs to be kept small. For that purpose, the fuel internal pressure must be reduced as much as possible, materials with small swelling and creep must be used, and interaction between the fuel bundle and wrapper tube must be mitigated.
 - (c) Fuel pellets must not melt at anticipated operational occurrences. (It should be noted that most fast reactor fuel designs do not allow fuel melting even at design basis accidents.) A melting limit of linear heat rate based on power to melting experiments and an adequate design criterion must be set up.

(3) Structure of fast reactor fuel element

According to the design principles above, the structure of fast reactor core fuel element is outlined here. Many MOX pellets along with the depleted UO₂ pellets as the axial blanket are inserted into a stainless steel fuel cladding. The plenum spring is inserted into the upper part of the fuel element to prevent the pellets from moving. The fuel element is sealed by welding the stainless steel end plugs into the top and bottom of the cladding. An adequate pellet-cladding initial gap is arranged and the gas plenum is provided, so that excess stress is avoided on the cladding or welds of the end plugs; this stress is due to the internal pressure of released FP gas and the cladding deformation caused by the difference of thermal expansion and swelling between the cladding and the pellet. Figure 4.3 showed the concept of the core fuel element.

In the blanket fuel element, many depleted UO₂ pellets are inserted into the stainless steel fuel cladding. In order to increase the fuel volume fraction for high breeding ratio, the diameter of the blanket fuel element is a little bit larger than that of the core fuel element. The shape and structure of the blanket fuel element are almost the same as those of the core fuel element.

(4) Major evaluation items in fuel element design

(a) Evaluation of cumulative damage fraction (CDF)

FP gas accumulates with burnup of fuel and that increases the cladding internal pressure. CDF is the evaluation item of cladding integrity associated with creep rupture and is defined below.

$$\text{CDF} = \int_0^t \frac{dt}{t_R(\sigma, T)} \quad (4.8)$$

t : Time

t_R : Creep rupture time (time to creep rupture under constant temperature and stress)

T : Cladding temperature

σ : Stress.

In the evaluation of CDF, cumulative fatigue fraction by thermal transients is added.

According to the definition of CDF, the fuel element ruptures when CDF reaches 1.0. In the design, the CDF limit is set taking an adequate margin to 1.0. Fuel integrity is assessed by ensuring that the evaluated CDF, considering various uncertainties, is below the limit.

(b) Evaluation of melting limit of linear heat rate and fuel temperature

In order to avoid fuel melting, the melting limit of the linear heat rate is identified by power to melting experiments. Based on the melting limit, the allowable design limit of the linear heat rate is set by considering various uncertainties and the operational overpower coefficient (ratio of the scram setpoint and rated power). In the core neutronics design,

the power distribution is flattened by plutonium enrichment zoning so that the maximum linear heat rate is below the allowable design limit.

The fuel temperature is calculated as below, using the maximum linear heat rate calculated by the core neutronics design, and the fuel design is assessed. This calculation also provides the initial condition of fuel temperature in the safety analysis of anticipated operational occurrences.

By assuming a constant power density Q , the one dimensional heat conduction equation in the radial direction of a cylinder is described as Eq. (4.9).

$$\frac{1}{r} \frac{d}{dr} \left(rk \frac{dT}{dr} \right) + Q = 0 \quad (4.9)$$

By integrating this equation,

$$rk \frac{dT}{dr} + Q \frac{r^2}{2} = C_1 \quad (4.10)$$

is obtained. By providing the boundary conditions as

$$\frac{dT}{dr} = 0 \text{ at } r = 0 \text{ (pellet center)}, T = T_s \text{ at } r = R_s \text{ (pellet surface)}$$

$C_1 = 0$ is obtained. By integrating Eq. (4.10),

$$\int_{T_s}^{T(r)} k(T) dT + \frac{Q}{2} \int_{R_s}^r r dr = 0 \quad (4.11)$$

is obtained. By integrating from the pellet surface to the pellet center and assuming $T = T_o$ at $r = 0$,

$$\int_{T_s}^{T_0} k(T) dT = \frac{Q}{4} R_s^2 \quad (4.12)$$

is obtained. By using $\chi = Q\pi R_s^2$ the relation between the power density and the linear heat rate is written as Eq. (4.13).

$$\chi = 4\pi \int_{T_s}^{T_0} k(T) dT \quad (4.13)$$

χ : Linear heat rate

k : Thermal conductivity of fuel pellet

T : Temperature

T_o : Pellet centerline temperature

T_s : Pellet surface temperature

The maximum fuel centerline temperature is estimated for normal operation and overpower conditions based on the cladding inner surface temperature and using the heat transfer coefficient between the pellet and cladding (gap conductance) and the thermal conductivity of the fuel pellet. In the case of overpower condition, the overpower coefficient is applied.

The gap conductance used for fuel design is based on irradiation test results from experimental reactors in Japan and overseas. The empirical correlations of the pellet thermal conductivity have been prepared by researchers in Japan and overseas as well. The thermal conductivity of MOX pellet, which has extensive operating experience as fast reactor fuel, is arranged as a function of the pellet density, O/M ratio and temperature.

It is known from the irradiation data that the MOX pellet structure is changed by irradiation under high temperature and high heat flux conditions. After being irradiated at high temperature, the internally fabricated pores in the pellet move towards the fuel center which has the peak temperature, so that the structure inside the pellet changes from that at the time of fabrication. In the post-irradiation examinations of fuel pellets which had been irradiated at high temperature, the following features have been observed: an unchanged region remained at the external layer of the pellet; an equiaxial crystal region was present inside the unchanged layer; a columnar crystal region existed inside the equiaxial crystal region; and a void was formed at the pellet center. The temperatures at the boundaries between the two regions and the densities of those structures have also been evaluated by post-irradiation examinations.

In the fuel element design, those data and correlations are installed into the fuel temperature evaluation model. The fuel temperature is calculated by solving the thermal conduction equation in consideration of the fuel restructuring.

[2] Design of fuel assembly

(1) Features of fast reactor fuel assembly

A fast reactor fuel assembly consists of triangularly arranged fuel elements and a containing wrapper tube (cf. Fig. 4.3). Positions of the fuel elements are kept by the wire spacers or the grid spacers, so that the coolant channels are ensured. The upper shielding is contained in the upper part of the wrapper tube. The top of the wrapper tube is connected to the handling head which has a gripper function for handling the fuel assembly. The lower shielding is also contained in the lower part of the wrapper tube. The bottom of the wrapper tube is connected to the entrance nozzle through which the coolant enters. The wrapper tube, along with the entrance nozzle, forms the individual coolant flow passage and hence enables flow distribution among the fuel

assemblies. The wrapper tube also protects the fuel element bundle and would act as one of the barriers against propagation of fuel damage during accident conditions.

Upper, lower and intermediate spacer pads are provided on the outer surface of the wrapper tube in order to keep the spacing between the neighboring assemblies and to take loads during operation including seismic load.

(2) Major design principles of fast reactor fuel assembly

For the design of a fuel assembly, the assembly size, i.e. the number of fuel elements, needs to be determined first. The following factors influence the assembly size.

- (a) Reactivity worth per assembly
- (b) Decay heat of an assembly
- (c) Weight of an assembly
- (d) Fuel cycle cost
- (e) Refueling time
- (f) Degrees of freedom for flow allocation
- (g) Degrees of freedom for control rod arrangement
- (h) Stable support of a fuel element bundle

Among them, (a), (b) and (c) increase with assembly size. High reactivity worth per assembly increases the degree of risk associated with a reactivity accident during fuel handling and criticality in case of submergence caused by an accident during transportation of the assemblies. High assembly decay heat or large assembly weight leads to excess loads on the cooling facility during fuel handling and on the refueling machines.

On the other hand, (d) and (e) decrease with increasing assembly size. Generally, as the number of fabricated assemblies is larger, the fuel fabrication cost is higher. Thus, larger assembly size reduces the fuel cycle cost including the fabrication cost. Also, larger assembly size means a smaller number of assemblies which shortens the time needed for refueling and hence improves the plant availability.

As for (f) and (g), the degrees of freedom decrease with increasing assembly size, i.e. decreasing the number of assemblies. As for (h), especially if the wire spacer is adopted, larger assembly size worsens the support because the degrees of freedom of the fuel elements' displacement increase with the number of the fuel elements, i.e. the assembly size.

From the above and some other considerations, an adequate assembly size is determined and then the assembly is designed based on two design principles.

- The assembly has and keeps sufficient mechanical and structural strength at normal operation and anticipated operational occurrences during the duration of service

- The assembly has and keeps sufficient mechanical and structural strength against normal loads during transporting and handling.

(3) Major evaluation items in fuel assembly design

(1) Stress evaluations

According to the design principles, sufficient strength of each component of the fuel assembly against various loads is confirmed and kept by evaluating the stresses associated with the loads at normal operation and anticipated operational occurrences by using the finite element method or other approaches.

(2) Duct-to-duct interaction (DDI)

DDI is evaluated by confirming that the neighboring wrapper tubes do not contact each other (i.e. the refueling function is not obstructed) due to expansion of the wrapper tube such as by thermal expansion, swelling and creep. In the DDI evaluation, bending of the wrapper tube due to thermal deformation by the temperature distribution and swelling by neutron irradiation must be considered as well as the expansion.

4.1.4 Nuclear Design

The core characteristics are both neutronic and thermal. Neutronic characteristics are obtained by the core nuclear design. In the nuclear design, the core configuration, the refueling plan and the plutonium enrichment are determined so that the core safely generates the designed thermal power, based on the plant and fuel basic specifications, throughout the plant life. Also, the core reactivity, breeding performance, neutron flux distribution, burnup characteristics, control rod worth, and reactivity coefficients are evaluated. The design point of those parameters are determined and coordinated with other design points as described in Fig. 4.4.

The nuclear design calculation methods appear earlier in Chap. 2.1. In the basic calculations of the nuclear design of fast reactors, multi-dimensional, multi-group diffusion calculation codes are mainly utilized.

[1] Multi-group reactor constants

In the nuclear design calculations of fast reactors, a wide range of neutron energies from thermal neutrons (0.025 eV) to fast neutrons (up to about 10 MeV) needs to be treated. The wide energy range is divided into many groups. The set of multi-group reactor constants, which are the averaged cross section of each nuclide within each energy group, are utilized for each group. Based on those sets of multi-group reactor constants, prepared by processing evaluated nuclear data files such as JENDL, the multi-group reactor constants for the design are made using the core configuration, the material composition and the temperature data of the actual core as input.

[2] Nuclear design calculations

The neutronic characteristics, such as the core reactivity, power distribution, burnup characteristics, and control rod worth, are evaluated using the multi-group reactor constants, the core geometry, etc. The reactivity coefficients are calculated by multi-dimensional diffusion and perturbation codes.

Owing to the recent progress in computer performance, the following improvements have been made.

- The number of energy groups is increased for better calculation accuracy. Three-dimensional calculation codes with detailed modeling of core geometry are mainly used.
- In cases for which the neutronic characteristics must be accurately calculated in geometries with strong heterogeneity or sharp spatial change in the neutron flux, multi-dimensional transport calculation codes are utilized and then the result of the diffusion calculation is corrected if necessary.
- In cases for which the neutronic characteristics must be accurately calculated in complex geometries, Monte-Carlo codes are utilized.

[3] Validation by calculating mock-up critical experiments

Mock-up critical experiments for simulating fast reactor cores have been conducted and their measurement data have been utilized for evaluating the accuracy of core nuclear design calculation methods. Based on those evaluations, the design calculation results can be corrected and the design specifications are then determined with accompanying prediction errors. In Japan, the major mock-up critical experiments done so far are those by the Fast Critical Assembly (FCA) for Joyo, the MOZART experiments [12] for Monju, and the JUPITER experiments [13] for a demonstration FBR plant.

4.1.5 Reactivity Characteristics [6]

Nuclear reactors are designed to have inherent power controllability, i.e. to have a negative power reactivity coefficient. Nuclear reactors are also designed to have excess reactivity for controlling the core against changes in the power as well as the burnup reactivity to allow its operation for the designed period. The excess reactivity is adequately designed so that the reactor is safely operated and shut down.

[1] Reactivity coefficients

The reactivity coefficients indicate the change in the reactivity against the temperatures of fuel, structure and coolant, and the coolant void fraction etc. They depend on the plutonium content, uranium content and burnup condition.

(a) Doppler coefficient: This is the ratio of the reactivity change and the change in the effective fuel temperature. The value is negative as long as the fissile enrichment is not too high. When the fuel temperature rises due to the increase in the power or other causes, thermal motions of nuclei

become stronger and the apparent width of the resonance absorption cross section curve of ^{238}U and ^{240}Pu is expanded. This increases resonance absorption of neutrons by those nuclei. Since the Doppler effect is mainly provided by the resonance absorptions of ^{238}U and ^{240}Pu , it gets stronger for the core with more neutrons at the resonance energy. The Doppler effect dominates the reactivity feedback against the change in the reactor conditions. Thus, the power reactivity coefficient, which is obtained by combining all the reactivity effects, is always kept negative for all the operating regions and hence the reactor has an inherent safety feature.

- (b) Fuel temperature coefficient excluding the Doppler effect: This is the ratio of the reactivity change by thermal expansion of fuel elements mainly in the axial direction to the change in the fuel temperature causing the thermal expansion.
- (c) Structure temperature coefficient: This is the ratio of the reactivity change by thermal expansion of structures to the change in the structure temperature causing the thermal expansion.
- (d) Coolant temperature coefficient: This is the ratio of the reactivity change by a decrease in the coolant density to the change in the coolant temperature causing the density change.
- (e) Core support plate temperature coefficient: This is the ratio of the reactivity change by enlarging the fuel assembly gap caused by thermal expansion of the core support plate to the change in the temperature of the core support plate.
- (f) Void reactivity: This is the reactivity change when a void is generated in the coolant. Fast reactors are designed so that the coolant does not evaporate at normal operation, anticipated abnormal occurrences and even design basis accidents, and that gas bubbles are not formed. For the purpose of defining and calculating the void reactivity, the following assumptions are made.
 - Gas bubbles formed in the primary system due to a certain cause pass through the core.
 - The coolant evaporates although it is technically not possible.

[2] Reactivity control

Reactivity of fast reactors is controlled by control rods. The functions of the control rods depends on the design philosophy. The description here is based on the Monju design as an example.

(1) Design principle of reactivity control system

(a) Reactor shutdown system

The reactor shutdown system, for emergency shutdown of the reactor at abnormal circumstances, consists of two independent systems, i.e. the primary shutdown system and the backup shutdown system. The regulating rods serve as the primary shutdown system, too. The backup shutdown rods have the function of being the backup shutdown system.

Even if one of the two systems does not work at emergency shutdown, the other system brings the reactor from the hot full power condition to the

cold shutdown condition with the designed reactivity shutdown margin, i.e. over $0.001\Delta k/k$ for example for the lowest design temperature. The designed margin, described above, must be achieved even if the control rod with the highest reactivity worth is fully withdrawn and stuck.

(b) Reactor control system

The necessary reactivity for operating the reactor, such as normal startup, normal shutdown and compensation for fuel burnup, is controlled by the regulating rods. The regulating rods consist of the fine control rods and the coarse control rods.

The fine control rods mainly regulate the reactivity against the changes in the temperatures of the fuel, structure and coolant. They automatically regulate the reactor power.

The coarse control rods mainly compensate the reactivity change by burnup of the fuel. Also, they can be used for regulating the reactivity change under conditions that are outside the range for the automatic control system of the fine control rods. In the case of Monju, for example, the coarse control rods regulate the reactivity under conditions from the cold shutdown condition to 30 % power condition.

Alternatively, the functions of the fine control rods and the coarse control rods might not be distinguished; and they are designed as regulating rods.

(2) Structures of control rods

(a) Regulating rod

The regulating rods serve as the primary shutdown system. The structure of the regulating rod is shown in Fig. 4.6. A control rod element consists of a stainless steel cladding containing B_4C pellets with enriched [10]B as neutron absorber. The control rod elements are contained in a protecting tube surrounded by a guide tube. Reactivity is regulated by moving the protecting tube up and down inside the guide tube.

^{10}B has relatively large absorption cross section even for high energy neutrons and is easy to be processed economically. Thus, it is widely used as the neutron absorber of fast reactors. On the other hand, ^{10}B generates helium gas by the (n, α) reaction. Since the lifetime of a control rod with sealed cladding is dominated by the internal pressure, more and more designs have adopted the bent type which releases the helium gas outside the cladding.

The regulating rods are inserted from the core top. The control rod drives are mounted on the top face of the core upper structure. The regulating rods are driven by the motors. The maximum rotating speed of the driving motor is physically limited so that the rod withdrawn speed is below the corresponding value. At emergency shutdown, the holding magnets are demagnetized and furthermore the regulating rods are inserted by acceleration using gas pressure.

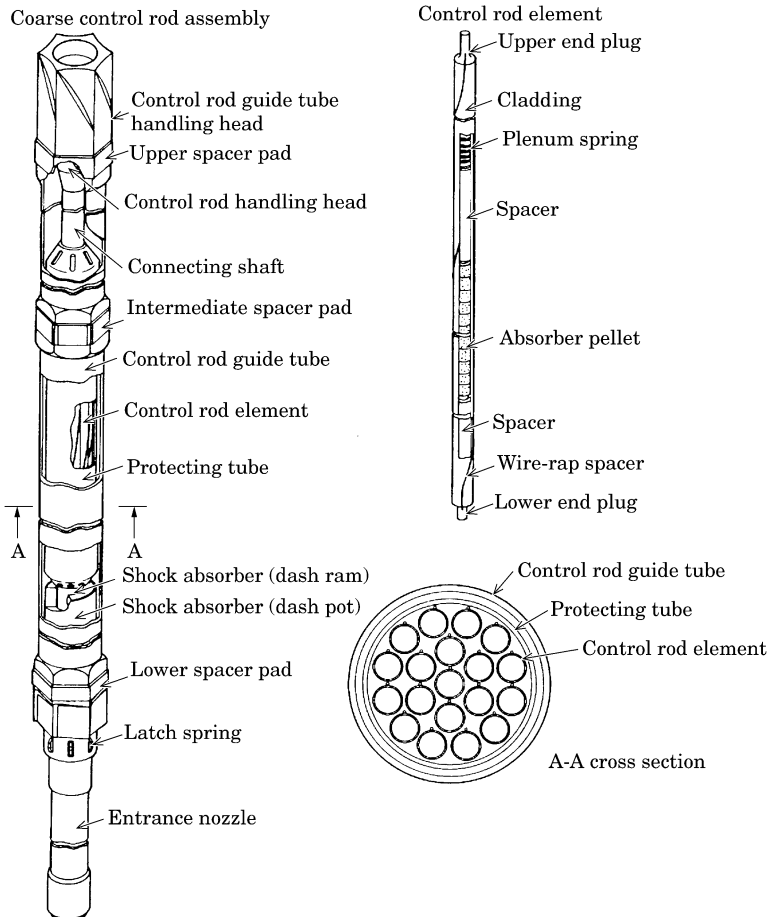


Fig. 4.6 Coarse control rod assembly of monju [6]

(b) Backup shutdown rod

The backup shutdown rods serve as the backup shutdown system. The structure of the backup shutdown rod is shown in Fig. 4.7. The parameters such as the enrichment of ^{10}B and cladding inner diameter are different from those of the regulating rod.

The backup shutdown rods are inserted from the core top. The control rod drives are mounted on the top face of the core upper structure. The backup shutdown rods are driven by motors. At emergency shutdown the holding magnets are demagnetized and furthermore the backup shutdown rods are inserted by acceleration using spring force.

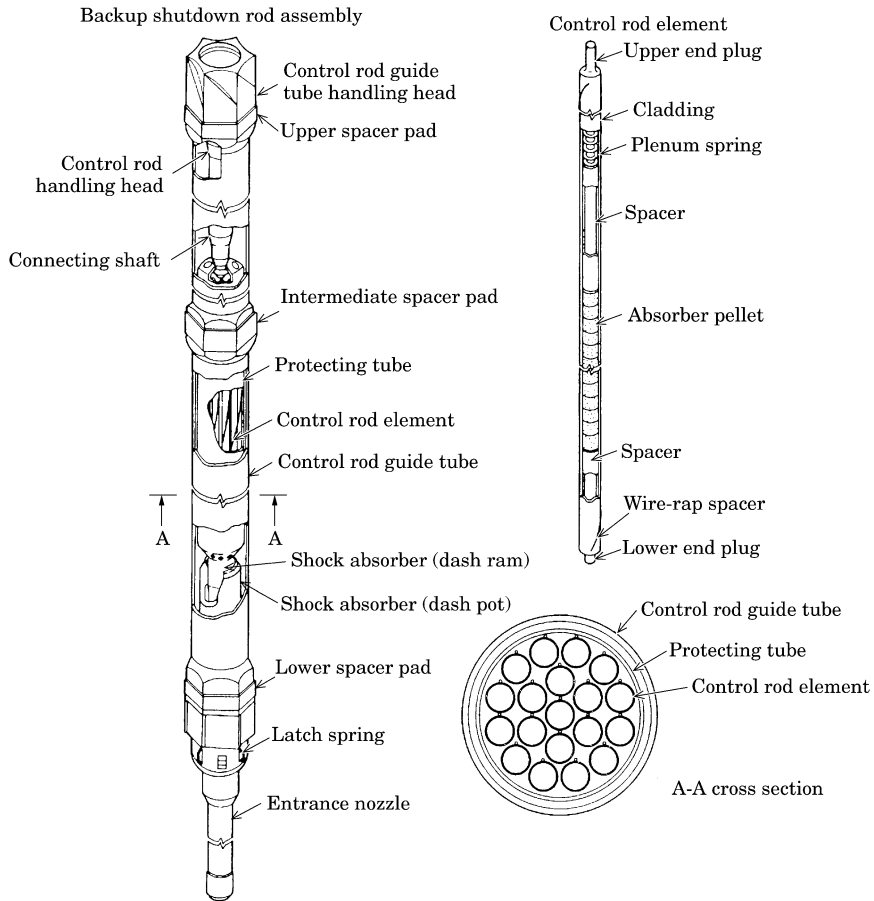


Fig. 4.7 Backup Shutdown Rod Assembly of Monju [6]

(3) Control rod arrangement and reactivity control

The number and arrangement of the control rods are determined to control the following reactivities. Examples of function of the control rods are shown in Table 4.3.

(a) Reactivities to be controlled

- (i) Reactivity of power compensation: This is the reactivity change between the hot full power condition and the cold shutdown condition. It is caused by the temperature changes in the fuel (including the Doppler effect), structure, coolant etc.
- (ii) Reactivity of burnup compensation: This corresponds to the loss of reactivity due to fuel burnup. It depends on the burnup of fissile materials, generation of the fission products, breeding of plutonium etc.

Table 4.3 Function and reactivity balance of Monju control rods [6] $(\times 10^{-2} \Delta k/k)$

Core		Initial core		Equilibrium core	
		Primary shutdown system	Backup shutdown system	Primary shutdown system	Backup shutdown system
Shutdown system		Regulating rod	Backup shutdown rod	Regulating rod	Backup shutdown rod
Control rod					
Necessary reactivity	Power compensation	1.5	1.5	1.7	1.7
	Burnup compensation	2.7	–	2.6	–
	Operation margin	0.3	–	0.3	–
	Absorption of error	1.0	–	1.0	–
	Sum of necessary reactivities	5.5	1.5	5.6	1.7
Control rod worth		7.0 ^a	5.4	7.0 ^a	5.8
Reactivity margin		1.5	3.9	1.4	4.1

^aAssuming that the control rod with the maximum reactivity worth is fully withdrawn and stuck

- (iii) Absorption of reactivity error: This is the prediction error in the design and it caused by the calculation error, fuel fabrication tolerance etc.
- (iv) Operation margin: This reactivity is to keep the control rods inserted even at the end of cycle so that the minimum required rate of change in the reactivity for load following is ensured.
- (v) Shutdown margin: The primary shutdown system and the backup shutdown system are each designed to have their own shutdown margin, so that they can independently keep the reactor subcritical at the cold shutdown condition.

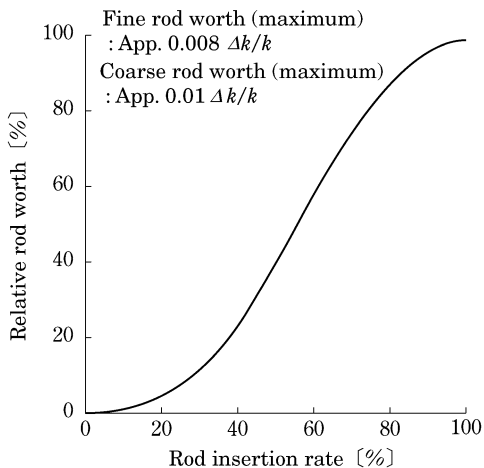
(b) Control rod arrangement

As shown in Fig. 4.3, the control rod assemblies are uniformly and symmetrically arranged in order to flatten the power distribution. As described before, the control rods have the functions of reactor shutdown and control of the power and burnup reactivity.

The coarse control rods compensate the burnup reactivity. They are withdrawn evenly after a certain period. The fine control rods are to be inserted to compensate the reactivity due to the coarse rods movements.

The main role of the fine control rods is regulating the power. To smoothly change the reactor power level during normal operation, the designed rate of change in reactivity needs to be ensured. The reactivity curve of the regulating rod is shown in Fig. 4.8. The rate of change in reactivity is relatively small in the upper and lower parts of the core. The movements of the fine rods are regulated so that the change in the reactivity per unit length of insertion is within a certain range. This is for ensuring the designed rate of change in reactivity is obtained by moving the fine control rods at a constant velocity.

Fig. 4.8 Reactivity insertion curve of Monju [6]



4.1.6 Power Distribution Characteristics [6]

[1] Power distribution characteristics

Since neutron mean free path is long and no FPs have a high absorption cross section, local distortion of the power distribution is small. The core performance is improved by flattening the overall (not the local) power distribution. Considerations for flattening the power distribution are as follows.

- (a) The core is divided into the inner core and the outer core. They have almost the same volume. The plutonium enrichment is higher in the outer core so that: the maximum linear heat rate is made equal between the two regions and the power distribution is flattened.
- (b) The scattered batch refueling method is applied. In this method, the refueled position is equally scattered in the core.
- (c) The coarse control rods and the fine control rods are driven so that abnormal power distribution does not occur. The coarse control rods and the fine control rods are equally withdrawn among each group (coarse or fine rod), respectively.

The regional power fractions change with the burnup. Accumulation of plutonium in the blanket region increases its power fraction. Examples of the regional power fractions are shown in Table 4.4.

[2] Stability of reactor power

A fast reactor core has a negative power reactivity coefficient mainly due to the Doppler effect. When a positive reactivity is inserted into the core, the reactor power and the temperature increase. Then the increase in the power is suppressed by the reactivity feedback and the power is stabilized.

Table 4.4 Power fractions of Monju [6]

(%)

Region	Cycle			
	Initial core ^a		Equilibrium core ^b	
	Beginning of cycle	End of cycle	Beginning of cycle	End of cycle
Inner core	53	55	53	53
Outer core	40	38	38	36
Sum of core regions	93	93	91	89
Radial blanket	5	5	6	7
Axial blanket	2	2	3	4
Sum of blanket regions	7	7	9	11

^aA core composed of only fresh fuels^bA core having equilibrium characteristics after periodic refueling

In fast reactors, the high energy of neutrons makes the mean free path relatively long, so that local distortion of the neutron flux distribution is small. Since the FPs do not have large cross sections for the major energy range of fast reactors, consideration of xenon is not necessary unlike that in LWRs.

4.1.7 Thermal-Hydraulic Design

[1] Basic principles of thermal-hydraulic design

Thermal-hydraulic design of fast reactors is made so that the allowable thermal design limit is not exceeded at normal operation and abnormal operational occurrences and that fuel integrity is kept until the designed burnup. The basic principles are explained below.

Normal operation indicates the conditions where startup, shutdown, operation in power and refueling are intentionally carried out and the operational condition is within the limit. *Anticipated operational occurrences* indicate the conditions where the operation is disturbed due to a single failure of equipment or its malfunction, which are anticipated during its lifetime, or a single operator failure. A condition having similar frequency and leading to an unplanned state is also an anticipated operational occurrence. The *allowable thermal design limit* indicates the limit of allowing fuel damage for safety design and continuous operation of the nuclear reactor facility.

The basic principles of fast reactor thermal-hydraulic design are, at normal operation and anticipated operational occurrences: (i) prevent sodium from boiling and (ii) prevent fuel from reaching the allowable design limit.

Item (i) is followed because there is a possibility of positive reactivity insertion due to boiling and an excess increase in the fuel cladding temperature due to change in heat transfer characteristics. For satisfying the allowable thermal design limit, the maximum fuel centerline temperature and the fuel cladding temperature are limited from the viewpoint of thermal-hydraulic

design. As for the maximum fuel centerline temperature, fuel melting is not allowed in the mainstream design in order to avoid failure of fuel cladding by excessive stress caused by thermal expansion of the fuel pellets. The design limit of the maximum fuel centerline temperature is determined by the melting limit test data with consideration of the design margin. As for the cladding temperature, the cladding temperature itself, which dominates the material properties, is limited instead of limiting the heat flux on the cladding surface because the heat transfer characteristic of sodium is better than that of water. For avoiding cladding failure by an increase in the cladding temperature for a short period at anticipated operational occurrences, the limit of maximum cladding temperature at anticipated operational occurrences is established. Stainless steel is generally used as the fuel cladding material of fast reactors. The limit of fuel cladding temperature at anticipated operational occurrences is determined based on out-of-pile rapid heat-up tests of irradiated target materials. Since the internal pressure creep dominates the mechanical strength of the fuel cladding for ensuring fuel integrity until designed burnup, the limit of fuel cladding temperature at normal operation, which dominates the creep strength, is determined based on the creep test data of the target materials. This limit for sodium cooled reactors is set as 650–700 °C in many designs.

In the thermal-hydraulic design of fast reactors, the flow allocation among the fuel assemblies is provided according to the power distribution in order to satisfy the allowable design limits above and to efficiently remove the heat generated in the reactor. That is the important feature of fast reactors compared to LWRs.

[2] Coolant flow allocation

The fast reactor core consists of the core fuel assemblies, blanket fuel assemblies for breeding, control rod assemblies for regulating power and reactivity, and radial shieldings. The heat generation of those components largely depends on the assembly type. Among the common assembly types, i.e. the core fuel assembly or blanket fuel assembly, the heat generation also depends on the loading position. In the thermal-hydraulic design of fast reactors, the coolant is adequately allocated among the assemblies in order to efficiently utilize the coolant led to the reactor and to satisfy the thermal design limits. As described in the list [1] of Sect. 4.1.7, the allowable thermal design limits consists of those for the fuel centerline temperature and for the fuel cladding temperature. The fuel centerline temperature is significantly influenced by the linear heat rate, while the fuel cladding temperature strongly depends on the coolant temperature. Thus, the flow allocation is designed with consideration of the maximum cladding temperature design limit so that this temperature is almost equal among the core fuel assemblies and blanket fuel assemblies.

The high pressure plenum and low pressure plenum are provided inside the reactor vessel, and coolant is supplied from the high pressure plenum to the core fuel assemblies with high heat generation and from the low pressure plenum to the blanket fuel assemblies with low heat generation. Since the coolant flow direction of sodium cooled reactors is from the lower part to the upper part of the reactor vessel, the flow allocation device is installed in the bottom of the fuel

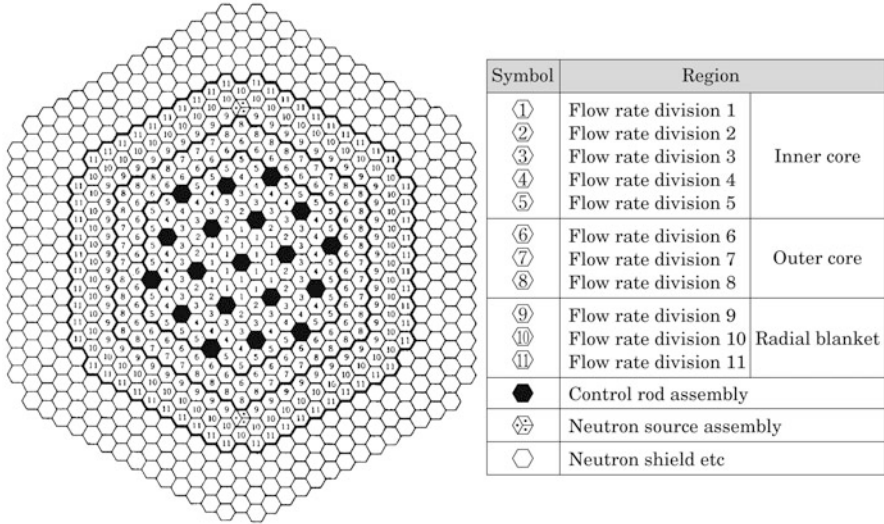


Fig. 4.9 Flow allocation of Monju [6]

assemblies. For example, the flow allocation device is installed in the connecting tubes which are between the upper and lower core support-plates. The entrance nozzles of the fuel assemblies are inserted into the connecting tubes. The designed flow rate is allocated by the combination of the flow allocation holes of the connecting tubes and the orifice diameter at the entrance nozzles.

An example of flow allocation design is shown in Fig. 4.9. In the flow allocation design, the necessary flow rates of the core and blanket fuel assemblies for satisfying the thermal design limits are calculated based on the evaluation of the cladding temperatures using the designed power distribution. The number of flow allocation regions is suppressed so that the flow allocation device is not complicated. To do that, the fuel assemblies are categorized as several groups. Within each group, the required flow rate is similar among the assemblies. Then, the flow rate for each group is determined. The flow allocation device is designed so that the pressure drops from the lower plenum to the upper plenum are equalized among all the flow paths with the flow allocation which is required for satisfying the thermal design limits. In this process, the pressure drop characteristics of each core components and the bypass of coolant flow are considered. The pressure drops at the flow allocation device and the core components are calculated using the pressure loss coefficients based on the experiments such as the water flow tests associated with the core internals, separate tests for the flow allocation device, and the simulated fuel assembly tests using water.

[3] Maximum coolant temperature and maximum cladding temperature

The coolant temperature and cladding temperature in the fuel assemblies are estimated by subchannel analysis. An example of the subchannel model is illustrated in Fig. 4.10. There are three types of subchannel. The inner subchannel

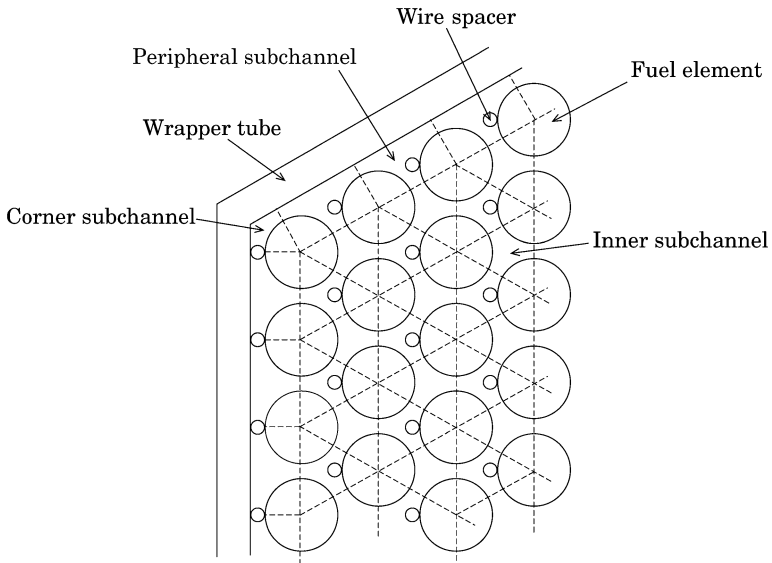


Fig. 4.10 Example of subchannel division model

is surrounded by three fuel elements, the peripheral subchannel is surrounded by two fuel elements and the inner wall of the wrapper tube, and the corner subchannel is surrounded by a fuel element and the wrapper tube corner. The three-dimensional thermal-hydraulic calculation is carried out in the subchannel analysis by modeling the fuel assembly as a set of parallel subchannels.

The coolant temperature distribution and cladding temperature distribution in each fuel assembly are calculated using the inlet flow rate determined by the flow allocation, and the power distribution among the fuel elements as the input conditions. In the subchannel analysis, the mixing of mass, momentum and energy between the neighboring subchannels is taken into account.

In the subchannel analysis, generally, the distributions of the coolant velocity and coolant temperature in the fuel assembly are obtained by solving mass, momentum and energy conservation equations in every axial node.

The design parameters used in the analysis are formulated depending on the analysis models. They are determined by experiments such as assembly flow tests using a simulated fuel assembly with the same dimensions as the actual one and coolant mixing tests. When the coolant temperature distribution in the assembly is obtained, the cladding temperature distribution is calculated according to the power distribution among the fuel elements. Consequently, the heat flux on the cladding surface is given by the power distribution; then the increase in the temperature from the coolant to the cladding surface is calculated using the heat transfer coefficient.

The maximum fuel temperature and maximum cladding temperature are estimated considering the engineering safety factors in order to secure enough design margin from the temperature distribution obtained by the subchannel analysis.

In the core thermal-hydraulic design, the nominal (most probable without any error margin) temperature distribution in the fuel assembly is calculated by the subchannel analysis first. Then, the *hot spot temperatures* of fuel centerline and fuel cladding are obtained considering the uncertainties of the calculated temperature caused by the tolerances of the design parameters etc. The hot spot temperatures are to be confirmed not to exceed the corresponding design limits. The temperature uncertainties are considered by multiplying the nominal temperatures by the engineering safety factors which are provided according to the errors of each parameter. The engineering safety factors are divided into two types. One is treated as a multiplication term by considering the systematic errors which must be considered cumulatively. The other is treated as a statistical term coming from random errors. An example of the former error is that of the power distribution. An example of the latter error is the fabrication tolerance of the fuel pellet.

Equation (4.14) is an example of the evaluation equation for the maximum temperature which includes consideration of the engineering safety factors.

$$T'_{HS} = T_{in} + \sum_{j=1}^l \prod_{i=1}^m G_{ij} \Delta T_j + \left[\sum_{k=1}^n \left\{ \sum_{j=1}^l (F_{kj} - 1) \prod_{i=1}^m G_{ij} \Delta T_j \right\}^2 \right]^{1/2} \quad (4.14)$$

In this equation, G_{ij} , F_{kj} are the factors of multiplication treatment and statistical treatment, respectively. ΔT_j is the nominal temperature rise of each position while m and n are the numbers of the multiplying factor and statistical factors, respectively.

$$\left. \begin{array}{l} T^1_{HS} : \text{Coolant} \\ T^2_{HS} : \text{Clad outer surface} \\ T^3_{HS} : \text{Clad inner surface} \\ T^4_{HS} : \text{Pellet surface} \\ T^5_{HS} : \text{Pellet centerline} \end{array} \right\} \text{Hot spots based on consideration of engineering safety factors}$$

$$\left. \begin{array}{l} \Delta T_1 = \Delta T_{Na} : \text{From assembly inlet to coolant} \\ \Delta T_2 = \Delta T_{flim} : \text{From coolant to clad outer surface} \\ \Delta T_3 = \Delta T_{clad} : \text{From clad outer surface to inner surface} \\ \Delta T_4 = \Delta T_{gap} : \text{From clad inner surface to pellet surface} \\ \Delta T_5 = \Delta T_{fuel} : \text{From pellet surface to pellet center} \end{array} \right\} \text{Nominal temperature rise}$$

As described above, the engineering safety factors are for estimating the maximum temperature rise in each position. By considering them, the fabrication tolerances, uncertainties of thermal-hydraulic parameters, power distribution uncertainty, and measurement uncertainty of the reactor thermal power, etc. are taken into account.

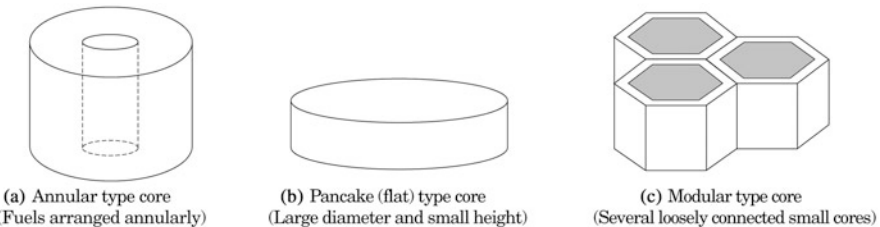


Fig. 4.11 Core concepts with low void reactivity

[4] Maximum fuel temperature

In the core thermal-hydraulic design, melting of the fuel pellets should be avoided at normal operation and anticipated operational occurrences. The maximum fuel centerline temperature with consideration of the engineering safety factors is confirmed to satisfy the design limit. As for the evaluation of the maximum fuel centerline temperature, see the list [1](4) of Sect. 4.1.3.

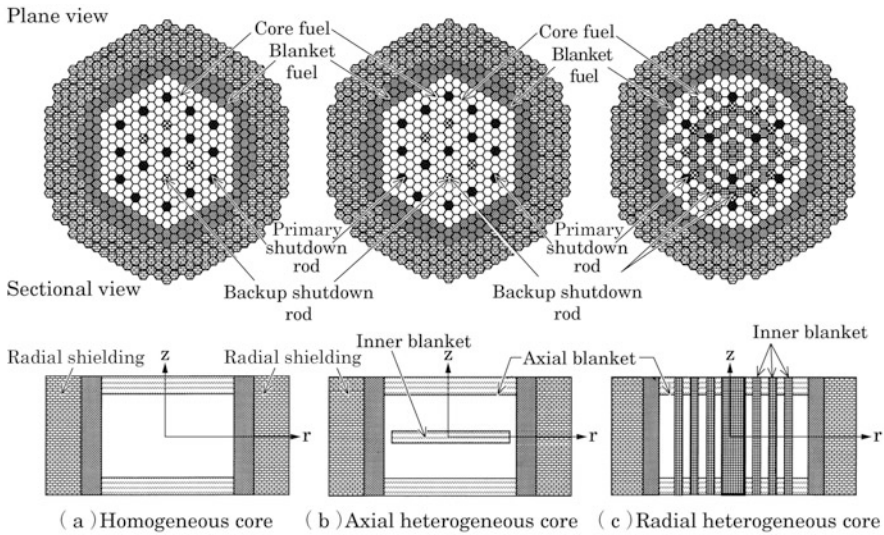
4.1.8 *Transitions in Core Design and Tendency in the Future*

[1] Transitions in development

From the beginning, the main purposes of fast reactor development have been improvements of both safety and economy.

(1) Reactor types

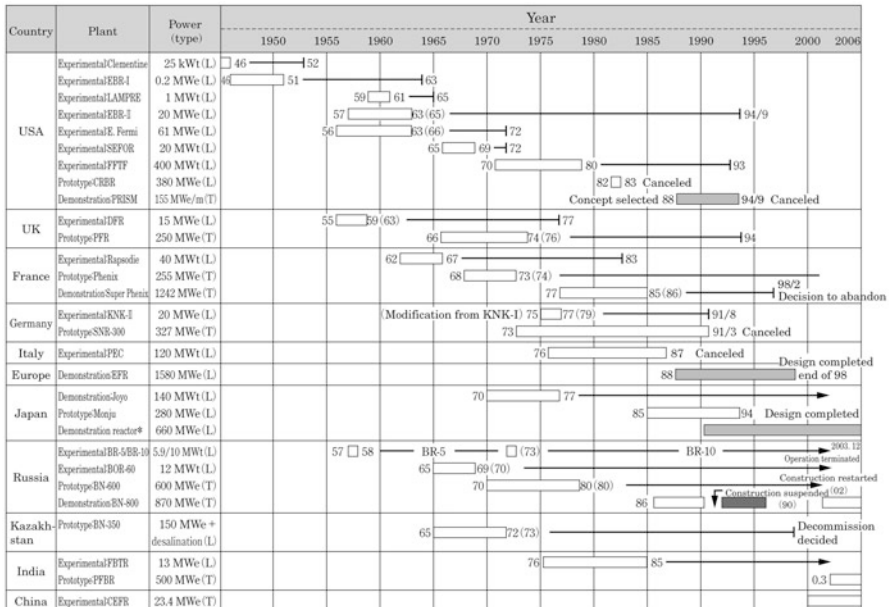
For core design, making the reactivity negative or as small as possible at coolant voiding has been one of the development goals for safety. Annular type, pancake (flat) type, and modular type core concepts were proposed, mainly in the US in the early study of large scale fast reactors. Those concepts are shown in Fig. 4.11. The common aim is increasing neutron leakage to the outside. In the 1980's, heterogeneous core concepts that had both reduced void reactivity and high breeding ratio were proposed in the US and France [14]. They are shown in Fig. 4.12. In those concepts, the blanket fuel assemblies are put into the core region or the blanket layer and upper and lower axial blankets are provided as well. The common aim is increasing neutron leakage from the core region to the blanket regions for higher breeding ratio. This kind of core concept has also been considered in Japan as a large scale fast reactor core. Simulated critical experiments were carried out under Japan-US collaboration as part of the JUPITER plan [13]. However, the actual designs of the prototype reactor and demonstration reactor (Fig. 4.13) adopted homogeneous cores which have a moderately flat shape, except that a heterogeneous core was considered in the uncompleted Clinch River Breeder **Reactor** Plant (**CRBRP**) of the US [9].



[Advantages and disadvantages of heterogeneous cores]

Advantages		Disadvantages	
<ul style="list-style-type: none"> Flat power distribution High breeding ratio and short doubling time Less positive void reactivity Small fast neutron flux and neutron exposure 		<ul style="list-style-type: none"> Tendency of larger fuel inventory Less negative Doppler coefficient Large change of power distribution with burnup 	

Fig. 4.12 Heterogeneous core concepts [15]



Start of construction □ First criticality — Shutdown → Under operation ■ Under plan

Type (L) : Loop type. (T) : Tank type

*Reactor type under consideration

Fig. 4.13 FBR developments worldwide [16]

(2) Coolant

The requirements for selection of fast reactor coolant are the following.

- (a) Neutron moderation is as little as possible.
- (b) Absorption cross section is as small as possible.
- (c) Cooling performance is high.

Requirement (c) is set because fast reactors have high power density. Various liquid metals were considered as fast reactor coolant. In the early days of fast reactor development, mercury was used in Clementine (US) and BR-2 (Soviet Union). NaK was used in the EBR-I (US), DFR (UK) and BR-5 (Soviet Union). Neither of these liquid metals has been utilized after those reactors due to the low boiling point and hence difficulty in achieving high thermal efficiency. Lead-bismuth, helium gas, etc were also considered as fast reactor coolant but their applications have been limited to design studies. Sodium does not moderate neutrons too much, and has a relatively small absorption cross section, a high boiling point and good cooling performance. Despite high chemical activity, sodium does not cause corrosion of materials. As a result, sodium was selected as the main option for fast reactor coolant in many countries including Japan [14, 17].

(3) Fuel

Besides MOX fuel, metal fuel, carbide fuel and nitride fuel have been considered as the core fuel of fast reactors.

In the early fast reactors i.e. the EBR-I and EBR-II (US) and DFR (UK), metal fuel was adopted from the viewpoint of high breeding ratio. However, the development was suspended due to the low burnup limit because of large irradiation swelling and the problem of eutectic alloy formation with cladding material. Later, improved alloy fuel was developed in the US in the 1980's and the Integral Fast Reactor (IFR) concept, where utilization of metal fuel and its reprocessing are combined, was proposed. The IFR was also researched in Japan. Carbide fuel and nitride fuel provide good breeding performance due to high heavy metal density, and enable high linear heat rate due to high thermal conductivity. Most of these fuel types have only been applied to design studies so far. Although operation experience of carbide fuel was and continues to be accumulated in the Indian experimental reactor FBTR, the Indian prototype reactor PFBR adopts MOX fuel. Oxygen in MOX fuel moderates neutrons and hence decreases the breeding ratio. That also enhances the Doppler effect and hence improves safety. Although low thermal conductivity makes the MOX fuel temperature relatively high, the high melting point of MOX fuel enables its operation under such high temperature conditions. Since MOX fuel is relatively stable after being irradiated, high burnup and long lifetime are possible. Also, oxide fuel has accumulated extensive experience as LWR fuel, which has made MOX fuel the mainstream for fast reactor fuel [14, 17].

[2] Tendency in the future

The fast reactor core designs so far have been mainly pursuing the breeding performance as seen in the so-called fast breeder reactor from the viewpoint of ensuring future energy sources. In the twenty-first century, significant growth of energy demand is expected mainly in developing countries. On the other hand, the issues of wasting natural resources and environmental destruction have recently become obvious. It has become internationally recognized that the world must go toward sustainable development with resource conservation and consideration of environmental issues as well as assurance of stable energy sources.

Japan, for example, has only small amounts of natural resources. It is essential to develop technologies which save resources, do not emit greenhouse gases, and lead to small loads on waste disposal. The FBR cycle was selected as one such technology. A high capacity for energy supply and the technologies for burning transuranium elements (TRU: Pu, Np, Am, Cm) have been developed for the FBR. The FBR must have high economy which is competitive with other power generation methods while ensuring safety as a major premise. Also, non-proliferation must be considered according to the world political situation. From this background, consideration of a concrete scenario for deploying the FBR cycle has been started in Japan. Japan's activities are attracting the world's rapidly increasing interests in FBR deployment, and international corroborations are strongly desired.

Taking Japanese experience as an example, it is important to develop, in the early stage, the FBR cycle which has international competitiveness by improving the performance of waste management and proliferation resistance and that goes toward a rational transition from the LWR cycle to the FBR cycle. This will contribute to sustainable development.

In the Fast Reactor Technology Development (FaCT) Project of Japan, the indexes of design targets are set from viewpoints of: safety; sustainability (environmental protection, waste management and resource efficiency); economy; and proliferation. Furthermore, they are determined in consideration of consistency to requirements of international collaborative programs that have already taken place such as GEN-IV*¹ and INPRO*².

*¹ GEN-IV is the fourth generation nuclear power plant system. The first generation indicates the early prototype reactors such as at Shippingport (PWR) and Dresden (BWR). The second generation indicates the following commercial reactors i.e. PWR, BWR, CANDU and VVER, RBMK. The third generation is the improved designs of the second generation systems. ABWR, APWR and EPR mainly pursue economy by scaling up. The reactors with the passive safety system such as AP1000 and ESBWR are also third generation. The fourth generation will follow the third generation and is assumed to have the following characteristics: (i) economically competitive with natural gas thermal power plants; (ii) higher proliferation resistance; (iii) higher safety; and (iv) minimum load for waste management.

*² INPRO (International Project on Innovative Nuclear Reactors and Fuel Cycles) is one of the IAEA programs to help prepare infrastructures aimed

toward deployment of innovative nuclear systems which have safety, economy, proliferation resistance, etc.

[3] Minor actinide fuel and reduction of environmental load

The spent fuel of LWRs contains minor actinides (MAs) i.e. Np, Am, Cm etc. as well as plutonium. In the conventional nuclear fuel cycle with high-decontamination reprocessing, those MAs are disposed in a deep geological repository as high-level radioactive waste and they will be supervised and stored long term. To reduce the environmental load, it is desirable to reduce the inventory of the high-level radioactive waste and to shorten the period for supervising it. The future fuel cycle is being researched in several countries toward reducing the MA inventory in the waste and hence reducing the environmental load by reloading the MAs to a reactor without separation from U and Pu. In such a fuel cycle, the decay time of the radioactive waste, defined as the period in which the radioactive toxicity decays to that of the amount of natural uranium needed for the equivalent electric power generation resulting in the production of the waste, may be shortened from several hundred thousand years to hundreds of years. The principle of transmuting the MAs in the reactor core is as follows. The value of (σ_c/σ_f) , i.e. the ratio of the capture cross section of a heavy nuclide σ_c to its fission cross section σ_f , is generally small for a fast neutron spectrum, and MAs, i.e. ^{237}Np and ^{241}Am having even number of neutrons, have a threshold energy of fission at several hundred keV. Thus, (σ_c/σ_f) quickly decreases for the energy above the threshold.

For this reason, the fraction of fission is high while that of build-up to heavier nuclei by successive neutron captures is small when MAs are transmuted by fast reactors. In other words, MAs can be utilized as the nuclear fuel. Even if the MA recycle is repeated in fast reactors, production of heavier nuclei is small compared to thermal reactors. This also implies that useless consumption of neutrons is smaller in fast reactors. In the case of thermal reactors, the MA nuclei with even numbers of neutrons which are not fissile are transmuted by capturing neutrons, thus the consumption of neutrons tends to be larger. In summary, MA transmutation by fast reactors has advantages from viewpoints of suppressing the production of heavier nuclei and neutron economy. The burnup chain including MA nuclei is shown in Fig. 4.14.

When MAs are utilized as fuel, two methods are considered. One is using driver fuel containing homogeneously distributed MAs (homogeneous loading). The other is separately fabricating MA fuel assemblies containing higher MA fraction and loading them into the core (heterogeneous loading). The core characteristics for each method are being researched. The influence of the homogeneous loading on the core characteristics is small. However, heat and neutron generations of the fresh fuel are large and the number of fuel assemblies needing special treatments is huge because all the fuel assemblies contain MAs. On the other hand, in the heterogeneous loading the number of such assemblies is limited. However, the influence on the core characteristics is relatively large. The loading position of the MA fuel assemblies must be suitably selected.

From the viewpoint of reducing the inventory of radioactive waste, transmutation of long-lived fission products (LLFPs) is desired as well as MA

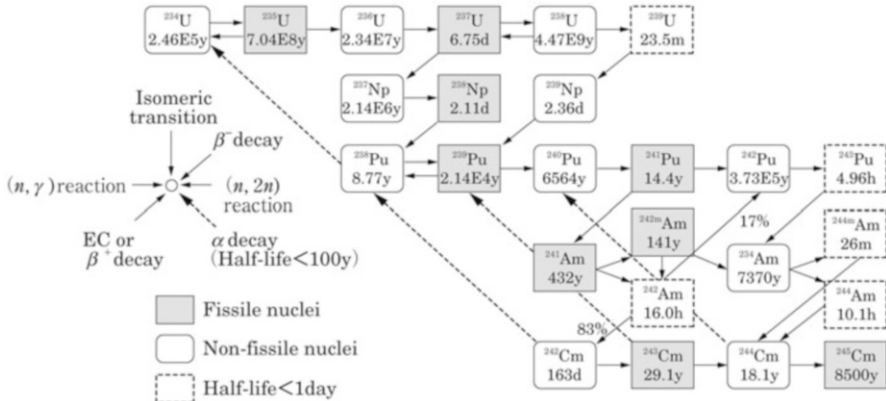


Fig. 4.14 Burnup chain [4]

nuclei. ^{129}I (half-life: 16 million years, ^{99}Tc (half-life: 210 thousand years) and ^{135}Cs (half-life: 2.3 million years), which are recognized to have potentially high environmental loads from viewpoint of inventory, half-life and mobility, are the targets of transmutation. The LLFP nuclei in the spent fuel are to be included in LLFP-containing fuel assemblies and reloaded to the reactor. As for ^{135}Cs , under the assumption of element separation (not isotope separation), reduction of its inventory by transmutation is difficult due to the new production from ^{133}Cs . Thus, ^{129}I and ^{99}Tc are the major targets. Since the principle of LLFP transmutation is neutron capture, lower neutron energy provides higher transmutation efficiency. When LLFPs are transmuted by fast reactors, moderator pins will be provided in the LLFP assemblies for improving the transmutation efficiency. The loading positions of the LLFP assemblies must be carefully chosen considering the influence on the core characteristics.

4.2 Design of High Temperature Gas-Cooled Reactors

4.2.1 Overview

The technologies of the high temperature gas-cooled reactors (HTGRs) are based on the designs and operating experiences with Magnox reactors and Advanced Gas-cooled Reactors (AGR)s. In AGRs, the outlet coolant temperature could not be elevated due to chemical reaction of the CO_2 coolant with the graphite structures. Thus, helium gas having high chemical stability is adopted as the coolant of the HTGRs, which enables high reactor outlet coolant temperature. Various gas-cooled reactors are compared in Table 4.5 [18–20]. Since metals could not be used as the fuel clad under the high temperature condition, coated particle fuel using ceramics coating was developed [21]. The coated particle fuel consists of spherical fuel kernels coated with pyrolytic carbon (PyC) and SiC. Utilization of the helium

Table 4.5 Comparison of various gas-cooled reactors

	Magnox reactor (CO ₂ cooled reactor)	Advanced gas-cooled reactor (AGR)	High-temperature gas-cooled reactor (HTGR)	Gas-cooled fast reactor	PWR as reference
Reactor	Tokai NPP unit 1 (587 MWt) [19]	Hinkley Point-B (1,500 MWt) [19]	THTR-300 (750 MWt) [19]	Conceptual design by JAEA (2,400 MWt) [20]	Ooi NPP unit 1 etc (3,411 MWt) [21]
Moderator	Graphite	Graphite	Graphite		Light water
Coolant	CO ₂ gas	CO ₂ gas	Helium gas		Light water
Fuel	Metal natural uranium (with Magnox alloy clad)	UO ₂ (with stainless steel clad)	Coated particle fuel	Pin type nitride fuel	UO ₂ (with Zircaloy-4 clad)
Reactor outlet coolant temperature (°C)	390	665	750	850	320
Power density (W/cm ³)	0.8	2.7	6		100
Burnup (GWd/t)	3.6	18	100	150	44

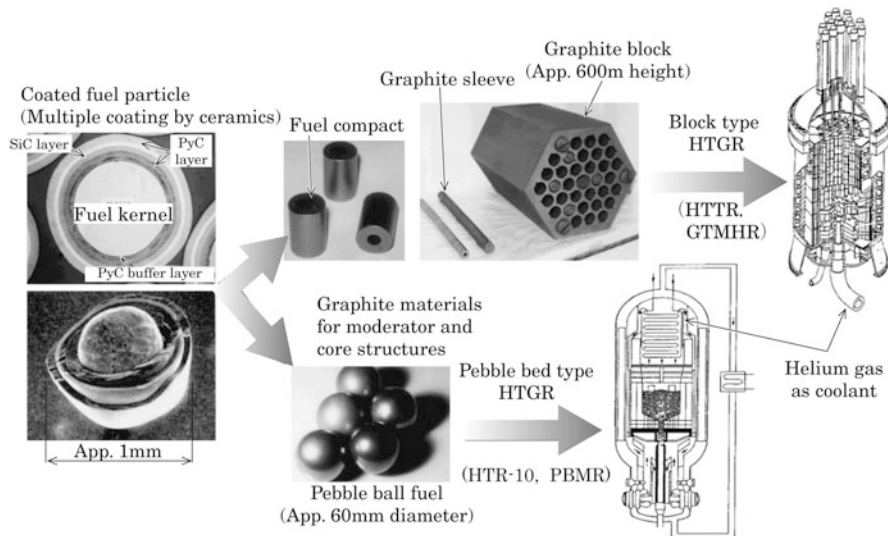


Fig. 4.15 Fuel of HTGRs

gas coolant and development of the coated particle fuel have enabled high reactor outlet coolant temperatures of nearly 1,000 °C to be reached. One characteristic of the HTGRs in terms of reactor physics is that the conversion ratio of fissile nuclei can be high due to the small absorption cross sections of the helium gas coolant and the graphite moderator. The high performance of the coated particle fuel against release of FPs, as well as the high conversion ratio, enables high burnup more than 100GWd/t.

The HTGRs are categorized as the pebble-bed type and the block type according to the fuel configuration. In the pebble bed type HTGRs, coated particle fuels are mixed with graphite powder. The mixture is formed as spherical fuel balls, each with a diameter of 6 cm. The reactor core is formed by disorderly piling up many fuel balls. The unique characteristic of pebble bed type HTGRs is the capability for continuous refueling during operation. The coolant flows in gaps around the fuel balls. The block type HTGRs use hexagonal block type fuel. The reactor core is formed by piling up blocks in the axial direction. Refueling is carried out by the refueling machine during shutdown period. Fuel configurations of those HTGRs are shown in Fig. 4.15. The specifications of constructed HTGRs are summarized in Table 4.6 [22].

The pebble bed type HTGRs, namely, the Arbeitsgemeinschaft Versuchsreaktor (AVR) [23] and Thorium Hochtemperatur Reaktor (THTR-300) [24] were constructed in Germany. The THTR-300 was a prototype power reactor. The Hochtemperatur Reaktor 10 MW (HTR-10) [25] was constructed in China as an experimental pebble bed type HTGR. In the Republic of South Africa, construction of the Pebble Bed Modular Reactor (PBMR) [26], which is a modular type HTGR with an annular core, was planned.

Table 4.6 Constructed HTGRs

Reactor	Dragon		Peach bottom		AVR		Fort St. Vrain		HTGR-300		HTGR		HTGR-10	
	Country	UK (OECD)	USA	Country	USA	Germany	USA	Germany	Japan	Germany	Japan	China	China	
Operation period	1964–1976	1966–1974	1966–1988	1974–1989	1983–1989	1998–	1983–1989	1998–	2000–	2000–	2000–	2000–	2000–	
Reactor power (MWt/MWe)	20/-	144/42	46/15	842/342	750/308	30/-	750/308	30/-	10/2.5	10/2.5	10/2.5	10/2.5	10/2.5	
Core diameter (m)	1.1	2.8	3.0	6.0	5.6	2.3	5.6	2.3	1.8	1.8	1.8	1.8	1.8	
Core height (m)	1.6	2.3	2.5	4.8	6.0	2.9	6.0	2.9	2.0	2.0	2.0	2.0	2.0	
Average core power density (W/cm ³)	14	8.3	2.5	6.3	6	2.5	6	2.5	2	2	2	2	2	
Fuel kernel	UO ₂	(Th,U)C ₂	UO ₂	(Th,U)C ₂	(Th,U)C ₂	UO ₂	UO ₂							
Fuel type	Rod	Rod	Pebble ball	Block (Multi-hole)	Pebble ball	Block (Pin-in-block)	Pebble ball	Block (Pin-in-block)	Pebble ball	Pebble ball	Pebble ball	Pebble ball	Pebble ball	
Core inlet coolant temperature (°C)	350	340	270	408	250	395	250	395	250	395	250	395	250	
Reactor outlet coolant Temperature (°C)	750	725	950	785	750	850/950	750	850/950	700	850/950	700	850/950	700	
Coolant pressure (MPa)	2	2.4	1.1	4.8	4	4	4	4	3	4	4	4	3	

Table 4.7 Major specifications of HTTR

Item	Specification
Reactor thermal power	30 MW
Primary coolant	Helium gas
Inlet coolant temperature	395 °C
Outlet coolant temperature	850 °C (During normal operation) 950 °C (During high-temperature test operation)
Primary coolant pressure	4 MPa
Core structure	Graphite
Effective core height	2.9 m
Equivalent core diameter	2.3 m
Average power density	2.5 MW/m ³
Fuel	Coated UO ₂ particle / Dispersed in graphite matrix
Uranium enrichment	3–10 wt% (Ave 5.9 wt%)
Type of fuel	Pin-in-block
Reactor pressure vessel	Steel (2 ^{1/4} Cr–1Mo)
Number of coolant loops	1 loop (with IHX and pressurized water cooler)

The block type HTGRs, namely, Fort St. Vrain (FSV) [27] in the US and the High Temperature Engineering Test Reactor (HTTR) in Japan were constructed. The HTTR has a thermal power of 30 MW and reactor outlet coolant temperature of 950 °C [28–30]. Its fuel type is the so-called pin-in-block type which is composed of fuel rods and a hexagonal graphite block (Fig. 4.15). The fuel rods are composed of fuel compacts loaded in a graphite sleeve. The fuel compacts are formed by mixing coated particle fuel with graphite powder. The major specifications of the HTTR are summarized in Table 4.7.

Since the reactor outlet coolant of LWRs is around 300 °C, their utilization is limited, namely, for electric power generation. On the other hand, helium gas having high chemical stability is used as the coolant for HTGRs and high reactor outlet temperature around 1,000 °C is possible, which enables high generating efficiency and utilization of HTGRs as a heat source particularly in the chemical industry. Thus, one of the HTGR advantages is its multi-purpose utilizations of nuclear energy.

Here, the core design of the HTTR is presented as an example of HTGRs. Also, the annular core design is described since it is noteworthy from the viewpoint of inherent safety.

4.2.2 Core, Fuel, and Control Rod Designs

[1] Core

The core of the HTTR is a layered structure of hexagonal fuel blocks, surrounded by the replaceable reflector. The replaceable reflector is further surrounded by the permanent reflector. The whole core structure is supported by the side shields and the core restraint mechanism which are provided outside

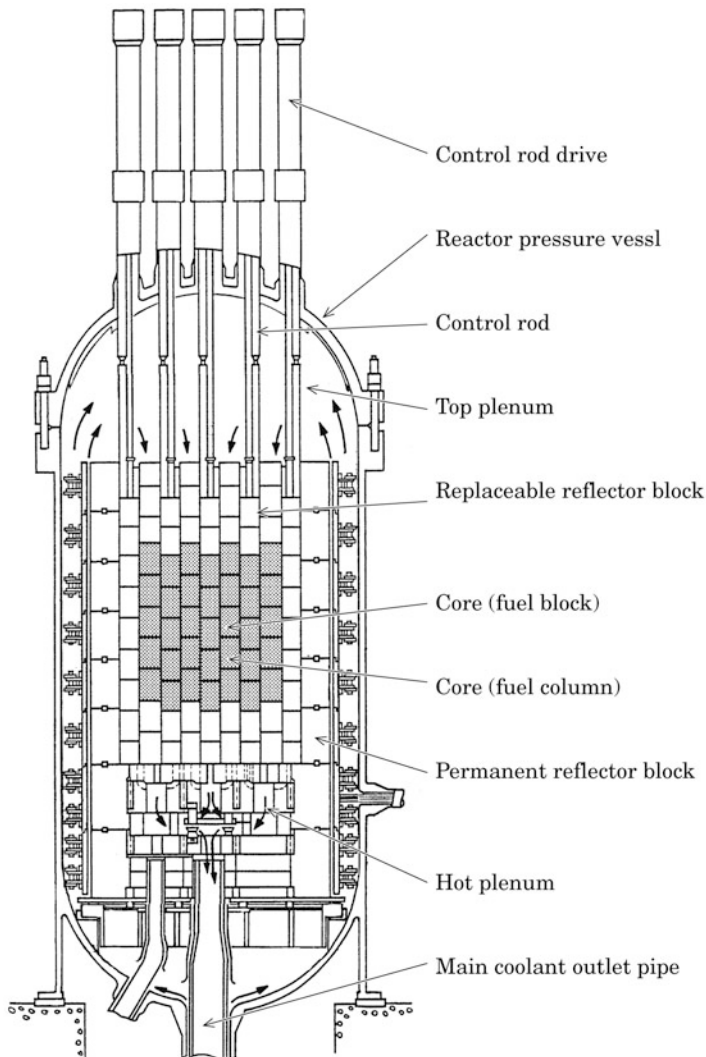


Fig. 4.16 Vertical cross sections of HTTR

of the permanent reflector. The fuel blocks are piled up into five layers. The top and bottom replaceable reflectors are placed above and below the fuel blocks, respectively. A set of hexagonal blocks i.e. five fuel blocks as well as top and bottom replaceable reflector blocks is called a column.

As shown in Fig. 4.16, the coolant entering into the reactor pressure vessel first flows upward from the lower region of the vessel through the space between the permanent reflector block and the vessel wall to the top plenum. It turns in the downward direction at the top plenum and enters the core. The

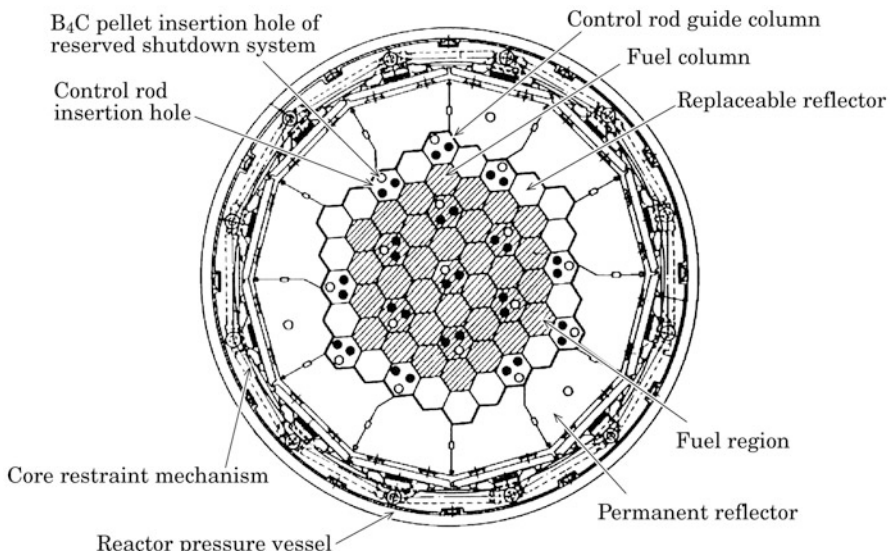


Fig. 4.17 Horizontal cross sections of HTTR

coolant flows in the annular channels between fuel rods and wall of cooling holes in the fuel block. It is heated up to 950 °C. The outflows of the heated coolant merge together in the hot plenum. Then, the coolant is led to the inner tube of the double-tube main coolant outlet pipe.

As shown in Fig. 4.17, control rod guide columns are provided in the core for inserting the control rods. A control rod guide column is a set of piled-up graphite blocks. Two of three holes are for inserting the control rods. The third is used for the reserve shut down system that drops B₄C pellets.

[2] Fuel block

The fuel type of the HTTR is the pin-in-block type where the fuel rods are inserted in a hexagonal graphite block as shown in Fig. 4.18. The coated particle fuels are mixed with graphite powder and pressed into an annular cylinder, which is called a fuel compact. Fourteen fuel compacts are inserted into a graphite sleeve to form a fuel rod. Thirty-three fuel rods are loaded into a hexagonal graphite block (36 cm in width and 58 cm in height), which forms a fuel block. Helium gas coolant flows downward in the spaces of a few millimeters between the fuel rods and wall of cooling holes in the fuel block. A fuel compact contains about 14 g of uranium which corresponds to about 13,000 coated particle fuels.

Three dowel pins are provided at the top of the fuel block and three dowel sockets are provided at its bottom. They are used for positioning when piling up the blocks. Holes for loading burnable poison are provided below each dowel pin. The burnable poison rod consists of B₄C pellets and it compensates burnup reactivity.

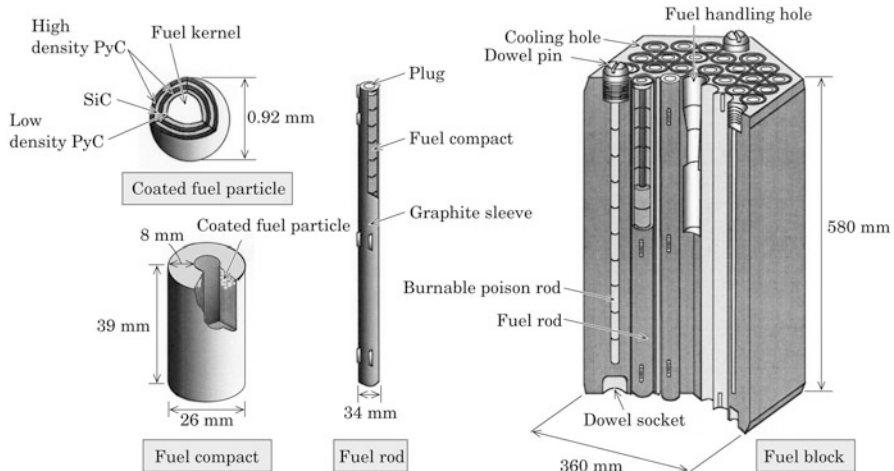


Fig. 4.18 Fuel of HTTR

[3] Coated particle fuel

The functions of the low density PyC layer (first layer) are to protect the inner high density PyC (second layer) layer by adsorbing fission fragments coming from the fuel kernel, and to provide a space for containing FP gas coming from the fuel kernel. The inner high density PyC (second layer) is provided for retention of FP gas. Short half-life of FP gas nuclei and their small diffusion coefficients in the high density PyC layer, as well as retention capability of the fuel kernel, ensure that FP gas release from the fuel is actually no problem as long as the second layer has no defects.

The SiC layer (third layer) has high retention capability for FP gas and metallic FP fragments. Due to the short half-life of these gas nuclei and their small diffusion coefficients, the SiC layer, the third layer has good retention capability of them just as the second layer does. The outer high density PyC layer (fourth layer) compresses the SiC layer externally by shrinking during irradiation. That prevents the SiC layer from experiencing a tensile load due to the internal gas pressure and hence avoids failure of the coated particle fuels.

[4] Allowable design limits of fuel and temperature [31, 32]

The characteristic feature of the coated particle fuels is retention of FPs by the ceramic coating layers. The principle of ensuring fuel integrity of LWRs is avoiding failure of the fuel clad, which contains FPs, by applying the criterion of the minimum critical heat flux ratio. On the other hand, since the characteristic of FP retention in the coated particle fuels is different from that in the LWR fuel, a new principle for ensuring fuel integrity is applied.

The mechanisms of FP gas release from the coated particle fuel can be categorized as below.

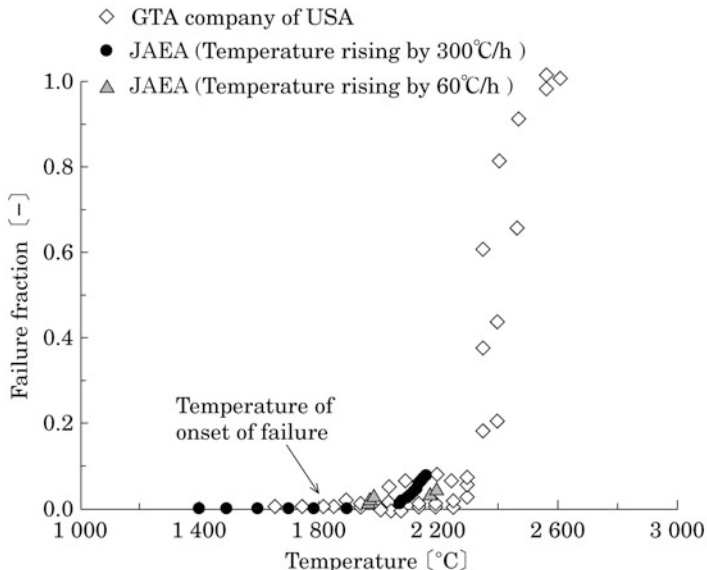


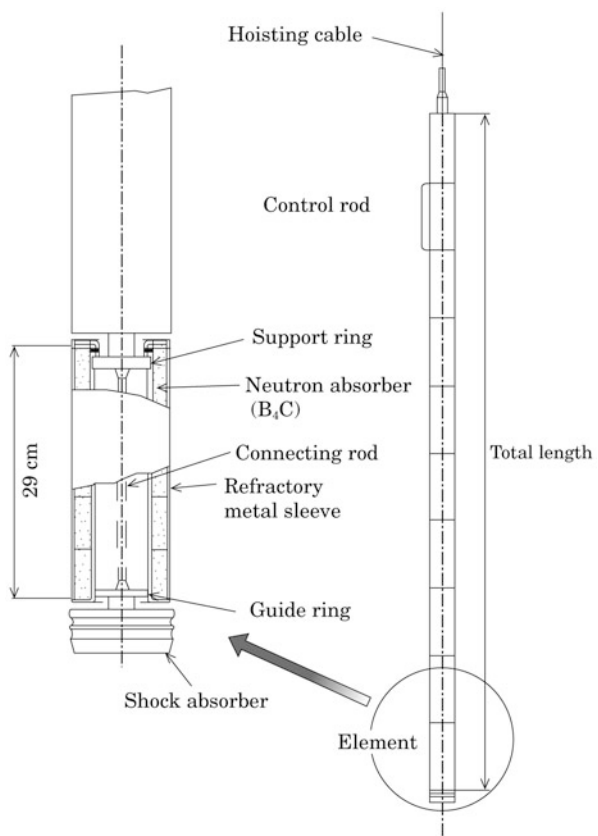
Fig. 4.19 Relation of temperature and fuel failure fraction of coated fuel particles

- (i) FP gas release from the coated particle fuels where the coating layers have failed at fabrication
- (ii) FP gas release from the intact coated particle fuels due to diffusion enhanced by heat up
- (iii) FP gas release due to failure of the coating layers during operation (additional failure)

The allowable design limit of the coated particle fuels is determined to keep failure of the coating layers associated with (iii) within an allowable range. The failure fraction associated with (i) is limited below 0.2 %. The diffusion of fission fragments associated with (ii) is much smaller than the release by (iii).

Various tests on failure of the coating layers have been carried out in several countries. Failure fractions of the coated particle fuels in some heating tests are shown in Fig. 4.19. Heating the coated particle fuels causes failure of the coating layers. Then fission gas (^{85}Kr) is abruptly released. The failure fraction is estimated by the release of radioactivity per coated particle fuel. From the figure, it can be seen that the failure fraction is almost zero below 1,800 °C, it gradually increases above 1,800 °C, and sharply increases around 2,200 °C. It is supposed that rapid thermal decomposition (thermal degradation) of the SiC layer above 2,200 °C leads to abrupt failure of the coating. The allowable design limit is set as 1,600 °C, taking a margin from 1,800 °C. In order to keep the fuel temperature below 1,600 °C at anticipated operational occurrences

Fig. 4.20 Control rod of HTTR



such as “Uncontrolled withdrawn of control rod at operation”, the limit of the fuel temperature at normal operation is set as 1,495 °C.

[5] Control rod

The structure of the control rod is shown in Fig. 4.20. The “element” consists of B₄C which is loaded in the refractory metal sleeve. The control rod (total length, about 3.1 m) is formed by axially connecting 10 elements using the connecting rod. The control rods are driven in pairs of two, and there are 16 pairs in total. The control rods are driven by hoisting the cable onto a drum using the control rod drive which is mounted in the stand pipe of the reactor pressure vessel. The control rods are inserted into the core from the top.

The reserve shutdown system is provided as backup to reactor shutdown system of the control rods. The reserve shut down system inserts negative reactivity into the core by dropping B₄C pellets into the hole in the control rod guide column.

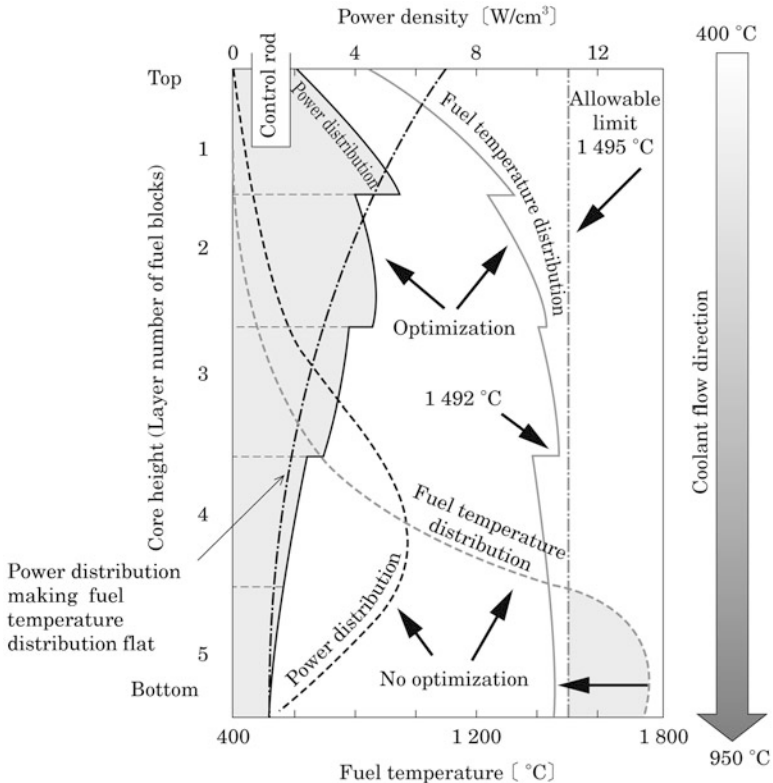


Fig. 4.21 Design of power distribution and fuel temperature distribution

4.2.3 Method of Achieving High Outlet Coolant Temperature

The reactor outlet coolant temperature of LWRs is around 300 °C and the temperature elevation from inlet to outlet is at most several tens of degrees. Thus, the power distribution is designed to be axially flat in LWRs. On the other hand, the reactor outlet coolant temperature is 950 °C and the temperature elevation from inlet to outlet is about 550 °C in the HTTR. Thus, special core design methods are necessary so that the fuel temperature at the core bottom where coolant temperature is high does not exceed the limit.

[1] Optimization of power distribution [33, 34]

If the power distribution is not optimized, the fuel temperature exceed the limit at the core bottom as shown in Fig. 4.21. The fuel temperature at the core bottom must be reduced by flattening the axial temperature distribution. The power distribution for flattening the axial temperature distribution is analytically obtained.

Fig. 4.22 Relation of coolant temperature and fuel temperature

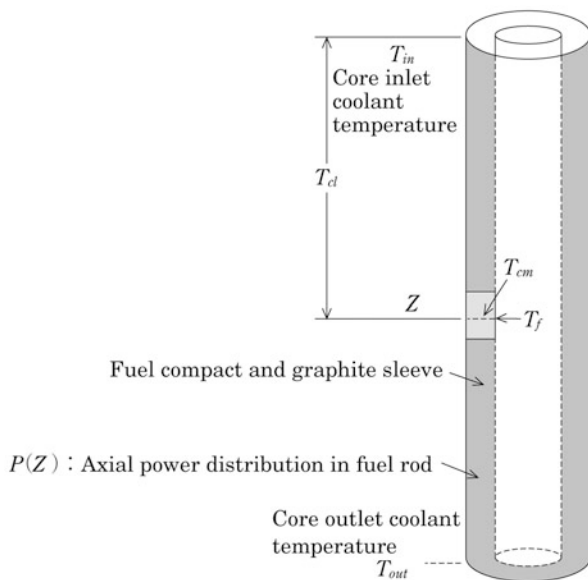


Figure 4.22 shows the relation of coolant temperature and fuel temperature. For the fuel rod, the inner surface temperature of the fuel compact $T_f(z)$ becomes high. This temperature needs to be reduced:

$$T_f(z) = T_{in} + T_{cl}(z) + T_{cm}(z) \quad (4.15)$$

where

T_{in} : Core inlet coolant temperature ($^{\circ}\text{C}$)

T_{cl} : Elevation of gas temperature from core inlet to axial position Z ($^{\circ}\text{C}$)

$$T_{cl}(z) = a \int P(z) dz \quad (4.16)$$

$P(z)$ indicates the axial power distribution and a is a factor which depends on coolant flow rate and coolant heat capacity. The heat capacity is regarded as constant.

$$T_{cm} : \text{Temperature elevation from surface of graphite sleeve to inner surface of fuel compact } (^{\circ}\text{C}) \quad (4.17)$$

$$T_{cm}(z) = bP(z)$$

Here, b is a factor which depends on fuel rod geometry and thermal conductivity. Although the thermal conductivity changes with temperature, it is regarded as constant.

Equation (4.18) is obtained by substituting Eqs. (4.16) and (4.20) into Eq. (4.16).

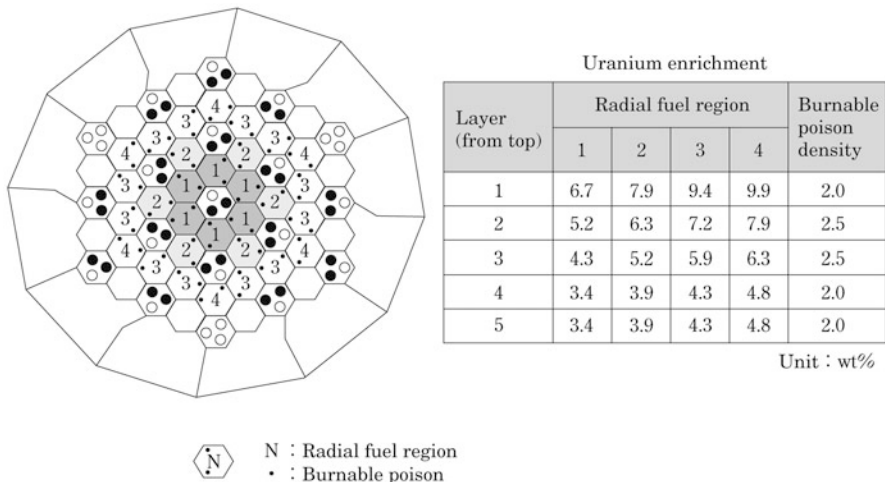


Fig. 4.23 Uranium enrichments of each fuel block in core

$$T_f(z) = T_{in} + a \int P(z) dz + b P(z) \quad (4.18)$$

By differentiating this equation under the condition $T_f(z) = constant$, which means axially flat distribution of fuel temperature, the following relation is obtained.

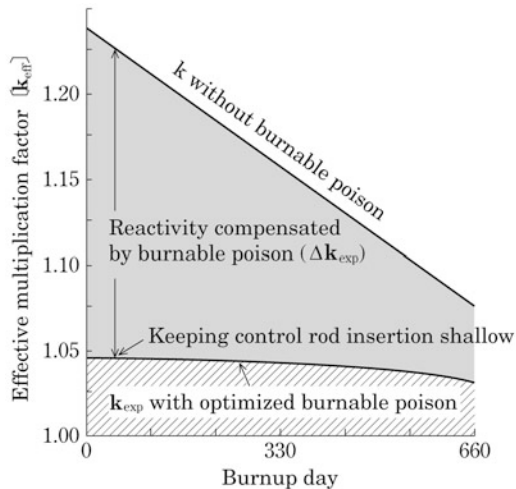
$$aP(z)dz = -bdp(z) \quad (4.19)$$

By solving this relation, the power distribution for achieving the axially flat distribution of fuel temperature is an exponential function.

$$P(z) = C \exp\left(-\frac{az}{b}\right) \quad (4.20)$$

C is an integration constant and determined to make T_{cl} of Eq. (4.16) the elevation of the coolant temperature in the core. Figure 4.21 shows the exponential power distribution for axially flattening the fuel temperature distribution of the HTTR. Such an optimized power distribution is achieved by making the uranium enrichment relatively high at the core top and relatively low at the core bottom. The fuel temperature distribution among the fuel columns is also flattened by making the uranium enrichment relatively high at the core peripheral region and relatively low at the core center region. The uranium enrichment division obtained by those adjustments is shown in Fig. 4.23. The number of enrichment divisions is 12. The minimum and maximum values are 3.4 wt% and 9.9 wt%, respectively. The core average enrichment is 5.9 wt%. The power

Fig. 4.24 Adjustment of k_{eff} for making control rod insertion shallow



distribution after the optimization is shown in Fig. 4.21. Due to shallow insertion of the control rods and other factors, the power distribution is not an exact exponential function at the core top.

[2] Preservation of optimized power distribution [35]

Since the fuel temperature must be kept below the limit throughout the burnup period, it is expected that the optimized power distribution is maintained. As shown in Fig. 4.24, high effective multiplication factor at the beginning of burnup period requires deep insertion of the control rods for compensating the excess reactivity. In such a case, the peak of power distribution like Fig. 4.21 (“No optimization” case) appears in core bottom and the fuel temperature there exceeds the limit. Thus, the control rod insertion, as illustrated in Fig. 4.21 (“Optimization” case), should be kept shallow throughout the burnup period. To do that, the effective multiplication factor should be made as small as possible while keeping the necessary reactivity for burnup like k_{exp} in Fig. 4.24. The reactivity which should be compensated by burnable poison (Δk_{exp}) is given by Eq. (4.21).

$$\Delta k_{\text{exp}} = k - k_{\text{exp}} \quad (4.21)$$

The multiplication factor is expressed as below by one-group theory:

$$k = \frac{\nu \Sigma_f}{\Sigma_a} \quad (4.22)$$

where

ν : Neutron yield per fission

Σ_f : Macroscopic fission cross section (1/cm)

Σ_a : Macroscopic absorption cross section (1/cm) excluding burnable poison

The multiplication factor k_{exp} which is made as small as possible by loading burnable poison is expressed as the next equation.

$$k_{\text{exp}} = \frac{\nu \Sigma_f}{\Sigma_a + \Sigma_{\text{exp}}} \quad (4.23)$$

Σ_{exp} is the adequate absorption cross section of burnable poison for achieving k_{exp} . From Eqs. (4.21), (4.22) and (4.23), Σ_{exp} is expressed as Eq. (4.24).

$$\Sigma_{\text{exp}} = \frac{\Delta k_{\text{exp}} \Sigma_a}{\Sigma_a + k_{\text{exp}}} \quad (4.24)$$

Burnable poison is a strong absorber and hence has a self-shielding effect. Thus, its effective absorption cross section Σ_{aBP} is expressed as:

$$\Sigma_{\text{aBP}} = f \sigma N \quad (4.25)$$

where

f : Self-shielding factor

σ : Microscopic absorption cross section of nuclide of burnable poison(barn)

N : Number of density of nuclides of burnable poison homogenized into fuel block (1/barn/cm)

f can be obtained by the empirical correlation below:

$$f = \frac{1}{1 + Cl \sigma N_{\text{BP}}} \quad (4.26)$$

where

C : Fitting factor

l : Factor depending on geometry of burnable poison (1/cm)(the radius is used for a rod type geometry)

N_{BP} : Number density of nuclides having absorption effect in burnable poison (1/barn/cm)

The change in the effective absorption cross section Σ_{aBP} can be obtained from Eqs. (4.25) and (4.26) by considering the change in the number density of nuclides N_{BP} . Among the changes in Σ_{aBP} for several burnable poisons with different geometries and nuclide number densities, that which is closest to the change in Σ_{exp} is the optimum one. Figure 4.25 shows the comparison of Σ_{exp} and several Σ_{aBP} which were considered in the design of burnable poison of the HTTR. From this figure, the optimum diameter (r) of the burnable poison rods was set as 0.7 cm. This optimization of burnable poison allows operation with shallow insertion of the control rods, as shown in Fig. 4.21, throughout the burnup period. Reference [35] describes details on optimization of the burnable poison.

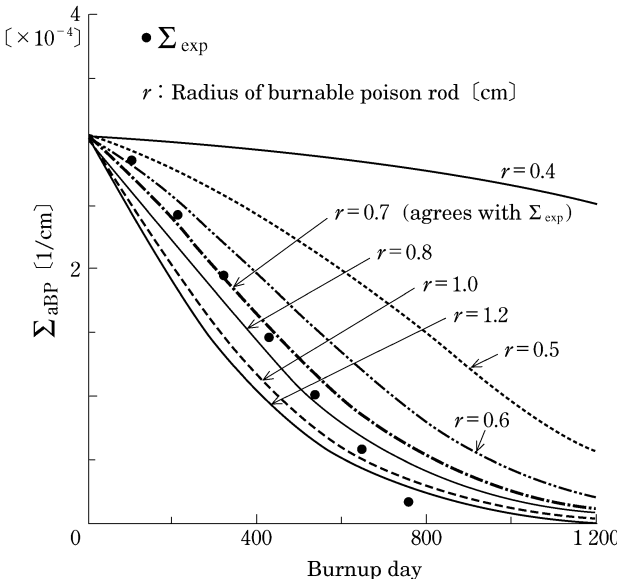


Fig. 4.25 Selection of burnable poison specifications

4.2.4 Nuclear Design

Reactor shutdown margin, power distribution, reactivity coefficients, etc. are important nuclear characteristics for ensuring performance and safety of nuclear reactors. Those nuclear characteristics are estimated using a nuclear design code system [36, 37]. The accuracy of the nuclear design code system of the HTTR was confirmed by comparison between calculated results and the experimental data of the Very High Temperature Reactor Critical Assembly (VHTRC). The nuclear design code system consists of the fuel cell calculation, the burnable poison cell calculation, the control rod cell calculation, and the core calculation. The codes and the process for HTTR are shown in Fig. 4.26.

[1] Nuclear design code system

(1) Fuel cell calculation

The 1 dimensional (D) cylindrical fuel cell models is used to obtain the average group constant of the fuel block. The neutron flux distribution in the cell is calculated by codes based on the collision probability method such as DELIGHT-7 [38]. The calculation process flow is shown in Fig. 4.27. Resonance absorption and neutron spectrum are calculated first, then the neutron flux distribution in the cell is calculated using the obtained a-few group microscopic constants. Next, the average group constants of the fuel rod are calculated, using the obtained neutron flux distribution. In this process, the double heterogeneity i.e. the coated particle fuels in a fuel

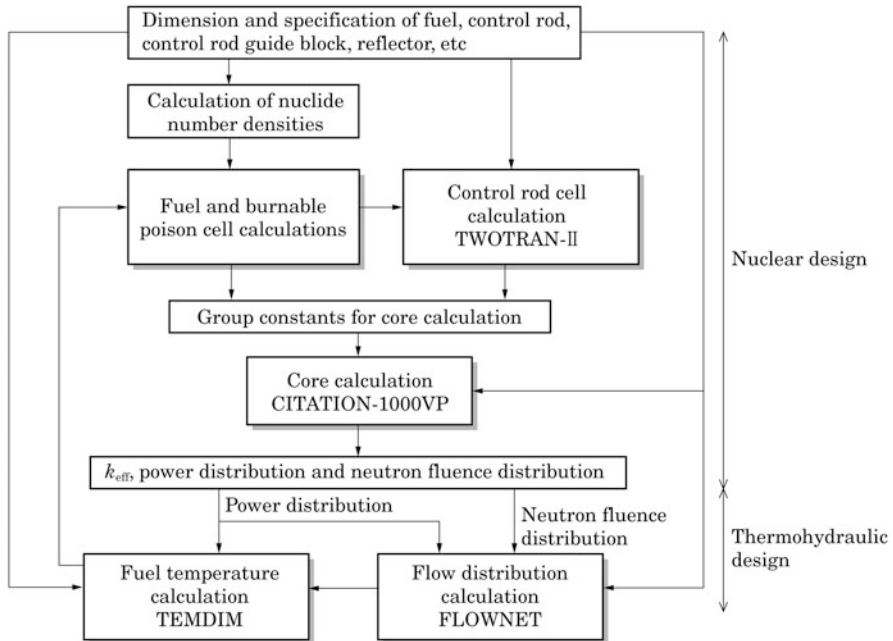


Fig. 4.26 Nuclear and thermohydraulic design codes and process flow

compact, and the fuel rods in a graphite block, is taken in to account. In this code, the neutron flux distribution in the burnable poison cell is calculated and the average group constants of the burnable poison are also calculated.

In the 1D cylindrical fuel cell model, as shown in Fig. 4.28, the material zones from the center to the outer boundary are the center gap, fuel compact, graphite sleeve, coolant channel, and graphite block. The cross section of the fuel cell model is the same as the fuel block cross section divided by the number of fuel rods, so that the calculated neutron spectrum in fuel cell is close to the actual one.

In the 1D cylindrical burnable poison cell model shown in Fig. 4.29, a burnable poison rod is surrounded by the material having the average group constants of the fuel rod which has been obtained in the fuel cell calculation. Since two burnable poison rods are loaded in a fuel block, the cross section of the surrounding fuel region is the same as one-half of the fuel block cross section.

(2) Control rod cell calculation

The control rod cell is used to obtain the average group constant of a pair of control rod inserted in graphite block. The neutron flux distribution in the cell is calculated by 2D transport codes such as TWOTRAN-II [39]. In this code, the neutron flux distribution in the strong neutron absorber of the control rod is calculated first. Using this flux distribution, the code

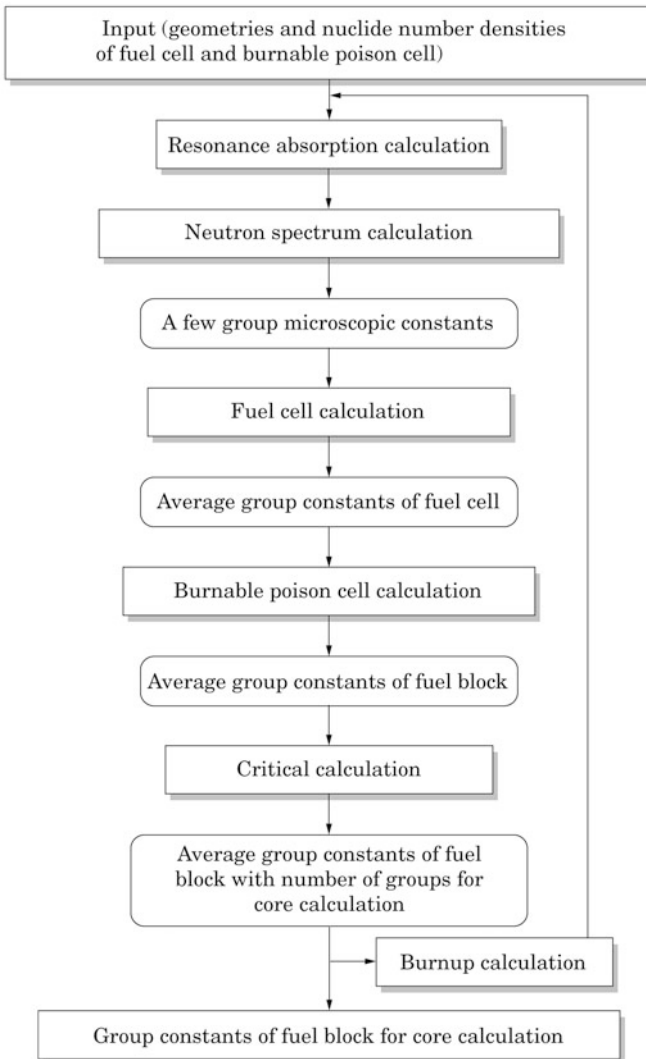


Fig. 4.27 Process flow of cell calculation

calculates the average group constants of a pair of control rods inserted in the graphite block. This code also calculates the average group constants of B₄C pellets inserted in the control rod guide block for reserve shutdown system.

For the control rod cell calculation, the 2D X-Y model is used as shown in Fig. 4.30. The model is for half of a control rod guide block in which a control rod is inserted and the surrounding fuel blocks. The average group constants of the control rod guide block where a control rod is inserted is

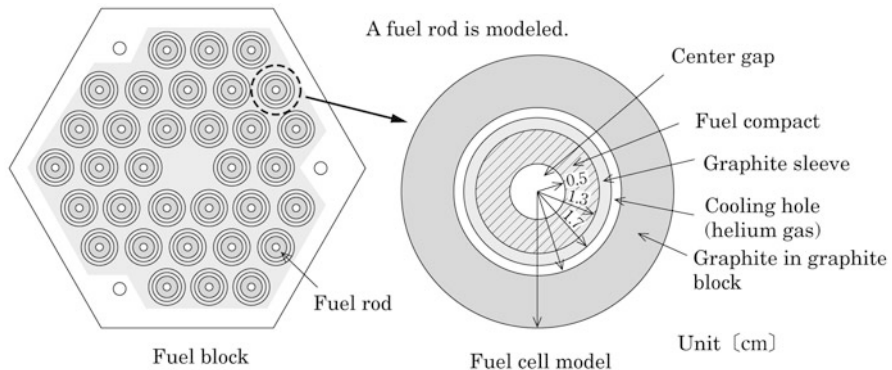


Fig. 4.28 One dimensional cylindrical fuel cell model for calculating group constants of homogenized fuel

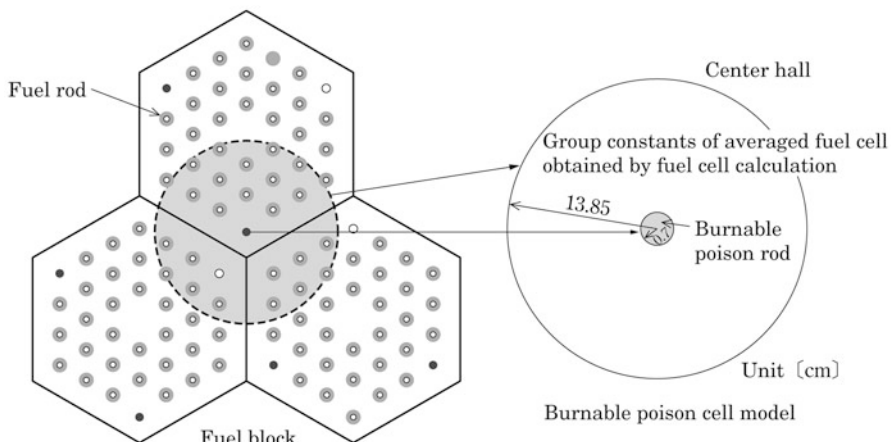


Fig. 4.29 One dimensional cylinder burnable poison cell model for calculating group constants of burnable poison

calculated by the flux-weighting method. Due to eccentricity of the control rod position from the block center, a one-half block model is used and the geometry of the neutron absorber is modeled by many micro rectangles.

(3) Core calculation

Diffusion calculation codes such as CITATION-1000VP are used for the core calculation [40, 41]. The effective multiplication factor, power distribution, reactivity coefficients, shutdown margin, etc are calculated using the core geometry and the average group constants obtained by the fuel cell calculation, burnup cell calculation, and control rod cell calculation. The power distribution obtained here is used for the fuel temperature calculation.

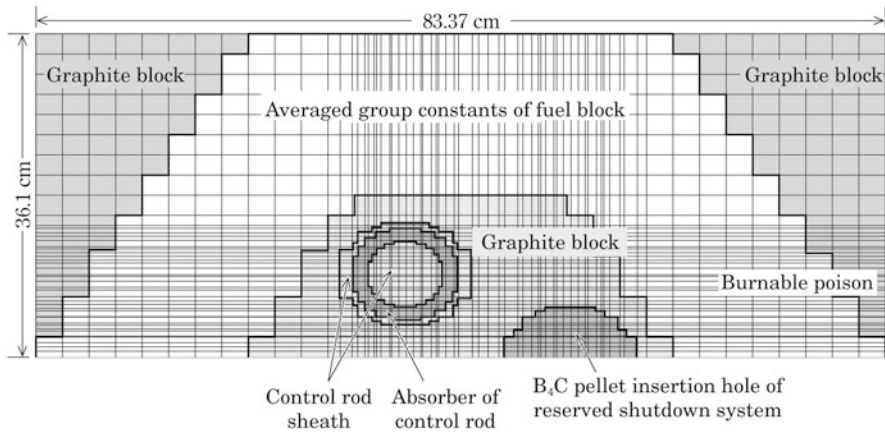


Fig. 4.30 Two dimensional control rod cell calculation model for calculating group constants of control rod

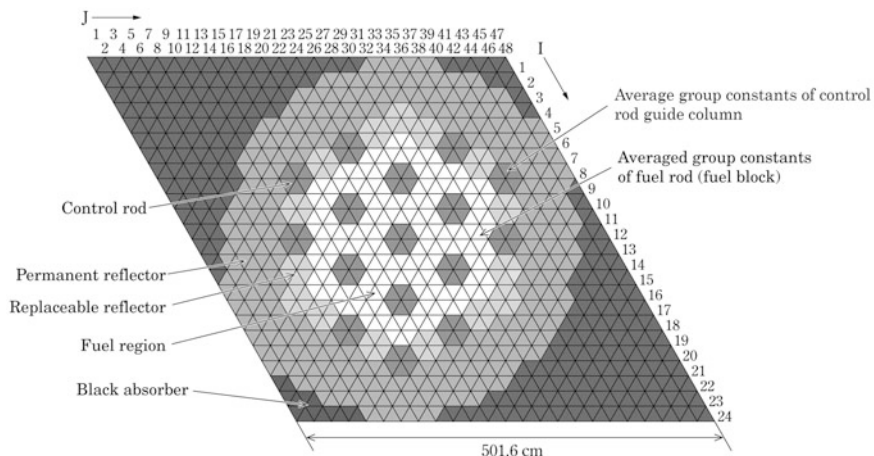


Fig. 4.31 Horizontal cross section of three dimensional triangular mesh model for core calculation

The horizontal cross section of the 3D triangular mesh model for the core calculation is shown in Fig. 4.31. Each fuel block is horizontally divided into 6 triangular meshes and axially divided into 4 meshes. The number density of the materials such as uranium and graphite, etc. are homogenized in each block.

[2] Validation of nuclear design code system

The nuclear design code system is validated by the experimental data of critical assemblies such as the VHTRC [42]. The VHTRC was constructed to study the nuclear characteristics of pin-in-block type HTGRs. The vertical cross section of

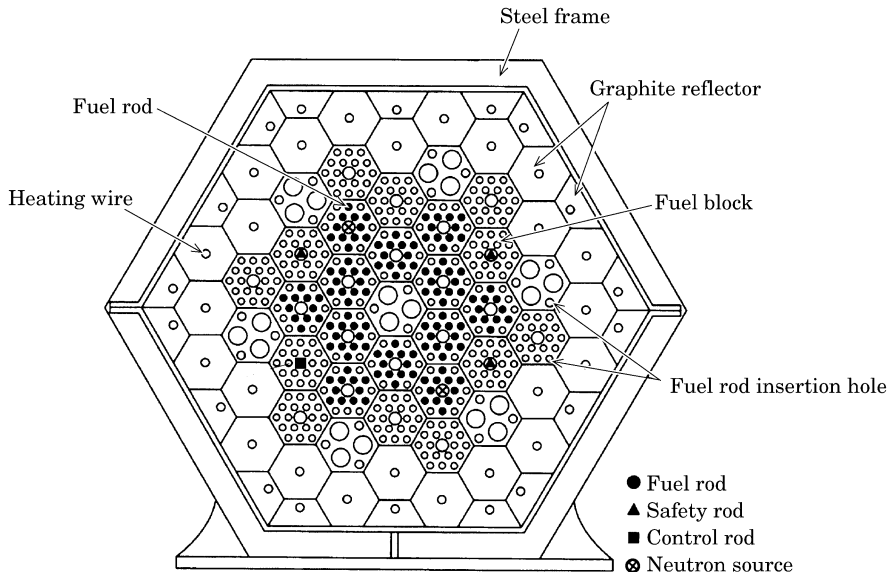


Fig. 4.32 Cross section of very high temperature reactor critical assembly (VHTRC)

Table 4.8 Comparison of VHTRC and HTTR major specifications

Reactor	VHTRC	HTTR
Core height (m)	2.4 (max)	2.9
Core diameter (m)	1.75 (max)	2.3
Fuel element	Hexagonal graphite block	Hexagonal graphite block
Fuel kernel of coated fuel particle	UO_2	UO_2
Diameter of coated fuel particle (μm)	599	600
Uranium enrichment (Wt%)	2, 4, 6	5.9 (average)
Moderator	Graphite	Graphite

the VHTRC is shown in Fig. 4.32. The VHTRC consists of two half assemblies. Each half assembly is formed by piling up the horizontal hexagonal graphite blocks and by fixing them into position by the steel frame. Each fuel block is equipped with the holes for loading fuel rods and inserting a control rod or a safety rod. The layout and loading number of the fuel rods can be easily changed. One of the half assemblies is fixed and the other is movable. Each fuel rod is formed by loading the fuel compacts into the graphite sleeve. Heating wires can be inserted into the graphite blocks so that experiments at desired temperatures can be done.

The major specifications of the VHTRC and the HTTR are compared in Table 4.8. The experimental data of the VHTRC, such as effective multiplication factor, control rod worth, burnable poison worth, power distribution (reaction rate distribution of copper) and temperature coefficients, were used for validation the nuclear design code system [43, 44].

(1) Effective multiplication factor

The effective multiplication factor is measured by the critical approach experiment where the fuel rods are sequentially loaded into the core. The effective multiplication factor for the ideal condition is calculated by correcting the measured one considering the effects of insertions and temperature. This ideal value is used for validation. The reactivity worth of insertions such as control rods, detectors, etc. is measured by the period method or the pulsed neutron technique.

Since the error between the experimental data and the predicted values was within $1\% \Delta k$, the calculation error used for the nuclear design of the HTTR was determined as $1\% \Delta k$.

(2) Control rod worth

The control rod worth is measured by inserting the mock-up control rod into the critical core and then measuring the subcriticality by the pulsed neutron technique. The error between the measured and calculated values was evaluated as 2.6 %. The calculation error was conservatively determined as 10 %.

The burnable poison worth was measured as well. Although the nuclear design code system accurately predicted the measured value, the calculation error was conservatively determined as 10 %.

(3) Power distribution

Using the proportional relationship among reaction rate of copper, neutron flux and fission rate, the calculations of the neutron flux distribution and the power distribution were validated by the measured reaction rate distribution of copper. In the measurement, copper foils were horizontally and axially inserted into the core and criticality was kept for a fixed period. The reaction rate of copper was obtained from the activation rates of the irradiated copper foils.

The calculated and measured axial reaction rate distributions of copper are shown in Fig. 4.33. The distribution is normalized so that the average reaction rate is 1.0. From that figure, the calculated distribution agrees well with the measured one in the fuel region. Since the errors between the calculation and the measurement were within 3 % for both radial and axial directions, the calculation error was determined as 3 %.

(4) Temperature reactivity coefficients [45]

The core was kept critical at room temperature and then the temperature was elevated using the heating wires. The subcriticality at the elevated temperature was measured by the pulsed neutron technique. From the relation between the temperature elevation and the decrease in the reactivity, the temperature reactivity coefficients were obtained. The measurements were carried out for temperatures to about 200 °C. The nuclear design code system well reproduced the measured values. The error was 6 % at maximum. The calculation error of the moderator temperature coefficient and the Doppler coefficient for the reactor transient analyses were determined as 10 %.

Fig. 4.33 Comparison of measured and calculated axial copper reaction rate distributions

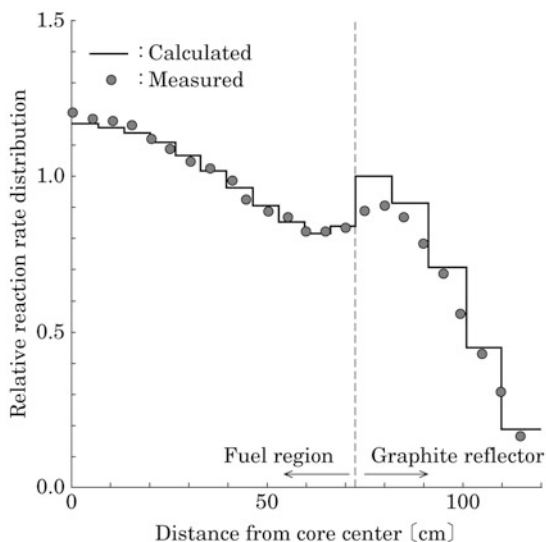


Table 4.9 Calculation errors considered in nuclear design

Index	Error between VHTRC measurement and calculation	Design error used for HTTR core design
Effective multiplication factor	1 % Δk	1 % Δk
Control rod reactivity worth	2.6 %	10 %
Burnable poison reactivity worth	\sim 0 %	10 %
Power distribution	2.9 %	3 %
Temperature reactivity coefficient	6 %	10 %

Based on those validations, the expected calculation errors in the nuclear design were determined. They are summarized in Table 4.9 with the errors used for core design [43].

[3] Nuclear design results of HTTR

The excess reactivity and the power distribution, etc. are described below as examples of nuclear design results [28].

(1) Excess reactivity

The excess reactivity is compensated by the control rods and the burnable poison. The power distribution is adjusted to keep the maximum fuel temperature below the limit. If the control rod insertion depth changes significantly with burnup, the power distribution changes, and hence there is a concern that the fuel temperature cannot be kept below the limit. Thus, the control rods are used for mainly the power level control and reactor shutdown. The reactivity change with burnup is compensated by the burnable poison. In this way, shallow insertion of the control rods is kept throughout the burnup period.

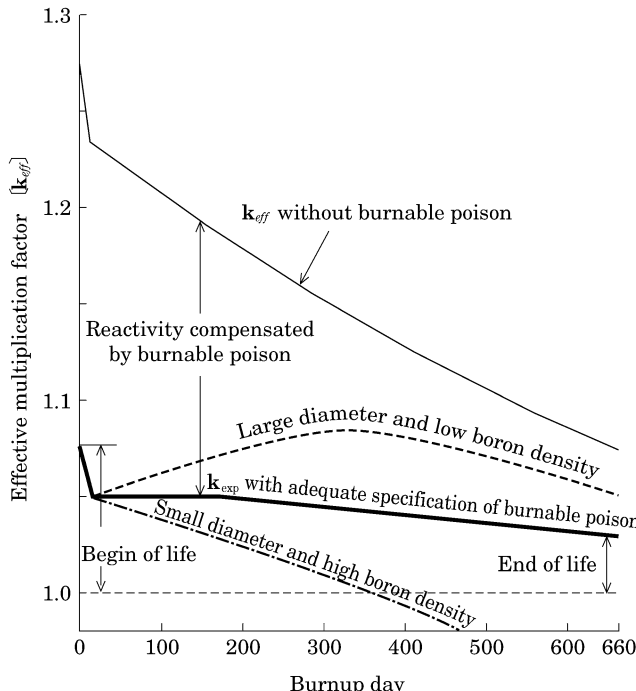


Fig. 4.34 Change of effective multiplication factor with burnup

In the nuclear design results, the effective multiplication factor changes with burnup (bold solid line) in Fig. 4.34. This line is the effective multiplication factor change that is calculated for full power operation with all the control rods fully withdrawn. If the burnable poison is not used, the effective multiplication factor is over 1.25 at the beginning of the burnup period and it rapidly decreases with burnup. It is difficult to compensate for such a change using only the control rods. If the compensation is made only by the control rods, it becomes difficult to keep the maximum fuel temperature below the limit at the beginning of the burnup period due to deep insertion of the control rods. With the burnable poison, the change of the effective multiplication factor is made small after accumulation of Xe at the beginning of the burnup period. The control rod insertion is kept almost constant throughout the burnup period. The control rods are slightly inserted in core and gradually withdrawn with burnup. Such a small change in the effective multiplication factor is owing to the adequate adjustment of the diameter and boron concentration of the burnable poison rods. With too large a diameter and too low a boron concentration, boron burns out rapidly and hence the excess reactivity recovers, which requires deep insertion of the control rods in the middle of burnup period. With too small a diameter and too high a boron concentration, on the other hand, the burnup of boron is too slow and hence

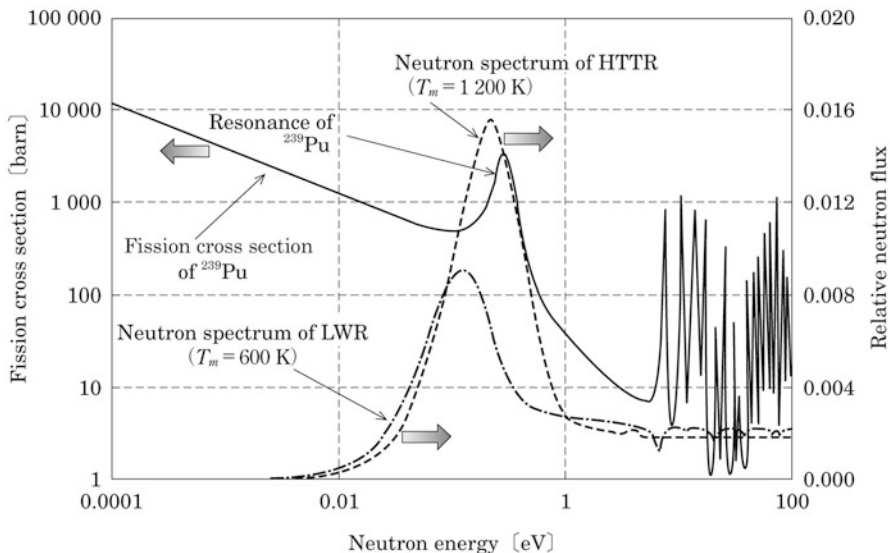


Fig. 4.35 Neutron spectra and fission cross section of ^{239}Pu

the excess reactivity decreases too fast, which makes it impossible to achieve the designed burnup days. In the HTTR core design, the diameter and boron concentration were suitably adjusted so that the changes in the control rod insertion depth and power distribution were kept small.

(2) Reactor shutdown margin

It is necessary to ensure sufficient shutdown margin even if the pair of control rods having the maximum reactivity worth is fully withdrawn (one rod stuck condition). In the assessment of the reactor shutdown margin, the total control rod worth with one rod stuck minus the calculation error is used as the available control rod worth. That available worth minus the maximum excess reactivity was confirmed to be more than $1\% \Delta k/k$ so that the reactor shutdown margin is sufficient.

(3) Temperature reactivity coefficient

A reactor core must have negative feedback characteristics to damp a change in the power level. The reactivity change against the change in the fuel temperature by $1\text{ }^{\circ}\text{C}$ i.e. the Doppler coefficient was confirmed to be negative for the entire operating region. The reactivity change against the change in the graphite temperature by $1\text{ }^{\circ}\text{C}$ i.e. the moderator temperature coefficient was also confirmed to be negative throughout the burnup period. However, it possibly becomes positive at the end of burnup cycle due to accumulation of ^{239}Pu . This is because the neutron spectrum shifts to higher energy by the elevation of graphite temperature and fission reaction rate due to resonance of ^{239}Pu increases as shown in Fig. 4.35. Shifting of the neutron spectrum decreases neutron absorption by Xe, which also

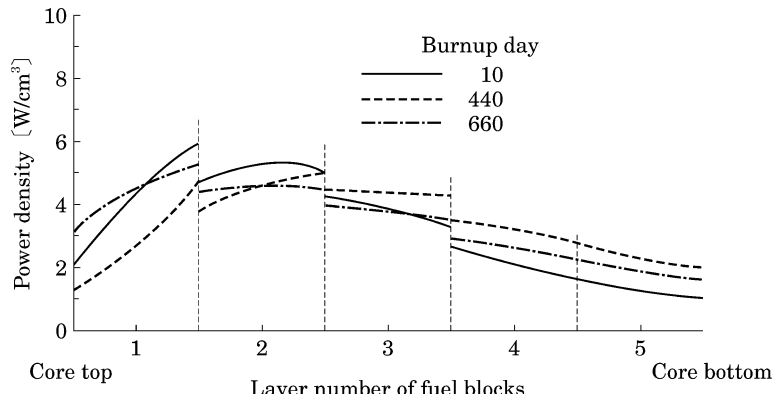


Fig. 4.36 Axial power distribution

possibly leads to a positive moderator temperature coefficient. Even if the moderator temperature coefficient is positive, the combined reactivity coefficient (combination of Doppler and moderator temperature coefficients) is kept negative for the entire operating region. Thus, inherent safety is ensured.

(4) Power distribution

The calculated axial power distribution is shown in Fig. 4.36. At the beginning of the burnup period, the power is relatively high in the core upper region having higher uranium enrichment and it is relatively low at the core lower region. The power density at the upper region gradually decreases with burnup. The control rods are gradually withdrawn from about 440 days and then the power density at the upper region increases again. Since such top peak distribution is achieved throughout the burnup period, the maximum fuel temperature is kept below the limit.

(5) Burnup

In order to achieve high burnup of spent fuel, it is better to increase the number of refueling batches. In the FSV reactor where the refueling method with multiple batches was adopted, the radial peaking factor was high because the fresh fuel columns were adjustment to the burnt fuel columns. The HTTR, which was aimed at achieving a high outlet gas temperature of 950 °C could not adopt the same multiple batch refueling method as of the FSV because such a method causes high fuel temperature in fresh fuel column. In the HTTR, all the fuel blocks are replaced at the same time (one batch method). As a result, the maximum burnup of spent fuel is 33G Wd/t which is lower than those of other types of HTGRs. For the commercial deployment of the block type HTGRs, the burnup of spent fuel should be increased by the axial fuel shuffling method [46]. In this method, an axially exponential power distribution can be achieved by loading the fresh fuel in the core upper region and the burnt fuel in the lower region.

4.2.5 Thermohydraulic Design

In the thermohydraulic design of the HTTR (see Fig. 4.26), the fuel temperature is calculated based on the power distribution from the nuclear design, the primary coolant flow rate, the engineering hot spot factors and the geometry of the fuel block.

The core components such as the fuel blocks, replaceable reflector blocks and control rod guide blocks have different heat generation. The fuel blocks also have different powers according to their uranium enrichment and loading position. Thus, the adequate core coolant flow rate which directly contributes to cooling the fuel is ensured. The coolant is distributed to each fuel block to keep the maximum fuel temperature as low as possible during normal operation.

[1] Thermohydraulic design codes

The thermohydraulic design consists of the flow distribution calculation and the resulting fuel temperature calculation (see Fig. 4.26). Since the HTTR core is formed by piling up the hexagonal graphite blocks, it is necessary in the fuel temperature calculation to consider not only the coolant flow in the cooling hole which directly contributes to cooling the fuel but also the coolant flow not directly contributing to fuel cooling such as the horizontal cross flow between the piled blocks, the gap flow between the columns, etc.

(1) Flow distribution calculation

The FLOWNET code [47] based on the flow network model is used for the flow distribution calculation. The coolant flow paths in the core are modeled as channels having equivalent length, area and hydraulic diameter. The flow channels are connected by equivalent paths of thermal conductivity. The channel data and heat transfer coefficient, etc. which have been measured beforehand by the hydraulic tests with the same scale as the actual core are conservatively corrected and adopted to the calculation.

The 1/6 core is modeled in the flow distribution calculation by considering the symmetry of the core [28]. The radial and axial flow network models are shown in Fig. 4.37. A column is modeled as a single flow channel. The flow channels including the gap flow paths are connected by horizontal flow paths and thermal conduction. The graphite blocks shrink due to neutron irradiation, which is taken into account for the gap size.

(2) Fuel temperature calculation

The fuel temperature is calculated based on the power distribution from the nuclear design and the coolant flow distribution from the flow distribution calculation considering the thermal conductivity of the fuel blocks and the engineering hot spot factors [48, 49]. The fuel temperature analysis code TEMDIM [50] is used. The core is represented by multi cylindrical channels, and the 2D temperature distribution and thermal deformation of each channel are calculated. Finally, the maximum fuel temperature is obtained by considering the engineering hot spot factors.

The calculation model of fuel rod is a cylindrical model which consists of fuel compacts, the gap between the fuel compact and the graphite sleeve,

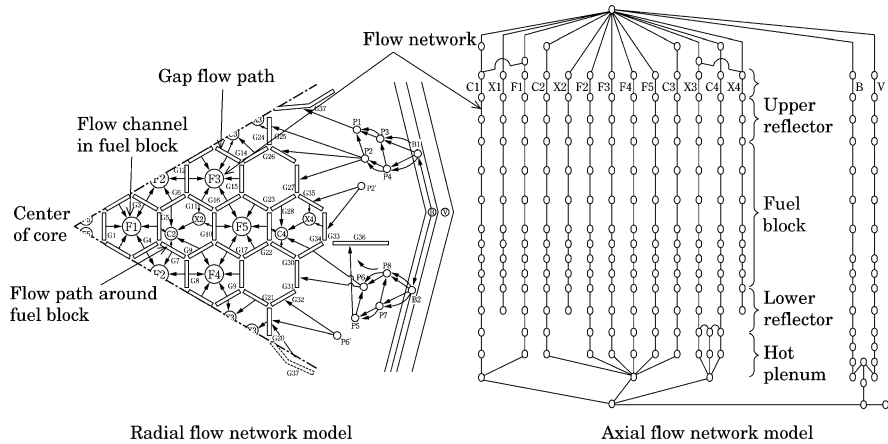


Fig. 4.37 Calculation model for coolant flow distribution in core

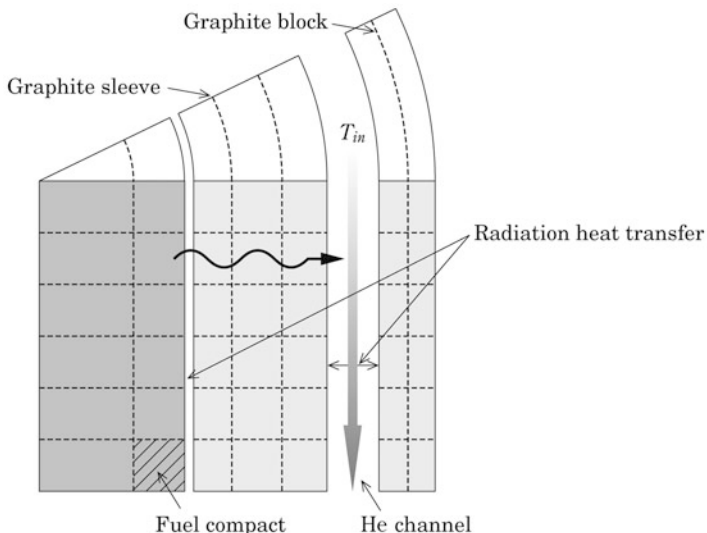


Fig. 4.38 Fuel temperature calculation model

the graphite sleeve, the coolant flow paths and the graphite block as shown in Fig. 4.38. The fuel rod is divided by radial and axial meshes. The power distribution from the nuclear design is corrected by considering the local power peaking and used for the fuel temperature calculation.

The nominal maximum fuel temperature is calculated based on the power distribution from the nuclear design and the coolant flow distribution. Based on this nominal temperature, the systematic maximum fuel temperature is evaluated using the engineering hot spot factors i.e. the random factors and the systematic factors [51]. The thermohydraulic design

must be made so that the systematic maximum fuel temperature does not exceed the allowable design limit (1,495 °C) for normal operation as introduced in the list [4] of Sect. 4.2.2.

The fuel temperature at any position is obtained by adding the temperature rises of each component to the inlet coolant temperature. Thus, the nominal temperature T^N of an arbitrary position is calculated as:

$$T^N = T_{in} + \sum_{i=1}^5 \Delta T_i^N \quad (4.27)$$

where

T_{in} : Core inlet coolant temperature (°C)

ΔT_i^N : Nominal temperature rise (°C)

$i = 1$: Coolant

2 : Flim

3 : Sleeve

4 : Gap

5 : Fuel compact

The evaluated maximum fuel temperature is the maximum value of the systematic fuel temperature. The systematic fuel temperature is obtained based on the nominal temperature rises ΔT_i^N , at an arbitrary burnup step and arbitrary region of interest (entire core or each column) considering the engineering hot spot factors, as shown in Eq. (4.28).

$$\begin{aligned} T_f &= T_{in} + \sum_{i=1}^5 \Delta T_i \\ &= T_{in} + \sum_{i=1}^5 \left[\prod_{j=1}^n f_{ij}^s \left\{ \sqrt{\sum_{k=1}^m (f_{ik}^R)^2} + 1 \right\} \right] \cdot \Delta T_i^N \end{aligned} \quad (4.28)$$

where

T_f : Systematic fuel temprature (°C)

ΔT_i : Temperature rise considering engineering hot spot factors (°C)

f_{ij}^s : Systematic factors associated with fuel rod

n : Number of systematic factors

f_{ik}^R : Random factors associated with fuel rod

m : Number of random factor

The maximum fuel temperature at an arbitrary burnup step and arbitrary region of interest is evaluated by Eq. (4.29) based on the systematic temperature:

$$T^{\max} = \text{Max}(T_f) \quad (4.29)$$

where

T^{\max} : Maximum fuel temperature (°C)

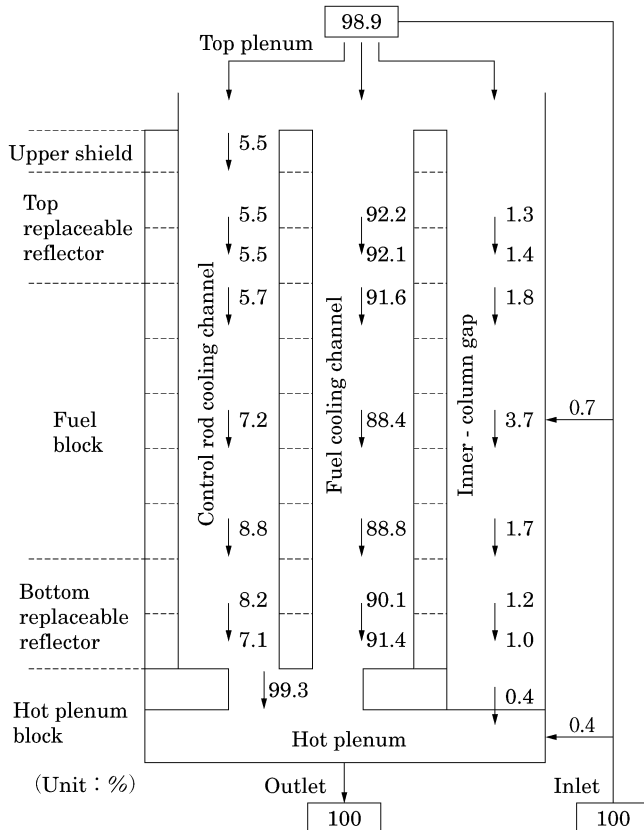


Fig. 4.39 Coolant flow distribution

[2] Overview of thermohydraulic design results of HTTR

The results of the flow distribution calculation for 950 °C operation are illustrated in Fig. 4.39 [28]. As the coolant flow in the core, there are gap flows between the blocks and gap flows between the permanent reflectors as well as the fuel channel flow directly cooling the fuel rods. The coolant flow rate directly contributing to the fuel cooling is about 88 % of the total flow rate. It shows the minimum value at the third block from the top of the fuel region. The flow reduction is occurred at the high temperature region, because the increase in the coolant temperature leads to increases in viscous resistance and hence pressure drop.

The calculated axial fuel temperature distribution is illustrated in Fig. 4.40 [28]. The solid lines indicate the nominal temperatures and the dashed line indicates the systematic temperature at the inner surface of the fuel compact. Since the coolant flow direction is downward, the coolant temperature increases from the top to the bottom. The fuel compact inner surface temperature is

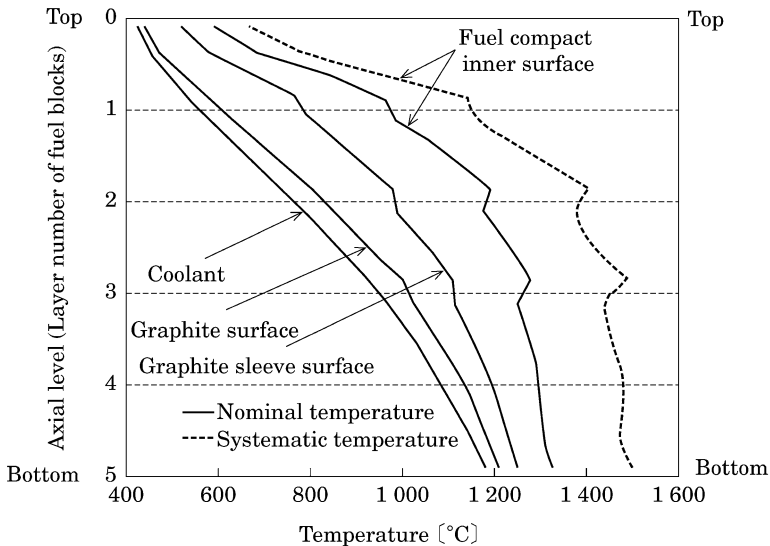


Fig. 4.40 Axial temperature distribution

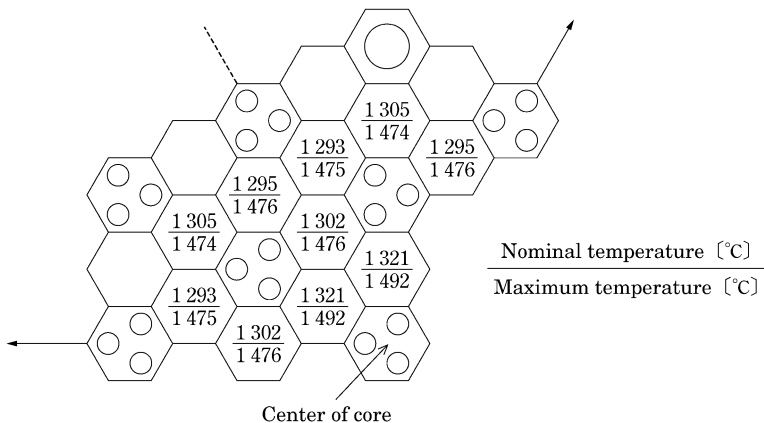
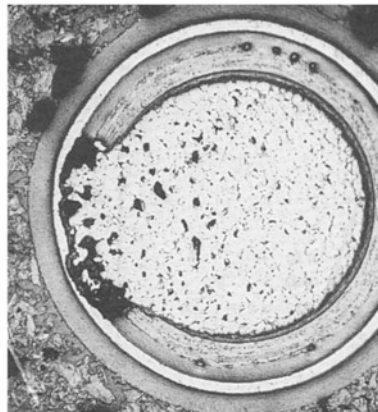


Fig. 4.41 Maximum temperatures of fuel columns at 950 °C operation

almost constant below the third layer. That is because the increase in the coolant temperature and the decrease in the power density along the axial direction cancel out each other.

The maximum fuel temperatures of each fuel column are shown in Fig. 4.41. This figure gives the maximum fuel temperature within the burnup period. The highest maximum temperature appears at the core inner region and it is 1,492 °C, which is below the limit of 1,495 °C for normal operation and does not reach the limit of 1,600 °C at anticipated abnormal occurrences. Thus, the thermal design limit is satisfied.



(Irradiation temperature : 1 690°C (Temperature gradient:164°C/cm),
Irradiation period: 84 days) ⁴⁹⁾

Fig. 4.42 Corrosion of coating layer by amoeba effect

4.2.6 Mechanical Design

In order to realize the core design, the mechanical design must be realized as well as the nuclear and thermohydraulic designs. In this section, the mechanical design of the fuel rod and the fuel block is described [52].

[1] Fuel rod

The fuel rod design must ensure integrity considering production and release of FPs, thermal expansion, irradiation creep, etc. The following conditions must be satisfied at normal operation and anticipated operational occurrences.

- (i) The failure fraction of the coating layers at fabrication must be made below a certain limit in order to avoid the release of FPs from the coated particle fuels. In the HTTR design, the limit is set as 0.2 % and the fraction of through-damaged particles of $2 \times 10^{-4} \%$ is achieved in the actual fabrication [53].
- (ii) In order to avoid failure of the coating layers, corrosion of the SiC layer caused by palladium, and degradation of the coating layers caused by migration of the fuel kernel, the maximum fuel temperature is kept below 1,600 °C. As already shown in Fig. 4.19, the failure fraction of the coating layers increases when the fuel temperature exceeds 1,800 °C. Migration of the fuel kernel is caused by its encroaching upon the coating layers along the temperature gradient; this is called the amoeba effect. The cross section of a coated particle fuel exhibiting the amoeba effect is shown in Fig. 4.42 [54]. Its mechanism is based on the following chemical formula.



At high temperature, the excess oxygen in the fuel kernel produces CO by reacting with the carbon in the low density PyC layer (first layer). At low temperature, the CO decomposes into C and CO₂, so that C accumulates there. Through the products of these reactions, the fuel kernel is pushed towards cracks formed at high temperature. The coated particle fuels are designed so that the fuel kernel does not reach the SiC layer.

- (iii) Cracking of the fuel rod by thermal expansion or irradiation deformation, which may threaten its structural integrity by mechanical interaction between the fuel compact and the graphite sleeve, is avoided. To do that, an adequate gap between the fuel compact and the graphite sleeve is provided in their fabrication.

[2] Fuel block

The following conditions must be satisfied for the fuel block.

- (i) The integrity of the fuel block must be maintained against loads during normal operation and anticipated operational occurrences. The sum of the loads to the graphite block and the stresses caused by the temperature gradient and irradiation deformation must be below the allowable stress of graphite.
- (ii) The gap between the fuel blocks needs to be as small as possible in order to reduce the coolant flow rate which is not contributing to fuel cooling. At the same time, the layout of the fuel blocks needs to be designed so that the refueling space is ensured.

4.2.7 Annular Core Design

The coolant depressurizes to atmospheric pressure due to a pipe break in the case of a primary coolant depressurization accident of HTGRs. In such case, it is difficult to remove the residual heat by using the primary cooling system because the air entering from pipe break may oxidize the graphite in the reactor. Therefore, the residual heat is conducted to the reactor vessel outer surface and is removed by the passive reactor vessel cooling system. This method has high inherent safety due to no use of active systems. However, the available reactor thermal power for removing the residual heat is about 200 MW. This is not large enough and not economical. From that background, the annular core in which fuel blocks at the core center region are replaced by graphite blocks was proposed for reducing the maximum fuel temperature which appeared in the core center as shown in Fig. 4.43 [55]. By taking advantage of its capability to enlarge the thermal power, originally proposed by K.Yamashita [55], the annular core with the thermal power of 600 MW was designed while keeping the inherent safety [56].

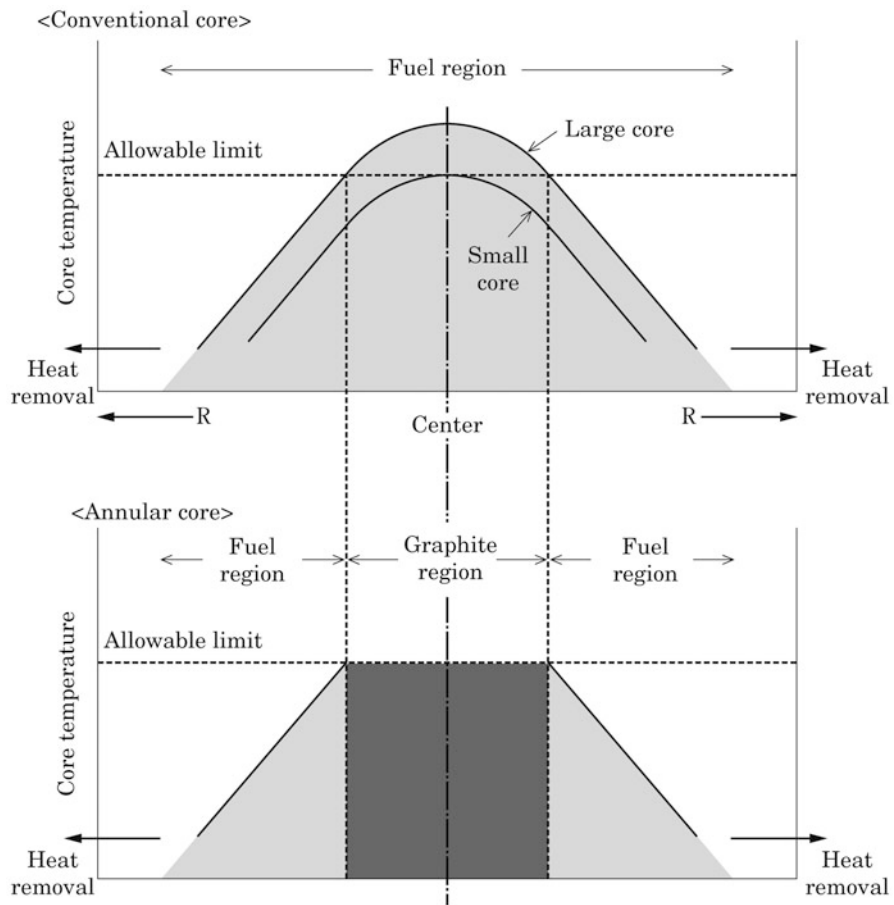


Fig. 4.43 Principle of keeping low fuel temperature of annular core at accident

The calculated results of a primary coolant depressurization accident for that design are shown in Fig. 4.44 [57]. The maximum fuel temperature appearing 70 h after the initiation of the accident was calculated as 1,595 °C which is below the limit of 1,600 °C. Thus, it was ensured that the additional failure of the coated particle fuels does not occur.

To calculate the fuel temperature of the annular core during accidents, thermal analysis codes such as TAC-NC are used. The TAC-NC code considers radiation heat transfer in the cooling holes and the gap between fuel blocks, natural convection in those spaces, etc.

Exercises of Chapter 4

1. Design a fast reactor core with an electric power of 1,000 MW under the following conditions.

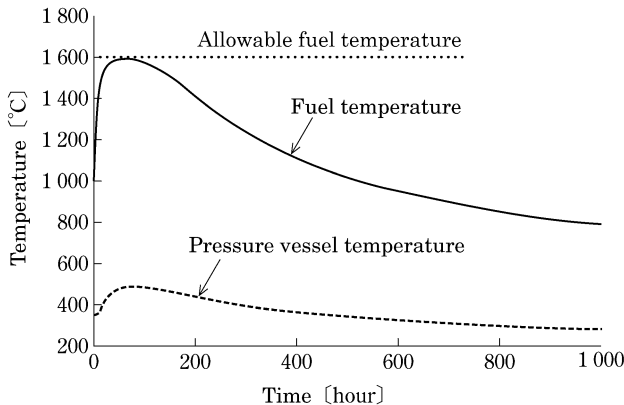


Fig. 4.44 Fuel temperature of annular core (600 MW) at primary coolant depressurization accident

- (i) Reactor thermal power: 2,500 MWt
 - (ii) Power fraction of core fuel: 92 %Power fraction of blanket fuel: 8 %
 - (iii) Average linear heat generation rate: 230 W/cm
 - (iv) Core height: 100 cm
 - (v) Number of fuel elements per assembly: 271
 - (vi) Radial blanket region 2 layers
2. Estimate the average discharged burnup of the core fuel after operating the reactor designed in problem 1 for 24 months. Assume MOX fuel and a dispersed refueling method with 3 batches. Other conditions are as below.
- (i) Diameter of fuel element: 8.5 mm
 - (ii) Clad thickness: 0.4 mm
 - (iii) Smear density of fuel (ρ_s): 9.5 g/cm³
3. Calculate the fuel centerline temperature of a fast reactor when the pellet surface temperature is 900 °C and the linear heat generation rate is 400 W/cm. Assume a constant thermal conductivity of 0.023 W/(cm•°C) in the fuel pellet without temperature dependency.
4. Explain the reason and the major limiting factors of flow distribution design in fast reactors.

References

1. Japanese translation by M. Narita, F. Fujita published from Gendaiougakusha Tokyo (1980), Duderstad JJ, Hamilton LJ (1976) Nuclear reactor analysis. John Wiley & Sons, inc. (in Japanese)
2. Ann S (1985) Fast breeder reactor. Dobunshoin, Tokyo (in Japanese)
3. Walter AE, Reynolds AB (1981) Fast breeder reactors. Pergamon Press, New York

4. Akahori M et al (2007) Nuclear handbook. Ohmsha, Tokyo (in Japanese)
5. Miki R (1972) Fast breeder reactors. Nikkan Kogyo Shimbun Ltd, Tokyo (in Japanese)
6. MONJU (2006) Update of licensing application report of "MONJU" (in Japanese)
7. PNC (1984) Technical report, No. 9, 51 (in Japanese)
8. Izumi K, Osada H, Hasegawa Y (1986) MHI technical report. No. 6, 23 (in Japanese)
9. Yuhara S (1992) Fundamental engineering course of fast breeder reactor: 14. Fundamental data base. Nucl Eng 6:68–79 (in Japanese)
10. Nakae N et al (1985) PNC technical report. No. 6, 70 (in Japanese)
11. Shibata K et al (2002) Japanese evaluated nuclear data library version 3 revision-3: JENDL-3.3. J Nucl Sci Technol 39:1125–1136
12. Zukeran A et al (1976) Mockup critical experiments for prototype fast breeder reactor "MONJU". J At Energy Soc Jpn 18(11):672–684 (in Japanese)
13. Mita T et al (1989) Outline of JUPITER-III program. J At Energy Soc Jpn 31(12):16–23 (in Japanese)
14. Mizoo N et al (1989) Fundamental engineering course of fast breeder reactor: 1. Outline of fast breeder reactor engineering. Nucl Eng 3:59–67 (in Japanese)
15. Japan Atomic Energy Relations Organization (1988) Materials for PR of FBR 1/2. (in Japanese)
16. Denki Shinbun (2009) The Nuclear Pocket Book Version 2009. (in Japanese)
17. Hayashi H, Yanagisawa T (2007) Fast breeder reactor: the past, the present and the future: (2) Changes of fast breeder reactor concept. J At Energy Soc Jpn 49(8):34–42 (in Japanese)
18. Asada T et al (1995) Nuclear handbook. Ohmsha, Tokyo (in Japanese)
19. Konomura M et al (2004) JNC technical report. No. 24, Supplement 2004.11, pp 47 (in Japanese)
20. Kanda M et al (2009) Nuclear power plant engineering. Ohmsha, Tokyo (in Japanese)
21. Stansfield O (1991) Evolution of HTGR coated particle fuel design. Energy 16(1/2):33–45
22. Fujimoto N (2006) Research on improvement of nuclear characteristic evaluation method for High Temperature Engineering Test Reactor (HTTR). JAEA-Review 2006-038 (in Japanese)
23. Ziermann E (1990) Review of 21 years of power operation at the AVR experimental nuclear power station in Jülich. Nucl Eng Des 121:135–142
24. Bäumer R et al (1990) Construction and operation experience with the 300-MW THTR nuclear power plant. Nucl Eng Des 121:155–166
25. Zhang Z, Yu S (2002) Future HTGR developments in China after the criticality of the HTR-10. Nucl Eng Des 218:249–257
26. Matzner D (2004) PBMR Project status and the way ahead. In: 2nd International topical meeting on high temperature reactor technology. Beijing, September, pp 22–24
27. Fort St (1970) Vraine nuclear generation station final safety analysis report, Docket-50267. Public Service Company of Colorado, Colorado
28. Saito S et al (1994) Design of high temperature engineering test reactor (HTTR), JAERI 1332
29. Yamashita K et al (2000) Startup core physics tests of High Temperature Engineering Test Reactor (HTTR): I. Test plan, fuel loading and nuclear characteristics tests. J At Energy Soc Jpn 42(1):30–42 (in Japanese)
30. Fujikawa M et al (2002) Rise-to-power test of the HTTR (High Temperature Engineering Test Reactor). Trans At Energy Soc Jpn 1(3):361–372 (in Japanese)
31. Fukuda K et al (1989) Research and development of HTGR fuels. JAERI-M 89-007 (in Japanese)
32. Hayashi K et al (1989) Assessment of fuel integrity of the High Temperature Engineering Test Reactor (HTTR) and its permissible design limit. JAERI-M 89-162 (in Japanese)
33. Yamashita K, Maruyama S et al (1992) Optimization of power distribution to achieve outlet gas-coolant temperature of 950 °C for HTTR. J Nucl Sci Tech 29(5):472–481
34. Yasuno T et al (1979) Design studies for the Mark-III core of experimental multi-purpose VHTR. JAERI-M 8399 (in Japanese)

35. Yamashita K (1994) Optimization method of Rod-Type Burnable Poisons for nuclear designs of HTGRs. *J Nucl Sci Tech* 31(9):979–985
36. Yamashita K et al (1996) Nuclear design of the high-temperature engineering test reactor (HTTR). *Nucl Sci Eng* 122:212–228
37. Fujimoto N et al (2004) Nuclear design. *Nucl Eng Des* 233:23–36
38. Shindo R et al (1990) DELIGHT-7: one dimensional cell burnup code for High Temperature Gas-Cooled Reactors (HTGR). JAERI-M 90–048 (in Japanese)
39. Latherop et al KD (1973) TWOTRAN-II: An interfaced exportable version of the TWOTRAN code for two-dimensional transport, LA-4848-MS. Los Alamos National Laboratory, Los Alamos
40. Harada H, Yamashita K (1989) The reactor core analysis code CITATION-1000VP for high temperature engineering. JAERI-M 89–135 (in Japanese)
41. Fowler TB et al (1971) Nuclear reactor core analysis code: CITATION, ORNL-TM-2496
42. Yasuda H et al (1990) Construction of VHTRC (Very high temperature reactor critical assembly), JAERI-1305
43. Yamashita K et al (1988) JAERI-M 88–245 (in Japanese)
44. Fujimoto N et al (2004) Validation of the nuclear design code system for the HTTR using the criticality assembly VHTRC. *Nucl Eng Des* 233:155–162
45. Yamashita K et al (1992) Analysis of overall temperature coefficient of reactivity of the VHTRC-1 core with a nuclear design code system for the high temperature engineering test reactor. *Nucl Sci Eng* 10:177–185
46. Yamashita K (1995) Upgrading of block type HTGRs' core with axial fuel shuffling. *J At Energy Soc Jpn* 37(3):213–216 (in Japanese)
47. S Maruyama et al (1988) Verification of in-vessel thermal and hydraulic analysis code FLOWNET. JAERI-M 88–138 (in Japanese)
48. Maruyama S et al (1988) Core thermal and hydraulic design of high temperature engineering test reactor (HTTR). JAERI-M 88–255 (in Japanese)
49. Maruyama S et al (1993) Evaluation of hot spot factors for thermal and hydraulic design of HTTR. *J Nucl Sci Tech* 30(11):1186–1194
50. Maruyama S et al (1988) Verification of fuel temperature analysis code TEMDIM. JAERI-M 88–170 (in Japanese)
51. Maruyama S et al (1988) Determination of hot spot factors for calculation of the maximum fuel temperatures in the core thermal and hydraulic design of HTTR. JAERI-M 88–250 (in Japanese)
52. Safety Analyses report of "HTTR" (1989, 1990) (in Japanese)
53. Sawa K, Tobita T, Mogi H, Shiozawa S, Yoshimuta S, Suzuki S, Deushi K (1999) Fabrication of the first-loading fuel of the high temperature engineering test reactor. *J Nucl Sci Technol* 36:683–690
54. Fukuda K et al (1989) Research and development of HTGR fuels. JAERI-M 89-007:264 (in Japanese)
55. Yamashita K (1983) A new HTR conception for a modular system with block-fuel elements and its comparison with an HTR with ball-shaped fuel elements. Jülich-1842, Kernforschungsanlage Jülich GmbH
56. Kunitomi K et al (2002) Design study on Gas Turbine High Temperature Reactor (GTHTR300). *Trans At Energy Soc Jpn* 1(4):352 (in Japanese)
57. Katanishi S, Kunitomi K (2007) Safety evaluation on the depressurization accident in the gas turbine high temperature reactor (GTHTR300). *Nucl Eng Des* 237(12–13):1372–1380

Answers for Exercises

Chapter 1

1. The burnup equations of ^{235}U and ^{239}Pu can be given by

$$\frac{dN^{25}(t)}{dt} = -\sigma_a^{25}\phi N^{25}(t)$$

$$\frac{dN^{49}(t)}{dt} = \sigma_c^{28}\phi N^{28} - \sigma_a^{49}\phi N^{49}(t)$$

For an initial condition of $N^{49}(0) = 0$, the atomic densities of ^{235}U and ^{239}Pu are obtained as

$$N^{25}(t) = N^{25}(0)e^{-\sigma_a^{25}\phi t}$$

$$N^{49}(t) = \frac{\sigma_c^{28}N^{28}}{\sigma_a^{49}}(1 - e^{-\sigma_a^{49}\phi t})$$

(Graph skip)

2. The production and destruction equations of ^{135}I and ^{135}Xe after changing neutron flux to ϕ_1 can be solved by using the equilibrium-state solutions at neutron flux ϕ_0 as initial conditions. The atomic densities of ^{135}I and ^{135}Xe can be obtained as

$$I(t) = \frac{\gamma_I \bar{\Sigma}_f}{\lambda_I} \{ \phi_0 e^{-\lambda_I t} + \phi_1 (1 - e^{-\lambda_I t}) \}$$

$$X(t) = \frac{(\gamma_I + \gamma_{Xe}) \bar{\Sigma}_f \phi_0}{\lambda_{Xe} + \bar{\sigma}_a^{Xe} \phi_0} e^{-(\lambda_{Xe} + \bar{\sigma}_a^{Xe} \phi_1)t} + \frac{(\gamma_I + \gamma_{Xe}) \bar{\Sigma}_f \phi_1}{\lambda_{Xe} + \bar{\sigma}_a^{Xe} \phi_1} (1 - e^{-(\lambda_{Xe} + \bar{\sigma}_a^{Xe} \phi_1)t}) \\ + \frac{\gamma_I \bar{\Sigma}_f (\phi_1 - \phi_0)}{\lambda_{Xe} + \bar{\sigma}_a^{Xe} \phi_1 - \lambda_I} (e^{-(\lambda_{Xe} + \bar{\sigma}_a^{Xe} \phi_1)t} - e^{-\lambda_I t})$$

where t represents time after the neutron flux change.

(Graph skip)

3. Skip
4. Skip
5. By the one-group first-order perturbation theory

$$\rho = \frac{(\nu\delta\bar{\Sigma}_f - \delta\bar{\Sigma}_a) \left[\int_{-L/12}^{L/12} \cos^2\left(\frac{\pi x}{L}\right) dx \right]^3}{\nu\bar{\Sigma}_f \left[\int_{-L/2}^{L/2} \cos^2\left(\frac{\pi x}{L}\right) dx \right]^3} = \frac{\nu\delta\bar{\Sigma}_f - \delta\bar{\Sigma}_a}{\nu\bar{\Sigma}_f} \left(\frac{1}{2\pi} + \frac{1}{6} \right)^3$$

The perturbation parts can be expressed in terms of temperature coefficient as

$$\delta\bar{\Sigma}_f = \frac{\partial\bar{\Sigma}_f}{\partial T} \Delta T = \bar{\Sigma}_f \left(a\alpha_{T_n}^{g_f} - \frac{1}{2T} - 3\theta \right) \Delta T$$

$$\delta\bar{\Sigma}_a = \left(\frac{\partial\bar{\Sigma}_a^F}{\partial T} + \frac{\partial\bar{\Sigma}_a^M}{\partial T} \right) \Delta T = \left\{ \bar{\Sigma}_a^F a\alpha_{T_n}^{g_F} + \bar{\Sigma}_a \left(-\frac{1}{2T} - 3\theta \right) \right\} \Delta T$$

where θ is the linear expansion coefficient of the medium, and $T_n = aT$ is assumed (T_n is the neutron temperature and T is the medium temperature). Substituting them into the reactivity expression gives

$$\rho = \left\{ a \left(\alpha_{T_n}^{g_F} - \frac{1}{\eta} \alpha_{T_n}^{g_M} \right) - \frac{3\bar{D}}{\nu\bar{\Sigma}_f} \left(\frac{\pi}{L} \right)^2 \left(\frac{1}{2T} + 3\theta \right) \right\} \left(\frac{1}{2\pi} + \frac{1}{6} \right)^3 \Delta T$$

where the criticality condition

$$\nu\bar{\Sigma}_f - \bar{\Sigma}_a = \bar{D}B^2 = 3\bar{D} \left(\frac{\pi}{L} \right)^2$$

is used.

Chapter 2

1. (a) Express atomic or molecular mass, density, and atomic number density as M , ρ (g/cm³), N (#/cm³) respectively. ²³⁵U enrichment (wt%) can be calculated as

$$\frac{N(^{235}\text{U})M(^{235}\text{U})}{N(^{235}\text{U})M(^{235}\text{U})+N(^{238}\text{U})M(^{238}\text{U})} \times 100 = 3.2 \quad (1.1)$$

According to Eq. (1.1), $N(^{235}\text{U}) : N(^{238}\text{U}) = 1 : 29.868$, namely, the ²³⁵U enrichment is 3.24 atm%.

$$M(\text{U}) = 0.324 \times M(^{235}\text{U}) + (1 - 0.324) \times M(^{238}\text{U}) = 237.075$$

$$M(\text{UO}_2) = M(\text{U}) + 2 \times M(\text{O}) = 269.075$$

$$\begin{aligned} N(\text{U}) &= N(\text{UO}_2) = \rho(\text{UO}_2)/M(\text{UO}_2) \times N_A \\ &= 10.4/269.075 \times (0.6022 \times 10^{24}) = 2.320 \times 10^{22} \text{ atoms/cm}^3 \end{aligned}$$

$$N(^{235}\text{U}) = N(\text{U}) \times 3.24/100 = 7.516 \times 10^{20} \text{ atoms/cm}^3$$

$$N(^{235}\text{U}) = N(\text{U}) \times (1 - 3.24/100) = 2.245 \times 10^{22} \text{ atoms/cm}^3$$

$$N(\text{O}) = N(\text{U}) \times 2 = 4.640 \times 10^{22} \text{ atoms/cm}^3$$

$$\begin{aligned} (\text{b}) \quad \Sigma_a(\text{UO}_2) &= N(^{235}\text{U})\sigma_a(^{235}\text{U}) + N(^{238}\text{U})\sigma_a(^{238}\text{U}) + N(\text{O})\sigma_a(\text{O}) \\ &= (7.516 \times 10^{20}) \times (50 \times 10^{-24}) + (2.245 \times 10^{22}) \\ &\quad \times (1.0 \times 10^{-24}) + (4.640 \times 10^{22}) \times (0.0025 \times 10^{-24}) \\ &= 6.014 \times 10^{-2} \text{ cm}^{-1} \end{aligned}$$

$$\begin{aligned} \Sigma_f(\text{UO}_2) &= N(^{235}\text{U})\sigma_f(^{235}\text{U}) + N(^{238}\text{U})\sigma_f(^{238}\text{U}) \\ &= (7.516 \times 10^{20}) \times (41 \times 10^{-2}) + (2.245 \times 10^{22}) \\ &\quad \times (0.1 \times 10^{-24}) \\ &= 3.306 \times 10^{-2} \text{ cm}^{-1} \end{aligned}$$

The probability that a neutron absorbed in pellet fissions, P_f , can be given by

$$\begin{aligned} P_f &= \Sigma_f(\text{UO}_2)/\Sigma_a(\text{UO}_2) = (3.306 \times 10^{-2})/(6.014 \times 10^{-2}) \\ &= 0.55 = 55\% \end{aligned}$$

(c) The mass of metal uranium included in a pellet, $w(\text{U})$ can be calculated as

$$\begin{aligned} \rho(\text{U}) &= N(^{235}\text{U})/N_A \times M(^{235}\text{U}) + N(^{238}\text{U})/N_A \times M(^{238}\text{U}) \\ &= 9.167 \text{ g/cm}^3 \end{aligned}$$

$$\begin{aligned} w(\text{U}) &= \rho(\text{U}) \times V_P \text{ (pellet volume)} \\ &= 9.167 \times (3.1416 \times (0.81/2)^2 \times 1.0) = 4.72 \text{ g} \\ &= 4.72 \times 10^{-6} \text{ ton} \end{aligned}$$

Initial Uranium Mass Included in a Fuel Assembly = $w(\text{U}) \times 366 \times 265 = 0.46 \text{ ton}$
 Uranium Loading Amount in Core (Metal Uranium Mass) = $0.46 \times 193 = 88 \text{ ton}$

(d) Since the pellet length is 1 cm, the linear power of fuel rod q' (W/cm) is equal to energy released from a pellet. Therefore,

$$\begin{aligned} q' &= \kappa \Sigma_f (\text{UO}_2) \phi V_p \\ &= (200 \times 1.602 \times 10^{-13}) \times (3.306 \times 10^{-2}) \times (3.2 \times 10^{14}) \times 0.515 \\ &= 175 \text{ W/pellet} = 175 \text{ W/cm} \end{aligned}$$

Since $w(\text{U}) = 4.72 \times 10^{-6}$ ton/pellet,

$$\begin{aligned} \text{Specific Power} &= (175 \text{ W/pellet}) / (4.72 \times 10^{-6} \text{ ton/pellet}) = 3.70 \times 10^7 \text{ W/ton} \\ &= 37 \text{ MW/ton} \end{aligned}$$

(e) Since burnup is a time integral of specific power,

$$\text{Burnup} = (36.0 \times 285) + (41.0 \times 290) + (38.0 \times 280) = 32800 \text{ MWd/ton}$$

(f) Total heat generation of pellet is,

$$\begin{aligned} \text{Burnup } 32800 \text{ MWd/ton} \times w(\text{U}) &= 32800 \times (4.72 \times 10^{-6}) \text{ ton/pellet} \\ &= 0.155 \text{ MWd} = 1.34 \times 10^{10} \text{ J.} \end{aligned}$$

The heat generation by uranium (^{235}U and ^{238}U) fission is
 $1.34 \times 10^{10} \text{ J} \times 2/3 = 8.92 \times 10^9 \text{ J.}$

Since the heat release per fission is $200 \times (1.602 \times 10^{-13}) \text{ J/fission}$,
Total number of uranium fission is $8.92 \times 10^9 / (200 \times 1.602 \times 10^{-13}) = 2.78 \times 10^{20}$ fission.

The number of ^{235}U fission is

$$\begin{aligned} (\text{Total number of } \text{uranium fission}) \times \Sigma_f(^{235}\text{U}) / \{\Sigma_f(^{235}\text{U}) + \Sigma_f(^{238}\text{U})\} &= (2.78 \times 10^{20}) \times 0.932 \\ &= 2.60 \times 10^{20} \text{ fission} \end{aligned}$$

Since the amount of ^{235}U decreases by other reactions such as the (n, γ) reaction, the number of ^{235}U absorption reaction is calculated as

$$\begin{aligned} \text{Number of } ^{235}\text{U absorption} &= (\text{Total number of } ^{235}\text{U fissions}) \times \Sigma_a(^{235}\text{U}) / \Sigma_f(^{235}\text{U}) \\ &= (2.60 \times 10^{20}) \times 1.22 \\ &= 3.17 \times 10^{20} \end{aligned}$$

which can be converted to ^{235}U mass as $(3.17 \times 10^{20}) / N_A \times M(^{235}\text{U}) = 0.12 \text{ g.}$

Therefore, ^{235}U decreased by about 0.12 g in a pellet of 32,800 MWd/ton burnup.

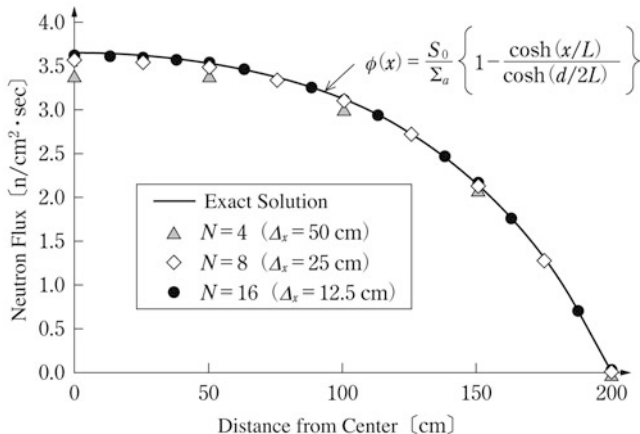
2. For example, for $N = 4$,

$$\begin{cases} a\phi_0 + b\phi_1 + a\phi_2 = S \\ a\phi_1 + b\phi_2 + a\phi_3 = S \\ a\phi_2 + b\phi_3 + a\phi_4 = S \\ \phi_0 = \phi_1 \text{ (Left boundary condition)} \\ \phi_4 = 0.0 \text{ (Right boundary condition)} \end{cases}$$

where

$$\Delta_x \equiv \frac{d/2}{N}, \quad a \equiv \left(\frac{1}{\Delta_x^2} \right), \quad b \equiv \left(\frac{-2}{\Delta_x^2} + \frac{-1}{D/\Sigma_a} \right), \quad S \equiv \left(-\frac{S_0}{D} \right)$$

Substitution of $d/2 = 200$ cm, $D = 1.0$ cm, $\Sigma_a = 2.5 \times 10^{-4}$ cm $^{-1}$, $S_0 = 1.0 \times 10^{-3}$ atoms/cm 2 s gives the following neutron flux distribution.



3. (a) Considering upscattering ($\Sigma_{2 \rightarrow 1}$) as zero,

$$\text{Fast group: } -D_1 V^2 \phi_1 + (\Sigma_{a,1} + \Sigma_{1 \rightarrow 2}) \phi_1 = \frac{\chi_1 (\nu_1 \Sigma_{f,1} \phi_1 + \nu_2 \Sigma_{f,2} \phi_2)}{k_{eff}}$$

$$\text{Thermal group: } -D_2 V^2 \phi_2 + \Sigma_{a,2} \phi_2 = \frac{\chi_2 (\nu_1 \Sigma_{f,1} \phi_1 + \nu_2 \Sigma_{f,2} \phi_2)}{k_{eff}} + \Sigma_{1 \rightarrow 2} \phi_1$$

- (b) For infinite medium, leakage is zero. $x_1 = 1$, $x_2 = 0.0$ give

$$(\Sigma_{a,1} + \Sigma_{1 \rightarrow 2}) \phi_1 = \frac{(\nu_1 \Sigma_{f,1} \phi_1 + \nu_2 \Sigma_{f,2} \phi_2)}{k_{eff}}$$

$$\Sigma_{a,2} \phi_2 = \Sigma_{1 \rightarrow 2} \phi_1$$

which can be rewritten as

$$\begin{aligned} k_\infty &= \frac{\nu_1 \Sigma_{f,1} \phi_1 + \nu_2 \Sigma_{f,2} \phi_2}{\Sigma_{a,1} \phi_1 + \Sigma_{a,2} \phi_2} = \frac{\text{Total Production Rate}}{\text{Total Absorption Rate}} \\ &= \frac{\nu_1 \Sigma_{f,1} + \nu_2 \Sigma_{f,2} (\Sigma_{1 \rightarrow 2} / \Sigma_{a,2})}{\Sigma_{a,1} + \Sigma_{1 \rightarrow 2}} = 1.318 \end{aligned}$$

4. Assuming the atomic densities of ^{135}I and ^{135}Xe as N^{I} and N^{Xe} , their variations with burnup time can be given by

$$\frac{dN^{\text{I}}}{dt} = \gamma^{\text{I}} \Sigma_f \Phi - \lambda^{\text{I}} N^{\text{I}}$$

$$\frac{dN^{\text{Xe}}}{dt} = \lambda^{\text{I}} N^{\text{I}} + \gamma^{\text{Xe}} \Sigma_f \Phi - (\lambda^{\text{Xe}} + \sigma_a^{\text{Xe}} \Phi) N^{\text{Xe}}$$

where λ^{I} and λ^{Xe} are the decay constants and Φ is one-group collapsed neutron flux.

Assuming $\sigma_0^i \approx 0$, the equilibrium atomic densities are obtained as

$$N_{\infty}^{\text{I}} = \frac{\gamma^{\text{I}} \Sigma_f \Phi}{\lambda^{\text{I}}}$$

$$N_{\infty}^{\text{Xe}} = \frac{\lambda^{\text{I}} N_{\infty}^{\text{I}} + \gamma^{\text{Xe}} \Sigma_f \Phi}{\lambda^{\text{Xe}} + \sigma_a^{\text{Xe}} \Phi} = \frac{(\gamma^{\text{I}} + \gamma^{\text{Xe}}) \Sigma_f \Phi}{\lambda^{\text{Xe}} + \sigma_a^{\text{Xe}} \Phi}$$

Assuming $\Phi \gg \lambda^{\text{Xe}} / \sigma_a^{\text{Xe}} = 7 \times 10^{12} \text{ n/cm}^2 \text{s}$, N_{∞}^{Xe} can be expressed as

$$N_{\infty}^{\text{Xe}} = \frac{(\gamma^{\text{I}} + \gamma^{\text{Xe}}) \Sigma_f}{\sigma_a^{\text{Xe}}}$$

$$5. \quad \frac{\partial(\rho h)}{\partial t} + \frac{\partial(\rho u h)}{\partial z} = \frac{P_e}{A} q'' - \frac{N_f}{N_w A_w} Q_w$$

where N_f is the number of fuel rods, and N_w is the number of water rods, and A_w is the cross-sectional area of water rod (m^2).

$$6. \quad \frac{\partial \rho_i}{\partial t} + \frac{\rho_i u_i - \rho_{i-1} u_{i-1}}{\Delta z} = 0$$

$$\frac{\partial(\rho_i h_i)}{\partial t} + \frac{\rho_i u_i h_i - \rho_{i-1} u_{i-1} h_{i-1}}{\Delta z} = \frac{P_e}{A} q_i''$$

$$\frac{P_{i-1} - P_i}{\Delta z} = \frac{\partial(\rho_i u_i)}{\partial t} + \frac{\rho_i u_i^2 - \rho_{i-1} u_{i-1}^2}{\Delta z} + \rho_i g \cos \theta + \frac{2f_i}{D_h} \rho_i u_{i-1}^2$$

$$\rho_i = \rho_i(P_i, h_i)$$

Chapter 3

1. The advanced standardization of LWRs has had the goal of improvements in reliability and availability, and reduction in exposure of radiation workers.

The first stage of advanced standardization in Japan took place from 1975 to 1977. In BWRs, there were improvements in the shape of the containment vessel head, security of maintenance space such as for the main steam isolation valve, and workability. Efforts were also made for reliability improvement by measures against stress corrosion cracking, automation of in-service inspection (ISI), and more efficient inspection (using remote and automatic techniques). In PWRs, *high tensile strength steel* for the containment vessel and the *prestressed concrete containment vessel* (PCCV) were developed. As a measure against fuel rod bowing for reliability improvement, the number of fuel rod grid spacers was increased from 8 to 9. *The eddy current technique* was developed to measure leakage from steam generator tubes, and improvements in its inspection accuracy and efficiency were made.

The second stage of advanced standardization was implemented from 1978 to 1980. There were improvements in operation and maintenance, efficient and regular inspections, and reduction in exposure of radiation workers.

The third stage was carried out from 1981 to 1985. The goals dealt with load following, longer cycle length, core performance improvements, more compact plant size, and shorter construction time. ABWRs and APWRs were developed. Internal pump, improved control rod drive mechanism, reinforced concrete containment vessel, high burnup fuel, and large-size turbine were developed and adopted in ABWRs.

The table presents an overview of the advanced standardization plan of LWRs.

	Improvements		
	PWR	BWR	SSC-resistant material (against fuel bowing)
Previous plant (800 and 1,100 MW class)	standard plant (800 and 1,100 MW class)	standard plant (800 and 1,100 MW class)	standard plant (1,300 and 1,500 MW class)
Availability factor	Depends on plant ~75 %	~80 %	SSC-resistant material (against fuel bowing)
Capacity factor	Depends on plant ~70 %	~75 %	Core design improvement
Regular inspection period	90–100 days	~85 days	Development of integrated reactor vessel head material Improvement of fuel inspection system
Worker exposure	(100 %) ~75 %	~50 %	Development of steam generator, Manipulator, mounter Improvement of Nozzle cap for steam generator water chamber
			Containment improvement

Source: Department of Nuclear Power Plant (1999) Agency for Natural Resources and Energy: nuclear handbook, 385

2. Calculation examples of 10×10 fuel specifications are as follows.

(a) Size Specifications of Water Rod

An approximate fuel rod pitch of 10×10 fuel assembly: $134/10 = 13.4$ mm. In the case that four rods are replaced with a large-diameter water rod in the same way of Step II fuel, if the water rod outer diameter and thickness are set as 26 mm, which is twice of the fuel rod arrangement, and 1.5 mm respectively, the cross-sectional area in two water rods is $2 \times (23)^2 \times \pi/4 = 831 \text{ mm}^2$. Thus, a non-boiling region larger than that of Step II fuel can be secured within channel box.

(b) Fuel Rod Specifications

The number of fuel rods becomes 92 excluding eight fuel rods which were replaced with two water rods.

The cross-sectional area of pellets in 60 fuel rods at Step II fuel can be obtained as

$$\text{Spellet} = \pi \times (10.4)^2 / 4 \times 60 = 5097 \text{ mm}^2$$

To maintain the same fuel inventory as Step II fuel, the pellet diameter will be

$$\text{Pellet Diameter} = (4\text{Spellet}/92/\pi)^{1/2} = 8.40 \text{ mm}$$

The cladding inner diameter will be given by applying the same gap between pellet and cladding as 0.18 mm of Step II fuel as

$$\text{Cladding Inner Diameter} = 8.40 + 0.18 = 8.58 \text{ mm}$$

Assuming the cladding thickness as 0.65 mm to maintain the same ratio between cladding thickness and cladding inner diameter, the cladding outer diameter will be

$$\text{Cladding Outer Diameter} = 8.58 + 2 \times 0.65 = 9.88 \text{ mm}$$

(c) Non-Boiling Region Area within Channel Box

Cross-sectional area of fuel rods and water rods within channel box is

$$= 92 \times (9.88)^2 \times \pi/4 + 2 \times (26)^2 \times \pi/4 = 8115 \text{ mm}^2$$

Cross-sectional area of non-boiling region within channel box is

$$= 179.3 - 81.1 = 98.1 \text{ cm}^2$$

which is almost the same as 99 cm^2 of Step II fuel.

3. (a) Cycle Burnup = (Specific Power) × (Cycle Length) × Load Factor

$$Bc(12) = 26.2 \times 365 \times 1.0 = 9563 \text{ MWd/t} = 9.563 \text{ GWd/t}$$

- (b) For cycle length = 12 months and discharge burnup = 45 GWd/t, the fuel batch size is given by

$$n(12) = 45 \div 9.563 = 4.7056$$

The core average burnup B_{EOC} can be calculated by the following equation

$$B_{EOC} = (2n - [n]) \times ([n] + 1) \times Bc/2n$$

Substituting $B_c(12)$ and the integer part of $n(12)$ gives

$$B_{EOC} = (2 \times 4.70 - 4) \times 5 \times 9.563 / (2 \times 4.70) = 27.5 \text{ GWd/t}$$

- (c) For cycle length = 15 months, the cycle burnup $Bc(15)$ is given by

$$Bc(15) = Bc(12) \times (15/12) = 11.95 \text{ GWd/t}$$

In the linear reactivity model, the sum of cycle length and discharge burnup has a constant relation in using the same fuel. Therefore, the discharge burnup $Bd(15)$ can be given by

$$Bd(15) = (Bd(12) + Bc(12)) - Bc(15) = 42.6 \text{ GWd/t}$$

The fuel batch size $n(15)$ becomes 3.56. Such a prolongation of operation cycle length with the same fuel decreases the discharge burnup.

4. (a) In BWRs, burnup reactivity decline is compensated by burnable poison (gadolinia) addition, core flow rate control, and control rod operation. Most of the burnup reactivity is controlled by burnable poison (gadolinia) added to pellets. The concentration of gadolinia is designed to be depleted out at EOC for fuel economy. Since BWR cores have negative void reactivity coefficients, the burnup reactivity decline can be compensated by changing the pumping speed of coolant recirculation pumps and increasing the core flow rate, namely, reducing the core void fraction, and by control rod operation as well. From the viewpoint of fuel economy, generally all control rods are designed to be withdrawn at EOC.
- (b) In ABWRs, since the core average void fraction is about 40 %, the void reactivity coefficient at the end of equilibrium cycle is about $-8 \times 10^{-4} \Delta k/k/\% \text{ void fraction}$. Therefore, change of the void fraction to 5 % gives a reactivity variation of about $4 \times 10^{-3} \Delta k/k$.

- (c) At BOC, the excess reactivity is controlled by control rod insertion at a core flow rate slightly lower than the rated one. Since the excess reactivity tends to increase during the first half of the operating cycle, the core flow rate is mainly reduced without moving control rods. When the core flow rate exceeds the range of the flow control, it is recovered by inserting control rods. Since the core reactivity tends to decrease during the latter half of the operating cycle, the core flow rate is increased by adjusting the recirculation flow rate and control rods are withdrawn when the core flow rate exceeds the range of the flow control.

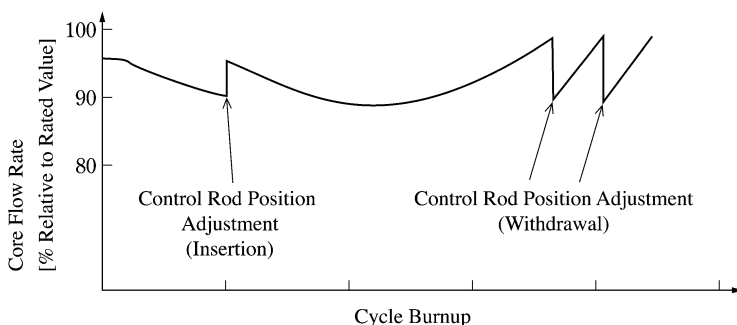


Figure Core flow rate and control rod position adjustment for reactivity control

5. Main challenges for high burnup:

- (a) Nuclear characteristics are changed as fuel enrichment increases; these changes include neutron spectrum hardening, more negative void reactivity coefficient, and control rod worth reduction.
- (b) At high burnup, the reactivity difference between fuel assemblies loaded in the core becomes large and mismatch of the fuel assembly power increases. As fuel enrichment increases, since the number of gadolinia-added fuel rods increases to control the excess reactivity, the local power peaking of a fuel assembly increases and the fuel linear heat generation rate increases.
- (c) The internal pressure of cladding increases.
- (d) The corrosion amount of cladding increases with increase in neutron irradiation and residence time in the core.

Countermeasures:

- (i) Increase in number and size of water rods

As a countermeasure for (a), H/U ratio increase and neutron spectrum softening are general countermeasures. Specially, the number of water rods has been increased to enlarge the non-boiling water region within a channel box and the arrangement of large-diameter water rods and the water channel has been implemented.

(ii) Increase in number of fuel rods

As a countermeasure for (b) and (c), an increase in the number of fuel rods is a general countermeasure. Fuel assemblies of 7×7 , 8×8 , and 9×9 designs have been implemented and the lattice arrangement has also been changed.

(iii) Improvement in corrosion resistance

As a countermeasure for (d), more easily fabricated high corrosion-resistant claddings with better composition have been developed and put into practical use.

(iv) Reduction in pressure drop of fuel assembly

From the viewpoint of fuel economy, items (i) and (ii) without reduction in fuel inventory cause an increase in pressure drop of a fuel assembly. Such an increased pressure drop leads to an increase in coolant pump capacity and less stability, so countermeasures against pressure drop are important. The designs of spacer and top tie plate of low pressure drop, and the use of a partial-length fuel rod have been implemented.

6. The cycle burnup at equilibrium cycle can be calculated as

$$2625/(0.46 \times 157) \times 413 = 15\,170 \text{ MWd/t}$$

The fuel assembly average burnup can be given by

1 Cycle Burned Fuel: 60 assemblies, 15,170 MWd/t

2 Cycle Burned Fuel: 60 assemblies, $15,170 \times 2$ MWd/t

3 Cycle Burned Fuel: 37 assemblies, $15,170 \times 3$ MWd/t

Therefore, the core average burnup at the end of equilibrium cycle is given by

$$(15\,170 \times 60 + 15\,170 \times 2 \times 60 + 15\,170 \times 3 \times 37)/(60 + 60 + 37) \\ = 28\,100 \text{ MWd/t}$$

7. Since the reactivity control by soluble boron in the primary coolant causes waste production, it is desirable that a core design with no use of soluble boron is realized to reduce waste. An idea is that the soluble boron is not to be used during normal operation, and to be used only for backup shutdown. Therefore, the following roles currently taken by soluble boron are needed to be substituted by other means.

- (i) Reactivity variation from cold to hot temperature: about 6 % $\Delta k/k$
- (ii) Reactivity decline during operating cycle: about 10 % $\Delta k/k$ or more
- (iii) Xe reactivity (maximum after shutdown): about 6 % $\Delta k/k$

As an alternative way for reactivity control, roles (i) and (iii) can be done by using control rods, and role (ii) can be done with gadolinia or burnable poison.

(a) Reactivity Controllability Enhancement of Control Rods

Reactivity controllability enhancement of control rods by about 12 % $\Delta k/k$ for (i) and (iii) is necessary which corresponds to three times as much as the current design. Two measures could be applied. One is to enhance the absorption capability of neutron absorbers and the other is to increase the number of rod cluster control assemblies. In the former, even enriched ^{10}B -containing B_4C does not attain twice the reactivity of the current Ag-In-Cd absorber. In the latter, the number of control rod clusters can be increased by a maximum 50 % due to limitation of the current design of the control rod drive mechanism (to increase more, development of a small control rod drive mechanism is needed). Thus, the reactivity controllability can be enhanced at most to twice as much as the current one even applying both measures. Therefore, it is also necessary to reduce the reactivity required for (i) and (iii). But, to realize the reduction, we have to considerably reduce the moderator-to-fuel volume ratio. However, since such a reduction in moderator-to-fuel volume ratio causes a reduction in control rod worth, it is necessary to get a balance between both.

(b) Excess Reactivity Controllability Enhancement by Gadolinia

The number of gadolinia-added fuel rods and fuel assemblies can be increased to control total reactivity corresponding to (ii). However, this is not practically easy because it gives rise to a deterioration of the power distribution. Numerous gadolinia-added fuel cause a higher power increase in high power fuel at early period of burnup because the reactivity increases further as burnup progresses at early period of burnup. This behavior is remarkable in the axial power distribution. The power variation goes into reverse as the burnup proceeds to some extent and then it leads to an oscillation in the axial power distribution as burnup progresses.

Thus, it is quite hard not to use soluble boron. In other words, it is recognized once again that the reactivity control by soluble boron is powerful and superior. By the way, the reactor of the nuclear power ship "Mutsu" was designed to use only control rods without soluble boron. Its control rods were not the cluster type but the cruciform type. The excess reactivity was smaller than that of conventional power plants and the power peaking factor was higher.

8. As shown in Fig. 3.38, the reactor can be controlled only by control rods until hot shutdown. Since the hot temperature condition is maintained for a while after shutdown, the reactivity varies mostly by accumulation and decay of Xe and its variation is compensated by adjusting the boron concentration. After the adjustment of the boron concentration, the criticality is generally attained by control rod withdrawal.

(i) 8 h later

The accumulation of Xe peaks and the reactivity of Xe increases (i.e. the reactivity of core decreases) by about 3 % $\Delta k/k$ (= 3,000 pcm) at 8 h after shutdown. The boron concentration is to be reduced by correspondingly

converting this reactivity (dilution). According to Fig. 3.45, the conversion is about 7 pcm/ppm. The boron concentration is diluted as 3,000/7≈430 ppm. It is noted that the limit of the dilution speed is 10 ppm/min or so, and further the speed becomes slower at low boron concentration. Therefore, it is necessary to start the dilution considerably before the expected criticality time.

- (ii) 20 h later
Accumulation of Xe is over, and it is back to almost the concentration at full power equilibrium (namely, the concentration at shutdown). Therefore, it is not necessary to adjust the boron concentration.
 - (iii) 90 h later
Xenon is almost gone, having decreased by about 3 % $\Delta k/k$ since shutdown. In other words, the boron concentration should be increased by about 430 ppm in the opposite direction to (i).
9. (i) As shown in Fig. 3.35, the boron concentration decrease by 120 ppm is required to move the moderator temperature coefficient to a more negative value by 2 pcm/°C. To realize that, the fuel loading pattern should be re-designed by additionally using 240 burnable poison rods. For example, 12 fuel assemblies containing 20 burnable poison rods can be prepared. However, the increase of 120 burnable poison rods leads to an increase in reactivity penalty at EOC by about 20 ppm (converted value to the soluble boron concentration). It is required to achieve the given cycle length considering the reactivity penalty.
- (ii) The same as in (i), it is necessary to reduce the boron concentration by 120 ppm which is compensated by control rods insertion. The boron worth at BOC is about 7 pcm/ppm from Fig. 3.45. Therefore, the reactivity of $120 \times 7 = 840$ pcm should be suppressed by control rod insertion. In Fig. 3.42, it corresponds to the insertion of control bank D to 50 steps (178 steps for control bank C). In other words, the moderator temperature coefficient can be maintained as negative at hot zero power if control bank D is restricted not to be withdrawn above 50 steps.

Chapter 4

1. Calculate the number of fuel assemblies from core thermal power as

$$\begin{aligned} \text{Total Length of Fuel Elements } (L) &= 2500 \times 10^6 \times 0.92 \div 230 \\ \text{Number of Fuel Elements } (N_{el}) &= L \div 100 \\ \text{Number of Fuel Assemblies } (N_a) &= N_{el} \div 271 \end{aligned}$$

Table 1 Number of assemblies of each layer in hexagonal arrangement

Layer number	Number of assemblies	Cumulative number of assemblies
1	1	1
2	6	7
3	12	19
4	18	37
5	24	61
6	30	91
7	36	127
8	42	169
9	48	217
10	54	271
11	60	331
12	66	397
13	72	469
14	78	547
15	84	631
16	90	721

Then, the number of fuel assemblies is 369.

- Guess the number of control rods (finally determined by evaluating control rod worth)

Set the number of control rods as a multiple of 6 or 3, considering usual symmetric arrangement of control rods. The number of control rods-to-fuel assemblies ratio of 7–10 % gives 30 or 36 control rods. From the viewpoint of control rods cost, the smaller number of control rods is the first candidate.

- Guess core arrangement

Take 397 or 403 fuel and control rod assemblies as a multiple of $6 + 1$. Divide the core into two almost equal volume regions and arrange the fuel assemblies. Consider a symmetric arrangement of control rods for power distribution flattening and place as many of the control rods in the inner core region as possible to increase their reactivity worth.

Table 1 shows the cumulative number of fuel assemblies per each layer when the fuel assemblies are placed in a hexagonal arrangement. Since the control rods are arranged in the inner core region, construct the inner core region using 217 fuel assemblies until the ninth layer and the outer core region with 180 fuel assemblies until the 12th layer. Figure 1 shows the arrangement of assemblies. Consider a uniform and symmetric distribution of 30 control rods. Figure 2 shows a core layout with control rods.

In the core design, the core characteristics (such as power distribution, control rod worth, and reactivity coefficients) are iteratively evaluated by changing the

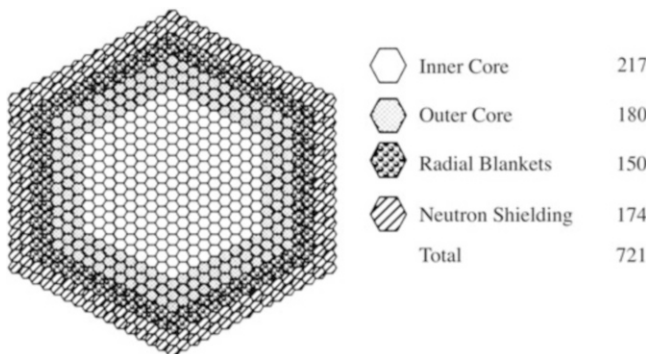


Fig. 1 Arrangement of assemblies

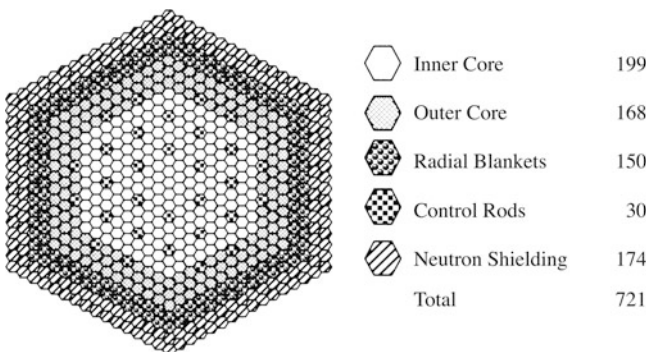


Fig. 2 Example of core layout (1,000 MWe)

core layout and finally the core layout for achieving the design targets are determined.

2. Calculate the fuel loading amount (W) as

$$W = \pi \left(\frac{\text{Cladding Inner Diameter}}{2} \right)^2 \times H_c \times N_e \times N_a \times \rho_s \times \text{Heavy Metal Fraction}$$

$$= 38.78 \text{ t}$$

Compute the burnup as

$$BU = Q \times \text{Core Power Fraction} \times D \times Nb/W$$

$$= 12.99 \times 10^4$$

$$= 130 \text{ GWd/t}$$

3. The relation of pellet temperature, linear power, and thermal conductivity can be given by

$$\chi = 4\pi \int_{T_s}^{T_0} k(T) dT$$

where

χ : Linear power

k : Thermal conductivity

T : Temperature

T_0 : Fuel centerline temperature

T_s : Fuel surface temperature

Assuming a constant thermal conductivity, then

$$k(T_0 - T_s) = \frac{\chi}{4\pi}$$

$$\therefore T_0 = T_s + \frac{\chi}{4\pi k}$$

Therefore, the pellet centerline temperature is calculated as 2,285 °C by

$$T_0 = 900 + \frac{400}{4 \times 3.14 \times 0.023} = 2285 \text{ [°C]}$$

4. The constituent components of fast reactor cores are characterized by fuel assemblies, blanket assemblies, control rod assemblies, and the radial shieldings, all of which produce quite different heats. For effective heat removal, it is necessary to distribute coolant flow rate adequately for each core component corresponding to each heat generation. The coolant flow allocation with no waste flow leads to a high core outlet temperature and high thermal efficiency and contributes to reduction in power generation cost.

In the thermal limitations of the fast reactor core thermal-hydraulic design, there are limits for fuel and cladding temperatures. While the fuel temperature is influenced by linear power of fuel, the cladding temperature is strongly dependent on coolant temperature. For a core flow allocation of fast reactors, therefore, coolant flow rate should be distributed to maintain the maximum cladding temperatures under the design limits for fuel and blanket assemblies at the rated core power. For a design of coolant flow allocation, fuel assemblies requiring nearly equal coolant flow should be classified into same flow allocation group and the number of core flow regions should be minimized in order to avoid complicated coolant flow control mechanism.

Index

A

Abnormal transients, 115–116
Absorption cross sections, 54
ABWR. *See* Advanced BWR (ABWR)
Accidents, 115–116
Adjoint operator, 40
Advanced BWR (ABWR), 152, 169
Advanced PWR (APWR), 209, 212–214
Advanced reactors, 231–301
Ag-In-Cd, 21
Angular neutron flux, 51
Annular core, 299–301
AO. *See* Axial offset (AO)
APWR. *See* Advanced PWR (APWR)
Axially two-zoned fuel, 157
Axial offset (AO), 201

B

Background cross section, 58
Bank, 194
Beginning of the cycle (BOC), 100
Block type, 269
BOC. *See* Beginning of the cycle (BOC)
Boiling transition, 137
Boiling water reactor (BWR), 130–178
Boltzmann equation, 49–51
Boric acid,
 concentration, 19
Boron, 19
Boron carbide, 21
Borosilicate glass, 19
Branching ratio, 66
Branch-off calculation, 69–70
Breeding performance, 238
Breeding ratio, 233, 240
Buildup, 6

Burnable neutron absorber, 19
Burnable poison rod, 178
Burnable poisons, 18–19, 68, 153–154, 197–198
Burnup, 8–9, 292
Burnup chain, 2, 66
Burnup equations, 2–6
BWR. *See* Boiling water reactor (BWR)

C

CAOC. *See* Constant axial offset control (CAOC)
CFD. *See* Computational fluid dynamics (CFD)
Channel box, 131
Channel stability (thermal-hydraulic stability), 113, 136
Chemical and volume control system, 190
Chemical shim, 19, 189
 $\chi(E)$, 50
Clinch River Breeder Reactor Plant (CRBRP), 262
Coated particle fuel, 267, 274
Cold shutdown, 37
Collision probability method, 62
Computational fluid dynamics (CFD), 102–103
Constant axial offset control (CAOC), 201, 203
Control cell core, 159
Control group, 194
Control of power distribution, 155–161
Control reactivity balance, 37
Control rod(s), 252–254, 276
 cluster, 178
 drive mechanism, 192
 guide tube, 178
 insertion limit, 194
 pattern, 158
 worth, 19–22, 147, 288

- Coolant flow rate control, 165
 Coolant temperature, 238
 Coolant temperature coefficient, 35–36
Core, 271–273
 - burnup calculation, 90–92
 - expansion effect, 36
 - management, 171–174, 220–223
 - performance calculation system, 174
 - performance monitoring, 174, 221–223
 - stability, 113, 136
- Coupled core calculation**, 83
CPR. *See* Critical power ratio (CPR)
CRBRP. *See* Clinch River Breeder Reactor Plant (CRBRP)
Critical heat flux, 181
Critical power ratio (CPR), 135
1/v Cross section, 29
Cross sections, 52–60
Cruciform control rod, 131, 152
Cumulative damage fraction, 245
- D**
Decay ratio, 136
Delayed neutron fraction, 215
Departure from nucleate boiling ratio (DNBR), 181
Depletion, 6
 - calculation, 67
- Design calculations**, 49–93
Design limits of fuel, 274–276
Differential boron worth, 197
Differential control rod worth, 194
Diffusion equation, 71
Dittus-Boelter correlation, 107
DNBR. *See* Departure from nucleate boiling ratio (DNBR)
Doppler coefficient, 189
Doppler effect, 24
Doppler feedback, 134
Doppler power coefficient, 189
Doppler temperature coefficient, 179, 189
Doubling time, 233
Down-scattering, 52
- E**
EBR-I, 264
Effective multiplication factor, 24, 288
Eigen value, 39
Eigen value problem, 78–80
Elastic scattering cross section, 54
ENDF-6, 55
Energy conservation equations, 94, 106
Engineering heat flux hot channel factor, 199
Engineering safety factors, 261
Envelope curve, 203
Equilibrium concentrations, 17
Equilibrium core, 99, 100
Equivalent fissile content method, 219, 242–243
Erbia, 19
Erbium, 19
 η value, 31
Excess reactivity, 150, 289–291
Ex-core neutron detectors, 222
- F**
Fast breeder reactor, 232
Fast fission factor, 24
Fast reactor fuel, 243–244
 - assembly, 247–249
 - element, 244
- Fast reactors**, 231–267
Feedback cross section, 89
FEMAXI-6, 120
Few-groups, 65
Fick's law, 71
First-order perturbation theory, 43
Fission product (FP), 9
 - poisoning, 9–18
- Fission source**, 78–80
Fission spectrum, 50
Fixed-source problem, 79
FP. *See* Fission product (FP)
Fuel assembly, 131
Fuel batch size, 138
Fuel block, 273–274, 299
Fuel cladding integrity, 119
Fuel design, 118
Fuel discharge burnup, 138
Fuel failure prevention, 135–136
Fuel integrity, 237
Fuel inventory, 138–139
Fuel loading amount, 240
Fuel loading pattern, 159, 209
Fuel management, 175–178
Fuel rod, 117–125, 298–299
 - behavior, 120–122
- Fuel shuffling**, 159
Fuel storage and handling facilities, 176–178, 224–225
Fuel temperature coefficient, 25–27, 179

G

Gadolinia, 19, 153
 Gadolinium, 19
 Gauss-Seidel method, 76
 Group collapsing, 63–65

H

Hafnium, 21
 Haling distribution, 160–161
 Heat flux hot channel factor, 181, 199
 Heavy metal, 9
 Heavy nuclides, 54
 High burnup, 162–164
 core, 214–215
 fuel, 165–167, 208
 High Temperature Engineering Test Reactor (HTTR), 282
 High-temperature gas-cooled reactors (HTGRs), 267
 Homogenization, 63–65
 HTGRs. *See* High-temperature gas-cooled reactors (HTGRs)
 HTTR. *See* High Temperature Engineering Test Reactor (HTTR)
 H/U ratio, 145–146, 184

I

^{135}I concentrations, 10
 Infinite dilution cross section, 57
 Infinite multiplication factor, 9
 Inherent reactivity, 22–37
 Initial loading core, 99
 Inner iteration, 76

J

Jens-Lottes correlation, 107

L

Lattice burnup, 65–69
 Lattice calculation, 60–70
 1/v Law, 54
 Linear stability analysis, 113
 Liquid metal fast breeder reactors (LMFBRs), 233–234
 LLFPs. *See* Long-lived fission products (LLFPs)
 LMFBR. *See* Liquid metal fast breeder reactors (LMFBRs),
 LOCA. *See* Loss of coolant accident (LOCA)
 Local power peaking, 155

Local power range monitors (LPRMs), 174
 Long-lived fission products (LLFPs), 266–267
 Long-term fuel management planning, 224
 Long-term reactivity changes, 19
 Loss of coolant accident, 116–117
 Low leakage core, 209–210
 LPRMs. *See* Local power range monitors (LPRMs)

M

Macroscopic cross sections, 52–53
 Mass conservation equation, 106
 Maximum fuel centerline temperature, 181
 Maximum linear heat generation rate, 141
 MCNP, 60
 MCPR. *See* Minimum critical power ratio (MCPR)
 MDNBR. *See* Minimum departure from nucleate boiling ratio (MDNBR)
 Metal fuel, 264
 Microscopic cross sections, 53–55
 Minimum critical power ratio (MCPR), 119, 135
 Minimum departure from nucleate boiling ratio (MDNBR), 119
 Minor actinides (MAs), 266–267
 Moderator temperature coefficient, 28–35, 147, 187–188
 Moderator temperature feedback, 134
 Moderator-to-fuel volume ratio, 146, 181, 184
 Momentum conservation equation, 94, 105
 Monte Carlo codes, 60
 MOSRA, 85
 MOX fuel, 209, 264
 MOX-fueled core, 167–169, 215–219
 Multi-dimensional diffusion equation, 74–76
 Multi-group cross sections, 55–59
 Multi-group diffusion equation, 38
 MVP, 60

N

Negative temperature feedback, 55
 Neutron flux, 51
 Neutron flux redistribution effect, 192
 Neutron infinite multiplication factor, 147
 Neutron spectrum, 51
 Neutron temperature, 30
 Neutron transport equation, 49–51, 60–63
 Newton’s law of cooling, 95
 NJOY, 59
 Nodal diffusion, 83–87

Non-leakage probabilities, 24
 Non-1/v factors, 29–31
 N-TH coupled core calculation, 87, 97–99
 Nuclear data, 52–60
 Nuclear design, 282–292
 Nuclear enthalpy rise hot channel factor, 181, 198–199

O

Open-loop transfer functions, 113
 Operating cycle length, 138
 Operation management, 173
 Out-in pattern, 209, 210
 Overlapping method, 194

P

PCI. *See* Pellet clad interaction (PCI)
 PCIOMR. *See* Pre-conditioning interim operating management recommendation (PCIOMR)
 PCMI. *See* Pellet cladding mechanical interaction (PCMI)
 PEACO, 59
 Pebble-bed, 269
 Pellet cladding mechanical interaction (PCMI), 120, 164
 Pellet clad interaction (PCI), 136, 161–162
 Perturbation theory, 38–45
 Plant control, 108–111
 Plant dynamics, 94–125
 Plant stability, 114, 136
 Plutonium content, 242
 Plutonium equivalent worths, 243
¹⁴⁹Pm, 16–18
 Post-shutdown buildup, 17
 Power coefficients, 22, 134–135
 Power defect, 190, 192
 Power density, 144
 Power distribution, 237, 256, 277–280, 288, 292
 control, 198–207
 oscillation, 207–209
 Power peaking factor, 140–144, 198–199
 Power range monitor (PRM), 174
 Pre-conditioning interim operating management recommendation (PCIOMR), 161–162
 PREPRO, 59
 Pressure coefficient, 36
 Pressurized water reactor (PWR), 127–130, 178–225
 PRM. *See* Power range monitor (PRM)

Production, 6
 Production-destruction equations, 10
 Prompt neutron lifetime, 216
 Proportional-integral-derivative (PID) control, 108
²³⁹Pu, 7
²⁴⁰Pu, 7
²⁴¹Pu, 7
²⁴²Pu, 7
 PWR. *See* Pressurized water reactor (PWR)
 Pyrolytic carbon, 267

Q

Quasi-static method, 93

R

RCCA. *See* Rod cluster control assembly (RCCA)
 Reactivity, 10, 13–152
 balance, 37
 changes, 6–8
 characteristics, 250–256
 coefficients, 187–189, 250–251
 control, 152–153, 189–198, 251–252
 control by coolant flow, 153
 insertion rate, 235
 worth, 21
 Reactor core calculation, 49–122
 Reactor power uprates, 170–171, 220
 Reactor shutdown, 234–235
 margin, 135, 291
 Reactor stability, 113–114
 Refueling batch number, 182
 Regional stability, 114, 136
 Reload core design, 171–173, 221
 Removal cross section, 77
 Resonance escape probability, 24, 25, 28
 Resonance integral, 25
 Rod cluster control assembly (RCCA), 179, 190–195

S

Safety analysis, 115–117
 Scatter-loading pattern, 159
 Schrock-Grossman correlation, 107–108
 Self-adjoint, 40
 Self controllability, 235, 237
 Self-shielding factor, 25, 58, 59
 Shadowing effect, 22
 Shutdown group, 194

- Shutdown margin, 37, 193
Single channel model, 89, 94
Six-factor formula, 9
SLAROM-UF, 59
Slowing-down neutron source, 77
 ^{149}Sm , 7, 14–18
 poisoning, 17
SOR. *See* Successive over relaxation (SOR)
Space-dependent kinetics calculation, 92–93
Spatial self-shielding effect, 62
Specific power, 138
Spectral shift operation, 165
SRAC, 59
SRNM. *See* Startup range neutron monitor (SRNM)
Stability, 113, 237
Stainless steel neutron reflector, 213
Standby liquid control system, 116
Startup, 111–112
Startup range neutron monitor (SRNM), 174
Structure temperature coefficient, 36
Stuck-rod criterion, 37
Subchannel analysis, 102
Successive over relaxation (SOR), 76
- T**
Temperature coefficients, 22–24, 26
Temperature reactivity coefficients, 288–289,
 291–292
Thermal disadvantage factor, 27, 28
Thermal-hydraulic design, 257–258
Thermal iteration, 78
Thermal utilization factor, 24, 27, 28
Thom correlation, 107
TIPs. *See* Traversing in-core probes (TIPs)
Transfer function, 113
Transmutation, 13, 67
- U**
 ^{235}U , 7
 ^{236}U , 8
Unit lattice, 144
Up-scattering, 52
Uranium-saving technology, 164–165
- V**
Void coefficient, 36
Void disappearance, 193
Void reactivity coefficient, 134, 147
- W**
Water gap, 131
Weighting spectrum, 57
Westcott factor, 29
Wigner-Seitz method, 21
Wrapper tube, 234
- X**
 ^{135}Xe , 7, 10–15
 buildup, 13–14
 concentrations, 10
 transients, 18
Xenon, 114
Xe oscillation, 208
Xe spatial oscillation stability, 136
- Z**
Zirconium liner fuel, 164